FATIGUE MECHANISMS:

ADVANCES IN QUANTITATIVE MEASUREMENT OF PHYSICAL DAMAGE

Lankford/Davidson/Morris/Wei, *editors*

ASTM STP 811

FATIGUE MECHANISMS: ADVANCES IN QUANTITATIVE MEASUREMENT OF PHYSICAL DAMAGE

A conference
sponsored by ASTM
Committees E-9 on Fatigue
and E-24 on Fracture Testing
Dearborn, Mich., 10-11 May 1982

ASTM SPECIAL TECHNICAL PUBLICATION 811
J. Lankford and D. L. Davidson, Southwest Research Institute, W. L. Morris, Rockwell International, and R. P. Wei, Lehigh University, editors

ASTM Publication Code Number (PCN)
04-811000-30

1916 Race Street, Philadelphia, Pa. 19103

Library of Congress Catalog Card Number: 82-73773

NOTE

The Society is not responsible, as a body,
for the statements and opinions
advanced in this publication.

Printed in Baltimore, Md. (b)
July 1983

Foreword

The International Conference on Quantitative Measurement of Fatigue Damage, sponsored by ASTM Committees E-9 on Fatigue and E-24 on Fracture Testing in cooperation with the Office of Naval Research, was held in Dearborn, Michigan, on 10-11 May 1982. James Lankford, Southwest Research Institute, served as conference chairman; D. L. Davidson, Southwest Research Institute, W. L. Morris, Rockwell International, and R. P. Wei, Lehigh University, served as co-chairmen. This volume, *Fatigue Mechanisms: Advances in Quantitative Measurement of Physical Damage*, has been edited by Messrs. Lankford, Davidson, Morris, and Wei.

Related ASTM Publications

Residual Stress Effects in Fatigue, STP 776 (1982), 04-776000-30

Rolling Contact Fatigue Testing of Bearing Steels, STP 771 (1982), 04-771000-02

Low-Cycle Fatigue and Life Prediction, STP 770 (1982), 04-770000-30

Design of Fatigue and Fracture Resistant Structures, STP 761 (1982), 04-761000-30

Methods and Models for Predicting Fatigue Crack Growth under Random Loading, STP 748 (1981), 04-748000-30

Statistical Analysis of Fatigue Data, STP 744 (1981), 04-744000-30

Fatigue Crack Growth Measurement and Data Analysis, STP 738 (1981), 04-738000-30

A Note of Appreciation to Reviewers

The quality of the papers that appear in this publication reflects not only the obvious efforts of the authors but also the unheralded, though essential, work of the reviewers. On behalf of ASTM we acknowledge with appreciation their dedication to high professional standards and their sacrifice of time and effort.

ASTM Committee on Publications

ASTM Editorial Staff

Janet R. Schroeder
Kathleen A. Greene
Rosemary Horstman
Helen M. Hoersch
Helen P. Mahy
Allan S. Kleinberg
Virginia M. Barishek

Contents

Growth of Small Cracks

FATIGUE CRACK GROWTH

Introduction

In 1978, ASTM sponsored an International Symposium on Fatigue Mechanisms, held in Kansas City, Missouri.[1] The present volume constitutes the proceedings of a follow-up to this earlier conference, with the goal of exploring advances in technology which might now permit more detailed quantitative measurement of fatigue damage. During the stages of formulating the conference, its theme was expanded from general consideration of damage measurement methods to an emphasis on both measurement and the ultimate use of cyclic damage parameters.

"Damage" is a term much discussed, and is often used in different ways by different investigators. For some researchers, cyclic damage consists of dislocation arrays, while for others "damage" means the presence of an actual fatigue crack. Evidently, at this time, fatigue damage remains in the eye of the beholder, and is dependent upon what aspect of fatigue is being studied. One is reminded of the story of the blind men describing an elephant, one feeling the trunk, another the ears, and so on. Although a unified definition of the term "cyclic damage" did not result from the conference discussions, many papers did report real progress in the measurement of damage parameters relevant to specific aspects of cyclic fatigue failure.

The conference was organized into two general areas: (*1*) crack initiation, fatigue lifetime, and the early (microcrack) stages of crack growth, and (*2*) fatigue damage associated with macroscopic-sized fatigue crack extension. In each case, authors attempted to achieve quantitative characterization of material "damage," together with mathematical models of the results in such form as would (at least) permit qualitative prediction of damage under different, but similar, conditions. Significant progress was recorded in certain cases.

Discussions of conference presentations have been included. The questions asked were presented in written form to the authors following the conference, and the replies contained in this volume represent their written responses, which in a few cases contain more detail than their verbal replies at the conference.

The Conference Organizing Committee is pleased to acknowledge the sup-

[1] *Fatigue Mechanisms, ASTM STP 675,* J. T. Fong, Ed., American Society for Testing and Materials, 1979.

port and encouragement of their own organizations, Southwest Research Institute, Lehigh University, and Rockwell International, in planning the conference. The committee also greatly appreciates the dedicated performance of the ASTM staff.

J. Lankford

Southwest Research Institute, San Antonio, Texas; symposium chairman and editor

D. L. Davidson

Southwest Research Institute, San Antonio, Texas; symposium co-chairman and editor

W. L. Morris

Rockwell International, Thousand Oaks, California; symposium co-chairman and editor

R. P. Wei

Lehigh University, Bethlehem, Pennsylvania; co-chairman and editor

Early Stages of Damage

Crack Initiation

Haël Mughrabi,[1] *Renhui Wang,*[2] *Klaus Differt,*[1] *and Uwe Essmann*[1]

Fatigue Crack Initiation by Cyclic Slip Irreversibilities in High-Cycle Fatigue

REFERENCE: Mughrabi, H., Wang, R., Differt, K., and Essmann, U., **"Fatigue Crack Initiation by Cyclic Slip Irreversibilities in High-Cycle Fatigue,"** *Fatigue Mechanisms: Advances in Quantitative Measurement of Physical Damage, ASTM STP 811*, J. Lankford, D. L. Davidson, W. L. Morris, and R. P. Wei, Eds., American Society for Testing and Materials, 1983, pp. 5-45.

ABSTRACT: Dislocation mechanisms of fatigue crack initiation in high-cycle fatigue are formulated, with special consideration given to those material properties which determine the cyclic slip mode. The models developed are related to pertinent experimental observations, referring mainly to copper mono- and polycrystals fatigued at room temperature. In particular, the following topics are considered: (*1*) the origin of cyclic slip irreversibilities in the bulk and near the surface, (*2*) computer simulations of surface roughening by random irreversible slip processes in planar- and wavy-slip materials, and (*3*) fatigue crack initiation by cyclic strain localization in persistent slip bands (PSBs) in mono- and polycrystalline wavy-slip materials. The evolution of the surface profile at emerging PSBs is described by a new semiquantitative model which is compared with other models. The model distinguishes between the rather rapid formation of extrusions and the more gradual development of surface roughness. It is shown that specific predictions regarding differences between PSB surface-profiles in mono- and polycrystals are borne out fully by the observations. In the case of copper polycrystals, the experiments show that PSBs are not only responsible for slip-band cracking in PSBs but also induce intergranular cracks. A model is proposed according to which cracks initiate as a result of the piling-up of PSB-matrix interface dislocations against the grain boundaries. Furthermore, the supporting role of environmental interaction and/or deformation-induced diffusion and grain boundary sliding is discussed.

KEY WORDS: high-cycle fatigue, irreversible slip, random slip, wavy slip, planar slip, annihilation of dislocations, cyclic strain localization, persistent slip bands, surface roughening, extrusions, transgranular and intergranular fatigue crack initiation, early fatigue crack propagation.

[1]Research Associate, Max-Planck-Institut für Metallforschung, Institut für Physik, 7000 Stuttgart 80, Federal Republic of Germany.

[2]Lecturer, Department of Physics, Wuhan University, Wuhan, People's Republic of China, and former Visiting Scientist, Max-Planck-Institut für Metallforschung, Institut für Physik, 7000 Stuttgart 80, Federal Republic of Germany.

About ten years ago Laird and Duquette [*1*] thoroughly reviewed the mechanisms of fatigue crack initiation.[3] One of their conclusions was that the models available at that time were "qualitatively and quantitatively inadequate." This conclusion is still largely valid today, in spite of the fact that significant progress has been made in several special cases of fatigue crack initiation and of early crack growth both in high-cycle (low-strain) fatigue and in low-cycle (high-strain) fatigue; see, for example, Refs *2* to *17*.

The present work confines itself to the study of the initiation (and early propagation) of fatigue cracks under conditions of high-cycle fatigue. One of the objectives of the introductory first part is to provide a general description in terms of dislocation processes of those microscopic events whose combined action is responsible for the initiation of fatigue cracks in many metals and alloys fatigued in the subcreep temperature range. These general concepts are then applied to fatigued face-centered-cubic (fcc) metals and alloys with the aim of deriving semiquantitative models of the near-surface dislocation behavior and of trans- and intergranular fatigue crack initiation. In particular, this involves the role of cyclic strain localization in persistent slip bands (PSBs), the evolution of surface roughness as a result of (localized) irreversible cyclic slip, and the interaction between PSBs and grain boundaries. The considerations are considerably facilitated by taking only one slip system into account, a simplification that appears justified in view of recent studies that show the predominance of single slip in high-cycle fatigue [*13,18–21*]. In the second part, recent experimental observations of the development of the surface topography and of the initiation of cracks in fatigued mono- and polycrystalline copper [*13,22,23*] are presented and discussed in terms of the concepts introduced earlier.

Basic Concepts

Origin of Cyclic Slip Irreversibilities

Irreversibilities of dislocation glide during cyclic straining arise whenever individual glide processes on a given glide plane are not perfectly reversed upon changing the sense of deformation. The classical example is the glide of a screw dislocation which undergoes cross slip before reversing its path [*24*]. In the absence of dislocation climb, the motion of edge dislocations is generally considered to be reversible, but see below. If we consider an expanding dislocation loop, however, the motion of different segment parts is correlated. As a consequence, for example, the irreversible cross slip of a segment of predominant screw character can give rise to an inequality of the forward and reverse glide of the remaining nonscrew segment and thus to a slip irreversibility of a more general type. We shall now consider the importance of the mutual anni-

[3]The italic numbers in brackets refer to the list of references appended to this paper.

hilation of pairs of unlike screw *and* edge dislocations and of the emergence of gliding edge dislocations at the surface as sources of irreversible slip.[4]

Cross slip is frequently induced by internal stresses and related in particular to the mutual attraction and annihilation of unlike screw dislocations [*25–27*] on glide planes spaced less than a critical annihilation distance y_s apart. As discussed elsewhere [*13*], y_s decreases not only with decreasing stacking fault energy, increasing strain rate, and decreasing temperature, but also with increasing yield stress and in the presence of short-range order. The parameter y_s is thus considered to be more suitable for characterizing the slip mode (wavy or planar) than just the stacking-fault energy.

During the process of irreversible cyclic deformation (fcc) metals and alloys spend a considerable fraction of their lifetime in steady-state cyclic saturation, where a dynamic balance exists between dislocation multiplication and annihilation [*28–31*]. Hence the mutual annihilation of unlike dislocations constitutes a major source of cyclic slip irreversibility which persists in cyclic saturation. In addition to the mutual annihilation of screw dislocations by stress-induced cross slip, there is strong evidence for the annihilation also of very closely spaced nonscrew (edge) dislocations of opposite sign which can be characterized by a (very small) annihilation distance y_e [*13,29,30,32*]. The mutual annihilation of unlike edge dislocations is an inescapable consequence of the easily verifiable argument that maintenance of cyclic saturation by a dynamic equilibrium between dislocation multiplication and annihilation must involve not only screw but also nonscrew dislocations [*30,33*].

If we confine ourselves to single slip with dislocations of type i with an annihilation distance y_i and Burgers vector $\mathbf{b}$ arranged in homogeneously distributed groups of n_i dislocations of the same sign, it can be shown [*29,30,34*] that annihilation of dislocations during steady-state cyclic deformation will not occur up to a shear strain amplitude $\gamma_{pl,i}$, provided

$$\beta = \frac{2\gamma_{pl,i} y_i}{b \cdot n_i} < 1 \tag{1}$$

If the criterion $\beta < 1$ is fulfilled, the same dislocations can move to-and-fro reversibly, whereas for $\beta = 1$ (or larger [*34*]), slip becomes irreversible and saturation will be maintained by a dynamic equilibrium between the generation and annihilation of dislocations.

Under conditions of partly irreversible cyclic slip, the slip irreversibility p can be defined as the ratio of the irreversible part $\gamma_{pl,irr}$ of the plastic shear strain amplitude γ_{pl} to γ_{pl} [*31,34*]:

$$p = \frac{\gamma_{pl,irr}}{\gamma_{pl}} \tag{2}$$

[4]Here and later the term *unlike* refers to a pair of dislocations which have the same Burgers vector but are of opposite sign.

So far, our discussion of irreversible cyclic slip has implicitly been confined to bulk behavior. In cyclic deformation, the near-surface processes which govern the initiation of fatigue cracks are of primary concern. Hence a distinction between irreversibility of cyclic slip processes occurring in the *bulk* and near the *surface* is necessary [*13*]. The following simple considerations show that the slip irreversibilities at the surface and in the bulk are rather similar for gliding screw dislocations but can be substantially different for gliding edge dislocations. For this purpose, we regard the generation of slip steps at the top face of a crystal, where the active Burgers vector has the largest component perpendicular to the surface. In the case of a screw dislocation gliding on the primary glide plane, its motion is perpendicular to its Burgers vector and parallel to the slip trace. The glide irreversibility will be governed mainly, as in the bulk, by the ease of cross slip, except that at the free surface the behavior can be modified somewhat by image forces [*35*]. An edge dislocation gliding towards the surface, on the other hand, with its direction of motion parallel to its Burgers vector and perpendicular to the slip trace, will emerge at the surface over the entire length of the generated slip line. Unless the edge dislocation is regenerated and returns into the crystal during reverse glide on its original glide plane, its emergence will constitute a source of irreversible slip which has no counterpart in the bulk behavior.

Evolution of Surface Roughness by Random Irreversible Glide Processes

The development of surface roughness by irreversible cyclic slip is well documented; see, in particular, Wood's early observations of taper sections of fatigued metals [*36*]. These observations led May [*37*] to develop a statistical model of surface roughening which was based on the assumption that slip lines in fatigue form by randomly distributed forward and reverse slip displacements. In light of our earlier conclusion that, during irreversible steady-state cyclic deformation, dislocations are continuously annihilated and newly generated (both in the bulk and near the surface), the assumption of random slip appears realistic [*14,15*].

On this basis, Differt and co-workers [*15*] studied the evolution of surface roughness due to randomly distributed forward and reverse (positive and negative) displacements by computer simulation. Surface-roughness profiles were obtained for random slip in glide regions composed of up to 5000 atomic glide planes, involving up to 4×10^6 individual (positive and negative) slip events. The dependence of the *average* surface roughness on the number of cycles N at a given plastic shear strain amplitude γ_{pl} could be characterized by the width w of the roughness profile which is defined as the difference between the largest positive and negative displacements parallel to $\mathbf{b}$. The mean width $\bar{w}$ is obtained as an average value based on ten computer simulations. If one considers

a large number of slip displacements due to groups of n dislocations (of the same sign), $\bar{w}$ can be expressed as

$$\bar{w} = \sqrt{6nbhpN\gamma_{pl}} \tag{3}$$

where h denotes the thickness of the glide region studied ($h = 1$ μm for the maximum number of 5000 glide planes spaced 0.2 nm apart that were studied). Equation 3 may be used to determine the product of n (the number of dislocations per group) and p (the slip irreversibility at the surface) by evaluating $\bar{w}$ for experimentally observed surface-roughness profiles such as those published by Lukáš and Klesnil [*38,39*] for fatigued copper and copper-zinc alloys.

The most important feature of the surface-roughness profile with respect to the initiation of fatigue cracks is the distribution of more or less deep and sharp notch-like valleys that form gradually during the process of irreversible random slip. This central aspect remains difficult to quantify as long as it is not possible to state at which stage severe notches are formed which begin to act as critical crack nuclei. However, the process of crack initiation can be characterized qualitatively by three stages [*15*] as follows. During an initial period of random irreversible slip a rough surface topography evolves. After this roughness has exceeded a critical magnitude in local regions, irreversible slip becomes accentuated in these regions and can no longer be considered random. In the final stage, the severeness of locally enhanced irreversible slip can lead to shear decohesion (Stage I crack initiation).

An important feature of surface-roughness profiles formed by random irreversible slip on only one slip system is that the characteristic wavelengths of the roughness profiles are significantly larger along the slip traces than in the direction perpendicular to the slip traces [*15*]. Thus the notchlike valleys that develop are long and narrow and represent more dangerous transgranular crack initiation sites than the much shorter surface irregularities that would evolve during random multiple slip in high-strain fatigue.

Irreversible Random Slip in Fatigued Planar-Slip Alloys

We now wish to consider the irreversibility and the development of surface roughness in fatigued planar-slip alloys such as Cu-30at.%Zn and Cu-10at.%Al. These materials are characterized by difficult cross slip—that is, by very small values of y_s—and the slip mode is coarse on a microscale due to the fact that the dislocations are arranged in (rather homogeneously distributed) groups of typically about 100 dislocations both in tensile deformation [*27,40,41*] and in fatigue [*42,43*]. The coarseness of the slip mode on a microscale is known to greatly enhance the susceptibility to fatigue crack initiation in single-phase planar slip and in age-hardened alloys; see, for example, Refs *11,12*, and *44*.

The annihilation distance y_s of screw dislocations in Cu-30at.%Zn (α-brass) and Cu-10at.%Al has been estimated as $y_s \approx 5$ nm [*13*] from the closest spacings of stable dislocation dipoles (multipoles) found in published transmission electron microscopy (TEM) micrographs [*40,41*]. We note that the value y_e for edge dislocations which is not known is presumably significantly smaller and can be assumed to be not very different from the value $y_e \approx 1.6$ nm found in pure copper [*30,32*]. In the discussion of slip irreversibility in the bulk we can hence confine ourselves for the sake of simplicity to the glide of groups of screw dislocations and assume that the latter make a contribution $\gamma_{pl,s} \approx 0.5\,\gamma_{pl}$ to the plastic shear strain amplitude γ_{pl}. With Eq 1 we then find for the screw dislocations, using $n_s \approx 100$, $y_s \approx 5$ nm, and $\gamma_{pl,s} \approx 0.5\,\gamma_{pl}$, that $\beta \ll 1$ for all values of γ_{pl} of interest. This implies that, in steady-state cyclic deformation, dislocation glide *in the bulk* should be largely reversible [*13*], as had been asserted earlier by Strutt [*43*]. On the other hand, however, Lukáš and Klesnil [*38,39*] have reported the development of a rough surface topography in fatigued Cu-30at.%Zn crystals, and Katagiri and co-workers [*45*] have observed the formation of Stage I shear cracks in the planar-slip bands of similarly fatigued polycrystals of the same material. These observations indicate clearly that cyclic slip *at the surface* is at least partly irreversible. Qualitatively, we attribute this slip irreversibility (which is suggested to be confined to the surface) to the emergence of nonscrew dislocation groups and possibly also to the enhancement of cross slip at the surface by image forces, as discussed earlier.

In a more quantitative approach, Differt and co-workers [*15*] have compared surface-roughness profiles obtained by computer simulation with the observations of Lukáš and Klesnil [*38,39*] on fatigued Cu-30at.%Zn crystals. Fig. 1*a* shows an example from the work of Lukáš and Klesnil [*38*], referring to a crystal fatigued for approximately 5×10^5 cycles at a constant axial stress amplitude $\sigma = \pm 82$ MPa. From earlier work of the same authors on polycrystalline material [*42*], it can be deduced that for this stress level $\gamma_{pl} \approx 10^{-4}$ in saturation. An example of a surface profile obtained by computer simulation is shown for comparison in Fig. 1*b*. This profile was generated by random slip of groups of 100 dislocations in a glide region containing 5000 glide planes ($h = 1$ μm) with 60 forward and reverse displacements, respectively. Inspection of the observations of Lukáš and Klesnil yields a mean profile width $\bar{w} \approx 0.5$ μm for $h = 7$ μm. In order to obtain agreement with the computer simulation (for $n = 100$, $h = 1$ μm, $b = 2.5 \times 10^{-10}$ m) we conclude from Eq 3 that the irreversibility at the surface must be $p \approx 0.5\%$ [*15*]. (It should be noted that, because the number of events is rather small in this case, Eq 3 can only provide a rough estimate.) For another example from the work of Lukáš and Klesnil [*39*], referring to $\sigma = \pm 118$ MPa, $N = 2 \times 10^4$, and $\gamma_{pl} \approx 4 \times 10^{-4}$, we have evaluated $\bar{w} \approx 0.75$ μm for $h = 8$ μm from the observations, and we find by comparison with Eq 3 that $p \approx 3\%$. These numbers depend, of course, on the experimental parameters employed, which are frequently not known with high accuracy. Thus, had we for example assumed $n = 50$ instead of

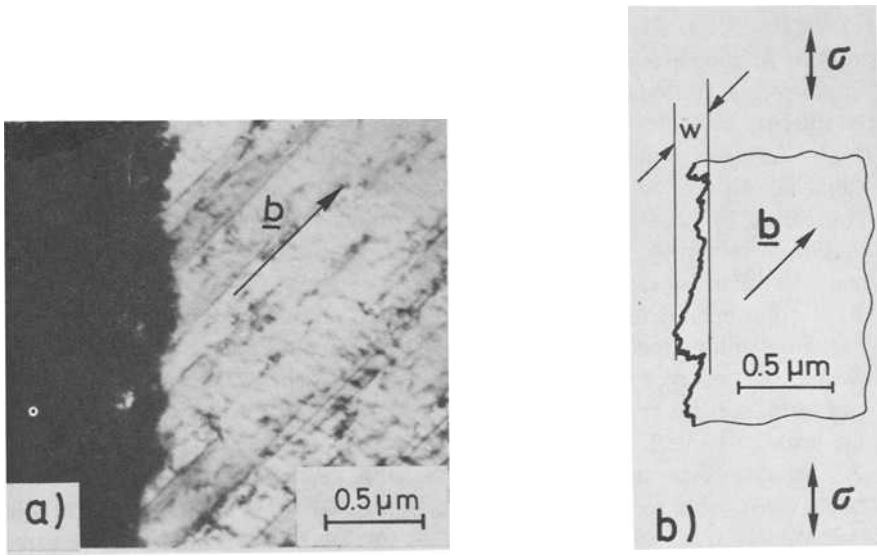

FIG. 1—*Evolution of surface roughness by random irreversible cyclic slip in a planar-slip material. Cu-30at.%Zn, at* $\gamma_{pl} \approx 10^{-4}$*; see text for details.* (a) *Experimentally observed roughness profile.* $N \approx 5 \times 10^5$*. From Lukáš and Klesnil* [38]. *Courtesy of the authors and of Akademie-Verlag.* (b) *Surface roughness profile generated by computer simulation. The profile corresponds to* $N \approx 1.5 \times 10^6$ *cycles for* $p \approx 0.5\%$*. From Ref* 15.

$n = 100$, then p would have been found to be twice as large as in the examples given.

The main conclusions from this comparison between computer simulation and observation are that in a planar-slip alloy such as Cu-30at.%Zn glide is largely reversible in the bulk but not at the surface [*13*] and that *the slip irreversibility at the surface increases with increasing* γ_{pl}. The slip irreversibility at the surface is rather small in absolute numbers but, because of the relatively large value of n, the effect on the roughness profile, compare Eq 3, is significant. Again, the question remains at what stage critical crack nuclei form which can develop into Stage I shear cracks such as those observed by Katagiri and co-workers [*45*].

Cyclic Strain Localization in Persistent Slip Bands

The most prominent cause of fatigue crack initiation in wavy-slip fcc metals fatigued in the high-cycle range is the localization of cyclic strain in persistent slip bands (PSBs) [*8,9,13,28,29,35,46–49*]. It has been demonstrated in experiments on single crystals of several fcc metals that a threshold value of γ_{pl} exists below which PSBs do not form [*13,28,29,50*]. Up to this threshold value so-called bundles or veins of clustered primary edge-dislocation dipoles

[*7,8,13,29,31,50–53*] form during cyclic hardening and stabilize in cyclic saturation. At the threshold value of γ_{pl}, cyclic hardening occurs up to a critical value τ_{PSB} of the shear stress amplitude at which the veins break down locally as the first PSBs develop in the form of thin lamellae (of ≈ 1 μm thickness) of high-slip activity parallel to the primary glide plane, embedded in the "matrix" dislocation distribution of dipolar veins. This process is usually accompanied by cyclic softening; see, for example, Ref *28*.

The threshold values of the plastic strain amplitude $\gamma_{pl,M}$, up to which the matrix is stable in saturation, and of the shear stress τ_{PSB} at which PSBs form, have so far been determined only for a limited number of pure fcc metals and for some dilute fcc solid-solution alloys in which PSBs form in a similar fashion. (For larger solute contents, slip becomes more planar and PSBs do not form; see, for example, Refs *38* and *39*.) These values of $\gamma_{pl,M}$ and of τ_{PSB} are listed in Table 1. It is estimated that these values are accurate within about 20 and 2%, respectively. Table 1 contains in addition similar data that have become available recently for some age-hardened alloys containing shearable precipitates [*21,54,55*]. Very interesting related results that have been obtained on fatigued spinodally decomposing alloys, in particular on Cu-4at.%Ti, by Sinning and Haasen [*16,56,57*] are more difficult to classify in this simple scheme and the reader is referred to the original publications.

The local breakdown of the metastable "matrix" dislocation distribution in pure metals and solid-solution alloys occurs after the veins have hardened to a critical extent at which they can no longer accommodate the imposed plastic strain amplitude [*8,13,28,29,35,48,49,58*]. In the case of age-hardened alloys, the formation of PSBs is essentially related to the localized repeated cutting

TABLE 1—*Threshold values of the plastic shear strain amplitudes* ($\gamma_{pl,M}$) *and the shear stress amplitudes* (τ_{PSB}) *for the formation of PSBs in fcc metals, solid solutions, and precipitation-hardened alloys at room temperature.*

Materials	$\gamma_{pl,M}$	τ_{PSB}, MPa	Ref
	PURE METALS		
Copper	6×10^{-5}	27.5	*28,50*
Nickel	10^{-4}	52	*29*
Silver	6×10^{-5}	17.5	*29*
	SOLID-SOLUTION ALLOYS		
Cu-2at.%Co	3×10^{-4}	27.5	*54*
Cu-2at.%Al	1.5×10^{-4}	33	*54*
	AGE-HARDENED ALLOYS		
Cu-1.4at.%Co, underaged	2×10^{-4}	66	*54,55*
Cu-2at.%Co, underaged	3×10^{-4}	73	*54,55*
Al-2.1at.%Zn-1.3at.%Mg, underaged	1.3×10^{-4}	97	*55*
Al-2.1at.%Zn-1.3at.%Mg, peak-aged	$< 2 \times 10^{-4}$	110	*55*
Al-2.4at.%Cu, peak-aged	1.5×10^{-5}	95	*21*

and degradation of the precipitates; see, for example, Refs *55* and *59* to *61*. The basic requirements for the formation of PSBs in single-phase materials have been summarized before [*29*], and the threshold conditions have been formulated in more quantitative terms recently for single-phase materials and for precipitation-hardened alloys [*58*].

Cyclic strain localization in PSBs in low-amplitude fatigue tests has the detrimental consequence that high-strain fatigue conditions prevail on a local scale and give rise to the initiation of cracks. The decisive difference with respect to overall low-cycle high-strain fatigue is that, since the localized deformation in PSBs is essentially confined to one slip system, the formed cracks are Stage I shear cracks which propagate only slowly. In pure fcc metals, the mean *local* shear strain amplitudes in PSBs are approximately $\gamma_{pl,PSB} \approx 7.5 \times 10^{-3}$ [*28,49,50*]. Thus an average *strain localization factor*

$$\frac{\gamma_{pl,PSB}}{\gamma_{pl,M}} \approx 10^2 \tag{4}$$

applies. We note, however, that according to recent work by Laird and co-workers [*62*] on copper crystals, $\gamma_{pl,PSB}$ can be considerably larger (or smaller) in individual PSBs. In age-hardened Al-2.4at.%Cu monocrystals, Cheng and co-workers have found that $\gamma_{pl,PSB}$ is as large as ≈ 0.5 [*21*]. This suggests that, in precipitation-hardened alloys containing PSBs, the strain localization factor is larger by more than one order of magnitude than in pure single-phase materials.

Surface Topography at Emerging PSBs

The PSBs studied so far in pure fcc metals consist of more or less equidistantly spaced dislocation walls which are densely packed with narrow edge-dislocation dipoles and which are separated by so-called channels of low dislocation density. The cyclic strain in the channels is carried mainly by gliding screw dislocations.[5] A detailed analysis involving the considerations underlying Eq 2, supplemented by additional more-refined evaluations [*14,29,30,34*], shows that steady-state cyclic deformation of PSBs in copper is characterized by the following features: (*1*) Dislocation glide is irreversible in the PSBs as opposed to the matrix and is governed by a dynamic balance between the generation of

[5]We take the opportunity to remark that in our previous publications it has always been emphasized that in the PSBs the screw dislocations carry the major part of the plastic strain [*13,29,30,49,58,63*] and that, contrary to recent statements by Laird and co-workers [*62*], we have not changed our views on this point, which are based on TEM. Irrespective of this, the main conclusion that Laird and co-workers derive from their surface observations at optical magnification, namely that the screw dislocations carry as much as one hundred times more strain than the edge dislocations, appears unjustified. Surface studies do not, as a matter of principle, permit us to distinguish the relative contributions of screw and edge dislocations to glide, and the lengths of individual slip lines and dislocation slip paths cannot be deduced at 200-fold magnification.

dislocations and the annihilation of screw dislocations in the channels ($y_s \approx 50$ nm) and of edge dislocations in the dislocation walls ($y_e \approx 1.6$ nm). (*2*) Point defects are formed in rather large numbers in the dislocation walls by the mutual annihilation of closely spaced unlike edge dislocations [*14,29,30,32,49*]. At the same time these point defects can be collected by dislocations located or passing within a capture distance y_p. Thus an equilibrium concentration of point defects is established in cyclic saturation, as originally concluded by Polák on the basis of electrical resistivity measurements [*64*]. Several arguments have been put forward suggesting that the point defects prevailing under equilibrium conditions have predominantly vacancy character [*14,30*] and that their *local* atomic concentration in the dislocation walls in saturation is given by

$$C_v^{sat} = \frac{y_e^2 \rho_e^{sat} b}{2 y_p} \tag{5}$$

Here ρ_e^{sat} is the *local* density of edge dislocations in the walls which is typically $\rho_e^{sat} \approx 5 \times 10^{15}$ m^{-2} [*30,31,53,65*]. In Eq 5, C_v^{sat} is larger by a factor of two than in the original publication [*14*] where it was supposed that a passing dislocation collects a point defect located within a capture distance y_p above *or* below the glide plane. Here, a vacancy-type defect is assumed to be collected by a dislocation only, if it lies within a capture distance y_p on the compression side of the glide plane. Assuming $y_p \approx b$, Eq 5 yields $C_v^{sat} \approx 6 \times 10^{-3}$. Since the walls occupy only about 10% of the PSB-volume, the *mean* atomic concentration of vacancy-type defects in the PSBs is $\bar{C}_v^{sat} \approx 0.1\, C_v^{sat} \approx 6 \times 10^{-4}$.

These features form the basis of a new model of the evolution of the surface profile at emerging PSBs which was put forward recently by Essmann, Goesele, and Mughrabi (EGM) [*14*]. In this model, the surface profile at emerging PSBs is caused by (*1*) the rather rapid formation of *extrusions* and (*2*) the more gradual development of *surface roughness* by random irreversible slip. These two features and their combined effects will now be discussed in more detail and compared with other related models.

Formation of Extrusions—It is shown by EGM that, during the process of glide and annihilation of edge dislocations, layers of dislocations are deposited at the PSB-matrix interfaces, as shown schematically in Fig. 2*a*. These interface dislocations correspond to multipolar arrays built up of interstitial-type dipoles. The number of atoms contained in the extra atomic planes is equivalent to the number of vacancies that prevail in the PSBs. Because of the interstitial nature of the interface dislocation-dipole layer, a residual internal compressive stress σ_{int} is set up in the PSB in the direction of **b**. This internal stress σ_{int} can be estimated as follows. The number m of interface dislocation-dipoles follows from

$$mb = \bar{C}_v^{sat} \cdot D \tag{6}$$

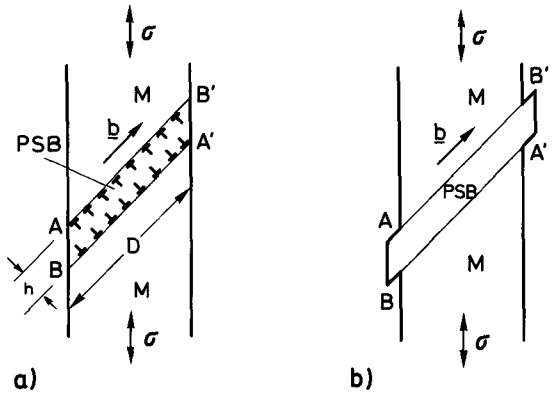

FIG. 2—*Formation of extrusions by emergence of PSB-matrix interface dislocations (schematically). M is matrix; σ is axial stress. After Ref* 14. (a) *Arrangement of interface dislocations corresponding to an interstitial-type dislocation-dipole layer. All other microstructural features (edge dislocation walls, screw dislocations) have been omitted for the sake of clarity.* (b) *Extrusions formed by emergence of interface dislocations.*

where D is the dimension of the PSB measured in the direction of **b**. The elastic compressive internal strain is given by

$$\epsilon_{\text{int}} = -\frac{mb}{D} = -\bar{C}_v^{\text{sat}} \tag{7}$$

Hence

$$\sigma_{\text{int}} = \epsilon_{\text{int}} \cdot E = -\bar{C}_v^{\text{sat}} \cdot E \tag{8}$$

where E is Young's modulus of elasticity. With $\bar{C}_v^{\text{sat}} \approx 6 \times 10^{-4}$, σ_{int} is found to be ≈ -6 MPa. A more rigorous calculation yields a slightly smaller value [*14*].

Under the action of the applied stress σ, the interface dislocations tend to glide out of the crystal at A and A' during the tensile phases and at B and B' during the compressive phases of cycling, respectively. This process leads to the formation of extrusions on both sides of the PSB, as indicated in Fig. 2*b*. Depending on the ability of the vacancy-type defects to migrate and to escape from the PSBs into the matrix, EGM consider two cases [*14*].

At *low temperatures* the vacancy-type defects cannot leave the PSB. The extrusions attain their maximum height when all interface dislocations have left the crystal. Thus the total height of the extruded material (in the direction of **b**) is given by

$$e = mb = \bar{C}_v^{\text{sat}} \cdot D \tag{9}$$

In other words, the heights of the extrusions on either side of the crystal are $0.5e$. For a specimen of 3 mm diameter ($D \approx 4.2$ mm), $0.5e \approx 1.2$ μm. Essmann and co-workers called these extrusions which cease to grow after all interface dislocations given by Eq 6 have left the crystal, *static extrusions*. Assuming that the emergence of the interface dislocations is not hindered seriously by other processes, *static extrusions are expected to form rather rapidly at the rate at which steady-state conditions are approached.*

At *higher temperatures* at which the vacancy-type defects become mobile, EGM consider the possibility that some of them can escape into the matrix. In this case the lost vacancies are replaced continuously by subsequent dislocation annihilation processes. Thus the number of interstitial-type dislocation-dipoles constituting the multipolar PSB-matrix interface dislocation layer will continue to increase beyond the value given by Eq 6, giving rise to *continuously growing extrusions*. The kinetics of this process have not been formulated quantitatively so far. EGM have noted that this process can only operate effectively in a thin PSB layer ($\approx$ 5 to 10 nm) at the PSB-matrix interface, since point defects located further away from the matrix will probably anneal out at dislocations within the PSB-walls before reaching the matrix. Thus continuous extrusion growth is considered to be a more probable process in very thin PSBs (such as those prevailing in fatigued age-hardened alloys) than in PSBs of about 1 μm thickness, as observed in pure fcc metals.

Surface Roughening by Random Irreversible Glide Processes—Surface slip steps at PSBs emerging at the top face of a crystal are formed mainly by screw dislocations gliding in channels bounded by the surface on one side and by dislocation walls on the other [*8,13,14,35,47-49*]. A statistical evaluation of the overall slip irreversibility p_{PSB} in PSBs has been performed by Essmann [*34*]. He finds for the slip irreversibility due to the glide of screw dislocations $\chi = 0.4$ and, by taking into account the correlation between the glide of screw and edge dislocations, finally obtains $p_{PSB} \approx 0.5\,\chi \approx 0.2$. The latter value is similar to an estimate by Woods [*31*] for Cu-5at.%Al. Using the value $p_{PSB} = 0.2$, Differt and co-workers [*15*] have studied by computer simulation the development of the surface topography due to random slip at emerging PSBs as a function of the number of cycles N. The calculations were performed for a typical thickness of the PSB, $h = 1$ μm, and γ_{pl} was replaced by the local value $\gamma_{pl,PSB} \approx 7.5 \times 10^{-3}$. It was assumed that $n_s = 1$—that is, that the screw dislocations act singly and not in groups—, since the groups of screw dislocations that have been observed in PSBs by TEM [*28,30,63*] are not believed to consist of dislocations on the same atomic plane. As described previously, the kinetics of the development of the surface roughness follow Eq 3; $\bar{w}$ increases proportionally to $\sqrt{N}$. Specifically, Eq 3 yields for PSBs in copper:

$$\bar{w}_{PSB} \approx 1.5 \times 10^{-3} \sqrt{N}\,[\mu m] \tag{10}$$

when N refers to the number of cycles *after* the PSB has been formed. Thus more than 10^5 cycles are required in order to generate a surface roughness with

a mean profile width $\bar{w}_{PSB} \approx 0.5$ μm in a surface region containing 5000 glide planes.

Combined Effect of Extrusions and Surface Roughness—Figure 3 shows schematically how the surface profile of a PSB is expected to develop as a function of N or cumulative plastic strain $\gamma_{pl,cum} = 4N \cdot \gamma_{pl,PSB}$. The diagram illustrates the case of a static extrusion that has stopped growing after saturation has been approached within 1000 cycles following the formation of the PSBs. Figure 4 shows an example of an actually computed PSB surface-profile with a static extrusion (for $D = 0.2$ cm) and a superimposed roughness profile generated by a total of 4×10^6 (positive and negative) random irreversible slip displacements corresponding to $N \approx 1.7 \times 10^5$ cycles.

Related Models of Extrusions and Intrusions—It is evident from Fig. 2 that, if the dislocation-dipole layer were of vacancy-type, then the emergence of the interface dislocations would give rise to the formation of intrusions [*14*]. In the EGM model, the point defects prevailing in cyclic saturation in this case would have to be predominantly of interstitial character. This possibility was also discussed but considered less probable [*14*]. Several other authors have recognized intuitively that dislocation-dipole arrays, similar to those discussed here, can give rise to extrusions and intrusions [*66–70*]. Some of these models have been worked out in detail under special assumptions [*69, 70*]. In their present form, these models do not incorporate some of the microscopic aspects evident from TEM observations but provide a detailed micromechanical description of the behavior of dipolar dislocation layers under alternating stresses. Most earlier dislocation models which have been reviewed by Laird and Duquette [*1*] differ from the present model in many respects, mainly because, unlike the

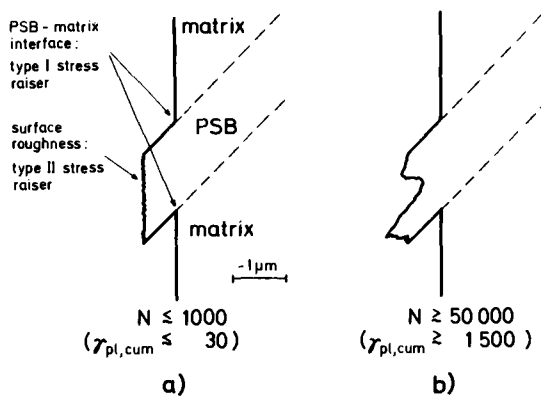

FIG. 3—*Development of stress raisers at extrusions (schematically).* $\gamma_{pl,cum} = 4N \cdot \gamma_{pl,PSB}$: *cumulative plastic shear strain in PSBs. From Ref* 14. *Courtesy of the authors and of Taylor & Francis.* (a) *Early stage. Rapid development of Type I stress raisers at slip offsets at the PSB-matrix interfaces.* (b) *Later stage. Formation of Type II stress raisers in surface roughness of extruded material.*

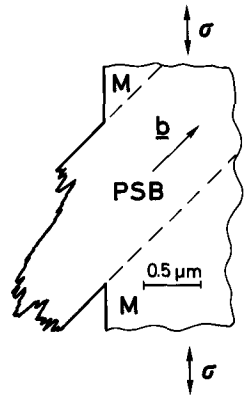

FIG. 4—*Constructed surface profile at emerging PSB, superposition of a static extrusion, and surface roughness due to random irreversible slip.* N ≈ *1.7* × *10*^{5}. *From Ref* 15.

present model, they are not based on detailed TEM evidence which has become available only quite recently.

In the framework of this study, a model developed by Brown and co-workers [*7,8,47*] is of considerable interest. This model is based on weak-beam TEM work which provided evidence that the narrow edge-dislocation dipoles which build up the veins in the matrix and the walls in the PSBs have predominantly vacancy character [*7*]. The authors assume that the density of these vacancy dipoles in the PSBs becomes larger than that in the matrix during cyclic saturation.[6] They then describe the long-range effect of this dislocation distribution by replacing each dislocation wall in the PSBs by a fictitious vacancy dislocation-dipole of height h. Thus the whole PSB can be modelled by a dislocation-dipole layer as in Fig. 2*a*, except that the dipoles have vacancy character and that the residual state of stress in the PSB is tensile in the direction of **b**. The authors estimate the residual elastic strains as $\epsilon_{int} = 2$ to 5×10^{-4} and obtain residual elastic *tensile* stresses of similar magnitude as the elastic *compressive* stresses in our model.

Because of the formal similarity between the two models, many of the detailed considerations of Brown and co-workers [*7,8*] relating to the state of stress and to the initiation of fatigue cracks can be applied also to our model. However, the fictitious vacancy dislocation-dipoles are not considered as glide dislocations that can emerge at the surface as in our case, and hence they play no crucial role in the development of the surface topography. (If they did, they would give rise to intrusions.) Rather, it is envisaged that motion of screw dislocations is responsible for the production of the vacancy-type dipoles [*47*]

[6]It appears to us that this assumption is crucial and not well supported by experimental observations. The available TEM [*53*] and X-ray line broadening [*65*] evidence indicates in fact that the *mean* density of dislocation dipoles in saturation is larger in the matrix than in the PSBs [*14*].

and, simultaneously, generates (rough) extrusions by a cross-slip mechanism [*8*] as in Mott's model [*24*].

Fatigue Crack Initiation at Emerging Persistent Slip Bands

Returning to Fig. 3, we note that two distinct types of stress raisers are predicted to develop at different stages of the fatigue process. The slip offsets at the PSB-matrix interface (Type I stress raisers) form early, whereas the notch-like valleys in the roughness profile of the PSB (Type II stress raisers) develop much more gradually. Hence it is suggested [*14*] that Stage I shear cracks develop first at the PSB-matrix interfaces and later also in the notch-like valleys, and that the fatal cracks may well be of the former type since these can develop into critical cracks at an earlier stage.

In the model of Brown and co-workers [*7,8,47*], it is proposed that the energy related to the state of residual stress can be released by the propagation of cracks along the PSB-matrix interfaces, and a simple estimate yields the crack initiation and propagation criterion for a PSB of thickness h:

$$\epsilon_{\text{int}}^2 > \frac{8\alpha_{\text{eff}}}{Eh} \tag{11}$$

where α_{eff} is an effective surface energy. Equation 11 indicates that for typical values of $|\epsilon_{\text{int}}| \approx 3 \times 10^{-4}$ and a value $\alpha_{\text{eff}} \approx 2\ \text{J/m}^2$, corresponding to a characteristic surface energy α_s, "brittle-type" crack propagation can be expected for $h \gtrsim 1$ mm [*7,8*]. For the reasons stated earlier, Eq 11 can also be applied to our model for a situation in which the interface dislocations are still in the crystal, and a similar result is obtained. In the case of significant plastic deformation at the crack tip, the effective surface energy α_{eff} would have to include both the surface energy α_s and a specific plastic deformation energy α_p, as in the Griffith-Orowan relation. However, TEM observations of Stage I crack tips in PSBs in copper show no evidence of a pronounced plastic zone [*9*]. Moreover, Brown [*8*] has estimated that the stresses at the tip of a Stage I crack of the type envisaged do not exceed the flow stress. He concludes that local stress fluctuations and/or environmental interaction—that is, a lowering of α_{eff} by surface reactions—will in fact be required to break the bonds at the crack tip.

Regarding the relative importance of Type I stress raisers at A, A' and B, B' respectively (Fig. 2*a*), Brown has performed a calculation of the stresses at these surface sites due to a dipolar dislocation array [*8*]. He concludes that, for a vacancy dislocation-dipole layer, very large tensile and compressive *surface stresses* prevail at B, B' and A, A' respectively. For an interstitial dislocation-dipole layer as shown in Fig. 2*a*, the situation would be reversed. Brown and co-workers [*7,8*] propose that immediately after its formation, the PSB will contain less vacancy dipoles than the matrix and will therefore be in a state of

compression (along **b**) which gives rise to the initiation of cracks at A and A', where the tensile stresses are largest. Later in saturation, the situation is suggested to be reversed and crack propagation will occur when the residual tensile stresses have become large enough. The application of similar considerations to our model, which does not predict a change in the sense of the residual stresses, indicates preferential initiation of cracks at A and A', as has been concluded also by other arguments [*14*]. It is worthwhile pointing out, however, that in our model, especially when the supply of interface dislocations has been exhausted (static extrusion), the sharper notches formed at B and B', as compared to those at A and A', could eventually become the more effective stress raisers. From the experimental point of view, it is interesting to note that Neumann [*44*] has in fact observed that fatigue crack initiation occurs preferentially at sites corresponding to A, A' in copper crystals. This observation has been confirmed more recently by Duquette [*71*] and by Hunsche and Neumann [*72*]. In addition, however, these authors noted that, following crack initiation at A, A', cracks eventually formed also at B, B' and that the fatal cracks were of the latter type.

These considerations emphasize the need for a description of the probability of fatigue crack initiation at slip offsets of given geometry. Valuable insight into this aspect has been obtained by Gräf and Hornbogen [*11*] in a study on a fatigued nickel-base superalloy (see also Ref *12*). These authors varied the slip distribution of this material by subjecting it to different heat treatments and were able to show clearly that the crack initiation probability increased with increasing coarseness of the slip distribution, that is, with increasing slip step height. In a recent detailed study of fatigue crack initiation at emerging PSBs in fatigued copper crystals Cheng and Laird [*17*] have come to a similar conclusion. They showed by their interferometric surface studies of localized slip in PSBs that there is a distribution of slip offsets in the PSB-distribution throughout the fatigue test and that the fatal crack originates in the PSB with the largest slip offset. Furthermore, they establish experimentally a relation between the slip offsets in the fatal PSB and the plastic shear strain amplitude γ_{pl}. Combining this with a criterion for crack initiation, based on a random-slip model of the evolution of notches, they finally obtain the following relation between the number of cycles N_i for crack initiation and γ_{pl}:

$$N_i^{0.78} \cdot \gamma_{pl} = K \tag{12}$$

From the experimental data of Cheng and Laird it follows that $K \approx 20$. Unlike the model of Brown and co-workers and our model, which emphasize the microscopic details of the dislocation processes, the model of Cheng and Laird has the major aim of establishing the number of cycles required for crack initiation by combining fairly general statistical considerations with empirical experimental data. Hence the three models are complementary in many respects.

Persistent Slip Bands and Fatigue Crack Initiation in Polycrystals

In order to explain some of the observations on fatigued polycrystals, which will be presented later, it is necessary to consider the role of PSBs in polycrystals with regard to both trans- and intergranular fatigue crack initiation. It has been shown recently by several authors that in fatigued single-phase fcc polycrystals PSBs form in a similar fashion as in single crystals in suitably orientated grains on slip systems with a high Schmid factor close to 0.5 [*13,18–21,23*]. Moreover, it could be shown that the threshold amplitudes for the formation of PSBs in fatigued copper polycrystals are related to those in copper monocrystals via

$$\sigma_{PSB} = \tau_{PSB} \cdot M \approx 58\,\text{MPa} \tag{13}$$

and

$$\Delta\epsilon_{pl,M} = \frac{2\gamma_{pl,M}}{M} \approx 5 \times 10^{-5} \tag{14}$$

Here σ_{PSB} and $\Delta\epsilon_{pl,M}$ refer to the threshold values of the axial stress amplitude and the plastic strain range, respectively, and M is an orientation factor slightly larger than two [*13,20,23*]. Based on the distinctly higher values of the stress and strain *fatigue limits* reported by Lukáš and co-workers [*73*] and by Hessler and co-workers [*74*], it was concluded that the PSB-thresholds correspond to fatigue crack initiation thresholds and represent lower limits to the fatigue limits at which cracks propagate [*20*].

We now consider the surface topography at emerging PSBs in a grain of a polycrystal for a situation in which the Burgers vector has a large component perpendicular to the surface, that is, comparable to the situation at the top face of a single crystal as in Figs. 2 to 4. Under these conditions the operation of the PSB will be almost unimpeded by constraints. In the model of Essmann and co-workers [*14*] the development of extrusions by the stepwise emergence of PSB-matrix interface dislocations can thus proceed as in single crystals, except that the interface dislocations can only emerge on one side, since the other side is blocked by the grain boundary. For a static extrusion the maximum height (in the direction of **b**) will thus be given by e in Eq 9, where D now denotes the grain diameter in the direction of **b**. For typical grain sizes of $D \approx 100\ \mu$m, the height of static (and of continuously growing) extrusions will thus be about two orders of magnitude smaller than in a single crystal of 1 cm diameter. The evolution of surface roughness by random slip, on the other hand, will be comparable to surface roughening in single crystals in correspondence with Eq 3. The major conclusion is therefore that, in fine-grained material, the extrusion effect will be greatly diminished. Hence the essentially unmodified

hill-and-valley surface roughening due to random slip can become the dominant feature responsible for the initiation of transgranular Stage I cracks.

Another case of interest is that of a PSB in a surface grain with the Burgers vector **b** lying roughly in the surface [*14,69*]. In this case the surface profile at the PSB will be only weakly developed (as on the side face of a single crystal). Significant effects are caused, however, due to the fact that in this case the grain boundaries (*1*) constrain the shear displacements in the PSB-lamella and (*2*) suppress the emergence of the PSB-matrix interface dislocations and thus the development of the (small) extrusions. As discussed in more detail elsewhere [*75*], the latter effect can initiate cracks at grain boundaries which we shall call *PSB-GB cracks*. Let us first consider the effects due to the constrained shear displacements in a PSB for the tensile phase (Fig. 5*a*). If the localized shear displacements in the PSB-lamella were unconstrained, and ignoring the much smaller deformations of the surrounding material, then the PSB-lamella would assume the parallelogram shape indicated by dashed lines. The displacements at the grain boundaries in the neighbourhood of A' and B' (and similarly at A and B) would be as also shown by dashed lines. Because of the relative rigidity of the surrounding material, however, the actual constrained configuration at A' and B' will be more as shown on the right-hand side of Fig. 5*a*. Thus the grain boundary will be subjected to transverse compressive stresses at B' and tensile stresses at A'. Simultaneously, however, the PSB-matrix interface dislocations are piled up against the grain boundaries at A and A', as shown in Fig. 5*b*. Compared with the long-range stress of these dislocation pile-ups, the short-range stress of the PSB-wall dislocation dipoles is insignificant. The pile-up effect counteracts that due to the overall shear displacement of the PSB-lamella. The latter effect can be characterized by the displacement s (Fig. 5*a*):

$$s = h \cdot \gamma_{\text{pl,PSB}} \tag{15}$$

In a very crude approximation, the effect due to the localized dislocation pile-ups will become dominant if the displacement mb due to m interface dislocations per pile-up exceeds $0.5s$; that is, if $mb > 0.5s$. Under the condition of static extrusion growth, m is given by Eq 6,[7] so that this condition can be expressed via Eq 15

$$D > \frac{h \cdot \gamma_{\text{pl,PSB}}}{2\,\bar{C}_v^{\text{sat}}} \tag{16}$$

For $h \approx 1\ \mu\text{m}$, $\bar{C}_v^{\text{sat}} \approx 6 \times 10^{-4}$ and $\gamma_{\text{pl,PSB}} \approx 7.5 \times 10^{-3}$; this means that for $D \gtrsim 6\ \mu\text{m}$ the interface-dislocation pile-up effect will become dominant. In

[7]It is worthwhile noting that the number of dislocations per PSB-matrix interface-dislocation pile-up is only a function of D and not, in addition, of the acting shear stress, as is usually the case for dislocation pile-ups.

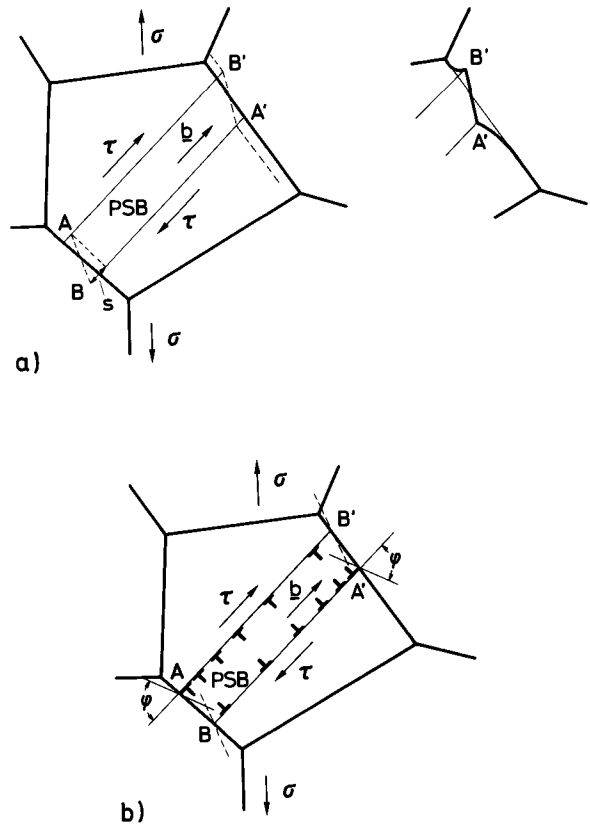

FIG. 5—*Interaction between PSBs and grain boundaries in polycrystals (schematically for tensile phase).* τ *is shear stress.* (a) *Effect due to homogeneous shear localized in a PSB bounded by grain boundaries. Distortion at grain boundary is indicated on the right.* (b) *Counteracting effect due to piling-up of PSB-matrix interface dislocations against grain boundaries.*

spite of the crudeness of Eq 16, which rests on a comparison between the displacements of a *localized* dislocation pile-up and an *homogeneous* shear, we can conclude that for most grain sizes of interest the major effect at the grain boundaries stems from the piling-up of the interface dislocations.

According to Stroh [*76*] (see also Ref *77*), the largest tensile stress at the head of a dislocation pile-up occurs across a plane making an angle $\phi = 70.5$ deg with the pile-up. These planes are indicated by the faint lines in Fig. 5*b*. (The corresponding planes that would play a role during compressive loading are indicated by faint dashed lines.) In many real situations these planes can lie almost in the grain boundary. Hence it appears probable that the repeated piling-up of the PSB-matrix interface dislocations under alternating stresses can cause grain boundary cracking of the type first envisaged by Zener [*78*]. In

this case Stroh's criterion for crack initiation at the head of a dislocation pile-up consisting of m dislocations subjected to a stress τ [*76, 77*] must be fulfilled. The necessary condition is

$$m\tau = \frac{3\pi^2\alpha_{\text{eff}}}{8b} \tag{17}$$

Assuming steady-state conditions as in the case of static extrusion growth, we can express m via *Eq* 6 and identify τ with τ_{PSB} acting in a PSB and obtain

$$D > \frac{3\pi^2\alpha_{\text{eff}}}{8\bar{C}_{\text{v}}^{\text{sat}} \cdot \tau_{\text{PSB}}} \tag{18}$$

In the case of "brittle-type" grain boundary cracking α_{eff} will be given by $\alpha_{\text{s}} - \frac{1}{2}\,\alpha_{\text{gb}}$, where α_{gb} is the grain boundary energy. For copper, typical values are $\alpha_{\text{s}} = 1.65\ \text{J/m}^2$ [*79*] and $\alpha_{\text{gb}} = 0.32\ \alpha_{\text{s}}$ [*80*]. Equation 18 implies for copper, with $\tau_{\text{PSB}} \approx 28$ MPa and $\bar{C}_{\text{v}}^{\text{sat}} \approx 6 \times 10^{-4}$, that for grain diameters $D \gtrsim 300\ \mu$m, PSBs can cause the initiation of "brittle-type" PSB-GB cracks.

Furthermore, in order to explain experimental observations of PSB-GB cracks (see below), it appears necessary to invoke also the facilitation of PSB-GB crack nucleation by environmental interaction. In analogy to the Stage I fatigue crack growth model of Duquette and Gell [*81*], we write for the effective surface energy in Eq 17:

$$\alpha_{\text{eff}} = \alpha_{\text{s}} - \tfrac{1}{2}\alpha_{\text{gb}} + \alpha_{\text{p}} - \alpha_{\text{ads}} \tag{19}$$

where not only the specific plastic-deformation energy α_{p} but also a possible lowering of α_{eff} by α_{ads}, due to gas adsorption or chemisorption, is taken into account. It is anticipated that, because of the substantial heat of formation of copper oxides ($\approx 1.6 \times 10^5$ J/mole [*82*]), the formation of a monolayer of oxide can reduce α_{eff} by a significant fraction of α_{s}. It is envisaged that PSB-GB cracks would thus initiate and spread by repetitive oxidation and "brittle-type" cracking (small α_{p}) at the PSB-GB crack tip during the tensile phases.

The only other model of PSB-GB fatigue crack initiation that has been worked out in some detail is that of Tanaka and Mura [*69*]. We refer the reader to the original publication for details.

Experimental Observations of Surface Features and Fatigue Crack Nucleation in Copper

Experimental Details

In this section we shall report on recent observations on fatigued copper mono- and polycrystals that were carried out specifically with the aim of check-

ing the applicability of the concepts outlined in the previous sections [*23*]. The single crystals were grown from high-purity (99.999%) copper and were orientated for single slip. The polycrystalline specimens were prepared from commercial-purity copper and were given different heat treatments in order to obtain specimens having small and large grain sizes of ≈ 25 and ≈ 400 μm, respectively. For comparison, some tests were also performed on high-purity polycrystalline material. The typical dimensions of the specimens were ≈ 4 mm diameter and ≈ 15 mm gage length, with some variations from case to case. With the exception of some preliminary experiments at temperatures of 77 and 403 K [*83*], all cyclic deformation tests were performed at room temperature on a servohydraulic MTS-machine in symmetric push-pull at controlled plastic strain amplitude, as described earlier [*28,29*]. The typical cyclic strain rates were in the range of 10^{-4} to 10^{-2} s^{-1}. For further details see Ref *23*.

All microscopic observations to be reported here were performed by scanning electron microscopy (SEM) on a Jeol JSM-35C microscope. Surface-roughness profiles were studied by the application of several complementary techniques that are more fully described elsewhere [*22,23*]. Briefly, the following three techniques were employed: (*1*) direct imaging of the surface relief at the edge of the specimens by viewing from the side, (*2*) quantitative evaluation of stereo picture pairs, and (*3*) deposition of a contamination line across the feature of interest by long exposure in the linescan mode and subsequent imaging under a large angle of tilt, so that local displacements of the contamination line could be interpreted as elevations or depressions.

Observations on Fatigued Single Crystals

Figure 6 shows examples of the surface profiles of "young" PSBs (Fig. 6*a*) that were formed within a cyclic deformation interval of ≈ 1000 cycles at $\gamma_{pl} = 2 \times 10^{-3}$ and of "old" PSBs (Fig. 6*b*) in a specimen cycled to failure after $N_f = 1.34 \times 10^5$ cycles. These pictures were obtained by direct relief-imaging. In both cases it is evident that material has been extruded. (Similar observations performed at emerging PSBs on the side face revealed no significant surface profile.) The height of the young PSBs (in the direction of **b**) after only 1000 cycles, corresponding to an average age of the extrusions of ≈ 500 cycles, is about 1 μm, whereas that of the much older extrusions is about 6 μm. This indicates that extrusion growth is rapid initially and becomes progressively slower subsequently. Detailed experiments at $\gamma_{pl} = 5 \times 10^{-4}$ to 2×10^{-3} and at 5 Hz have shown that the initial rate of extrusion growth is about 10 nm/cycle and decreases to a very small value of ≈ 0.03 nm/cycle after $\approx 10^5$ cycles [*23*]. The extrusion height after about 10^5 cycles is larger than that of a static extrusion, estimated to be about 2 μm by Eq 9 for $D \approx 6$ mm, by about a factor of three. Preliminary experiments on copper crystals fatigued at 77, 295, and 403 K have shown that the extrusion heights observed after about 4×10^4 cycles at

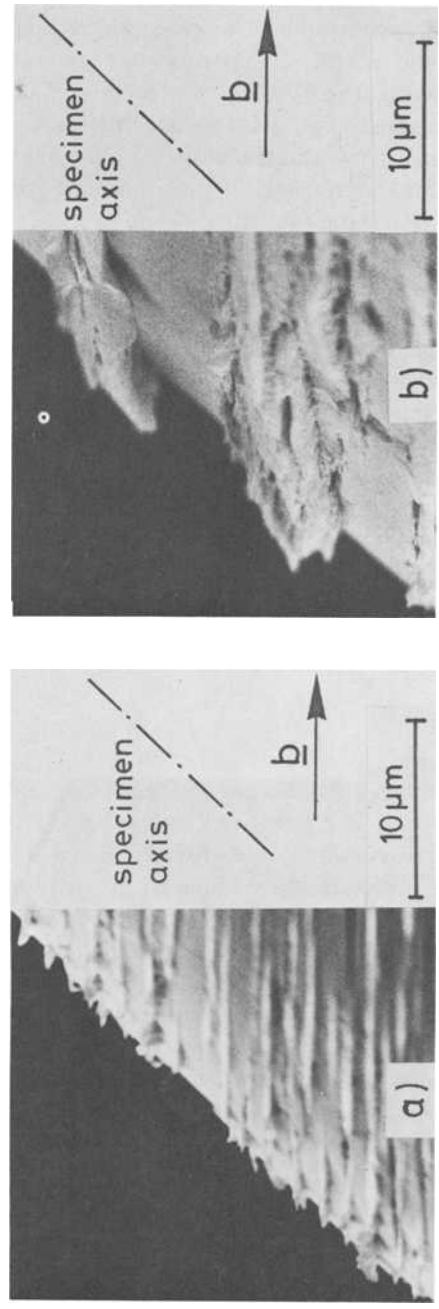

FIG. 6—*Observations of PSB surface-profiles by direct SEM relief-imaging. Fatigued copper crystals:* γ_{pl} 2×10^{-3}. *From Ref 23.* (a) *"Young" PSBs formed in a deformation interval of 1000 cycles.* (b) *"Old" PSBs after cycling till failure:* $N_f = 1.34 \times 10^5$.

$\gamma_{pl} = 2 \times 10^{-3}$ are about 4 μm in all cases [*83*]. This result indicates that the rate of extrusion growth does not depend markedly on temperature.

Imaging by the contamination-line technique is very suitable to determine the shape of (young) extrusions (Fig. 7). The typical shape is a rounded triangular profile, as displayed by the locally distorted contamination lines, when viewed after a strong tilt of 60 deg around the contamination line which was originally deposited at right angles to the PSB (Fig. 7*a*). Figure 7*b* shows the surface profile of the same PSB at another position. Three features are particularly interesting:

1. There is a notch-like intrusion at the PSB-matrix interface (marked by an arrow) which corresponds to site A (or A') in Fig. 2. A similar notch is lacking at the PSB-site in Fig. 7*a*.
2. At the bottom right there is a ribbon-like, much more pronounced extrusion, with a height of ≈ 2 μm over a length of some microns.
3. The surface of the extrusions is smooth and displays no detectable surface roughening.

Compared with the surface profiles of young PSBs, it is evident from Fig. 6*b* that old PSBs have rough surface profiles. The surface roughness is difficult to evaluate quantitatively because of the complex surface profile due to pronounced ribbon-like extrusions and because of the difficulty of distinguishing the surface roughness from adjacent extrusions due to other closely neighboring PSBs.[8] Furthermore, several microcracks are apparent at the PSB-matrix interfaces and within the PSBs. A view of the top face, in particular, shows microcracks at PSB-matrix interfaces corresponding to sites A and A' in Fig. 2. An example pertaining to the same specimen shown in Fig. 6*B* is presented in Fig. 8.

According to these observations, extrusions are clearly the dominant feature at emerging PSBs. However, one further feature, lacking in Figs. 6 to 8, which is observed fairly commonly, though by far not as frequently as extrusions, is shown in Fig. 9. In this case the surface topography displays not only extrusions, as evidenced by the displacements of the contamination lines, but also sharp extended notch-like valleys. It was observed repeatedly that these notches occur at local compression slip steps of typically $\lesssim 1$ μm in height. This can also be inferred from the contamination-line profile traversing such a notch in Fig. 9. These notches either appear isolated parallel to the trace of the PSBs or alternate along a PSB with pronounced ribbon-like extrusions. It appears possible that these notches are in fact microcracks.

[8]Work in progress has shown that while ribbon-like extrusions are common features of crystals fatigued at 293 and 403 K, such extrusions are not observed after fatigue at 77 K. In the latter case, an undisturbed surface roughness profile which is superimposed on a bulky extrusion is clearly recognizable [*83*].

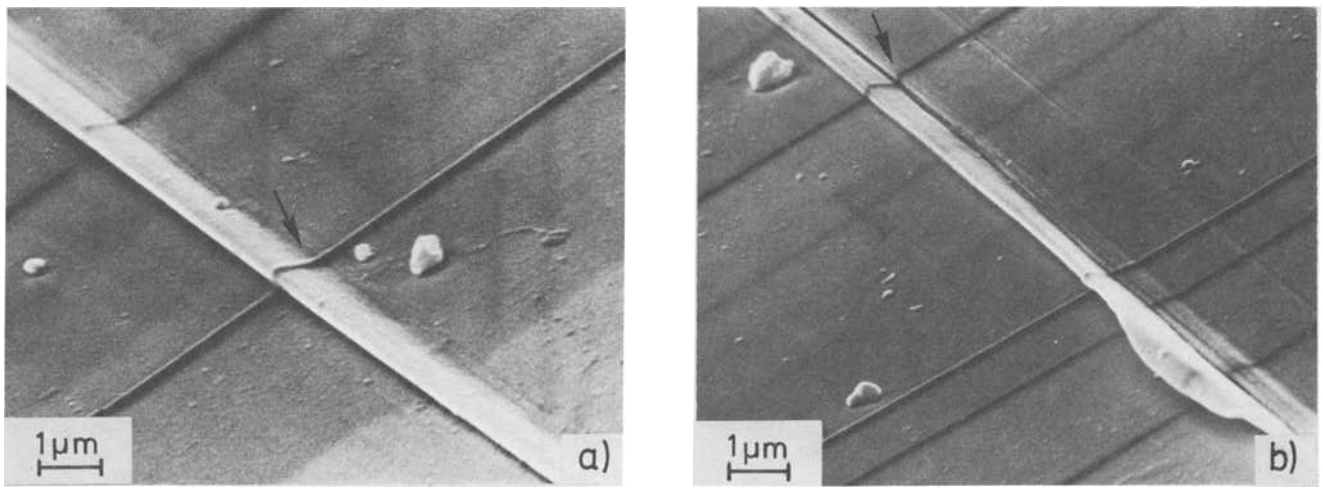

FIG. 7—*Surface profiles of "young" PSBs observed by SEM contamination-line technique. Copper crystal, top face,* $\gamma_{pl} = 5 \times 10^{-4}$*, age of PSBs is* ≈ *500 cycles. Angle of tilt is 60 deg. Displacements of the contamination lines parallel to PSB-trace reflect the actual profile at* ≈ *85% of the nominal magnification. From Ref* 23. (a) *Rounded triangular shape of extrusion. Arrow indicates PSB-matrix interface corresponding to* A,A′. (b) *Other part of same PSB as in* (a). *Note ribbon-like extrusion growth at bottom right and development of small "intrusion" at PSB-matrix interface corresponding to* A,A′ *(marked by arrow).*

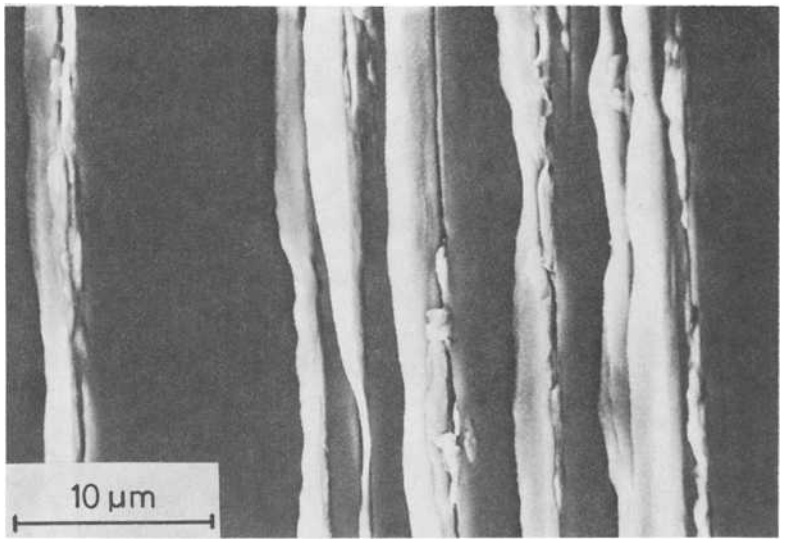

FIG. 8—*Fatigue cracks at PSB-matrix interfaces corresponding to* A,A'. *Top face of same copper crystal as in Fig. 6*b. *From Ref* 23.

Observations on Fatigued Polycrystals

Figure 10*a* shows PSBs in a surface grain of a copper polycrystal fatigued to failure. The traces of the PSBs shown are approximately perpendicular to the stress axis. Thus the situation is comparable to that of PSBs emerging at the top face of a single crystal. As described in detail elsewhere [*22,23*], the stress axis was inclined to the plane of the figure so that the active Burgers vector is roughly perpendicular to the picture. For the PSB region contained within the dashed lines, the surface profile was evaluated quantitatively from a pair of stereo micrographs. The result shown in Fig. 10*b* reveals that the surface topography is essentially a hill-and-valley profile with typical wavelengths of ≈ 0.3 and ≈ 2 μm across and along the PSB, respectively. There is no detectable overall extrusion effect, and the surface roughness is well described by Eqs 3 and 10, with a mean profile width $\bar{w} \approx 0.4$ μm.

An example of a more pronounced surface profile of an emerging PSB is shown in Fig. 11, which shows a PSB extending from one grain boundary to the next and which is marked by three traversing contamination lines. Because of the large angle of tilt under which the picture has been taken, the picture appears somewhat distorted. In particular, the direction along the PSB appears strongly compressed. This specimen had been deformed at small, successively increasing values of $\Delta\epsilon_{pl}$ till a final value of $\Delta\epsilon_{pl} = 6 \times 10^{-4}$ was attained. The age of the PSB is about 700 000 cycles and thus much higher than that of the PSB shown in Fig. 10. Accordingly, the roughness profile is much more

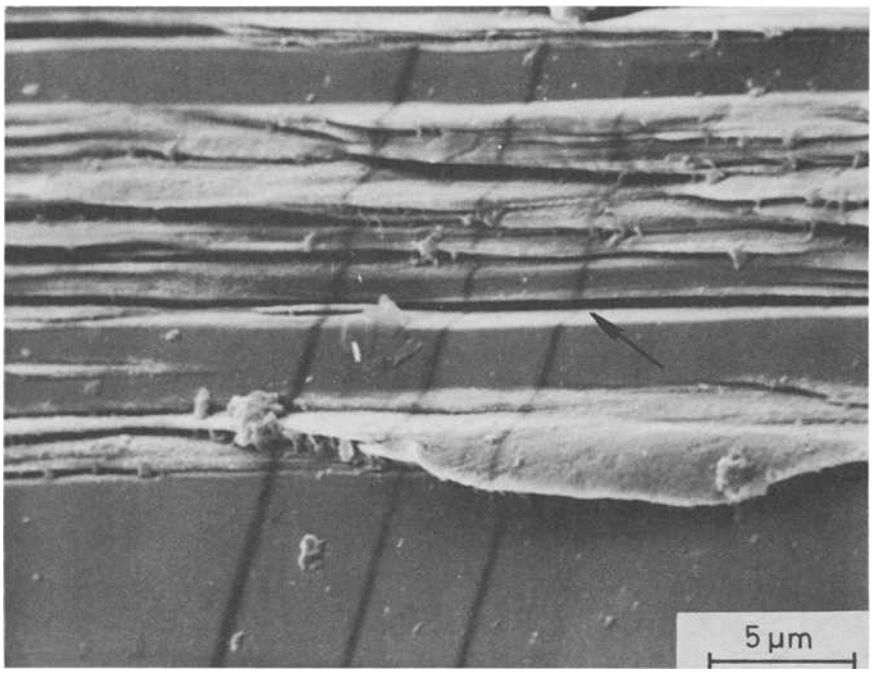

FIG. 9—*Surface profile at top face of copper crystal fatigued for* N = 1.1×10^4 *cycles at* $\gamma_{pl} = 4 \times 10^{-3}$. *Observation by SEM contamination-line technique. Angle of tilt is 30 deg. Displacements of contamination lines along PSB-traces reflect actual profile at* ≈ *50% of the nominal magnification. Note ribbon-like extrusion at bottom right and notch-like "intrusion" associated with compression slip step (marked by arrow). From Ref* 23.

strongly developed, with a mean profile width of $\bar{w} \approx 1$ μm, again in very reasonable agreement with Eqs 3 and 10. In addition, there is a superimposed effect of a net extrusion whose height is estimated to be 0.1 to 0.2 μm from stereo micrographs.

It appeared that, after a large number of cycles, many of the PSBs did contain microcracks, although their unambiguous identification was difficult. On the other hand, there was clear evidence for accumulation of fatigue damage at grain boundary sites, where PSBs impinged, and PSB-GB cracks were easily recognizable on SEM micrographs of all specimens fatigued to failure. Figs. 12*a–d* show typical examples. These findings can be summarized as follows:

1. PSBs responsible for fatigue damage at grain boundaries were generally observed to act co-operatively and to widen at the damaged grain boundaries, indicating the tendency towards less severely localized slip (Figs. 12*a–d*).
2. PSB-GB cracks were more frequent in the coarse-grained specimens, but occurred also abundantly in the fine-grained specimens.
3. The fatigue damage at grain boundaries caused by PSBs ranged from

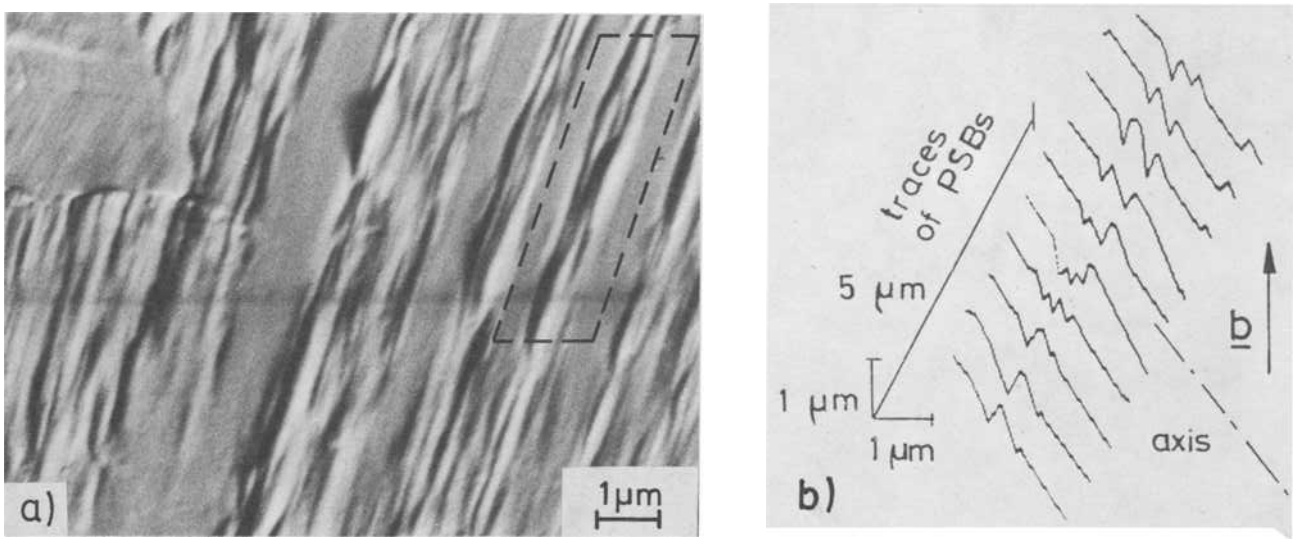

FIG. 10—*Surface profiles of emerging PSBs in fatigued copper polycrystal, grain size* $\approx 25\ \mu m$, $\Delta\epsilon_{pl} = 2 \times 10^{-3}$, $N_f = 3 \times 10^4$. *From Refs* 22 *and* 23. *Courtesy of the authors and of Riederer-Verlag.* (a) *View of emerging PSBs in a grain. Specimen axis tilted out of plane of picture so that active Burgers vector is approximately perpendicular to picture. Projection of specimen axis parallel to horizontal contamination line.* (b) *Stereometric reconstruction of ten equidistantly spaced surface profiles across PSB framed by dashed lines in* (a).

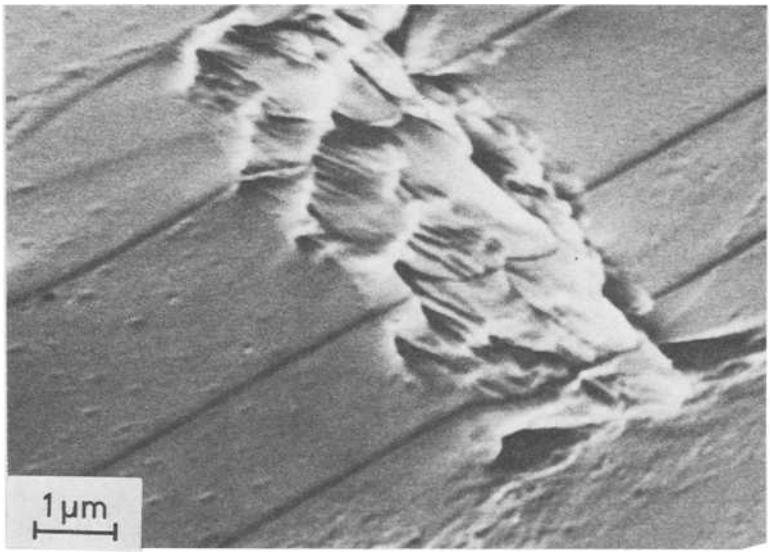

FIG. 11—*Surface profile at "old" emerging PSB extending from grain boundary to grain boundary; D ≈ 25 μm; see text for details. The displacements at the three contamination lines along the PSB-trace reflect the actual profile at ≈85% of the nominal magnification. Displacements to the right and left indicate elevations and depressions, respectively. From Ref 23.*

severe fragmentation (Fig. 12*c*), step formation (Fig. 12*a*), and development of void-type cavities, (Fig. 12*d*), reminiscent of high-temperature fatigue [*84*], to widely opened cracks (Fig. 12*b*).

4. Similar observations were made on high-purity specimens.

Observations of fatigue fracture surfaces (Figs. 13 and 14) indicated that a mixed-type, partly trans- and partly intercrystalline fracture mode prevailed in the vicinity of the crack nucleation site. At low $\Delta\epsilon_{pl}$ (2×10^{-4}), this type of fracture mode was evident from the surface of the specimen (Fig. 13*b*) to a crack depth as large as ≈2.5 mm (Fig. 13*c*), and only at larger depths did typical Stage II fatigue striations become apparent (Fig. 13*d*). We hence consider the mixed-mode fracture surface which is perpendicular to the stress axis only on the average macroscopic but not on the microscopic scale as a Stage I fracture surface. This type of mixed-mode Stage I fracture was also typical of the early stage of crack propagation at much higher $\Delta\epsilon_{pl}$ (10^{-2}) (Fig. 14*b*). In this case, however, the transition to Stage II crack propagation occurred at a much earlier stage at a crack depth of only a few grain diameters.

Discussion

The rapid initial growth of extrusions immediately after PSBs have been formed and the much slower subsequent growth observed in this study sub-

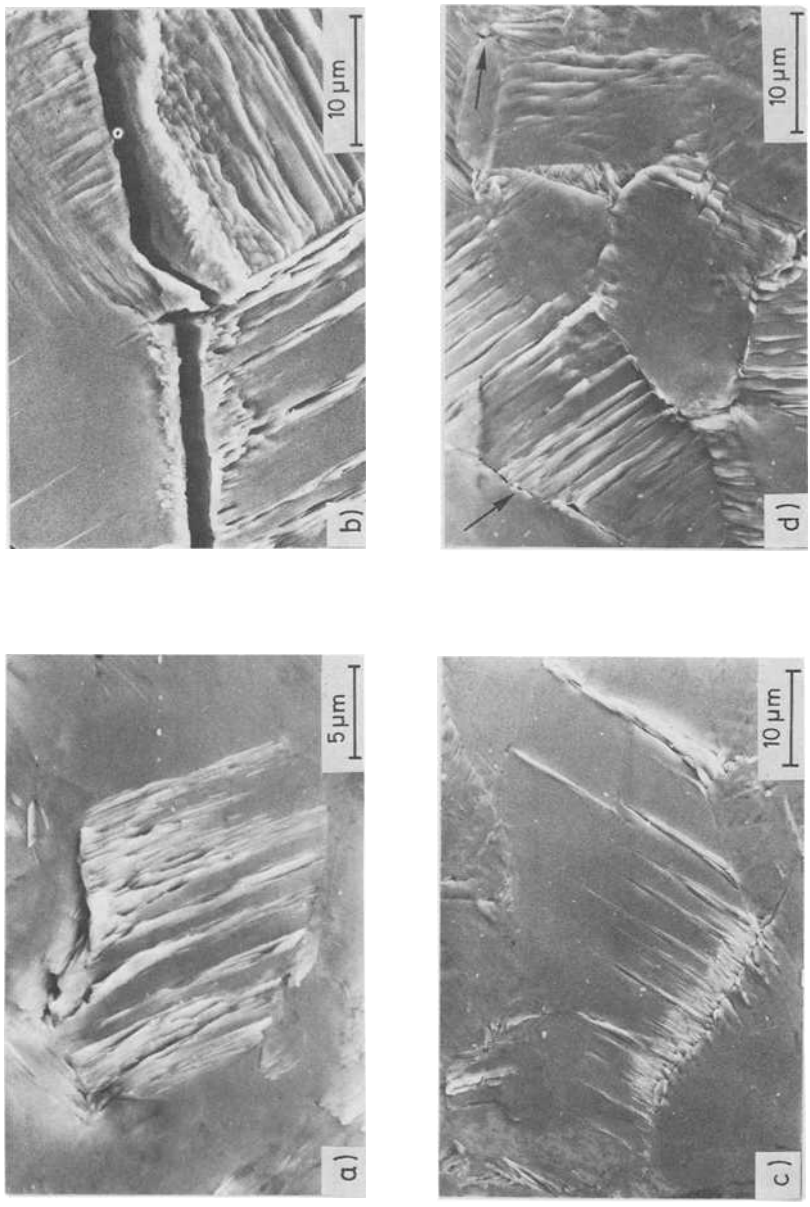

FIG. 12—*Examples of fatigue damage at grain boundaries due to impinging PSBs. Stress axis horizontal in* (a), (c), and (d) *and vertical in* (b). *From Ref* 23. (a) $\Delta\epsilon_{pl} = 2 \times 10^{-4}$, $N_f = 8.3 \times 10^5$, $D \approx 25$ *µm*. (b) $\Delta\epsilon_{pl} = 2 \times 10^{-4}$, $N_f = 2.2 \times 10^5$, $D \approx 400$ *µm*. (c) $\Delta\epsilon_{pl}$ *increased stepwise till* $\Delta\epsilon_{pl} = 6 \times 10^{-4}$, $D \approx 25$ *µm*. (d) $\Delta\epsilon_{pl}$ *increased stepwise till* $\Delta\epsilon_{pl} = 3 \times 10^{-3}$, $D \approx 25$ *µm*.

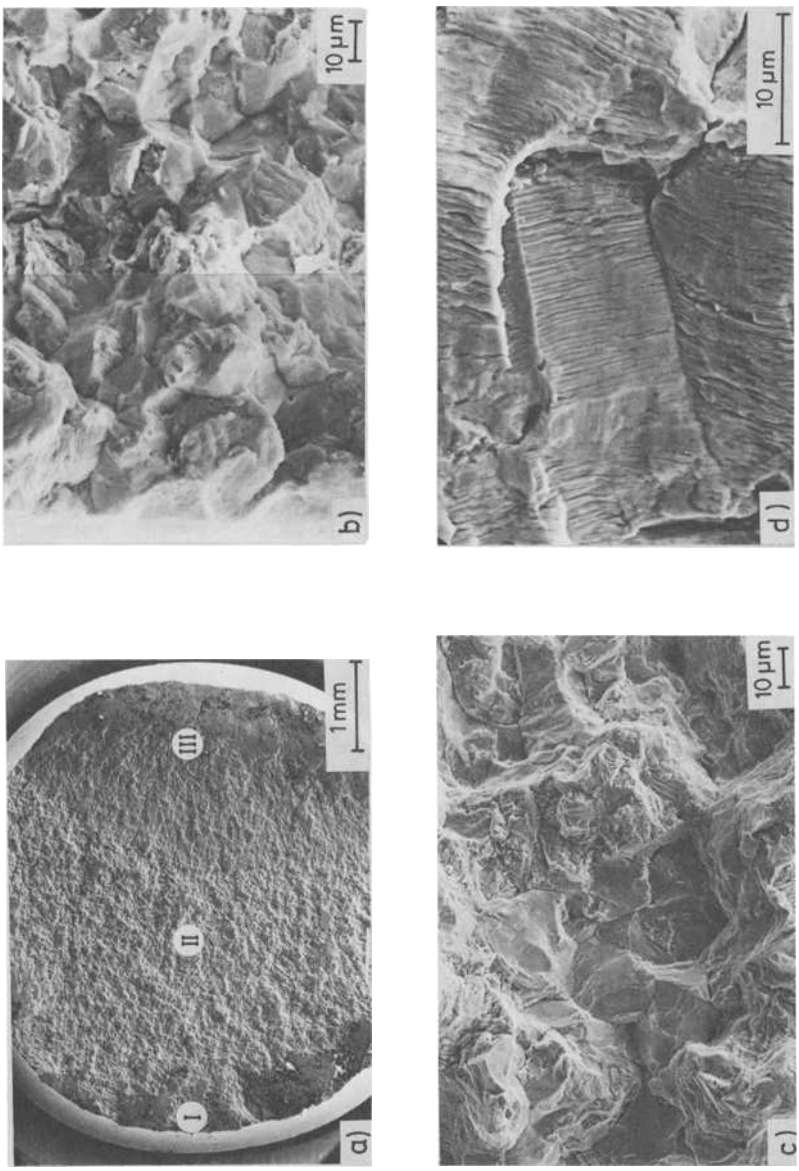

FIG. 13—*Fracture surface of copper polycrystal* (D ≈ 25 µm), *fatigued at* $\Delta\epsilon_{pl} = 2 \times 10^{-4}$, $N_f \approx 6 \times 10^5$. *From Ref* 23. (a) *Low-magnification view.* (b) *Site I in* (a) *at higher magnification; note original surface on left.* (c) *Site II in* (a) *at higher magnification.* (d) *Site III in* (a) *at higher magnification.*

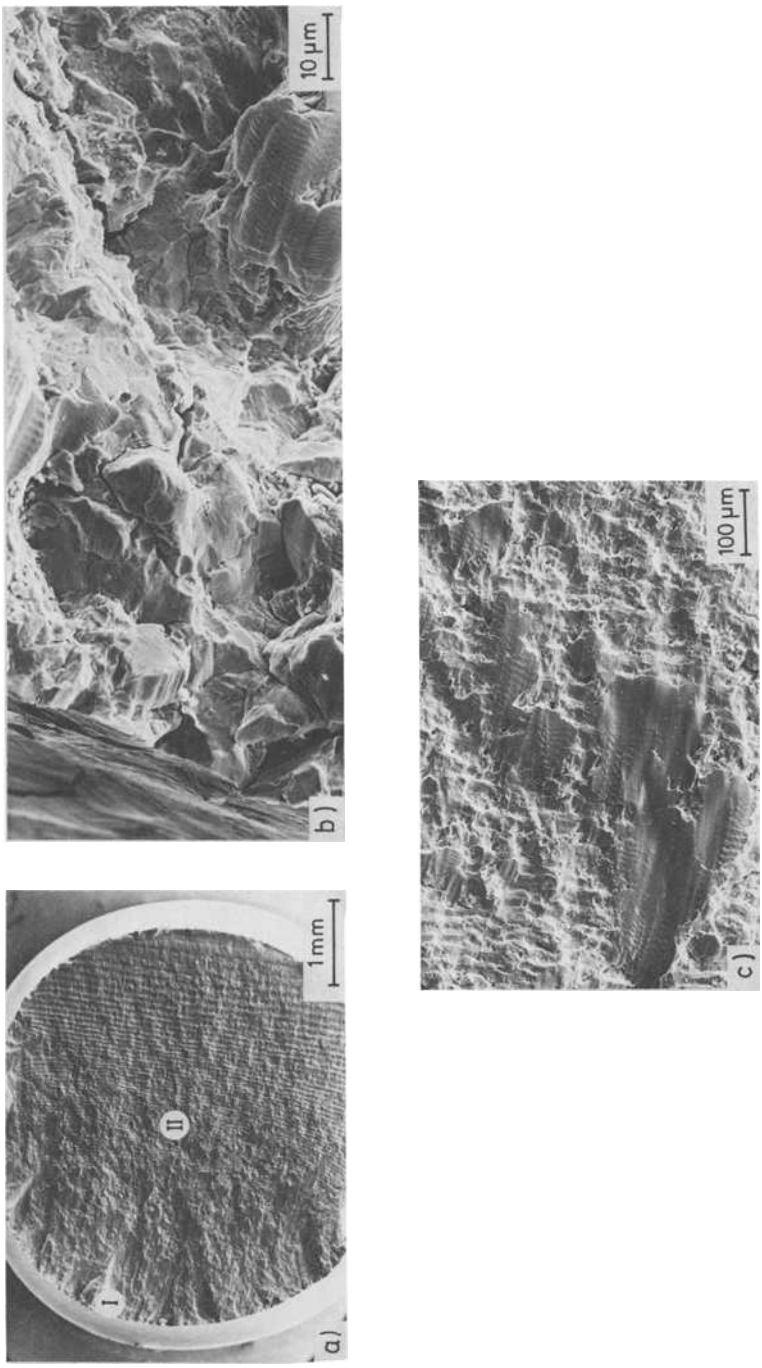

FIG. 14—*Fracture surface of copper polycrystal* (D ≈ 25 µm) *prefatigued at* $\Delta\epsilon_{pl} = 0.005$ *and fatigued to failure at* $\Delta\epsilon_{pl} = 0.01$. *From Ref* 23. (a) *Low-magnification view.* (b) *Site I in* (a); *note original surface on left.* (c) *Site II in* (a).

stantiate earlier more qualitative work [*33,85*]. The early extrusion growth can be understood in the EGM-model as the rapid initial development of static extrusions. Furthermore, the model provides an explanation for the triangular shape of young extrusions [*14*]. It appears to us that the rapid initial extrusion growth is not easy to understand in the model of Brown and co-workers [*7,8,47*], in particular if, as they assume, the density of vacancy dislocation-dipoles were initially higher in the matrix than in the PSBs. In this case one should expect that intrusions are formed first and then turn gradually into extrusions.

The rapid decrease of the rate of extrusion growth with increasing number of cycles conforms to the prediction of the EGM-model of static extrusion growth. The observed persistence of very slow extrusion growth even after a large number of cycles is in agreement with very recent work of Hunsche and Neumann [*72*]. This observation is in contrast to the simple model according to which static extrusion growth should terminate after all PSB-matrix interface dislocations have emerged. Since the rate of extrusion growth does not appear to depend significantly on temperature, it seems inappropriate to attribute this slow late extrusion growth to continuous extrusion growth caused by the loss of mobile vacancy-type defects to the matrix. As discussed, this latter process should in any case be significant only in a thin layer at the PSB-matrix interface. The absence of a temperature-dependence of extrusion growth suggests that long-range migration of vacancy-type defects plays a minor role in the extrusion process and that the vacancy-type defects are collected by the dislocations in the PSB-walls in a stress-induced, largely athermal process that requires only a small number of jumps because of the high dislocation (sink) density.

For these reasons the persistence of slow extrusion growth must be considered as an indication of a small but real deviation from steady-state conditions that is manifest even after a large number of cycles. This conclusion is substantiated by TEM observations showing that, late in the fatigue test, increasing secondary slip activity in the PSBs gradually transforms the primary edge-dislocation PSB-walls into a cell structure [*23,35,51*] in a process of "secondary" cyclic hardening [*23*]. With the participation of dislocations of different Burgers vectors, the simplified picture of an equilibrium between defect production and annihilation by primary glide only can no longer be expected to hold accurately.

The effect of gradual surface roughening at emerging PSBs in fatigued single crystals was evident but could not be evaluated satisfactorily because of the dominance of complicated extrusions. We note, however, that the PSB surface roughness evident in the TEM work of Lukáš and co-workers [*51*] is in good accord with the concept of random irreversible slip. Furthermore, in our polycrystals of small grain size, the disturbing extrusion effect was almost absent, as predicted by the model outlined earlier. Hence the surface roughness could

be evaluated quantitatively and was found to be in remarkably good agreement with our earlier considerations of random irreversible slip in PSBs.

We infer from these observations that net extrusions, as also proposed by Mecke and Blochwitz [*86*], and hill-and-valley roughness profiles arising from random slip are the dominant features of the surface topography and not the strict pairwise occurrence of extrusions and intrusions characteristic of most earlier models (see the review by Laird and Duquette [*1*]). These different views can be reconciled as follows. In our model, intrusion-like deepenings occur as a part of the hill-and-valley profiles (Figs. 10 and 11) and in the form of microcracks which initiate at the PSB-matrix interfaces (Figs. 6*b*, 7*b*, and 8) and within emerging PSBs (Fig. 6*b*). These microcracks correspond presumably to early Stage I shear cracks.

In addition, two other features of interest should be mentioned, namely the isolated sharp intrusion-like notches associated with slip steps and the narrow pronounced ribbon-like extrusions, both of which were only observed on the single crystals. The notch-like features are rather different from the more typical PSB surface profiles and are difficult to account for in virtually all microscopic PSB-models. They could be due to a more macroscopic mechanism at slip steps similar to that suggested long ago by Ewing and Humfrey [*88*]. On the other hand, the possibility exists that these "unexpected" notches bear some relation to the rather large local strain concentrations of uncertain origin that occur *within* PSBs, as reported recently by Laird and co-workers [*62*]. These authors, in their interferometric observations at about 200-fold magnification, would presumably not have recognized these very narrow notch-like features but would have detected any strain localization associated with them. Regarding the narrow ribbon-like extrusions, it seems possible that they form by continuous extrusion growth limited to thin layers at the PSB-matrix interface from which the vacancy-type defects which are known to be mobile at room temperature [*87*] can escape into the matrix [*14*]. This conclusion is substantiated by the observation that such ribbon-like extrusions are not observed after fatigue at low temperatures (77 K) at which vacancies cannot migrate [*83*].

The described crack initiation sites are in basic agreement with TEM observations by Katagiri and co-workers [*9*] and more or less as expected both in our model and in that of Brown and co-workers [*7,8,47*]. However, the Stage I crack initiation criterion expressed by Eq 11, which is based on a strain-energy release argument [*7*], can hardly explain the formation of cracks at the PSB-matrix interface of PSBs having thicknesses as small as $h \approx 1\ \mu$m (Figs. 6*b* and 8). This is presumably true, even when it is assumed that the effective surface energy α_{eff} is reduced substantially by environmental interaction (oxidation) [*81*]. As shown recently [*23*], Stage I cracks can also initiate and propagate in high vacuum, though at a much reduced rate, in fatigued copper single crystals of single-slip orientation. This is in contrast to the absence of Stage I

cracks in ⟨100⟩-orientated crystals fatigued in vacuum [*89*]. Taking all the facts together, we favor the interpretation that the (rather small) internal strain energy is largely released by the emergence of the PSB-matrix interface dislocations; this emergence is accompanied by the rapid development of extrusions and Type I stress raisers, as indicated in Figs. 2 and 3. It is then plausible to propose that Stage I cracks can initiate subsequently at these stress raisers. Alternatively, in terms of Brown's model [*8*], the experimental observations would suggest that the large tensile surface stresses at the PSB-matrix interfaces are more essential to Stage I crack initiation than the energy criterion (Eq 11) and could explain also the initiation of cracks at thin PSBs ($h \approx 1$ μm).

In the case of polycrystals of small grain size, the role of the PSB-matrix interfaces appears to be less significant for crack initiation than in single crystals, since the extrusion effect is so small. Thus slip-band cracking is expected to occur mainly in the notches formed in the roughness profile due to random irreversible slip, that is, at Type II stress raisers (Fig. 3). The abundance of PSB-GB cracks at low plastic strain amplitudes just above the strain fatigue limit [*73*] comes somewhat as a surprise. It can be inferred from the fracture surfaces (Figs. 13 and 14) that trans- and intergranular cracking are roughly of comparable significance. In general, grain boundary cracking has been considered more typical of low-cycle high-strain fatigue [*1,2,90,91*]. Figueroa and Laird [*92*], however, have made similar observations at low amplitudes. Since in our study the behavior was essentially unaltered in high-purity copper polycrystals, we exclude the possibility of grain boundary embrittlement by segregation effects.

The observations show that the PSB-GB crack initiation mechanism is effective in copper at room temperature for significantly smaller grain sizes than the lower limit $D \approx 300$ μm, as estimated for "brittle-type" PSB-GB cracks ($\alpha_{eff} \approx 1.4\,J/m^2$) under conditions as in the case of static extrusion growth by the use of Eq 18. This discrepancy would become even larger if one assumed that PSB-GB cracking is largely plasticity-controlled; that is, if the contribution α_p to α_{eff} (Eq 19) were dominant. The unlikeliness of such an assumption follows also from an evaluation of the fatigue lifetime of copper at the strain fatigue limit in the framework of the foregoing model of PSB-GB cracking which leads to the conclusion that α_{eff} is comparable in magnitude to α_s, implying that α_p is presumably small [*75*]. On the other hand, studies on single crystals have shown that, because of the discussed deviations from true cyclic saturation, the extrusion heights attained after, for example, $N_f \approx 10^5$ cycles, are several times larger than predicted for static extrusion growth by Eq 9. Thus the number m of PSB-matrix interface dislocations per pile-up (Fig. 5*b*) can be expected to be correspondingly larger than the value given by Eq 6 which was used in deriving Eq 18. This consideration reduces the lower limit for the grain size D at which "brittle-type" PSB-GB cracks can form according to Eq

18 and makes it much more compatible with the small grain size of $\approx 25\ \mu m$ for which PSB-GB cracks were observed in this study.

The main implication of these considerations, namely that PSB-GB cracking of copper polycrystals in air is indeed a quasi-brittle process with little plastic crack tip blunting, requires further attention. Coffin [*93*] has noted that, for a large number of materials, fatigue in air leads to intergranular cracking, whereas fatigue in vacuum causes only transgranular cracking. The possible role of oxidation can be inferred from a recent study by Auger spectroscopy which revealed that the surface of fatigued copper was preferentially enriched with oxygen at emerging PSBs [*94*]—that is, at the sites of localized strain—, as had already been suggested many years ago [*46*]. It is therefore proposed that surface oxidation facilitates the initiation of PSB-GB cracks in copper fatigued in air and stabilizes them during subsequent propagation, rendering the cracking process quasi-brittle. Presumably oxidation embrittles the crack tip and lowers α_{eff} significantly, as suggested by Snowden [*95*] for the case of intergranular fatigue failure of lead in air. At the same time any other effects due, for example, to hydrogen cannot be excluded. Our observations suggest furthermore that PSB-GB cracking is facilitated not only by environmental effects but also by the co-operative action of several neighboring PSBs and by processes more important in high-temperature fatigue [*84*] such as deformation-induced vacancy migration and coalescence at grain boundaries and grain boundary sliding. Further experiments in controlled atmospheres and at different temperatures would be desirable in order to clarify the relative significance of these different mechanisms in promoting PSB-GB cracks.

Conclusions

The results of the present work on high-cycle fatigue crack initiation mechanisms in single-phase fcc metals and alloys can be summarized as follows:

1. In planar-slip materials, random irreversible slip of large dislocation groups gives rise to a pronounced surface roughness and thereby leads to slip-band cracking.

2. Fatigue damage in wavy-slip materials results mainly from cyclic strain localization in PSBs.

3. In single crystals, fatigue damage due to PSBs originates from stress raisers at the edges of rapidly forming extrusions and from surface roughening of the extruded material by random irreversible slip. In addition, other less well characterized features play a role.

4. In polycrystals, the extrusion effect at PSBs is small and slip-band cracking is largely due to the surface roughening at emerging PSBs by random irreversible slip. Furthermore, PSBs promote the initiation of grain boundary cracks by a pile-up mechanism.

5. The available evidence indicates that not only slip-band cracking but also grain boundary cracking due to PSBs are facilitated by environmental interaction (oxidation).

6. Semiquantitative models based on detailed microscopic data have been formulated for the aforementioned cases of fatigue crack initiation and have been shown to be in substantial agreement with recent experimental observations.

Acknowledgments

The authors are grateful to Dr. U. Goesele for several useful discussions and to Drs. L. M. Brown, A. S. Cheng, and C. Laird for making available their manuscripts prior to publication. Furthermore, they express their appreciation to the reviewers for helpful comments on the original manuscript.

References

[1] Laird, C. and Duquette, D. J. in *Corrosion Fatigue*, A. J. McEvily and R. W. Staehle, Eds., National Association of Corrosion Engineers, Houston, Tex., 1972, pp. 88-117.

[2] Kim, W. H. and Laird, C., *Acta Metallurgica*, Vol. 26, 1978, pp. 777-787 and 789-799.

[3] Kim, Y. H. and Fine, M. E. in *Proceedings*, 5th International Conference on the Strength of Metals and Alloys, Aachen, P. Haasen, V. Gerold, and G. Kostorz, Eds., Pergamon Press, Elmsford, New York, 1979, Vol. 2, pp. 1131-1136.

[4] Fine, M. E., *Metallurgical Transactions*, Vol. 11A, 1980, pp. 365-379.

[5] Ruppen, J., Bhowal, P., Eylon, D., and McEvily, A. J. in *Fatigue Mechanisms, ASTM STP 675*, J. T. Fong, Ed., American Society for Testing and Materials, 1979, pp. 47-68.

[6] Morris, W. L., James, M. R., and Buck, O., *Engineering Fracture Mechanics*, Vol. 13, 1980, pp. 213-221.

[7] Antonopoulos, J. G., Brown, L. M., and Winter, A. T., *Philosophical Magazine*, Vol. 34, 1976, pp. 549-563.

[8] Brown, L. M. in *Proceedings*, International Conference on Dislocation Modelling of Physical Systems, Gainesville, Fla., 1980, M. F. Ashby, R. Bullough, C. S. Hartley, and J. P. Hirth, Eds., Pergamon Press, Elmsford, N.Y., 1981, pp. 51-68.

[9] Katagiri, K., Omura, A., Koyanagi, K., Awatani, J., Shiraishi, T., and Kaneshiro, H., *Metallurgical Transactions*, Vol. 8A, 1977, pp. 1769-1773.

[10] Katagiri, K., Awatani, J., Omura, A., Koyanagi, K., and Shiraishi, T. in *Fatigue Mechanisms, ASTM STP 675*, J. T. Fong, Ed., American Society for Testing and Materials, 1979, pp. 106-128.

[11] Gräf, M. and Hornbogen, E., *Scripta Metallurgica*, Vol. 12, 1978, pp. 147-150.

[12] Gräf, M. and Verpoort, C. in *Proceedings*, Fifth International Conference on the Strength of Metals and Alloys, Aachen, P. Haasen, V. Gerold, and G. Kostorz, Eds., Pergamon Press, Elmsford, N.Y., Vol. 2, pp. 1207-1212.

[13] Mughrabi, H. and Wang, R. in *Proceedings*, International Symposium on Defects and Fracture, Tuczno, Poland, 1980, G. C. Sih and H. Zorski, Eds., Martinus Nijhoff Publishers, The Hague, Boston, London, 1982, pp. 15-28.

[14] Essmann, U., Goesele, U., and Mughrabi, H., *Philosophical Magazine A*, Vol. 44, 1981, pp. 405-426.

[15] Differt, K., Essmann, U., and Mughrabi, H. to be submitted to *Philosophical Magazine*.

[16] Sinning, H.-R., Doctorate thesis, Göttingen University, West Germany, 1981.

[17] Cheng, A. S. and Laird, C., *Fatigue of Engineering Materials and Structures*, Vol. 4, 1982, pp. 331-341 and 343-353.

[18] Rasmussen, K. V. and Pedersen, O. B., *Acta Metallurgica*, Vol. 28, 1980, pp. 1467-1478.

[19] Klaffke, D. and Maennig, W., *Materialprüfung*, Vol. 22, 1980, pp. 65-74.

[20] Mughrabi, H. and Wang, R. in *Deformation of Polycrystals: Mechanisms and Microstruc-*

tures, Proceedings of the Second Risø International Symposium on Metallurgy and Materials Science, N. Hansen, A. Horsewell, T. Leffers, and H. Lilholt, Eds., 1981, pp. 87-98.

[*21*] Cheng, A. S., Figueroa, J. C., Laird, C., and Lee, J. K. in *Deformation of Polycrystals: Mechanisms and Microstructures*, Proceedings of the Second Risø International Symposium on Metallurgy and Materials Science, N. Hansen, A. Horsewell, T. Leffers, and H. Lilholt, Eds., 1981, pp. 405-415.

[*22*] Wang, R., Bauer, B., and Mughrabi, H., *Zeitschrift für Metallkunde*, Vol. 73, 1982, pp. 30-34.

[*23*] Wang, R., Doctorate thesis, Stuttgart University, Federal Republic of Germany, 1982.

[*24*] Mott, N. F., *Acta Metallurgica*, Vol. 6, 1958, pp. 195-197.

[*25*] Essmann, U., *Acta Metallurgica*, Vol. 12, 1964, pp. 1468-1470.

[*26*] Basinski, Z. S., *Discussions of the Faraday Society*, Vol. 38, 1964, pp. 93-102.

[*27*] Steeds, J. W. and Hazzledine, P. M., *Discussions of the Faraday Society*, Vol. 38, 1964, pp. 103-110.

[*28*] Mughrabi, H., *Materials Science and Engineering*, Vol. 33, 1978, pp. 207-233.

[*29*] Mughrabi, H., Ackermann, F., and Herz, K. in *Fatigue Mechanisms, ASTM STP 675*, J. T. Fong, Ed., American Society for Testing and Materials, 1979, pp. 69-105.

[*30*] Essmann, U. and Mughrabi, H., *Philosophical Magazine A*, Vol. 40, 1979, pp. 731-756.

[*31*] Woods, P. J., *Philosophical Magazine*, Vol. 28, 1973, pp. 155-191.

[*32*] Essmann, U. and Rapp, M., *Acta Metallurgica*, Vol. 21, 1973, pp. 1305-1317.

[*33*] Backofen, W. A. in *Fracture*, B. L. Averbach, D. K. Felbeck, G. T. Hahn, and D. A. Thomas, Eds., MIT Press and John Wiley, 1959, pp. 435-449.

[*34*] Essmann, U., *Philosophical Magazine A*, Vol. 45, 1982, pp. 171-190.

[*35*] Kuhlmann-Wilsdorf, D. and Laird, C., *Materials Science and Engineering*, Vol. 27, 1977, pp. 137-156.

[*36*] Wood, W. A., *Philosophical Magazine*, Vol. 3, 1958, pp. 692-699.

[*37*] May, A. N., *Nature* (London), Vol. 185, 1960, pp. 303-304.

[*38*] Lukáš, P. and Klesnil, M., *Physica Status Solidi (a)*, Vol. 5, 1971, pp. 247-258.

[*39*] Lukáš, P. and Klesnil, M. *Physica Status Solidi (a)*, Vol. 5, 1971, pp. 247-258.

[*40*] Pande, C. S. and Hazzledine, P. M., *Philosophical Magazine*, Vol. 24, 1971, pp. 1039-1057.

[*41*] Neuhäuser, H., Koropp, J., and Heege, R., *Acta Metallurgica*, Vol. 23, 1975, pp. 441-453.

[*42*] Lukáš, P. and Klesnil, M., *Physica Status Solidi*, Vol. 21, 1967, pp. 717-731.

[*43*] Strutt, P. R., *Journal of the Australian Institute of Metals*, Vol. 8, 1963, pp. 115-126.

[*44*] Neumann, P., *Zeitschrift für Metallkunde*, Vol. 58, 1967, pp. 780-789.

[*45*] Katagiri, K., Omura, A., Koyanagi, K., Awatani, J., Shiraishi, T., and Kanegiro, H. in *Fracture 1977*, Proceedings of the Fourth International Conference on Fracture, Waterloo, University of Waterloo Press, Ontario, Canada, Vol. 2, 1977, pp. 695-702.

[*46*] Thompson, N., Wadsworth, N. J., and Louat, N., *Philosophical Magazine*, Vol. 1, 1956, pp. 113-126.

[*47*] Brown, L. M. in *Proceedings*, "Fatigue 1977" Conference, Cambridge, U.K., *Metal Science*, Vol. 11, 1977, pp. 315-320.

[*48*] Laird, C. in *Fatigue and Microstructure*, 1978 ASM Materials Science Seminar, St. Louis, American Society for Metals, Metals Park, Ohio, 1979, pp. 149-203.

[*49*] Mughrabi, H. in *Proceedings*, Fifth International Conference on the Strength of Metals and Alloys, Aachen, 1979, P. Haasen, V. Gerold, and G. Kostorz, Eds., Pergamon Press, Elmsford, N.Y., Vol. 3, 1980, pp. 1615-1638.

[*50*] Mughrabi, H., Herz, K., and Ackermann, F. in *Proceedings*, Fourth International Conference on the Strength of Metals and Alloys, Nancy, Vol. 3, 1976, pp. 1244-1248.

[*51*] Lukáš, P., Klesnil, M., and Krejči, J., *Physica Status Solidi*, Vol. 27, 1968, pp. 545-558.

[*52*] Basinski, S. J., Basinski, Z. S., and Howie, A., *Philosophical Magazine*, Vol. 19, 1969, pp. 899-924.

[*53*] Antonopoulos, J. G. and Winter, A. T., *Philosophical Magazine*, Vol. 33, 1976, pp. 87-95.

[*54*] Wilhelm, M. and Everwin, P. in *Proceedings*, Fifth International Conference on the Strength of Metals and Alloys, Aachen, P. Haasen, V. Gerold, and E. Kostorz, Eds., Pergamon Press, Elmsford, N.Y., Vol. 2, 1979, pp. 1089-1094.

[55] Wilhelm, M., *Materials Science and Engineering*, Vol. 48, 1981, pp. 91-106.
[56] Sinning, H.-R. and Haasen, P., *Scripta Metallurgica*, Vol. 15, 1981, pp. 85-90.
[57] Sinning, H.-R. and Haasen, P., *Zeitschrift für Metallkunde*, Vol. 72, 1981, pp. 807-812.
[58] Mughrabi, H. in *Proceedings*, Fourth International Conference on Continuum Models of Discrete Systems, Stockholm, O. Brulin, and R. K. T. Hsieh, Eds., 1981, North-Holland, The Hague, The Netherlands, 1981, pp. 241-257.
[59] Vogel, W., Wilhelm, M., and Gerold, V., *Acta Metallurgica*, Vol. 30, 1982, pp. 21-30.
[60] Laird, C. in *Treatise on Materials Science and Technology, Vol. 6: Plastic Deformation of Materials*, Academic Press, New York, 1975, pp. 101-162.
[61] Stoltz, R. E. and Pineau, A. G., *Materials Science and Engineering*, Vol. 34, 1978, pp. 275-284.
[62] Laird, C., Finney, J. M., and Kuhlmann-Wilsdorf, D., *Materials Science and Engineering*, Vol. 50, 1981, pp. 127-136.
[63] Mughrabi, H. in *Proceedings*, Third International Conference on the Strength of Metals and Alloys, Cambridge, Vol. 1, 1973, pp. 407-409.
[64] Polák, J., *Scripta Metallurgica*, Vol. 4, 1970, pp. 761-764.
[65] Wilkens, M., Herz, K., and Mughrabi, H., *Zeitschrift für Metallkunde*, Vol. 71, 1980, pp. 376-384.
[66] Lin, T. H. and Ito, Y. M., *Proceedings of the National Academy of Sciences*, Vol. 62, 1969, pp. 631-635.
[67] Neumann, P., *Acta Metallurgica*, Vol. 17, 1969, pp. 1219-1225, and unpublished work.
[68] Fine, M. E. and Ritchie, R. O. in *Fatigue and Microstructure*, 1978 ASM Materials Science Seminar, St. Louis, American Society for Metals, Metals Park, Ohio, 1979, pp. 245-278.
[69] Tanaka, K. and Mura, T., *Journal of Applied Mechanics*, Vol. 103, 1981, pp. 97-103.
[70] Lin, T. H. and Ito, Y. M., *Journal of Mechanics and Physics of Solids*, Vol. 17, 1969, pp. 511-523.
[71] Duquette, D. J., personal communication, 1979.
[72] Hunsche, A. and Neumann, P., presented at Spring Meeting of the German Physical Society, 1982, *Verhandlungen der DPG (VI)*, Vol. 17, 1982, pp. 896-897.
[73] Lukáš, P., Klesnil, M., and Polák, P., *Materials Science and Engineerig*, Vol. 15, 1974, pp. 239-245.
[74] Hessler, W., Müllner, H., Weiss, B., and Stickler, R., *Metal Science Journal*, Vol. 15, 1981, pp. 225-230.
[75] Mughrabi, H. in *Proceedings*, Second International Symposium and Seventh Canadian Fracture Conference on Defects, Fracture and Fatigue, Mont Gabriel, Quebec, Canada, 30 May-5 June 1982, J. W. Provan and G. C. Sih, Eds., Martinus Nijhoff Publishers, The Hague, Boston, London, in press.
[76] Stroh, A. N., *Advances in Physics*, Vol. 6, 1957, pp. 418-465.
[77] Smith, E. and Barnby, J. T., *Metal Science Journal*, Vol. 1, 1967, pp. 56-64.
[78] Zener, C., *Transactions of the American Society for Metals*, Vol. 40, 1948, pp. 3-31.
[79] Inman, M. C., McLean, D., and Tipler, H. R., *Proceedings of the Royal Society*, Vol. A273, 1963, pp. 538-557.
[80] Hondros, E., "Energetics of Solid-Liquid Interfaces," in *Interfaces*, R. C. Gifkins, Ed., Butterworths, London, 1969, p. 77.
[81] Duquette, D. J. and Gell, M., *Metallurgical Transactions*, Vol. 2, 1971, pp. 1325-1331.
[82] Volsky, A. and Sergievskaya, E., *Theory of Metallurgical Processes*, Mir Publishers, Moscow, 1971, p. 148.
[83] Mughrabi, H., unpublished work, 1982.
[84] Bhat, S. P. and Laird, C. in *Fatigue Mechanisms, ASTM STP 675*, J. T. Fong, Ed., American Society for Testing and Materials, 1979, pp. 592-623.
[85] Avery, D. H. and Backofen, W. A. in *Fracture of Solids*, D. G. Drucker and J. J. Gilman, Eds., Interscience Publishers, New York, 1963, pp. 339-382.
[86] Mecke, K. and Blochwitz, C., *Physica Status Solidi (a)*, Vol. 61, 1980, pp. K5-K7.
[87] Ramsteiner, F., Lampert, G., Seeger, A., and Schüle, W., *Physica Status Solidi*, Vol. 8, 1965, pp. 863-879.
[88] Ewing, J. A. and Humfrey, J. C. W., *Philosophical Transactions A*, Vol. 200, 1902, pp. 241-250.
[89] Neumann, P., Vehoff, M., and Fuhlrott, H. in *Fracture 1977*, Proceedings of the Fourth In-

ternational Conference on Fracture, Waterloo, University of Waterloo Press, Vol. 2, 1977, pp. 1313-1324.
[90] Laird, C. and Smith, G. C., *Philosophical Magazine*, Vol. 8, 1963, pp. 1945-1963.
[91] Boettner, R. C., Laird, C., and McEvily, A. J., Jr., *Transactions of the Metallurgical Society of AIME*, Vol. 233, 1965, pp. 379-387.
[92] Figueroa, J. C. and Laird, C., personal communication, 1979.
[93] Coffin, L. F., *Proceedings of the Institution of Mechanical Engineers*, Vol. 188, 1974, pp. 109-127.
[94] Fischer, H., Wang, R., and Mughrabi, H., unpublished work, 1981.
[95] Snowden, K. U., *Acta Metallurgica*, Vol. 12, 1964, pp. 295-303.

DISCUSSION

E. E. Underwood[1] *(written discussion)*—Surface roughness appears to play an important role in the research described by the authors. The results quoted on persistent slip bands, using stereopictures of the profiles, or the contamination line technique, look very impressive.

One method for the quantitative characterization of an irregular curve is that proposed by E. W. Behrens,[2] in connection with a study of roughness parameters for the trace through a fracture surface.[3] This parameter is easily visualized because it is physically related to the ratio of mean height to mean period of the trace peaks.

Behrens' profile roughness parameter P_R is defined by

$$P_R = \tfrac{1}{2} \int_{x_1}^{x_2} P(x)dx/L_T \tag{20}$$

where x_1 and x_2 are positions of the test line below and above the trace (or profile) where no intersections are possible. The test line (of length L_T) is displaced parallel to itself and the crack propagation direction between x_1 and x_2. The number of intersections measured as a function of test line position x is $P(x)$.

The working equation can be expressed by

$$P_R \simeq \frac{\Delta x}{2L_T} \sum_i P_i \tag{21}$$

where Δx is the displacement of the test line, and ΣP_i is the total number of intersections of the test line between positions x_1 and x_2.

[1]Chemical Engineering/Metallurgy, Georgia Institute of Technology, Atlanta, Ga. 30332.
[2]Private communication to E. E. Underwood, Sept. 1977.
[3]Underwood, E. E., "Quantitative Fractography—A Preliminary Analysis," unpublished document, 10 March 1979.

This procedure has been applied to the four traces published by Krasowsky and Stepanenko.[4] Table 2 summarizes the results. The duplicate readings give an idea of the variation to be expected.

Even though the important characteristics of undulating surface traces are expressed in terms of a single number, as the authors point out, more detailed information, such as the tendency for a notch to develop, may be required. It is possible that the curves obtained by plots of P_R versus the fatigue parameter may reveal the occurrence of this more localized phenomenon (notching).

H. Mughrabi et al (authors' closure)—The appearance of a critical notch, at which a crack can initiate, is a localized event that occurs somewhere within a PSB, where the statistical fluctuations, responsible in our model for the development of surface roughness, accumulate to an extreme situation in the form of a deep and narrow valley.

In our work the roughness profile was characterized by several parameters, and the mean profile width used in the present paper was one of them. Although, as shown in the paper, the mean profile width is a useful quantity for comparison of computed and observed roughness profiles, it is not specific enough to reveal critical notch effects. We are therefore very interested in Professor Underwood's comments and agree that Behrens' roughness parameter P_R may possibly provide a suitable characterization of extreme situations corresponding to notches. In order to check this, some further studies will be necessary. We are very grateful for this useful hint.

TABLE 2—*Results of procedure discussed by E. E. Underwood applied to the four traces of Krasowsky and Stepanenko.*[a]

Figure	Trace	ΣP_i	L_T, mm	P_R
5	I′	53	87	0.305
8	I′	57	86.5	0.330
6	II′	66	90	0.367
8	II′	69	88	0.392
5	I″	52	71	0.366
8	I″	50	72	0.347
6	II″	52	77	0.338
8	II″	52	76.5	0.340

[a]*International Journal of Fracture*, Vol. 15, No. 3, June 1979, p. 203.

[4]Krasowsky, A. J. and Stepanenko, V. A., *International Journal of Fracture*, Vol. 15, No. 3, June 1979, p. 203.

A. J. McEvily[5] (*written discussion*)—This comment and question has to do with the schematic of a slip band in a single crystal which you showed. For this case an extrusion is depicted at each of the opposite ends of the PSB. Sometime ago Boettner tested under cyclic loading a single crystal of rectangular cross section and noted that at a corner an intrusion on one face was coupled with an extrusion on the face around the corner. All slip bands away from the corner showed only extrusions. The question then in your case is: Did you in fact observe extrusions at opposite ends of a PSB?

H. Mughrabi et al (*authors' closure*)—We appreciate Professor McEvily's question and his comments. Yes, we have checked the point raised by him in almost all cases by looking at the surface profile of one and the same PSB at the two opposite top faces of the crystal and have always found extrusions at both ends. In addition, we have recently performed an experiment similar to the one performed by Dr. Boettner that was described by Professor McEvily and we have not observed intrusions coupled with extrusions.

[5]Professor, Department of Metallurgy, University of Connecticut, Storrs, Conn. 06268.

Michael R. James[1] *and Winfred L. Morris*[1]

The Role of Microplastic Deformation in Fatigue Crack Initiation

REFERENCE: James, M. R. and Morris, W. L., **"The Role of Microplastic Deformation in Fatigue Crack Initiation,"** *Fatigue Mechanisms: Advances in Quantitative Measurement of Physical Damage, ASTM STP 811*, J. Lankford, D. L. Davidson, W. L. Morris, and R. P. Wei, Eds., American Society for Testing and Materials, 1983, pp. 46-70.

ABSTRACT: A reference gage technique is used to measure the localized plastic strains which develop within individual surface grains during cyclic loading of Al 2219-T851. These are found to increase more rapidly in grains having large distances of slip between grain boundaries in the plane of the surface. Further fatigue causes cyclic hardening of the surface in the large grains as manifest by a reduction in the microplastic deformation. Maximum values of the local plastic strain and the cycles needed to achieve them are observed to be a function of environmental humidity and of internal hydrogen content.

Humid air is found to decrease the development of microplasticity when compared with fatigue in dry air. Increased quantities of internal hydrogen (although in contents less than 1 ppm) substantially increase the rate of development of microplasticity early during fatigue and later accelerates cyclic hardening of the surface. A model based on a critical fracture strain criterion is formulated and used to calculate the numbers of constituent particles in the alloy fractured during fatigue. The model satisfactorily predicts the enhancement of particle fracture in alloys that contain hydrogen or that are fatigued in dry air. We conclude that the principal effect of these environmental factors on particle fracture arises because they alter the propensity of the surface to undergo microplastic deformation.

KEY WORDS: fatigue, crack initiation, crack nucleation, particle fracture, microplasticity, microstructure, aluminum alloys, environmental effects

The surface of an alloy is a favorable site for fatigue crack initiation. It is exposed to the ambient environment, and its mechanical properties are altered from those of the bulk by surface oxide and by the partial absence of constraints on the deformation. Pioneering research by Thompson et al [*1*] demonstrated that initial fatigue damage can be concentrated very near the surface.[2] They found that periodic removal of shallow surface layers during fatigue extended the fatigue life of commercially pure copper. Kramer [*2*] has

[1]Member Technical Staff, Rockwell International Science Center, Thousand Oaks, Calif. 91360.

[2]The italic numbers in brackets refer to the list of references appended to this paper.

subsequently reported the same effect for a number of materials. But despite many eloquent studies of dislocation structure precursive to fatigue crack initiation, quantitative models of initiation have been slow in developing. Until recently, there has not been a strong need for such insight. Now, new lifetime prediction techniques require models that predict cycles to crack formation from the localized microstructure at potential sites of crack initiation [*3*]. A major constraint to the rapid success of recent efforts in initiation modeling has been the extreme difficulty in measuring localized changes in the mechanical properties of the surface which are associated with fatigue. Consequently, there is still no consensus regarding the manner in which fatigue induced deformation in the alloy matrix actually leads to crack formation.

Contemporary theories separate the crack initiation process into two parts. Dislocation models are used to calculate the degree of localized microplastic strains developed within individual grains; the strains are sensitive to local grain size and thus microstructure as well as other ancillary factors such as the environment. The actual cycles to crack initiation are subsequently determined by imposing a fracture criterion which is determined by the nature of the cracking site. For instance, in modeling constituent particle fracture, both Chang et al [*4*] and Tanaka and Mura [*5*] assumed that a particle breaks when the elastic strain energy in the particle equals the energy required to form the new fracture surface. Elastic strain within the particle arises from dislocation pile-ups at the matrix-particle interface. There is ample qualitative evidence, however, that microplasticity is not the only driving force for crack initiation. For example, in Al 2219-T851, the crack initiation habit changes with cyclic stress amplitude as well as with cycles (Fig. 1). Certainly, each fracture mode requires its own initiation criterion. However, all three modes of cracking cannot be responsive to microplasticity alone because their order of occurrence changes with cyclic stress amplitude.

Consequently, the state of deformation of the matrix precursive to crack initiation must be characterized by other factors in addition to its degree of microplasticity. The hardness of the surface appears to be one such factor. Fifteen years ago, Grosskreutz [*6*] examined near-surface dislocation structures in Al 1100 and found them to be sensitive to the mechanical properties of the surface oxide. Dislocation tangles indicative of hardening in strained samples were more easily developed under the thick coherent oxides which formed in humid air. Subsequently, Kramer [*2*] has argued that hardening of the surface is *required* for fatigue crack initiation. Supporting this, Pangborn et al [*7*] have recently presented data for an Al 2024-T3 alloy that show a correlation between localized hardening and fatigue lifetime. Their X-ray double-crystal diffractometry technique involving high-resolution imaging of the lattice distortion is biased towards determination of the excess dislocation density in the largest surface grains. It appears, then, that cyclic hardening of the matrix material within a large grain in 2024 may be a precursor to cracking in the grain.

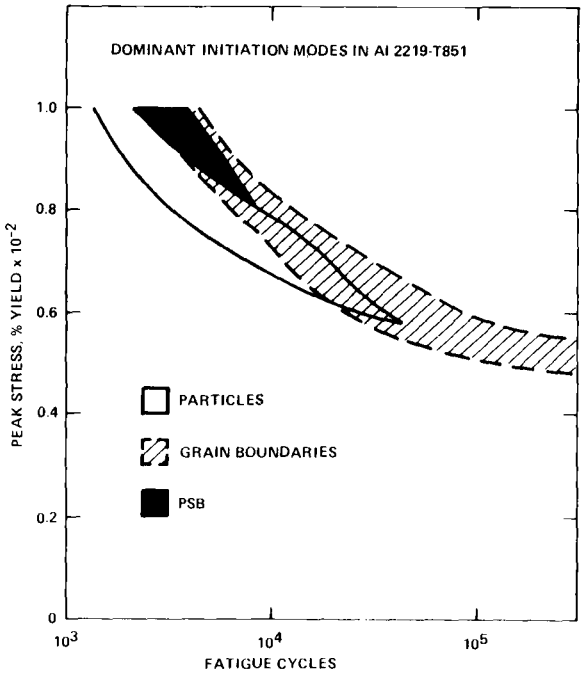

FIG. 1—*Several microcrack initiation modes are active in Al 2219-T851 and are dominant at different cyclic stress amplitude regimes which tend to overlap as illustrated here.*

In this paper, we examine the influence on crack initiation of both localized microplasticity and cyclic surface hardening by measuring local plastic strains within individual grains. Effects of humidity and heat-to-heat variations in the alloy hydrogen content are also assessed by this method. The microplastic response of the alloy surface is characterized by using a reference gage technique described previously [*8*] and summarized briefly here. Measurements on Al 2219-T851 show that the localized plastic strains which occur at peak tensile loads within individual grains increase progressively with fatigue at a rate which increases with grain size. While the microplasticity initially increases more rapidly within large grains, its development is ultimately retarded by cyclic hardening of the surface. Furthermore, the maximum microplastic strains obtained during fatigue are affected both by the atmospheric humidity and by the internal hydrogen content of the alloy. At the stress amplitude employed, crack initiation in the 2219 alloy takes place at constituent particles, apparently at a critical value of local plastic strain, and thus the rate of particle fracture is sensitive to both humidity and to alloy hydrogen content.

We show that internal hydrogen substantially increases the early development of microplasticity and enhances the rate of particle fracture. Heat-to-heat variations in hydrogen content as small as 1 ppm have an important effect

on the fatigue lifetime of Al 2219-T851. Moist air, however, has an opposite effect in that the development of microplasticity is delayed and the maximum plastic strain is decreased from that attained in dry air. Apparently, the principal effect of humidity on crack initiation in 2219 does not arise from hydrogen liberated by oxidization.

Experimental Procedures

Both crack initiation and localized microplasticity data were obtained with flexural fatigue specimens such as shown mounted in a loading jig in Fig. 2. Specimens were machined from plate stock with the principal stress axis parallel to the rolling direction. The mechanical properties and grain size of each heat studied are given in Table 1. To minimize residual surface stresses developed during machining, each specimen was milled with decreasing cutting depths and then mechanically polished with 0.05-μm alumina (Al_2O_3) powder to a mirror finish. Results are given for specimens fatigued in stroke control in fully reversed loading in either a dry air state or in laboratory air at 50 to 60% relative humidity. The numbers of constituent particles fractured by fatigue were determined by scanning electron microscopy (SEM) by using the jig in Fig. 2 to place the surface in tension and open the cracks for improved visibility.

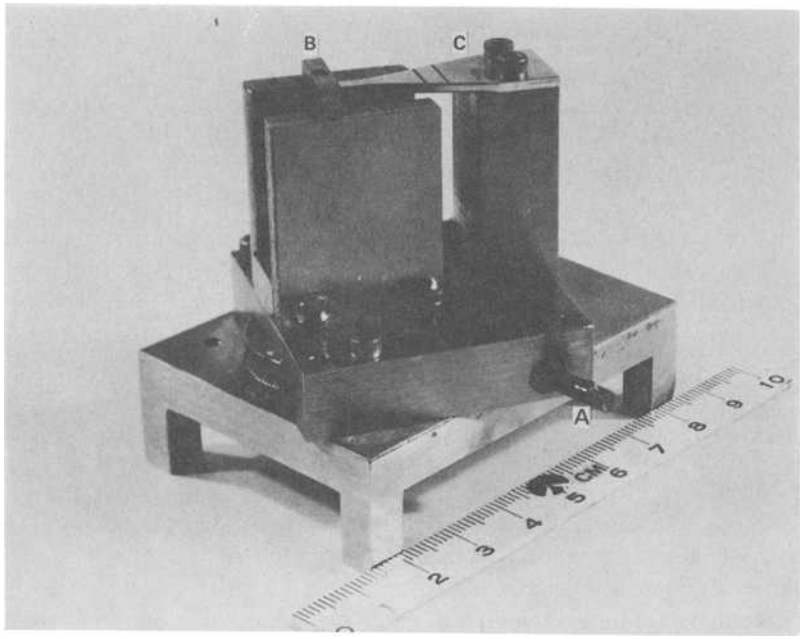

FIG. 2—*Specimen C is loaded in flexure by puller bar B which is moved through a worm gear attached to shaft A, which in turn is connected to the outside of our SEM through a rotary feedthrough. Data are taken only in the region marked on the specimen by parallel lines.*

TABLE 1—*Material properties.*

	Heat II	Heat III
	CHEMICAL COMPOSITION, %[a]	
Silicon	0.05	0.07
Iron	0.22	0.24
Copper	6.02	5.94
Manganese	0.29	0.31
Magnesium	0.008	<0.001
Zinc	0.04	0.03
Titanium	0.07	0.04
Vanadium	0.13	0.11
Zirconium	0.18	0.15
Oxygen	0.0031	0.0024
Nitrogen	0.003	0.001
Hydrogen	high[b]	low[b]
	GRAIN SIZE, μm	
Longitudinal	45	80
Transverse	30	60
	YIELD STRENGTH, MPa	
	358	358

[a] Data from Luvak Inc., Boylston, Mass.
[b] All less than 1 ppm. Ranking by bubble densities.

Initially, the dry environment was achieved by covering the entire fatigue machine with a box purged with dry nitrogen for approximately 12 h until the measured relative humidity was less than 1%. Subsequently, we found that specimens coated by a flexible stopping off medium (Locamit, W. Canning and Co. Ltd.) had the same particle fracture behavior as in the dry nitrogen environment. The dry environment data presented here were obtained in this way.

Microplasticity Measurements

Theories of crack initiation at constituent particles, based upon strain energy density concepts, associate fracture with a peak tensile plastic strain in a grain containing a particle. With repeated cyclic loading, the surface yields microplastically while the bulk remains elastic. Only the largest grains at the surface experience substantial microplasticity, so a technique is needed that can determine the magnitude of the tensile plastic strains within these grains. Ideally, one needs to know the width of the local stress-strain hysteresis loops versus cycles and local grain size, to evaluate the energy criterion for fracture.

A method that provides approximate loop widths within individual grains

has been devised. It involves the use of thin mica flakes as reference gages to determine surface displacements over 20 μm gage lengths. The procedural details of this method have been published elsewhere [8]. Here we discuss the nature of the data which the technique provides.

A specimen is fatigued in air in fully reversed loading and loading is interrupted at zero load (Point 1, Fig. 3*a*) after completing the compression half cycle. Reference gages of mica flakes are placed on the sample, which is then transferred to a loading jig in an SEM. Residual strains within individual grains are measured over the gage length ℓ (Fig. 3*b*) by determining the relative displacements between the sample surface and mica at Points x_1 and x_2, for

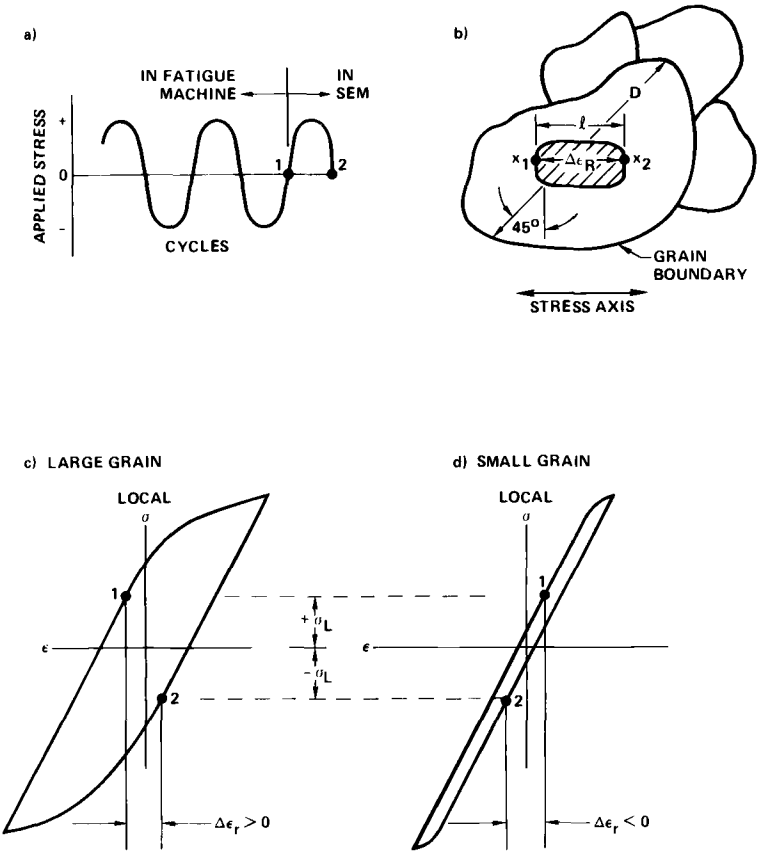

FIG. 3—*Reference gage technique for measuring local microplastic deformation within individual grains.* (a) *Specimen is unloaded from compression half cycle after fatigue.* (b) *Residual strain is measured from the relative displacements between the sample surface and the mica reference gage over a tensile load cycle in the SEM.* (c) *In the large grains,* $\Delta\epsilon_r$ *is the sum of the tensile plastic strain and the elastic reaction strain and is positive.* (d) *After unloading, small grains are driven into elastic compression and* $\Delta\epsilon_r$ *is negative.*

loading over a tensile cycle (that is, from Points 1 to 2, Fig. 3*a*). This involves taking micrographs before and after loading at Points x_1 and x_2, which are then processed by a stereoscopic technique to obtain displacements. These are converted to residual strain ($\Delta\epsilon_r$), measured parallel to the principal stress axis. Resulting strain sensitivity is approximately 0.005%. It appears at least for Al 2219-T851 that the microplasticity is contained in a thin layer near the surface, and therefore the shear stress which supports the axial strain will be in the plane of the surface and at ± 45 deg to the stress axis. For this reason a correlation is sought between $\Delta\epsilon_r$ and the maximum grain dimension D measured at ± 45 deg to the stress axis in data presented later.

If the local *stresses* were identically zero when the applied stress was zero, then $\Delta\epsilon_r/2$ would be the half width of the hysteresis loop ($\Delta\epsilon_p$). Because of local constraints of the microplastic deformation, however, the local stress will tend to the compressive after a tensile cycle, and tensile after a compressive cycle. We illustrate the consequence of this for a small grain (Fig. 3*d*) in which the microplastic deformation is small, neighboring a large grain (Fig. 3*c*) in which the microplasticity is large. For this particular case, the local stress σ_L arising from plastic strain in the large grain is the same in both grains. In both cases, $\Delta\epsilon_r$ is the sum of the plastic strains and an elastic reaction strain which arises from σ_L. In the large grain, $\Delta\epsilon_r$ is positive for loading from 1 to 2 and negative for loading from 2 to 1. The small grain experiences principally the elastic reaction and $\Delta\epsilon_r$ is negative for loading from 1 to 2. For the large grain we anticipate that $\sigma_L \propto \Delta\epsilon_p$, and since $\Delta\epsilon_r = 2\Delta\epsilon_p + \text{constant} \cdot \sigma_L$ we later make the approximation that $\Delta\epsilon_p \propto \Delta\epsilon_r$ for large grains. This proportionality also assumes that the reversible plastic strain which takes place on unloading to zero load is negligible, or at least does not change with fatigue. The Bauschinger effect is small in high-strength aluminum alloys, at least prior to reversal of the load.

Hydrogen Content Measurements

Heat-to-heat variations in the fatigue behavior of aluminum alloys are common. These are apparently in response to factors such as alloy grain size, and to small fluctuations in composition within the normal range. It appears that small amounts of hydrogen at the 1 ppm level can substantially affect the ductility of the matrix of aluminum. The reference gage technique allows the true ductility of the alloy matrix to be measured at the surface. We have found two heats of Al 2219-T851 which differ markedly in crack initiation behavior. Gas extraction analysis shows that the hydrogen contents of these are both less than 1 ppm (Table 1). The relative hydrogen contents of these two materials have been ranked as low (Heat III) and high (Heat II), based on counting of the number of gas bubbles (Fig. 4) formed in the materials after 3 h of annealing at 515°C. A histogram of numbers versus bubble diameter is given for the two

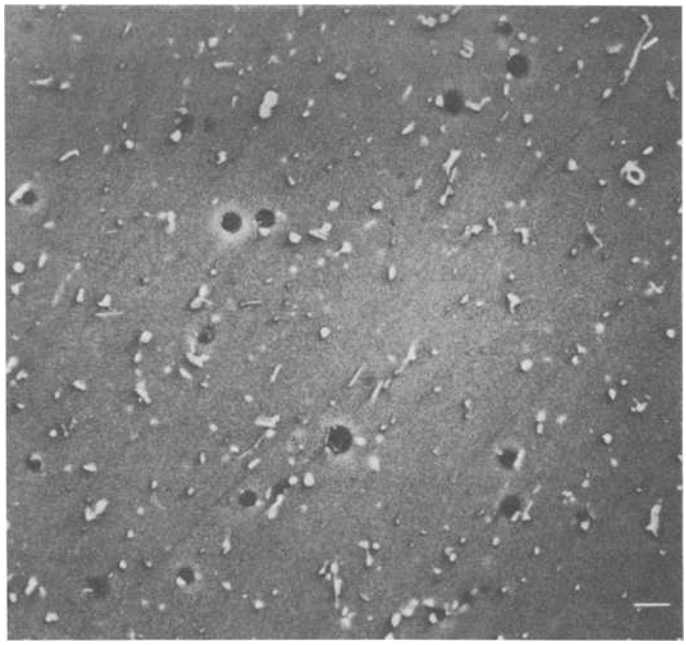

FIG. 4—*Scanning electron micrograph of voids at constituent particle sites in Heat II. These are typically hemispherical, suggestive of bubbles. Bar is 10 μm.*

materials in Fig. 5;[3] this was obtained by sectioning and polishing 0.15-cm-thick slabs of the alloys after the annealing procedure.

Microplasticity measurements presented later show a substantial difference between Heat II and Heat III materials which is attributed to differences in their hydrogen content. To substantiate our hypothesis as to the role of hydrogen, microplasticity measurements were also made on Heat III material which had been charged to increase its hydrogen content. Charging was done in a salt bath using a modified form of the procedure developed by Elkholy et al [*9*]. The apparatus is illustrated in Fig. 6. The salt consists of $NaHSO_4$, $KHSO_4$, and Na_2SO_4 in the proportions 37.5/42.5/160 by weight. Sufficient water was added to produce a melting temperature of 150°C. Charging was done for 4 h

[3]The total area under the curve $F(D)$ in Fig. 5 must equal the total number of bubbles per square centimetre. This is given by

$$\#/\text{cm}^2 = \int_0^{D_{\max}} F(D)dD$$

where D is the bubble diameter. Since dD has units of μm, $F(D)$ must have units of $\#/\text{cm}^2$ μm.

Another way of looking at this is to note that there are (in all probability) zero bubbles with a diameter of exactly 5 μm, but $1200/\text{cm}^2$ within the interval of 4.5 to 5.5 μm. This is found by extracting the value of $1200/\text{cm}^2$ μm from Fig. 5 and multiplying it by the 1 μm unit interval.

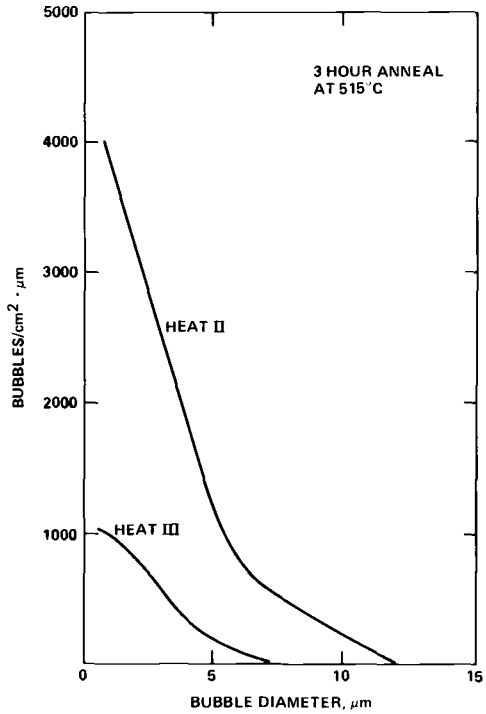

FIG. 5—*Histogram of the diameter of bubbles sectioned at the surface of specimens taken from the center of the plate stock for Heats II and III. Plotted on the ordinate is the number of bubbles per unit area per unit length in bubble diameter. Specimens were annealed for 3 h at 515°C.*

at a current of 200 mA/cm^2. Best results were obtained if no additional water was added during charging. When this technique was successfully employed, the specimen surface was not corrosively attacked. Massive amounts of hydrogen were clearly driven into the material, as seen when subsequently annealing samples to determine hydrogen content. Grains are actually lifted out of the surface by gas formed at the boundaries after annealing (Fig. 7). The actual fatigue samples were not annealed after hydrogen charging and particle fracture remained the primary crack initiation mode. Specimens exposed to the salt, but not in the charging loop, showed no significant change in microplasticity behavior from the uncharged material.

Results

The deformation which leads to the fractue of constituent particles in Al 2219-T851 apparently takes place in a shallow layer near the surface. Particles tend to be more readily fractured in grains having a large surface cross section. Also, polishing to remove only a few microns of the surface noticeably alters

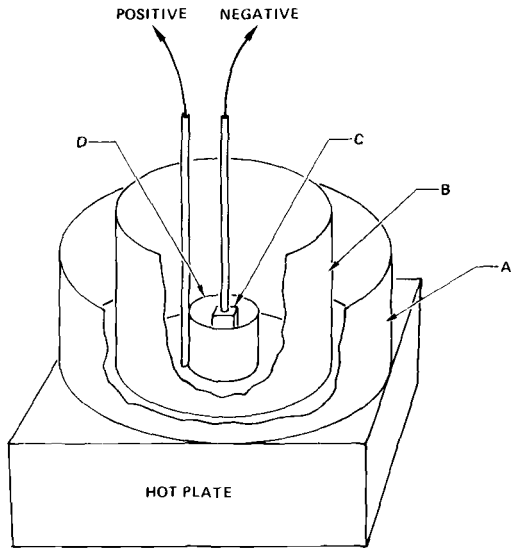

FIG. 6—*Schematic drawing of the salt bath apparatus used for hydrogen charging.* (a) *Outer quartz beaker containing diffusion pump oil.* (b) *Inner quartz beaker containing salt.* (c) *Specimen.* (d) *Platinum anode. Although not shown, the charging beaker is also covered by a watch glass.*

the state of cyclic hardening of the material and affects early crack growth. Consequently, we have sought a correlation between the residual strain $\Delta\epsilon_r$ and grain size, to establish the effect of slip distance on the development of microplasticity. Data are presented for the low hydrogen content Heat III in moist and in dry air, and for Heat II and hydrogen charged Heat III in moist air. The Heat II material apparently has a high as-received hydrogen content (Fig. 5). The development of localized microplasticity is found to be very sensitive to environmental humidity and internal hydrogen. These factors also alter the propensity for particle fracture during fatigue as shown by experimentally determined fractured particle densities. We conclude by demonstrating that the measured number of particles fractured by fatigue can be related to $\Delta\epsilon_r$ using a simple model.

Microplasticity Results

A correlation is sought between values of $\Delta\epsilon_r$ (which are measured parallel to the principal stress axis) and the size of the grain containing the measurement site. The size parameter evaluated is the maximum grain width D measured at ± 45 deg to the principal stress axis (Fig. 3*b*); these are the approximate directions of slip responsible for the observed axial microplasticity, if as reported earlier the deformation is concentrated near the surface. All results were ob-

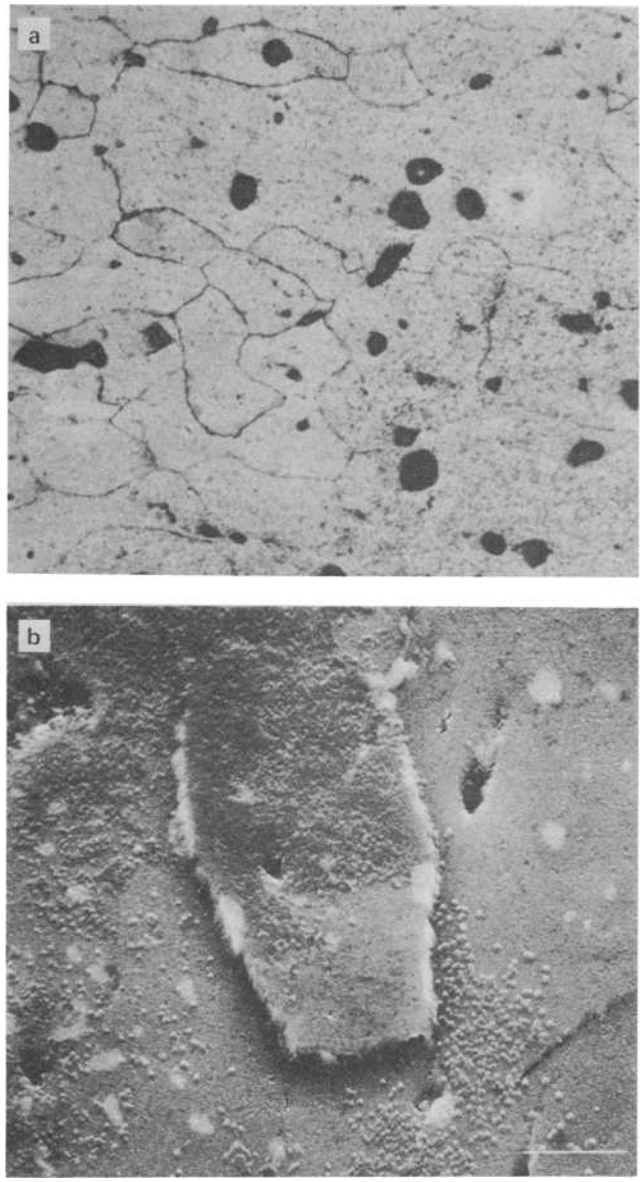

FIG. 7—*Micrographs of the surface of a Heat III specimen after hydrogen charging and a 3-h anneal at 515°C, showing damage to grain boundaries.* (a) *Optical photograph at ×250; the pits are at the sites of constituent particles etched out during charging.* (b) *Scanning electron micrograph showing lifting of a grain out of the surface (bar is 10 μm).*

tained for loading at a cyclic stress amplitude of ± 270 MPa, or at nominally 75% of the yield strength.

Results in Figs. 8 and 9 are from Ref *10* and are for Heat III fatigued in 50% relative humidity air. On the first loading cycle the strain is elastic. With increasing fatigue, plastic strains develop more rapidly at sites of large slip. The strain measurement sensitivity is better than $\pm 0.005\%$ strain, as attested by the results at zero fatigue cycles in Fig. 8. The scatter in values of $\Delta\epsilon_r$ from grain to grain of the same size is real and probably arises from variations in grain crystallographic orientation and depth. $\Delta\epsilon_r$ also depends on the properties of other grains near each measurement site. Small grains in which $\Delta\epsilon_r$ is compressive are found to lie near large grains in which $\Delta\epsilon_r$ is tensile.

We digress for a moment to note that this last result means σ_L must be compressive for all grains after a tensile load cycle. The summation of σ_L over the specimen will produce a macroscopic residual stress which, if large enough, could be measured by X-ray diffraction. For fully reversed loading, this stress is reversed on each half cycle and appears to be small. In tension-tension load-

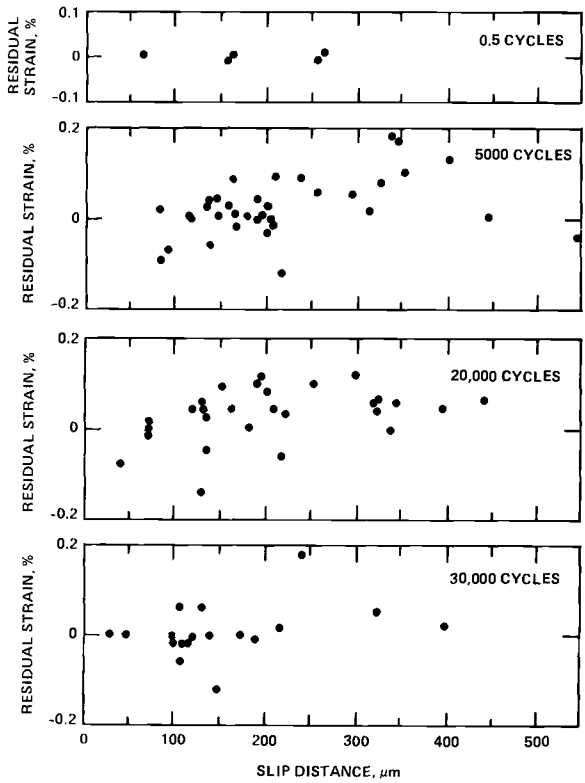

FIG. 8—*Residual strain $\Delta\epsilon_r$ as a function of slip distance for four intervals of fatigue at a cyclic stress amplitude of ± 270 MPa for Heat III in 50% relative humidity air.*

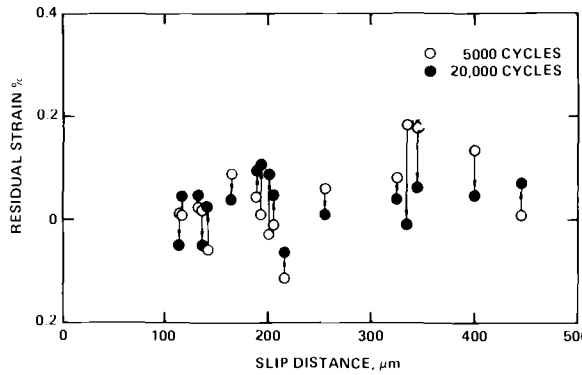

FIG. 9—*Trends in development of residual plastic strain are determined by repeated measurements at the same sites for the same material and loading conditions as in Fig. 8. From 5 to 20 × 10^3 cycles hardening has reduced the peak plastic strains in the largest grains, while they continue to increase in 200-μm grains.*

ing, however, the strain ratchets and a net compressive stress develops as reported by Zurek et al [*11*]. For Al 7075-T6, these authors showed that the magnitude of the residual stress increases with alloy grain size, a result anticipated from the present microplasticity studies.

With increasing fatigue, $\Delta\epsilon_r$ reaches a peak value and begins to fall, suggestive of localized hardening. Referring again to Fig. 3, we note that the local stress-strain hysteresis loops actually open and then close. This happens earlier for the larger grains, as seen in Fig. 8. Because of the statistical scatter in values of $\Delta\epsilon_r$, this behavior is not conclusively demonstrated by Fig. 8. Figure 9 shows results of an experiment in which mica particles were retained at the same locations for measurements after both 5 × 10^3 and 20 × 10^3 cycles. It can be seen that the magnitude of the total strain $\Delta\epsilon_r$ has begun to decrease in the 400-μm grains after 20 × 10^3 cycles, but is continuing to increase in 200-μm grains. To ensure that $\Delta\epsilon_r$ data are truely representative of the local matrix properties, strain measurements were made only in areas which were distant from microcracks and free of any large constituent particles.

Atmospheric humidity and internal hydrogen both have striking effects on the development of localized microplasticity with fatigue. Samples of Heat III cycled in dry air (~0% relative humidity) have substantially *increased* peak values of $\Delta\epsilon_r$ (Fig. 10) at 20 × 10^3 cycles compared with the 50% relative humidity data in Fig. 8. Thus humidity decreases the peak microplastic strain.

The effect of internal hydrogen is to increase the initial rate of development of microplasticity for values of $\Delta\epsilon_r$ up to 0.2 to 0.3% (Figs. 11 and 12). Thereafter, with additional fatigue, the surface rapidly hardens. The strains in the larger grains become predominantly elastic later during the fatigue lifetime, resulting in $\Delta\epsilon_r \simeq 0$ or $\Delta\epsilon_r < 0$ if there is tensile plasticity in nearby grains. This effect is quite clear for Heat II material fatigued in 50% relative humidity

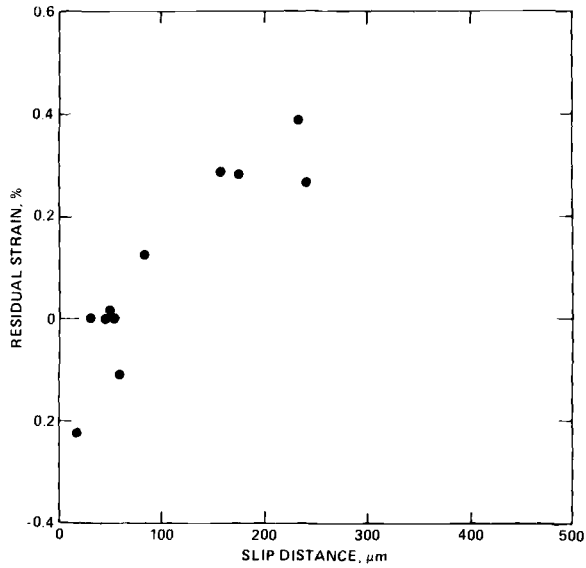

FIG. 10—*Measured residual cyclic strain is plotted versus the maximum slip distance through the measurement site for a Heat III sample cycled in dry air for 20 × 10³ cycles at ±270 MPa. Note that no mica flakes were found in grains with D > 50 μm where a decrease in $\Delta\epsilon_r$ might be evident.*

even though the grain size of this material is only half of that in Heat III (Fig. 11). The changes in $\Delta\epsilon_r$ for hydrogen-charged Heat III material are in the same direction, but even more pronounced (Fig. 12). In this case, the sample could only be fatigued to 15 000 cycles before substantial surface cracking developed. All the data at 15 000 cycles exhibited compressive $\Delta\epsilon_r$-values; this indicated that only the numerous grains with sizes less than 50 μm were still being plastically deformed. Unfortunately $\Delta\epsilon_r$ could not be measured in these small grains because the mica flakes invariably lay on a grain boundary.

Fractured Constituent Particle Results

In Al 2219-T851 most constituent particles are β-phase (Cu_2FeAl_7) and range in size from 1 to 25 μm [*12*]. The particle size distribution for Heats II and III are essentially the same, and are given in Fig. 13. Larger particles tend to fracture first during fatigue [*13*]. This is apparently a consequence of a critical strain energy criterion for fracture. Also, constituent particles within the large grains tend to fracture first, in response to the more rapid development of microplasticity within those grains [*10,13*]. The numbers of particles per unit area fractured during fatigue change with environmental humidity and with internal hydrogen content. More particles are broken in those 2219 materials in which peak values of $\Delta\epsilon_r$ are large and are reached rapidly. To quantify this

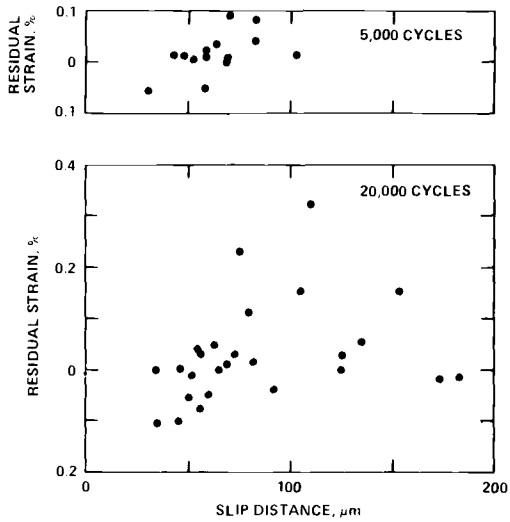

FIG. 11—*Measured residual strain versus maximum slip distance for Heat II material which is high in internal hydrogen content.*

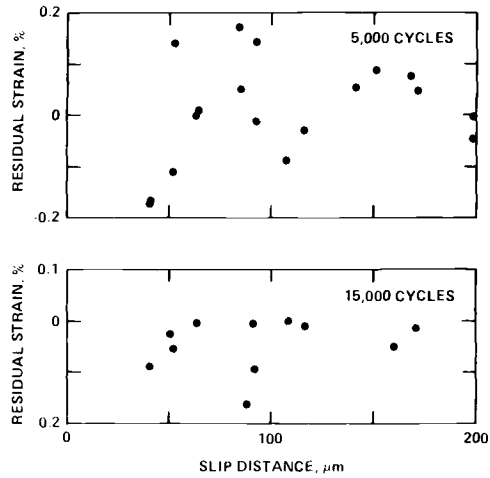

FIG. 12—*Measured residual strain versus maximum slip distance for hydrogen-charged Al 2219-T851 Heat III material.*

observation, counts were made of the numbers of particles fractured during fatigue as a function of their maximum distance of slip (at ± 45 deg) from the grain boundaries. Specimens were fatigued, and both fractured and unbroken particles were located by SEM. Later, the specimens were chemically etched to reveal the grain boundaries so that the ratio of fractured particles to total

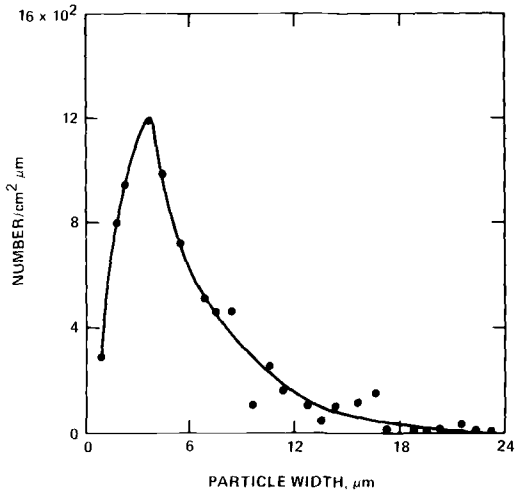

FIG. 13—*A histogram of the intermetallic particle width for Heat II and Heat III materials combined. Plotted on the ordinate is the number of particles per unit area per unit length in particle width. The dimension measured is normal to the applied stress axis and hence is normal to the rolling direction.*

available particles (>2 μm) having a given maximum slip distance could be determined. Figure 14 compares four cases of measured and predicted numbers of broken particles (plotted as a probability) versus slip distance. The cyclic stress amplitude for all experiments was ± 270 MPa, the same as used to measure $\Delta\epsilon_r$. The slip distance D is defined as illustrated in Fig. 15. The curves in Fig. 14 are predicted by the model described subsequently. We have assumed that the environment alters only the surface microplasticity (that is, $\Delta\epsilon_r$), not the particle fracture energy, and have calculated the number of fracture events by using the measured values of $\Delta\epsilon_r$. The statistical errors are especially large for large D because the number of particles having a slip distance more than 150 μm in an individual specimen is small.

Consistent with our microplasticity observations, particles in the larger grains have a greater probability of fracture. Also, comparatively more particles are fractured in those materials containing more hydrogen [that is, in hydrogen-charged Heat III (Fig. 14*a*) and Heat II (Fig. 14*b*)]. The effect of hydrogen in Heat III is so dramatic that it took only 5000 fatigue cycles (Fig. 14*a*) to fracture more particles than in the uncharged material fatigued for 20×10^3 cycles (Fig. 14*d*).

Fewer particles are broken for Heat III fatigued in moist air (Fig. 14*d*) than in dry air (Fig. 14*c*). Given the severe approximation made in the model used in making the predictions shown, the agreement between theory and experiment is good and strongly indicative of the major role of localized plasticity in

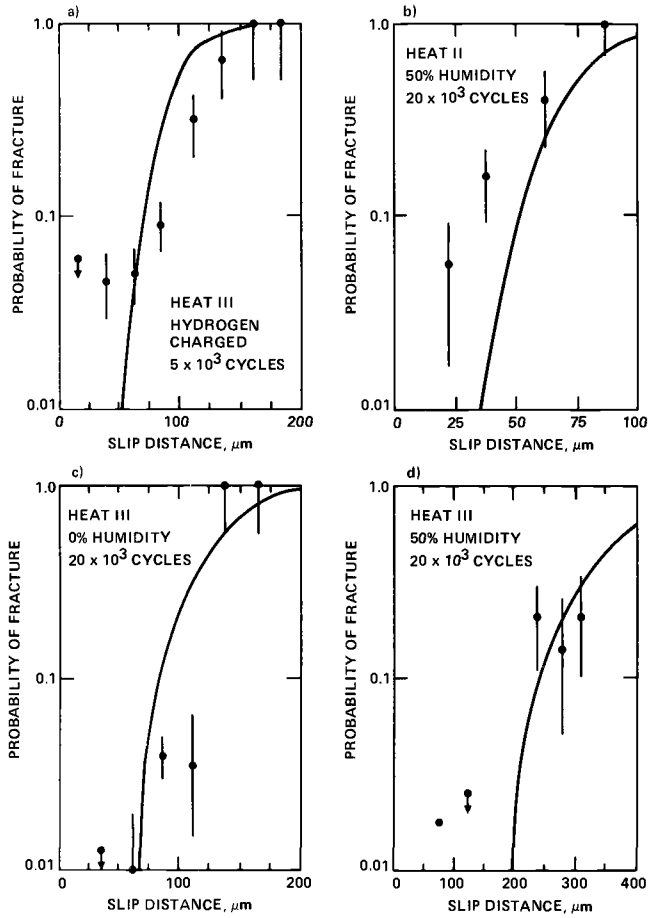

FIG. 14—*Probability of a particle being fractured versus slip distance for Al 2219-T851 for both heats. Data are plotted as a histogram over 25 or 50 μm intervals in slip distance. The bars denote statistical measurement error. The solid curves are predicted from the particle fracture model.*

particle fracture. One anomalous observation is that for Heat III fatigued in moist air, more particles are fractured in small grains than predicted.

Particle Fracture Model

We present a model to predict from measured values of $\Delta\epsilon_r$, the fraction of particles having a maximum slip distance D from a grain boundary which will have fractured by N fatigue cycles. We neglect the effect of crystallographic orientation of the grains on $\Delta\epsilon_r$ and define from experimental values of $\Delta\epsilon_r$ a parameter $\Delta\epsilon_{pmax}$ (N, D), which is the maximum plastic strain that occurs in a grain at or before N cycles. An expression is derived to relate $\Delta\epsilon_{pmax}$ to the size

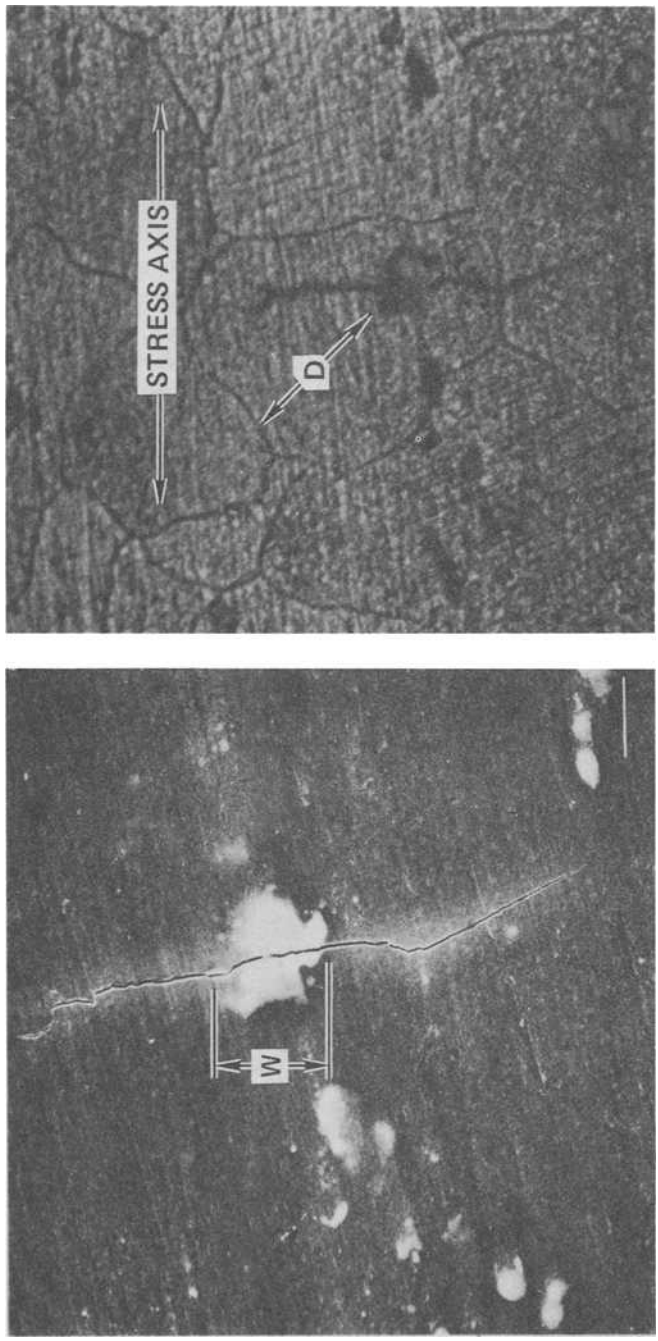

FIG. 15—(a) *Scanning electron micrograph of a fractured intermetallic particle. Particle width* w *is measured normal to the stress axis. The bar in the lower right corner represents 10 μm.* (b) *Optical micrograph illustrating the slip distance* D *as the maximum distance from particle to grain boundary at 45 deg to the stress axis. The sample has been etched to reveal the grain boundaries after fatigue. The view is normal to the surface.*

of the smallest particle w_{min} having slip distance D which will fracture by N cycles. The percentage of particles fractured is then determined by using the measured distribution in particle sizes given in Fig. 13, and is simply the number of particles larger than w_{min} divided by the total number of particles. $\Delta\epsilon_{pmax}$ changes with both alloy hydrogen content and with ambient humidity, and the predicted effect of these parameters on particle fracture, given in Fig. 14, derives entirely from their effect on $\Delta\epsilon_{pmax}$.

If $\Delta\epsilon_r$ is measured after N cycles, a maximum upper bound in residual strain ($\Delta\epsilon_{rub}$) is found which has a peak at an intermediate grain size (Fig. 16) caused by hardening of the larger grains. Models of both Chang et al [4] and Tanaka and Mura [5] predict that $\Delta\epsilon_{rub} \propto D$ for small D. This trend is partially obscurred in our data by the compressive reaction strains in the small grains. For grains larger than those with the peak $\Delta\epsilon_{rub}$, the plastic strain was greater earlier during fatigue. The quantity $\Delta\epsilon_{rmax}$ (N, D) is defined to be the maximum value of residual strain experienced at or prior to N cycles, and is illustrated by the dashed line in Fig. 16. To obtain an estimate of the localized plasticity for particle fracture modeling, we assume, as discussed earlier, that $\Delta\epsilon_{pmax} \propto \Delta\epsilon_{rmax}$. For clarity, we have displaced these two quantities in Fig. 16, but because one proportionality constant is used in the model described subsequently, it suffices to set $\Delta\epsilon_{pmax} = \Delta\epsilon_{rmax}$. To reiterate, the difference between $\Delta\epsilon_{pmax}$ and $\Delta\epsilon_{rmax}$ is that the estimated compressive reaction strains have been added to $\Delta\epsilon_{rmax}$ to obtain $\Delta\epsilon_{pmax}$. Finally, as shown in Fig. 16, a linear approximation is made by setting $\Delta\epsilon_{pmax} = \alpha D$. Parameter α is determined for each of the four combinations of N and material listed in Table 2, by placing an upper bound line of the form $\Delta\epsilon_{rmax} = \alpha D$ through the experimental microplasticity data given earlier.

A criterion for fracture proposed by Chang et al [4] is that, at fracture, the stored elastic strain energy within the particle is equal to the energy required to produce the fracture surface. Thus for a spherical particle

$$\frac{4\pi}{3}\left(\frac{w}{2}\right)^3\left(\frac{E}{2}\right)(\Delta\epsilon_{pmax})^2 = 2\pi\gamma\left(\frac{w}{2}\right)^2 \tag{1}$$

where γ is a surface energy per area, w is the width of the particle, and E is the elastic modulus of the particle. Actually, the physical constraints of the matrix modulus are also important [5], but for a given alloy can be treated as a modification to E. We make the approximation that all constituent particles have the same value of γ, and hence for a given plasticity the smallest particle which will fracture has width

$$w_{min} = \beta/(\Delta\epsilon_{pmax})^2 \tag{2}$$

where β is a parameter dependent on γ and the relative particle and matrix moduli. A value for β is chosen based on the experimental observation that all

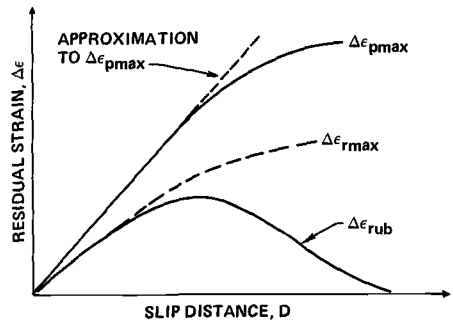

FIG. 16—*Schematic representation of the change in residual strain* $\Delta\epsilon_r$ *as a function of slip distance with increasing fatigue.*

TABLE 2—*Approximate values of* $\Delta\epsilon_{pmax}$ (N,D).

Material	Cycles (N)	$\Delta\epsilon_{pmax}$ versus D, μm^{-1}
Heat III, hydrogen charged	5×10^3	2.24×10^{-5}
Heat III, 0% humidity	20×10^3	1.73×10^{-5}
Heat III, 50% humidity	20×10^3	0.6×10^{-5}
Heat II, 50% humidity	20×10^3	2.97×10^{-5}

particles of diameter 2 μm and wider are fractured in the hydrogen-charged Heat III material for D in the range of 150 to 175 μm. $\Delta\epsilon_{pmax} = 0.00363$ for $D =$ 160 μm in this material, so

$$\begin{aligned} \beta &= 2\,\mu m \cdot (0.00363)^2 \\ &= 2.63 \times 10^{-5}\,\mu m \end{aligned} \tag{3}$$

The predicted fraction of particles having slip distance D which are fractured was calculated for the four cases considered in Fig. 14 by using Eq 2. $\Delta\epsilon_{pmax}$ for a given D was extracted from Table 2, and w_{min} was found using $\beta = 2.63 \times 10^{-5}$ μm. Finally, we assumed that all particles larger than w_{min} fractured, and determined the resulting fraction of the total available for fracture by integration of the distribution in particle sizes for the alloy which is given in Fig. 13.

Discussion

Measurements of surface microplasticity characterize the mechanical properties of the alloy matrix at the surface and provide a unique means to investi-

gate fatigue crack initiation. One might anticipate that hydrogen and environmental humidity would decrease the fracture strength of constituent particles, as well as alter the ductility of the matrix. These possibilities were examined separately by using microplasticity measurements to determine the effect of environment on the local matrix ductility within individual grains, and by comparing values of localized plastic strain with the propensity for particles to fracture. With one exception discussed later, we conclude that the substantial effects of environmental humidity and of internal hydrogen on the numbers of particles in Al 2219-T851 fractured during fatigue is due to the changes these factors induce in the local ductility of the alloy matrix at the surface.

Internal hydrogen *increases* the initial rate of formation of localized plasticity within individual surface grains.[4] Conversely, humid air *decreases* the formation of local matrix plasticity, as compared to that for fatigue in dry air. This trend is valid for small plastic strains in the range of 0.2 to 0.3%, and is persuasive evidence that the effect of humidity on surface ductility does not arise from hydrogen liberated by oxidation.

In Table 3, we use the parameter α to rank the four investigated combinations of environment according to their effect on matrix ductility. α is the material parameter in the relationship $\Delta\epsilon_{pmax}(N) = \alpha D$, and has been extracted by analysis of microplasticity data as discussed earlier. Since $\alpha(N)$ is a function of fatigue cycles N, only the three combinations for which data were obtained at 20 000 cycles can be compared directly. The fatigue lifetime of hydrogen-charged Heat III material was too short to experimentally determine α accurately at 20 000 cycles. A crude estimate suggested by the theory of Chang et al [4] is that $\alpha(20\,000) = 4 \cdot \alpha(5000)$; this has been used to provide the value listed in Table 3.

Naturally, combinations of materials and environment giving smaller values of α are those which display the least microplasticity, and in which the fewest particles are fractured by fatigue. It appears that hydrogen increases the rate of formation of localized plastic strain in 2219 fatigued in 50% humidity by a factor of 5 to 15 depending on the alloy hydrogen content. The amounts of hydrogen that lead to these changes are too small to accurately characterize, but for Heat II are known to be less than 1 ppm by weight. One concern was that aging of the 2219 during charging in the hot salt might have contributed to its change in properties. This appears not to be the case; charging induced only minor surface damage which was removed by polishing prior to fatigue. Also, two specimens exposed to the hot salt but placed outside of the charging loop retained the fatigue lifetime and microplasticity characteristic of uncharged material.

We draw three conclusions from the agreement between predicted and measured numbers of constituent particles fractured by fatigue (Fig. 14). Firstly,

[4]The local microplasticity measurement senses the plasticity in the matrix of the individual grains and we cannot say from this how the hydrogen affects the grain boundaries. We did not, however, see an increase in grain boundary fracture events in the high-hydrogen materials.

TABLE 3—*Effect of environment on local matrix ductility.*

Material	Environment	α (20 000), μm^{-1}
Heat III, low hydrogen	50% relative humidity	0.6×10^{-5}
Heat III, low hydrogen	0% relative humidity	1.73×10^{-5}
Heat II high hydrogen	50% relative humidity	2.97×10^{-5}
Heat III, hydrogen charged	50% relative humidity	8.96×10^{-5}

at the cyclic stress amplitude used, elastic strain in the particles resulting from localized microplasticity substantially exceeds the elastic strain from the external load, and is the prime factor in particle fracture. Secondly, the surface energy of the fracture plane is essentially the same for the preponderance of the particles, and is insensitive to either hydrogen content or to humidity. Thirdly, hydrogen and humidity act to induce changes in numbers of particles fractured by altering the propensity of the matrix at the surface to undergo microplastic deformation. Because of the simplistic nature of the model of particle fracture, however, small direct effects of the environment on particle fracture energy would not be unambiguously detectable. Also, not shown in Fig. 14 is an error band around the predicted values that results from the measurement of $\Delta\epsilon_r$, which further precludes the detection of such small effects.

Actually, quite by accident, we discovered one anomaly which suggests that not all the particles have the same fracture surface energy. In the Heat III material fatigued in 50% humidity, more particles were fractured in 75-μm grains than predicted. We might have been content to ascribe this difference to the simplicity of our fracture model, but, after chemical etching of the surface to expose the grain boundaries for slip distance measurements, we discovered that these fractured particles belong to a subset ($<3\%$) which was heavily attacked by the acid. These probably have a smaller than average γ. Their chemical composition is indistinguishable (as measured by energy dispersive X-ray analysis) from the remainder of the particles. Perhaps their lower fracture energy is related to their structure.

A complete theory of constituent particle fracture by fatigue should include modeling of the development of localized microplasticity and of the cyclic hardening of the surface which limits it. Elsewhere [*10*] we have discussed the functional form of models which can be used to predict $\Delta\epsilon_{pmax}$. These were semiempirical and required material parameters which can be difficult to measure and which we therefore treated as empirical constants. The approach incorporated the effects on particle fracture of grain crystallographic orientation and of cyclic hardening of the surface. Consistent with the aforementioned new observations, it was necessary to assume that the constituent par-

ticles have a range in γ-values to explain the excess fracture of small particles at low cyclic stress amplitude.

A more fundamental derivation of an expression to predict $\Delta\epsilon_{pmax}$ is needed. Results reported here on the effect of environment on microplasticity may provide some guidance for this by indicating the mechanisms which control its development. Because internal hydrogen increases microplasticity of the matrix at small plastic strains, while humidity decreases microplasticity, we attribute the humidity effect to surface oxide. Grosskreutz [*6*] has reported that tenacious oxides of aluminum can lead to near-surface tangling of dislocations in monotonically loaded specimens. We believe that the same mechanism is responsible for the small ductility of the surface when fatigued in humid air. Presumably, the oxide inhibits motion of dislocations through the surface. Apparently, at small strains, hydrogen does not cross the surface oxide barrier, and so leaves the material unaffected.

In hydrogen-rich 2219, cyclic hardening of the surface is very rapid after $\Delta\epsilon_r$ exceeds 0.2 to 0.3%. Similar responses of nickel [*14*] and iron alloys [*15,16*] to hydrogen in monotonically loaded specimens have been reported, and consist of apparent enhanced ductility at small plastic strains and decreased ductility at large strains.

We report elsewhere [*3*] that the plastic deformation associated with short surface crack growth in Al 2219-T851 is less in the hydrogen-rich material. This is yet another, and the more typically observed, manifestation of the embrittlement of hydrogen at large plastic strains. Thus it appears that hydrogen degrades the fatigue performance of Al 2219-T851 in two ways. At small strains it enhances microplasticity and accelerates crack initiation. At large strains it reduces ductility and accelerates crack propagation. It is hoped that continued research will ultimately allow these processes to be accurately modeled.

Acknowledgments

The research was funded by the Office of Naval Research under Contract N00014-79-C-0334. R. V. Inman and R. M. Govan are thanked for their help in specimen preparation and scanning electron microscopy.

References

[*1*] Thompson, N. T., Wadsworth, N. J., and Louat, N., *Philosophical Magazine*, Vol. 1, 1956, p. 113.
[*2*] Kramer, I. R., *Metallurgical Transactions*, Vol. 5A, 1974, p. 1735.
[*3*] Morris, W. L. and James, M. R., this publication, pp. 179-206.
[*4*] Chang, R., Morris, W. L., and Buck, O., *Scripta Metallurgica*, Vol. 13, 1979, p. 191.
[*5*] Tanaka, K. and Mura, T., *Metallurgical Transactions*, Vol. 13A, 1982, p. 117.
[*6*] Grosskreutz, J. C., *Surface Science*, Vol. 8, 1967, p. 173.
[*7*] Pangborn, R. N., Weissman, S., and Kramer, I. K., *Metallurgical Transactions*, Vol. 12A, 1981, p. 109.

[8] Morris, W. L., Inman, R. V., and James, M. R., *Journal of Materials Science*, Vol. 17, 1982, p. 1413.
[9] Elkholy, A., Galland, J., Axou, P., and Bastien, P., *Comptes Rendus Hebdomadaires des Seances de L'Academie des Sciences, Series C*, Vol. 284, 1977, p. 363.
[10] James, M. R. and Morris, W. L., *Materials Science and Engineering*, Vol. 56, 1982, p. 63.
[11] Zurek, A. K., James, M. R., and Morris, W. L., "The Effect of Grain Size on Fatigue Growth of Short Cracks," accepted by *Metallurgical Transactions A*.
[12] Morris, W. L., *Metallurgical Transactions*, Vol. 9A, 1978, p. 1345.
[13] Morris, W. L. and James, M. R., *Metallurgical Transactions*, Vol. 11A, 1980, p. 850.
[14] Heubaum, F. and Birnbaum, H. K., "The Effect of Hydrogen on the Fracture and Slip Behavior of Nickel," ONR Technical Report, Contract USN 00014-75-C-1012, Office of Naval Research Laboratory, March 1981.
[15] Kimura, H., Matsui, H., Kimura, A., Kimura, T., and Oguri, K. in *Hydrogen Effects in Metals*, I. M. Bernstein and A. W. Thompson, Eds., AIME, Warrendale, Pa., 1981, p. 191.
[16] Hirth, J. P. *Metallurgical Transactions*, Vol. 11A, 1980, p. 861.

DISCUSSION

Larry Mueller[1] (*written document*)—What were your microflakes made of? How did you attach them? Can you obtain these commercially?

M. R. James and W. L. Morris (*authors' closure*)—These questions are specifically answered in the paper. Also, more information is available in Ref *8*.

D. L. Davidson[2] (*written discussion*)—How was your low humidity quantified? Should it be stated in ppm water vapor rather than relative humidity? Have you measured your oxide thicknesses (by sputtering and Auger) to verify your hypothesis that the oxide is thicker in the water vapor environment?

M. R. James and W. L. Morris (*authors' closure*)—The definition of low humidity and the methods used to obtain it are given in the paper. We have not, as yet, determined the oxide thickness as suggested. It is not clear if it is the oxide thickness or the tenacity with which it adheres to the substrate which is important to local surface microplasticity.

Carl Alstetter[3] (*written discussion*)—You state that hydrogen increases the ductility. I think you must be cautious in the use of the word "ductility" to describe an increased microplasticity. Ductility has the traditional and conventional meaning of percent elongation or percent reduction of area in a tension test. Do you mean that hydrogen increases ductility, defined in this way? If not, it would be better not to use "ductility increase due to hydrogen."

[1]Alcoa, Alcoa Technical Center, Alcoa Center, Pa. 15069.
[2]Staff Scientist, Southwest Research Institute, San Antonio, Tex. 78284.
[3]University of Illinois, Urbana, Ill.

M. R. James and W. L. Morris (authors' closure)—You are correct. Hydrogen does not increase the reduction in area in a conventional tension test. In the alloys we studied, it alters only the mechanical properties of the matrix material within individual surface grains. We have referred to this in the paper as "microplasticity" or "local matrix ductility."

A. J. McEvily[4] *(written discussion)*—You observe that hydrogen promotes microplastic behavior. Do you have an explanation for this effect?

M. R. James and W. L. Morris (authors' closure)—We cannot provide an adequate explanation for this effect, which occurs at the low strain amplitudes obtained in these experiments. References are given in the paper to similar effects of hydrogen on bulk ductility where other authors attribute the effect to changes in dislocation character and mobility. Apparently, no quantitative model of the mechanism is available.

[4]Professor, Department of Metallurgy, University of Connecticut, Storrs, Conn. 06268.

Jeffrey L. Field,[1] *Farhoud Behnaz,*[1] *and Robert N. Pangborn*[1]

Characterization of Microplasticity Developed During Fatigue

REFERENCE: Field, J. L., Behnaz, F., and Pangborn, R. N., **"Characterization of Microplasticity Developed During Fatigue,"** *Fatigue Mechanisms: Advances in Quantitative Measurement of Physical Damage, ASTM STP 811*, J. Lankford, D. L. Davidson, W. L. Morris, and R. P. Wei, Eds., American Society for Testing and Materials, 1983, pp. 71-94.

ABSTRACT: X-ray line-broadening studies and stress analyses were employed to characterize quantitatively the fatigue-induced lattice deformation and change in the residual stress prior to crack initiation. Measurements were made after surface layer removals to evaluate surface and subsurface microplasticity, and X-rays with different penetration capability were used in order to facilitate a similar comparison nondestructively. At high maximum stress amplitudes imposed by bending fatigue, rapid distortion of the surface layer followed by an extended period of recovery contrasted with a more steady accumulation of lattice imperfection in the subsurface region. Concomitant modification of residual stresses during the cycling included the development of a maximum compressive stress early in the life and a transition to tension during the intermediate life fractions, reaching a peak tensile stress when the line breadths for the near-surface and subsurface converged. The differentiation in surface and subsurface line broadening during cycling at high and low maximum stress levels was accredited to the operation of different crack initiation mechanisms, and the potential for postponing crack initiation through surface layer removal was investigated.

KEY WORDS: fatigue damage, X-ray diffraction, microplasticity, slip lines, dislocation density, X-ray residual stress analysis, recovery mechanisms, stress relaxation, crack initiation

A reliable means for accurate and nondestructive assessment of cumulative fatigue damage has been sought for many years, for both fundamental and practical reasons [*1*].[2] X-ray diffraction methods are sensitive to the changes in internal structure of crystalline solids and thus represent a poten-

[1]Graduate Research Assistant, Graduate Research Assistant, and Assistant Professor of Engineering Mechanics, respectively, Department of Engineering Science and Mechanics, The Pennsylvania State University, University Park, PA. 16802.

[2]The italic numbers in brackets refer to the list of references appended to this paper.

tially useful approach to fatigue damage measurement. However, their application in the past has met with only limited success. For example, many investigators have reported the introduction of cold work during the very early or late stages of fatigue, but have had difficulty diagnosing the mechanisms contributing to damage during intermediate life fractions. The lattice distortion due to cold work is manifested by the asterism of diffraction spots for fatigued single crystals [*2,3*] or the broadening of diffraction lines for polycrystalline metals [*1,4,5*]. In addition to the invariance of the X-ray patterns after the initial fatigue cycles, observations of line broadening for fatiguing in the safe range of stresses below the fatigue or endurance limit [*6*], and a transient stage featuring peak sharpening for initially cold-worked specimens [*7*], have hampered direct correlation of X-ray data to accrued damage. X-ray microbeam techniques have been successfully applied to resolve the fatigue-induced misorientation of individual grains of a specimen and to distinguish on that basis which grains represent potential sites for microcracking [*8*]. Again, however, the changes were restricted to the initial and terminal portions of life.

Residual stresses have also been monitored during fatigue in various modes. The intrinsic residual stresses are a function of the manufacturing process, component fabrication or forming procedure, and surface finishing or heat treatments employed. Significant gradients in the stress with depth from the surface will often exist [*9*] unless a stress relief anneal is performed. Subsequent fatiguing will then modify the magnitude and distribution of these residual stresses [*10*], which can exert considerable influence on the mechanical behavior and failure of the component [*11*]. These changes have therefore been investigated for potential utilization as an indicator of incipient cracking or cumulative damage [*1,8–10,12–14*].

The often conflicting trends reported in the literature to date and the multimodal character of the residual stress changes measured during cycling imply a strong dependence of such measurements on the particular metal or alloy investigated, its initial condition, and the mode and amplitude imposed in the fatigue testing. The differences in sign and sense of change at the onset of failure, in particular, hinder any attempt to propose a unified rationale for crack initiation on the basis of residual stress analyses.

Recent investigations, conducted using double crystal diffractometry (DCD) modified for application to polycrystalline materials [*15*], have yielded a more consistent criterion on which to base an estimate of remaining life. The primary departure in approach from that of prior investigations was the study's focus on both the surface and subsurface response to fatigue cycling. By removing surface layers incrementally, followed by X-ray analysis at each depth, the distortion induced in grains located at the surface could be compared to the deformation incurred by grains in the underlying and bulk regions after any amount of fatiguing. A nondestructive method giving comparable results was also devised by selection of appropriate X-ray targets to vary

the penetration and thus the average depth from which the grain reflections were obtained. The capability of the DCD method to resolve the rocking curves for individual grains, whose location could be determined by backward-tracing topography using the same camera, permitted identification of those grains experiencing localized deformation [*16*]. Studies of spectrum amplitude fatigue showed that the accrued damage due to cycling could be monitored to a terminal or critical excess dislocation density at failure [*17*]. Preliminary investigations indicated that conventional line-broadening analysis could also be utilized to follow the progressive accumulation of damage during push-pull fatigue of Al 2024, if deeply penetrating Mo K_α radiation was employed to probe the subsurface layers, several grain diameters beneath the rapidly deformed surface layer.

The goals of the current investigation include a more comprehensive evaluation of microplasticity and its distribution in depth, particularly in relation to fatigue crack initiation. The choice of reduced-section, bending specimens for the study provides better control of crack initiation and a planar surface on which to conduct the X-ray diffraction analysis. The pure bending mode of fatigue maintains the normal stress state of the fully reversed axial loading while introducing an applied stress gradient from the surface to bulk. The X-ray line broadening can be interpreted in terms of changes in root mean square (rms) strain and particle size [*18–20*]. These parameters, in conjunction with fatigue-induced modification of the residual stress, can be viewed as both precursors of, and contributors to, crack initiation. Therefore emphasis was placed on correlation of the X-ray data to crack initiation mechanisms known to be operative in the alloy studied.

Al 2024 is prone to localized deformation during fatigue, which occurs by repetitive cutting of shearable precipitates resulting in slip bands comparable to the persistent slip bands (PSBs) of high stacking-fault energy (SFE) materials, or by concentration of the plastic deformation in the precipitate-free zones (PFZs) along grain boundaries due to aging inhomogeneity [*21,22*]. The surface roughness associated with slip band emergence on the surface may induce transgranular cracking. Grain boundaries impede the spreading of slip bands. For high SFE metals, propagation of the damage has been proposed to occur by PSB initiation in adjacent grains or by cyclic strain localization at the grain boundaries [*23*] leading to intergranular cracking. Impurity inclusions represent another significant contributor to fatigue crack initiation and failure. The phenomena involved have been classified [*24*] into three distinct types: interfacial debonding [*25*] resulting in the emination of slip band cracks into the matrix, cracking or debonding of the inclusion by impinging slip bands [*26,27*], and cracking along coarse slip bands radiating from inclusions which are neither cracked nor debonded [*28*]. The latter mechanism was observed by Kung and Fine as part of a comprehensive study of fatigue crack initiation and early growth in Al 2024-T4. These investigators also reported a transition in the dominant crack nuclea-

tion mechanism on the basis of the magnitude of the applied stress amplitude. At low stress amplitudes, crack initiation occurred at slip bands associated with constituent particles. At high stress amplitudes, a more general slip band cracking due to intrusion and extrusion formation was observed. The local stress associated with the transition lies between the monotonic and cyclic 0.2% offset yield strengths reported in an earlier paper [*29*]. Below the transition, a large crack could form from a single source, while above the transition, coalescence of microcracks led to the formation of a macrocrack. A primary focus of the current investigation, then, will be to determine the qualitative and quantitative differences in the X-ray diffraction data obtained when fatigue stress levels are applied to activate those contrasting cracking mechanisms.

Experimental Procedure

Test specimens were machined from as-received plates of Al 2024. The specimen dimensions and four-point bending configuration are shown in Fig. 1. The rolling direction was parallel to the long dimension, and semicircular side grooves were introduced to provide a reduced section in the central, constant moment portion of the length. The specimens were mechanically polished, followed by solution treatment at 495°C for 1 h and quenching in ice water. Natural aging of the recrystallized structure was allowed to occur

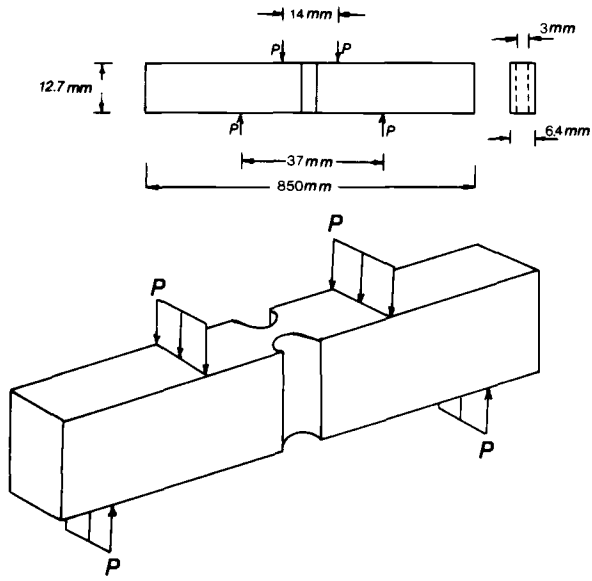

FIG. 1—*Specimen geometry and loading configuration for four-point bending fatigue of Al 2024-T4.*

for one week. All specimens were subsequently polished with 6-μm diamond paste and electropolished in a 1:3 HNO_3—CH_3OH solution at −25°C to remove 50 μm from all surfaces prior to testing. The 0.2% offset yield strength for the Al 2024-T4 was found to be 327 MPa, and the average grain size in the transverse direction was about 20 μm. Light etching also revealed nearly spherical S-phase particles and irregularly-shaped, elongated, β-phase particles.

Tension-tension bend testing was conducted under constant load control using an Instron cycler operated at 25 Hz. The four-point bending jig was designed with a keyhole to permit observation at 50 times magnification of the specimen surface subject to tension. Loads were selected to provide maximum stresses at the outer fibers both above and below the monotonic yield stress and to maintain a minimum applied moment equal to 15% of the maximum. The maximum tensile stresses calculated on the basis of inelastic bending theory were used to construct the *S-N* curve shown in Fig. 2. Several specimens were tested at each of four maximum moments to estimate the average number of cycles for crack initiation. Additional tests were con-

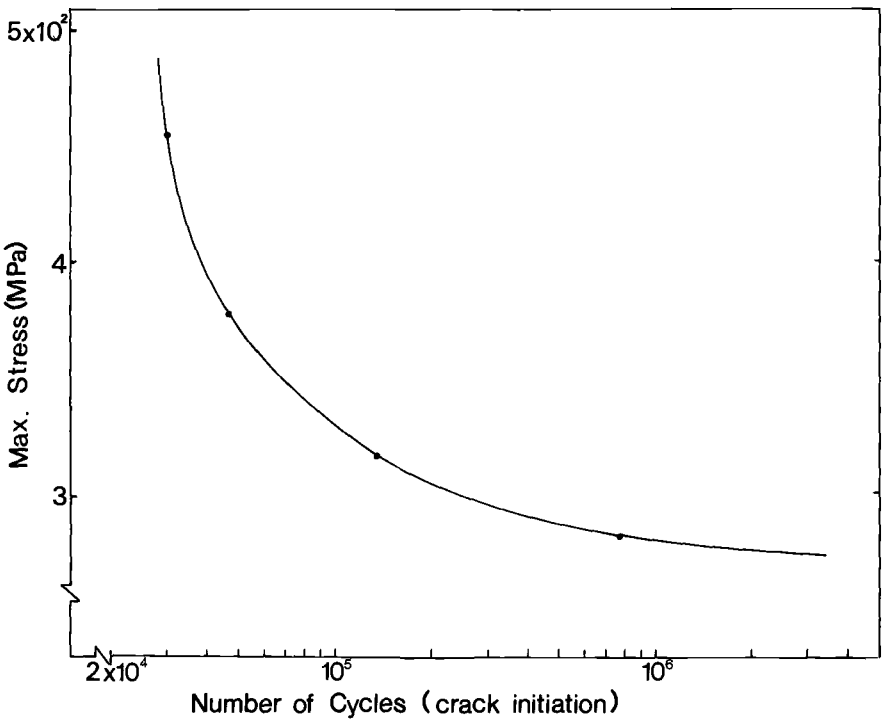

FIG. 2—S-N *curve for fatigue crack initiation in pure (tension-tension) bending of Al 2024-T4. The two intermediate stress levels were employed in the X-ray diffraction studies.*

ducted with periodic interruption of the cycling to permit scanning of the surface for microcracks using an optical metallographic microscope. After cracks of about 100 μm in length were first noted, their growth was monitored by successive measurements after short intervals of cycling. Backward extrapolation of a log-log plot of crack length (a) versus number of fatigue cycles (N) was used to identify the cycles to initiation (N_i) for each specimen, where an initiated crack was taken for convenience as 25 μm in length. Table 1 summarizes the results of initial testing, including the proportion of the number of cycles to failure (N_f) consumed by crack initiation.

The X-ray line-broadening analysis was carried out using a GE XRD-5 diffractometer, modified for step scanning and coupled to an Apple II Plus microcomputer to provide control signals and record the counter-timer output. A collimated beam with 1.5 mm width and 3.2 mm length was incident on the specimen surface subjected to cyclic tensile stress and centered at the location of the minimum cross section. The long dimension of the incident beam area was oriented so as to traverse the specimen from fillet to fillet. The entire span of the most highly stressed region therefore contributed to the measurements, averaging the deformations at the specimen edges where crack initiation was most probable with those at the midsection. Step scanning of the diffraction lines from the {111}, {200}, {222}, and {400} crystallographic planes was accomplished at 0.005-deg intervals and counting times of 30 or 40 s. Ni-filtered Cu K_α and Zr-filtered Mo K_α radiations were employed in the analysis. The $K\alpha_1/K\alpha_2$ doublet separation was performed according to the Rachinger correction [*30*], after which the halfwidths (peak width at half the maximum intensity) and integral breadths (integrated intensity divided by peak height) were computed and compared. Correction for instrumental broadening was achieved using the line-breadths obtained for annealed and polished specimens in conjunction with the breadths measured after fatiguing, such that the corrected integral breadth $\bar{\beta} = (\beta_m^2 - \beta_o^2)^{1/2}$, where β_m is the measured integral breadth and β_o is the integral breadth of the undeformed specimen. The studies of line broadening as a function of the fraction of precrack fatigue life involved two different procedures. The first involved the cycling of each specimen to a selected fraction of life based on

TABLE 1—*Comparative crack initiation data for tension-tension bending of Al 2024-T4.*

Maximum Stress (σ_{max}), MPa	Average Number of Cycles to Crack Initiation (N_i)	Fraction of Life for Crack Initiation (N_i/N_f)
464	3.7×10^4 ($\pm 6\%$) [a]	0.54
386	4.7×10^4 ($\pm 11\%$)	0.74
325	1.4×10^5 ($\pm 18\%$)	0.86
292	7.7×10^5 ($\pm 25\%$)	0.96

[a]Percent spread of data about mean value for five specimens tested.

the average life from previous tests. Immediately after X-ray analysis, each specimen was cycled to crack initiation, and the actual fractions of life represented by the diffraction data were adjusted accordingly. Other specimens were subjected to a sequence of cycling blocks with X-ray analysis conducted at the end of each block. In this way, the changes in line breadth could be monitored for a single specimen at regular fractions of life. Inherent to this procedure, however, is the longer hold time required for the multiple X-ray measurements, during which relaxation could occur. For the studies in depth, specimens were simply cycled to fractions of life determined from the previously compiled average number of cycles to crack initiation at each stress level. Surface layers of increasing thickness were removed stepwise by electropolishing, and the line broadening at each depth was measured using Cu K_α radiation.

The X-ray residual stress analyses were carried out by the single exposure technique using a cylindrical, back reflection camera, a double-aperture collimator tube, an inclination angle between the incident beam and specimen surface normal of 45 deg, and a high-purity copper reference powder applied to the specimen surface. Each film is thus self-calibrating, and correction for variation in specimen-to-film distance is simplified. The shifts in position of the lines from both the {422} and {511}/{333} crystallographic planes were measured for use in computing the residual stress in the Al 2024 specimens. The line corresponding to the {420} crystallographic planes for copper, which falls at a diffraction angle between these two, was used for calibration purposes.

Results

The initial X-ray measurements were conducted on specimens cycled at the higher of the two applied moments ($\sigma_{max} = 386$ MPa) selected for study so as to favor slip band cracking as the dominant initiation mechanism. Figure 3 shows the corrected integral breadths measured using Cu K_α radiation as a function of the fraction of precrack fatigue life (N/N_i). All four diffraction lines monitored display a similar dependence on the life fraction featuring three stages: a rapid broadening during the first 10 to 15% of life, line sharpening during the intermediate portion of the life to a minimum breadth at 75 to 95% of life, followed by broadening during the cycles imposed just prior to crack initiation. The specimens cycled to selected fractions of life for X-ray analysis and fatigued immediately thereafter to failure, and those cycled and analyzed stepwise to failure, exhibit nearly identical broadening characteristics. As indicated in Fig. 3, the maximum penetration, assuming a reflected to incident intensity ratio of $1/e$, varies from about 12 to 28 μm for the diffraction lines analyzed. Figure 4 shows the concomitant changes in relative peak intensity for the four lines during the life, revealing the normal inverse relationship between reflected intensities and line breadths.

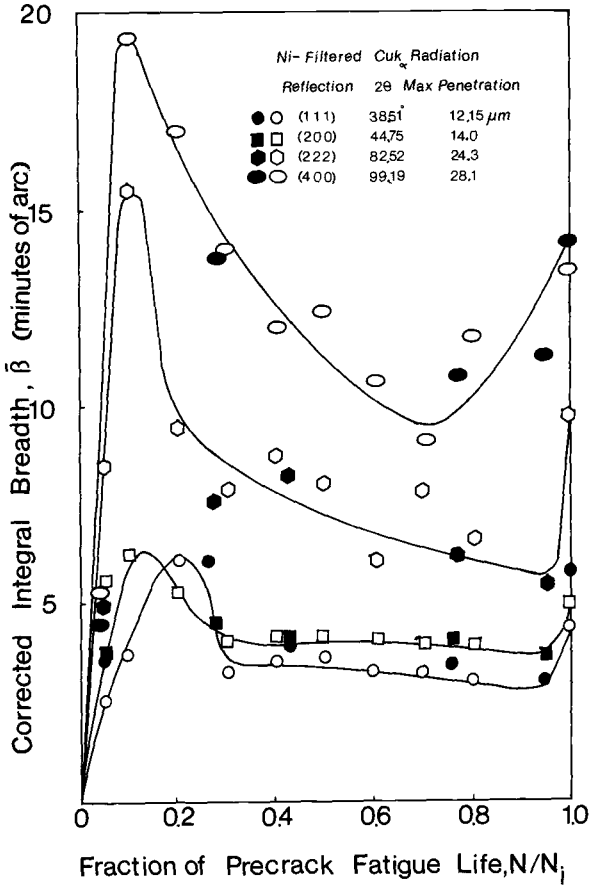

FIG. 3—*Line broadening measured using Cu K_α radiation as a function of the fraction of precrack fatigue life at σ_{max} = 386 MPa. Solid symbols represent specimens cycled to a single fraction of life and subsequently fatigued to failure. Open symbols correspond to specimens cycled stepwise to failure.*

Similar measurements taken using Mo K_α radiation disclosed a fatigue response in sharp contrast to that obtained when Cu K_α radiation was employed. As illustrated by Fig. 5, the same diffraction lines broaden rapidly during the initial cycles and continue to increase in breadth throughout the intermediate life fractions, reaching a maximum at about 75% of life. Figure 6 displays the as-recorded and Rachinger-corrected (200) peaks typical of undeformed (annealed) and fatigued specimens. A transient decline in breadths ends at about 95% of life and broadening is again evident at the onset of cracking. The maximum depth sampled by the deeper-penetrating Mo K_α radiation is seen to be about 56 to 130 μm, or an average of four to five grain thicknesses.

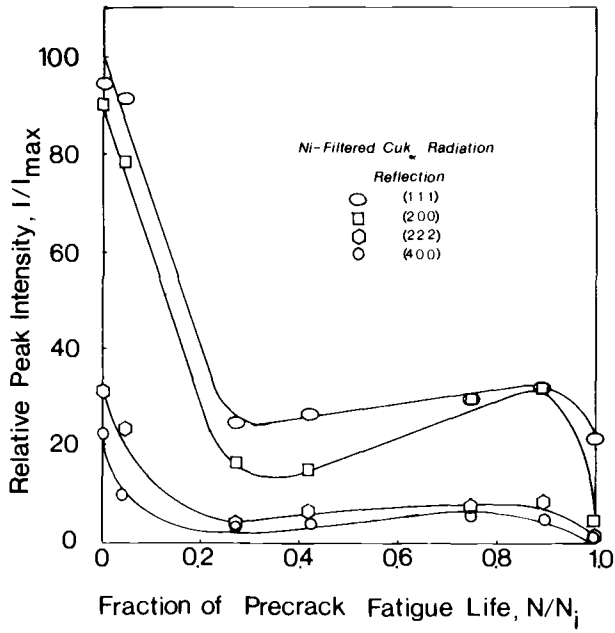

FIG. 4—*Dependence of the relative peak intensity of X-ray lines on the fraction of precrack fatigue life, where* I *is the Rachinger-corrected peak intensity and* I_{max} *is the as-measured peak intensity reflected from the* {*111*} *crystallographic planes of a virgin specimen.*

Reduction of the line breadths obtained with Mo K_α radiation was accomplished according to the formulation [*20*]

$$\overline{\beta}^2 = \beta_D^2 + \beta_\epsilon^2 = (\lambda/D\cos\theta)^2 + [4(1.25)\langle\epsilon^2\rangle^{1/2}\sin\theta/\cos\theta]^2$$

where Gaussian distribution functions are used to represent the particle size and strain contributions, β_D and β_ϵ respectively, to the corrected integral breadth, λ is the X-ray wavelength, D is the particle size, θ is the Bragg angle, and $\langle\epsilon^2\rangle^{1/2}$ is the rms strain. Rearrangement of this expression to facilitate plotting of the experimental data from the two families of crystallographic planes analyzed yielded a change in rms strain from 0.51×10^{-3} at $N/N_i = 0.04$ to 1.32×10^{-3} at $N/N_i = 1.0$, and a reduction in particle size from a nearly constant value of 0.15 μm over the first 40% of life to 0.073 μm over the final 25% of the precrack life. The enhancement in rms strain is the dominant contribution to the fatigue-induced broadening during the first half of the precrack fatigue life and continues to increase as a smaller domain size is produced by fatigue-induced substructure formation. Therefore, by using the dependence of the strain-controlled broadening on the diffraction angle, namely $\beta_\epsilon = 5\langle\epsilon^2\rangle^{1/2}\tan\theta$ [*19*], the four curves in each of Figs. 3 and 5 can be

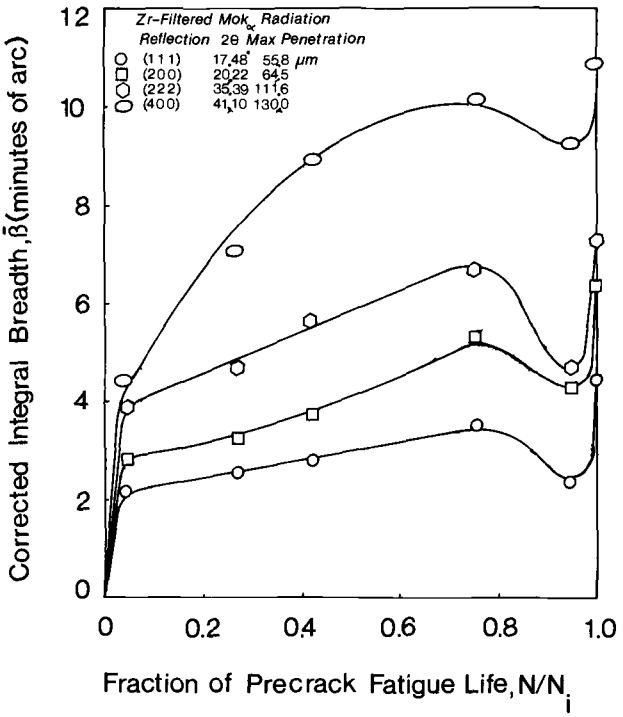

FIG. 5—*Line broadening measured using Mo K_α radiation as a function of precrack fatigue life at σ_{max} = 386 MPa.*

condensed into one. For each type of radiation used and for each fraction of life, the data collected for each $hk\ell$ reflection are adjusted according to the expression

$$\bar{\beta} = (\bar{\beta}_{hk\ell}/\tan\theta_{hk\ell})(\tan\theta)_{avg}$$

where $\bar{\beta}_{hk\ell}$ and $\theta_{hk\ell}$ are the corrected integral breadth and corresponding Bragg angle for each $hk\ell$ line, and $(\tan\theta)_{avg}$ represents the average of the tangents of the Bragg angles of all the diffraction peaks monitored. A quantity representative of the broadening for all four peaks combined is then obtained by averaging these values. The reduced data for the X-ray analyses conducted with copper and molybdenum radiation are displayed by the curves in Fig. 7. The error bands correspond to the total spread about each condensed data point. These curves demonstrate the marked difference in behavior exhibited by near-surface grains relative to those located at greater depths. While the curve generated with copper radiation indicates that lattice distortion is incurred rapidly in the surface layers due to dislocation generation and multiplication, and molybdenum radiation averages the

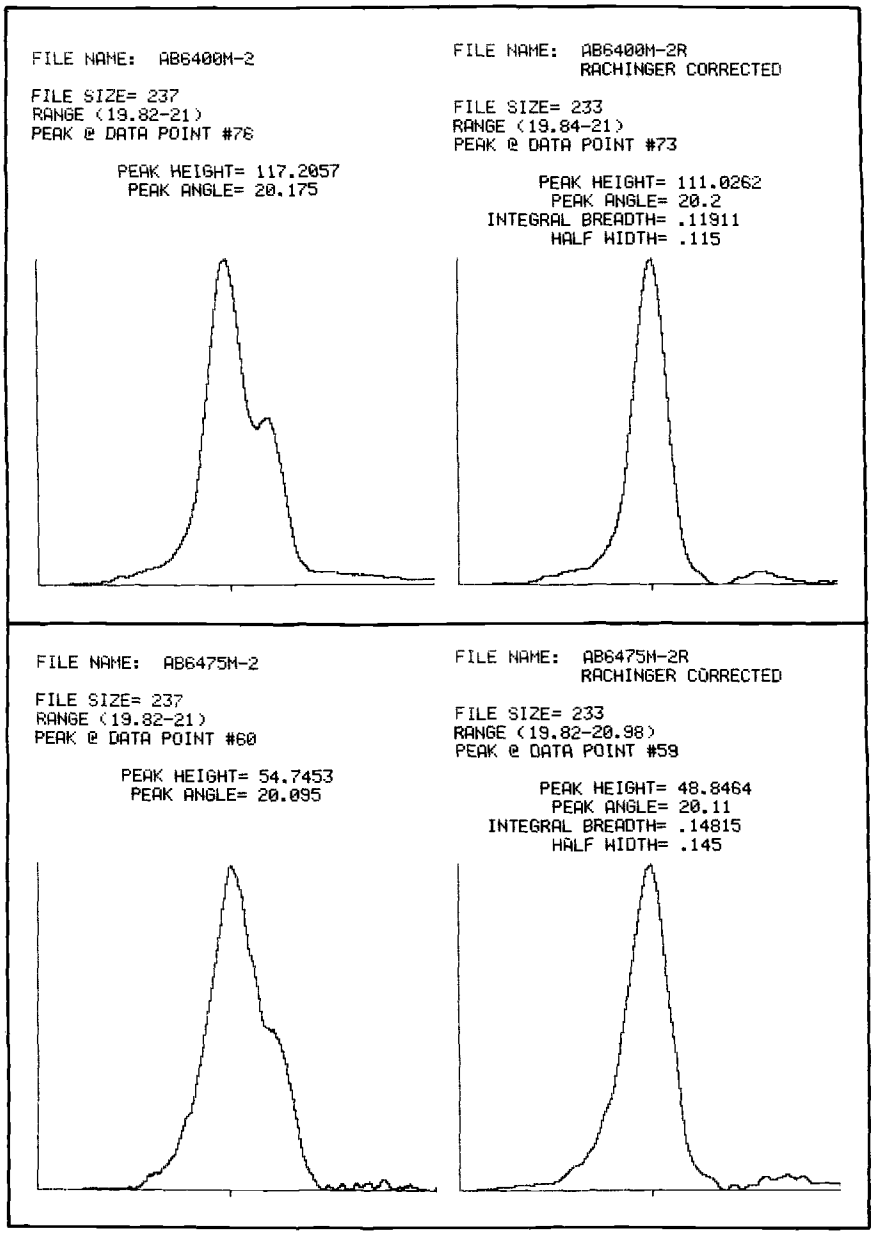

FIG. 6—*Diffraction peaks recorded for the {200} crystallographic planes.* (top) *Profiles for virgin specimen before and after* $K\alpha_1/K\alpha_2$ *doublet separation.* (bottom) *Uncorrected and corrected profiles for specimen cycled to 75% of precrack fatigue life.*

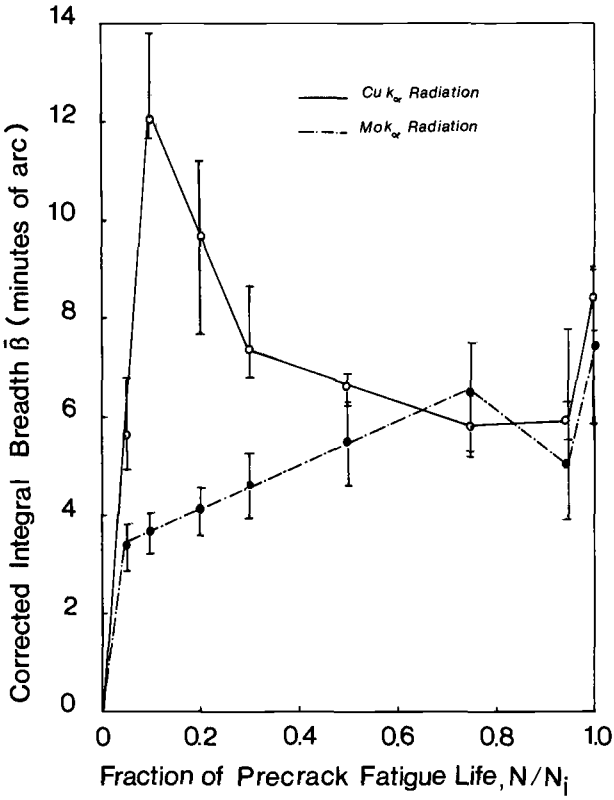

FIG. 7—*Superposition of line-broadening curves obtained with Cu K_α and Mo K_α radiations. Average maximum penetrations for lines monitored are 20 and 90 μm respectively.*

deformation accrued to a much thicker layer and displays a more gradual damage accumulation. The decline in breadths recorded using copper radiation over the period of life from $N/N_i = 0.10$ to 0.75 is indicative of cyclic recovery, the result of rearrangement of the dislocations, decreasing density and increasing free lengths. A similar trend was observed by Weiss and coworkers for bending fatigue of Al 7050 plate [*31*]. The breadths of diffraction lines recorded using Cr K_α and Cu K_α were found by these investigators to increase in most cases until 15 to 25% of life, followed by an abrupt decline to a value only slightly higher than measured prior to fatigue. It was proposed that this indicates cyclic softening of the surface layer and is connected with the original compressive residual stress of the test specimens. Further cycling caused the integral breadths to increase again. Referring again to Fig. 7, it may be seen that the two curves converge at $N/N_i \approx 0.65$; subsequently, multiplication and interaction of dislocations in both the near-surface and subsurface layers, accompanied by the emergence of coarse slip lines at the surface as later described, leads to crack initiation.

Further investigation of the deformation gradient in the surface layers was carried out by incremental removal of surface layers of specimens cycled to various fractions of life. The results of X-ray line-broadening analyses for three such specimens are collected in Fig. 8. Although all three profiles show considerable oscillation in the breadth values close to the original surface of the specimens, a more general trend is also evident. Superimposing the curves as in Fig. 9, and neglecting the near-surface variability, reveals that the steep gradient obtained after fatiguing for 5% of the life is gradually reduced in severity during progressive cycling. At 75% of life, the surface breadths have declined from their value at 25%, while those of subsurface layers have increased, so that the line breadths are almost constant with depth. Spark erosion planing to remove larger layer thicknesses, followed by electropolishing, was carried out on the specimen cycled to 75% of life to

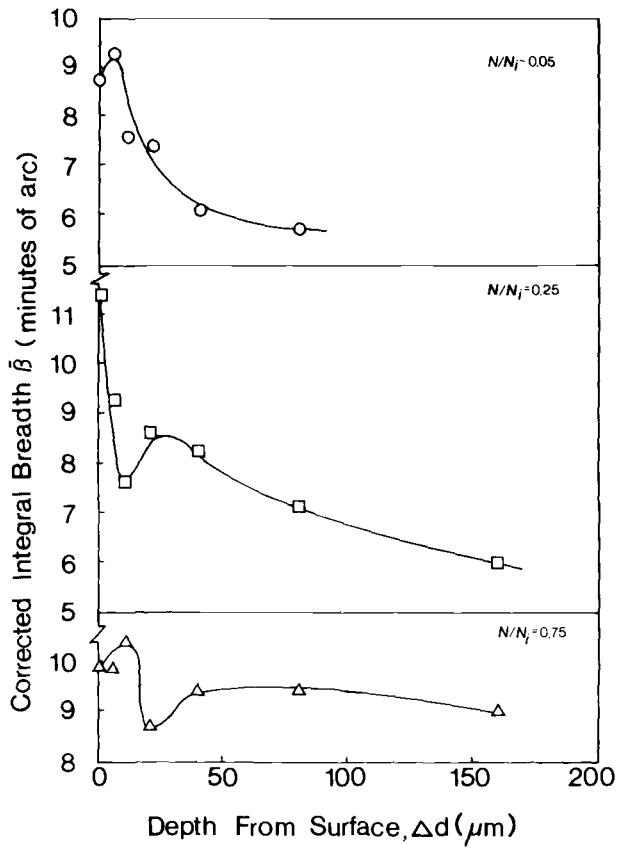

FIG. 8—*Depth profiles for selected fractions of precrack life* (N/N_f) *derived by line-broadening analyses after stepwise surface layer removals. Data for each depth correspond to average over maximum layer analyzed by Cu* K_α *radiation of about 28 μm thickness.*

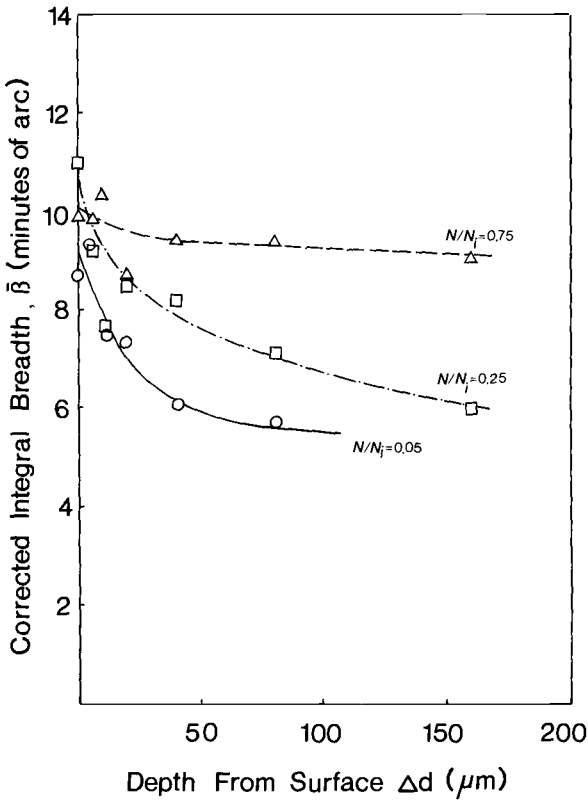

FIG. 9—*Superposition of depth profiles shown in Fig. 8 for various fractions of precrack fatigue life.*

allow X-ray analysis at much greater depths than shown in Figs. 8 and 9. The results gave a gradual and nearly linear decline in the integral breadths from about 9 min of arc at 320 μm from the original surface to less than 5 min of arc at approximately the neutral axis. This suggests that the accumulation of dislocations in the surface layer and associated stress field due to pileups activate dislocation sources in the underlying material. At progressively higher fractions of life, dislocation multiplication and interaction occurs in successively deeper regions of the specimen. As a result, sufficient stress is developed and exerted in the vicinity of the neutral axis to cause an increase in dislocation density of grains subject to little stress due to flexure.

Previous studies [*15*] disclosed that for push-pull cycling, stress amplitudes below the fatigue strength produce measurable distortions only in the surface layer. At higher stress amplitudes, however, the dislocation density increased throughout the specimen cross section, with that of bulk material lagging behind the surfaces layer until incipient failure. A similar behavior was ex-

hibited during bending fatigue, for which it can be argued that under the combined influence of the applied stress and the back stresses associated with dislocation accumulation at the surface early in the life, the subsurface dislocation density is gradually elevated to a level comparable to the surface value. Slip lines were observed to have emerged on selected surface grains at this later stage of life. Between $N/N_i = 0.80$ and 1.0, they spread to adjacent grains and became deeper and coarser. A number of small cracks usually appeared in directions closely associated with coarse slip lines, some of which eventually intersected to form a main crack (Fig. 10). In agreement with the observations by Kung and Fine [*28*], the cracks were not formed at constituent particles and tended to propagate through β-phase particles and in the interfaces between S-phase particles and the matrix.

In order to better understand the modifications in line broadening which take place during fatigue, X-ray residual stress measurements were carried out using Cu K_α radiation. The results shown in Fig. 11 reveal transitions in the residual stress dependence on the fraction of life which correspond closely to the stages of line broadening identified previously. The rapid enhancement of the compressive residual stresses at the surface during the first 20% of life coincides with the stage featuring rapid line broadening. This is to be expected as the surface grains subject to plastic deformation under tension-tension cycling are placed in residual compression on unloading due to stresses exerted by the less-strained underlying regions. During the intermediate life fractions, the residual stress is transformed from a peak compressive value of about -100 MPa to a nearly equivalent maximum value in tension at 60 to 70% of life. Figure 7 shows that the change in sign of the surface residual stresses is accompanied by a reduction in the line breadths measured at the surface and gradual enhancement of those recorded using more deeply penetrating incident radiation. The development of a peak tensile stress corresponds to the fraction of life at which the curves representative of the line broadening measured with Cu K_α and Mo K_α converge. Thereafter, the residual stress relaxes towards zero as crack initiation is approached. This final period of stress relaxation coincides with the appearance of slip lines on the surface. It is apparent, therefore, that despite the high degree of distortion incurred at the surface early in the life, crack initiation is impeded by the concomitant generation of compressive residual stress. A number of factors apparently contribute to the initiation of surface cracks including (*1*) the transformation of the residual stresses to tensile character, (*2*) the terminal buildup of dislocations in the surface layer with concomitant dislocation accumulation in the subsurface material, and (*3*) the formation of coarse slip lines, which can develop into surface intrusions. This sequence of events, and the collective enhancement of the applied stress attributable to them, provides the stress concentration required for crack nucleation at the surface.

The results from preliminary investigations conducted at a lower maximum applied moment are summarized in Fig. 12. Here it can be seen that

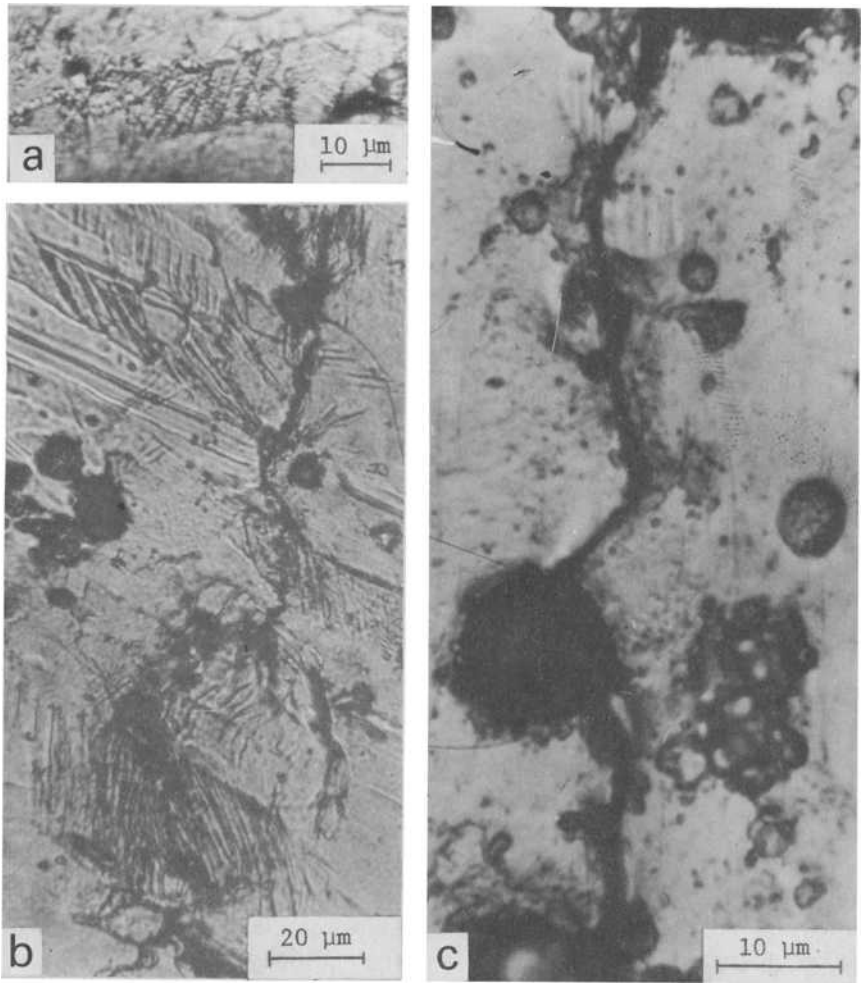

FIG. 10—*Optical micrographs of Al 2024.* (a) *Slip lines emerging prior to crack initiation.* (b) *Coarse slip lines in vicinity of growing fatigue crack.* (c) *Crack propagation through and around constituent particles (unetched).*

the surface layer analyzed by Cu K_α radiation does not incur the high level of distortion introduced by cycling at higher maximum stress. During the initial cycles, both the surface and the subsurface region probed by Mo K_α radiation give comparable degrees of broadening. Beyond 20% of life, the surface undergoes recovery manifested by reduced line breadths, while the subsurface line broadening continues at a reduced rate. At about 75% of the precrack fatigue life, the distortion at the surface begins to accrue rapidly again, with the line breadths reaching values similar to those measured using Mo K_α

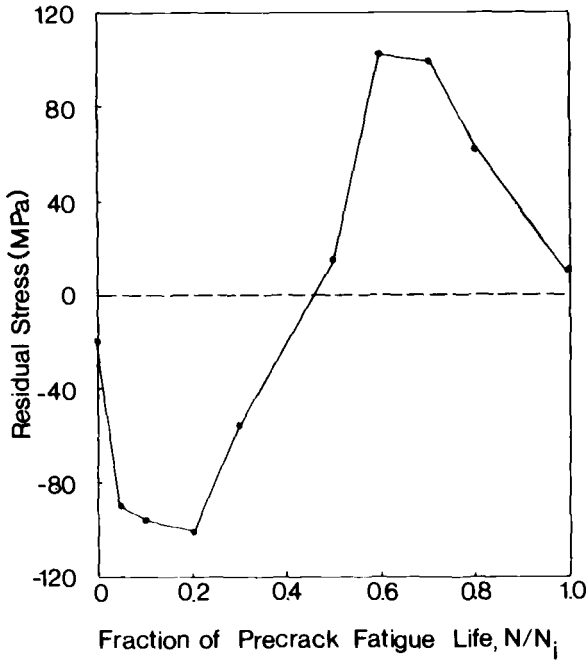

FIG. 11—*Modification of surface residual stress as a function of the fraction of precrack fatigue life.*

radiation prior to crack initiation. While the relative values of the breadths measured with the two radiations differ from those measured for the higher maximum stress level over most of the life, the comparability of line breadths for the near-surface and subsurface again appears to represent a distribution of damage conducive to crack initiation. Although not yet confirmed by direct observation, it is proposed that the difference in behavior identified by X-ray diffraction analyses of specimens fatigued at low as compared to high maximum stresses may be due to the initiation of cracks at coarse slip lines radiating from constituent particles [*28*]. These investigators found that 95% of the cracks were initiated by this mechanism at the lower stresses, and that the cracks formed were associated primarily with 2 to 3% of the particles greater than 2 μm in size, and usually with those greater than 6 μm in size. It should be emphasized that while the early-life line broadening at the surface cannot be used to estimate cumulative damage since the trend is later reversed, this does not imply that no fatigue damage has been incurred. Figure 13 demonstrates quite the opposite. Plotted in this figure are line-broadening data obtained during an experimental sequence consisting of (*1*) precycling a specimen to 15% of the average, precrack fatigue life at the higher of the maximum bending moments used in this study, (*2*) electrolytic removal of a surface layer of

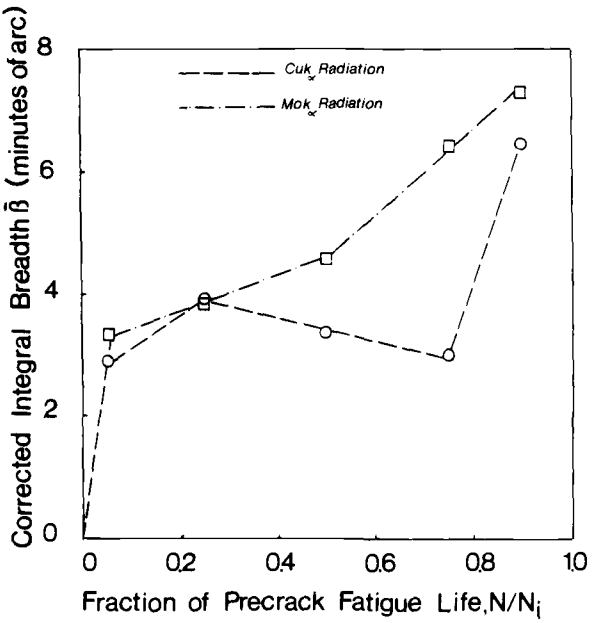

FIG. 12—*Superposition of line-broadening data obtained with Cu K_α and Mo K_α radiations as a function of the fraction of precrack fatigue life for Al 2024-T4 cycled at low stress level* (σ_{max} = *325 MPa*).

100 μm thickness (from both loaded surfaces of the specimen), and (*3*) resumption of the cycling to eventual crack initiation. It can be seen that the reduced line breadths measured after surface removal increase again when the fatiguing is continued. After 10 to 15% of the normal life, they attain a maximum and begin to decrease at a rate typical of that found in the earlier studies for the intermediate life fractions. The cycling required to regenerate a high dislocation density at the new surface represents, approximately, the extension of the normal life achieved by the surface removal treatment. Further experiments of this type indicated that surface removal after precycling to fractions of life between 0.05 and 0.25 yields extensions of life approximately equal to the amount of precycling, or essentially full recovery of the original life. Significant improvements in fatigue life were not obtained as a result of surface removal when precycling was carried past 50% of life; at least for the limited number of tests conducted, extensions of life were much less then the amount of precycling and generally lay within the total scatter of initiation data for this stress level of 20 to 25% (Table 1). Very large net increases in the normal life were obtained previously for axially fatigued specimens given a surface layer removal treatment, even when the precycling was carried to 95% of life [*15*]. This was ascribed to the instability of the bulk dislocation structure when cycling is resumed after elimination of the highly deformed surface layer.

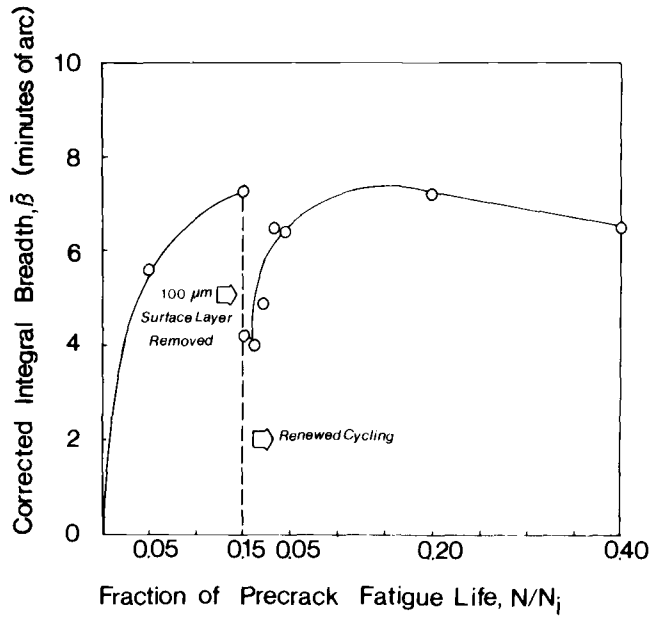

FIG. 13—*Change in integral breadths measured with Cu K_α radiation during an experimental sequence consisting of precycling to a given percent of life, removal of a 100-μm-thick surface layer by electropolishing, and renewed cycling to 40% of life.*

The diminishing returns realized with the treatment when applied to bending fatigue specimens require further verification, but may result from the differences in stress distribution and resultant depth profiles of induced distortion between the flexural and axial fatigue modes.

Summary and Conclusions

The study illustrates the importance of combining more than one technique, and of monitoring fatigue-affected structural changes at both the surface and in the subsurface, in order to both measure damage quantitatively and contribute to the fundamental understanding of damage mechanisms. These conclusions are founded on the following findings: (*1*) the inherent surface-sensitivity associated with fatigue cycling which obscures other significant manifestations of damage, such as the progressive lattice distortion and dislocation accumulation in the subsurface region; (*2*) the transient nature of the parameters measured by a particular technique, exemplified by the reduction in surface line breadths during intermediate life fractions, and the alterations in sign and sense of change exhibited by residual stresses during the life; and (*3*) the reversibility or reduction of fatigue damage through judicious treatment, demonstrated by the cyclic regeneration of a surface layer

with high dislocation density required after that formed during precycling is removed, thereby delaying crack initiation and promoting an extension of the normal life. In relation to these aspects of fatigue processes, this investigation has shown that (*1*) near-surface and sub-surface X-ray line broadening can be measured nondestructively using incident radiation with different penetration capabilities and compared with one another to provide a more definitive characterization of cumulative damage, (*2*) companion analyses of induced residual stresses utilizing essentially the same instrumentation disclose large modifications in the internal stress distribution during precisely that stage of life for which the changes in line breadth are more gradual, and (*3*) integrated measurements of this type provide indirect evidence of the microplasticity and its distribution developed during fatigue at different stress levels and reveal a strong correlation to the various origins for crack initiation which have been identified by direct observation.

References

[*1*] Weiss, V., Oshida, Y. and Wu, A., *Fatigue of Engineering Materials and Structures*, Vol. 1, 1979, pp. 333-341.

[*2*] Gough, H. G. and Wood, W. A., *Proceedings of the Royal Society* (London), Vol. A154, 1936, pp. 510-539.

[*3*] Spencer, R. G. and Marshall, J. W., *Journal of Applied Physics*, Vol. 12, 1941, pp. 191-196.

[*4*] Bennett, J. A., *Journal of Research of the National Bureau of Standards*, Vol. 46, 1951, pp. 457-461.

[*5*] Taira, S., Gotto, T. and Nakano, Y. in *Proceedings*, 12th Japanese Congress of Materials Research, Society of Materials Science, Kyoto, Japan, 1969, pp. 8-14.

[*6*] Barrett, C. S., *Metals and Alloys*, Vol. 8, 1937, p. 13.

[*7*] Gould, R. W. and Pittella, C. F., *Advanced X-ray Analysis*, Vol. 16, 1973, pp. 354-366.

[*8*] Taira, S. and Hayashi, K. in *Proceedings*, 9th Japanese Congress of Testing Materials, Society of Materials Science, Kyoto, Japan, 1966, pp. 1-6.

[*9*] James, M. R. in *Proceedings*, Spring Meeting of the Society for Experimental Stress Analysis, Dearborn, Mich., 1981, pp. 84-86.

[*10*] Boggs, B. and Byrne, J. G., *Metallurgical Transactions*, Vol. 4, 1973, pp. 2153-2157.

[*11*] Syren, B., Wohlfahrt, H. and Macherauch, E. in *Proceedings*, 2nd International Conference on Mechanical Behavior of Materials, Boston, 1976, pp. 212-235.

[*12*] Koves, G., *Microstructural Science*, Vol. 4, 1976, pp. 233-243.

[*13*] Koves, G., *Advanced X-ray Analysis*, Vol. 13, 1970, pp. 468-486.

[*14*] Weiss, V., Oshida, Y. and Wu, A., *Journal of Nondestructive Evaluation*, Vol. 1, 1980, pp. 207-213.

[*15*] Pangborn, R. N., Weissmann, S. and Kramer, I. R., *Metallurgical Transactions*, Vol. 12A, 1981, pp. 109-120.

[*16*] Weissmann, S., *Accuracy in Powder Diffraction, NBS Special Publication 567*, 1980, pp. 411-431.

[*17*] Pangborn, R. N., Weissmann, S. and Kramer, I. R., *Advanced X-ray Analysis*, Vol. 24, 1981, pp. 203-208.

[*18*] Stokes, A. R. and Wilson, J. C., *Proceedings of the Physical Society* (London), Vol. 56, 1944, p. 174.

[*19*] Scherrer, P., *Nachrichten von der Königlichen Gesellschaft der Wissenschaften zu Göttingen*, Vol. 2, 1918, p. 98.

[*20*] Klug, H. P. and Alexander, L. E., *X-ray Diffraction Procedures for Polycrystalline and Amorphous Materials*, 2nd ed., Wiley, New York, 1974, pp. 661-665.

[21] Mughrabi, H., *Strength of Metals and Alloys*, Vol. 3, 1979, pp. 1615-1638.
[22] Grosskreutz, J. C., *Metallurgical Transactions*, Vol. 3, 1972, pp. 1255-1262.
[23] Laird, C. and Duquette, D. J., *Corrosion Fatigue*, National Association of Corrosion Engineers, Houston, 1972, pp. 88-117.
[24] Tanaka, K. and Mura, T., *Metallurgical Transactions*, Vol. 13A, 1982, pp. 117-123.
[25] Grosskreutz, J. C. and Shaw, G. G. in *Proceedings*, 2nd International Conference on Fracture, Chapman and Hall, London, 1969, pp. 620-629.
[26] Morris, W. L., Buck, O. and Marcus, H. L., *Metallurgical Transactions*, Vol. 7A, 1976, pp. 1161-1165.
[27] Morris, W. L., *Metallurgical Transactions*, Vol. 9A, 1978, pp. 1345-1348.
[28] Kung, C. Y. and Fine, M. E., *Metallurgical Transactions*, Vol. 10A, 1979, pp. 603-610.
[29] McKittrick, J., Liaw, P. K., Kwun, S. I. and Fine, M. E., *Metallurgical Transactions*, Vol. 12A, 1981, pp. 1535-1539.
[30] Rachinger, W. A., *Journal of Scientific Instruments*, Vol. 25, 1948, p. 254.
[31] Weiss, V. and Wu, A. Y., "Feasibility Study of Fatigue Damage Characterization in 7050 Aluminum," Final Report, David W. Taylor Naval Ship R&D Center, Annapolis, Md., Jan. 1981.

DISCUSSION

J. G. Byrne[1] (*written discussion*)—I would merely like to point out, in relation to the history of applying Fourier analysis of the broadening of X-ray lines to fatigue studies, that, so far as I know, my associates and I were probably the first practitioners. The work of Taira which the authors mentioned was contemporary, but of a qualitative film nature. In fact, we too were predated by Ogilvie and Mall, although the latter results were never published. In more recent work of ours, involving copper and steels, we have coupled X-ray and positron measurements to relate dislocation cell and vacancy formation during fatigue. I find the authors' work very interesting, especially the depth studies, and am glad to see X-ray measurements coming into more frequent use in fatigue. I might point out also that positrons may be used for depth profiling via utilization of positron sources of different energy.

J. Field et al (*authors' closure*)—We appreciate the comments by Professor Byrne and the pioneering work he and his associates conducted in applying Fourier analysis to X-ray line broadening during fatigue. As indicated in the concluding section of our paper, we heartily endorse the use of more than one experimental method to follow the microstructural changes that occur during cycling. Only in this way can the individual contributions of a variety of mechanisms be evaluated to provide a more comprehensive understanding of the progression towards fatigue failure. Our studies of the variation in line

[1]Department of Materials Science and Engineering, University of Utah, Salt Lake City, Utah 84112.

breadth with depth from the surface have also been useful in monitoring the fatigue deformation preceding crack initiation. The utilization of positron sources of different energy for nondestructive depth profiling is a suggestion well worth pursuing, and could yield information on changes occurring both prior to and after cracks are initiated.

M. R. James[2] (*written discussion*)—Was the fatigue loading fully reversed, or tension-tension bending? Did you identify any other crack initiation mode, such as grain boundary cracking, or was it 100% slip band cracking?

J. Field et al (*authors' closure*)—The fatigue loading was carried out by four-point beam bending in tension-tension. The generation of compressive residual stresses on unloading would therefore be expected at the tensile surface. Later in the fatigue life, relaxation of these compressive stresses occurred and eventually they changed in sign (Fig. 7). Since the residual stress measurements were confined to the surface layer probed by Cu K_α radiation, the distribution and fatigue-induced modification of residual stresses in depth is not yet known. The near-surface effects identified in this study, however, are presumed to be related to the concomitant changes in lattice distortion manifested by the X-ray line breadths occurring in the surface layer and subsurface regions. Line broadening both at the surface and in the subsurface, accompanied by relaxation of the tensile residual stresses, occurred as microcracks were formed. The fatigue cracks initiated at the stress levels employed in these investigations were associated with coarse slip lines. No propensity for grain boundary cracking was identified.

David Cameron[3] (*written discussion*)—What was the initiation criterion employed? How was it observed?

J. Field et al (*authors' closure*)—The procedures and criterion employed for crack initiation are described in the Experimental Procedure section of our paper. Since the proportion of the total life consumed by the initiation stage is dependent on the applied stress level, the practice of plotting X-ray diffraction data versus the fraction of the fatigue life to failure (N/N_f) can lead to some confusion. Often it is not clear which changes in the diffraction patterns can be ascribed to fatigue deformation incurred prior to crack initiation and which are related to the microplasticity associated with the opening of numerous microcracks or propagating macrocracks. Admittedly, the definition of an initiated crack is often a function of the detection capability, and the actual contribution of the first crack detected to eventual failure is

[2]Rockwell International Science Center, Thousand Oaks, Calif. 91360.

[3]Structural Integrity Laboratories, Department of Mechanical Engineering, University of Toronto, Ontario, Canada.

not always known. However, if the criterion for establishing crack initiation is clearly stated and the X-ray data plotted versus N/N_i, some of the ambiguity in interpreting the data can be alleviated.

H. Mughrabi[4] (*written discussion*)—I have a remark and a question. The remark first. When using X-ray techniques one has to be careful about whether one is measuring the amount of lattice plane *bending* (rocking curve measurements) or the elastic strains, that is, local changes in lattice plane *spacings*, as evidenced by X-ray line broadening. The former type of measurement permits the determination of the density of *local excess dislocations* of one sign, but not of the *total* dislocation density, which one can only obtain from the X-ray line broadening. In general, it is important to note that a high local excess dislocation density is not necessarily equivalent to a high total dislocation density. This is particularly true for measurements at the original surface of the deformed specimen, where preferential dislocations egress, or piling up can give rise to more significant lattice bending than in the bulk, irrespective of the total dislocation densities at the surface or in the bulk.

My question is related to how you unload your fatigued specimens before performing residual stress measurements, since unloading from reverse stressing can reverse the signs of residual stresses observed after unloading from forward stressing. If I have understood correctly your response to Dr. James's question, you have not performed fully reversed fatigue tests, but rather pulsating tension tests, and have therefore always unloaded from tension. Is this true?

J. Field et al (*authors' closure*)—We agree with the basic content of the remarks concerning what lattice distortions are measured with X-ray rocking curve and X-ray line broadening techniques. We would add that in our experience in applying X-ray double-crystal diffractometry (modified for analyses of polycrystalline materials) and conventional line-broadening methods to metal fatigue, the changes in local excess dislocation density and total dislocation density have paralleled one another.

All specimens were cycled in tension-tension bending and were thus unloaded from tension for subsequent residual stress analysis.

D. L. Davidson[5] (*written discussion*)—In your figures showing broadening versus depth, you removed some material (how?) and then quote a broadening for that depth. But the penetration of the X-rays is 70 to 90 μm. How is the number in your figures for depth defined? Is it depth of material removed, or the limits of beam penetration, or some mean value?

[4]Max-Planck-Institut für Metallforschung, Institut für Physik, Stuttgart, Federal Republic of Germany.

[5]Southwest Research Institute, San Antonio, Tex. 78284.

J. Field et al (authors' closure)—In generating the depth profiles, surface layer removal was accomplished by electropolishing the top and bottom surfaces of the specimen simultaneously using the same solution and conditions employed in the initial surface preparation. The depths indicated on the graphs represent the layer thickness removed from the surface analyzed, in this case the tensile surface, and are assumed by necessity to be one half of the total change in thickness of the specimen after each polishing step. The layer probed by the Cu K_α radiation used to conduct the depth studies is about 30 μm in thickness for the highest angle diffraction peak monitored.

J. G. Cabañas-Moreno,[1] *M. S. Yang,*[1] *J. R. Weertman,*[1]
M. Roth,[2] *Z. Y. Zhang,*[2] *G. D. Wignall,*[3] *and W. C. Koehler*[3]

Studies of Grain Boundary Cavitation by Small-Angle Neutron Scattering

REFERENCE: Cabañas-Moreno, J. G., Yang, M. S., Weertman, J. R., Roth, M., Zhang, Z. Y., Wignall, G. D., and Koehler, W. C., **"Studies of Grain Boundary Cavitation by Small-Angle Neutron Scattering,"** *Fatigue Mechanisms: Advances in Quantitative Measurement of Physical Damage, ASTM STP 811*, J. Lankford, D. L. Davidson, W. L. Morris, and R. P. Wei, Eds., American Society for Testing and Materials, 1983, pp. 95–114.

ABSTRACT: Small-angle neutron scattering has been used to study the process of fatigue-induced grain boundary cavitation in two model materials, pure copper and a Cu-7Al alloy, fatigued at elevated temperature. Values have been obtained from the scattering data for void volume fraction, and number density of the voids and their size distribution, as a function of fatigue time. The growth rate of individual voids has been calculated and found to be in good agreement with a recent theory of fatigue-induced cavitation. Copper and copper-aluminum show opposite responses to the effect of fatigue temperature on cavitation. An increase in the temperature of fatigue produces an increase in the total void volume growth rate and the void nucleation rate in the case of copper, a decrease in copper-aluminum. The process of grain boundary cavitation is shown to be very sensitive to the movement of the grain boundaries. Grain boundary migration can cause cavitated boundaries to shed their voids into the matrix. The number and size distribution of cavities in a specimen appear to be related to the extent of grain growth which occurs during fatigue.

KEY WORDS: fatigue (high temperature), grain boundary cavitation, copper, copper-aluminum, small-angle neutron scattering, void nucleation, void growth rate, grain boundary migration, grain growth

The phenomenon of grain boundary cavitation (GBC) occurs frequently in metals, alloys, and ceramics which are subjected to static or fatigue loading at elevated temperatures. It usually involves a marked loss of ductility and,

[1]Department of Materials Science and Engineering and the Materials Research Center, Northwestern University, Evanston, Ill. 60201.
[2]Institut Laue-Langevin, Grenoble, France. Dr. Zhang is presently at the Institute of Physics, Chinese Academy of Sciences, Beijing, China.
[3]Oak Ridge National Laboratory, Oak Ridge, Tenn. 37830.

by itself or acting in combination with other processes (for example, fatigue crack growth), is a major cause of mechanical failure.

The process of GBC involves (*1*) the nucleation and (*2*) the growth of cavities at grain boundaries. Therefore a characterization of GBC requires a knowledge of the kinetics of nucleation *and* of growth. This knowledge could be used to determine, for example, the mechanisms whereby cavities are nucleated and how they grow, and the influence on cavitation of material parameters (grain size, composition, etc.) and testing variables (temperature, stress, strain, rate of deformation, etc.). Such information is essential for accurate predictions of lifetimes under service conditions.

The literature is replete with theoretical models for the growth of cavities in creep [*1-7*].[4] Much less attention has been given to fatigue cavitation [*7-10*]. On the experimental side the precision measurement of density [*11-13*] is probably the only method to have produced useful quantitative data of *total* cavity volumes per unit volume of sample. However, it is impossible, using this technique, to separate the influence of continued void nucleation from individual void growth. Few attempts have been made to measure nucleation rates, and low-resolution techniques for void detection frequently were used [*12,14*]. Argon et al [*15*] have recently commented on the importance of detection of extremely small voids in the determination of nucleation rates.

In the past few years our research group has been using small-angle neutron scattering (SANS) [*16-18*] and high-voltage electron microscopy (HVEM) [*19*] to study GBC in pure copper and in copper-aluminum alloys. The complementary techniques of SANS and HVEM are perhaps unmatched in their ability to provide both detailed information and statistical data of great sensitivity on the cavitation process [*19,20*]. The choice of materials has been dictated mainly by the need for a simple, stable microstructure in which the scattering from causes other than voids is as small as possible. The copper-aluminum alloys have a lower stacking fault energy than pure copper, even at the elevated temperatures of the fatigue testing [*21*]. They are single phase, so there is no problem with small-angle scattering from precipitates, nor does there seem to be appreciable clustering of one element or the other which could cause additional scattering [*22*]. It is hoped that a comparison of cavitation in copper with that in the copper-aluminum alloys will provide information on the influence of stacking fault energy on GBC.

In this paper we report the results of our SANS study of fatigue cavitation in pure copper and in one of the copper-aluminum alloys. We also will discuss the unique advantages of the SANS technique, as well as its limitations in the study of GBC.

[4]The italic numbers in brackets refer to the list of references appended to this paper.

A number of texts and review articles have been written (for example, Refs *20, 23,* and *24*) on the subject of small-angle neutron scattering and the methods whereby the data are analyzed. The reader should consult these for a detailed treatment. Briefly, scattering measurements are carried out by directing a monoenergetic aligned beam of neutrons along an evacuated flight path onto (and through) a specimen. The scattered neutrons are recorded on a position sensitive detector placed some meters behind the specimen. Rather long wavelength neutrons ($\simeq$ 0.5 to 1 nm) are used in order to eliminate any double Bragg scattering. A typical specimen thickness is 5 mm and the cross section irradiated is about 100 mm^2. The extent of scattering as read by the detector is corrected for instrumentation and absorption effects, radially averaged, and converted to the differential scattering cross section per unit volume of specimen, $d\Sigma/d\Omega$. The final result is a curve of $d\Sigma/d\Omega$ versus the scattering vector q for each specimen. (Here $q = 4\pi \sin \theta/\lambda$, where θ is the Bragg angle and λ is the wavelength of the neutrons.) Typically the scattering curves can be measured over the range of $q \simeq 0.03$ nm^{-1} to $\simeq 2$ nm^{-1}. In order to carry out a complete analysis of the data, however, it is necessary to know $d\Sigma/d\Omega$ over all of reciprocal space. Fortunately, at sufficiently small values of q the measured scattering follows the Guinier law [*25*], which can be used to determine extrapolated values of $d\Sigma/d\Omega$ down to zero q. Similarly, at the upper end of the measurable q's the scattering is governed by Porod behavior [*26*] and thus the measured data can be extrapolated out to $q \rightarrow \infty$. The total volume fraction of the scattering entities (here voids) is obtained from the integration of $d\Sigma/d\Omega$ over all of reciprocal space. The total surface area of the scatterers per unit sample volume can be found from the behavior of the scattering curve in the Porod region. A knowledge of $d\Sigma/d\Omega$ over all values of q permits an inversion of the scattering curve to obtain a size distribution of the scatterers.

Experimental Details

The materials studied were high-purity copper (99.999% pure) and copper containing 7% aluminum (15 atomic percent). The alloy was prepared from 99.999% pure elements. Flat tension specimens with a 9.5 mm gage length and 6.5 by 6.5 mm cross section were fatigued in fully reversed loading with a servohydraulic testing machine. All fatiguing was carried out in an environment of purified argon. Details of the experimental setup and testing conditions can be found elsewhere [*17,18,27-29*].

We have investigated the effect of (*1*) stress, (*2*) temperature, and (*3*) frequency of cycling. The experimental conditions are summarized in Table 1. The SANS measurements for pure copper were made at the Institut Laue-Langevin (Grenoble, France), and those for the copper-aluminum alloys were carried out at the Oak Ridge National Laboratory (Oak Ridge, Tennessee).

TABLE 1—*High-temperature fatigue conditions.*

Material and Temperature	Stress Amplitude (Fully Reversed), MPa	Frequency, Hz	Fatigue Time, s	Variables Investigated
Copper				
405°C[a]	34.0	17.0	1.5×10^2 to 1.2×10^4	temperature and composition
486°C	34.0	17.0	4.5×10^1 to 4.5×10^3	
567°C	34.0	17.0	1.5×10^1 to 1.5×10^3	
Cu-7Al				
390°C	68.0	17.0	6.0×10^2 to 1.8×10^4	
480°C	68.0	17.0	6.0×10^2 to 6.0×10^3	
570°C	68.0	17.0	1.0×10^2 to 6.0×10^2	
Copper				
405°C	20.7	17.0	4.5×10^2 to 3.6×10^4	stress amplitude
405°C	34.0	17.0	1.5×10^2 to 1.2×10^4	
405°C	48.3	17.0	6.0×10^1 to 1.2×10^4	
Copper				
405°C	34.0	1.7	1.5×10^3 to 1.2×10^5	frequency
405°C	34.0	17.0	1.5×10^2 to 1.2×10^4	
405°C	34.0	68.0	1.1×10^2 to 2.9×10^3	

[a]First three rows of data from work of R. Page, J. R. Weertman, and M. Roth [*17, 18*].

Results

Effect of Cavitation on the Scattering Curve

There are a variety of sources of small-angle scattering [*30*]. Therefore it is necessary to determine what fraction of a scattering curve taken from a fatigued specimen actually is produced by the cavities. Figure 1 shows log-log plots of the differential scattering cross section $d\Sigma/d\Omega$ versus the scattering vector q for three copper-aluminum specimens. Two of the specimens had been fatigued for 2×10^5 cycles under the same loading conditions. However, one was fatigued at 390°C, the other at room temperature. The third specimen was unfatigued. It can be seen that the difference in scattering is insignificant between that coming from the specimen fatigued at room temperature, which contains a high dislocation density but no voids, and that from the annealed control specimen. On the other hand, the specimen fatigued at 390°C shows a considerable enhancement in scattering. It is concluded that the difference between $d\Sigma/d\Omega$ of a fatigued specimen and of the control specimen represents that portion of the scattering curve of the fatigued material which arises from voids.

In order to make sure that the increase in scattering produced by high-temperature fatigue truly is a grain boundary phenomenon, the scattering

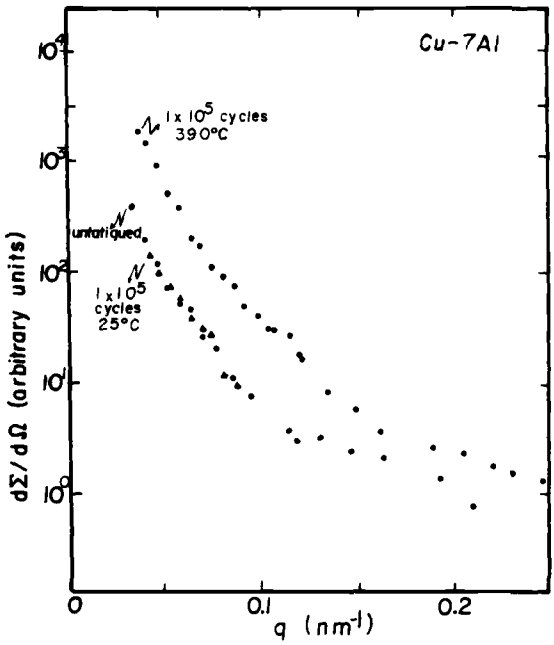

FIG. 1—*Differential scattering cross section,* $d\Sigma/d\Omega$, *as a function of scattering vector* q *for three Cu-7Al specimens. One specimen (solid circles) was fatigued for* 10^5 *cycles at 390°C, 17 Hz, in fully reversed loading (stress amplitude = 68.0 MPa). A second specimen was fatigued at room temperature under identical loading conditions (solid triangles). The third specimen (open circles) was unfatigued.*

from a copper single crystal which had been heavily fatigued at 405°C was compared with scattering from a similar but unfatigued single crystal. (This experiment is described in Ref *18*.) No appreciable difference in the scattering behavior of the two crystals was found. Later examination by transmission electron microscopy (TEM) showed that the fatigued sample contained a well-developed subgrain structure. Evidently neither the dislocations nor the vacancies generated during fatigue make a significant contribution to the small-angle scattering. No precipitates have been seen in either the copper or the copper-aluminum alloys during extensive examination in the HVEM. In view of all this evidence it is concluded that the source of the increased scattering in polycrystalline specimens produced by high-temperature fatigue is grain boundary cavitation.

Effect of Temperature on Cavitation

Analysis of the scattering data by well-known procedures [*20,24*] yields some quantitative measures of the extent of cavitation, such as the void vol-

ume fraction V_f and the total surface area of the cavities per unit volume of material. Figure 2 shows the effect of fatigue temperature on the void volume fraction which develops in pure copper and in the copper-aluminum alloy. The copper data are taken from the work of Page et al [*17,18*]. (Note that the 480°C copper-aluminum curves in Figs. 2 and 4 have been drawn without taking into account the middle datum point. The specimen fatigued for 2100 s at 480°C was found to have experienced some unusual grain growth. This specimen is discussed again in a later section.) It can be seen that the values of V_f range over some three orders of magnitude and extend to void volume fractions of less than one part in a million. The variation of V_f with fatigue time is in itself a measure of the damage that has occurred. However, in order to study the cavitation process a more sophisticated analysis of the SANS data is required.

There are a number of techniques [*31-33*] for the determination of the distribution of sizes of scattering entities which has given rise to a known (measured) scattering curve. We have used the method developed by Schmidt and co-workers [*31*]. Before carrying out the inversion from scattering curve to size distribution it is necessary to know the shape of the particles.

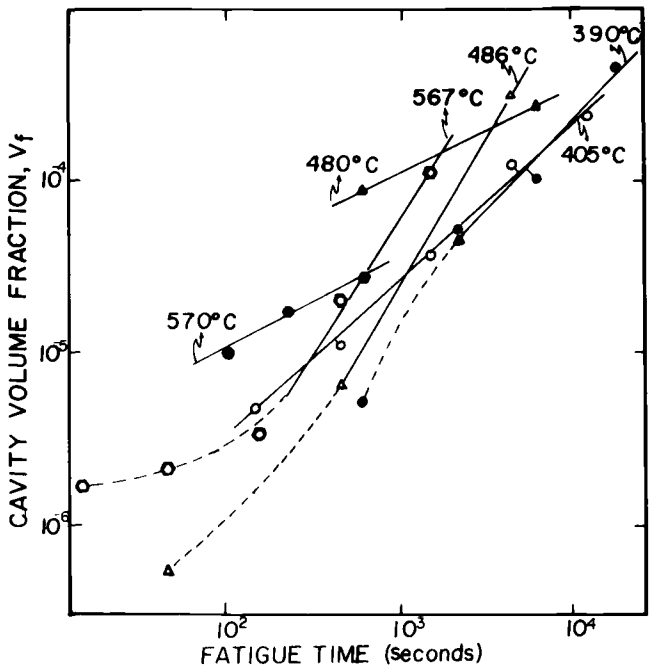

FIG. 2—*Void volume fraction as a function of fatigue time for specimens fatigued at various temperatures. Open symbols: pure copper; closed symbols: Cu-7Al. Solid lines: linear portion of curves. Copper results taken from the work of Page et al* [17,18]. *All results have been normalized to a grain size of 60 μm.*

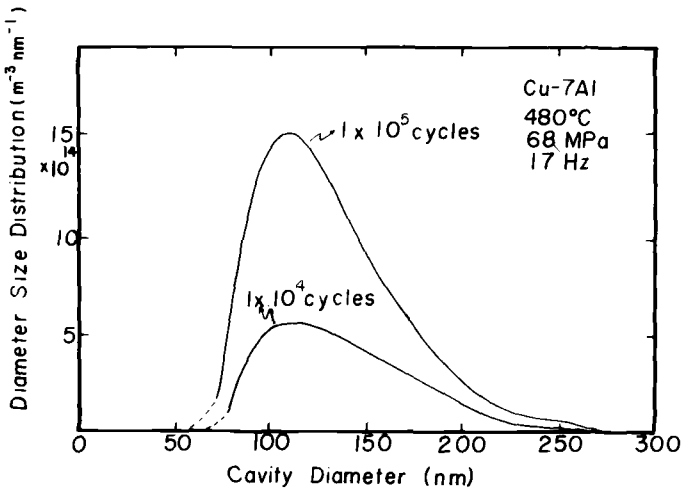

FIG. 3—*Size distribution curves of voids in Cu-7Al fatigued at 480°C, 17 Hz, with a stress amplitude of 68.0 MPa. Specimens cycled for 10^4 and 10^5 cycles. Results have been normalized to a grain size of 60 μm.*

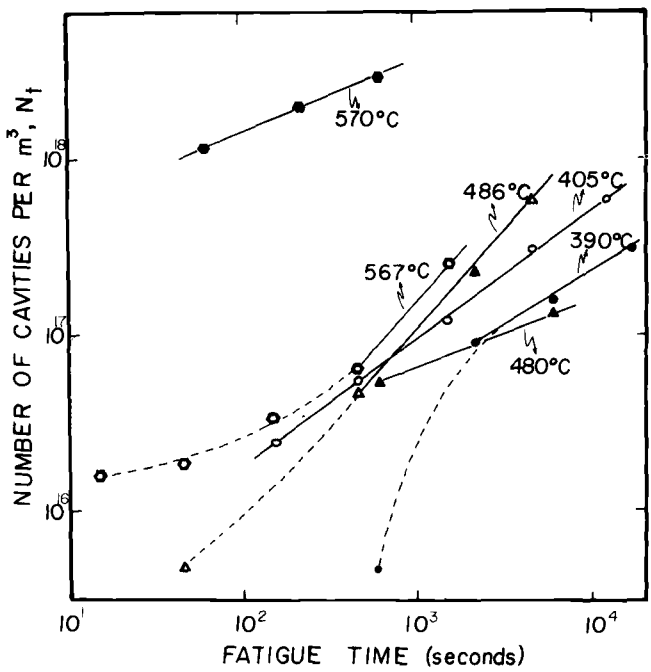

FIG. 4—*Number of cavities per unit volume as a function of fatigue time for specimens fatigued at various temperatures. Open symbols: pure copper; closed symbols: Cu-7Al. Solid lines: linear portion of curves. All results normalized to a grain size of 60 μm. Copper results taken from the work of Page et al* [17,18].

Previous HVEM studies [*19,34*] have shown that voids less than about 1 μm in size in copper and copper-aluminum fatigued at elevated temperature are roughly spherical. Two examples of a size distribution curve are shown in Fig. 3. The total number of voids per unit volume of material, N_T, can be found by measuring the area under the distribution curves. The results are presented in Fig. 4. It can be seen that, on log-log plots, the dependence on fatigue time of both V_f and N_T becomes linear after a short initial period of fatiguing. Values for V_f and N_T in the linear region are given in Table 2. In the case of copper, the growth rate of the total void volume V_f increases with increasing temperature of fatigue. The nucleation rate also rises with the fatigue temperature. The growth rates of V_f and N_T in the copper-aluminum alloy decrease as the fatigue temperature is increased. It appears that in the early stages of fatigue both the void volume fraction and the number of voids are larger in alloy specimens tested at 480 or 570°C than in the pure copper fatigued at the corresponding temperature. However, this situation is reversed as fatigue proceeds, because of the lower growth and nucleation rates in the copper-aluminum alloy. As regards an explanation for the opposite temperature dependence of the void nucleation rate in copper and in copper-aluminum, it is highly suggestive that the stacking fault energy of copper drops with increasing temperature [*35*] whereas that of copper-aluminum rises [*21*]. (The precise role of stacking fault energy in influencing GBC is not fully understood. It appears that stress concentrations which lead to intergranular cracking in planar slip metals are quickly relaxed through cross slip in high stacking fault energy material. It has been observed [*19,34,36*] that voids nucleate in the copper and copper-aluminum alloys at points which experience high stress concentration during grain boundary sliding, namely, at grain boundary serrations.)

Effects of Stress Amplitude and Frequency of Cycling on Cavitation

Figures 5 and 6 show the change in cavitation brought about by varying the fatigue stress amplitude from 20.7 to 48.0 MPa in a copper fatigued in fully reversed loading at 405°C at a frequency of 17 Hz. It can be seen from a comparison of the two figures that the increase in V_f in going from 34.0 to 48.3 MPa is related to an enhancement of the nucleation rate. The size distributions in copper fatigued at these two stress levels are similar in appearance. Lowering the stress level to 20.7 MPa produces a large drop in V_f but the number of cavities remains high. Most of the size distribution curves in this series of specimens are much narrower and peak at a lower void diameter than the distributions of the 34.0 and 48.3 MPa series (Fig. 7).

The result of varying frequency of cycling while keeping stress amplitude and temperature constant is shown in Figs. 8 and 9. Higher frequencies hasten cavitation very substantially. Slow cycling, like low stress amplitudes, leads to a large number of very small cavities.

TABLE 2—*Experimental and theoretical values of* V_f, N_T, *and* $\dot{v}$.

Material and Experimental Conditions	Void Volume Fraction (V_f)	No. Density of Voids (N_T), m^{-3}	Individual Void Growth Rate (Experimental) ($\dot{v}_{exp}$), $m^3 s^{-1}$	Individual Void Growth Rate (Theoretical) ($\dot{v}_{th}$), $m^3 s^{-1}$[b]	
				Sintering Stress = 0	Sintering Stress = Stress Amplitude
			PURE COPPER[a]		
405°C, 34.0 MPa, 17.0 Hz	$4.4 \times 10^{-8} t^{0.93}$	$4.4 \times 10^{14} t^{0.78}$	$1.6 \times 10^{-23} t^{-0.86}$	$8.9 \times 10^{-24} t^{-0.69}$	$3.7 \times 10^{-24} t^{-0.82}$
486°C, 34.0 MPa, 17.0 Hz	$2.8 \times 10^{-10} t^{1.6}$	$2.5 \times 10^{13} t^{1.2}$	$7.2 \times 10^{-24} t^{-0.55}$	$1.6 \times 10^{-23} t^{-0.69}$	$5.1 \times 10^{-24} t^{-0.82}$
567°C, 34.0 MPa, 17.0 Hz	$1.6 \times 10^{-9} t^{1.5}$	$1.5 \times 10^{13} t^{1.3}$	$2.6 \times 10^{-23} t^{-0.80}$	$2.5 \times 10^{-23} t^{-0.69}$	$6.6 \times 10^{-24} t^{-0.82}$
405°C, 20.7 MPa, 17.0 Hz	$4.9 \times 10^{-8} t^{0.61}$	$1.8 \times 10^{16} t^{0.40}$	$6.4 \times 10^{-25} t^{-0.79}$	$5.4 \times 10^{-24} t^{-0.69}$	$2.2 \times 10^{-24} t^{-0.82}$
405°C, 34.0 MPa, 17.0 Hz	$7.0 \times 10^{-8} t^{0.82}$	$3.9 \times 10^{14} t^{0.80}$	$2.5 \times 10^{-24} t^{-0.99}$	$8.9 \times 10^{-24} t^{-0.69}$	$3.7 \times 10^{-24} t^{-0.82}$
405°C, 48.3 MPa, 17.0 Hz	$4.3 \times 10^{-8} t^{0.98}$	$5.1 \times 10^{14} t^{0.83}$	$1.4 \times 10^{-23} t^{-0.85}$	$1.3 \times 10^{-23} t^{-0.69}$	$5.2 \times 10^{-24} t^{-0.82}$
405°C, 34.0 MPa, 1.7 Hz	$3.2 \times 10^{-9} t^{0.85}$	$3.7 \times 10^{16} t^{0.30}$	$8.2 \times 10^{-26} t^{-0.45}$	$8.9 \times 10^{-24} t^{-0.69}$	$3.7 \times 10^{-24} t^{-0.82}$
405°C, 34.0 MPa, 17.0 Hz	$7.0 \times 10^{-8} t^{0.82}$	$3.9 \times 10^{14} t^{0.80}$	$2.5 \times 10^{-24} t^{-0.99}$	$8.9 \times 10^{-24} t^{-0.69}$	$3.7 \times 10^{-24} t^{-0.82}$
405°C, 34.0 MPa, 68.0 Hz	$1.5 \times 10^{-7} t^{0.83}$	$6.9 \times 10^{14} t^{0.80}$	$6.5 \times 10^{-24} t^{-0.97}$	$8.9 \times 10^{-24} t^{-0.69}$	$3.7 \times 10^{-24} t^{-0.82}$
			Cu-7Al		
390°C, 68.0 MPa, 17.0 Hz	$1.0 \times 10^{-8} t^{1.1}$	$1.3 \times 10^{15} t^{0.62}$	$5.1 \times 10^{-24} t^{-0.52}$	$1.8 \times 10^{-23} t^{-0.69}$	$7.4 \times 10^{-24} t^{-0.82}$
480°C, 68.0 MPa, 17.0 Hz	$4.5 \times 10^{-6} t^{0.47}$	$4.0 \times 10^{15} t^{0.39}$	$8.6 \times 10^{-23} t^{-0.92}$	$3.2 \times 10^{-23} t^{-0.69}$	$1.0 \times 10^{-23} t^{-0.82}$
570°C, 68.0 MPa, 17.0 Hz	$1.9 \times 10^{-6} t^{0.45}$	$1.9 \times 10^{17} t^{0.43}$	$1.7 \times 10^{-25} t^{-0.92}$	$5.0 \times 10^{-23} t^{-0.69}$	$1.4 \times 10^{-23} t^{-0.82}$

[a]First three rows of data from work of R. Page, J. R. Weertman, and M. Roth [*17,18*].
[b]See Ref *17* for values of physical quantities used in calculation of $\dot{v}_{th}$.

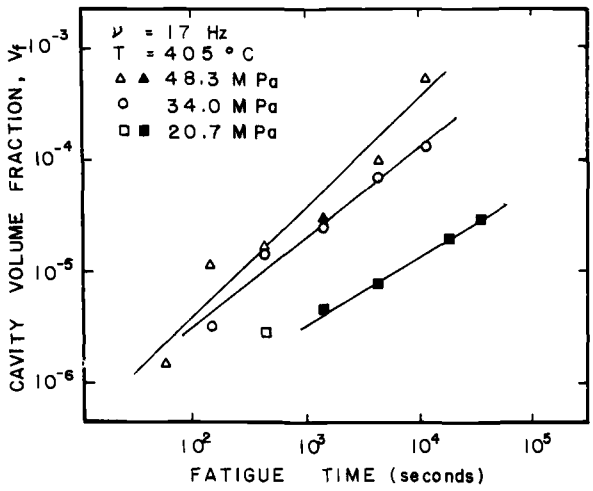

FIG. 5—*Total void volume fraction as a function of fatigue time for copper tested at several stress amplitudes. All specimens were fatigued at 405°C at a frequency of 17 Hz in fully reversed loading. Solid points indicate specimens with a narrow void size distribution curve which peaks at a very small diameter. All results normalized to a grain size of 60 μm.*

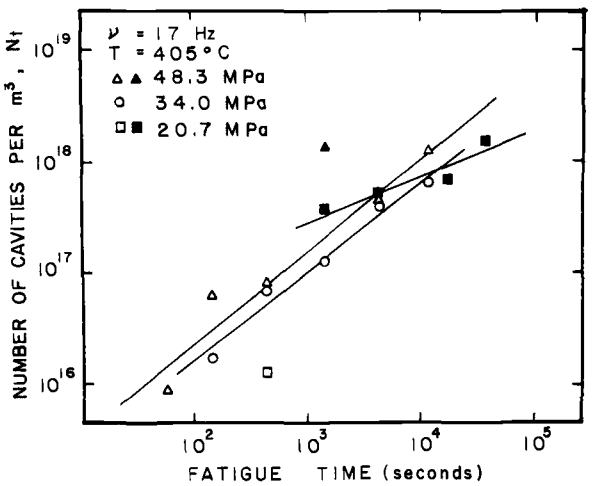

FIG. 6—*Number of voids per unit volume as a function of fatigue time for copper tested at several amplitudes. Test conditions and meaning of solid points same as in Fig. 5.*

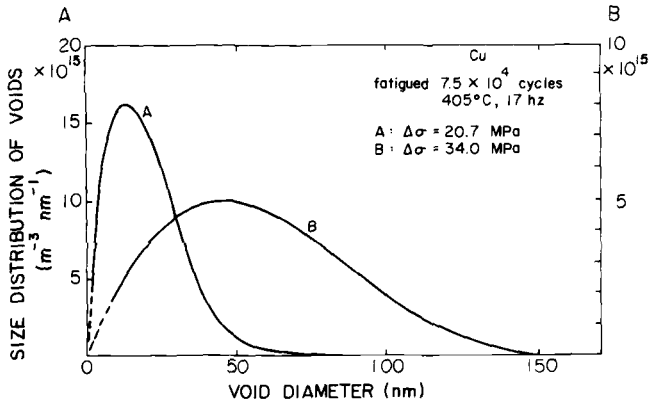

FIG. 7—*Curve A: size distribution of voids in a copper specimen fatigued for 7.5 × 10⁴ cycles at a stress amplitude of 20.7 MPa, 405°C, 17 Hz. Curve B: size distribution of voids in copper fatigued for 7.5 × 10⁴ cycles at 34.0 MPa, 405°C, 17 Hz. Note the difference in scales between A and B. Results normalized to a grain size of 60 μm.*

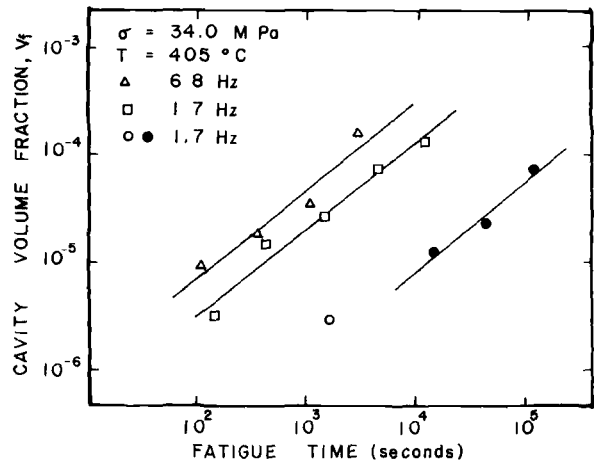

FIG. 8—*Total void volume fraction as a function of fatigue time for copper cycled at several frequencies. All specimens were fatigued at 405°C in fully reversed loading with a stress amplitude of 34.0 MPa. Results normalized to a grain size of 60 μm. Solid points have same meaning as in Fig. 5.*

Fatigue-Induced Cavitation in Model Materials

The results presented in the previous sections demonstrate that small-angle neutron scattering is a sensitive technique for quantifying fatigue damage when it appears in the form of cavitation. There should be important technological applications for SANS as a method of nondestructure testing.

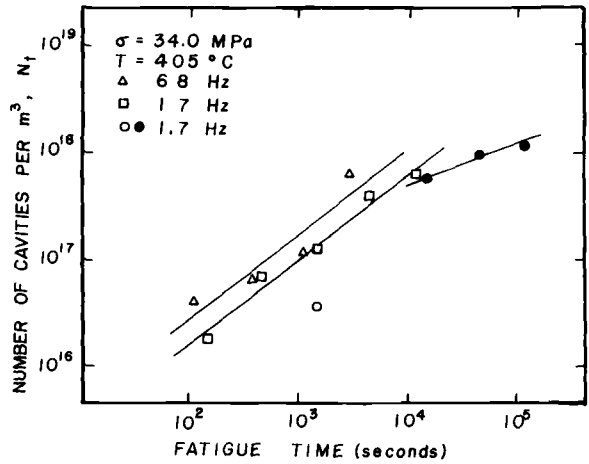

FIG. 9—*Number of voids per unit volume as a function of fatigue time for copper tested at several cycling frequencies. Test conditions and meaning of solid points as in Fig. 8.*

Furthermore, in a simple model system such as pure copper or copper-aluminum, SANS permits an examination into the basic mechanisms of GBC. For example, since both the total void volume fraction and the number density of voids can be determined, the growth rate $\dot{v}$ of individual voids can be found. The calculation of $\dot{v}$ is especially simple for that portion of the fatigue life of a specimen in which V_f and N_T vary approximately exponentially with time (straight-line region of the curves in Figs. 2, 4, 5, 6, 8, and 9). Values of $\dot{v}$ ($\dot{v}_{exp}$) obtained in this manner are listed in Table 2. The growth of the individual voids appears to be highly transient. Also given in Table 2 are values of $\dot{v}$ ($\dot{v}_{th}$) calculated from a recent theory of fatigue-induced cavitation [*10*]. This theory is concerned with the transient diffusion of vacancies down grain boundaries in the immediate vicinity of a newly nucleated void, before a steady-state stress field has had time to become established. Briefly, it is shown in Ref *10* that after a void has been nucleated it takes a certain amount of time before the normal stress acting across a grain boundary during the compressive half of the symmetric loading cycle becomes equal to the normal stress during the tensile half. While this period of unbalanced stress persists a void can experience a very rapid net growth. The two columns of $\dot{v}_{th}$ have been calculated on the assumption that the cavities experience (*1*) no stress caused by surface energy forces or the pressure of gas trapped in the voids, and (*2*) a mean sintering stress equal in magnitude to the amplitude of the cyclic stress. As discussed in Refs *10* and *17*, the value of $\dot{v}_{exp}$ might reasonably be expected to lie somewhere within these estimates. It can be seen that for both copper and copper-aluminum the agreement between theory and experiment is quite acceptable. The observed time dependence of

$\dot{\nu}_{exp}$ is similar to the predicted behavior, and the numerical coefficients, with the exception of copper and copper-aluminum tested under conditions leading to the high density of extremely small voids, are similar to the theoretical values. These results are strong evidence that the small ($< \sim 0.1$ μm radius) fatigue-induced cavities in copper and copper-aluminum which scatter neutrons grow by vacancy diffusion, not by plastic deformation. This finding is in agreement with HVEM observations on fatigue cavities in these two materials [*19,34*].

A complicating factor in the study of cavitation in very pure metals is the extreme mobility of the grain boundaries. The grains change both their size and their shape under the stimulus of fatigue at elevated temperatures [*37*]. A diamond grain configuration, in which most of the boundaries are oriented for maximum shear, develops within a few minutes in pure copper fatigued under the conditions of the present experiment [*36*]. A cavitated boundary which migrates may leave some of its voids behind in the matrix, where they slowly shrink under the influence of surface forces (Fig. 10). Strings of small cavities within the matrix which paralleled a nearby boundary were observed frequently in HVEM studies of the fatigued copper [*34,38*]. The negative

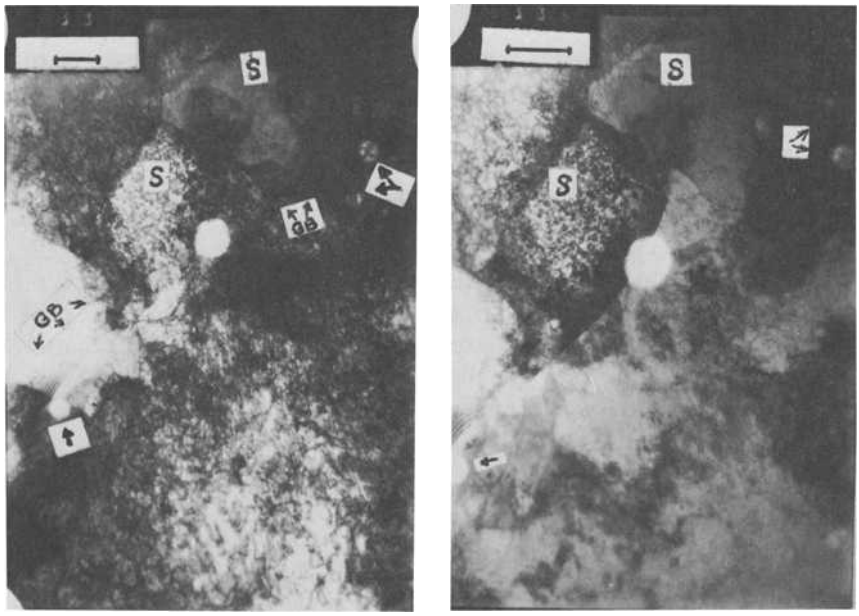

FIG. 10—*HVEM micrographs showing spherical cavities (arrows) near a grain boundary (GB). Two small subgrains (S) also can be observed. The diffraction condition was varied between the two micrographs in order to show the GB location more clearly. The specimen is Cu-2.2Al (5 at. % Al) fatigued at 420°C and 17 Hz in reverse bending. The marker indicates 0.5* μm. From *Ref* 34. *(Micrographs taken at the Argonne National Laboratory.)*

growth of these abandoned cavities will affect the value of $\dot{v}$ calculated from the SANS data. This point is discussed in Ref *18*.

Grain boundary motion (especially sliding) also has a marked effect on cavity nucleation [*37*]. If the motion involves migration as well, the more rapidly a grain boundary moves the larger are the number of cavities left in the matrix. All the values for V_f and N_T given in this paper have been "normalized" to a 60 μm grain size; that is, they have been scaled to take into account the variation with grain size of grain boundary area per unit volume of material. However, the normalization does not correct for the effect on cavitation of variations in grain boundary mobilities. Page [*27*] observed some irregularities in the scattering curve of copper fatigued at 567°C. The copper-aluminum specimen fatigued at 480°C for 2100 s (Fig. 2) appears to have a smaller void volume fraction than the specimen tested for 600 s. Both the copper and copper-aluminum specimens which showed anomalous scattering behavior were found to contain a number of very large grains after fatiguing. From Figs. 5 and 6 it can be seen that, for most of the specimens fatigued at the lowest stress level (20.7 MPa), the size distribution of the cavities was narrow and peaked at a very small void diameter. Similar size distributions were found in most of the specimens fatigued at the slowest cycling frequency (Figs. 8 and 9). Metallographic examination revealed that the grain growth during fatigue in many of the specimens containing a population of very small voids was significantly less than in specimens with the usual void size distribution. This correlation between grain growth and void size was especially strong in the case of samples fatigued at the low stress amplitude. In view of the examples just cited it is evident that grain boundary mobility has a strong influence on void nucleation and growth. The grain growth during fatigue in apparently similar specimens can differ markedly. It appears, therefore, that there is an element of uncertainty in the actual extent of cavitation which will be produced in a given material, even though the usual test parameters such as temperature, fatiguing variables, material purity, and processing history are well specified. Note that it is unlikely that the detailed information on the variability of cavitation behavior would be obtained by any currently available measuring technique other than SANS.

Summary

1. High-temperature fatigue produces a marked increase in the small-angle neutron scattering from specimens of pure copper and a Cu-7Al alloy. This increase can be attributed to the presence of fatigue-induced grain boundary cavities.

2. The SANS data have been used to calculate void volume fraction as a function of fatigue time under a number of test conditions. Void volume fractions at least as small as 10^{-6} can be measured. The presence of cavities can be detected after a few seconds of fatiguing. Small-angle neutron scattering

is a sensitive, nondestructive method for assessing fatigue damage when it occurs in the form of cavitation. In model systems SANS provides detailed information which can be used to study the mechanisms of grain boundary cavitation.

3. The growth rate of individual voids was calculated from values of the void volume fraction and the number density of cavities (obtained from the scattering data). In the case of both copper and copper-aluminum the growth of the voids is very transient. Good agreement is found between the growth rates obtained from the scattering data and rates predicted by a theory of fatigue-induced cavitation.

4. Pure copper and the copper-aluminum alloy show opposite responses to the effect of fatigue temperature on cavitation. An increase in the temperature of fatigue produces an increase in the total void volume growth rate and void nucleation rate in the case of copper, a decrease in copper-aluminum.

5. Cavitation is strongly influenced by movement of the grain boundaries. Grain boundary migration can cause cavitated boundaries to leave some of their voids behind in the matrix. The size distribution of voids found in fatigued samples is related to the extent of grain growth during fatigue. A population of very small voids was found in samples which experienced little grain growth.

Acknowledgments

The HVEM study was carried out at the Argonne National Laboratory. We are grateful to Dr. A. Taylor and Mr. A. Philippides for their expert assistance.

We wish to acknowledge the invaluable help of B. R. Weertman with the SANS measurements carried out at the Institut Laue-Langevin.

Extensive use was made of the facilities of Northwestern University's Materials Research Center, funded by the NSF-MRL program.

This research was supported by NSF-MRL Grant DMR-7923573, NSF Grant DMR-7826026, and the government of Mexico.

References

[1] Hull, D. and Rimmer, D. E., *Philosophical Magazine*, Vol. 4, 1959, pp. 673-687.
[2] Speight, M. V. and Harris, J. E., *Metal Science Journal*, Vol. 1, 1967, pp. 83-85.
[3] Raj, R. and Ashby, M. F., *Acta Metallurgica*, Vol. 23, 1975, pp. 653-666.
[4] Dobeš, F. and Čadek, J., *Scripta Metallurgica*, Vol. 4, 1970, pp. 1005-1008.
[5] Hancock, J. W., *Metal Science*, Vol. 10, 1976, pp. 319-325.
[6] Beere, W. and Speight, M. V., *Metal Science*, Vol. 12, 1978, pp. 172-176.
[7] Weertman, J., *Metallurgical Transactions*, Vol. 5, 1974, pp. 1743-1751.
[8] Skelton, R. P., *Philosophical Magazine*, Vol. 14, 1966, pp. 563-572.
[9] Trinkaus, H., *Scripta Metallurgica*, Vol. 15, 1981, pp. 825-828.
[10] Weertman, J. R., *Canadian Metallurgical Quarterly*, Vol. 18, 1979, pp. 73-81.
[11] Boettner, R. C. and Robertson, W. D., *Transactions of the Metallurgical Society of AIME*, Vol. 221, 1961, pp. 613-622.

[12] Gittins, A., *Metal Science Journal*, Vol. 1, 1967, pp. 214-216.
[13] Miller, D. A. and Langdon, T. G., *Metallurgical Transactions* A, Vol. 11A, 1980, pp. 955-962.
[14] Rozenberg, V. M., Shalimova, A. V. and Zvereva, T. S., *Fiz. metal. metalloved.*, Vol. 25, 1968, pp. 326-332.
[15] Argon, A. S., Chen, I. W., and Lau, C. W. in *Creep-Fatigue Environment Interactions*, R. M. Pelloux and N. S. Stoloff, Eds., The Metallurgical Society of AIME, Warrendale, Pa., 1980, pp. 46-85.
[16] Saegusa, T., Weertman, J. R., Cohen, J. B., and Roth, M., *Journal of Applied Crystallography*, Vol. 11, 1978, pp. 602-604.
[17] Page, R., Weertman, J. R., and Roth, M., *Scripta Metallurgica*, Vol. 14, 1980, pp. 773-777.
[18] Page, R., Weertman, J. R., and Roth, M., *Acta Metallurgica*, Vol. 30, 1982, pp. 1357-1366.
[19] Page, R. and Weertman, J. R., *Acta Metallurgica*, Vol. 29, 1981, pp. 527-535.
[20] Weertman, J. R. in *Nondestructive Evaluation: Microstructural Characterization and Reliability Strategies*, O. Buck and S. M. Wolf, Eds., The Metallurgical Society of AIME, Warrendale, Pa., 1981, pp. 147-168.
[21] Saka, H., Sueki, Y., and Imura, T., *Philosophical Magazine*, Vol. 37A, 1978, pp. 273-289.
[22] Epperson, J. E., Kostorz, G., Ortiz, C., Fürnrohr, P., and Gerstenberg, K. W., *Acta Metallurgica*, Vol. 27, 1979, pp. 1363-1372.
[23] *Treatise on Materials Science and Engineering*, Vol. 15, *Neutron Scattering*, G. Kostorz, Ed., Academic Press, New York, 1979.
[24] Guinier, A. and Fournet, G., *Small-Angle Scattering of X-Rays*, Wiley, New York, 1955.
[25] Guinier, A., *Ann. Phys.* (Paris), Vol. 12, 1939, pp. 161-237.
[26] Porod, G., *Kolloid Z.*, Vol. 125, 1952, pp. 51-57, 109-122.
[27] Page R., "High Voltage Electron Microscopy and Small-Angle Neutron Scattering Investigation of Grain Boundary Cavitation in High Purity Copper," Ph.D. thesis, Northwestern University, Evanston, Ill., 1980.
[28] Cabañas-Moreno, J., "A Study of Grain Boundary Cavitation in Copper-Aluminum Alloys by Small-Angle Neutron Scattering and High Voltage Electron Microscopy," Ph.D. thesis, Northwestern University, Evanston, Ill., 1982.
[29] Yang, M., Weertman, J. R., and Roth, M., to be published.
[30] Gerold, V. and Kostorz, G., *Journal of Applied Crystallography*, Vol. 11, 1978, pp. 376-404.
[31] Fedorova, I. S. and Schmidt, P. W., *Journal of Applied Crystallography*, Vol. 11, 1978, pp. 405-411.
[32] Vonk, C. G., *Journal of Applied Crystallography*, Vol. 9, 1976, pp. 433-440.
[33] Glatter, O., *Journal of Applied Crystallography*, Vol. 13, 1980, pp. 7-13.
[34] Cabañas-Moreno, J. and Weertman, J. R., to be published.
[35] Murr, L. E., *Scripta Metallurgica*, Vol. 6, 1972, pp. 203-208.
[36] Saegusa, T. and Weertman, J. R., *Scripta Metallurgica*, Vol. 12, 1978, pp. 187-191.
[37] Westwood, H. J. and Taplin, D. M. R., *Metallurgical Transactions*, Vol. 3, 1972, pp. 1959-1965.
[38] Page, R. and Weertman, J. R., unpublished results.

DISCUSSION

J. T. Fong[1] (*written discussion*)—When a fatigue test at a high temperature is interrupted to allow SANS to probe the voids in the specimen at am-

[1]National Bureau of Standards, Washington, D.C. 20234.

bient temperature, is it obvious that the state of microstructure is unaffected by the cooling that is necessary for this experiment?

J. G. Cabañas-Moreno et al (authors' closure)—There may be some shrinkage of voids driven by surface tension forces as a specimen cools. (The load was removed during cooling.) However, the cooling rate is very rapid just after the power to the furnace is turned off. If the growth of the grain boundary voids takes place by a vacancy diffusion mechanism (and there is much evidence that it does), a modest drop in temperature will greatly slow down this activated process. Thereafter, even if the specimen cools very slowly, little further change in void size will take place. We do not know what other microstructural changes might occur which would contribute to the small angle scattering. Certainly the scattering from any dislocations generated or lost would be negligible compared with that from the voids.

E. E. Underwood[2] *(written discussion)*—Other than to compliment the authors on a beautiful piece of work, well-done, I wonder if the analysis published by DeHoff on the "Growth Path Envelope" would be of interest.[3] This analysis was developed for the determination of the time variation of the geometry of particles in a structure. Although DeHoff dealt with particles of known shape, the spherical voids obtained in the present study are completely equivalent to particles in this case.

Briefly, DeHoff derives a simple relationship between the particle size distribution function at any time and functions of the nucleation and growth rates. Using a graphical technique, the time dependence of the volume fraction, surface area, and total curvature can be calculated and compared with experiment.

J. G. Cabañas-Moreno et al (authors' closure)—Thank you for the comment and the suggestion. No, we did not know of DeHoff's analysis, but we shall certainly look into it.

A. K. Chakrabarti[4] *(written discussion)*—Did you experimentally observe the number and size of the vacancies present in the copper and copper-aluminum alloys after heating up, holding for 1 h, and cooling down (without any fatigue, as a check on the effect of temperature on the base material vacancy concentration)? Could there be a number of vacancies already present in the base material, so that as one applies fatigue cycles the already present vacancies would start growing to accommodate the damage? Would diffusion at 350

[2]Chemical Engineering/Metallurgy, Georgia Institute of Technology, Atlanta, Ga. 30332.

[3]DeHoff, R. T., *Metallurgical Transactions*, Vol. 2, 1971, p. 521.

[4]Materials Research and Engineering, Detroit Diesel Allison, Division of General Motors Corporation, Indianapolis, Ind. 46206.

to 450°C in copper be fast enough to grow vacancies on the order of 100 Å in 15 s?

J. G. Cabañas-Moreno et al (authors' closure)—With our method of measurement it is not possible to determine the number and size of the voids present in a sample which simply was heated without load for an hour, then cooled. (We assume that by the term "vacancy" you mean vacancy cluster, that is, void.) After our specimens were machined all of them were annealed in purified argon at 500°C for 8 h, then slowly cooled. Scattering from one of these unfatigued specimens was subtracted from the scattering of each of the fatigued samples in order to eliminate the scattering from causes other than voids. It is from this *difference* in scattering that the void volume fraction, void size distribution, etc., are calculated.

It is possible but very unlikely that the samples contained any nucleated voids before fatiguing began. The samples were completely recrystallized after machining. Whatever the nucleation mechanism is, it must be very fast. Extrapolation of void volume fraction versus fatigue time back to zero fatigue time shows no measurable incubation time. (Such curves are shown in Ref *18* of our paper.)

It is difficult to answer the last part of this question. Firstly, it is necessary to know the initial size of the void. For example, if the nucleation mechanism consists of voids opening up at ledges in sliding grain boundaries, the initial void size will be on the same order of magnitude as the ledge height. Secondly, the magnitude of the stress driving the diffusion must be specified. Then the effect of surface tension forces must be considered. Finally, the mechanism of growth must be specified. The transient growth model described in Ref. *10* of our paper and mentioned by us in the present work has been used to calculate the rate of growth of individual voids in material fatigued under conditions which led to observable voids in 15 s (stress amplitude = 34 MPa, temperature = 567°C, cycling frequency = 17 Hz). These rates of growth, calculated with the assumption of (*1*) zero surface forces, and (*2*) surface forces equal in magnitude to the stress amplitude, are given in Table 2. It can be seen that, in either case, in 15 s the predicted growth in volume is greater than the volume of a 100-Å sphere.

H. Mughrabi[5] *(written discussion)*—At the moment I am very impressed by the new data that you have presented. I recall that a while ago a paper by Kettanen, Lepisto, and Kostorz appeared in which they presented low-angle neutron scattering on copper crystals fatigued at room temperature.[6] These authors concluded that little void-like vacancy agglomerates exist in fatigued

[5]Max-Planck-Institut für Metallforschung, Institut für Physik, Stuttgart, Federal Republic of Germany.

[6]*Acta Metallurgica*, Vol. 29, 1981, pp. 969-972.

single crystals, though the mean defect diameter of $\approx$ 2 nm inferred by these authors appears to be outside the diameter distribution you studied. Could you please comment? Furthermore, I should like to ask your opinion regarding the use of positron lifetime studies as a further technique to investigate void deformation.

J. G. Cabañas-Moreno et al (authors' closure)—We hope you continue to be impressed! We were very interested in the paper by Kettanen et al when it came out. The voids they studied appear to be far smaller than those we found in our copper fatigued at elevated temperature. In fact the size of the voids they deduced from their SANS measurements put them at the limit of this experimental technique, and the difference in scattering between their heavily and lightly fatigued samples was just above the noise level.

We had already done a rather similar experiment early in our SANS measurements. It is briefly described in our present paper. We compared the scattering from a single crystal of copper fatigued for 3.6×10^6 cycles at 405°C (one half the melting temperature), 17 Hz, and strain amplitude of 0.035%, with the scattering from a similar but unfatigued copper single crystal. The difference in scattering from the two crystals was negligible—just at the noise level. We performed this experiment with the single crystals to make sure that the observed increase in scattering with high-temperature fatigue in polycrystalline crystals really *is* associated with grain boundaries.

I believe that positron annihilation measurements are most useful when the voids are very small, a few nanometres or less in diameter. Thus positron annihilation could be a valuable complement to SANS in the study of voids.

H. Mughrabi (written discussion)—As a trained physicist, I find the variation of certain mechanisms as a function of characteristic parameters such as temperature most illustrative. We have not heard much about low-temperature fatigue at this conference, but certain aspects of high-temperature fatigue have been presented. You have described to us in detail the rapid development of small cavities at the grain boundaries during high-temperature fatigue of copper, but have not explained what role these *small* cavities play in the failure process. I should appreciate your comment on that. In the presentation of Drs. Manson and Halford, on the other hand, it was clear that the much larger cavities they saw with conventional optical microscopy did cause grain boundary fatigue cracking. The question I have here relates to the differences in lifetime for the cp-mode in air and in vacuum, respectively. In the cp-mode the grain boundaries are strongly cavitated throughout the material, presumably regardless of the environment. If this is so, it is surprising to me that the fatigue lifetime in vacuum is so significantly larger than in air, as shown by Drs. Manson and Halford, since the specimens are thoroughly fatigue damaged over the entire cross section in either case. Or do

you perhaps find that, while a significant difference exists, other fatigue modes (for example, pc) exhibit an even larger difference in fatigue lifetimes in air and in vacuum?

J. G. Cabañas-Moreno et al (authors' closure)—A variety of fates appears to await the grain boundary cavities once they are nucleated in the copper samples during high-temperature fatigue. Because of the extreme mobility of the boundaries many of the voids are left behind in the matrix by the rapidly migrating boundaries. These voids do not grow any further (rather they probably shrink as the result of surface tension) and it is not expected that such voids contribute to failure. Of the voids which remain on boundaries a certain fraction are located at points of stress concentration (for example, a serration on the boundary), and these voids continue to grow until they coalesce with their neighbors. Analysis of the stress field in the vicinity of a grain boundary void in material subjected to high-temperature fatigue shows that large normal stresses appear close to the tips of the voids (see Ref *10* of our paper). Such stresses are likely to nucleate additional voids in the close neighborhood of the original void. Thus nucleation is continuous and the voids do not have to grow to such a large size before they coalesce. (Such stringers of voids have been observed in the TEM. See Ref *19* of our paper.)

In summary, it appears that a significant fraction of the small voids detected by SANS in the fatigued copper actually do *not* contribute to the failure process. The situation will be different in a material with less mobile grain boundaries.

William J. Baxter[1]

Oxide Films: Quantitative Sensors of Metal Fatigue

REFERENCE: Baxter, W. J., **"Oxide Films: Quantitative Sensors of Metal Fatigue,"** *Fatigue Mechanisms: Advances in Quantitative Measurement of Physical Damage, ASTM STP 811*, J. Lankford, D. L. Davidson, W. L. Morris, and R. P. Wei, Eds., American Society for Testing and Materials, 1983, pp. 115-136.

ABSTRACT: An electrochemical technique is described that images and quantitatively measures the distribution and severity of fatigue damage. The technique is based upon (*1*) the creation of microcracks in a surface anodic oxide film during fatigue of the underlying metal, and (*2*) the detection of these microcracks by contacting the surface with a gel electrode. When a voltage pulse is applied, current passes through the fatigue-induced microcracks in the oxide film. An image of the sites of current flow is retained in the surface of the gel, while the total charge flow is a measure of the extent of rupture of the oxide film. The capabilities of the technique are illustrated by measurements on aluminum alloys. The distribution of surface fatigue damage may be mapped as early as 1% of the fatigue life, while fatigue cracks $\geq$ 10 μm long are easily imaged.

KEY WORDS: metal fatigue, microcracks, oxide films, gel electrode

A quantitative measure of the development of fatigue damage in metals could provide the basis of an abbreviated testing technique for the prediction of fatigue life. This would permit rapid design iteration, with the conventional and time-consuming procedure of testing to failure being reserved for final validation. But the measurement of fatigue damage is an old problem which has resisted the efforts of many investigators employing a variety of techniques [*1*].[2] This paper describes a simple electrochemical technique, hereafter referred to as *gel electrode*, in which an adherent surface oxide film essentially functions as a discriminator. The surface oxide film is formed prior to the application of the fatigue loading; during the early stages of a fatigue test "damage" accumulates in the underlying metal and produces micro-

[1]Senior Staff Research Scientist, Physics Department, General Motors Research Laboratories, Warren, Mich. 48090.

[2]The italic numbers in brackets refer to the list of references appended to this paper.

cracks in the oxide film. After fatigue loading the density and distribution of the microcracks are measured and imaged with the gel electrode.

The fatigue-induced rupturing of thin surface oxide films was first studied extensively by the exoelectron method [*2,3*] that is, by the photoelectrons which are emitted preferentially from the metal surfaces freshly exposed by the microcracks in the surface oxide film. The intensity of the exoelectron emission from localized regions was found to provide a quantitative measure of the severity of the fatigue deformation in those regions. Deformation was detected as early as ~1% of the fatigue life, and the fatigue life could be predicted for a range of cyclic stress amplitudes. The technique was restricted, however, by the need to perform the fatigue test in a vacuum to prevent reoxidation of the microcracks.

The gel electrode method [*4,5*] does not suffer from this drawback, so fatigue testing may be performed under normal atmospheric conditions. The procedure is a modified version of a technique developed by Klein [*6*] for the study of defective sites in anodic oxide films. The microcracks in the oxide are detected by contacting the specimen with a dried surface film on a gel-electrolyte, containing potassium iodide (KI) and starch, and applying a voltage pulse to stimulate a corrosion current which flows preferentially to the microcracks. This current anodically oxidizes the KI to release iodine ions, which react with the starch to form a black complex. These complexes are retained in the skin of the gel and provide an accurate spatial representation of the sites of the microcracks in the oxide film, that is, the sites of fatigue damage.

The initial investigations of this new technique were confined to the imaging of fatigue cracks in 6061-T6 aluminum [*4*], and the detection of fatigue deformation in 1100-0 aluminum [*5*]. This paper illustrates the more general applicability of the technique with results from 7075-T6, 2024-T4 and T3, 6061-T6 and 1100-0 aluminum. Two regimes of application of the technique are described:

1. Images produced by short current pulses (10 ms) provide good spatial resolution but low sensitivity. Nevertheless, fatigue cracks only 10 μm long are detected, and the charge flow during image formation is a measure of the crack length.
2. Long current pulses (5 s) overexpose the image, but increase the sensitivity so that fatigue deformation is measured as early as 0.2% of the fatigue life. This sensitivity surpasses the capabilities of optical and scanning electron microscopy.

The Oxide Film

For the surface oxide to function as a reliable and quantitative discriminator of fatigue of the underlying metal, the fracture properties of the

film must be consistent and reproducible from specimen to specimen. Experience with the exoelectron method [*7-9*] has established that, for aluminum alloys, consistent results may be obtained by establishing a standard specimen preparation procedure and controlling the oxide thickness by the voltage applied during anodization. (For details see next section.)

The choice of oxide thickness is a compromise. Thick oxides (~ 100 nm) are not well suited because they rupture independently of the microstructural details of the deformation in the substrate metal [*8*]. On the other hand, the gel electrode method requires that the oxide thickness must be greater than that of the natural oxide (4 nm) which spontaneously reforms in the fatigue-induced microcracks. This condition ensures that during gel electrode imaging, the electrically driven corrosion currents will pass primarily through the thin oxide in the microcracks and not elsewhere. In these experiments, an oxide thickness of 14 nm was selected. While such an oxide can suppress some of the surface fatigue deformation in soft 1100-0 aluminum [*9*], it nevertheless develops microcracks which are intimately related to the deformation accumulated in the substrate metal. This is illustrated by the micrographs in Fig. 1, which were obtained with a photoelectron microscope [*10*]. In these micrographs the sources of exoelectrons appear as white regions and demonstrate the systematic increase in the density of microcracks with continued fatigue cycling. This series of micrographs is a clear demonstration of the role of the oxide film as a discriminator of the accumulation of fatigue deformation in the substrate metal.

Experimental Procedure

The procedure consists of three steps: (*1*) specimen preparation including anodization to produce a surface oxide film 14 nm thick, (*2*) fatigue cycling of the specimen, and (*3*) gel electrode printing of the microcracks in the oxide film.

Specimen Preparation

Specimens of 7075-T6, 6061-T6, 2024-T3 and 1100-0 aluminum were machined from sheet material 1.5 mm thick to produce a conventional tapered bending fatigue specimen. When the sole experimental objective was to image fatigue cracks, a small notch was filed in one edge to accelerate the process of crack initiation. The specimens of 2024-T4 aluminum were machined from 10-mm-diameter rod to form a gage section of 6.5 mm diameter and 30 mm long. Some of the specimens were mechanically polished to aid subsequent examination by optical and scanning electron microscopy, but polishing is not necessary for successful gel electrode imaging. The other specimens were cleaned in chromic acid at 70°C. All specimens were then an-

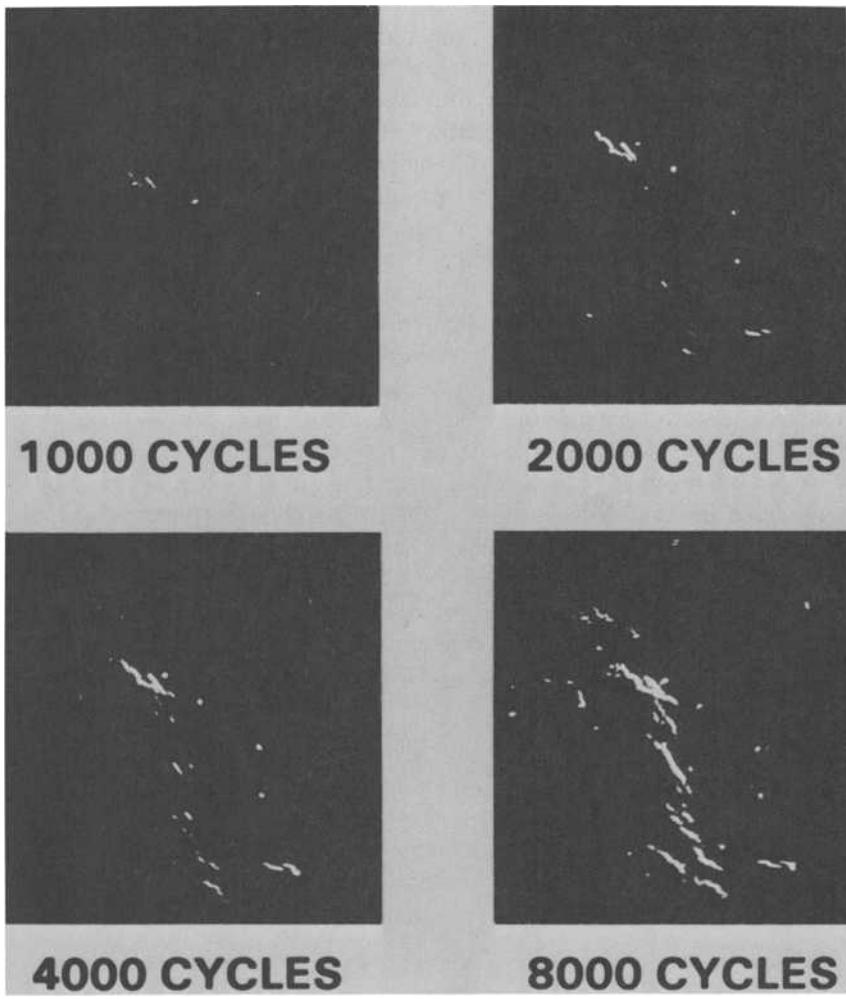

FIG. 1—*Photoelectron micrographs of the same region of a specimen of 1100 aluminum as a function of the number of fatigue cycles. The white regions (exoelectrons) define the development of microcracks in the 14-nm oxide film.*

odized in a 3% solution of tartaric acid at a potential of 10 V to form a surface oxide film 14 nm thick [*11*].

Fatigue Cycling

The flat sheet specimens were fatigued by reverse bending and required $\sim 10^5$ cycles to initiate a fatigue crack at the notch. In the absence of a notch the strain amplitude was increased to cause failure after $\sim 10^5$ cycles. The

cylindrical specimens of 2024-T4 aluminum were fatigued in torsion to produce a surface cyclic strain of $\pm 6.5 \times 10^{-3}$.

Gel Electrode Imaging

The electrolyte consists of an agar gel containing 0.2*m* potassium iodide, 0.05*m* borax, and 30 g of starch per litre. For most of the experiments, this warm fluid mixture was dispensed into small lengths (~ 3 cm) of plastic tube 6 mm in diameter. The plastic tube was over-filled so that, upon cooling, the liquid formed a smooth hemispherical gel tip at one end of the tube (Fig. 2). A piece of aluminum wire was sealed into the other end of the tube to serve as a cathode. In approximately 5 min a flexible skin formed on the gel tip. This tip was then pressed gently against the surface of the specimen and a pulse of negative potential was applied to the cathode.

In the case of the torsion fatigue specimens a simple and effective large-area mapping technique was developed (Fig. 3). Two pieces of white polyurethane foam were coated with a thin layer of the gel and then dried for 5 min. These flexible gel electrodes were held with the specimen sandwiched between them, the flexible gel wrapping around and contacting the entire gage section. An aluminum wire contacted the gel at the edge of the sandwich to provide a

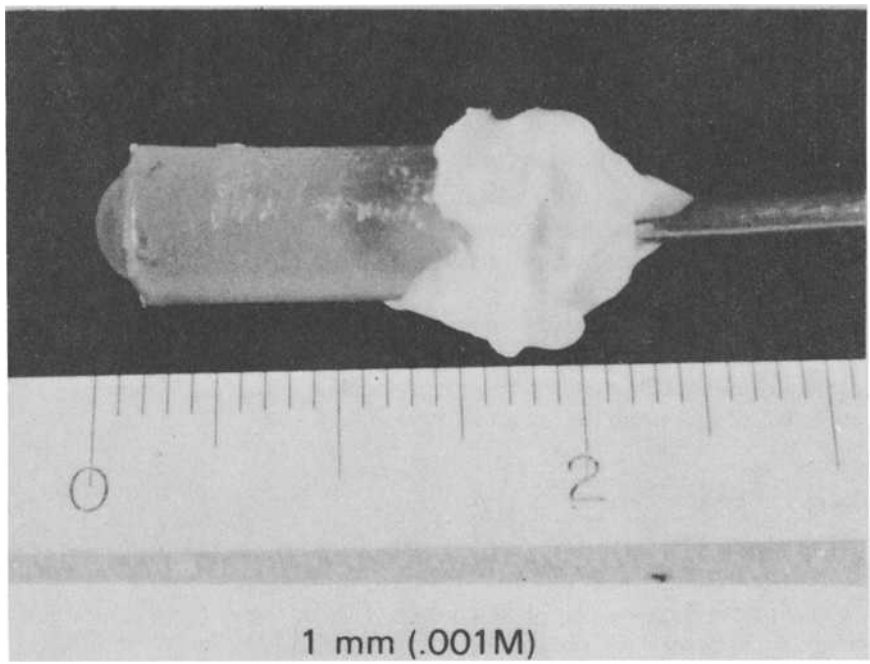

FIG. 2—*Photograph of plastic tube containing a cathode and the gel electrolyte.*

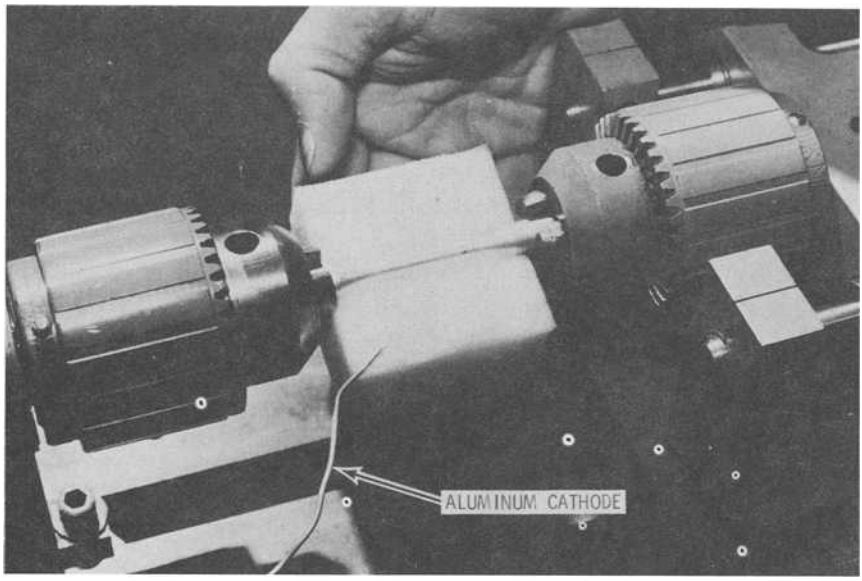

FIG. 3—*Photograph of one half of a gel electrode sandwich being held in contact with a torsional fatigue specimen. The gel coating on the polyurethane foam wraps around half of the specimen.*

cathode. Again a negative voltage pulse was applied to the cathode. In this way an image of the total surface was formed without removing the specimen from the fatigue machine.

The images formed in the skin of the gel were viewed and photographed with an optical microscope. These images were then correlated with observations of the specimens in a scanning electron microscope (SEM). The latter also provided the basis for independent measurements of the length of any fatigue cracks.

The flow of current during image formation was recorded on a Nicolet digital oscilloscope and stored on magnetic disks. This information was later displayed on an *X-Y* recorder, and the total charge flow during imaging was obtained by measuring the area under the curve.

Images of Fatigue Cracks

The sensitivity and spatial resolution attainable are determined to some extent by the charge flow, and this can be controlled by the duration of the voltage pulse. For a 10-V pulse, a duration of 100 ms consistently produces an image which is clearly visible to the unaided eye (Fig. 4), but subsequent examination of the gel with an optical microscope reveals that the image is overexposed, so that some of the more subtle features are not resolvable. A

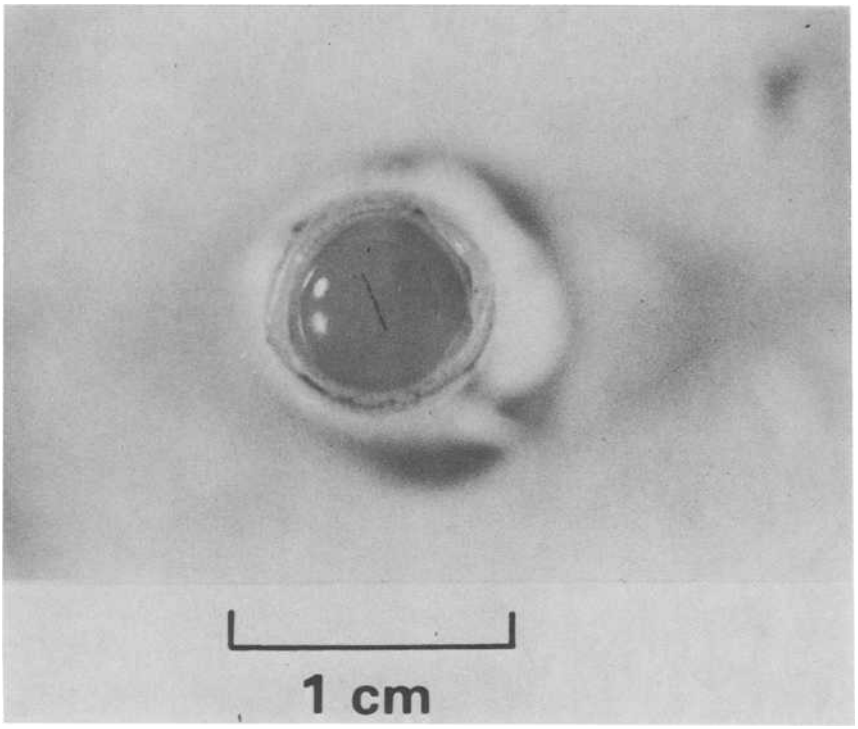

FIG. 4—*Photograph of a gel tip showing an image of a fatigue crack 1.7 mm long in a specimen of 2024-T3 aluminum. Image formed by a 10-V pulse of 100-ms duration.*

pulse of 1-ms duration produces an image with good spatial resolution, but it is so faint that it is difficult to photograph with an optical microscope. A pulse of 10-ms duration is in general the best compromise, providing an image with sufficient spatial resolution and contrast to permit direct correlation with scanning electron micrographs of the specimen itself. Unless specified to the contrary, all the images presented here were formed with 10-V pulses of 10-ms duration.

7075 Aluminum

The photograph in Fig. 5*a* shows a magnified gel electrode image of two parallel fatigue cracks in a polished specimen of 7075-T6 aluminum. This particular image is easily correlated with its mirror image in the optical micrograph of the specimen in Fig. 5*b*. The main crack is 1.1 mm long and the irregularities are faithfully recorded by the gel electrode image. More interesting is the clear resolution of the shorter crack, which is 160 μm long and is located only 20 μm away from the main crack. Note also that the scratches on the surface do not contribute to the gel electrode image.

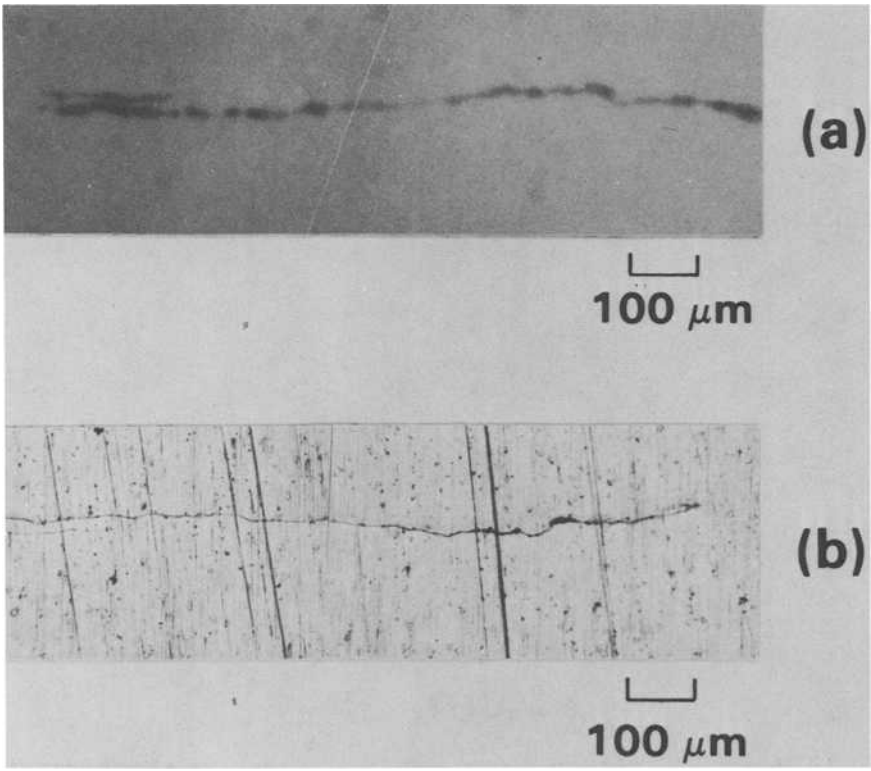

FIG. 5—(a) *Gel electrode image and* (b) *optical micrograph of two parallel fatigue cracks in 7075-T6 aluminum. Gel electrode image formed by a 10-V pulse of 10-ms duration.*

2024 Aluminum

Figure 6 shows a magnified view of a portion of a gel electrode image obtained from a torsional fatigue specimen of 2024-T4 aluminum. This image is noteworthy for its complexity, containing many distinctive features which facilitate direct correlation with microscopic examination of the specimen itself. For example, the scanning electron micrograph in Fig. 7 shows the dual nature of the main crack corresponding to the central portion of the image in Fig. 6. Note that Fig. 6 is an inverted mirror of Fig. 7. All the irregularities and secondary branches are rendered clearly visible by the gel electrode image, except where the spatial resolution is insufficient. For example, the twin cracks at location E are only separated by 15 μm, so they appear as a single, broad line in the gel electrode image. Similarly, the very broad section at location D in Fig. 6 actually results from the presence of three cracks: there is a small secondary crack between the two main cracks (Fig. 7). Another feature of interest in this gel electrode image is the large spot at location B. This

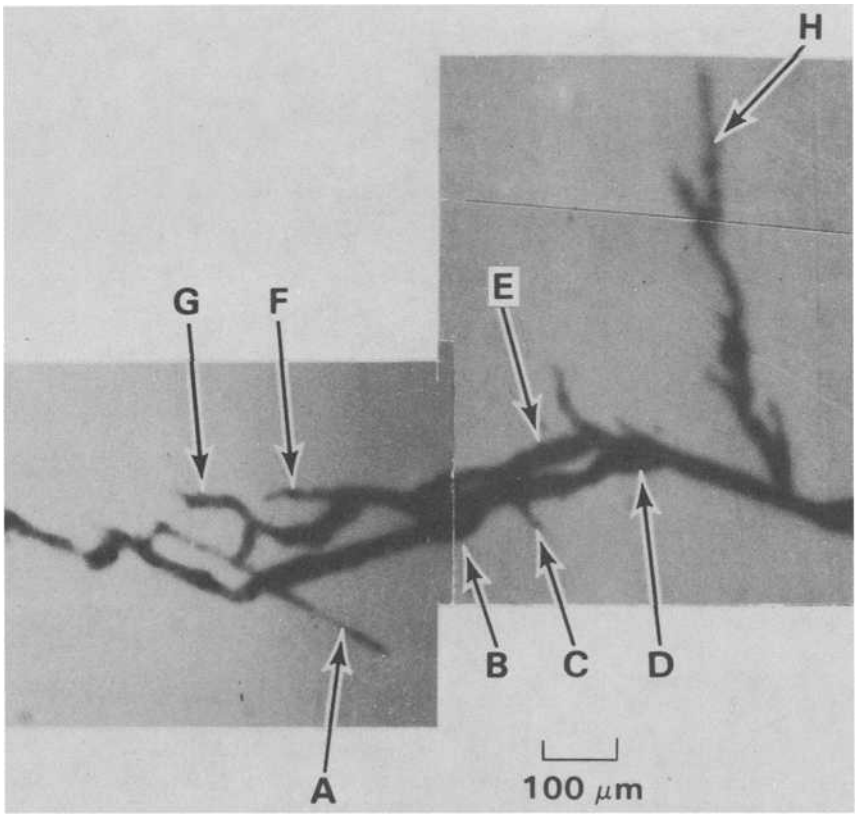

FIG. 6—*Magnified portion of a gel electrode image of a complexity of fatigue cracks in a specimen of 2024-T4 aluminum fatigued in torsion. Image formed by a 10-V, 10-ms pulse.*

resulted from the presence of a pronounced extrusion emanating from the fatigue crack (Fig. 7). This extrusion provided a localized but large area of contact with the gel.

Even though the image in Fig. 6 was formed with only a 10-ms pulse, the most subtle of secondary cracks were clearly imaged. Indeed this was just one of many instances where, without the guidance of the gel electrode image, many of the secondary cracks would have been overlooked during examination of the specimen in the SEM. For example, the micrograph in Fig. 8 shows a portion of the secondary crack corresponding to location H in Fig. 6.

The gel electrode image shown in Fig. 9*a* was obtained from the area around a notch in a specimen of 2024-T3 aluminum, and revealed that several fatigue cracks had been initiated along the edge of the notch. This situation arose because this particular specimen was too heavily etched, so that in addition to the main crack (C), which is ~280 μm long, several other small cracks grew from etch pits. For example, the feature C_1 in Fig. 9*a* was traced to the

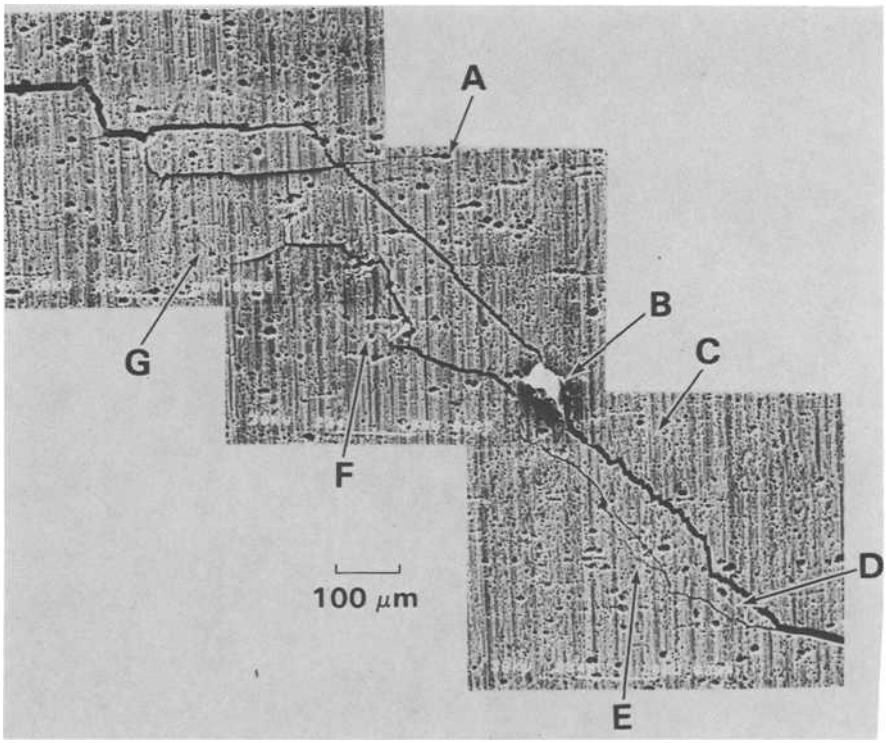

FIG. 7—*Scanning electron micrograph of the fatigue cracks in 2024-T4 aluminum corresponding to the central portion (reversed) of the gel electrode image shown in Fig. 6.*

presence of very faint hairline cracks barely discernible in the SEM (Fig. 9*b*). Each of these cracks is only ~ 10 μm in length.

If a single fatigue crack is only ~ 10 μm in length, the image formed by a 10-ms pulse is often simply a spot rather than a linear feature. While this represents the limit of resolution of an image formed in this way, it is not the limit of sensitivity, because on several occasions the fatigue damage associated with spots in the gel image could not be identified with the SEM. This aspect, namely the detection of fatigue deformation, is discussed in a later section.

Charge Flow and Crack Length

The *X-Y* recordings of three oscilloscope traces in Fig. 10 show the current transients associated with the formation of images with 10-V, 10-ms pulses. The lower current trace was obtained from a region with no fatigue cracks; after an initial rapid decay associated with charging the capacitor formed by

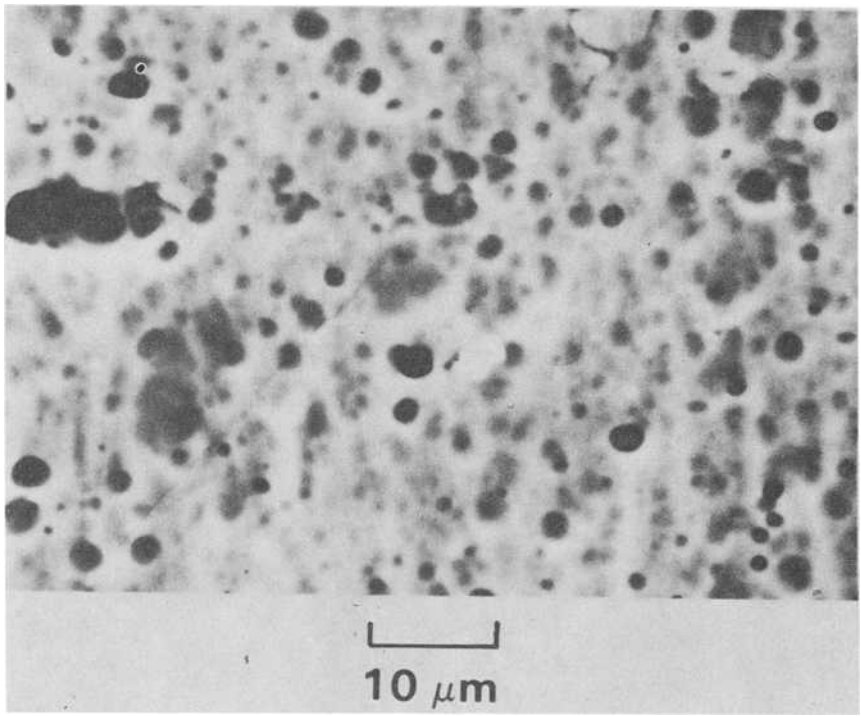

FIG. 8—*Scanning electron micrograph of the secondary crack corresponding to location H in Fig. 6.*

the gel electrode, oxide film, and metal substrate, the current stabilized at a level of $\sim 10^{-1}$ mA. The other two current traces were obtained during imaging of cracks 0.7 and 1.75 mm long. After the initial charging transient, the current stabilized at 0.48 and 1.2 mA respectively. (These currents continue at approximately these levels during imaging with 100-ms pulses.)

The total flow of charge during the formation of an image of a fatigue crack is proportional to the total length of the crack being imaged. This is illustrated in Fig. 11 by measurements on several alloys. The line drawn through the data is given by

$$Q = 1.25 \times 10^{-5} \ell \, C$$

where ℓ is the length of the crack in millimetres. Within the limits of the experimental scatter evident in Fig. 11, this result is independent of the alloy composition.

Many sources of the scatter in Fig. 11 can be understood in terms of the

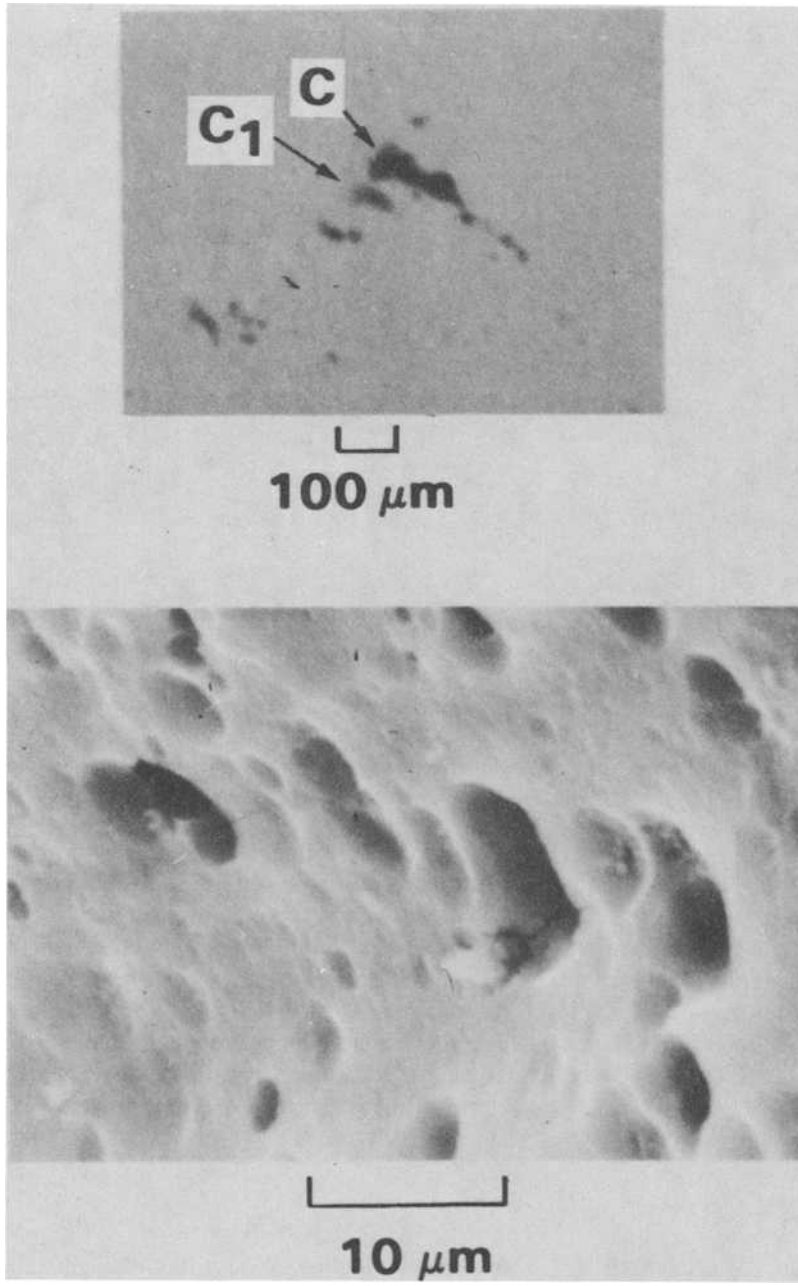

FIG. 9—(a) *Gel electrode image of several fatigue cracks initiated at a notch in a specimen of 2024-T3 aluminum. Image formed by a 10-V, 10-ms pulse.* (b) *Scanning electron micrograph of cracks responsible for feature* C_1 *in* (a).

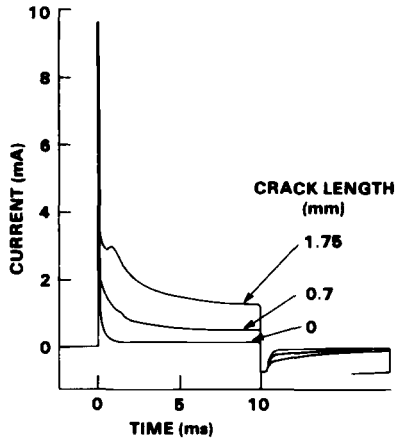

FIG. 10—*Oscilloscopic traces of the current flow during imaging of fatigue crack in 2024-T3 aluminum.*

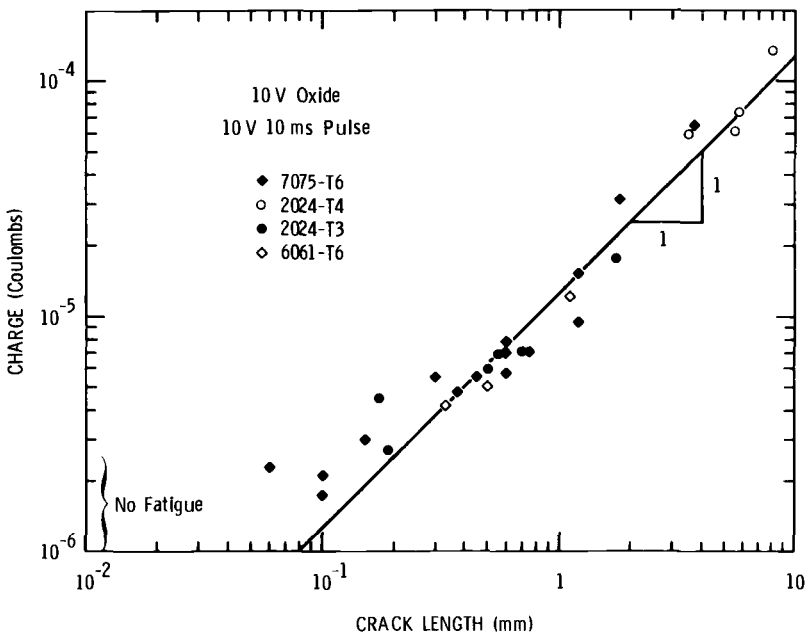

FIG. 11—*Effect of crack length on the charge flow during the formation of an image with a 10-V, 10-ms pulse.*

information contained in the images themselves. For example, the image in Fig. 6 showed that irregularities in the density of the image, which simply manifest irregularities in the current density, can arise from (*1*) variations in the width of a crack, (*2*) the presence of extrusions, and (*3*) the extent of secondary cracking. If the latter is at all extensive, as in Fig. 6, then this also introduces errors in the measurement of total crack length.

The apparent deviation from linearity in Fig. 11 for cracks shorter than ~ 200 μm is due primarily to the flow of current to locations other than the crack itself. For example, the conductive gel tip typically contacts an area of 0.13 cm^2 of the oxide coated surface of the metal, forming a capacitance of ~ 0.1 μF. Thus, even in the absence of any fatigue cracks, when a 10-V pulse is applied 10^{-6} C will flow to charge up this capacitance. This factor alone can account for most of the aforementioned deviation from linearity.

It should also be noted that the recorded values of charge flow to regions without fatigue cracks can vary from specimen to specimen, as indicated by the bracket (lower left) in Fig. 11. This variation is believed to arise from imperfections in the oxide film, which permit small leakage currents to flow. (The original problem investigated by Klein [*6*].) The presence of these unpredictable currents limits the sensitivity of charge flow measurements for the detection of fatigue cracks. Thus experience to date indicates that cracks ≥ 200 μm long can be reliably detected by charge flow measurements. On the other hand, the images themselves do not suffer from this limitation, since a small uniform charge flow does not create a visible image. Thus, as demonstrated in the previous section, image inspection by optical microscopy can definitely reveal the presence of fatigue cracks as short as 10 μm.

Measurement of Fatigue Deformation

The purpose of this series of experiments was to evaluate the ultimate sensitivity provided by a 14-nm oxide film in combination with gel electrode imaging. One limitation was that relatively little current should pass through the intact regions of the 14-nm oxide film. On the basis of preliminary measurements on nonfatigued specimens a 5-V, 5-s pulse was selected as appropriate.

Surveys of Damage Distribution

All the specimens were fatigued by reverse bending and had the conventional tapered geometry designed to provide a uniform distribution of surface strain along the gage section. Each specimen was surveyed along the length of each side by contacting a series of gel tips at intervals of ~ 5 mm along the center line, as illustrated schematically in Fig. 12*a*. The oscilloscope traces in Fig. 12*b* show the current flow to the gel tips at the locations specified in Fig. 12*a* for a specimen of 1100-0 aluminum which had been fatigued for

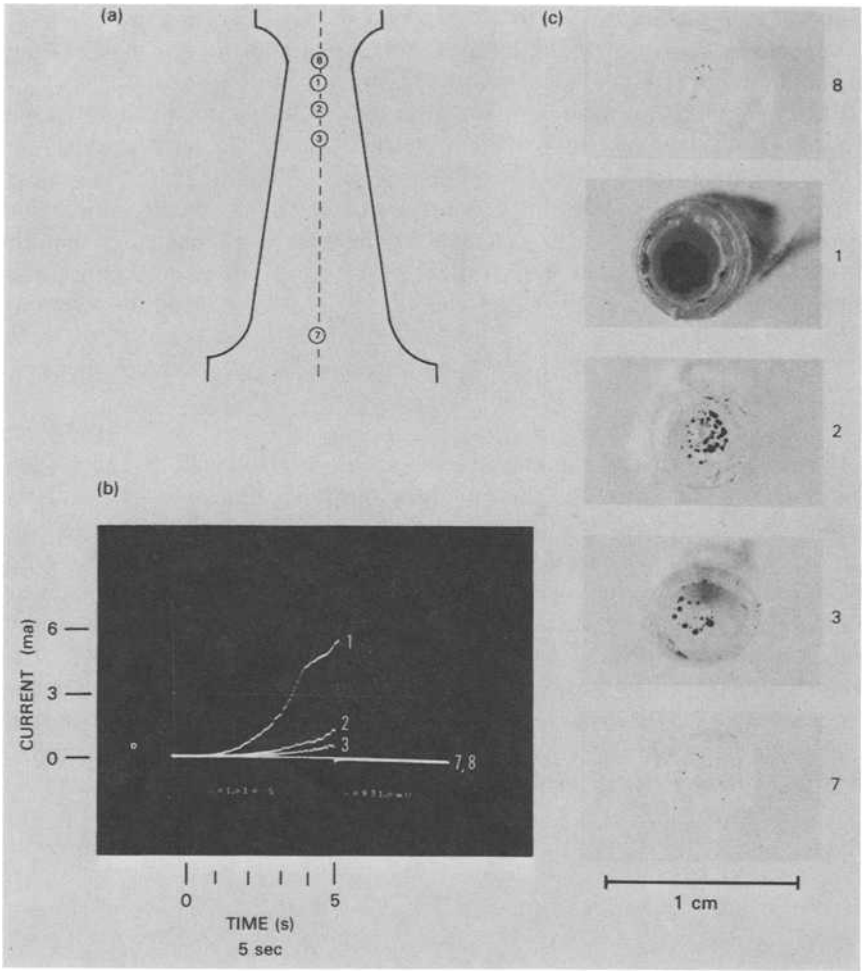

FIG. 12—*Gel electrode measurements with a 5-V, 5-s pulse on a specimen of 1100-0 aluminum fatigued for 10^4 cycles ($\approx 10\%$ of fatigue life).* (a) *Specimen geometry showing locations of gel tip contact.* (b) *Oscilloscopic traces of current flow at these locations.* (c) *Gel tips after imaging.*

10 000 cycles ($\approx 10\%$ of life). It should be noted that on the time scale shown in Fig. 12*b* the initial charging transient and constant current regimes (see Fig. 10) are not resolved. Instead, the current appears simply to increase with time, and during this stage the total charge flow is very much greater than that which flows during the initial 10 ms.

The appearance of the gel tips is illustrated by the photographs in Fig. 12*c*. The images are obviously severely overexposed and consist simply of a distribution of black spots. The density of these spots, however, does correlate with the magnitude of the current flow, and both depict a definite,

nonuniform distribution of surface fatigue damage. The damage is most severe at location 1, where there has been the greatest disruption of the 14-nm oxide, permitting the largest flow of charge during imaging.

The longitudinal distribution of charge flow is usually quite similar on the two surfaces of the specimen. This is illustrated in Fig. 13 for a specimen of 6061-T6 aluminum fatigued for only 10^3 cycles. (To convert the measured charge flow to charge density, the area of contact was determined from the corresponding image on the gel tip.) Although this specimen was at only $\sim 0.7\%$ of its fatigue life, the distribution of fatigue damage is clearly defined, and the maximum value of charge density is $\sim \times 10$ the background value for nonfatigued regions.

Severity of the Deformation

The density of charge flow increases substantially with additional fatigue cycling. This is also true for the density of spots that develop on the gel tips, which provide a good visual indication of the severity of the fatigue. This is illustrated by the photographs in Fig. 14, which show the appearance of a series of tips after imaging the region of most severe fatigue damage (that is, maximum charge flow) in a series of specimens of 6061-T6 aluminum fatigued by different amounts. Even in the absence of fatigue, a few spots always develop, varying in number from specimen to specimen, or from region to region of the same specimen. These spots are believed to be associated with the presence of defects in the 14-nm oxide film (that is, the effect studied by Klein [*6*]). While this is clearly a small effect in comparison to the spot density obtained after only 1000 fatigue cycles ($\sim 0.7\%$ life), it does eventually limit the sensitivity of the technique.

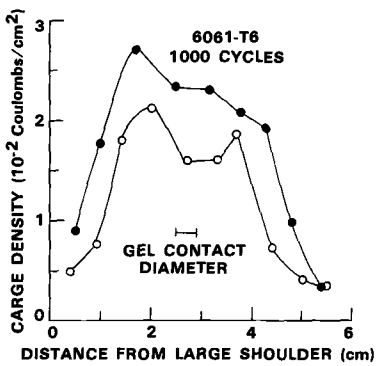

FIG. 13—*Distribution of charge density that flowed during gel electrode imaging with 5-V, 5-s pulses at a series of locations along the two surfaces of a specimen of 6061-T6 aluminum. Specimen at* $\approx 0.7\%$ *of fatigue life.*

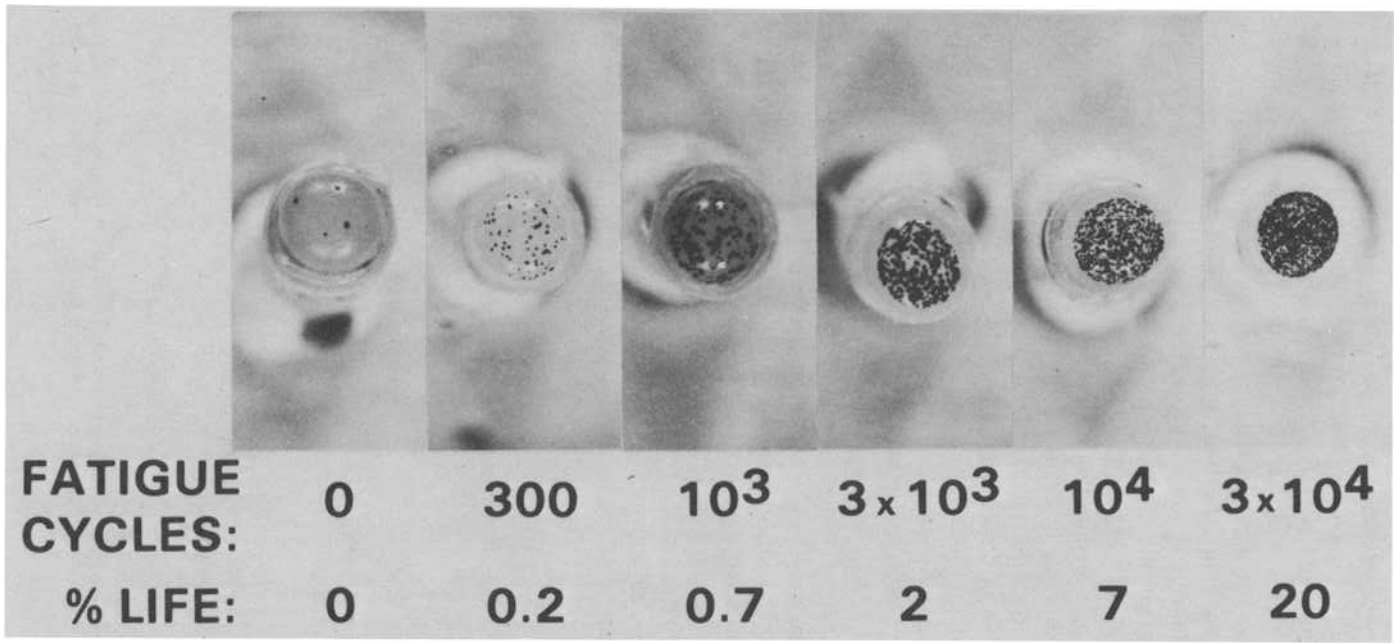

FIG. 14—*A series of gel electrode tips after imaging at the locations of maximum charge flow on a series of specimens of 6061-T6 aluminum fatigued by different amounts. Images formed with a 5-V, 5-s pulse.*

From a quantitative viewpoint, the significant parameter is the maximum value of charge density observed to flow during imaging. The effect of the number of fatigue cycles on the observed maximum charge density, for a large number of specimens of 6061-T6 aluminum, is summarized in Fig. 15. Each data point represents a different specimen. The range of charge density observed to flow to nonfatigued regions is also indicated. While this background again limits the ultimate sensitivity of the gel electrode technique, fatigue damage is still readily detected as early as 300 cycles, that is, ~0.2% of the fatigue life. Thereafter there is a systematic increase in the density of charge flow with increasing fatigue cycles. The scatter, which has been drawn to encompass all data points, is found to be a factor of 4 in width, most of which is considered to originate from specimen-to-specimen variations. This specimen variation is evident in the factor of 3 in the range of fatigue lives (N_f in Fig. 15) encountered for similar specimens fatigued under identical conditions. Thus the quantitative relationship evident in Fig. 15 provides a basis for measuring the severity of the fatigue damage and for estimating the fatigue life. For example, if a charge flow of 5×10^{-2} C/cm^2 is measured, then the specimen has consumed between 0.7 and 3% of its life.

This ability to detect fatigue damage earlier than 1% of the fatigue life demonstrates that the development of microcracks in a surface oxide film (in conjunction with the gel electrode imaging) provides the basis of a very sensitive and quantitative tool for the assessment of fatigue damage. During subsequent microscopic examination of many of the specimens, it was found that this sensitivity for the detection of surface fatigue surpassed the capabilities of optical and scanning electron microscopy. The only features encountered in the SEM, for example, were artifacts produced by the gel elec-

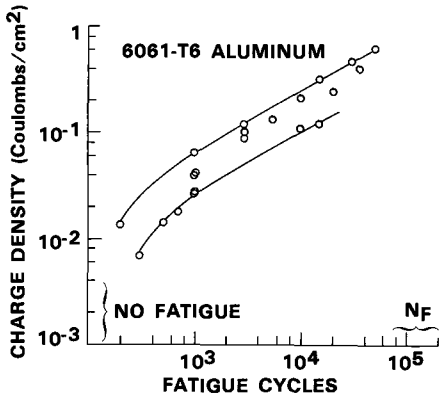

FIG. 15—*Effect of the number of fatigue cycles on the maximum value of charge density which flowed to specimens of 6061-T6 aluminum during gel electrode imaging with 5-V, 5-s pulses.* N_f *indicates the range of fatigue lives observed for similar specimens tested under the same conditions.*

trode imaging process, and these only occurred in regions where the current flow had indicated the presence of fatigue-induced microcracks in the oxide. These artifacts were corrosion products of the type shown in the scanning electron micrograph in Fig. 16.

Summary

Strongly adherent, thin surface oxide films on metals can play the role of a sensitive and quantitative discriminator of the development of fatigue damage in the underlying metal. An accumulation of surface damage can produce microcracks in the surface oxide film. These microcracks may be conveniently detected, and their density and distribution measured and imaged by a gel electrode technique. This combination of oxide film and gel electrode provides a new tool for the study and assessment of surface fatigue damage in metals, with a sensitivity that exceeds the capabilities of optical or scanning electron microscopy.

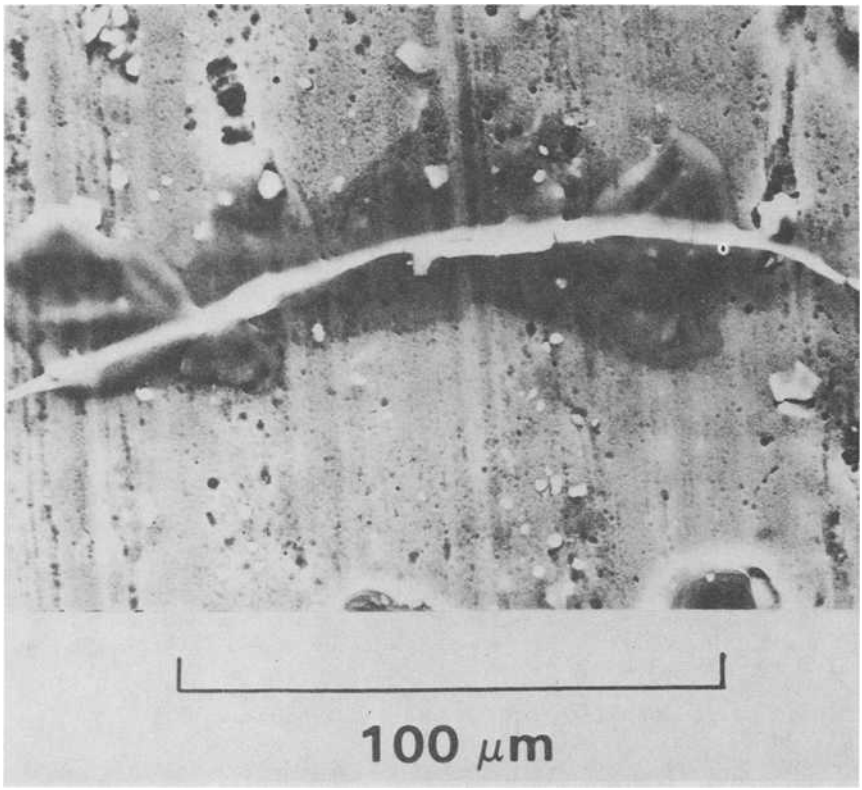

FIG. 16—*Scanning electron micrograph showing a typical corrosion artifact produced by the current flow during gel electrode imaging of a fatigued specimen with a 5-V, 5-s pulse.*

The specimen preparation prior to fatigue loading is minimal, requiring only cleaning of the surface and the anodic deposition of a thin surface oxide film. After fatigue loading, the extent of the microcracks in the oxide is determined by pressing a gel electrode against the surface, applying a voltage pulse, and measuring the current which flows through the microcracks. The gel electrode retains a clear visual image of the location of the sites of current flow, providing additional information on the distribution of the microcracks in the oxide and hence the fatigue damage in the metal.

Experiments on a range of aluminum alloys have demonstrated the following capabilities:

1. Fatigue cracks in the metal, some as short as only ~ 10 μm in length, may be consistently detected and located with the gel electrode image.
2. The flow of charge during imaging of a fatigue crack is proportional to the crack length and independent of the composition of all alloys studied to date. This charge flow provides an alternative measure of crack length and can detect cracks as short as 200 μm.
3. Fatigue deformation may be detected as early as 0.2% of the fatigue life.
4. The flow of charge is a measure of the severity of the fatigue deformation, and provides a basis for the early prediction of fatigue life.

Acknowledgments

The author is very grateful for the assistance of D. W. Gorkiewicz in performing this investigation, to S. R. Rouze for the photoelectron micrographs in Fig. 1, and to W. Lange for the scanning electron micrographs.

References

[1] Barton, J. R. and Kusenberger, F. N. in *Metal Fatigue Damage—Mechanism, Detection, Avoidance, and Repair, ASTM STP 495*, American Society for Testing and Materials, 1971, pp. 123-227.
[2] Baxter, W. J., *Metallurgical Transactions*, Vol. 8A, 1977, pp. 899-904.
[3] Baxter, W. J. in *Electron and Positron Spectroscopies in Materials Science and Engineering*, O. Buck, J. K. Tien, and H. L. Marcus, Eds., Academic Press, New York, 1979, pp. 35-53.
[4] Baxter, W. J., *Metallurgical Transactions*, Vol. 13A, 1982, pp. 1413-1419.
[5] Baxter, W. J., *Metallurgical Transactions*, Vol. 13A, 1982, pp. 1421-1427.
[6] Klein, G. P., *Journal of the Electrochemical Society*, Vol. 113, 1966, pp. 345-348.
[7] Arnott, D. R., Baxter, W. J., and Rouze, S. R., *Journal of the Electrochemical Society*, Vol. 128, 1981, pp. 843-847.
[8] Baxter, W. J. and Rouze, S. R., *Journal of Applied Physics*, Vol. 49, 1978, pp. 4233-4237.
[9] Baxter, W. J. and Rouze, S. R., *Metallurgical Transactions*, Vol. 13A, 1982, pp. 1573-1575.
[10] Baxter, W. J. and Rouze, S. R., *Review of Scientific Instruments*, Vol. 44, 1973, pp. 1628-1629.
[11] Grosskreutz, J. C., *Journal of the Electrochemical Society*, Vol. 116, 1969, pp. 1232-1237.

DISCUSSION

B. Cina[1] (*written discussion*)—In order to ascertain whether the indications of cracks observed in the several aluminum alloys fatigue tested derive from the metal or from what could be presumed to be the more brittle oxide, has the author applied a single cycle of tensile stress of magnitude equal to that of the maximum stress in his fatigue tests to each of these alloys?

In a similar connection, the observation of cracking very early on in the monotonic tensile testing of the 1100 aluminum alloy, a highly ductile material, is surprising if interpreted solely in terms of the metal.

W. J. Baxter (*author's closure*)—Based upon observations with both the gel electrode technique and the photoelectron microscope, a single cycle at the stress levels of our fatigue experiments does not rupture the oxide film. The films are, in fact, surprisingly ductile, the onset of rupture in a tension test occurring at a macroscopic strain of $\sim 2 \times 10^{-2}$ due to the emergence of slip steps in the underlying metal. Thus during a fatigue test the oxide is not ruptured until slip band extrusions develop.

L. Mueller[2] (*written discussion*)—Can you use this technique on specimens where the oxide layer has not been built up beyond the natural thickness? How dependent is this technique on the cleanliness of the specimen? Can this technique be used in the field?

W. J. Baxter (*author's closure*)—The answer to your first question is no. The technique relies upon the presence of thinner oxide films in the fatigue zone than elsewhere, so that the current flows preferentially to the fatigue damaged region. Concerning the other questions you raise, I believe that the technique can in principle be used in service, although the limitations have yet to be investigated. Accumulations of dirt should certainly be removed, but with care. A major concern would be avoidance of removal of the oxide film from the surface by processes such as abrasion or corrosion.

H. Mughrabi[3] (*written discussion*)—Could it be that the intentionally deposited oxide layers enhance the rate of crack initiation of the base metal after they have fractured locally?

[1]Israel Aircraft Industries, Ltd., Lod, Israel.

[2]Alcoa, Alcoa Technical Center, Alcoa Center, Pa. 15069.

[3]Max-Planck-Institut für Metallforschung, Institut für Physik, Stuttgart, Federal Republic of Germany.

W. J. Baxter (author's closure)—I have no reason to believe that this happens. The presence of these very thin (14 nm) oxide films does not influence the fatigue life of our specimens. I think film thicknesses $\gtrsim 10^3$ nm are required to influence the base metal in the manner that you suggest.

A. K. Chakrabarti[4] *(written discussion)*—Since the oxide layer is of different material than the alloy, it may deform and crack earlier than the parent material. Is there a one-to-one correlation between indication and actual damage?

Extrusions, intrusions, and grain boundary/sub-boundary rotation may cause cracking of the oxide layer, but the material itself may not be damaged severely. Therefore, all indications detected by this method may not represent a true level of damage corresponding to material discontinuity.

W. J. Baxter (author's closure)—Microcracks develop in the oxide film prior to the appearance of a fatigue crack in the metal at the sites of the development of slip band extrusions in the metal. Since in the case of unidirectional tensile deformation a strain of $\sim 2 \times 10^{-2}$ is required to rupture the oxide, however, there will be an analogous threshold of severity of slip band extrusion. (Conversely, minor or unimportant fatigue damage will not be detected.) The correlation between the gel electrode image and the actual microscopic damage is very convincing for even minute fatigue cracks, but a similar direct correlation with precrack fatigue deformation (that is, persistent slip bands) has yet to be demonstrated. However, exoelectron studies (see, for example, Ref *3* in the list of references appended to the paper) have established such a correlation between fatigue deformation and the microcracks in thin oxide films. Furthermore, the similarity between the increase of exoelectron emission and the increase of charge flow to the gel electrode during the early stages of fatigue indicates that the gel electrode measurements will be correlated with the actual fatigue damage in due course.

N. Ranganathan[5] *(written discussion)*—Can this technique be used to quantify strains in the plastic zone around a fatigue crack? If so, can you provide details on this subject?

W. J. Baxter (author's closure)—This is certainly an aspect that needs to be investigated. The strain distribution could be quantified by measuring the charge flow at various locations with a very small gel electrode. Because of the limited spatial resolution of the technique, however, only quite large plastic zones could be mapped.

[4]Materials Research and Engineering, Detroit Diesel Allison, Division of General Motors Corporation, Indianapolis, Ind. 46206.

[5]ENSMA, Poitiers, France.

Early Stages of Damage

Fatigue Lifetime

Guy C. Pluvinage[1] *and Michel N. Raguet*[1]

Physical and Mechanical Measurements of Damage in Low-Cycle Fatigue: Applications for Two-Level Tests

REFERENCE: Pluvinage, G. C. and Raguet, M. N., **"Physical and Mechanical Measurements of Damage in Low-Cycle Fatigue: Applications for Two-Level Tests,"** *Fatigue Mechanisms: Advances in Quantitative Measurement of Physical Damage, ASTM STP 811*, J. Lankford, D. L. Davidson, W. L. Morris, and R. P. Wei, Eds., American Society for Testing and Materials, 1983, pp. 139-150.

ABSTRACT: Physical and mechanical measurements of damage during low-cycle fatigue are made on steel by eight different methods. The decrease in load at constant strain amplitude is chosen as damage parameter to predict the cyclic life during two-level temperature and strain tests.

KEY WORDS: steel, low-cycle fatigue, high temperature, damage, cyclic life

In the case of structures under mechanical or thermal cycles, the problem of estimating the fatigue life is essential for engineers. Many fatigue life prediction methods which have been widely developed during recent years use the damage concept initially introduced by Katchanov [*1*] for creep problems.[2]

Most authors [*2,3*] have used continuous damage models and consider only cracks and microcracks as damage, ignoring other forms of damage such as the formation of point, line, or planar defects which appear especially during the shakedown period of the material. The definitions and evaluation methods of damage are, at the present time, a much debated question. The methods may be divided into two categories:

1. Those which affect the quantification of defects, especially the crack density.

[1]Professor and Graduate Student, respectively, Laboratoire de Fiabilité Mécanique, University of Metz, Metz, France.

[2]The italic numbers in brackets refer to the list of references appended to this paper.

2. Those which examine the evolution of a property of the material, an evolution resulting from the introduction of defects. Properties which have been correlated with damage evolution include resistivity [4], ductility [5], fatigue limit [6], Young's modulus [7], mechanical energy dissipation [8], plastic strain [2], and residual life [9].

The authors have chosen to define damage D_x as the change in a property X of a material. By using this definition, it results that (1) damage can be negative, (2) some defects have no influence on damage, and (3) no microstructural model is needed to characterize the influence of a defect. The damage correlated with the various properties gives evidence of the nonlinear character of the damage function as a lifetime prediction function. The forms of the curves obtained are quite different, and are generally dependent on the loading level, the higher levels corresponding to a higher damage level.

The models proposed for two-level tests may be divided into two cases:

1. There is no interaction of the first level upon the second (Fig. 1*a*).
2. There is interaction of the first level upon the rate of the damage accumulation of the second level (Fig. 1*b*) [10,11].

We must also point out the following assumption: the transition between two different levels is made horizontally, that is, at a constant damage.

At σ_1, damage accumulates along path OAC until point A is reached, whereupon the stress level is changed to σ_2. The damage then begins to accumulate along path OBC, which is the path along which damage would have accumulated if the stress had been equal to σ_2. In Fig. 1*b* this is not the case; that is, after the load change, damage accumulates along the new line BD. Here β is the fraction of the specimen's life spent and D is the damage parameter defined as the change of a property.

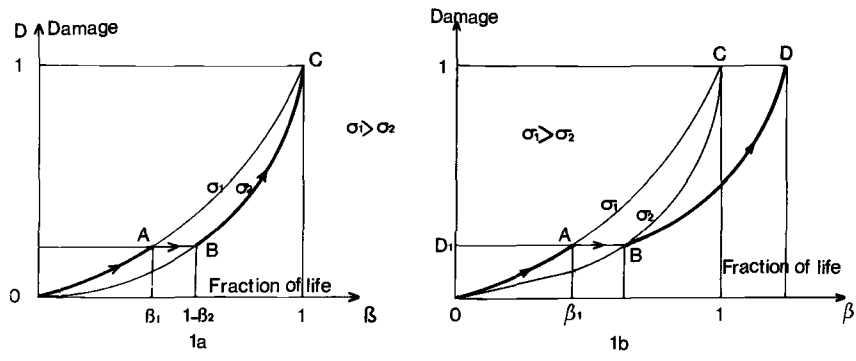

FIG. 1—*Damage accumulation curves for two-level tests.* (a) *Without interaction.* (b) *With interaction.*

Characterization of Damage D_x by the Study of the Material Property Evolution During Low-Cycle Fatigue

In order to evaluate in different ways damage evolution during low-cycle fatigue at high temperature, we have carried out experiments on a bainitic steel. Strain-controlled cyclic tests were performed on cylindrical specimens using a servohydraulic machine. The specimens were heated in an electric furnace. The testing parameters were:

Total strain amplitude:	0.64% and 0.73%
Temperature:	573°C and 610°C
Strain rate:	$3.2 \times 10^{-3}\ s^{-1}$

The defects that developed during the plastic strain cycles, dislocations, cells, and microcracks were characterized using optical and transmission electron microscopy, and were compared with the changes of applied load level. In Fig. 2, the damage D_F is considered to be the load drop and is plotted versus the fraction of life $\beta = N/N_R$ (N_R is the number of cycles to failure). The damage is defined as

$$D_F = \frac{F_0 - F_N}{F_0 - F_R}$$

where F_0 is the value of the load for the virgin material, F_R is the value of the load when failure occurs, and F_N is the value of the load after N cycles of strain. The normalized cumulative length of the microcracks $\ell/\ell_F = L$ is also plotted versus the fraction of life β on the same diagram (ℓ_F is the cumulative length of the microcracks at failure).

The virgin material shows dislocations clustered without apparent order. After cycling through $\beta = 0.07$, we observe the dislocations becoming organized into cell walls. Cycling for a larger fraction of the lifetime does not result in the evolution of the cell size, but the cell walls get thinner until failure ($\beta = 1$). Similarly, we observed by an optical microscope, microcracks in specimens which were sliced on planes parallel to the direction of loading. We repeated this for each of the specimens cycled at different fractions of life.

It was found that the material goes through several stages, consisting of the movement of dislocations, their migration into cell walls, the nucleation of microcracks, and finally the development of a dominant crack. Three major stages on the curve of load drop can be observed: (*1*) the evolution of the dislocations and their arrangement into cell walls, (*2*) the thinning of cell walls and nucleation of microcracks, and (*3*) the propagation of one or more microcracks.

The influence of these different kinds of defects on a set of physical and mechanical properties was investigated in similar conditions of loading in order to compare damage definitions. The following measurements were made:

1. *Electrical resistance* of the specimen, measured under constant-intensity current with a high-sensitivity voltmeter.

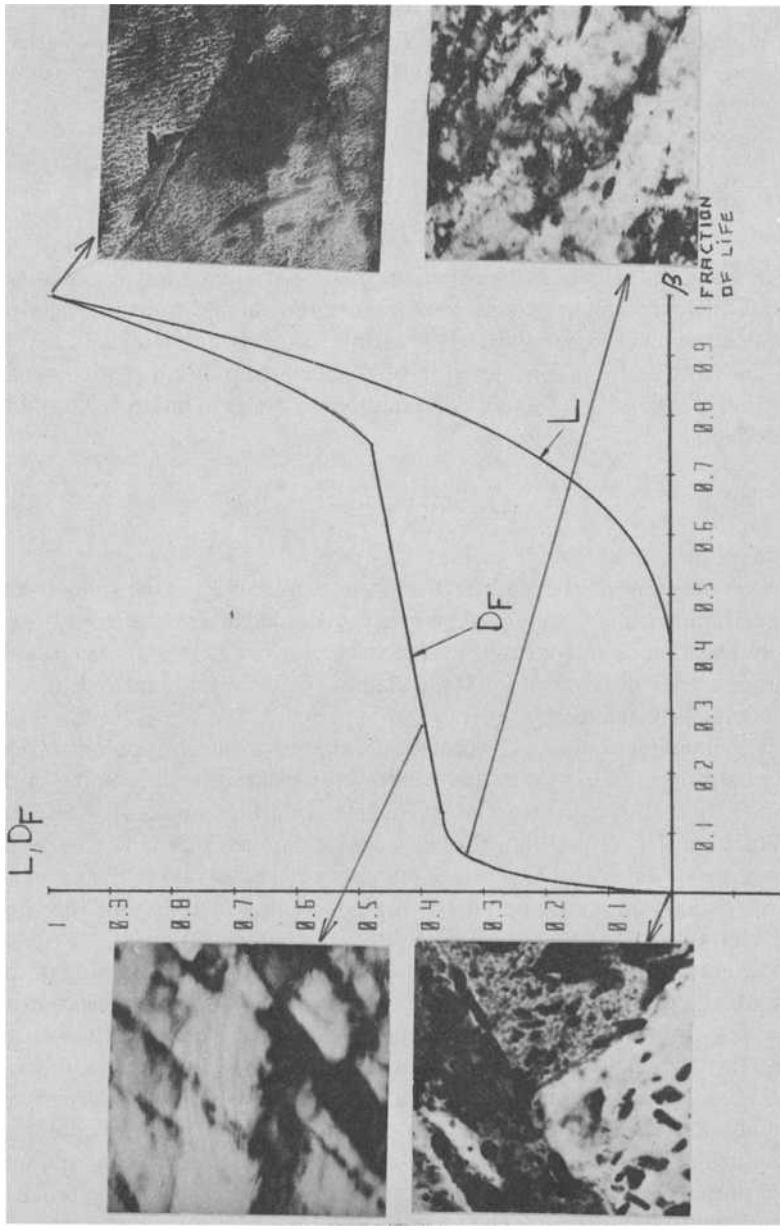

FIG. 2—*Crack and dislocation evolution during low-cycle fatigue of a bainitic steel.*

2. *Density*, obtained by a double weighing of the specimen in air and then in a liquid (the sensitivity of the balance was 10^{-7} g).

3. *Ductility* (strain to fracture), measured by compressing a cylindrical portion of the cycled specimen.

4. *Brinell hardness*.

5. *Limit of reversibility*, defined as the applied stress for which a residual deformation $\epsilon = 10^{-5}$ after relaxation of 1 h is observed.

6. *Young's modulus*, defined as being the slope of the elastic portion of the hysteresis loops.

7. *Number of cycles* for a second level of strain or temperature defined as $D_1 = 1 - \beta_2$.

8. *Load drop* during strain-controlled tests (for softening materials).

In order to compare these values, they were normalized on a linear scale between 0 (undeformed material) and 1 (failure).

The "damage" according to the authors' definition is given by

$$D_x = \frac{X_0 - X_n}{X_0 - X_R}$$

where X_0 is the value of the considered property for the undeformed material, and X_R is the value of the considered property after N cycles of strain. The evolution of each of the foregoing eight properties as a fraction of lifetime may be seen in Fig. 3.

It is clear that damage evolution versus lifetime strongly depends on the property used as damage indicator. It is possible to put the eight properties into three categories:

1. Those which are sensitive to the formation of macrocracks (1 and 6).
2. Those which are sensitive to the migration of the dislocations (2 and 4).
3. Those which are sensitive to both of the above (3, 5, and 8).

The evolution of mechanical properties is sensitive to all types of defects, as we can see on the evolution curves of the limit of reversibility, ductility, and load drop. All eight properties give evidence of the three stages. Among the last-named three methods, only load drop allows continuous measurements and is not destructive. We therefore use the load drop method to study the two-level tests.

Tests with Two Levels of Strain or Temperature or Both

As shown in Fig. 4, the one-level damage curves $D_F = f(\beta)$ are a function of the temperature and the strain. These curves are called "elementary curves of damage." For the two-level tests (of temperature or strain), the change of level of the cyclic load range F is marked by a decrease (or an increase) in load without

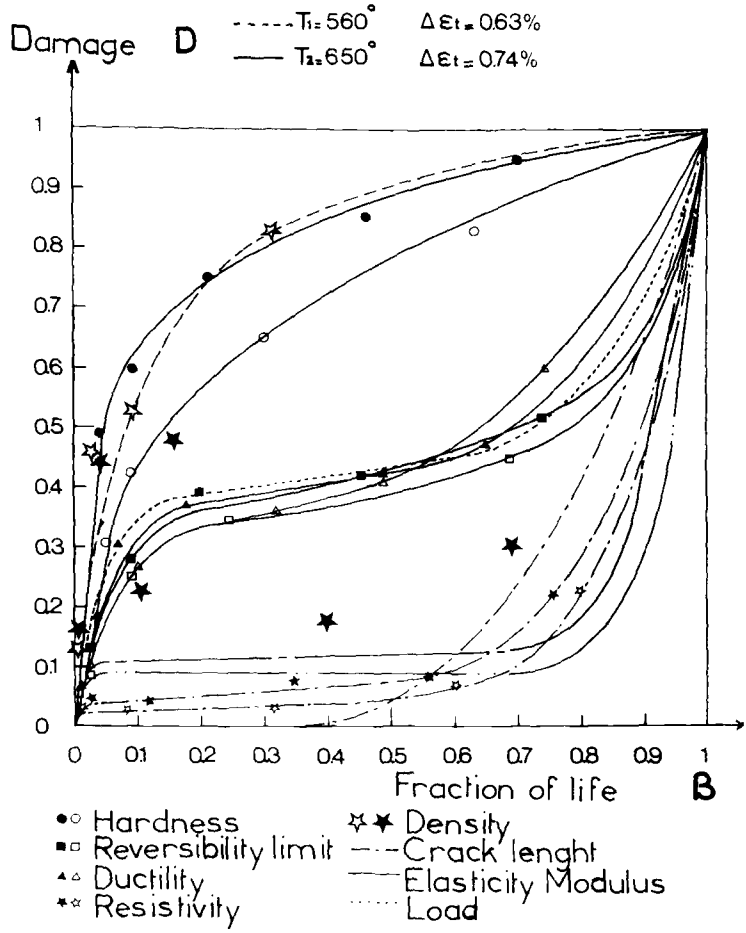

FIG. 3—*Damage evolution curves measured by eight different methods.*

any possibility of reaching the elementary curve at the second level, when this second level is applied alone (Fig. 5). The gap between the elementary curve and the actual curve at this second level is called ΔF, and is defined in Fig. 6 as positive or negative.

The shape of the actual curve after the second level is applied is not modified, and characterizes the influence on the load of defects accumulated at two different strain levels for the same fraction of life β_1.

In agreement with other work [*12*], the two-level tests do not often follow the theoretical results of Miner's Law [*13*] (Fig. 7):

$$\Sigma \frac{N_i}{N_{Ri}} = 1$$

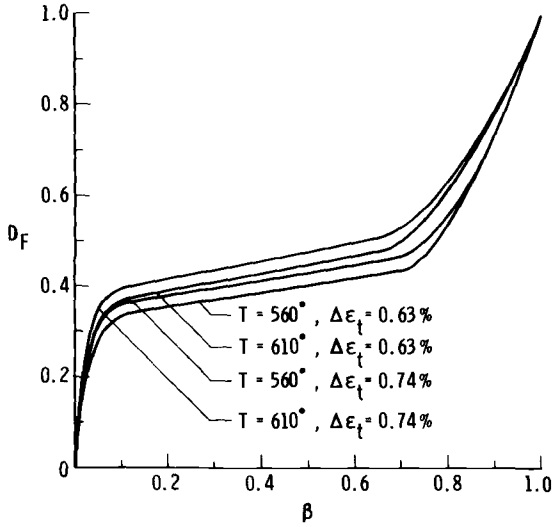

FIG. 4—*Damage evolution curves for four different conditions of strain and temperature.*

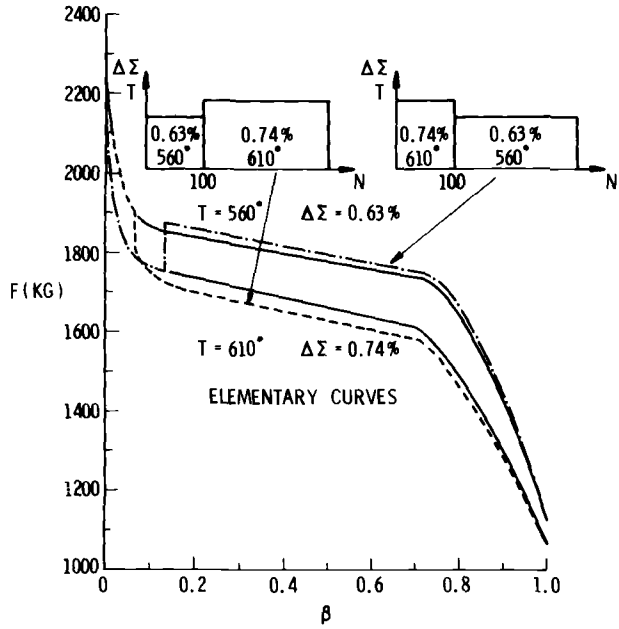

FIG. 5—*Load evolution for two-level strain-controlled tests.*

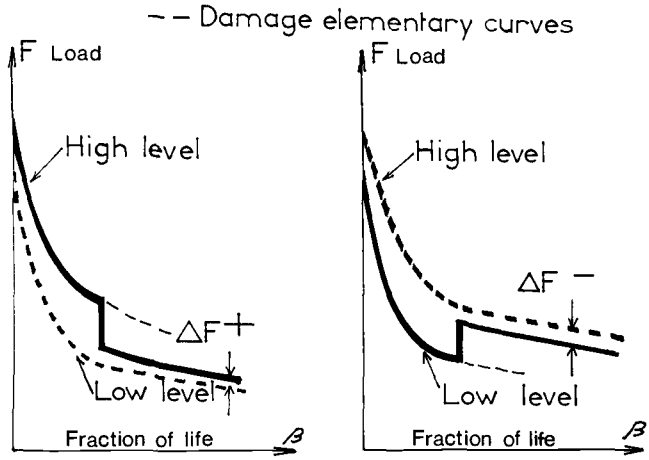

FIG. 6—*Definition of the gap* ΔF.

The value obtained by Miner's parameters versus gap ΔF are plotted in Fig. 8; a linear correlation between these two parameters is observed (correlation coefficient = 0.85).

Next, we varied the experimental conditions in order to obtain a maximum gap as opposed to the theoretical results of Miner's Law. These experimental conditions were characterized by two parameters:

1. The fraction of life at the first level β_1.
2. The ratio of the number of cycles to failure at the first level, and at the second level when they are applied alone, N_{R1}/N_{R2}.

These parameters characterize at the same time the strain and the temperature level.

Results can be seen in Fig. 9, which was drawn from 40 specimens. The relation $\Delta F = (N_{R1}/N_{R2}, \beta)$ shows that the maximum gap is obtained when $\beta_1 = 0.07$, with a loading ratio of $N_{R1}/N_{R2} = 2$.

Discussion

The quantitative measurement of fatigue damage appears to be strongly dependent on the damage definition. Two possibilities for this damage definition exist:

1. Damage is considered as the presence of defects.
2. Damage is considered as the alteration of a property.

The first way presents difficulties; several kinds of defects exist generally at the same time, and for a particular type of defect, several parameters can be used

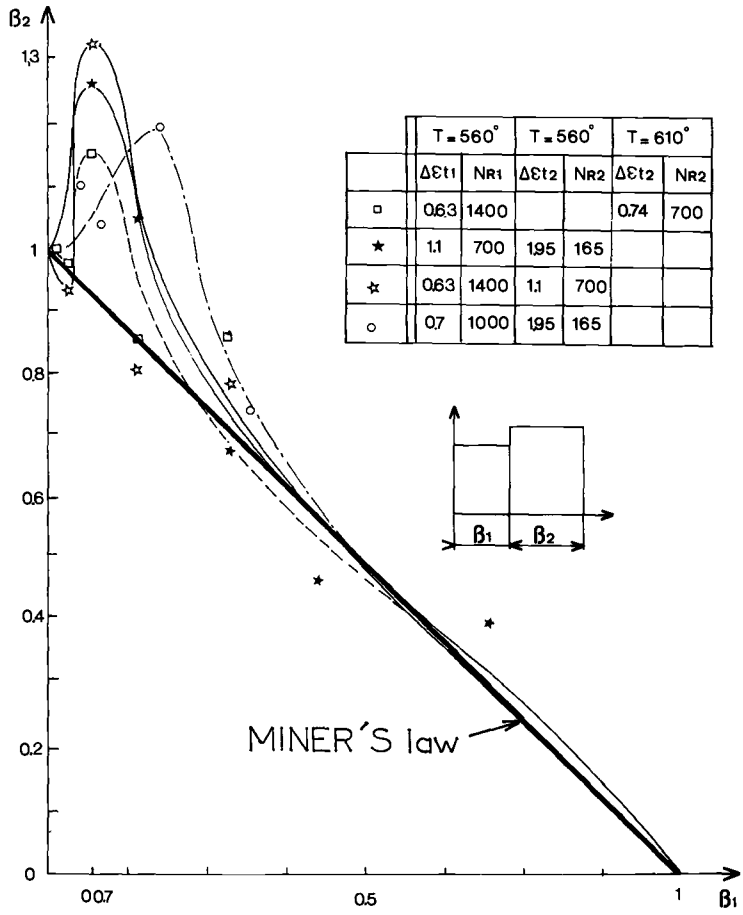

	T = 560°		T = 560°		T = 610°	
	Δεt1	NR1	Δεt2	NR2	Δεt2	NR2
□	0.63	1400			0.74	700
★	1.1	700	1.95	165		
☆	0.63	1400	1.1	700		
○	0.7	1000	1.95	165		

FIG. 7—*Fraction of life at second level versus fraction of life at first level* [$\beta_2 = f(\beta_1)$].

(geometry, size distribution, etc.). The problem of adding the effects of different kinds of defects to obtain "total damage" has not yet been solved.

The relation between defects and the alteration of a property is complex. It has been studied in some simple cases through the relation between microcracks and elasticity, using the effective stress concept of Katchanov [7]. Comparison of the cumulative length of the microcrack curve (Fig. 2) is made with the evolution of Young's modulus versus fraction of life (Fig. 3); a difference in the shapes of these two damage curves is evident, owing to cyclic softening before crack nucleation, and shows the influence of two kinds of defects. The examination of the evolution of a property seems easier for a quantitative measurement of fatigue damage. The material is considered as a black box and no attention is given to defects. Unfortunately, the damage evolution curve is

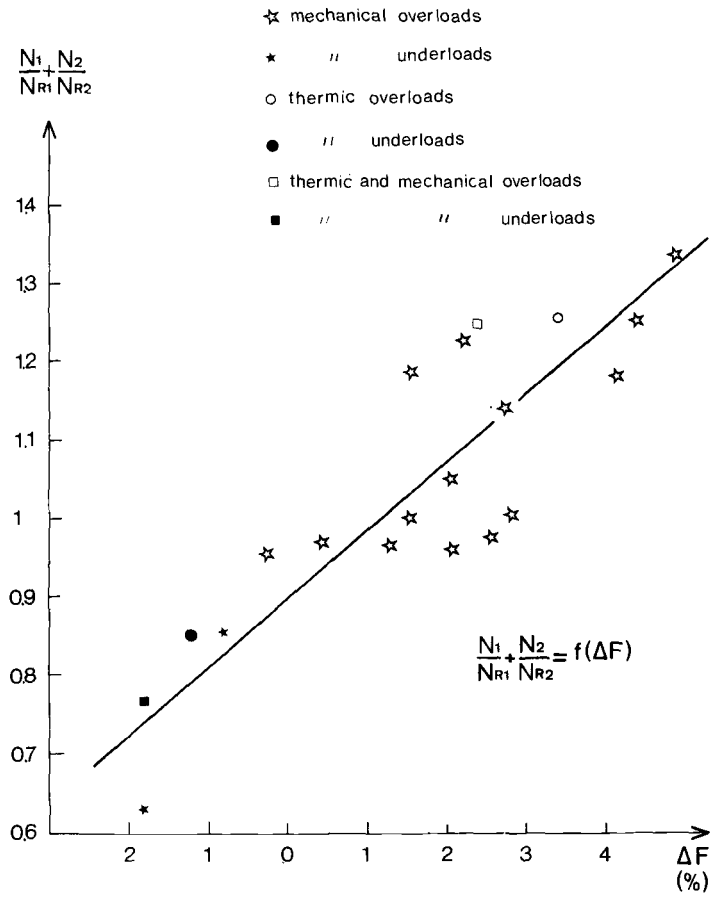

FIG. 8—*Correlation between Miner's parameter and gap* ΔF.

strongly dependent on the property used as damage indicator (Fig. 3); however, it always presents three stages.

The choice of the properties used as damage indicators is based on sensitivity. Nondestructive methods are preferred. For these reasons, the load drop was chosen.

It can be seen in Fig. 7 that two-level tests give a memory effect. This memory effect is characterized by a deviation from Miner's Law. The relation between damage and memory effects can be seen by the same two approaches.

The memory effect can be considered as a disturbance of the damage evolution curve, or as a different distribution of defects at a given fraction of life β. During the first cycling level which is, for example, higher than the second one, the material damage is mainly characterized by a dislocation density, a cell size, or a microcrack density (Fig. 2). Mechanical cycling at a second level

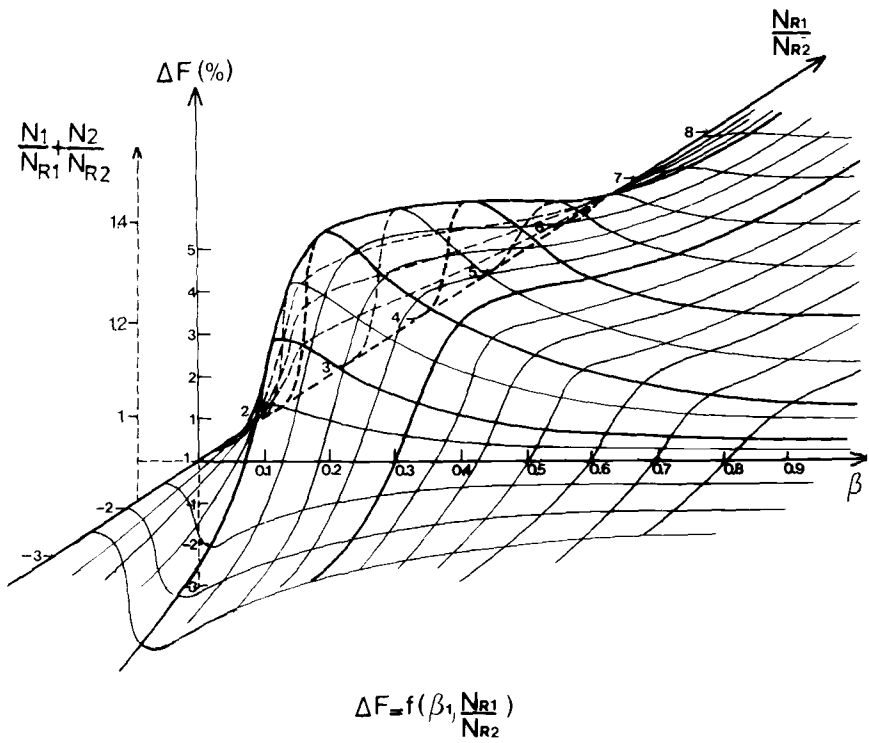

FIG. 9—*Miner's parameter evolution versus experimental conditions.*

during the same fraction of life can lead to a different dislocation density, a bigger cell size, or a larger microcrack density. When the second level is applied, a new defect distribution is produced by the annihilation of some dislocations and by the destruction of cells. But the new distribution uses old cell walls or the old part of the dislocation distribution. These debris on a microstructural scale give the memory effect. This is easier when the cells are improperly formed—that is, at the beginning of cyclic life ($\beta < 0.1$)—and explains the maximum of memory effect for $\beta = 0.07$. The new defect distribution yields under the applied strain ϵ_2 to a different load drop.

Conclusions

The quantitative measurement of fatigue damage always depends on the properties that are used as damage indicators.

The memory effect that appears in two, or multilevel, tests can be considered as a different damage evolution curve under the same applied strain, and measured by the load gap.

References

[1] Kachanov, L. M., *Izvestiia Akademii Nauk S.S.S.R., Teck. Nauk.*, No. 8, 1958, pp. 26-31.
[2] Chaboche, J. L., *Revue Française de Mécanique*, No. 50-51, 1974, p. 7182.
[3] Shanley, F. R., "A Theory of Fatigue Based on Unbonding during Reserved Slip," *The Rand Corporation Report*, 1955, p. 350.
[4] Cailletaud, G., Policella, M., and Baudin, G., "Mesure de Déformation et d'Endommagement par Méthode Electrique," *Recherche Aérospatiale*, 1980-1981, pp. 47-58.
[5] Polhemus, J. F., Spaeth, C. E., and Vogel, W. M. in *Fatigue at Elevated Temperatures, ASTM STP 520*, American Society for Testing and Materials, 1973, pp. 625-636.
[6] Henry, D. L., *Transactions of ASME*, Vol. 77, 1955, pp. 913-918.
[7] Lemaitre, J. in *Proceedings*, Third Congress Français de Mécanique, Grenoble, 1977, pp. SD1-SD2.
[8] Gatts, R. R., *Journal of Basic Engineering, Transactions of ASME*, Vol. 83, No. 4, 1961, pp. 529-540.
[9] Kommer, S. in *Proceedings of ASTM*, American Society for Testing and Materials, Vol. 45, 1945, pp. 532-543.
[10] Corten, H. T. and Dolan, J. T. in *Proceedings*, International Conference on Fatigue of Metals, Institution of Mechanical Engineers, 1956, pp. 235-246.
[11] Chaboche, J. L. in *Proceedings*, International Conference of Fracture (ICF) 5, Vol. 3, 1981, p. 1381.
[12] Manson, S. S., Freche, J. C., Ensign, C. R., "Application of a Double Linear Damage Rule to Cumulative Fatigue," ASA TND 38-39, 1967.
[13] Miner, M., *Journal of Applied Mechanics*, Vol. 27, 1945, pp. 159-164.

Klaus Rahka[1] *and Campbell Laird*[2]

In Situ Indications of Ductility Evolution During High-Temperature Fatigue Testing with and without Hold Times

REFERENCE: Rahka, K. and Laird, C., "***In Situ* Indications of Ductility Evolution During High-Temperature Fatigue Testing with and without Hold Times,"** *Fatigue Mechanisms: Advances in Quantitative Measurement of Physical Damage, ASTM STP 811*, J. Lankford, D. L. Davidson, W. L. Morris, and R. P. Wei, Eds., American Society for Testing and Materials, 1983, pp. 151-175.

ABSTRACT: It has been reported in the literature that high-temperature fatigue exposure initially leads to an increase in the subsequently measured creep ductility, whereas prolonged fatigue exposure lowers the creep ductility in low-alloy Cr-Mo-V-steel. In the work now being initially reported an aim has been to observe microstructural changes due to high-temperature strain-controlled fatigue exposure with or without hold times. The controlled strain was the principal (axial) strain. For test response variables, the load and diametral strain were measured. While the cycle-to-cycle flow stress was observed to decrease monotonically—that is, the material cyclically softened—, the diametral strain range initially increased and subsequently decreased. It is concluded from the similarity in behavior between the changes in post-fatigue creep ductility (lateral contraction at fracture, RA) and *in situ* diametral strain range that the *in situ* diametral strain range is a powerful means of observing ductility changes due to fatigue. The effect of hold time at the tensile limit of the cycle is to reduce the diametral strain range as a whole and to speed up the drop in diametral strain range after it passes its maximum value. The maximum is generally reached during the few tens of initial cycles. The subsequent exhaustion of ductility develops quite rapidly at first but then slows down until the onset of cracking eventually speeds up the ductility exhaustion rate. In all cases the diametral strain amplitude behaved in a more strongly changing manner than the flow stress, indicating more sensitivity to the microstructural damage than the drop in the flow stress.

KEY WORDS: fatigue, high temperature, hold time, creep ductility, creep-fatigue, damage

[1]Technical Research Center of Finland (VTT/MET), Espoo, Finland; formerly at Department of Materials Science and Engineering/K1, University of Pennsylvania, Philadelphia, Pa. 19104 (on leave from Technical Research Center of Finland).

[2]Department of Materials Science and Engineering/K1, University of Pennsylvania, Philadelphia, Pa. 19104.

Nomenclature

T Temperature, °C, K, °F
T_γ Austenitization temperature
M Tempering parameter
t Time, h
Δe_a Axial strain range, %
Δe_d Diametral strain range, %
r^2 Regression correlation coefficient

Recently, a concept of ductility exhaustion was proposed by Priest and Ellison [*1*] in the context of analyzing creep-fatigue damage in a Cr-Mo-V steel.[3] This ductility exhaustion was reported to occur in cyclic strain-controlled testing with holds in tension for a preset time [*2*]. The effect was not pronounced with holds in compression. The strength of the effect of tension was associated with the drop in the stress, due to relaxation, during the holds [*3*]. At low stress in pure creep experiments, a low-ductility creep fracture has been observed [*3*] which is different from that at high stress, and the "relaxed" stress during holds in fatigue cycling fell below the threshold needed to cause a low-ductility fracture. In other reports, a life prediction model was developed [*4,5*]. The model is based on the existence and magnitude of the creep ductility transition stress; that is, cyclic strain-controlled tests with tensile hold are thought to behave similarly to creep at low stress.

The principal damage observed during low stress creep and strain cycling with tensile hold was grain boundary cavitation after an initial softening; however, except for the volumes immediately adjacent to the grain boundaries, few changes were observed in the microstructure that could be held as indications of damage other than that definitely related to cavitation [*6*]. It is noteworthy that other work on roughly the same kind of steel and using the same kind of cycling has not revealed as strong an effect of tensile hold on the reduction of fatigue life. Nor has such a particular relation been established between the fracture mechanisms which occur in strain cycling with tensile hold and those in low stress creep [*7,8*]. Indeed, compression hold was reported to be possibly even more damaging than tensile hold; that is, fatigue life was reduced more [*8*]. Evidently, the factor which differentiates these results must be sought in the basis of the ductility exhaustion concept of Ellison et al [*1-6*], namely the sharply stress dependent creep ductility of the steel used in their experiments. Therefore, firstly, a brief survey of factors affecting creep ductility is given, and this provides the perspective by which the steel used in our experiments was chosen.

Secondly, studies aimed at describing the development of creep and creep-fatigue damage are reviewed. Finally, we present our *in situ* observations of

[3]The italic numbers in brackets refer to the list of references appended to this paper.

high-temperature fatigue damage evolution in a modern production forging having a nominal composition of 1Cr-1Mo-¼V. Since Coffin's work [*9*] provides a suggestion that the ductility exhaustion concept for an initially ductile metal subjected to loading involving cycling can be interpreted more generally than implied by Ellison et al [*1-6*], the discussion focuses on ductility exhaustion as indicated by diametral strain response and its relation to micromechanisms occurring throughout the bulk of a specimen (that is, including grain interiors).

This discussion will lead to a new definition to creep-fatigue damage based on the ductility exhaustion of the bulk microstructure, which seems to be strong in materials with a cyclic softening response and especially strong for tests conducted at moderate strain amplitudes (on the order of ±1%).

Creep Ductility of 1Cr-1Mo-¼V Steel

If we confine attention to creep behavior at temperatures not far removed from 550°C, the typical operating temperature of a rotor steel, we note that the creep ductility (elongation or reduction of area at fracture of a load-controlled creep specimen) of 1Cr-1Mo-¼V low-alloy steel is particularly sensitive to exposure stress and three main metallurgical factors [*7,10-19*]: (*1*) austenitization temperature and cooling rate, (*2*) tempering temperature and time, and (*3*) impurity level (P, S, Sn, Sb, As, Al). Within the scope of our work we regard of marginal importance the factors of alloying, including carbon [*20*], possibly vanadium [*15*], and even molybdenum [*3,19,21,22*].

Regarding austenitization temperature, it is sufficient to note here that two ranges, 1020 to 1050°C and 950 to 970°C, are desirable from a creep strength point of view, optimum strength being reached with the higher range [*7,10,11,14,16,21*]. However, since the higher range leads to low ductility [*7,10,11,14,16,20,23-25*] and hence notch sensitivity in creep [*11*], experience has worked in favor of the lower range for austenitization of turbine rotor shafts. In the late 1970s ductility was increasingly emphasized (see, for example, Refs *26* to *28*). In the last 25 years, the recommended time and temperature of tempering have increased from a tempering time and temperature parameter [*29*] value of $M = T\,(\mathrm{K})\,(20 + \log t) = 19\,155$ [*10*] to 20 833 [*22*]. This indicates increased emphasis on ductility through tempering, supposedly for the benefit of electricity consumers. Indeed, it can be said that notch sensitivity has been optimized with the aim of obtaining a ratio of unity between notch and smooth creep strength at low stress [*10*], as far as heat treatment [*22*] is concerned.

In the last ten years, there has been an increased focus on the harmful effect of residual impurities on creep ductility [*17,18,19,23,25*], and the harmful effect of inclusions, particularly those which are sulfur related, on the resistance to crack initiation of a machine component exposed to fatigue loads [*27,28*]. Improvements in fatigue properties to date are promising [*22,30*]. It

is noteworthy that creep ductility values appear insensitive to inclusion count when the count is high, whereas fatigue life is sensitive [*28*]. A compilation of the stress-dependent creep ductility values of 1Cr-1Mo-¼V steel taken from the literature is shown in Fig. 1. The graph indicates the significant difference in creep ductility between the steel of the present investigation [*22*]

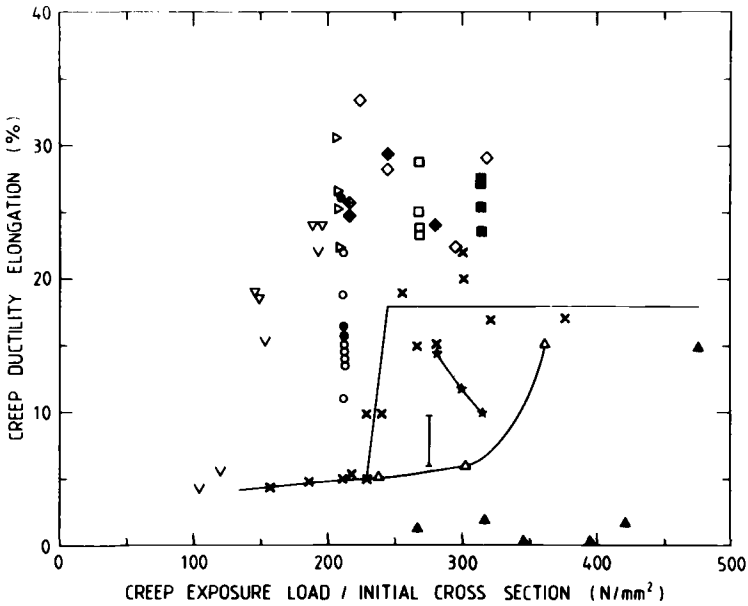

■ Westinghouse rotor steel used in this work [*22*], 538°C, M = 20 830
□ Westinghouse rotor steel used in this work, 565°C
▷ Westinghouse rotor steel used in this work, 593°C
Impurity index = 0.35 [*19*]
● Roan and Seth [*19*], 593°C, M = 20 066
Impurity index = 0.35
○ Roan and Seth [*19*], 593°C, M = 20 066
Impurity index = 0.27 − 0.70
▽ Goldhoff and Beattie [*14*], 568°C
1000 h and 5000 h elongation
◇ Jaske and Mindlin [*31*], 538°C
◆ Jaske and Mindlin [*31*], 565°C
also used by Curran and Wundt [*32*] and Leven [*8*]
⊕ Kramer and Randolph [*27,28*], failed Gallatin rotor
v Murphy and Branch [*20*], 575°C, 0.13C
× Ellison et al [*1-6*], 565°C
Ellison transition stress = 245 N/mm²
Norton and Strang [*21*]
★ Krempl and Walker [*7*], high-ductility variant
△ Stone and Murray [*15*], 565°C
▲ Goldhoff [*33*], 538°C, T_γ = 998°C (reduction of area)

FIG. 1—*General survey of creep ductility/exposure stress interdependence. All data for* T_γ = *950 to 975°C except that of Goldhoff et al, which shows the effect of a higher austenitization temperature.*

(which is the same as that used elsewhere [*30*]), that of Ref *8*, and that of Ellison et al [*1-6*]. The higher creep ductility of modern rotors, such as used in our study, points up the significance of alloying (Mo, V), heat treatment, and impurities, and diminishes the importance of the ductility exhaustion concept advanced by Priest and Ellison [*1*]. However, low-stress long-time creep testing would be needed for a fully exhaustive evaluation of this point. It is believed that part of this evaluation is provided by the results presented subsequently. The creep ductility values reported by Ellison and Paterson [*3*] and Priest and Ellison [*1*] are higher than the values presented by Goldhoff [*33*], Woodford and Goldhoff [*34*], Stone and Murray [*15*], and Norton and Strang [*21*]. Also, the "high-ductility" variant of Krempl and Walker [*7*] falls below the values of Ellison et al [*1,3*] probably and mainly because of insufficient tempering. The main differences between the steels of lower ductility are summarized in Table 1. The systematic differences between the ductility reported by Ellison et al and the higher ductilities reported by others are summarized in Table 2.

As noted previously, creep ductility usually increases with increasing tempering parameter for long hold times in tempering. A typical correlation is shown in Fig. 2 [*10*]. Aside from this main trend, an exceptionally high ductility is shown for short-time tempering (which may be unrealistic in production) for intermediate tempering parameter values, provided the temperature is high. Figure 2 also indicates the tempering parameter of the steel used in this work. Again, as mentioned previously, this parameter has increased from about 19 000 in 1955 to 20 830 in 1982.

Creep Fatigue and Creep-Fatigue Damage

Apart from low-ductility variants of 1Cr-1Mo-¼V steel, where a significant creep and creep fatigue damage is provided by grain boundary cavita-

TABLE 1—*Clearly identifiable factors that lower the creep ductility below that of the steel used by Ellison et al* [1-6].

Parameter	Ellison et al [*1-6*]	Goldhoff [*33,35-37*]	Stone and Murray [*15*]	Norton and Strang [*21*]	Krempl and Walker [*7*]	Viswanathan [*17*]
T_γ	975°C	higher	...	...	...	...
M	20 760	lower	lower	(lower)	lower	lower
% C	0.24	higher	...	...	...	...
% Mo	0.6	...	...	lower	...	...
% V	0.29	...	higher	slightly higher	...	...
% impurities	P = 0.016	...	...	...	...	...
	S = 0.01	...	...	...	...	...
% Al	not recorded	...	...	...	...	probably higher

TABLE 2—*Clearly identifiable factors that raise the creep ductility above that of the steel used by Ellison et al* [1-6].

Parameter	This Work	Goldhoff and Beattie [14]	Jaske and Mindlin [31]	Roan and Seth [19]	Murphy and Branch [20]
T_γ	lower	lower	...	lower	lower
M	slightly higher	...	...	...	...
% C	...	...	...	...	lower
% Mo	higher	higher	higher	higher	...
% V	...	...	...	...	...
% impurities (P + S)[a]	lower	...	...	lower	lower

[a]Impurities other than P and S could not be included because they are not reported by Ellison and Paterson [3].

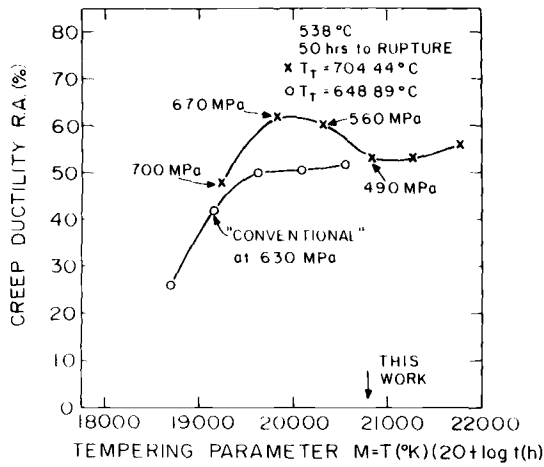

FIG. 2—*Effect of tempering parameter on creep ductility for 50-h creep strength. Creep exposure stresses required for such a creep strength are indicated. Note that ductilities are exceptionally high for intermediate time tempering at high temperature.*

tion [1-6], the principal damage process prior to cracking, which occurs late in life, is softening [7,8,28,31,32,37], that is, strength decay. The interaction of the creep and fatigue damage with respect to specimen life is therefore (roughly speaking) synergistic (Fig. 3) [32]. However, large fractions of fatigue damage and small fractions of creep damage can interact benignly [8]. The basis for calculating interaction is provided, of course, by the linear damage summation rule. Generally, "pretreatment" by fatigue shortens creep life, whereas a small fraction of creep damage (exposure time/rupture time) can extend subsequent fatigue life over that life with no creep damage at all [8]. In the tests cited in Fig. 3 the Cr-Mo-V steel had a creep ductility at

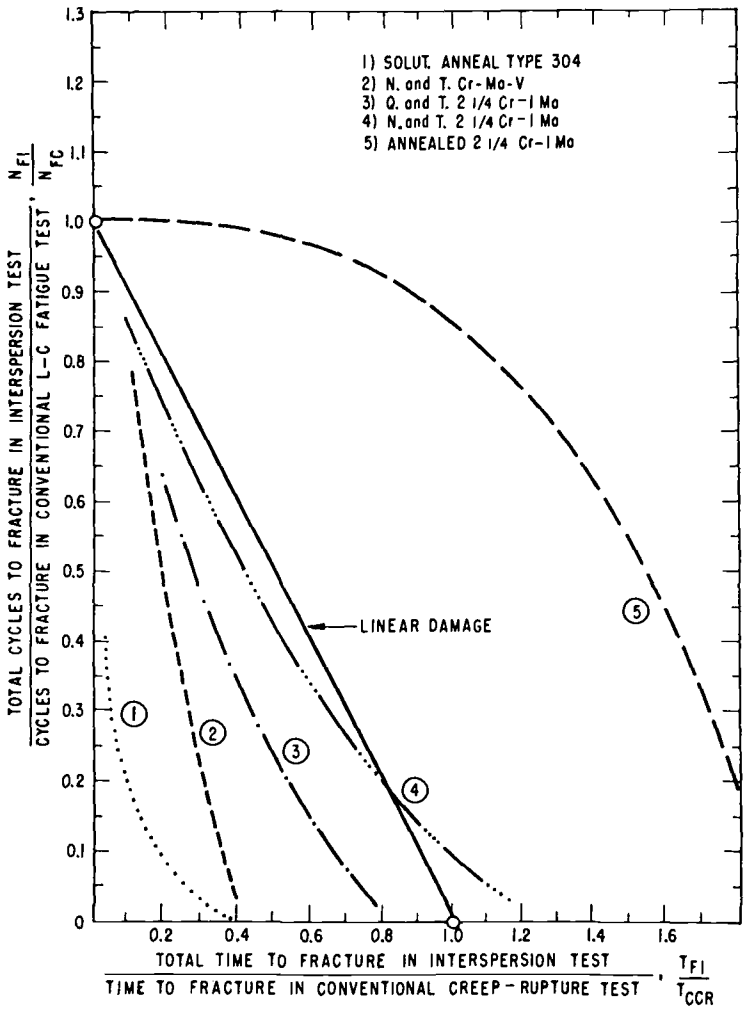

FIG. 3—*Comparison of actual test results with the linear damage summation rule for the interaction of fatigue and creep in 1Cr-1Mo-¼V steel and other steels* [8,30,32]. *Note that creep fatigue damage can be synergistic (specimen failure points fall on the left side of the linear damage line) in 1Cr-1Mo-¼V steel heat-treated for service as a rotor shaft.*

high stresses of the same range as in the material in this work, but exposure stresses and strains were in general rather high.

Damage caused by low stress in creep, fatigue, or creep-fatigue, other than softening or cracking, has not been extensively treated in the published literature. Of course, microstructural changes observed by microscopy have received attention in some investigations, particularly carbide reactions in Cr-Mo-V-steel [*6,14,16*], as well as changes of dislocation substructure in

relation to carbides [*6*]. Older literature abounds with suggestions that carbide reactions strongly influence the brittle behavior and notch sensitivity of Cr-Mo-V steel in creep [*11-13,33-36,38*]. Cases in which changes in carbide morphology have been detected, however, seem to be those where a low value of the tempering parameter was used; thus the carbides were not as stable as those produced today by higher tempering values. One result of this is the occurrence during testing of reactions comparable to those of ageing solids, and such reactions are therefore understood to cause low ductility and notch sensitivity. In the case of a modern, higher ductility rotor forging, carbide reactions have been observed to be subtle [*30*]. Thus low-ductility problems are today understood to be especially relevant to other areas of steel technology (for example, in welding or brazing) when the control over metallurgical treatment may be much poorer than that used for the smelting, forging, and heat treatment of rotor shafts.

Observations of the dislocation substructure produced by exposure have led to several conclusions. Dislocations form substructures in load-controlled creep if the exposure stress is large enough to cause significant strain accumulation. In fatigue, dislocation subcell formation and microstructural alignment occurs, but sequential-fatigue, low-stress creep tests lead to little detectable change in either the carbides or the bulk grain structure, because the main damage process occurs at grain boundaries [*6*].

Apart from these damage observations, an important and quite different indication of fatigue damage at 565°C is provided by Ellison and Paterson [*3*] in the form of the creep ductility after fatigue with continuous cycling. Note that this ductility (Fig. 4) rises for small fractions of fatigue damage and decays for larger fractions. Our results will be compared with this indication.

From tests designed to explore the time dependence of fatigue damage it has been concluded that a lowering of the frequency of cycling shortens high-temperature fatigue life, measured by the number of cycles to failure [*8*]. In

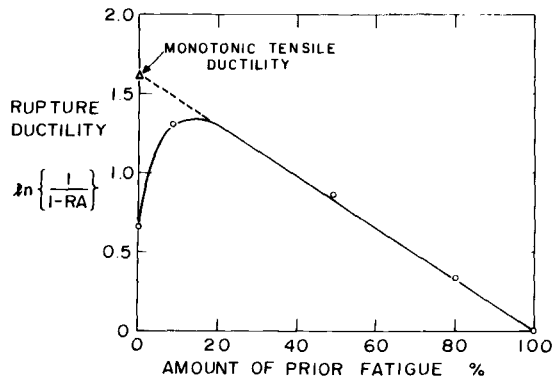

FIG. 4—*Post-fatigue creep ductility according to Ellison and Paterson* [3].

the work reported by Leven [*8*], the effect of lowering of the cyclic frequency by introduction of hold at the peak tensile strain was to reduce the fatigue life too. However, the reduction was not by far as large as that found by Ellison et al [*1-5*]. Neither was grain boundary cavitation reported to dominate in the cracking mechanism in the work reported by Leven [*8*] as was the case in the experiments of Ellison et al [*1-5*]. Therefore it is believed that a creep-fatigue damage mechanism dominated by grain boundary cavitation may not be as important in modern rotor shafts as postulated by Ellison et al [*1-5*] for their steel and we shall focus on deformation mechanism based damage. Since a potential source of ductility exhaustion by microcrack formation may be introduced by surface oxidation and cracking during cycling, some measures have been taken to ensure that oxidation-related effects are also of secondary importance in this work.

Test Material and Experimental Details

The chemical composition of the test material, which came from a commercial rotor forging, is presented in Table 3. The austenitizing was performed at 950°C with air cooling, and the tempering was done at about 670°C with subsequent stress relieving to a total tempering parameter $M = T\,(\mathrm{K})\,[20 + \log t(h)] = 20\,830$. At room temperature the tensile strength was 775 MPa and the 0.2% offset yield strength was 620 MPa. The creep ductility given in Fig. 1 is in the high range, primarily because of low impurity content and long tempering. The ingot had a pronouncedly low sulfur and inclusion content [*30*]. The tests performed were of the axial strain-controlled type using smooth specimens. Gage section length was 12 mm and the diameter was roughly 5 mm. Both were measured from each specimen to give an accurate basis for the calculation of strain. For response quantities, both load and transverse strain were measured with the usual aim of studying strength response (softening); the transverse strain was measured to indicate the nature of the plasticity in the specimen as a function of exposure cycles and time. The extensometers used for measuring axial and diametral strain are shown in Fig. 5. The transducers were an Instron gage for axial strain, which was joined to the specimen with a water-cooled "scissor" adapter equipped with quartz tips, and, for diametral strain, a standard high-temperature diametral gage, manufactured by MTS. This gage also had quartz rods for attachment to the specimen. The specimens were heated by novel

TABLE 3—*Composition of the Cr-Mo-V rotor steel.*

C	Mn	P	S	Si	Ni	Cr	V	Mo	Sn	As	Al	Cu	Sb
0.29	0.71	0.010	0.003	0.21	0.34	1.16	0.24	1.29	0.01	0.004	0.005	0.04	0.0007

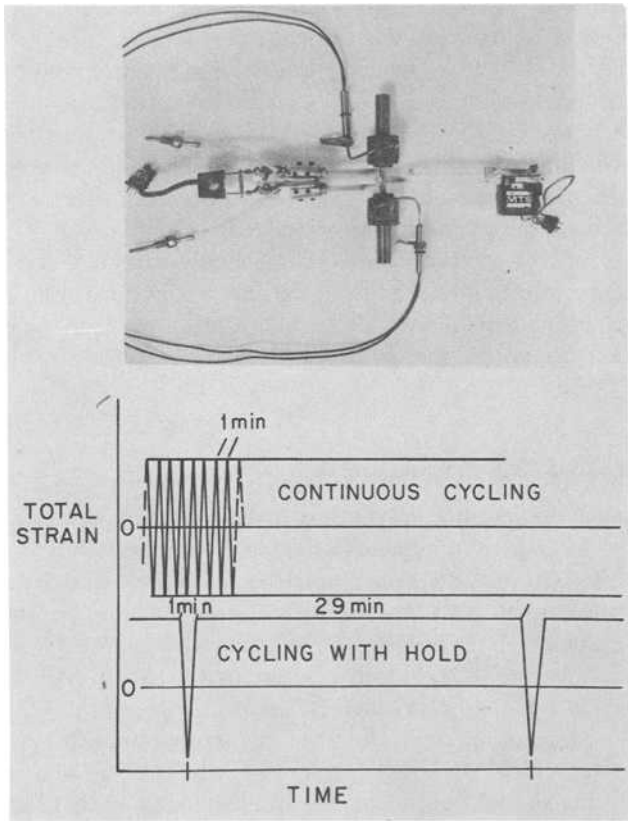

FIG. 5—*Test configuration and controlling waveforms for axial strain. The strain transducers are Instron and MTS standard instruments. Heating of the specimen was by noninductively wound resistance heaters located at the specimen shoulders.*

miniature resistance heaters produced by ARI Industries. These blind end double-lead heaters were noninductively wound and were located around both shoulders of the specimen (Fig. 5).

All tests were performed at 550°C in a chamber with dehumidified, deoxygenated argon. Some oxidation occurred, however, which is shown in Fig. 6. This is not believed to invalidate the conclusions of the paper, because oxide-connected crack embryos were found to be minute even at long-time exposures. All tests were run in a CGS servohydraulic testing rig. The controlling waveforms are shown in Fig. 5: (*1*) a 1 cycle/min, zero-symmetric sawtooth waveform for continuous cycling, and (*2*) cycling with hold having the same transient phase and a 29-min hold at peak tensile strain during each cycle. The typical load and diametral strain response for a cycle with hold is shown in Fig. 7.

FIG. 6—*Section of specimen cycled with 29-min hold in tension;* $\Delta e = \pm 0.7\%$ *for 349 cycles.*

Test Results

The typical softening response in continuous cycling is shown in Fig. 8. Figure 9 shows the corresponding cyclic softening curves for cycling with 29-min hold in tension, including the value of the cycle-dependent relaxed stress. Both show a relatively evident stabilization. Therefore, since the locus of stabilized stress-strain hysteresis peaks can be thought to form a cyclic stress-strain curve, the stabilized relaxed stress—by analogy—can be thought to give the relaxed cyclic stress-strain curve. Since results at other strain levels are not yet available for our material, the relaxed cyclic stress-strain curve obtained by Ellison and Paterson [*2*] is shown (Fig. 10) with the results of our tests inserted. The stress response of our steel to strain cycling with hold shows that it is softer than that of Ellison and Paterson. The particular

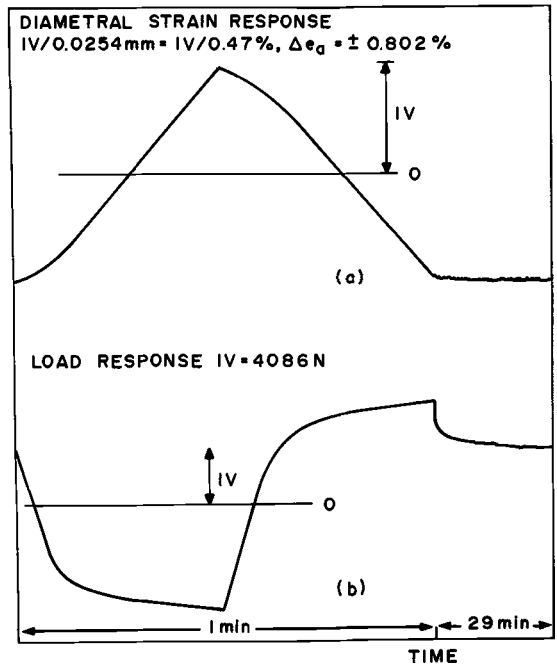

FIG. 7—*Load and diametral strain response for a cycle with hold.*

reason for this is not known, but the small differences in austenitization temperature and tempering, and the large difference in heat-treated forging size, all indicate possibly a higher strength for Ellison and Paterson's steel.

The results of special interest in the present work are the variations with cycling of the ratio of diametral strain range to axial range for tests conducted under axial strain control and with zero-symmetric strain. These variations are shown in Figs. 11 and 12 for cycling without and with holds, respectively. The ordinate in these figures essentially measures the Poisson's ratio for the peaks of the cycle. For the first few cycles, the ratio shows the expected value of 0.5. With increasing cycles, the value increases and then it systematically decreases towards a value of 0.3, *in spite of the fact that plastic strain cycling is maintained.* When we first observed this astonishing result, we were disturbed and believed that some testing anomaly must have caused it. An intensive effort to uncover such an anomaly produced no satisfactory explanation and we are forced to the position that the result is a true one. It is interesting that the decline of the Poisson's ratio can be associated with a decrease of ductility, and, in some sense, the response is similar to the behavior of the post-fatigue creep ductility reported in passing by Ellison and Paterson [2]. Note that the decline in Poisson's ratio occurs faster for cycling

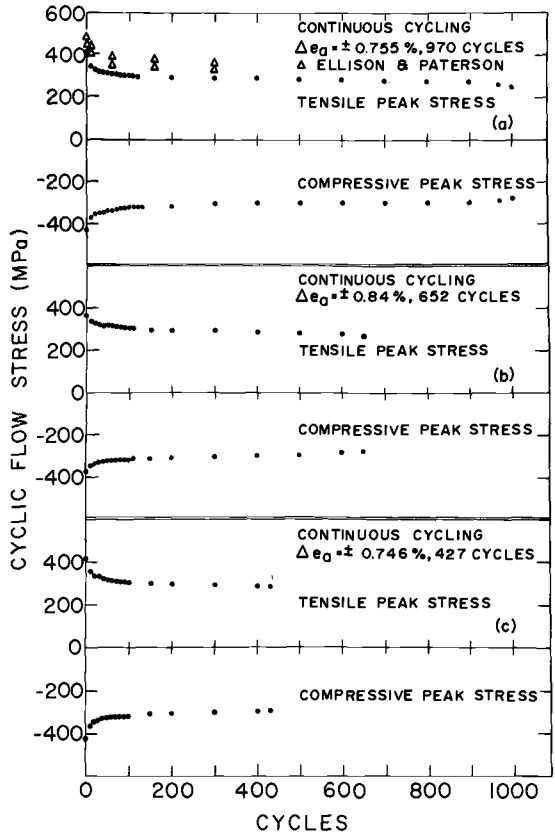

FIG. 8—*Cyclic softening during continuous cycling in total strain control with* $\Delta e = \pm 0.755\%$ (a), $\pm 0.840\%$ (b), *and* $\pm 0.746\%$ (c), *for this work and Ellison and Paterson* [2].

with holds than without holds. We do not yet know how this behavior depends on the magnitude of the strain amplitude.

Microstructural observations of "damage" have been made by optical microscopy, SEM, and TEM. They have not revealed any significant changes in carbide size, morphology, or density, although possible carbide agglomeration may exist. This judgement is based on examinations of many areas per specimen. The principal results apply to variations in the arrangement of dislocation substructures; these are shown in Figs. 13 and 14. The dislocation subboundaries undergo minor reorganization for continuous cycling, and dislocation annihilation and apparent reorganization of subboundaries occur on a major scale in cycling with hold. The clear result is thus the remarkable drop in dislocation density in cycling with hold compared with that without hold, and the differences in the behavior of the Poisson's ratio for the two modes of cycling. Indeed, this indicates a strong dependence of damage

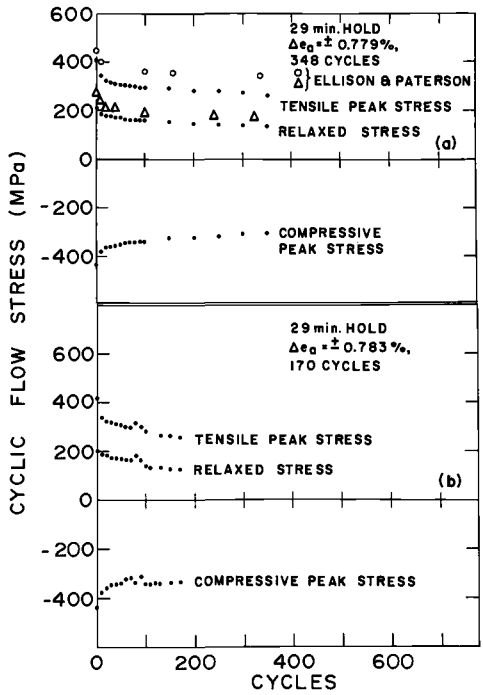

FIG. 9—*Cyclic softening and relaxation during total strain-controlled cycling with 1-cpm cycle and 29-min hold at every tensile strain peak, for this work and Ellison and Paterson* [2].

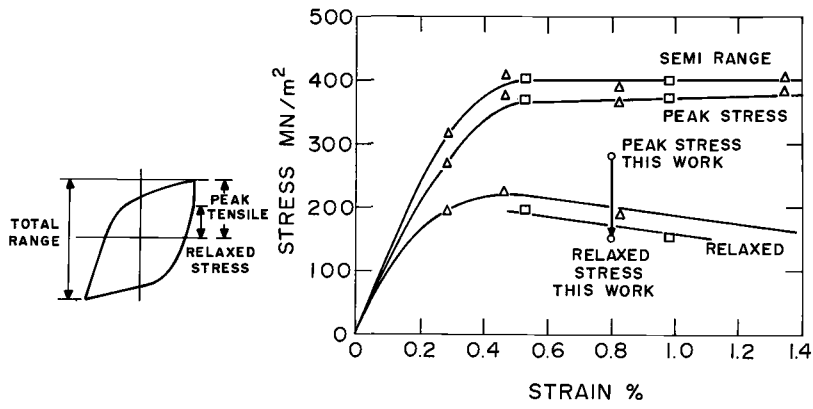

FIG. 10—*Cyclic stress strain curves according to Ellison and Paterson* [2]. *The result for this work is inserted.*

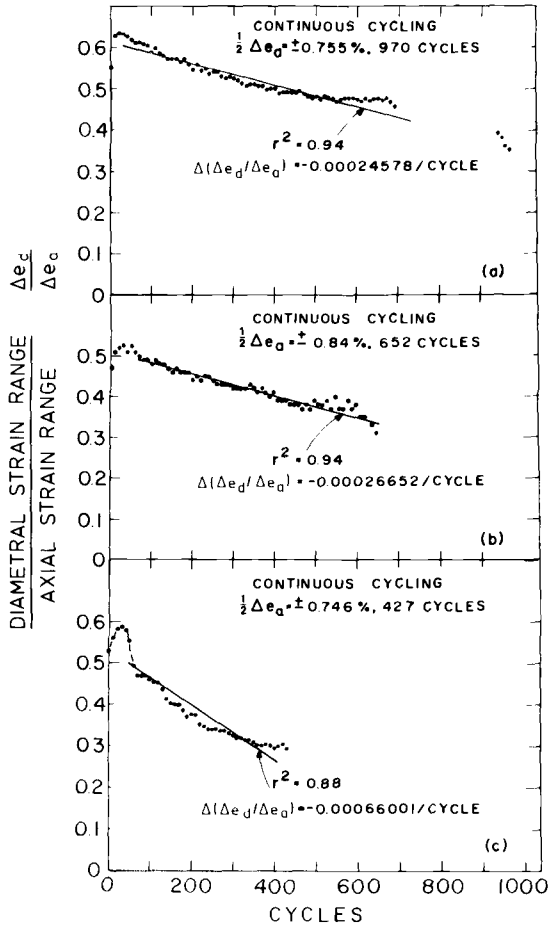

FIG. 11—*Variation of diametrical strain range to axial strain range in continuous cycling for the same specimens illustrated in Fig. 8.*

(both to the microstructure and to the ductility) on the damaging input (the axial strain waveform in our case).

Discussion

Creep and creep-fatigue interaction damage has been exclusively described in the literature on the basis of strength, microstructural variation, or cracking mode; that is, the typical mechanical damage for 1Cr-1Mo-¼ V steel is softening, which might generally be considered to accelerate damage [*32,37*]. Conversely, since for example 2¼Cr-1Mo steel is creep hardening [*39*], the creep-fatigue interaction is at least sometimes "healing"; that is, the linear

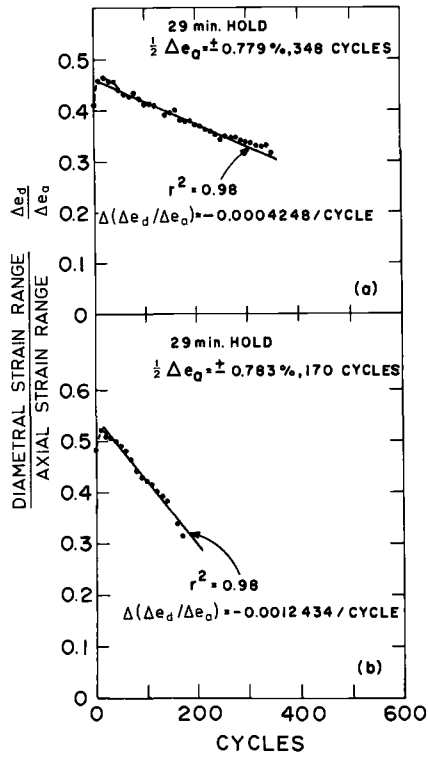

FIG. 12—*Variation of diametral strain range to axial strain range in cycling with hold time for the same specimens as illustrated in Fig. 9.* r^2 *indicates the value of a regression correlation.*

damage summation can be conservative, especially for annealed 2¼Cr-1Mo steel [*32*]. If the description of the mechanical response is limited to strength, it may be that it can tell us something about the relative rates at which damage can accumulate, a softening response giving a greater interaction rate than a hardening response at the strain ranges in question. It is clear, however, that damage estimation based on strength or hardness alone would lead to confusion in materials whose cyclic flow stress is stable or in circumstances where the strength did not vary. For example, if the material flow stress were stable to the exposure conditions, a strength-based damage parameter would not indicate change, whereas clearly the specimen would suffer damage by fatigue, creep, or creep-fatigue. Further, since the cyclic stress response in strain-controlled cycling typically shows a saturation behavior in the course of the initial cycles both in cycling with hold and without hold, it is concluded that a measure of strength response alone (flow stress or hardness) is a quite inadequate assessment of the accumulation of mechanical damage in general. Because we have found here that the Poisson's ratio declines in a

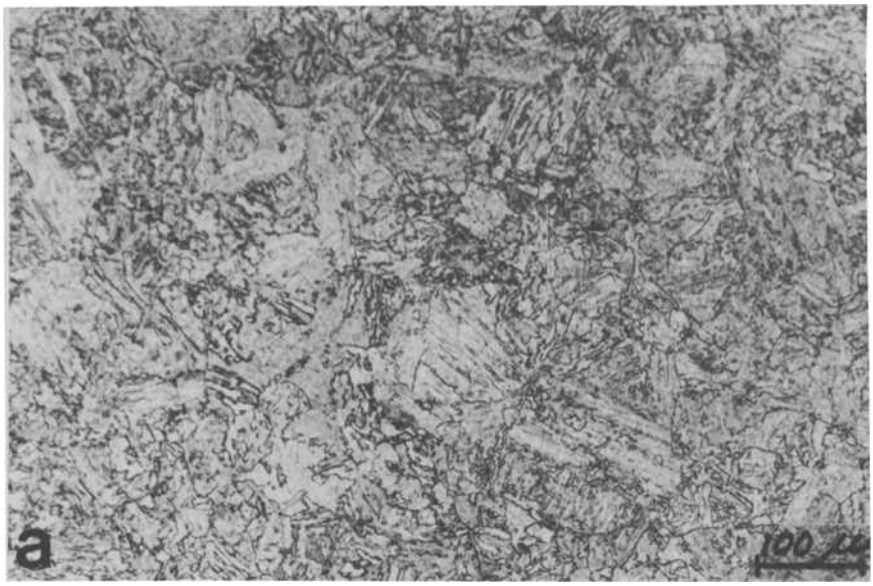

FIG. 13*a*—*Optical micrograph of material in the virgin state.*

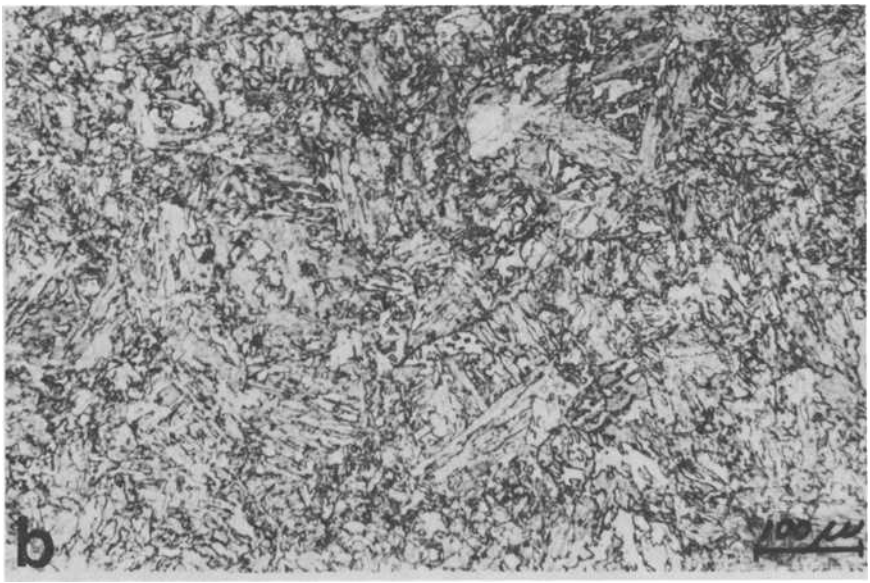

FIG. 13*b*—*Optical micrograph of material cycled continuously for 400 cycles.*

FIG. 13*c*—*Optical micrograph of material cycled with holds for 349 cycles.*

systematic fashion, and this decline is presumably connected with a change of ductility, we naturally propose to study the response of the secondary (diametral) strain as well as the microstructure. Some aspects of ductility have been studied by Coffin [*9*] and indicated by Ellison et al [*1-6*].

When it comes to mechanical behavior, the secondary strain has been studied by different means ever since it was defined by Poisson [*40*]. Quite recently it was used in thermal fatigue evaluation by Carden [*41*], but to the authors' knowledge it has not been studied as an "independent" *in situ* response in fatigue testing. Of course, it has often been used as a control parameter at large strain amplitudes in cyclic tests, when buckling of a cylindrical specimen would have been a problem in axial strain control.

Typical results to date (Figs. 11 and 12) indicate that, in continuous cycling with constant limits of total primary strain, the transverse secondary strain range first rises—incident with the fast initial softening—often to unusually high values (Poisson's ratio may climb above 0.5, for reasons provided subsequently) and thereafter decays at a rate that is much more pronounced than, for example, the softening rate. In cycling with tensile hold—that is, with stress relaxation at each tensile peak—the diametral strain range first rises again, but stays at a lower value than in continuous cycling. Subsequently (with 29-min hold) the decay in secondary strain range is

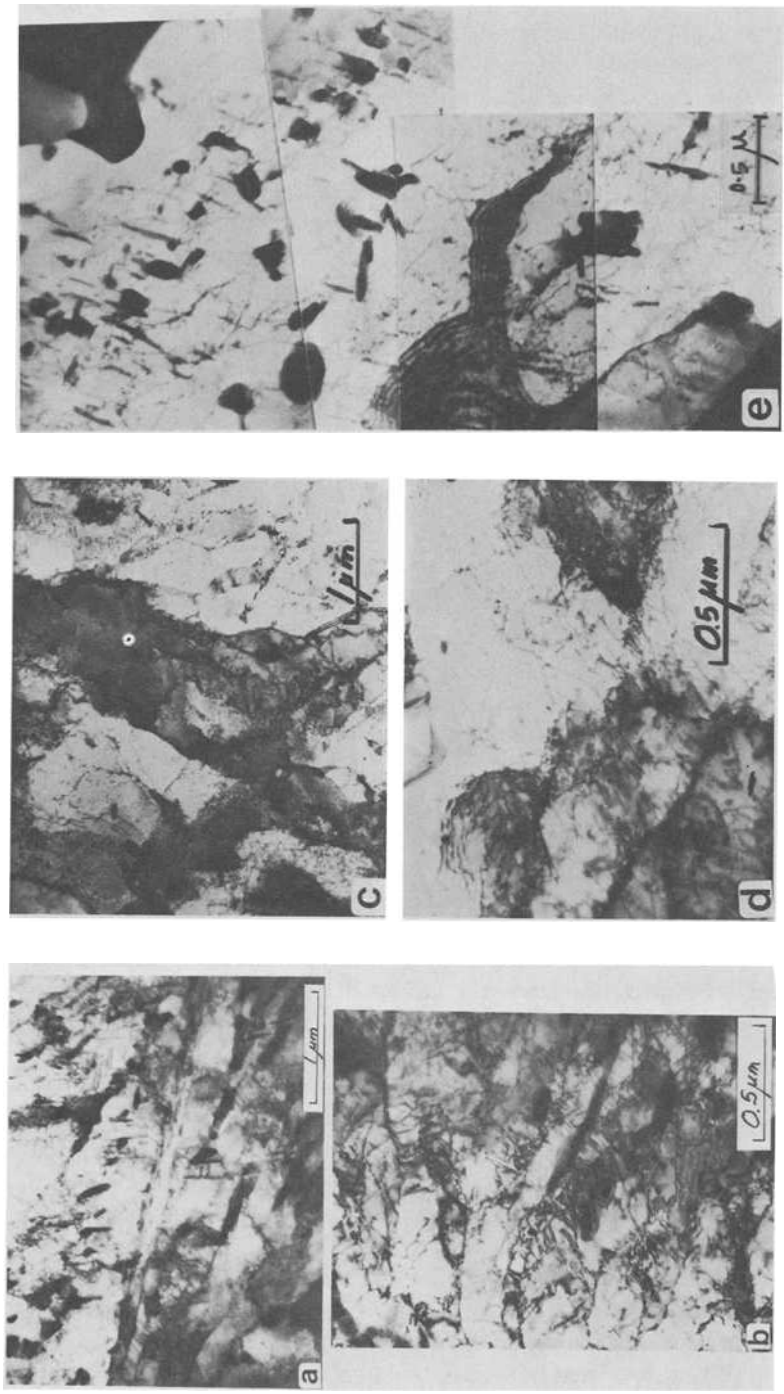

FIG. 14—*Typical TEM micrographs of* (a) *and* (b) *virgin, and* (c) *and* (d) *exposed material, 400 cycles continuous cycling, and* (e) *exposed material, 349 cycles with 29-min hold in tension.*

on an average twice as fast per cycle as in continuous cycling, indicating for this hold time a doubled damage rate compared with that of regular fatigue.

It is of relevance to note that crack embryos of minute size could be observed in the post-test sections (Fig. 6). For the exposures studied by us, however, they formed only late during the softening phase. Even then the crack depths formed were minute compared with those reported by Ellison et al [*1-6*]. Moreover, we detected no early internal cavitation. It is believed therefore that the observed behavior in the transverse strain range is purely a response of the specimen bulk behavior and is not affected by cracking in this material until late in life. At this stage a clear drop in transverse strain range can be seen. The ultimate drop in diametral strain range is especially clear in the case of a specimen cycled continuously for about 1000 cycles. Also, a Poisson's ratio approaching 0 was seen during unloading from tension as a significant crack started to grow.

In all tests, a typical feature of the behavior of the diametral strain range was an initial fast rise. Sometimes the transverse strain range became larger than half of the longitudinal range, which indicated some nonconservative behavior in the material. Although the corresponding specific volume change, $\sim 0.06\%$, is small, it is believed that this behavior is mainly an outcome of macroscopic strain concentration. This may have resulted in part from a compelled specimen design, which means that the cylindrical section had to be made about 0.005 mm (0.002 in.) thinner in the center of the gage length. The purpose of this thinning was partly to provide clear diametral "point" response and partly because otherwise the axial gage wedge pressure required to position the extensometer would have had to be larger. This would have led to unacceptable denting of the specimen at the wedge site, the reason being plastic instability due to dual loading [*42*]. For the same reason a "feather touch" was assured for the diametral gage with a pressure-relieving spring to minimize any waist effect due to this instrument. We are confident that the surprising initial increase of transverse strain with respect to axial strain is mainly caused by macroscopic strain concentration because we could observe it. Since the material is subject to work-softening, strain concentrations persisted.

The role of mean strain accumulation in fatigue, as a fundamental feature for cracking, has been suggested in the past [*43*] and studied [*9*], but even in this context the diametral strain has not received the kind of treatment given in the present work. While the primary mean strain in our work was kept at zero—that is, no drift was allowed in the control—, some drift in diametral mean strain was observed. The report of such observed drift is not a primary object of this paper. However, it can be reported that, in experiments considered to be successful, the change in diametral mean strain was generally found similar to the change in axial strain range. Some irregularities between tests, particularly at the later stages, were observed; that is, in some tests failure (the end of test is defined here as initiation of cracking) was preceded by

monotonic contraction. In others, the drift in mean strain having been initially contractual, it later reversed itself and caused recovery of the original diameter. In all, the drift aspect deserves more attention and will be reported when a full picture emerges (this involves testing at other strain amplitudes). In the light of our results to date, however, drift does not seem to provide the dominant mechanism for fatigue or creep-fatigue damage. Instead, bulk change in ductility associated with the response of the diametral strain range (the mechanism of which we still do not understand) is suggested to indicate the answer. In the majority of practical cases, of course, such behavior will operate in combination with drift, ratchetting, and similar kinds of phenomena.

It seems clear that a pronounced difference exists between the detailed microstructure produced by continuous cycling and that produced by cycling with 29-min hold. Apparently both dislocation density and subgrain morphology are concerned (Figs. 13 and 14). The remarkable fact seems to be that along with the differences for the two kinds of test, the microstructural impressions do not provide one single image of the damage state (fraction of life) of the material. Rather, the microstructure is dependent on test waveform. Both for cycling with hold and for continuous cycling, the transverse strain ranges are comparable, however, approaching a value of 30% of the axial (controlling) strain range as damage is accumulated. This value, 30% of the longitudinal strain, is roughly the Poisson's ratio for elastic behavior of steel. Since the behavior tends to apparent elasticity, it can be understood to indicate zero ductility.

The exhaustion of ductility as described here does not mean a cessation of plasticity—that is, sudden fracture without a yield—, but only that microstructural conditions of deformation have developed that are favorable to a lowered ductility and hence gradual cracking, provided at least that the same loading pattern continues. The microstructural patterns at the early crack growth stage (late in our test) indicate significant differences for cycling with hold and continuous cycling. Hence a model based on dislocation density does not seem to provide a model for the yield strength as it may do for some cases at a lower temperature [*44*]. Rather, it seems as if a stress dependence of the dislocation density in creep [*45,46*] should be understood to apply for creep fatigue as well. The significant stress must be taken to be the peak stress for continuous cycling and the relaxed stress for cycling with hold. More detailed evaluation of this point is underway.

The drop in ductility (diametral strain range in our case) seems to lend itself best for determining the *rate* of damage accumulation, whereas the dislocation structure is part of a picture of the history-dependent *state* of damage. In order to simplify the *rate* aspect, a linear regression analysis was done on the results of diametral strain range versus cycles. This analysis yielded the data presented in Table 4 and in Figs. 11 and 12.

By using the approximate constant decremental rate of the diametral strain range, we may calculate a damage rate on the following basis. Virgin

material has a capacity to suffer damage which is related to full plasticity; that is, the difference between the total strain (total diametral strain range) and the elastic strain (regarded as equal to zero ductility, namely $\Delta e_d/\Delta e_a = 0.3$). In the ideal case, therefore, plasticity is given by $0.5 - 0.3 = 0.2$. Consumption of this capacity of ductility is equivalent to the number of cycles to incubate cracking, which can be estimated by taking the quotient of the virgin state (100%) ductility and the percent damage per cycle read from Table 4; that is, in the case of continuous cycling the estimate is 100%/0.2% per cycle = 500 cycles and with hold the estimate is 100%/0.42% per cycle = 240 cycles. Cycling with 29-min hold therefore gives a damage rate/cycle roughly twice as high as in continuous cycling, and a crack incubation count which is half as great. Because of the apparent variation in strain localization from specimen to specimen we have averaged the change in diametral strain range per cycle for the different tests recorded. The calculated number of cycles for exhaustion of ductility naturally corresponds fairly well with the experimental mean values, 682 for continuous cycling and 259 cycles with hold.

Conclusions

This report is the first from a DOE-sponsored project on the characterization of creep-fatigue damage in a 1Cr-1Mo-¼V rotor steel, and it focuses on damage in the early stages of life. Inter-relationships of literature results have been developed, as well as results from a new experimental approach based on transverse (diametral) strain range response in strain-controlled testing with the total axial strain amplitude held constant. In addition, observations of the damaged microstructure are presented. The following conclusions are drawn:

1. A recently proposed ductility exhaustion mechanism [*1-6*] of creep fatigue damage in 1Cr-Mo-V steel is found not to be general because it is intimately connected to low-ductility, intergranular creep cracking, which is sensitive to steel treatment.

2. Early high-temperature fatigue and creep-fatigue damage rate is uniquely characterized by the diametral (secondary) strain range response in a manner

TABLE 4—*Drop in diametral strain range as approximated by a linear regression curve fit.*

	Total Cycles	$\Delta e_d/\Delta e_a$ per Cycle	% Damage per Cycle (Mean)
Continuous tests	970	0.00025	0.20
	650	0.00027	
	427	0.00066	
29-min hold in tension	348	0.00042	0.42
	170	0.00124	

which resembles literature data [2] on post-fatigue creep ductility and fatigue data with superimposed monotonic strain [9]. The data are not yet sufficient to determine how this behavior is dependent on strain amplitude.

3. In the rotor steel tested by us, a hold time of 0.5 h at the tensile maximum strain leads to a ductility exhaustion damage rate based on secondary strain response that is roughly twice as fast per cycle as in continuous cycling.

4. Microstructural features on a fine scale (apparent dislocation density and subgrain morphology) seem to describe the amount of fatigue or creep fatigue damage as dependent on damaging input (waveform, load, axial strain, or diametral strain). Indeed, the dependence of this microstructure on the input waveform seems to indicate a picture of service history that may provide invaluable information in practice. A need for further effort in this direction is obvious.

Acknowledgments

The professional support of Mr. Raymond de la Veaux during test implementation is gratefully acknowledged. Inspiring discussions with the fatigue group at the University of Pennsylvania are remembered (KR) with gratitude. Support in the form of test material from Westinghouse, Lester, Pennsylvania, and the Metals Properties Council is also acknowledged. This work is the first public report on steel from an ongoing DOE-sponsored research project (DE-AC02-80ER105170). Basic support from the National Science Foundation to the Mechanical Testing Facility of LRSM under Grant DMR79-23647 is acknowledged, as is personal Finnish support (KR) from the Technical Research Center of Finland (VTT), the Walter Ahlström Foundation, and the Emil Aaltonen Foundation.

References

[1] Priest, R. H. and Ellison, E. G., *Materials Science and Engineering*, Vol. 49, 1981, pp. 7-17.

[2] Ellison, E. G. and Paterson, A. J. F., *Proceedings of the Institution of Mechanical Engineers*, Vol. 190, Dec. 1976, pp. 331-338.

[3] Ellison, E. G. and Paterson, A. J. F., *Proceedings of the Institution of Mechanical Engineers*, Vol. 190, Dec. 1976, pp. 319-330.

[4] Paterson, A. J. F. and Ellison, E. G., *Proceedings of the Institution of Mechanical Engineers*, Vol. 190, Dec. 1976, pp. 339-348.

[5] Ellison, E. G. in *AGARD Conference Proceedings No. 243: Characterization of Low-Cycle High-Temperature Fatigue by the Strain Range Partitioning Method*, 46th Meeting of the AGARD SCM Panel, Aalborg, Denmark, 11-12 April 1978, Paper 14, pp. 14-1—14-9.

[6] Bartlett, R. A., Plumbridge, W. J., Chung, T. E., and Ellison, E. G. in *Fracture 1977*, D. M. R. Taplin, Ed., Vol. 2, 1 CF 4, Waterloo, Canada, 19-24 June 1977, pp. 831-837.

[7] Krempl, E. and Walker, C. D. in *Fatigue at High Temperature, ASTM STP 459*, American Society for Testing and Materials, 1969, pp. 75-99.

[8] Leven, M., *Experimental Mechanics*, Vol. 13, Sept. 1973, pp. 353-372.

[9] Coffin, L. F., Jr., in *Achievement of High Fatigue Resistance in Metals and Alloys, ASTM STP 467*, American Society for Testing and Materials, 1970, pp. 53-76.

[10] Jones, M. H., Newman, P. P., Sachs, G., and Brown, W. F., *Transactions of the American Society for Metals*, Vol. 47, 1955, pp. 926-956.
[11] Werner, F. E., Eichelberger, T. W., and Hamer, E. K., *Transactions of the American Society for Metals*, Vol. 52, 1960, pp. 376-403.
[12] Woodhead, J. H., *Journal of the Iron and Steel Institute*, Sept. 1966, pp. 894-896.
[13] Discussion, *Journal of the Iron and Steel Institute*, Sept. 1966, pp. 896-904.
[14] Goldhoff, R. M. and Beattie, H. J., *Transactions of AIME*, Vol. 233, Sept. 1965, pp. 1743-1756.
[15] Stone, P. G. and Murray, J. D., *Journal of the Iron and Steel Institute*, Nov. 1965, pp. 1094-1107.
[16] Relander, K. and Geiger, T., *Journal of Engineering for Power, Transactions of ASME*, April 1967, pp. 238-246.
[17] Viswanathan, R., *Metals Engineering Quarterly*, Nov. 1975, pp. 50-56.
[18] Tu, L. K. L. and Seth, B. B., *Metals Technology*, March 1978, pp. 79-91.
[19] Roan, D. F. and Seth, B. B. in *Ductility and Toughness Considerations in Elevated Temperature Service*, A. D. Schaefer, Ed., ASME Winter Meeting, San Francisco, 10-15 Dec. 1978, ASME-MPC-8, 1978, pp. 79-97.
[20] Murphy, M. C. and Branch, G. D., *Journal of the Iron and Steel Institute*, Oct. 1969, pp. 1347-1364.
[21] Norton, J. F. and Strang, A., *Journal of the Iron and Steel Institute*, Feb. 1969, pp. 193-203.
[22] Bethlehem laboratory sheet on 1Cr-1Mo-¼V rotor steel supplied for this work by Westinghouse, Bethlehem, Pa., courtesy B. B. Seth.
[23] Tipler, H. R. and Hopkins, B. E., *Metal Science*, Feb. 1976, pp. 47-56.
[24] Tipler, H. R., Taylor, L. H., Thomas, G. B., Williamson, J., Branch, G. D., and Hopkins, B. E., *Metals Technology*, May 1975, pp. 206-219.
[25] Hopkins, B. E., Tipler, H. R., and Branch, G. D., *Journal of the Iron and Steel Institute*, Sept. 1971, pp. 745-746.
[26] Jaffee, R. I., *Metallurgical Transactions A*, Vol. 10A, Feb. 1979, pp. 139-164.
[27] Kramer, L. D. and Randolph, D. D., "Metallurgical Considerations," Part 1 of Analysis of the Tennessee Valley Authority, Gallatin Unit No. 2 Turbine Rotor Burst, Westinghouse paper, presented at ASME Winter Meeting, New York, 5-10 Dec. 1976.
[28] Kramer, L. D. in *Fractography in Failure Analysis, ASTM STP 645*, American Society for Testing and Materials, 1978, pp. 249-274.
[29] Hollomon, J. H. and Jaffee, L. D., *Transactions of AIME*, Vol. 162, 1945, pp. 223-249.
[30] Swaminathan, V. P., "Advanced Technology High-Temperature Cr-Mo-V Steam Turbine Rotors," presented at ASM Conference on Solution to Materials Problems in Power Plants, Philadelphia, 2-3 Dec. 1980.
[31] Jaske, C. E. and Mindlin, H., "Elevated-Temperature Low-Cycle Fatigue Behaviour of a 2¼Cr-1Mo and a 1Cr-1Mo-¼V Steel," in *Symposium on 2¼Cr-1Mo Steel in Pressure Vessels and Piping*, ASME G11, A. O. Schaefer, Ed., 16-17 Sept. 1971, Denver, ASME, New York, 1971.
[32] Curran, R. M. and Wundt, B. M., "A Study of Low-Cycle Fatigue and Creep Interactions in Steels at Elevated Temperatures," presented at 1974 ASME Winter Meeting, in *Current Work on Behaviour of Materials at Elevated Temperatures*, A. O. Schaefer, Ed., ASME-MPC, New York, 1974, pp. 1-104.
[33] Goldhoff, R. M., contribution to Discussion, in *Joint International Conference on Creep*, 25-29 Aug. 1963, New York, and 30 Sept.-4 Oct. 1963, London, ASME/ASTM/Institution of Mechanical Engineers, Vol. II—Discussion, Institution of Mechanical Engineers, London, 1963, p. D121.
[34] Woodford, D. A. and Goldhoff, R. M., *Materials Science and Engineering*, Vol. 5, 1969-1970, pp. 303-324.
[35] Goldhoff, R. M., *Journal of Basic Engineering*.
[36] Goldhoff, R. M., "Stress Concentration and Size Effects in a Cr-Mo-V Steel at Elevated Temperatures," Paper 8, in *Joint International Conference on Creep*, 25-29 Aug. 1963, New York, and 30 Sept.-4 Oct. 1963, London, ASME/ASTM/Institution of Mechanical Engineers, Institution of Mechanical Engineers, London, 1963, pp. 4-11—4-32.
[37] Goldhoff, R. M. and Woodford, D. A. in *Testing for Prediction of Material Performance*

in Structures and Components, ASTM STP 515, American Society for Testing and Materials, 1972, pp. 89-106.

[*38*] Brozzo, P., "A Method for the Extrapolation of Creep and Stress-Rupture Data of Complex Alloys," Paper 67, in *Joint International Conference on Creep*, 25-29 Aug. 1963, New York, and 30 Sept.-4 Oct. 1963, London, ASME/ASTM/Institution of Mechanical Engineers, Institution of Mechanical Engineers, London, 1963, pp. 6-77—6-85.

[*39*] Lonsdale, D. and Flewitt, P. E. J., *Metals Science and Engineering*, Vol. 39, 1979, pp. 217-219.

[*40*] Köster, W. and Franz, H., *Metallurgical Review*, Vol. 6, No. 21, 1961, pp. 1-55.

[*41*] Carden, A. E. in *Manual on Low Cycle Fatigue Testing, ASTM STP 465*, American Society for Testing and Materials, 1970, pp. 163-188.

[*42*] Coffin, L. F., *Journal of Basic Engineering, Transactions of ASME*, Sept. 1960, pp. 671-682.

[*43*] McClintock, F., *Fracture of Solids*, Interscience Publishers, New York, 1963, pp. 65-102.

[*44*] Törrönen, K., "Microstructural Parameters and Yielding in a Quenched and Tempered Cr-Mo-V Pressure Vessel Steel," Ph.D. thesis, VTT Publication 22, Technical Research Center of Finland, Espoo, 1979.

[*45*] McLean, D. and Hale, K. F., "Structural Processes in Creep," ISI Special Report 70, Iron and Steel Institute, London, 1961, p. 19.

[*46*] Lagneborg, R., *International Metals Reviews*, Review 165, Vol. 17, 1972, pp. 130-146.

Early Stages of Damage

Growth of Small Cracks

Winfred L. Morris[1] *and Michael R. James*[1]

Statistical Aspects of Fatigue Failure Due To Alloy Microstructure

REFERENCE: Morris, W. L. and James, M. R., **"Statistical Aspects of Fatigue Failure Due to Alloy Microstructure,"** *Fatigue Mechanisms: Advances in Quantitative Measurement of Physical Damage, ASTM STP 811*, J. Lankford, D. L. Davidson, W. L. Morris, and R. P. Wei, Eds., American Society for Testing and Materials, 1983, pp. 179-206.

ABSTRACT: The elements of a methodology are described to calculate the scatter in fatigue lifetime which arises from statistical variations in alloy microstructure from sample to sample within a uniform heat of material, and from variations in mean grain size and in the ductility of the alloy surface from heat-to-heat. The modeling is formulated for certain structural aluminum alloys for which the dominant mode of crack initiation is by fracture of constituent particles near the alloy surface. For one of these, an Al 2219-T851 alloy, small amounts of internal hydrogen at contents less than 1 ppm are found to affect surface ductility and both crack initiation and early growth. The application of models of crack initiation and short crack growth to predict the combined effects of grain size and hydrogen on fatigue lifetime is demonstrated for smooth bar specimens of two heats of Al 2219-T851. Experiments confirm predictions that fatigue lifetime is increased by decreasing both grain size and alloy hydrogen content.

The models used to predict fatigue lifetime are discussed individually and deal with both the initiation and the early growth of surface fatigue cracks. They are evaluated by comparing predicted and measured mean and stochastic trends in rates of initiation and growth in Al 2219-T851 and Al 7075-T6. The paper concludes with a short treatment of the implication of the statistical nature of the fatigue failure process to prediction of the occurrence of failures of low probability, very early in the service lifetime.

KEY WORDS: fatigue, microstructure, mathematical modeling, micromechanics, crack initiation, short crack growth

Modern design and in-service maintenance strategies called Repairability, Retirement-for-Cause, and Damage Tolerant Design will be employed with increasing sophistication in the coming years to increase the service lifetime of high-performance aircraft. These methods all rely on an ability to accurately predict the fatigue propagation of short cracks. In their optimum forms, Repairability and Retirement-for-Cause will also require accurate predictions of

[1]Rockwell International Science Center, Thousand Oaks, Calif. 91360.

crack initiation. Methods for such predictions range from adequate to nonexistent, depending on materials and loading requirements. A special problem is that a reliable and inexpensive method of predicting the probability of early fatigue failure is not available. Large-scale fatigue testing in which hundreds of specimens are broken is too expensive; and unfortunately, extrapolation of the early failure characteristics of an alloy from a few experimental results is unreliable, as demonstrated by Bloomer and Roylance [*1*] and by Korbacher [*2*] for polycrystalline aluminum and copper, respectively.[2] Neither Weibull or lognormal distributions were adequate for such extrapolation, apparently because the mechanisms controlling early and mean fatigue lifetime are different.

To replace extensive fatigue testing, Provan [*3*], Ghonem and Provan [*4*], and McCartney [*5*] have proposed models that allow failure statistics to be calculated from alloy microstructure. These idealize the fatigue failure process and remain to be verified. Alternatively, we have pursued the formulation of a statistical model of fatigue failure which seeks to accurately represent microscopic processes of crack initiation and short crack growth and their relationship to alloy microstructure. Since this approach was first outlined [*6*], we have learned that these processes are much more varied and complex than originally anticipated. Progress has been made, however, and we show in this paper that the scatter in fatigue lifetime of a Al 2219-T851 alloy can be calculated from its grain size and internal hydrogen content.

Experimental Procedure

Growth rate data were obtained by using small tapered cantilever beam specimens of the type illustrated in Fig. 1. All aluminum alloys were machined with progressively decreasing cutting depths and then mechanically polished, ending with 0.05-μm Al_2O_3 powder. This procedure minimizes residual stresses on the specimen surface. Grain size and yield strength of the various aluminum alloys studied are listed in Table 1. Specimens were fatigued in bending under fully reversed loading in laboratory air of approximately 50% relative humidity. Crack lengths were measured at intervals by using an optical microscope equipped with a jig to load the specimen in tension for improved visability. A similar jig was used in a scanning electron microscope for crack tip opening displacement measurements, and to count fractured constituent particles (Fig. 1).

Two heats of Al 2219-T851 used in this study, denoted II and III, have substantially different crack initiation and growth behavior which we attribute to hydrogen content. Hydrogen contents of less than 1 ppm appear to affect the fatigue properties of this alloy. These are too small to be reliably measured by gas extraction analysis; commercially measured contents for both heats are

[2]The italic numbers in brackets refer to the list of references appended to this paper.

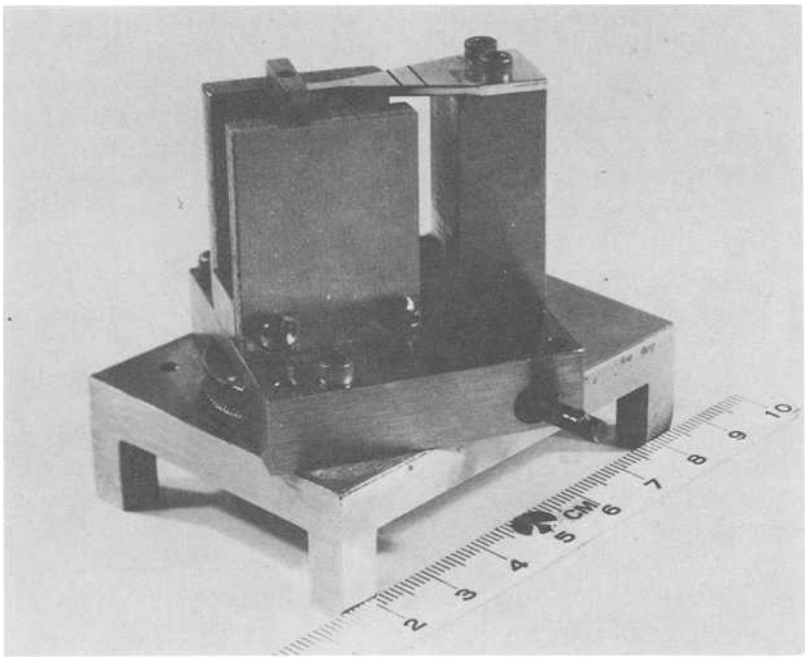

FIG. 1—*Tapered cantilever beam flexural fatigue specimen mounted in loading jig. To avoid the stress concentration at the gripping points, data are taken between the parallel lines marked on the specimen.*

TABLE 1—*Alloy properties.*

Material	Transverse Grain Size, μm	Hydrogen Content	Yield Strength, MPa
Al 2219-T851 (Heat II)	30	high	360
Al 2219-T851 (Heat III)	60	low	360
Al 7075-T6	12, 130	unknown	500 to 510

less than 1 ppm. A qualitative technique was employed to rank the amount of hydrogen in the two materials. Samples 0.15 cm thick were annealed at 515°C, and the number of gas bubbles formed in the interior of subsequently sectioned and polished specimens was determined by optical microscopy. Peak densities of bubbles were formed after 3 h. A histogram, for this annealing time, of bubble number versus diameter for the two heats is given in Fig. 2. We infer that Heat II contains substantially more hydrogen than does Heat III. Such differences in hydrogen content might be a function of the amount of scrap metal used in preparing the melt.

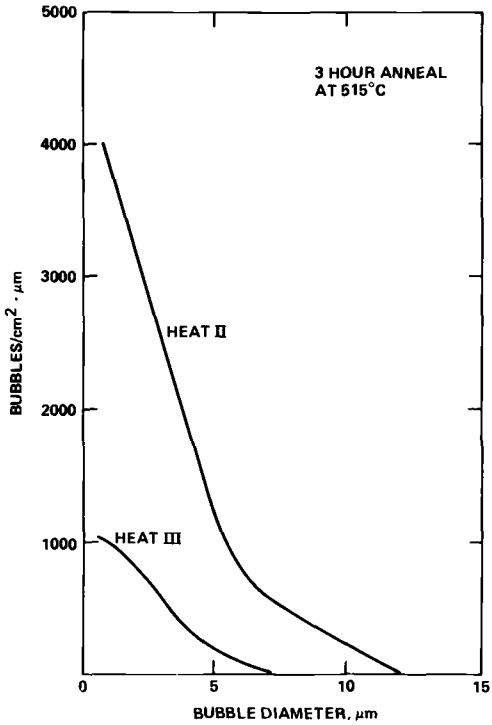

FIG. 2—*Histogram of the number of bubbles found on the surface of specimens of Al 2219-T851 after annealing for 3 h at 515°C.*

Statistical Model of Constituent Particle Fracture

The earliest crack initiation events occur because of unusual combinations of alloy microstructure in the vicinity of an initiation site. These are frequently responsible for the ultimate fatigue failure of a component, especially at low cyclic stress amplitude where few cracks are initiated. The statistical scatter in lifetime due to crack initiation can be quite important, as pointed out by work of Hunter and Fricke [*7-9*] over 25 years ago.

Common sites of fatigue crack initiation in structural aluminum alloys are at constituent particles, in slip bands, or at grain boundaries. The wealth of information of fatigue-induced dislocation structures has provided only partial guidance to the formulation of models of crack initiation at such sites. A difficulty has been the identification of appropriate criteria for crack formation.

It is also now realized that fatigue-induced changes in the mechanical properties of the surface are complex. Pangborn et al [*10*] have demonstrated, using X-ray diffraction rocking curve measurements on Al 2024-T3, that the near-surface excess dislocation density increases during fatigue, ultimately

reaching a saturation level. Their measurement technique favors the analysis of large grains, and it appears that cracking begins first in these grains after the excess density reaches saturation. Pangborn et al interpret this as the point of maximum surface hardening.

Recently, we have been able to measure fatigue-induced local plastic strains ($\Delta\epsilon_p$) within individual surface grains. This is accomplished by comparing displacements in the surface to flakes of mica placed in the grains as a reference [*11*]. As reported elsewhere in this volume [*12*], we find that it is important to distinguish microplasticity and hardness of the surface when devising initiation models. $\Delta\epsilon_p$ first increases as new mobile dislocations are generated within a grain on each loading cycle. $\Delta\epsilon_p$ reaches a peak and then decreases as the mobility of the dislocations progressively decreases. For Al 2219-T851, indentation hardness and measurements of the duration of retarded crack growth at grain boundaries show that the cyclic hardening of the surface associated with reduced mobility begins long before $\Delta\epsilon_p$ reaches its peak. Peak values of $\Delta\epsilon_p$ are reached more rapidly in larger grains and in Al 2219-T851 containing larger quantities (but still trace amounts) of internal hydrogen. At least for crack initiation by particle fracture, it appears that the major stochastic elements are the effect of grain size on the local plastic strain $\Delta\epsilon_p$ and the relationship between $\Delta\epsilon_p$, particle size, and the propensity for particle fracture. These factors are considered here.

Particle Fracture Model

Constituent particles are common sites of crack initiation in those alloys in which particles exceed 5 μm in size. There is substantial evidence that the fracture of constituent particles requires a critical value of $\Delta\epsilon_p$, that is, plastic strain within a grain, which is larger the smaller the particle. Chang et al [*13*] and Tanaka and Mura [*14*] have proposed models of particle fracture which employ a strain energy fracture criterion. The strain energy within a particle, induced by a pile-up of dislocations at the particle-matrix interface, is equated with the surface energy required to create the fracture. Cycles needed to develop the pile-up, which is equivalent to the number of cycles required to reach a critical value of $\Delta\epsilon_p$, can be calculated for an elastic-perfectly-plastic material. We have reported [*15*] for Al 2219-T851 that the dependence of the rate of particle fracture upon cyclic stress amplitude predicted by both models is not as strong as is experimentally observed; far fewer particles are fractured at low stress amplitude than predicted. We have proposed [*15*] an empirical modification to the Chang model [*13*] to account for the reduction in $\Delta\epsilon_p$ resulting from cyclic hardening of the surface. This allows our observations to be modeled, but involves too many adjustable parameters to be entirely satisfactory. Furthermore, the model only correctly predicts the behavior of $\Delta\epsilon_p$ as it is increasing. Fortunately, this is the regime of importance to crack initiation. This model is used later and is stated here for completeness. The equations relate a

progressive increase in mobile dislocation density (η), and in local friction stress (τ_i) to cycles, cyclic stress amplitude, and to the size of individual grains and the particles they contain.

Microplastic Development Equations

$$\frac{d\eta}{dN} = K_1 D_{max}(\tau_e - \tau_i - K_2\eta) \qquad \text{at } N = 0, \eta = 0 \tag{1}$$

$$\frac{d\tau_i}{dN} = \theta(\tau_e - \tau_i) \qquad \text{at } N = 0, \tau_i = \tau_0 \tag{2}$$

$$\Delta\epsilon_p \propto \eta \tag{3}$$

Fracture Criterion

$$\text{strain energy} = \text{surface energy}$$

$$E w^3 \frac{\eta^2}{2} \propto 2\gamma w^2, \qquad \gamma_{min} \leq \gamma \leq \gamma_{max} \tag{4}$$

where E is the elastic modulus of the particle, N is the number of fatigue cycles, and D_{max} and w are the distance of slip from particle to grain boundary and particle sizes, respectively. τ_e is an effective local shear stress, which is proportional to the applied stress but is modified to account for the effect of grain crystallographic orientation on propensity for slip parallel to the surface [*16*]. γ is the fracture surface energy which lies in a range from γ_{min} to γ_{max}, τ_0 is the friction stress at $N = 0$ fatigue cycles, and K_1 and K_2 are material parameters. The model is used to calculate the number of particles fractured during fatigue by numerical integration over the various combinations of grain and particle sizes and grain crystallographic orientations present in the alloy at the surface.

Results and Discussion

The general trend in Al 2219-T851 is for large particles in the large grains to fracture first [*16*] as would be anticipated from Eqs 1 and 4. Kung and Fine [*17*] and Grosskreutz and Shaw [*18*] have reported the same effect of particle size in other alloys. The statistical effects of grain size and their orientation are, however, quite important and must be considered in predicting numbers of particles fractured during fatigue.

In Fig. 3 we illustrate the effect of grain size on particle fracture by comparing predicted (from Eqs 1 to 4) and measured numbers of fracture events as a

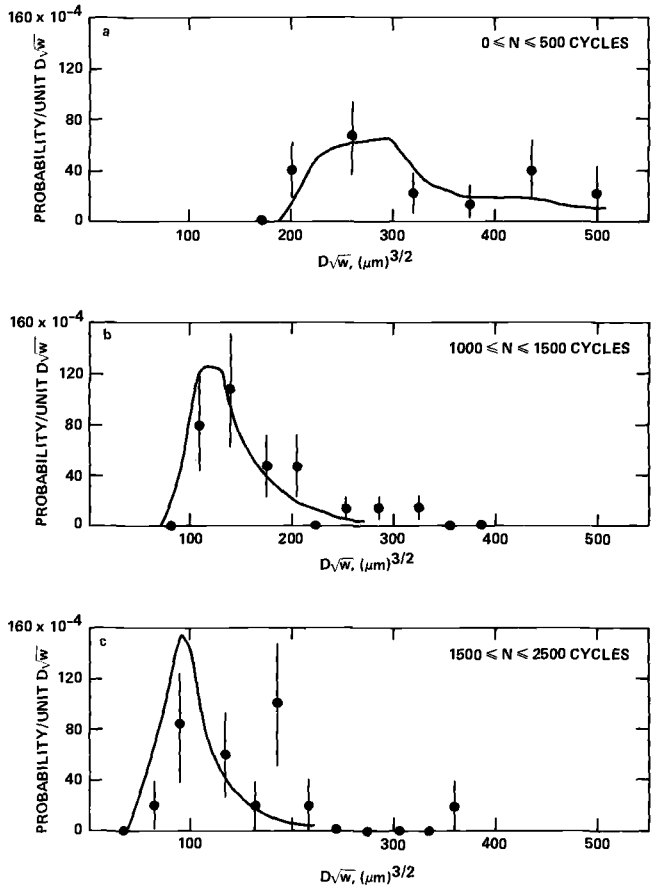

FIG. 3—*Comparison of predicted (solid line) and experimentally determined probabilities of particle fracture as a function of the product* $D_{max}\sqrt{w}$, *for various increments in fatigue at a cyclic stress amplitude of* ± 330 *MPa.*

function of $D_{max}\sqrt{w}$ for Al 2219-T851 (Heat III). For the special case of large cyclic stress amplitude (± 330 MPa), cyclic hardening can be neglected and the product of slip distance and particle size determines the probability of fracture. Predictions are made using the D_{max} and particle size distributions given in Fig. 4. Once each particle breaks, it produces a crack the size of the particle.

In a rolled alloy, the grain cross section is commonly largest in the rolling plane. Smooth bar samples, the fatigue lifetimes of which we characterize later, were machined with their axis parallel to the rolling direction. On these, the size of the surface grains varies with location about the circumference of the bar. Fewer particles are fractured on the side of the bar containing the

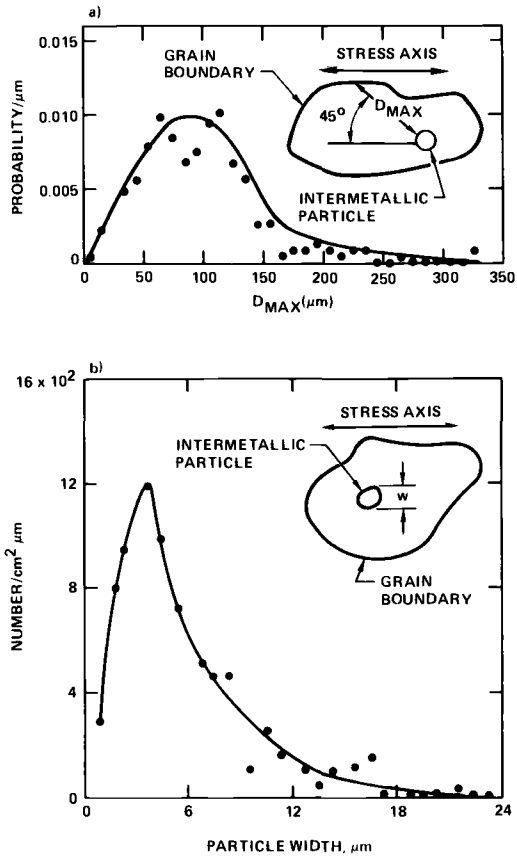

FIG. 4—*Distributions in particle to grain boundary slip distance and in constituent particle sizes of 2219 Heat III material. Data points are experimental and solid line is the curve fit used in the computer simulation.*

smallest grains (Fig. 5). The curves are of the form $1/D_{max}$, where in this case D_{max} is that of the largest slip distance in ten values.

Early Growth

Linear elastic fracture mechanics (LEFM) is not always adequate to predict crack growth rate. Problems are encountered when cracks are short and/or growing through regions of large plastic deformation, or where crack growth is affected by time-dependent processes such as can occur at high temperature or in aggressive environments. Mechanisms have been discovered which account for experimental observations of growth rates both faster and slower than expected from LEFM; they are reviewed separately here.

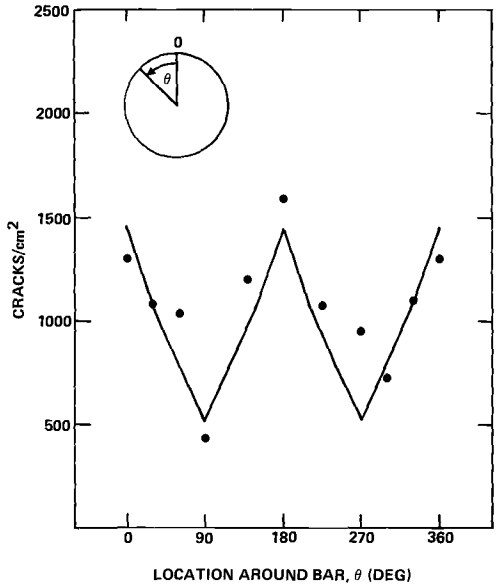

FIG. 5—*Numbers of particles fractured around the circumference of a smooth bar varies because the grain size (see inset) changes with location around the bar.*

Growth Rates Faster Than LEFM Predictions—Short fatigue cracks often propagate more rapidly than expected from LEFM [*19-23*]. One manifestation of this is that crack growth rates increase with cyclic stress amplitude (σ_a) for fixed cyclic stress intensity (ΔK). Consequently, threshold values of cyclic stress intensity (ΔK_{th}), which must be exceeded to produce crack growth, are a function of crack length. ΔK_{th} for a Al 2219-T851 alloy (Heat III), given in Fig. 6, is typical of the variation with crack length (a) that has been reported. At sufficient lengths, ΔK_{th} approaches an equilibrium value (ΔK_0) for a fixed R-ratio. To rationalize this behavior, El Haddad et al [*24*] have hypothesized that short cracks behave as if they were a length a_0 longer than their true length. This leads to the result

$$\Delta K_{th} = \Delta K_0 \sqrt{a/(a + a_0)} \tag{5}$$

As prescribed by El Haddad et al, a_0 can be calculated from ΔK_0 and the alloy endurance limit. For steels, a_0 increases with alloy grain size and decreases with alloy yield strength [*24,25*]. The solid curve in Fig. 6 is predicted using Eq 5 by setting $a_0 = 60$ μm, the average grain size ($\Delta K_0 = 1.95$ MPa $\sqrt{m}$). This expression frequently provides a good empirical description of the relationship of crack length to ΔK_{th}. While the model has been successfully

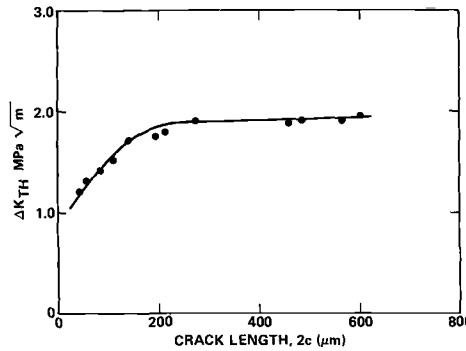

FIG. 6—ΔK_{th} *increases with crack length in a 60-μm grain size Al 2219-T851 alloy, reaching the equilibrium value of* ΔK_0 *at a crack length of 250 μm. Solid curve is from Eq 5 using* $a_0 = 60$ *μm.*

employed [*26*], there is an absence of physical insight into why it works and when it might fail.

Several models based on mechanistic concepts have been advanced to explain the small thresholds and rapid growth of short cracks. We have reported elsewhere [*27,28*] that the effectiveness of fracture surface roughness in propping open short surface cracks in a fine-grained Ti 6Al-2Sn-4Zr-6Mo alloy increases with crack length. Roughness prevents full crack closure on unloading and causes the effective cyclic stress intensity to be less than that calculated from the applied stress range. In this alloy, ΔK_{th} is smaller than ΔK_0 for very short cracks because they close more completely at minimum load. High-strength materials having a large grain size and low ductility should react most strongly to this mechanism.

Smith [*29*] and Yang and Liu [*30*] conclude that LEFM will underestimate growth rates for short cracks because of a large ratio of plastic zone size to crack length. Yang and Liu have proposed an elastic-plastic unzipping model to calculate an effective cyclic stress intensity (ΔK_{eff}), to replace LEFM values in this case. However, for small cracks, the plastic zone size is confined by the grain boundaries in certain aluminum alloys [*31*]. It is not clear how their model might respond to such constraints.

Tanaka and co-workers [*32-34*] have predicted that propagation is restrained by a backstress created by dislocations trapped between the crack tip and grain boundary. Furthermore, they hypothesize that a critical value of $\Delta K(\Delta K_{th}^*)$ must be exceeded for growth to proceed into a new grain. For long cracks at low cyclic stress amplitude it is argued that this mechanism determines the threshold value of cyclic stress intensity, once an appropriate correction for crack closure has been made. At sufficiently high cyclic stress amplitude, boundaries no longer permanently stop crack growth and the threshold decreases. Morris et al [*35*] report that the grain boundary blockage transition

with stress amplitude is gradual, and that at intermediate stresses propagation is only temporarily interrupted by boundaries in a Al 2219-T851 alloy. Chang et al [*13*] have proposed a model which rationalizes renewed growth in terms of the fatigue-induced microplastic deformation of the grain at a short crack tip. The model is not correct for long cracks. Recent results by Zurek et al [*36*] suggest that $\Delta K \leq \Delta K_{th}$* for this mechanism to be active.

In addition, for cracks with lengths on the order of the grain size special circumstances arise which may accelerate growth rates. Lankford [*37*] reports decreasing growth rates for cracks within single grains of Al 7075-T6 which he attributes to propagation out of a region of local stress intensification. Also, early growth is more likely to be crystallographic and more rapid because of an absence of Mode I closure stress [*38*].

Growth Rates Slower Than LEFM Predictions—Two mechanisms have been reported which rationalize decreasing growth rates with increased cyclic stress amplitudes. One of these is crack closure arising from residual plasticity at the crack tip [*31*]. For short cracks the plastic zone size is subject to noncontinuum conditions, and can be substantially larger than anticipated as a crack enters a large grain. Growth can be slowed by the Mode I closure stress which develops, and completely stopped if the ratio of grain size to crack length is on the order of unity [*35*]. Crystallographic cracks are not affected because the associated deformation is in the plane of the crack. Another mechanism that can decrease the growth rate of short cracks arises if compressive residual stresses develop at the alloy surface during fatigue. Recently, Zurek et al [*36*] have discovered such compressive stresses can develop in aluminum alloys fatigued at positive load ratios, even if the stress amplitude is less than the bulk yield stress. The surface stress apparently results from microplastic creep of the surface and can be of sufficient magnitude to substantially decrease crack growth rate.

The mechanisms of plasticity-induced crack closure and the intermittent interruption of propagation of cracks by grain boundaries appear to be of special importance to short crack propagation in aluminum alloys. A distribution in the size of grains in the crack path leads to stochastic variations in rates of growth of individual cracks from both mechanisms. Consequences of these two phenomena on both mean and stochastic growth behavior are examined next.

Plasticity-Induced Crack Closure

An empirical expression for the effective cyclic stress intensity resulting from variations in crack closure stress with crack location relative to grain boundaries has been proposed [*31*]. It states

$$\Delta K_{\text{eff}} = F(a/2c)\sigma_a(1 - \alpha z_0/2c)\sqrt{2c} \tag{6}$$

where $2c$ is crack length, z_0 is the distance of the surface crack front to the next grain boundary, σ_a is the cyclic stress amplitude, a is crack depth, $F(a/2c)$ is a shape factor approximately equal to unity, and α is a material parameter with values from alloy to alloy in the range of 0.5 to 1.2. $F(a/2c) = 1.12$ for $a/2c = 0.4$, and in the absence of closure [*28*]

$$\Delta K = \Delta K_{\text{eff}} = 1.12\,\sigma_a\sqrt{2c} \tag{7}$$

If one does an experiment in which the closure stress is a hidden variable, the expected relationship of growth rate to ΔK and σ_a is found by eliminating $2c$ from Eq 6 to obtain

$$\Delta K_{\text{eff}} = \Delta K\left[1 - \alpha z_0\left(\frac{1.12\,\sigma_a}{\Delta K}\right)^2\right] \tag{8}$$

and a resulting growth rate of

$$\frac{dc}{dN} = A\,\Delta K_{\text{eff}}{}^n \tag{9}$$

where material parameter n has a value near 2.0, and $\Delta K_{\text{eff}} = 0$ if the term in brackets is negative.

If z_0 is measured at increments during fatigue, Eq 9 can be used to predict the rates of growth of the two surface tips of individual cracks. Predicted and experimentally determined rates compared in Fig. 7 were obtained in this way for a crystallographic (a) and a noncrystallographic crack (b) propagated in Al 2219-T851. To improve the accuracy in calculation of ΔK, crack depth was determined by measuring crack compliance. The large dips in rates of growth in (b) occur as the crack tips enter a new grain and a larger closure stress develops. For the crystallographic crack $\alpha = 0$, and the small fluctuations in growth rate are associated with brief interruptions of growth by grain boundaries, an effect modeled in the next section.

Mean growth rates for an ensemble of cracks can be predicted from Eqs 8 and 9 by making an appropriate average over z_0. Such a technique is used elsewhere to assess the effect of alloy grain size and of σ_a on mean growth rates in a Al 7075-T6 alloy [*36*]. Naturally, the average value of z_0 increases with grain size. Confirmed by experiment in Ref *36* are the predictions, apparent from Eq 8, that mean growth rates at a given ΔK decrease if either σ_a or alloy grain sizes is increased.

The implications of Eq 8 to stochastic variations in growth rate from closure stress are assessed here, using a computer simulation to follow the propagation of an ensemble of cracks through a field of grains whose rates of growth are given by Eqs 8 and 9. The calculations are done for two mean grain sizes (12

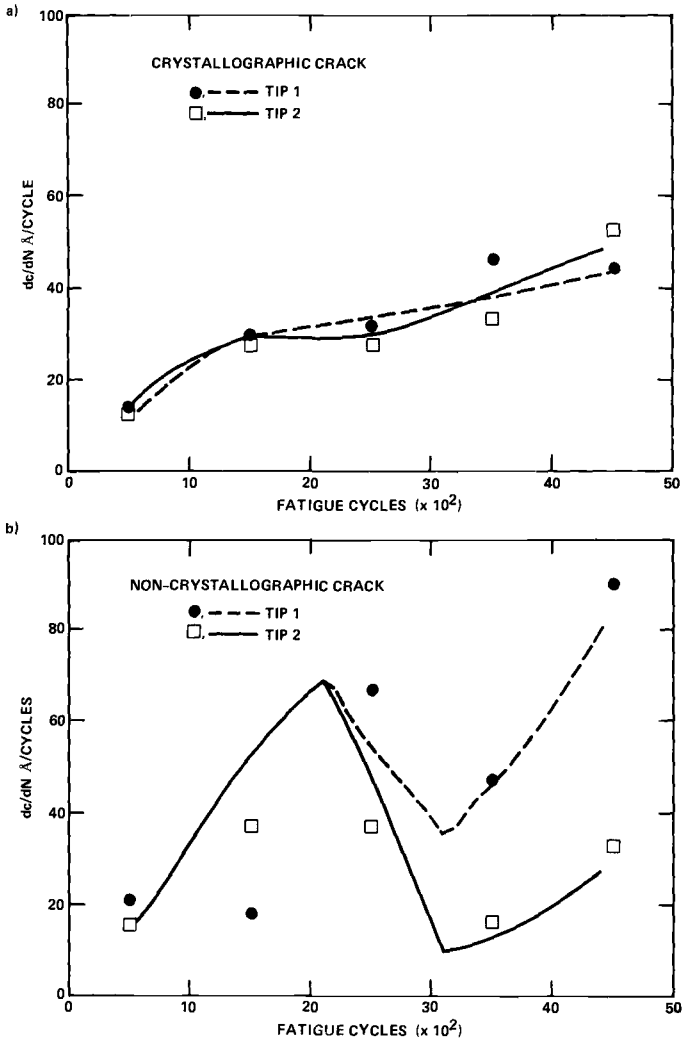

FIG. 7—*Comparison of measured and predicted rates of growth of crystallographic and noncrystallographic cracks in an Al 2219-T851 alloy (Heat III). Curves are obtained using Eq 9 and values of* ΔK_{eff} *calculated from Eq 5 by measuring the location of the crack tip relative to the grain boundaries. Data are given for each surface crack tip.*

and 130 μm mean distances of slip at ± 45 deg to the principal stress axis) by Monte Carlo selection of the size of grains in the crack path, from an experimentally determined distribution (Fig. 8). An expected standard deviation in growth rates is obtained which is substantially greater in the 130-μm (Fig. 9) than in the 12-μm (Fig. 10) alloy. The experimental data, taken from Ref *36*, show substantially the same trends except that the experimental scatter is

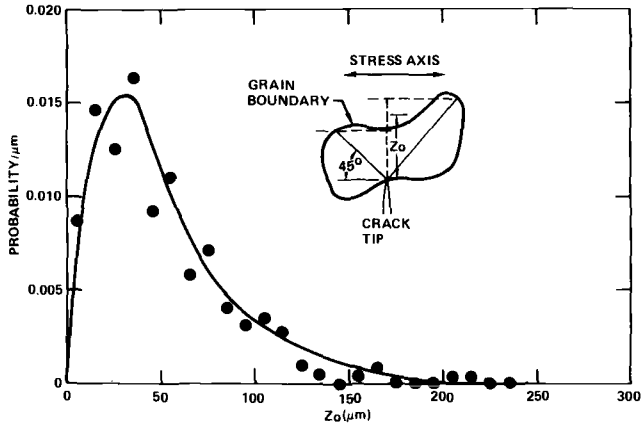

FIG. 8—*Typical alloy microstructure distribution in the direction of crack propagation is obtained using an average of the two 45-deg distances to the next grain boundary, for a crack entering the grain at arbitrary location. The curve is fit to the data points given here for Al 2219-T851. Actual values used to calculate the closure stress for 130-μm and 12-μm average grain sizes are obtained by setting the average of the curve to these values.*

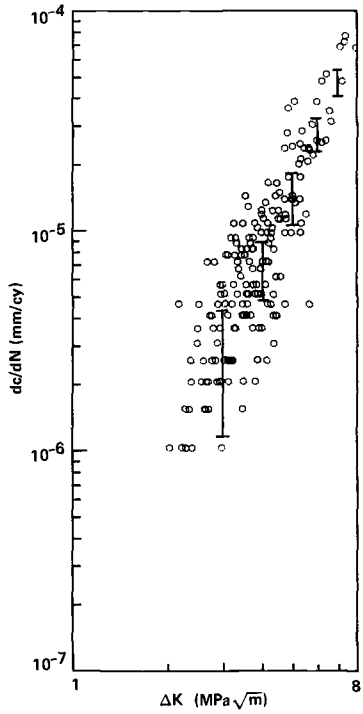

FIG. 9—*Growth rate data for Al 7075-T6 (130-μm grain size) cycled at ±300 MPa,* R = −1. *ΔK was calculated from Eq 7. The error bars represent the expected scatter (one standard deviation) obtained using a computer simulation of growth rate based on closure stress.*

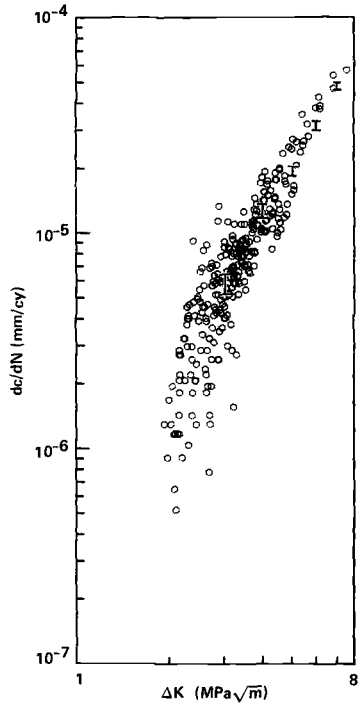

FIG. 10—*Growth rate data for Al 7075-T6, having a 12-μm grain size obtained by thermomechanical grain refinement, cycled at ±300 MPa,* R = −1. *The error bars, representing the expected scatter as in Fig. 9, are smaller than in the coarse grain material because of the small closure stress* ($z_0 \leq 12$ *μm on average*).

larger. A major additional source of experimental scatter is the assumption of an average value of $F(a/2c)$. Propagation rate is slightly faster in the fine grain material as a consequence of a smaller average closure stress.

Grain Boundary Blockage

Crack growth rates in Al 2219-T851 at small cyclic stress amplitudes depend upon σ_a in a manner consistent with grain boundary blockage concepts (Fig. 11). For ΔK less than a critical value (ΔK_c) the growth rate is sensitive to cyclic stress amplitude. At sufficiently large cyclic stress, the transition at ΔK_c disappears and rates are bounded by an extension of the power law regime. The blockage process has been characterized for short cracks in Al 2219-T851 by measuring the crack tip opening displacement (CTOD) during fatigue of tips stopped temporarily by boundaries. A progressive increase in CTOD is found until growth renews (Fig. 12). A conclusion based upon limited data is that propagation begins when the CTOD reaches a critical value giving a cyclic

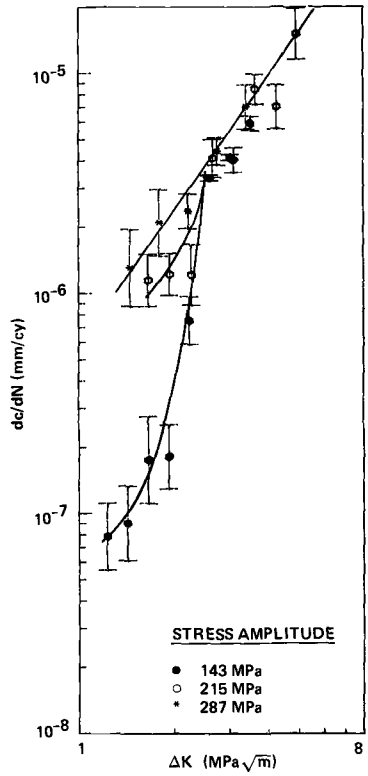

FIG. 11—*Short crack growth rate data for Al 2219-T851 at three cyclic stress amplitudes. The data points are averages from a large number of cracks and the error bar represents the 70% confidence limit in the average. The low stress amplitude data (longer crack length) shows a threshold in growth rate below a critical* ΔK *of* ~ 2.8 *MPa*$\sqrt{m}$ *attributed to the blockage of growth by grain boundaries. The* $\sigma_a = \pm 215$ *MPa data show a similar retardation of growth below* ΔK_c, *but the growth rate is faster. Blockage is less effective because, as seen in Eq 10, the cycles of retarded growth are less for higher stress amplitude. At* $\sigma_a = \pm 287$ *MPa, grain boundary blockage is insignificant and growth rate below* ΔK_c *follows the same power law growth as above* ΔK_c. *(The increase in growth rate at very low* ΔK *for* $\sigma_a = \pm 143$ *MPa occurs because the crack length is less than a grain diameter.)*

stress intensity equivalent to ΔK_c. (Actually, we are unsure if the critical value is dependent on the cyclic stress intensity (that is, ΔK_c) or on the maximum stress intensity (that is, K_c) [*36*]). We employ the model proposed by Chang et al [*13*] and later modified [*15,35*] to describe the stochastic effect of this phenomenon. This sets the requirement for a renewed growth after ΔN cycle as

$$1 \leq \int_N^{N+\Delta N} \beta D\, \sigma_a(\sigma_a - \sigma_0)\, \Delta K\, e^{-\theta N}\, dN \tag{10}$$

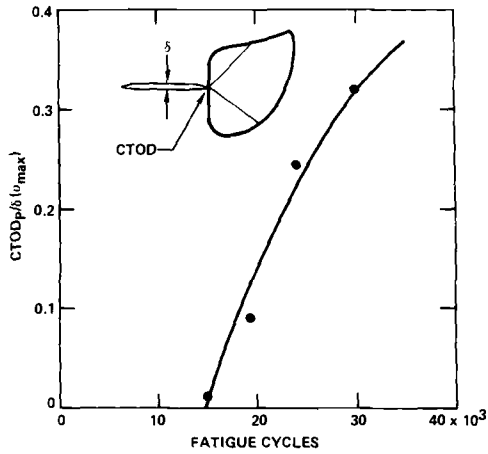

FIG. 12—*Crack tip opening displacement of a nonpropagating surface crack stopped by a grain boundary increases progressively with fatigue.*

where θ and β are material parameters, D is the grain size at the crack tip, and σ_0 is a friction stress. The expression derives from a consideration of the consequences of the progressive fatigue-induced microplastic deformation of the grain at the crack tip, which leads to a monotonically increasing CTOD. The model neglects the linear elastic contribution to ΔK, and so is clearly in error for long cracks. In the present paper this problem has been dealt with by setting $\beta = \infty$ for $\Delta K \geq \Delta K_c$.

The expression predicts that the duration of growth blockage by boundaries will increase with cycles due to hardening of the surface via the term $e^{-\theta N}$. A consequence, illustrated in Fig. 13, is that surface cracks initiated in a prefatigued Al 2219-T851 specimen propagate more slowly than the average. A stochastic effect of the grain size is anticipated, which arises because the blocking effect of small grains is greater since they are less prone to microplastic deformation. We believe this is at least qualitatively correct. In Fig. 14, predicted distributions in cycles for an ensemble of cracks to propagate from 80 to 500 μm in length are compared. The calculated values are obtained from a computerized simulation of propagation which combines the stochastic effects of both closure stress and grain boundary blockage based upon Eq 10.

Lifetime Predictions

The stochastic models of constituent particle fracture and early growth are combined to calculate the effect of alloy grain size and material coefficients on the mean lifetime of smooth bars of Al 2219-T851, and the statistical scatter around the mean. Material coefficients used are sensitive to alloy hydrogen

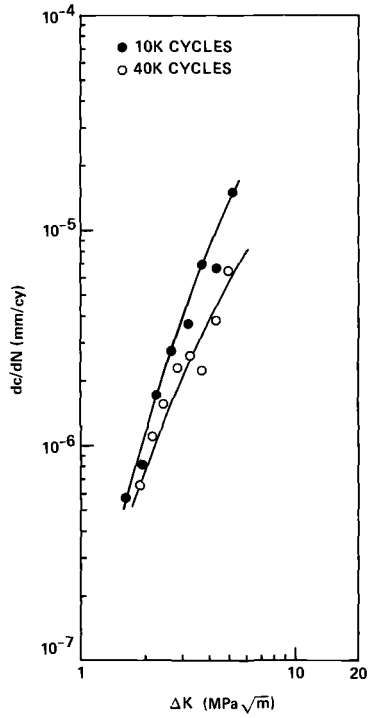

FIG. 13—*Crack growth rate in Al 2219-T851 as a function of* ΔK *for two increments in cycles to crack initiation, 10K cycles and 40K cycles. Cracks were initiated by embrittling 50-μm-diameter areas on the surface with ink [38]. Cracks initiated later in fatigue lifetime grow more slowly on the average because they are more readily stopped by grain boundaries. Fully reversed loading at* ± 225 *MPa. The data points given are averages over a large ensemble of cracks (see Ref* 36 *for averaging procedure).*

content and the measurement of these is reported elsewhere [*12*]. Those sensitive to environment are listed in Table 2.

A typical bar of Heat II material contains 100×10^3 grains at the surface. Only a subset of these can be modeled, and to ensure that the predicted lifetimes converge to realistic averages it is necessary to force the Monte Carlo calculation to consider only local microstructures in which initiation is sufficiently early to potentially affect lifetime. This amounts to modeling of events associated with large particles and large grains near the tails of the size distributions in these quantities (Figs. 4 and 8). The procedure used to achieve this has been described previously [*6*], and differs only in slight changes to the deterministic laws (as presented in the section on Early Growth) used once a microstructure has been generated. The simulation follows the stochastic propagation of 300 of the earliest initiated cracks in a simulated fatigue specimen, and the lifetime is determined by the crack which reaches critical size first.

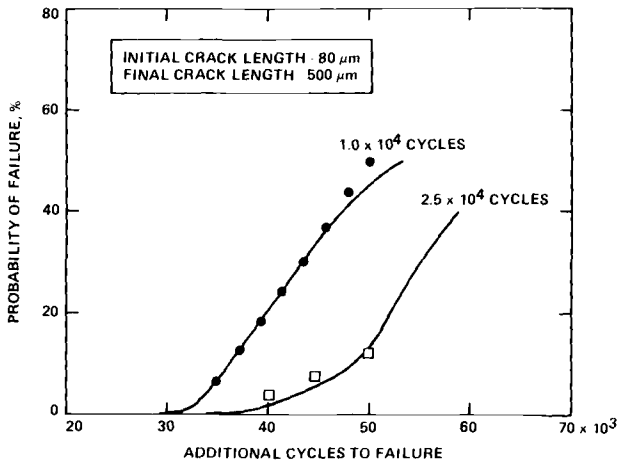

FIG. 14—*Statistical scatter in the fatigue cycles for cracks to propagate from 80 to 500 μm lengths in 2219 Heat III material fatigued at ±225 MPa. Shift in the data with cycles to initiation of the 80-μm crack is caused by an increase in the blockage period. Curves are predicted values obtained using a Monte Carlo simulation of crack growth.*

TABLE 2—*Effect of environment on material parameters.*

	θ, cycle^{-1}		α	
Al 2219-T851	Dry Air	Moist Air	Dry Air	Moist Air
Heat II (high hydrogen)	$<1 \times 10^{-6}$	$<1 \times 10^{-6}$	0.80	0.74
Heat III (low hydrogen)	1×10^{-5}	3.5×10^{-5}	1.02	0.80

Repetition of the simulation for new local microstructures is used to generate predicted statistical variations in lifetime.

Results

One capability of the computer simulation of fatigue failure was first assessed by comparing the predicted and experimentally determined distributions in crack length for the Heat III 2219 alloy at three cyclic stress amplitudes. These results are given in Fig. 15, and the comparison appears to be satisfactory. The number of cycles to failure for fully reversed loading of smooth bar samples of Heat III at three cyclic stress amplitudes is given in Fig. 16. To complete the predicted failure calculation, we added to the lifetime for each specimen the number of cycles determined by LEFM, for a crack to grow from 500 μm to critical size. Predictions and experimental results for Heats II and III at one cyclic stress amplitude are compared in Fig. 17.

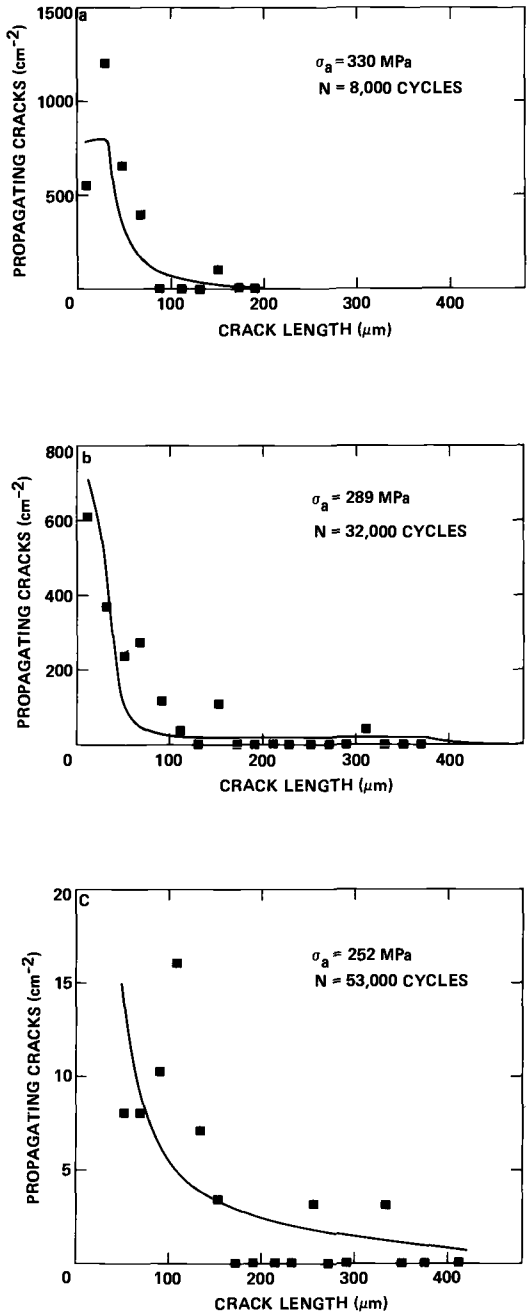

FIG. 15—*Comparison of predicted and measured distribution in surface crack length in Al 2219-T851 (Heat III) for three cyclic stress amplitudes.*

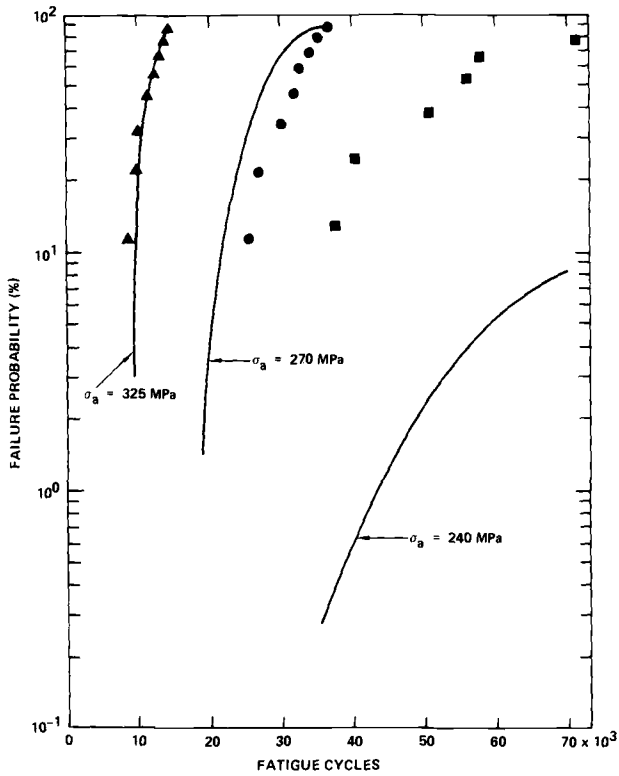

FIG. 16—*Failure probability versus cycles to failure for smooth bar specimens of Al 2219-T851 (Heat III) for three cyclic stress amplitudes. Symbols are experimental data points and solid lines represent the predicted lifetime curves obtained with a Monte Carlo simulation of fatigue failure. Disparity between simulation and actual lifetime for the low cyclic stress amplitude is attributed to the absence of grain boundary cracking in the model.*

One form of output of the fatigue simulation is a listing of the fatigue cycles to initiate each crack in a bar and its length at failure. We find from this that the crack that grows to critical size is usually among the earliest, but not necessarily the first, to be initiated during fatigue. This trend is especially true for Heat III material, for which growth later in lifetime is slowed by the increasing duration of blockage. Certain special combinations of large grain and particle sizes, and particle location, enhance rapid particle fracture and rapid early growth. Although the accuracy with which the model predicts mean fatigue lifetime is highly sensitive to the accuracy of the numerous material coefficients needed to describe initiation and growth processes, the scatter in lifetime predicted by the model is closely related to its ability to depict the occurrence of the local combinations of alloy microstructure which lead to failure. To better evaluate this capability, coefficient A has been increased by

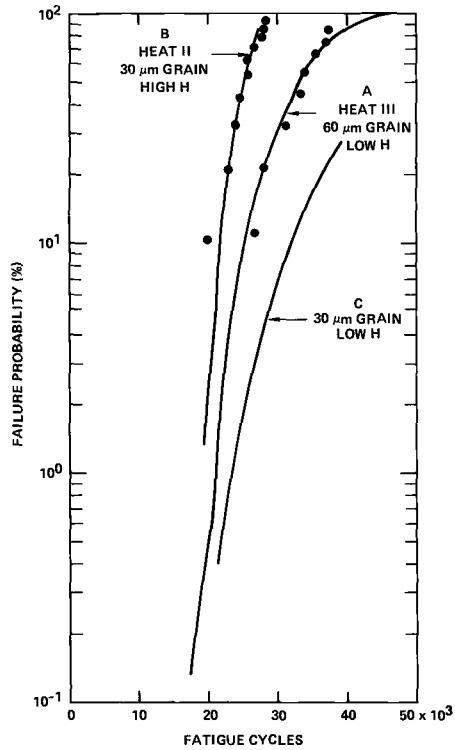

FIG. 17—*Effect of alloy grain size and hydrogen content on the scatter in lifetime for three cases. Data are from smooth bars, and curves are obtained by a Monte Carlo simulation of crack initiation and growth for 1000 simulated fatigue specimens of each material.*

7% over the experimentally determined value to superimpose the predicted and measured mean lifetime of alloy A in Fig. 17. The predicted distribution in fatigue lifetimes involves no curve fitting, and the agreement strongly suggests that the major source of scatter in lifetime is correctly represented by the model.

Discussion

We believe that the ultimate application of the aforementioned procedure will be to calculate the probability of the early fatigue failure of materials from their microstructure. Much remains to be learned about initiation and growth mechanisms before this can be done for an arbitrary structural aluminum alloy and random loading history. The disparity in Fig. 16 between predicted and measured distributions in lifetimes for the Heat III material fatigued at ± 240 MPa, for instance, arises from a growth mode not included in the model. As the surface cyclically hardens and transgranular propagation is

suppressed, early growth continues in a slower intergranular mode. Nevertheless, at higher amplitudes for which the initiation and early growth phenomena are more accurately represented, it appears that the model is already capable of reasonable accuracy. To understand the basic mechanisms of initiation and early growth is not the only important task, however. The source of heat-to-heat variation in the mechanical properties of the surface, as altered by the environment, must also be identified and modeled. Trace amounts of hydrogen are responsible for the poorer performance of Heat II in fatigue, for instance. Surprisingly, this happens even though the mean grain size is only half that of Heat III. In Fig. 17, we also show the improved lifetimes predicted for a hypothetical small grain material free of hydrogen. It remains to be seen if other trace elements can affect the fatigue performance in similar ways.

Unusually early fatigue failures which occur at low probabilities can arise not only from mechanisms that can be analytically modeled, but also from happenstances not amenable to analysis. The former consist of the types of events we have considered here and arise from combinations of microstructures which have a low probability of occurrence, but which lead to rapid crack initiation and growth if they are present. The latter phenomena include anomalies more likely to arise, for example, from unnoticed porosity or foreign debris in cast materials.

Since early fracture probabilities are derived from the product of a number of unlikely microstructural combinations, it is not necessary to know the extremes of each individual distribution (such as grain size) with high accuracy. However, we do believe that more accuracy in both the D_{max} and w distributions at large sizes is required than is presented here, even to make accurate predictions at probabilities of failure of 1×10^{-3}. One must also be aware of additional mechanisms that might further assist early failure. For instance, incorporated in the growth models we used to predict fatigue lifetime is a simulation of the coalescence of two adjacent cracks. We have not discussed this because such coalescence is sufficiently rare that it is predicted to enhance failure only at probabilities outside the range of our experimental data. Herein is an important reason why the extrapolation of early failure probabilities from limited fatigue data cannot be trusted. The mechanisms that govern early failure can differ and have different statistics from those that control the mean lifetime. Clearly, there is a large amount of work ahead before the full potential of microscopic failure modeling can be realized. But for the future, such efforts hold the substantial promise of providing advanced capabilities of designing structures obtainable in no other way.

Acknowledgments

The effects of hydrogen and of relative humidity on incubation and crack closure stresses were determined as part of a program supported by the Office of Naval Research under Contract N00014-79-C-0334. The remainder of the

research was supported by Rockwell International IR&D funds. We thank Dr. J. A. Wert for preparing the Al 7075-T6 material in several grain sizes.

References

[1] Bloomer, N. T. and Roylance, T. F., *The Aeronautical Quarterly*, Vol. 16, 1965, p. 307.
[2] Korbacher, G. K., *Experimental Mechanics*, Vol. 11, 1971, p. 540.
[3] Provan, J. W. in *Fracture 1977*, Vol. 2, Waterloo, Canada (19-24 June 1977), p. 1169.
[4] Ghonem, H. and Provan, J. W., *Engineering Fracture Mechanics*, Vol. 13, 1980, p. 963.
[5] McCartney, L. N., *International Journal of Fracture*, Vol. 15, 1979, p. 477.
[6] Morris, W. L., James, M. R., and Buck, O., *Engineering Fracture Mechanics*, Vol. 13, 1980, p. 213.
[7] Hunter, M. S. and Fricke, W. G., Jr., in *Proceedings*, American Society for Testing and Materials, Vol. 54, 1954, p. 717.
[8] Hunter, M. S. and Fricke, W. G., Jr., in *Proceedings*, American Society for Testing and Materials, Vol. 55, 1955, p. 942.
[9] Hunter, M. S. and Fricke, W. G., Jr., in *Proceedings* American Society for Testing and Materials, Vol. 56, 1956, p. 1038.
[10] Pangborn, R. N., Weissman, S., and Kramer, I. K., *Metallurgical Transactions*, Vol. 12A, 1981, p. 109.
[11] Morris, W. L., Inman, R. V., and James, M. R., *Journal of Materials Science*, Vol. 17, 1982, p. 1413.
[12] James, M. R. and Morris, W. L., this publication, pp. 46-70.
[13] Chang, R., Morris, W. L., and Buck, O., *Scripta Metallurgica*, Vol. 13, 1979, p. 191.
[14] Tanaka, K. and Mura, T., *Metallurgical Transactions*, Vol. 13A, 1982, p. 117.
[15] James, M. R. and Morris, W. L., *Materials Science and Engineering*, Vol. 56, 1982, p. 63.
[16] Morris, W. L. and James, M. R., *Metallurgical Transactions*, Vol. 11A, 1980, p. 850.
[17] Kung, C. Y. and Fine, M. E., *Metallurgical Transactions*, Vol. 10A, 1979, p. 603.
[18] Grosskreutz, J. C. and Shaw, G. G. in *Proceedings*, 2nd International Conference on Fracture, P. L. Pratt, Ed., Chapman and Hall, London, 1969, p. 620.
[19] Frost, N. E., *Proceedings of the Institution of Mechanical Engineers*, Vol. 173, 1959, p. 811.
[20] Pearson, S., *Engineering Fracture Mechanics*, Vol. 7, 1975, p. 235.
[21] Kitagawa, H. and Takahashi, S. in *Proceedings*, 2nd International Conference on Mechanical Behavior of Materials, Boston, Aug. 1976, p. 627.
[22] Fine, M. E. and Ritchie, R. O., *Fatigue and Fracture*, ASM, Metals Park, Ohio, 1979, p. 245.
[23] Hill, S. J. and Boutle, N. F. in *Fracture 1977*, Vol. 2, ICF4, Waterloo, Canada, 19-24 June 1977, p. 1233.
[24] El Haddad, M. H., Smith, K. M., and Topper, T. H., *Transactions of ASME, Journal of Engineering Materials and Technology*, Vol. 101, 1979, p. 42.
[25] El Haddad, M. H., Topper, T. H., and Topper, T. N., *Transactions of ASME, Journal of Engineering Materials and Technology*, Vol. 103, 1981, p. 91.
[26] El Haddad, M. H., Dowling, N. E., Topper, T. H., and Smith, K. N., *International Journal of Fracture*, Vol. 16, 1980, p. 15.
[27] Morris, W. L., James, M. R., and Buck, O., "A Simple Model of Stress Intensity Range Threshold and Crack Closure Stress," *Engineering Fracture Mechanics*, in press.
[28] James, M. R. and Morris, W. L., *Metallurgical Transactions*, Vol. 14A, 1983, p. 153.
[29] Smith, R. A., *International Journal of Fracture*, Vol. 13, 1977, p. 717.
[30] Yang, C. Y. and Liu, H. W., *Scripta Metallurgica*, Vol. 14, 1979, p. 785.
[31] Morris, W. L., *Metallurgical Transactions*, Vol. 11A, 1980, p. 1117.
[32] Taira, S., Tanaka, K., and Nakai, Y., *Mechanics Research Communications*, Vol. 5, 1978, p. 375.
[33] Taira, S., Tanaka, K., and Hoshina, M. in *Fatigue Mechanisms, ASTM STP 675*, American Society for Testing and Materials, 1979, pp. 135-173.
[34] Tanaka, K., Nakai, Y., and Yamashita, M., *International Journal of Fracture*, Vol. 17, 1981, p. 532.

[35] Morris, W. L., James, M. R., and Buck, O., *Metallurgical Transactions*, Vol. 12A, 1981, p. 57.
[36] Zurek, A. K., James, M. R., and Morris, W. L., "The Effect of Grain Size on Fatigue Growth of Short Cracks," accepted by *Metallurgical Transactions A*.
[37] Lankford, J. M., *Fatigue of Engineering Materials and Structures*, Vol. 5, 1982, p. 233.
[38] Morris, W. L., James, M. R., and Buck, O., *Nondestructive Evaluation: Microstructural Characterization and Reliability Strategies*, O. Buck and S. M. Wolf, Eds., AIME, 1981, p. 387.

DISCUSSION

H. Mughrabi[1] *(written discussion)*—You have discussed cyclic surface hardening in the case of fatigued aluminum alloys. I am not quite sure, however, whether I really understand what you mean by this, since you also stated that after pulsating tension, the surface region is found to be in a state of residual compressive stress. According to my understanding, if this is the case, the surface has yielded in tension at a lower local yield stress than the bulk and, accordingly, the bulk retains residual tensile stresses after unloading; these balance the residual compressive stresses in the surface layer. This is, however, rather different from the compressive residual surface stresses present, for example, in shot-peened material. In the latter case, it is clear that the surface region has been strained plastically while the bulk has not. Accordingly, there is a surface region with a higher dislocation content than in the bulk. In all other cases that are not so evident, I would indeed very much like to see direct observational evidence of the (preferential) surface hardening envisaged. Would you please comment on this, and sort out my problems in understanding what you said?

W. L. Morris and M. R. James (authors' closure)—Further details on our studies of the microplastic deformation of surfaces are given by us in another paper in this volume.[2] By measuring the local stress-strain hysteresis loop in individual grains in aluminum alloys, we find that the surface is initially elastic for cyclic loading at amplitudes less than the bulk cyclic yield strength. With fatigue, the local hysteresis loops open, more rapidly so within the large grains as they become microplastic. However, with continued fatigue the hysteresis loops begin to close, especially within the large grains, and at some sites the deformation ultimately returns to elastic. It is this later phase which we interpret as resulting from localized hardening of the surface.

Your reference to compressive residual stresses is a separate problem which

[1]Max-Planck-Institut für Metallforschung, Institut für Physik, Stuttgart, Federal Republic of Germany.

[2]"The Role of Microplastic Deformation in Fatigue Crack Initiation," pp. 46-70.

occurs in tension-tension loading. Although not discussed here, more information can be found in Ref *36* of our paper.

J. R. Davidson[3] (*written discussion*)—Your first data slide showed that, for very small cracks, the growth rate decreased, then increased with ΔK. Jim Newman, at NASA-Langley Research Center, has shown that crack closure predicts this. He is, however, wary about considering cracks with lengths of the same length as grains, for crack closure, as he uses it in his computer program, is formulated from continuum theory. Even so, your figure, and Newman's independent results, are remarkably similar (also compare the results of David Davidson, Southwest Research Institute, who indicates seeing similar results).

Would the initiation phase contribute more scatter to life than the stochastic part of the growth phase?

W. L. Morris and M. R. James (*authors' closure*)—The slide you refer to comes from Fig. 1 in Ref *36* and shows the erratic growth of a single short crack as it encounters grain boundaries in its path. For Al 7075-T6, if one averages the growth rates of a large ensemble of short cracks, however, the average growth rate continually increases with ΔK.

Regarding your question on scatter, cyclic stress amplitude is an important parameter. At high amplitudes, the number of initiation events is large and a major source of scatter in lifetime comes from the processes of early growth and crack coalescence. At low stress amplitude, the number of initiation events is small and stochastic fluctuations in the rates of occurrence of these has an important effect on the scatter in lifetime.

J. T. Fong[4] (*written discussion*)—Computer simulation of stochastic processes involving more than two random variables, such as your problem of creating a crack propagation process, is a subject that could be evaluated through a statistical analysis based on sampling theory. The result should include an estimate of the uncertainties that depends on a limited sample size. What is your sample size and your estimate of these uncertainties?

W. L. Morris and M. R. James (*authors' closure*)—Your question is difficult to answer quickly because it necessitates an explanation of the computer simulation philosophy. To accurately represent lifetime resulting from stochastic crack initiation and growth processes, the simulation is designed to consider only those cracking events which can occur sufficiently early to potentially effect fatigue lifetime. Obviously, this entails a restriction of the phase space from which the microstructural parameters are selected, as is described

[3]NASA-Langley Research Center, Hampton, Va. 23665.
[4]National Bureau of Standards, Washington, D.C. 20234.

in Ref *6* of our paper. Without restriction, at least 10^7 selections would be required to represent a single fracture bar. A randomly selected subset of these, corresponding to a small subset of the 10^5 grains present on the surface of the bar, would yield unrealistically large lifetimes as it is the rare combination of large particles in large grains that accelerates crack initiation. Our method forces the simulation to consider only the 300 earliest forming cracks from such rare combinations of microstructure for each fatigue bar, involving selection of about 10^4 microstructural parameters. The crack which leads to failure in the simulation is usually among the first 30 that initiate and increasing the simulation to 300 cracks typically shortens lifetimes by less than a few percent. Thus we believe this number represents an upper bound of the statistical error in lifetime for a single bar. We have not done a similar analysis to determine the uncertainty in the stochastic variation in lifetimes predicted by our technique.

E. E. Underwood[5] (*written discussion*)—This study represents a considerable effort in the quantification of microstructural parameters important to the authors' model. My question concerns the choice of D and w measurements, and whether more easily obtained quantitative parameters could have been used, rather than individual measurements of lengths across grains (D) and across fractured surface particles (w).

For example, alternative approaches appear possible that are based on statistically exact equations, and that involve considerably less measurement time.[6,7] A "size" parameter for grains that seem most directly related to the three-dimensional slip paths in randomly oriented, equiaxed polycrystals is the mean intercept length $\bar{L}_3$.[6] One half of this mean "path" through the grains could possibly be used for the authors' 45-deg D-dimension, without serious changes to their curves or conclusions. If the grains are nonequiaxed, the extent of elongation with respect to the stress axis can be evaluated easily by means of a parameter, Degree of Orientation, which gives a numerical assessment of mean grain elongation.

Also, the authors' w-parameter, which appears to be the *projected* length of a crack through a surface particle, can be measured rapidly and accurately with an electronic pencil, such as found in the Zeiss Videomat, or any automatic image analysis equipment that has operator-interactive capability. The straight-line distance between the two crack ends is obtained simply by touching the two crack ends. If the true crack length is desired, the operator merely traces the crack from one end to the other.

These or other quantitative measurements can be performed quickly and efficiently. Depending on the specific parameters required for the model,

[5]Chemical Engineering/Metallurgy, Georgia Institute of Technology, Atlanta, Ga. 30332.

[6]Underwood, E. E., *Quantitative Stereology*, Addison-Wesley, Reading, Mass., 1970.

[7]Underwood, E. E. and Starke, E. A., Jr., in *Fatigue Mechanisms, ASTM STP 675*, American Society for Testing and Materials, 1979, pp. 633-682.

specific quantities, or combinations of quantities, can be obtained that should satisfy the particular need.

W. L. Morris and M. R. James (authors' closure)—This comment by Professor Underwood is indeed relevant, especially in light of Dr. Fong's question. The statistical distributions in grain and particle sizes are important to our model and time consuming to obtain. The approaches Professor Underwood suggests are perfectly suitable for these. We have found that the grain size distribution is accurately approximated by a two-parameter Weibull distribution which, if verified, should allow the sample size to be reduced in determining these distributions.

K. Tanaka,[1] *M. Hojo,*[2] *and Y. Nakai*[3]

Fatigue Crack Initiation and Early Propagation in 3% Silicon Iron

REFERENCE: Tanaka, K., Hojo, M., and Nakai, Y., **"Fatigue Crack Initiation and Early Propagation in 3% Silicon Iron,"** *Fatigue Mechanisms: Advances in Quantitative Measurement of Physical Damage, ASTM STP 811*, J. Lankford, D. L. Davidson, W. L. Morris, and R. P. Wei, Eds., American Society for Testing and Materials, 1983, pp. 207–232.

ABSTRACT: The etching susceptibility of dislocations in 3% silicon iron is used to study the initiation and early propagation of small fatigue cracks in smooth specimens subjected to completely reversed cyclic bending. The condition for crack initiation along grain boundaries, which is the dominant mode of crack initiation, is derived from the crystallographic relationship of adjacent grains relative to the stress axis and grain boundary. The propagation behavior of small cracks was compared with that of long through-cracks. Most of the small cracks begin to decelerate, departing from the relation between the rate and the effective stress intensity range for long cracks when the growth path changes from the grain boundary or slip band to the noncrystallographic or transitional path. Some cracks become nonpropagating, while others accelerate again in accordance with the relation between the rate and the stress intensity range for long cracks. Since the crack growth rate is expressed as a unique power function of the size of the highly strained region near the crack, except for slip band cracks, it is concluded that the crack closure is primarily responsible for the anomalous growth behavior of small cracks. Some discussion is given on the influence of the grain size on the fatigue process of the smooth specimen.

KEY WORDS: fatigue (materials), crack initiation, crack propagation, small cracks, crack closure, fracture mechanics, silicon iron, etch pit, microstructure, threshold condition

The fatigue process of smooth specimens is composed of the crack initiation and propagation phases. When the length of cracks is above several times the grain size, the growth rate is predictable from the fracture mechanics data of long through-crack propagation, provided that the difference in

[1]Department of Mechanical Engineering and Mechanics, Lehigh University, Bethlehem, Pa. 18015.
[2]Industrial Products Research Institute, Agency of Industrial Science and Technology, M.I.T.I., Tsukuba, Ibaraki, Japan.
[3]Department of Engineering Science, Kyoto University, Kyoto, Japan.

crack closure is taken into account [*1,2*].[4] The influence of the material microstructure is minimal in this stage of crack propagation. On the other hand, the stages of crack initiation and early growth are much influenced by the material microstructure. The site of crack initiation varies with the microstructure of materials [*3*]. The grain boundary has been reported to act as a barrier against crack growth in the early stage in aluminum alloys by Morris [*4-7*], tempered martensite and super alloy by Lankford et al [*8,9*], and low-carbon steel by Tanaka et al [*10,11*]. The mode of crack growth and the crack closure stress are dependent on the crack length as well as the material [*4-7,10,11*]. The slip character may play an important role in the microstructure-sensitive nature of the initiation and early propagation of small cracks.

In the present paper, fatigue tests on smooth specimens of 3% silicon iron were conducted, and the initiation and early propagation of small cracks were studied based on the etch-pit observation of slip deformation. The growth behavior of small cracks were compared with that of long cracks. The etching susceptibility of dislocations in this alloy has been used to examine the plastic deformation attending large fatigue crack growth [*12,13*]. No such work has been conducted with the initiation and early propagation of small cracks in smooth specimen fatigue.

Experimental Procedure

The experimental material used in the present experiment was 3% silicon iron with the chemical composition (in weight percent) of 3.02Si, 0.007C, 0.15Mn, 0.013P, 0.004S, 0.46A1, balance Fe. The same material was used in our previous study of fatigue growth of long through-cracks [*13*]. After machining, specimens were heat-treated under two different conditions: annealing at 875°C for 0.5 h and at 1100°C for 2 h followed by forced air cooling. The former annealing produced the grain size 130 μm and the latter 600 μm. The material with a grain size of 130 μm, designated as Material S, has a yield stress of σ_Y = 431 MPa and a tensile strength of σ_B = 576 MPa, and the material with a grain size of 600 μm, designated as Material L, has σ_Y = 365 MPa and σ_B = 534 MPa. The surface of all specimens was finally finished by electropolishing with Morris reagent [*14*]. Special care was taken not to etch the grain boundary, because the etched grain boundary acted as a crack initiator and also made the detection of crack initiation difficult.

The specimen has a minimum cross section of width 14 mm and thickness 4 mm (Fig. 1) [*1*] and has a weak stress concentration with the elastic stress concentration factor 1.04 under plane bending [*15*]. The applied stress amplitude described in the following sections is the nominal stress multiplied by 1.04.

The fatigue tests were performed in a resonance-type bending test machine

[4]The italic numbers in brackets refer to the list of references appended to this paper.

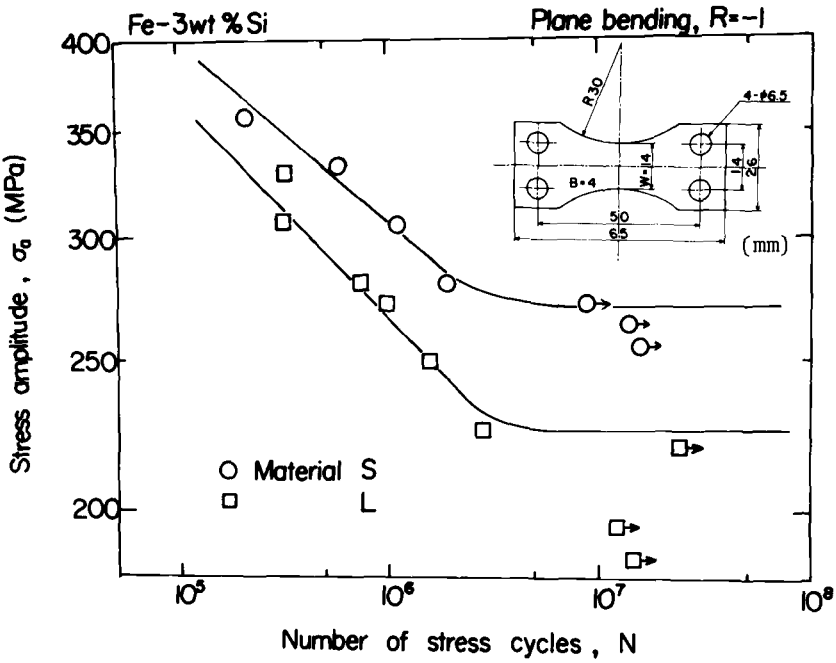

FIG. 1—S-N *curves.*

operated at a frequency of 33.3 Hz. The specimens were subjected to a fully reversed plane bending moment; that is, the ratio of the maximum to minimum stress, R, was -1.

During fatigue tests, the machine was stopped and the specimen removed. Small cracks on the specimen surface were examined with an optical microscope at ×150 to ×600 magnifications. The crack length measured is the projected length on the plane perpendicular to the stress axis. The fatigue test was ended at the time when the longest crack was about 3 mm in length. The fatigue specimens were aged at 150°C for 1 h and then etched with Morris reagent [*14*] to reveal the etch pit pattern around a fatigue crack. The grain structure of the material was also developed after etching. Cleavage cracking was not observed within this experimental range in fractographic observation.

S-N Curve and Microscopic Observation

Figure 1 indicates the relation between the stress amplitude σ_a and the number of stress cycles to failure. The fatigue limits of Materials S and L are 270 and 225 MPa, respectively. The detailed observations of fatigue crack initiation and its early growth were conducted for the cases of $\sigma_a = 280$ ($\sigma_a/\sigma_Y = 0.65$) and 331 MPa ($\sigma_a/\sigma_Y = 0.77$) for Material S and $\sigma_a = 240$

($\sigma_a/\sigma_Y = 0.66$) and 280 MPa ($\sigma_a/\sigma_Y = 0.77$) for Material L. The macroscopic plastic strain was not detected with the strain gage during fatigue under these stress amplitudes. Four corners of the specimen are designated by A, B, C, D, and cracks initiated closer to each corner are identified by the corner designation and an arbitrary number.

The micrographs of the specimen surface in the stage of crack initiation are shown in Fig. 2, and those of the specimens of Material S etched after fatigue are presented in Fig. 3. In these micrographs, the stress axis is horizontal and the upper direction is toward the specimen corner. The crack initiation site is indicated by letter N in Fig. 3.

The initiation site of fatigue cracks is mainly along the grain boundary for the cases of Material S at $\sigma_a = 331$ MPa and of Material L at $\sigma_a = 240$ and 280 MPa. For the case of Material S at $\sigma_a = 280$ MPa, about one third of the cracks nucleates along slip bands. Figure 2*b* indicates the crack initiation along the slip bands impinging on the grain boundary (see Fig. 3*c*). Figures 2*a* and 2*c* are grain boundary cracks. (The micrograph corresponding to Fig. 2*a* after fatigue is Fig. 3*e*.) Figure 2*d* is a micrograph of the crack shown in Fig. 2*c* at the later stage of fatigue.

In the optical microscopic observation of the polished specimen surface during fatigue, a dark line first appears and then the line darkens mostly without elongating its length (compare Fig. 2*c* with Fig. 2*d*). A crack can be identified when a clear propagation of the dark line is detected. The fraction of the crack initiation life to the total life is from 20 to 30%. The length of fatigue cracks at initiation was between 20 to 70 μm for Material S, and between 100 and 400 μm for Material L.

Fatigue cracks initiated along slip bands (Figs. 3*a* and 3*c*) and along grain boundaries (Figs. 3*b*, 3*d*, and 3*e*) begin to propagate into grains. Their propagation path in the early stage is frequently affected by the slip system, but growth is not along the slip, as denoted by T in Fig. 3*c*). A jagged crack shape indicates that the crack is propagating from one plane to another; thus the growth mode is a mixture of slip band, crystallographic mode, and Stage II mode. Since this type of crack growth is most frequently observed in the early stage, it is called here the transition mode. As a crack continues to grow, the crack propagation mode becomes mostly of Stage II type.

In the following sections, the crystallographic orientation relationship for grain boundary crack initiation will be first discussed, and then a detailed quantitative analysis of early crack propagation will be conducted in comparison with the long through-crack propagation reported in the previous study [*13*]. The data of long cracks obtained so far are only for the case of Material S, so the strict comparison will be restricted to the case of Material S.

Crack Initiation

Some grain boundary cracks nucleated at the corner of the specimen. For such cracks, it is possible to determine the orientation of slip planes against

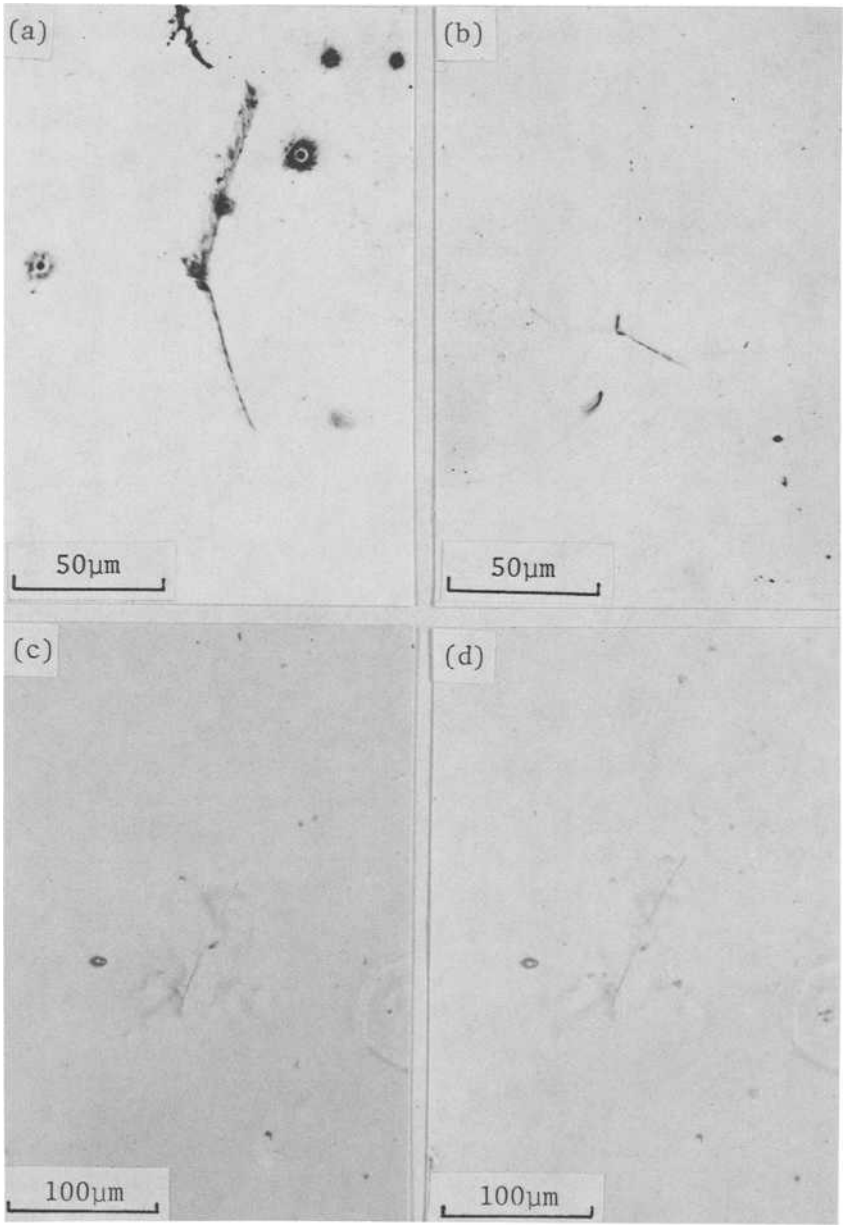

FIG. 2—*Micrographs of crack initiation.* (a) *Crack B16, Material S,* $\sigma_a = 331$ *MPa,* $N = 5.2 \times 10^5$. (b) *Crack B2, Material S,* $\sigma_a = 331$ *MPa,* $N = 1.2 \times 10^5$. (c) and (d) *Crack B7, Material L,* $\sigma_a = 240$ *MPa,* $N = 6.3 \times 10^5$ *and* 8.4×10^5.

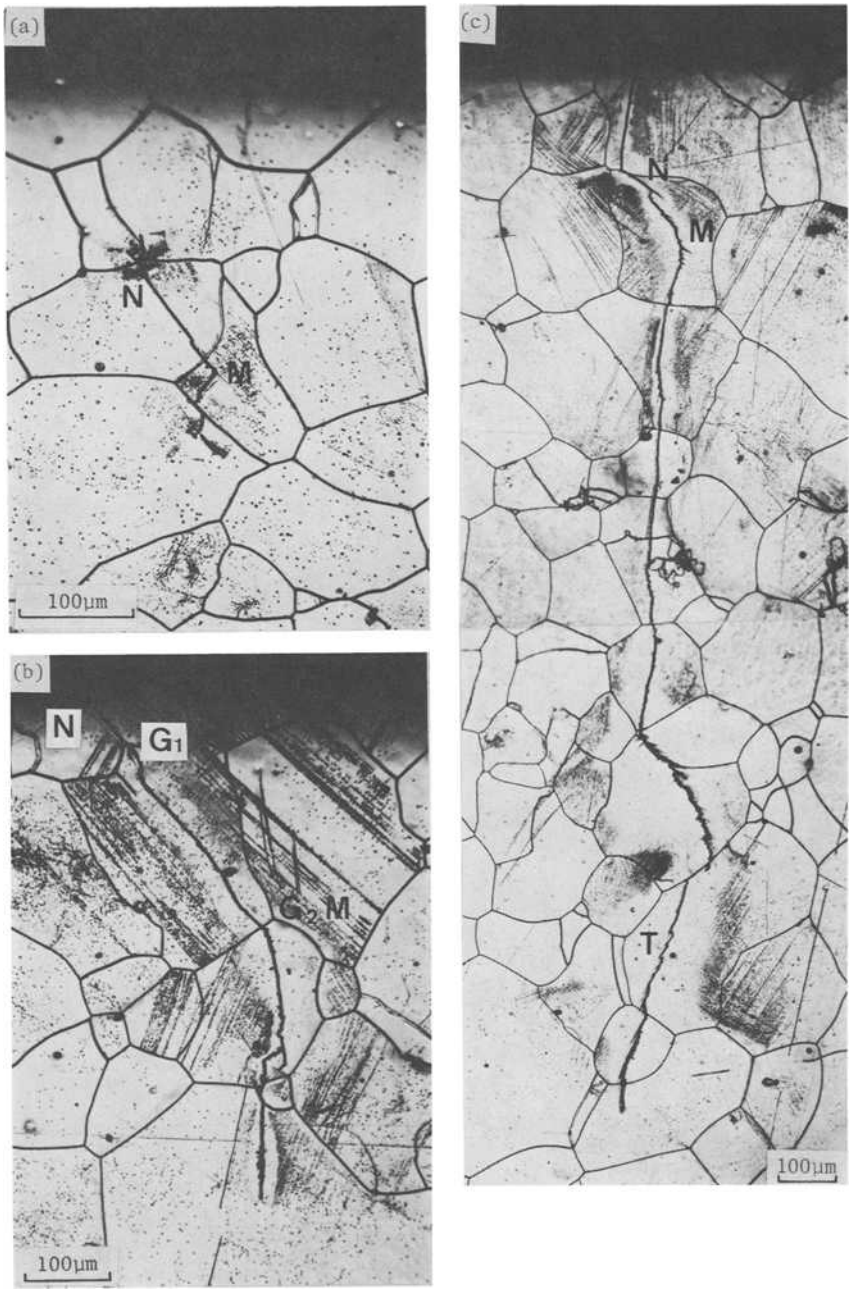

FIGS. 3*a*, 3*b*, and 3*c*—*Micrographs of Material S etched after fatigue.* (a) *Crack C4,* σ_a = *280 MPa.* (b) *Crack B1,* σ_a = *331 MPa.* (c) *Crack B2,* σ_a = *331 MPa.*

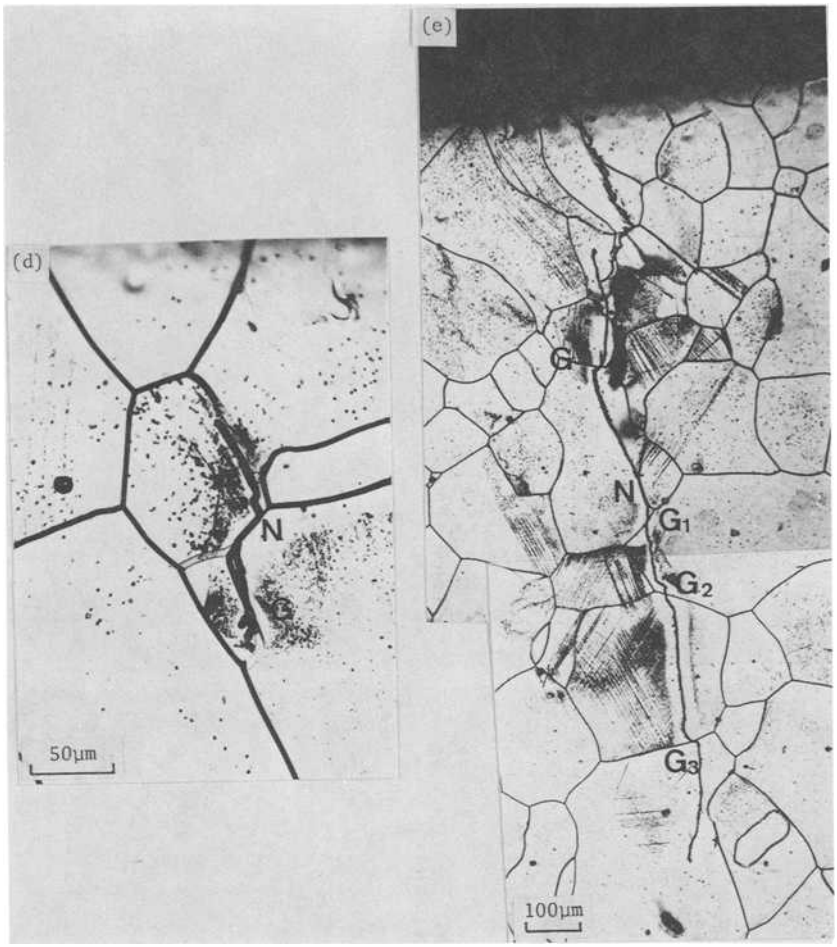

FIGS. 3*d* and 3*e*—*Micrographs of Material S etched after fatigue.* (d) *Crack A3,* $\sigma_a = 331$ *MPa.* (e) *Crack B16,* $\sigma_a = 331$ *MPa.*

the stress axis and the grain boundary from two micrographs taken from two surfaces of the specimen. Figure 4 presents two micrographs of such a crack, where Fig. 4*a* is the micrograph taken from the side surface and Fig. 4*b* is from the front surface.

Figure 5 illustrates the slip plane within a grain located at the specimen corner. The line *CK* is the slip trace of the slip plane *CKLM* seen on the front surface *ABCD*, and *CM* is that seen on the side surface *BCGF*. The corner line of the specimen is *BC* parallel to the stress axis (y axis). The angle α is the angle between slip trace and stress axis on the front surface; α' is the angle on the side surface as shown. From angles α and α', the normal *HP* of

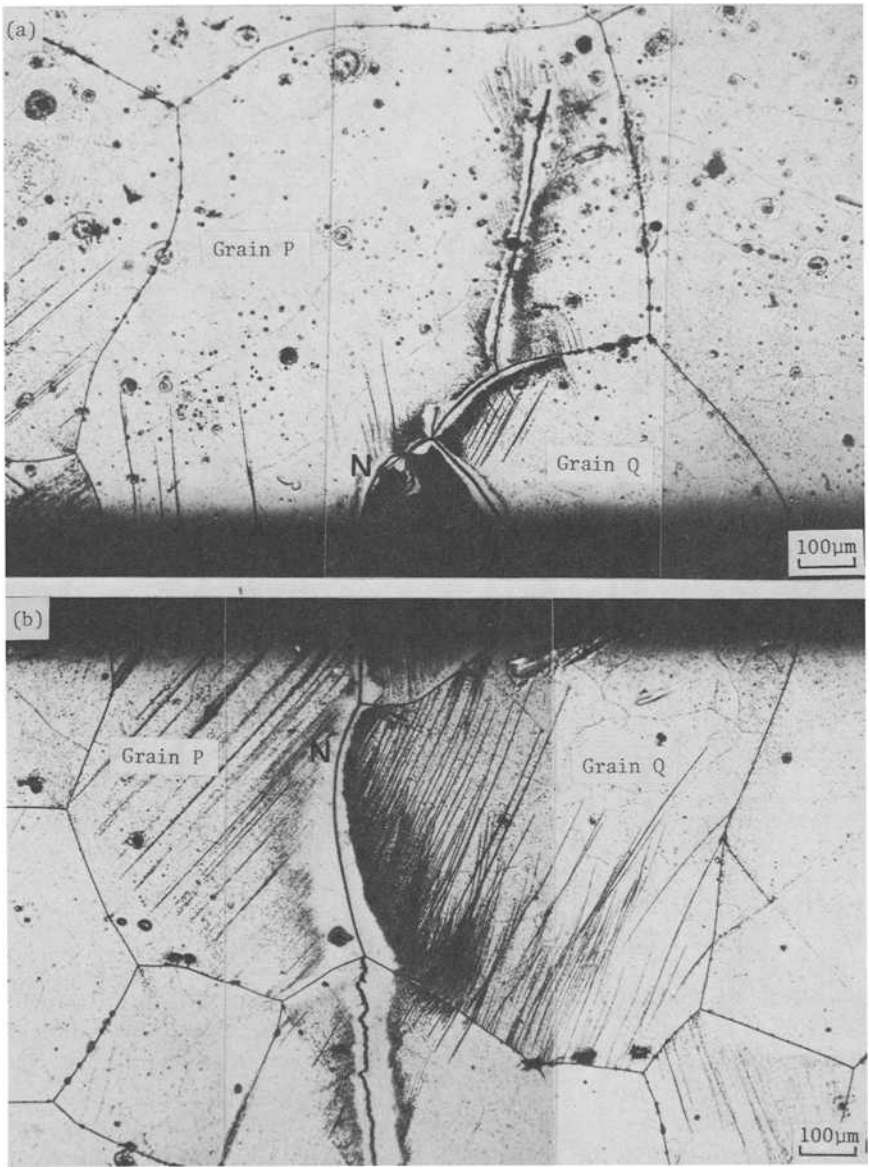

FIG. 4—*Micrographs of Crack A1 initiated at grain boundary. Material L,* $\sigma_a = 280$ *MPa.* (a) *Side surface.* (b) *Surface.*

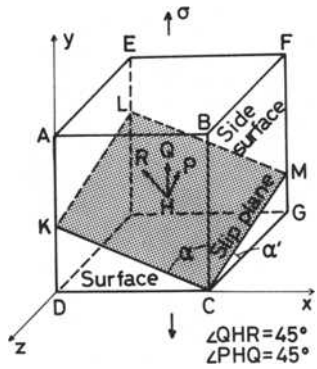

FIG. 5—Orientation of slip plane in a grain located at the specimen corner.

the slip plane can be determined. When the angle $\angle PHQ$ equals 45 deg, the maximum shear stress is resolved on the slip plane (HQ is parallel to the stress axis, HR is the slip direction). In this case, the following relation between α and α' can be obtained:

$$\cot^2\alpha + \tan^2\alpha' = 1 \tag{1}$$

By assuming that the grain boundary is the plane formed by the intersections of the grain boundary with the front and side surfaces (a curved line is approximated by a straight line), an approximate angle θ between the stress axis and the grain boundary plane can be determined.

The orientation relationship was examined for the case of Material L under $\sigma_a = 331$ MPa. Measurements of α, α' and θ were possible only for four cracks. The data on α and α' of two grains adjacent to a grain boundary crack are presented in Fig. 6 together with θ, where the line indicates Eq 1. The angle between the normal of the slip plane and that of the grain boundary was high (around 50 to 65 deg) in one of two adjacent grains, whose data are denoted by the solid marks in Fig. 6. The angle in the other grain was about 40 deg. From the results of four cracks, it seems necessary that the primary slip system in one and only one grain has the maximum shear stress. This slip plane intersects the grain boundary at a higher angle in three cases out of four.

For a grain boundary cracking, it is also required that the normal stress should act on the grain boundary plane. Figure 7 shows an example of a dark line along the grain boundary and the slip bands impinge the grain boundary (the stress axis is horizontal). It did not become a propagating crack. The grain boundary where a propagating crack is formed has a relatively high angle against the stress axis, as seen in Figs. 3*b*, 3*d*, and 3*e*, and also in the four cases shown in Fig. 6.

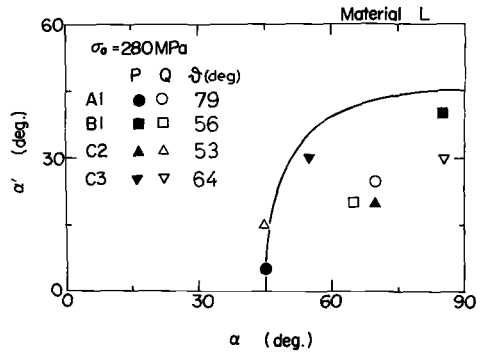

FIG. 6—*Angles of slip traces.*

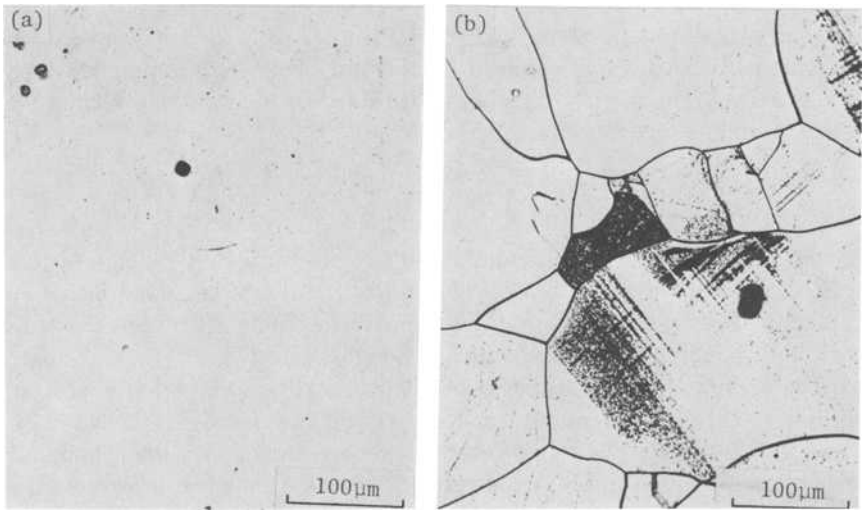

FIG. 7—*Micrographs of fatigue specimen of Material S under* σ_a = *331 MPa.* (a) *Polished surface.* (b) *Etched surface.*

The crystallographic requirements for fatigue crack initiation at the grain boundary was studied by Kim and Laird [*16*] with pure copper under high strain cycling. The requirement for normal stress on the grain boundary is confirmed by the present experiment. They also pointed out that the incompatibility of slip between two adjacent grains was responsible for crack nucleation. This requirement was met in their experiment when the slip on the most active slip system in either one or both of the adjoining grains was directed at the intersection of the boundary with the specimen surface. The present result concerned with low strain fatigue suggests another mechanism

that produces the plastic incompatibility between two adjoining grains. The incompatibility caused by the active slip in one grain impinging the grain boundary at high angles, not necessarily directing at the intersection of the boundary with the specimen surface, can also cause crack initiation, and this incompatibility seems to be pronounced when the slip in the other grain is not under the maximum shear stress. This type of grain boundary crack initiation was theoretically analyzed by Tanaka and Mura [*17*]. They ascribed the crack initiation to the stress concentration caused by the stacking of double-layer dislocation arrays piling up at the grain boundary. When the number of slip bands stacked is small or the stress concentration is insufficient, the crack nucleates along the slip band. This type of slip band cracking is seen in Figs. *3a* and *3c*. The theory predicts that the number of dislocation dipoles is an indicator of the fatigue damage. A quantitative comparison of the damage accumulation modeled in the theory with the experimental observation of dislocations needs to be done in the future.

Crack Propagation Behavior

In order to examine the detailed behavior of fatigue crack growth, the increment of the crack length was measured separately for each tip of a surface embedded crack. The increment of the crack length toward the specimen corner is denoted by u and that in the opposite direction by ℓ. Propagation curves of three cracks, C4, B1, and B16, are presented in Figs. 8*a*, 8*b*, and 8*c*, whose micrographs are given in Figs. *3a*, *3b*, and *3e*, respectively. Crack C4 nucleated along the slip band and propagated mainly downward. After passing a grain boundary, it changes the direction and slows down. The upper tip is branched. Crack B1 nucleated along the grain boundary and prop-

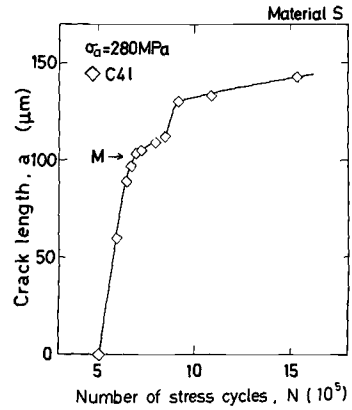

FIG. 8*a*—*Crack propagation curves of Material S under* $\sigma_a = 331$ *MPa; Crack C4*ℓ.

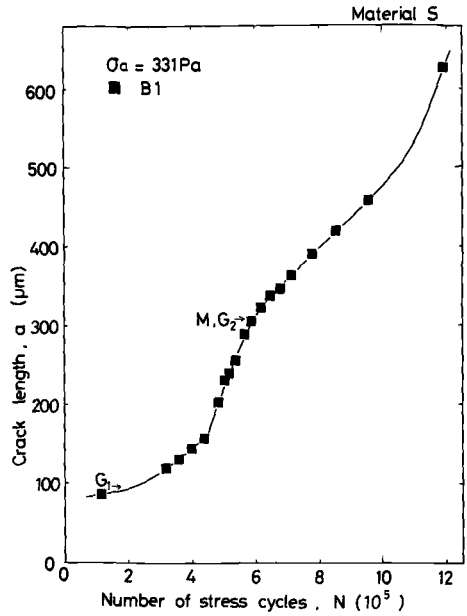

FIG. 8*b*—*Crack propagation curves of Material S under* $\sigma_a = 331$ *MPa; Crack B1.*

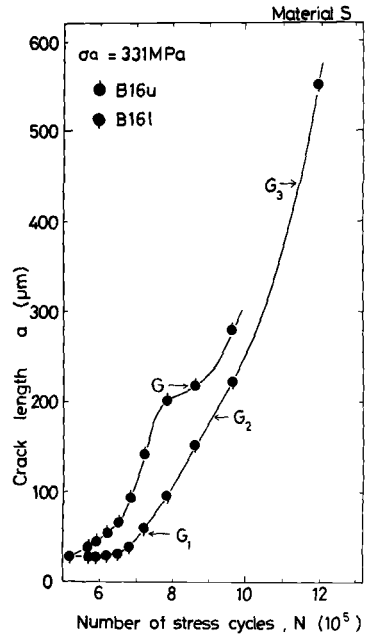

FIG. 8*c*—*Crack propagation curves of Material S under* $\sigma_a = 331$ *MPa; Crack B16.*

agated over the boundary G1 along slip band. The growth mode changed to noncrystallographic or of Stage II type after crossing the boundary G2. The crack begins to decelerate and then accelerate. Crack 16, nucleated along the grain boundary and propagating within a grain, decelerates before reaching to the boundary G, while the grain boundaries, G1, G2, and G3, have no such influence on the crack growth. A more detailed discussion of the interaction of crack growth and microstructure in Materials S and L is presented elsewhere [*18*]. Most cracks showed the irregular growth behavior affected by the microstructure in their early propagation stage. The irregular behavior was mainly caused by the growth mode change and much less frequently by the blocking of the grain boundary.

In order to correlate the crack propagation rate to the stress intensity factor, the shape of both surface and corner cracks was observed by breaking at a liquid nitrogen temperature several other specimens fatigued under the same stress amplitudes to various number of stress cycles. Corner cracks were shaped roughly as a quarter ellipse, the surface embedded cracks as a half ellipse. The ratio λ of the crack depth c to the crack length a on the surface (the half crack length for embedded crack) was measured and correlated to a. The relation between λ and a was found to be almost independent of the stress amplitude and the grain size [*18*]. For the present experiment, λ was estimated through this relation for surface cracks and was actually measured for corner cracks. The stress intensity factor at the crack tip on the surface was calculated from a and λ by using the equations proposed by Nakai and Tanaka [*10*]. The effect of the specimen edge on the stress intensity factor was neglected. This is not serious, because most of the rate data for small embedded cracks were taken rather away from the edge.

The crack propagation rate da/dN in Material S is plotted against the stress intensity range ΔK in Fig. 9*a* for the cases when the grain boundary blocking was not involved. The value of ΔK equals the maximum stress intensity factor K_{max} for the present experiment under $R = -1$. The dashed lines drawn in the figure indicate the relations of da/dN versus ΔK and da/dN versus ΔK_{eff} obtained for long through-crack propagation in Material S under $R = -1$, where ΔK_{eff} is the effective stress intensity factor defined by $\Delta K_{eff} = K_{max} - K_{op}$ (K_{op} is the stress intensity factor at the crack tip opening) [*13*]. As seen in the figure, the da/dN-ΔK relations of Crack D3 ($\sigma_a = 280$ MPa), B1 and B2ℓ ($\sigma_a = 331$ MPa), are close to the da/dN-ΔK_{eff} relation for long cracks in the early stage, and the rate decreases and then increases again, merging into the da/dN-ΔK relation for long cracks. Crack C4ℓ ($\sigma_a = 280$ MPa) propagates in the initial stage faster than that given by the da/dN-ΔK_{eff} relation of long cracks. Cracks A1ℓ, C4ℓ ($\sigma_a = 280$ MPa), and D2 ($\sigma_a = 331$ MPa) become nonpropagating. The ΔK-value at nonpropagation is between the threshold values of ΔK and ΔK_{eff} for long cracks. The rate of Crack D2ℓ ($\sigma_a = 280$ MPa) gradually transfers from the da/dN-ΔK_{eff} relation to the da/dN-ΔK relation for long cracks.

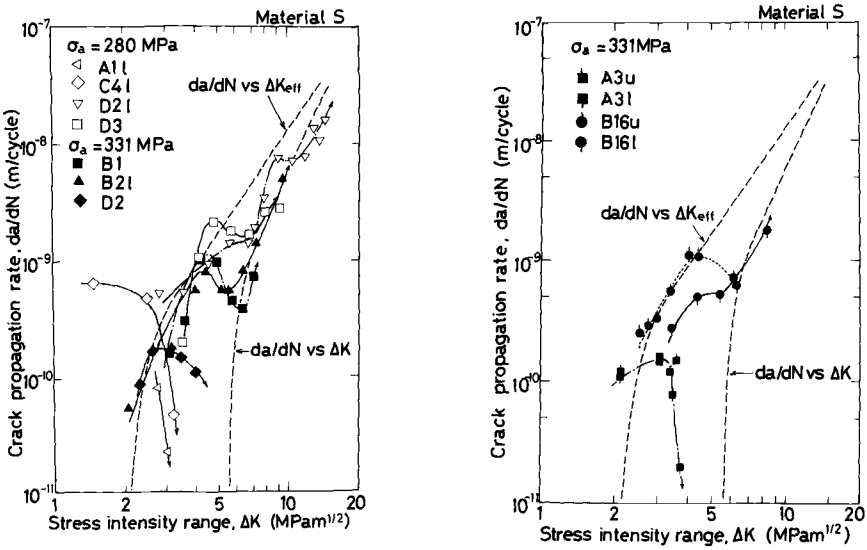

FIG. 9—*Relation between crack propagation rate and stress intensity range in Material S.*

In the sigmoidal variation of the da/dN-ΔK relation for small cracks, the point where the rate dropped rather sharply was determined and the corresponding micrographs were examined. This point is indicated by letter M in Figs. 3*a* to 3*c*. From a careful comparative examination including other cases, it can be concluded that the crack growth path is crystallographic, along slip bands or grain boundaries, before the point of deceleration, and of Stage II or of the transition type after that point. The results are summarized in Table 1, together with the crack length and ΔK at the rate-decreasing point. The mean length is 149 μm and the mean value of ΔK is 3.8 MPa$\sqrt{\text{m}}$.

The rate of Cracks B16 and A3 in Material S, which were decelerated by the grain boundary, is plotted against ΔK in Fig. 9*b*. A general trend is largely similar to the data presented in Fig. 9*a*. Both cracks were decelerated by the grain boundary denoted by G in Figs. 3*d* and 3*e*. The deceleration took place at distances about 50 and 12 μm from crack tip to boundary for Cracks B16 and A3, respectively. The grain boundary effect on crack deceleration may depend on the slip orientation in the grain next to the crack tip. When the slip system in the grain is easy to operate, the grain boundary does not act as a barrier, but it can influence the growth rate through growth-mode change or it has no essential effect.

For the case of Material L, the growth behavior of small cracks was also sigmoidal although the variation of the rate was larger than in the case of Material S [*18*]. The irregular behavior of crack growth was mostly caused by the change in crack growth mode. The results are summarized in Table 1. At

TABLE 1—*Growth mode, crack length, and stress intensity factor characteristics of anomalous small crack growth.*

Material	Stress Amplitude (σ_a), MPa	Crack Designation	Rate-Decreasing Point				Merging Point	
			Growth Mode Before the Point	Growth Mode After the Point	Crack Length (a), μm	SIF (ΔK), MPa$\sqrt{\text{m}}$	Crack Length (a), μm	SIF (ΔK), MPa$\sqrt{\text{m}}$
S	280	C4ℓ[a]	slip band	transition	55	2.8	...	...
		D3	grain boundary	Stage II	200	3.6	650	6.8
	331	B1	slip band	Stage II	310	5.4	390	6.1
		B2ℓ	slip band	Stage II	120	4.9	210	6.2
		D2[a]	grain boundary	Stage II	60	2.3	...	...
L	240	B6ℓ	grain boundary	Stage II	390	5.8	600[b]	6.6[b]
		B8ℓ[a]	grain boundary	Stage II	260	3.6	...	...
	280	A1	grain boundary	Stage II	590	6.2	760[b]	7.1[b]
		B2u	grain boundary	Stage II	250	5.7	400[b]	6.8[b]

[a]Nonpropagating cracks.
[b]At the minimum rate point.

the rate-decreasing point, the mean crack length is 373 μm and the mean ΔK value is 5.3 MPa$\sqrt{\text{m}}$.

To pursue the fail-safety prediction of a structural component with a small crack, one of the important problems will be the condition where the results of small crack growth merge with the long crack data obtained in ordinary tests of linear fracture mechanics. Taylor and Knott [*19*] have suggested that the condition is determined by the crack length. This length was found to be about four times the grain size in a cast nickel aluminum bronze (the grain size 100 μm). According to Lankford's result [*20*] with a 7075-T6 aluminum alloy (grain size 80 μm), the total length at merge was 180 μm, that is, about two times the grain size. He interpreted the merging condition as the monotonic plastic zone being equal to the grain size. As seen in Fig. 5, merging occurs at the minimum rate point in the near-threshold region below the growth rate of 2×10^{-9} m/cycle. The crack length and ΔK are given in Table 1 for Material S. The crack length a at merge is about 1.5 and 5 times the grain size, which does not contradict Taylor-Knott's data. However, the merging points seem to be independent of the stress amplitude, in contradiction to the constant crack length criterion. The monotonic plastic zone ζ_F was found in the previous long crack study of Material S [*13*] to be a function of K_{max} as

$$\zeta_F = 0.45\,(K_{max}/\sigma_Y)^2 \tag{2}$$

where σ_Y is the yield stress. If this equation is used, the monotonic plastic zone ζ_F calculated from ΔK $(=K_{max})$ = 6 to 7 MPa$\sqrt{\text{m}}$ for Material S is 87 to 120 μm. The applied stresses relative to the yield stress is 0.65 to 0.77 in the present experiment, so the actual ζ_F will be higher than those calculated. Therefore the present data do not contradict the condition proposed by Lankford [*20*]. Since the relations of da/dN-ΔK and $\zeta_F - K_{max}$ for long cracks in Material L are not yet obtained, it is difficult to examine the grain size effect. In Table 1, the crack length a and ΔK at the minimum rate point are given, which can be regarded as those at merge. The values are larger in Material L than in Material S.

Taylor [*19*] and Lankford [*20*] did not report the data of small crack growth after meeting the da/dN-ΔK relation for long cracks. The results presented in Fig. 5 show that the growth rate of small cracks increases following the long crack growth law. The ratio of the monotonic plastic zone ζ_F (estimated by Eq 2) to the crack length a is around 0.5 to 0.3 in the range of ΔK = 8 to 10 MPa$\sqrt{\text{m}}$ (a = 350 to 800 μm), so the scale of the monotonic plastic zone is beyond a condition of small-scale yielding for local plasticity. However, the condition of the small-scale yielding for fatigue crack growth is not yet well defined. According to ASTM Test for Constant-Load-Amplitude Fatigue Crack Growth Rate above 10^{-8} m/Cycle (E 647-81), the size requirement for center cracked plate is to be below the net section yielding due to the

maximum load. In the present study, no loop expansion was detected with the strain gage measurement, so macroscopic, net-section yielding was not involved. The small-scale yielding condition based on the crack tip opening seems to be more appropriate in fatigue crack growth. By using the Dugdale model, the deviation in crack tip opening displacement from the small-scale yielding equation is 23% while that in plastic zone size is 70% at the stress level corresponding to the ratio of plastic zone size to crack length 0.5 [*21*]. Based on this criterion, fairly good agreement in growth behavior between small and long cracks seems reasonable in the present experiment.

Highly Strained Region Around Crack

In the micrographs shown in Fig. 3 the white region without etch pits can be seen within the dark etched region close to the crack. This white region has high plastic strain and is interpreted as the cyclic plastic zone in the case of fatigue [*12,13*]. The material used in the present experiment has a similar etching response to tensile strains as that used by Hahn et al [*12*]. In tensile deformation, the white region begins to appear at about 6% strain and cover almost everywhere at about 10% strain [*13*]. Hahn et al indicated that the monotonic tensile strain was equivalent to the total accumulated strain in cyclic straining [*12*]. As seen in Fig. 3, the etching response of each grain seems to be not uniform and even dark etch pits can not be seen near the crack in several grains. In the case of tensile deformation, a plastic strain of 0.3% was found to be enough to yield a fairly uniform covering of dark etch pits by using the same etching condition [*13*]. Although the reason is not clear, the etching sensitivity of dislocations in 3% silicon iron seems to be dependent not only on plastic strain, but also on the crystallographic orientation. Therefore, in the present study, the width of the white region perpendicular to a crack was measured at several locations where it was clearly visible. Because the crack length measurement had to be done without knowing the position of the grain boundary or near-tip etch pit pattern, the data points in the propagation curves such as shown in Fig. 8 were obtained rather arbitrarily. When the width of the white region changed dramatically during two successive measurements of crack length, the width was averaged and correlated to the crack growth rate calculated from two lengths. An example of such cases is the extension from G1 to G2 (Fig. 3*e*) of Crack B16 whose growth curve is shown in Fig. 8c.

Figure 10 shows the relation between the width of the white region 2η (m) and the crack propagation rate da/dN (m/cycle) for Material S. The same marks are used to indicate the data as in Fig. 9 and the circles are the data obtained for the other cracks. Although there is scatter, the relation between da/dN and η can be approximated above the rate 3×10^{-10} m/cycle by

$$da/dN = 4.9 \times 10^{-3}(2\eta)^{1.5} \tag{3}$$

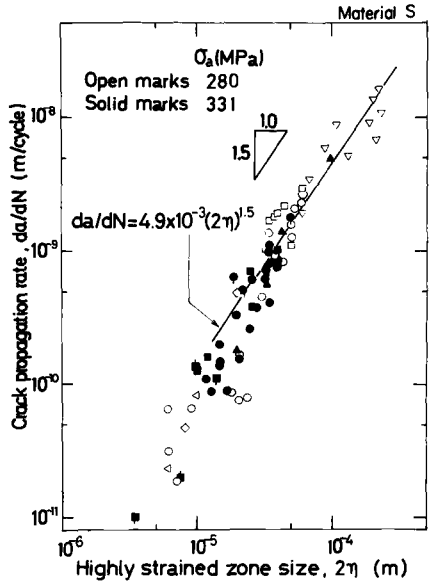

FIG. 10—*Relation between crack propagation rate and highly strained zone size.*

In the region below 3×10^{-10} m/cycle, 2η is between 4 and 30 μm. It should be noted that the rate can be correlated uniquely to 2η, even though anomalous behavior is observed in the da/dN-ΔK relation in the early stage. The same relation was obtained for the case of Material L although the scatter of data is large [*18*]. In Fig. 10, the data of slip band crack growth are not included in the region above 3×10^{-10} m/cycle, because the measurement of 2η was not successful. The data of slip band growth of Crack A3u are below this rate. The etch pit patterns at slip band growth of Crack C4 and B1 are not clear (Figs. 3*a* and 3*b*). The white region near slip band cracking of Crack B2 (Fig. 3*c*) is supposed to be made during crack initiation. Therefore Eq 3 is confirmed for cracks propagating along the grain boundary, or in transitional or Stage II mode. For slip band crack growth, the deformation in the crack growth direction seem to be more important than that in the perpendicular direction [*22*], so the relation between da/dN and η may be different. Further study is necessary. For cracks propagating in the other modes, a unique relation, Eq 3, between da/dN and 2η suggests the importance of crack closure as analyzed based on the results of the long-crack study given below.

In our previous study of long through-cracks in the same Material S [*13*], da/dN is expressed by the following function of 2η measured in the interior of the specimen in the same rate region of 3×10^{-10} to 2×10^{-8} m/cycle:

$$da/dN = 2.0 \times 10^{-2}(2\eta)^{1.5} \tag{4}$$

It was also found that the highly strained region 2η (m) is a unique function of the effective stress intensity range ΔK_{eff} (MPa$\sqrt{\text{m}}$) for long cracks

$$2\eta = 0.14(\Delta K_{\text{eff}}/\sigma_{\text{Y}})^2 \tag{5}$$

The relation between da/dN (m/cycle) and ΔK_{eff} (MPa$\sqrt{\text{m}}$) for long cracks is obtained from Eqs 3 and 4 as

$$da/dN = 1.3 \times 10^{-11}(\Delta K_{\text{eff}})^{3.0} \tag{6}$$

This relation is the same as that obtained from the measurement of ΔK_{eff}, which is shown by the dashed line in Fig. 9. Since the value of 2η measured in the present study for surface cracks is much smaller than the grain size and crack size, and the grain boundary normally does not block the highly strained region, a second power relation similar to Eq 5 is expected between 2η and ΔK_{eff} for surface cracks. Therefore it can be concluded that the variation of crack closure is primarily responsible for the anomalous variation of the rate versus ΔK shown in Fig. 9. If we assume that Eq 6 is also applicable to the case of surface cracks, the ratio of the 2η-value measured on the specimen surface for surface cracks to that measured in the specimen interior for long cracks is calculated by Eqs 3 and 4 as 2.6, which is a reasonable factor for converting the crack tip plasticity in the plane strain condition to that in the plane stress condition [*13,23*].

Since Elber [*24*] pointed out the significance of crack closure in fatigue crack propagation, a number of research has been reported which shows that the increase in crack closure level slows down the fatigue crack propagation rate, especially in the near-threshold region [*25-28*]. In the present material, the increase in crack closure was also shown to be the primary cause of the rate decrease of long cracks in the near-threshold region, deviating from the Paris law in the intermediate rate region [*13*]. However, most of the previous works have been conducted with long cracks, and the crack closure studies of small cracks are very few. Morris measured the crack closure for small cracks with the grain size dimension in 7075-T851 aluminum alloy [*5*] and 2219-T851 alloy [*4,6,7*]. He observed that a slip band crack less than the grain size was very low [*5*] and that the irregularity of crack path or the fracture surface mismatch was a main reason for crack closure in this length region [*4,6*]. The closure stress of Stage II cracks of the grain size order was found to increase roughly in proportion to the distance to the next grain boundary ahead of the crack tip [*7*]. The crack closure in this case was explained to be caused by residual plastic strain. From the discussion with respect to Fig. 9 and the agreement of the early crack growth with the long-crack da/dN-ΔK_{eff} rela-

tion, it is reasonable to regard the opening stress intensity K_{op} as zero when the crack is propagating along the grain boundary, and K_{op} begins to increase as it grows in the mode of Stage II or transitional type. A slip band crack, for example Crack C4ℓ (Fig. 9*a*), can propagate faster than predicted from the da/dN-ΔK_{eff} relation for long cracks, and the assumption of zero opening stress is not enough to explain this type of fast growth. The mode of crack growth or local microplasticity [*20*] may be significant.

The plasticity-induced crack closure of a semi-infinite crack propagating under a constant ΔK condition was analyzed by Budiansky and Hutchinson [*29*], who based their analysis on the Dugdale yield model. The present authors applied this model to a small crack under the assumption of the constant residual stretch attached to the crack face [*30*]. The crack closure level calculated increases as the crack length becomes large. Also, the finite-element simulation indicated that the crack closure increased as the crack grew from the initial ideal crack without residual extension [*31*]. Therefore it is reasonable that the plasticity-induced crack closure increases with the crack increment made by Stage II mode growth, which is consistent with the foregoing explanation of anomalous behavior of small crack growth based on the crack closure. Roughness-induced crack closure which may play some role in transional mode growth will have a similar dependency of crack length, although the theoretical analysis is not yet completed.

According to the Budiansky-Hutchinson crack closure model [*29*], the crack closure level increases with the maximum value of crack tip opening displacement and reduces by its cyclic component. Thus the Morris result on the grain boundary effect on crack closure is consistent with the prediction. But the grain boundary effect on crack closure in the present experiment seems to be contradictory. As described in the preceding section, Cracks B16ℓ and A3ℓ began to decelerate at distances 50 and 12 μm from the grain boundary G. If Eq 2 is used, the ζ_F-value calculated at the rate-decreasing point are 65 μm (K_{max} = 5.1 MPa$\sqrt{m}$) for B16u and 15 μm (K_{max} = 2.4 MPa$\sqrt{m}$) for A3ℓ. Therefore the rate begins to decrease when the monotonic plastic zone hits the grain boundary. In the long-crack study [*13*], this condition was also coincidental with the transition from the Paris law region to the near-threshold region, that is, the point where the crack closure begins to increase. The blocking of the monotonic plastic zone reduces the maximum crack tip opening displacement [*32*], so the crack closure should decrease according to the Budiansky-Hutchinson model [*29*].

In order to explain the effect of the structure-sensitive plasticity on crack closure, a dislocation model similar to that proposed by Kanninen et al [*33*] seems to be more appropriate than the Dugdale-type strip yield model. They represent the residual plasticity of Stage II crack by dislocations and evaluate the crack closure load from the back stress field of residual dislocations. Although they try to model the macroscopic residual plasticity for Stage II crack by super-dislocations, the model can also be used for physical disloca-

tions with a special configuration relative to the crack. Figure 11 illustrates the residual dislocations around cracks propagating along the slip band (*a*) and in Stage II fashion (*b*). The stress intensity factor produced by the dislocations parallel to the crack shown in Fig. 11*a* is nearly zero. On the other hand, the dislocations inclined to the crack shown in Fig. 11*b* (Kanninen et al model) give a negative value of the stress intensity factor, which means the opening stress intensity factor is positive. For the grain boundary crack, the zero K_{op} can be derived if we regard the impinging slip bands as made of dislocation dipoles, which is assumed in the fatigue crack initiation theory by Tanaka and Mura [*17*]. Based on the dislocation model, the increase in crack closure due to the grain boundary can be explained by considering the secondary dislocations or cross-slipped dislocations stacked near the grain boundary (Figs. 11*c* and 11*d*). Since those dislocations are closer to the crack than the dislocations formed without any grain boundary blocking, the back stress causing crack closure will be larger. A detailed analysis will be the subject of a future study. Also, the actual measurement of crack closure is necessary to substantiate the foregoing discussion.

Influence of Grain Size on Fatigue Process

The growth behavior of small cracks in the present material is more sensitive to the mode or the path of crack propagation than to the interaction with the grain boundary. To investigate the influence of the grain size on the growth mode, the average characteristics are studied. At several values of ΔK, the growth mode was identified for all cracks observed, and the percentage of number of cracks propagating in each mode was measured.

Figure 12 shows the variation of the percentage of each mode as a function

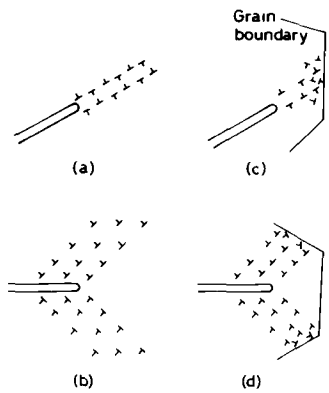

FIG. 11—*Crack and residual dislocations.* (a) *Slip band crack.* (b) *Stage II crack (Kanninen et al model).* (c) *Slip band crack blocked by grain boundary.* (d) *Stage II crack blocked by grain boundary.*

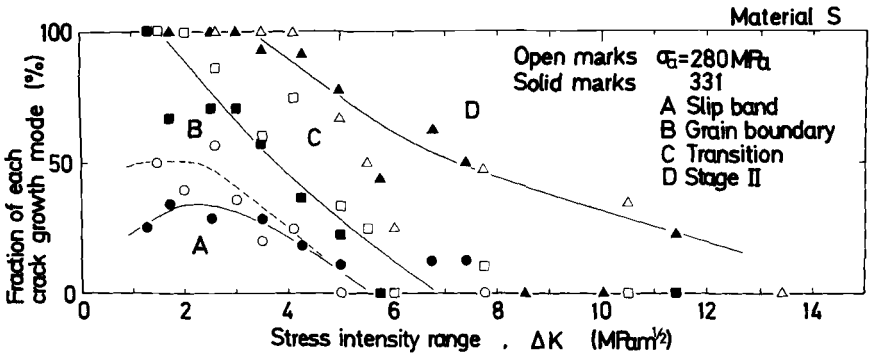

(a) Material S

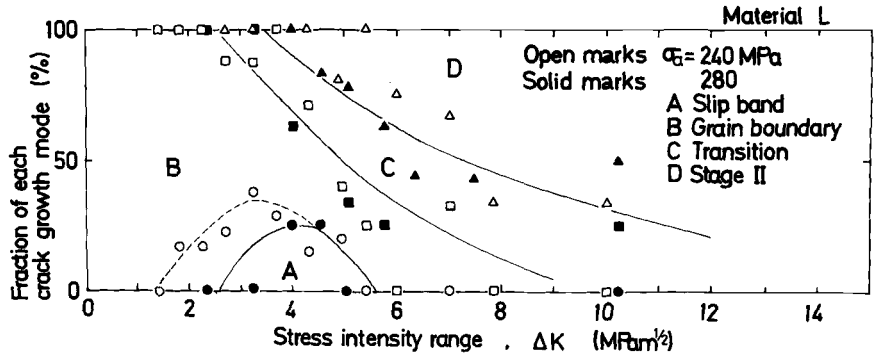

(b) Material L

FIG. 12—*Variation of crack growth mode with stress intensity range.* (a) *Material S.* (b) *Material L.*

of ΔK. The ordinate is the accumulated fraction of each mode. The regions denoted by A, B, C, and D indicate the fractions of slip band, grain boundary, transitional, and Stage II modes, respectively. The circles, squares, and triangles are the experimental data used to draw the dividing lines. Therefore the fraction of each mode at a certain ΔK equals the segment of a vertical line cut by each dividing line. In this section we discuss which factor, the crack size (grain size) or ΔK, controls and determines the fraction of each mode. If the crack size is the controlling factor, the data indicated by the solid marks corresponding to the higher stress shift to the right. On the other hand, if ΔK is controlling, the solid and open marks are coincidental. From this point of

view, the fractions of Stage II and transitional modes are controlled by ΔK, while the fraction of slip band cracking seems to be controlled by the grain size. The dividing lines are drawn based on this consideration. A statistical treatment is necessary for more precise discussion.

The ΔK-value at the maximum fraction of slip band cracking is summarized in Table 2. The length $2a_s$ for an embedded crack corresponding to this ΔK is calculated. The ratio of $2a_s$ to the grain size is about 0.4. Therefore it can be concluded that the slip band cracking is more closely related to the grain size than to ΔK. This is consistent with results from low-carbon steels [*34*]. In experiments with low-carbon steel of grain size 50 μm, the slip band cracking did not transfer to other types of cracking until its length was over the grain size; that is, $2a_s/d$ was about unity. There seems to be a limiting value of the grain size above which the slip band cracking does not spread over one grain. The ΔK-value where the sum of the fractions of slip band cracking and grain boundary cracking equals 50% is given in Table 2. This value is independent of the stress amplitude and tends to be larger in Material L. The ΔK value to 50% fraction of Stage II cracking is 7.2 MPa$\sqrt{\text{m}}$. It is interesting to see that this value coincides with the transition from the near-threshold region to the Paris law region in the da/dN-ΔK relation for long cracks shown in Fig. 9.

The influence of grain size on the fatigue life of the smooth specimen is mainly in the stages of the crack initiation and the early crystallographic growth. The sigmoidal variation of small cracks obviously suggests that the fatigue limit of the present material is determined by the condition of the nonpropagating small cracks and that the length of those cracks increases with grain size. To derive the total life curve, statistical analysis of the granular structure will be necessary.

Conclusions

1. The initiation site of fatigue cracks is mainly along the grain boundary in 3% silicon iron. In optical microscopic observation, a dark line first appears and then the line darkens without elongating its length until it becomes a crack. It is necessary for grain boundary crack initiation that the primary slip system of only one of two adjacent grains is subjected to the cycling of the maximum resolved shear stress and that the slip bands impinge at about 50 to 65 deg on the grain boundary.

2. Small cracks propagate along the grain boundary or the slip band in the early stage and then change their mode to transitional or Stage II type. Most of the cracks first accelerate following the relation between the rate da/dN and the effective stress intensity range ΔK_{eff} for long cracks, and then decrease approaching to the da/dN-ΔK relation for long cracks. After merging, the rate increases in accordance with the long crack growth law. Some cracks become nonpropagating. Slip band cracks can propagate faster than

TABLE 2—*Average characteristics of the fatigue process.*

Material	Stress Amplitude (σ_a), MPa	Initiation Crack Length (a_i), μm	Maximum Fraction of Slip Band Cracking			50% Fraction of Crystallographic Cracking (ΔK), MPa$\sqrt{m}$	50% Fraction of Stage II Cracking (ΔK), MPa$\sqrt{m}$
			Stress Intensity Factor (ΔK) MPa$\sqrt{m}$	Crack Length (a_s), μm	$2a_s/d$		
S (d = 130 μm)	280	20 to 70	1.8	22	0.34	3.7	7.2
	331		2.3	26	0.40		
L (d = 600 μm)	240	100 to 400	3.4	100	0.37	5.0	7.2
	280		4.1	120	0.40		

predicted from the da/dN-ΔK_{eff} relation for long cracks. The stress intensity factor for nonpropagating small cracks is between the threshold values of ΔK_{eff} and ΔK for long crack growth.

3. Micrographic observation indicated that deceleration of small cracks in the early stage took place mostly when the growth path changed from slip band or grain boundary to noncrystallographic path, and much less frequently when the crack approached to the grain boundary.

4. While the relation between da/dN and ΔK is irregular for small cracks, the rate was found to be expressed as a unique power function of the size of the highly strained region near the crack, except for slip band cracks. The irregular behavior of the da/dN-ΔK relation for small cracks was ascribed primarily to the crack closure behavior due to the growth mode change.

5. Based on the average characteristics of the small crack growth mode, it can be concluded that the slip band cracking is more closely related to the grain size than to ΔK, and that the transition to Stage II or transitional mode is more likely controlled by ΔK than by grain size.

References

[1] Taira, S., Tanaka, K., and Hoshina, M. in *Fatigue Mechanisms, ASTM STP 675*, American Society for Testing and Materials, 1979, pp. 135-173.

[2] Tanaka, K., Hoshide, T., and Maekawa, O., *Engineering Fracture Mechanics*, Vol. 16, 1982, pp. 207-220.

[3] Laird, C. and Duquette, D. J. in *Corrosion Fatigue*, O. F. Devereux, A. J. McEvily, and R. W. Staehle, Eds., NACE 2, 1972, pp. 88-117.

[4] Morris, W. L., *Metallurgical Transactions A*, Vol. 8A, 1977, pp. 1079-1085.

[5] Morris, W. L., *Metallurgical Transactions A*, Vol. 8A, 1977, pp. 1087-1093.

[6] Morris, W. L., *Metallurgical Transactions A*, Vol. 10A, 1979, pp. 5-11.

[7] Morris, W. L., *Metallurgical Transactions A*, Vol. 11A, 1980, pp. 1117-1123.

[8] Lankford, J., *Engineering Fracture Mechanics*, Vol. 9, 1977, pp. 617-624.

[9] Lankford, J., Cook, T. S., and Sheldon, G. P., *International Journal of Fracture*, Vol. 17, 1981, pp. 143-155.

[10] Nakai, Y. and Tanaka, K. in *Proceedings*, 23rd Japan Congress on Materials Research, 1980, pp. 106-112.

[11] Tanaka, K., Nakai, Y., and Yamashita, M., *International Journal of Fracture*, Vol. 17, 1981, pp. 519-533.

[12] Hahn, G. T., Hoagland, R. G., and Rosenfield, A. R., *Metallurgical Transactions A*, Vol. 3, 1972, pp. 1189-1202.

[13] Tanaka, K., Hojo, M., and Nakai, Y., *Material Science and Engineering*, Vol. 55, 1982, pp. 85-96.

[14] Morris, C. E., *Metal Progress*, Vol. 56, 1949, p. 696.

[15] Neuber, H., *Kerbspannungslehre*, 2nd ed. Springer-Verlag, Berlin, 1958, p. 73.

[16] Kim, W. H. and Laird, C., *Acta Metallurgica*, Vol. 26, 1978, pp. 789-799.

[17] Tanaka, K. and Mura, T., *Journal of Applied Mechanics, Transactions of ASME*, Vol. 48, 1981, pp. 97-103.

[18] Hojo, M., Tanaka, K., and Nakai, Y., "Etch-Pit Study of Early Fatigue Crack Propagation in 3% Silicon Iron," *Journal of the Society of Materials Science* (Japan), to be published.

[19] Taylor, D. and Knott, J. F., *Fatigue of Engineering Materials and Structures*, Vol. 4, 1981, pp. 147-155.

[20] Lankford, J., "The Growth of Small Fatigue Cracks in 7075-T6 Aluminum," *Journal of Engineering Materials and Structures*, to be published.

[21] Rice, J. R. in *Fracture*, H. Liebowitz, Ed., Academic Press, New York, Vol. 2, 1968, pp. 191-311.
[22] Laird, C. in *Fatigue and Microstructure*, American Society for Metals, Metals Park, Ohio, 1979, pp. 149-203.
[23] Lankford, J., Davidson, D. L., and Cook, T. S. in *Cyclic Stress-Strain and Plastic Deformation Aspects of Fatigue Crack Growth, ASTM STP 637*, American Society for Testing and Materials, 1977, pp. 36-55.
[24] Elber, W. in *Damage Tolerance in Aircraft Structures, ASTM STP 486*, American Society for Testing and Materials, 1971, pp. 203-242.
[25] Ritchie, R. O., Suresh, S., and Moss, C. M., *Journal of Engineering Materials and Technology, Transactions of ASME*, Vol. 102, 1980, pp. 293-299.
[26] Halliday, M. D. and Beevers, C. J., *Journal of Testing and Evaluation*, Vol. 9, 1981, pp. 195-201.
[27] Minakawa, K. and McEvily, A. J., *Scripta Metallurgica*, Vol. 15, 1981, pp. 633-636.
[28] Nakai, Y., Tanaka, K., and Nakanishi, T., *Engineering Fracture Mechanics*, Vol. 15, 1981, pp. 291-302.
[29] Budiansky, B. and Hutchinson, J. W., *Journal of Applied Mechanics, Transactions of ASME*, Vol. 45, 1978, pp. 267-276.
[30] Nakai, Y., Tanaka, K., and Yamashita, M., "An Analysis of Closure Behavior of Small Fatigue Cracks," *Journal of the Society of Material Science* (Japan), to be published.
[31] Ohji, K., Ogura, K., and Ohkubo, Y., *Engineering Fracture Mechanics*, Vol. 7, 1975, pp. 457-464.
[32] Taira, S., Tanaka, K., and Nakai, Y., *Mechanics Research Communications*, Vol. 5, 1978, pp. 375-381.
[33] Kanninen, M. F., Atkinson, C., and Feddersen, C. E. in *Cyclic Stress-Strain and Plastic Deformation Aspects of Fatigue Crack Growth, ASTM STP 637*, American Society for Testing and Materials, 1977, pp. 122-140.
[34] Tanaka, K., Nakai, Y., and Maekawa, O., *Journal of the Society of Materials Science* (Japan), Vol. 31, 1982, pp. 376-382.

DISCUSSION

R. W. Hertzberg[1] (*written discussion*)—Did you measure closure stresses for the short cracks? If so, how did you accomplish this task?

K. Tanaka et al (*authors' closure*)—We did not measure closure stresses for the short cracks in the present study.

[1]Lehigh University, Bethlehem, Pa. 18015.

Hideo Kitagawa,[1] *Yuji Nakasone,*[2] *and Satoru Miyashita*[3]

Measurement of Fatigue Damage by Randomly Distributed Small Cracks Data

REFERENCE: Kitagawa, H., Nakasone, Y., and Miyashita, S., **"Measurement of Fatigue Damage by Randomly Distributed Small Cracks Data,"** *Fatigue Mechanisms: Advances in Quantitative Measurement of Physical Damage, ASTM STP 811,* J. Lankford, D. L. Davidson, W. L. Morris, and R. P. Wei, Eds., American Society for Testing and Materials, 1983, pp. 233-263.

ABSTRACT: During the fatigue process of unnotched smooth materials, small surface cracks often initiate, grow, and coalesce; these cracks are randomly distributed over the material surfaces in terms of size and location. This paper investigates the probabilistic laws these cracks follow, and proposes a quantitative method for the fatigue damage evaluation and residual-fatigue-life prediction of the materials. This method can be carried out in two ways. One is based on the variation of the statistical parameters (for example, the mean etc.) of the crack surface-length distribution with the number of load cycles. The other is based on the growth rate of the distributed small cracks and on the crack length distribution function.

The procedures of the method are described by taking the example of corrosion fatigue of a weldable structural steel, HT 60. The first step is the preparation of specimens having small cracks randomly distributed over their surfaces; the second step is the sampling of statistical data on the cracks from these specimens and from real structures; and, finally, the third step is fatigue damage evaluation and residual-life prediction based on various statistical treatments of the data obtained.

For the test of the goodness of the model and data in the present study, a Monte Carlo simulation analysis was made, which can deal with the initiation, growth, and coalescence behavior of distributed cracks.

Finally, the characteristic features and the scope of application of the method are described, and some comments are made on its applications to other fatigue fracture processes.

KEY WORDS: fatigue, quantitative measurement, fatigue damage evaluation, life prediction, inspection, small cracks, surface cracks, crack growth, statistical analysis, Monte Carlo simulation, fracture mechanics, corrosion fatigue

[1]Professor, Institute of Industrial Science, University of Tokyo, Tokyo, Japan.

[2]Researcher, National Research Institute for Metals, Tokyo, Japan; formerly, Graduate Student, University of Tokyo, Tokyo, Japan.

[3]Research Engineer, Topy Industries Ltd., Tokyo, Japan.

This paper proposes a quantitative method for evaluation of the damage or the life of structures subjected to fatigue. The method comprises statistical measurements and analyses of small cracks randomly distributed over smooth unnotched materials. Sizes and locations of these small cracks can be considered to be random variables.

Mechanism of fracture, role of distributed small cracks, etc., in fatigue processes of smooth unnotched materials are essential problems to solve; nevertheless, these problems are not discussed here. Instead, the present paper investigates and utilizes only the statistical regularity of correspondence between the degree of the progress of fatigue fracture process and the variation in the crack length distribution of distributed small cracks to make a quantitative evaluation of fatigue damage and residual life prediction.

Fracture mechanics has already been applied to the evaluation of the integrity and reliability of large welded structures. In conventional fracture mechanics, residual lives and strength of cracked materials often are calculated mainly by, say, integrating the growth rate of a relatively large independent single crack which existed before service or initiated from a crack-like flaw.

The present paper, however, proposes a new method for a quantitative evaluation of the fatigue process of structural components having smooth unnotched surfaces—in which preservice-existing cracks, crack-like flaws, or sharp notches are not allowed to exist—by the use of data of the distributed small surface cracks which initiate during service.

Methodology and Procedures of the Method (An Example of Its Application to a Corrosion Fatigue Problem)

The methodology and procedures of the method are described by using the corrosion fatigue process of smooth unnotched steel in pure water as a typical example of the fatigue fracture process related to distributed small cracks, during which fatigue damage has yet to measured quantitatively. The method can be applied, not only to the example described here but to other cases such as low-cycle fatigue, elevated-temperature fatigue, etc., if suitable modifications are made with some limitations taken into consideration (see the section on Objectives of the Method and Notes on Its Application to Other Fatigue Processes). This example uses results obtained from corrosion fatigue experiments which employed specimens of a simple shape; nevertheless, the method can be applied, almost as it is, to dangerous portions in real structures.

The method is comprised of three steps: (*1*) preparation of corrosion fatigue specimens over which numerous corrosion pits and small cracks are randomly distributed, (*2*) sampling of data on sizes and locations of these pits and cracks, and (*3*) analyses of these data and fatigue damage evaluation and life prediction based on these analyses. Figures 1*a* and 1*b* illustrate

the methodology and procedures of the method, which are described in detail in the following sections.

First Step: Preparation of Small-Cracks-Distributed Specimens

The first step of the method in this example is corrosion fatigue experiments, which, if necessary, can be replaced by other types of fatigue experiments. These corrosion fatigue experiments employed sheet specimens of as-rolled weldable structural steel, HT 60, having a tensile strength of 588 MPa. This HT 60 steel greatly reduces its fatigue strength in corrosive environments, which has now become one of the most serious problems to solve. The geometry of the specimens is illustrated in Fig. 2.

The specimens were subjected to cyclic axial tension loads having a sinusoidal waveform on a 10-ton horizontal-type hydraulic servofatigue tester. The loading frequency was 10 Hz and the stress ratio (R) was approximately zero.

The corrosive was pure water, deionized by ion exchange resin, in which the specimens were soaked, being kept horizontal throughout the corrosion fatigue tests (Fig. 3).

Each specimen was coated with silicone rubber except for a central area of 25 by 30 mm on its top surface in order to obtain uniform corrosion conditions as well as to avoid crack initiation at the edge of the specimen (Fig. 2).

All the corrosion fatigue experiments were conducted at stress levels sufficiently lower than the fatigue limit in air of this material; that is, $\Delta\sigma_\omega = 470$ MPa. In this stress range, fracture is considered to be caused mainly by distributed small cracks; this characterizes corrosion fatigue fracture. Figure 4 shows the resultant S-N curves.

Second Step: Sampling of Data on Corrosion Pits and on Distributed Small Cracks

Numerous corrosion pits and small surface cracks initiating from these pits were observed distributed randomly over the corrosion-fatigue specimen surface obtained in the first step. The sizes and locations of these pits and cracks can be regarded as random variables. The sizes and number of these defects generally become larger as time (or the number of load cycles) and applied stress level increase. Figure 5 shows an example of corrosion pits and cracks distributed over one of the corrosion-fatigued specimens.

The sampling of data on corrosion pits and on distributed small cracks involved two procedures (Fig. 1a). One procedure was used for investigating the statistical distributions of sizes and locations of corrosion pits and of distributed small cracks at various stages of the corrosion fatigue process. In this procedure (left-hand side of Fig. 1a) fifteen different specimens were used for the measurements of sizes and locations of pits and cracks at five load cycle ratios of $N/N_f = 0.2$, 0.4, 0.6, 0.8, and 1.0 for three applied stress

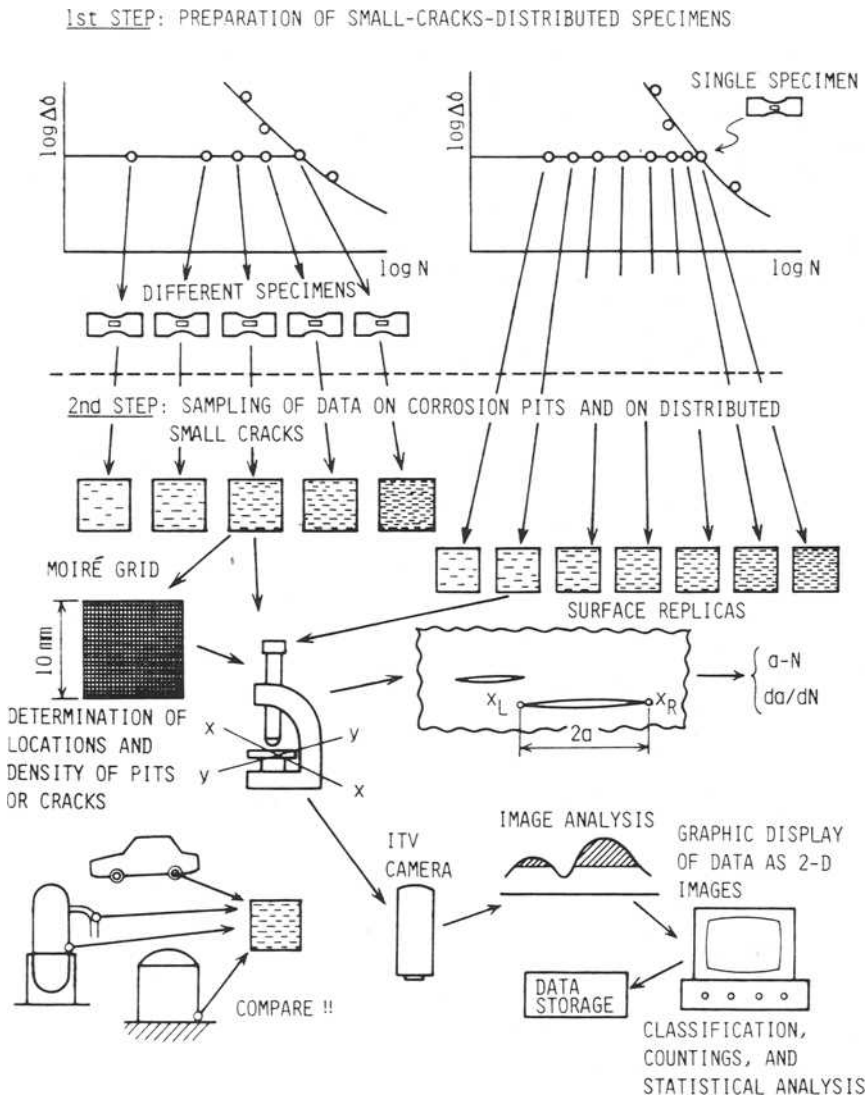

FIG. 1*a*—*Schematic representation of the procedures of the method (Part 1).*

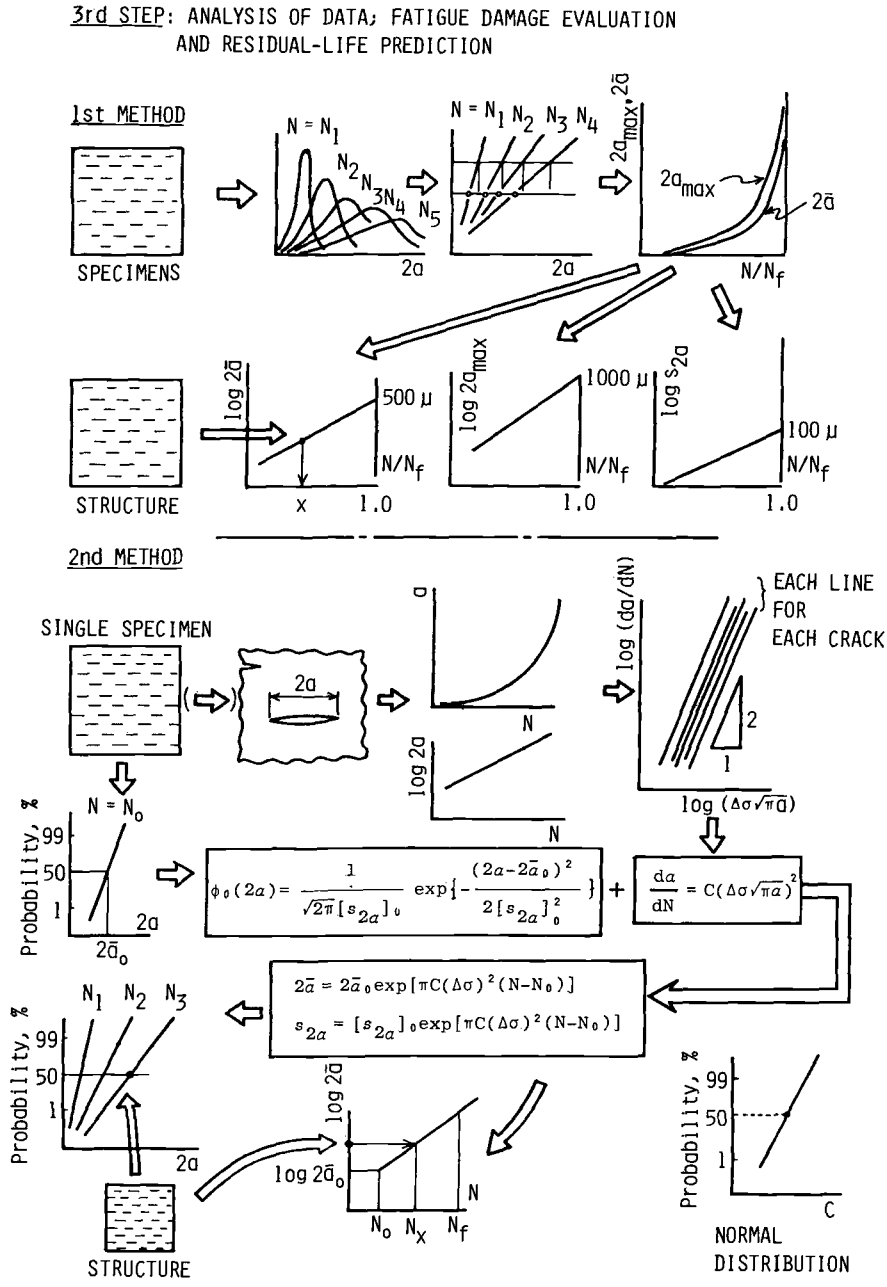

FIG. 1*b*—*Schematic representation of the procedures of the method (Part 2).*

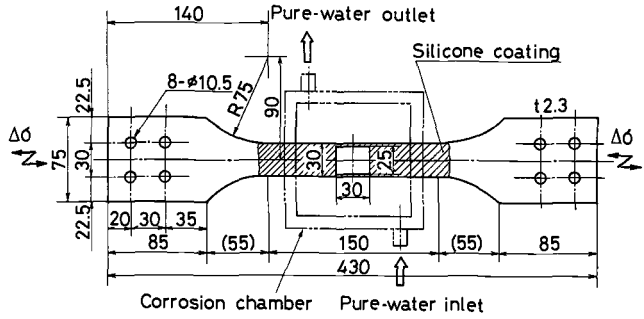

FIG. 2—*Corrosion fatigue specimen geometry, in millimetres.*

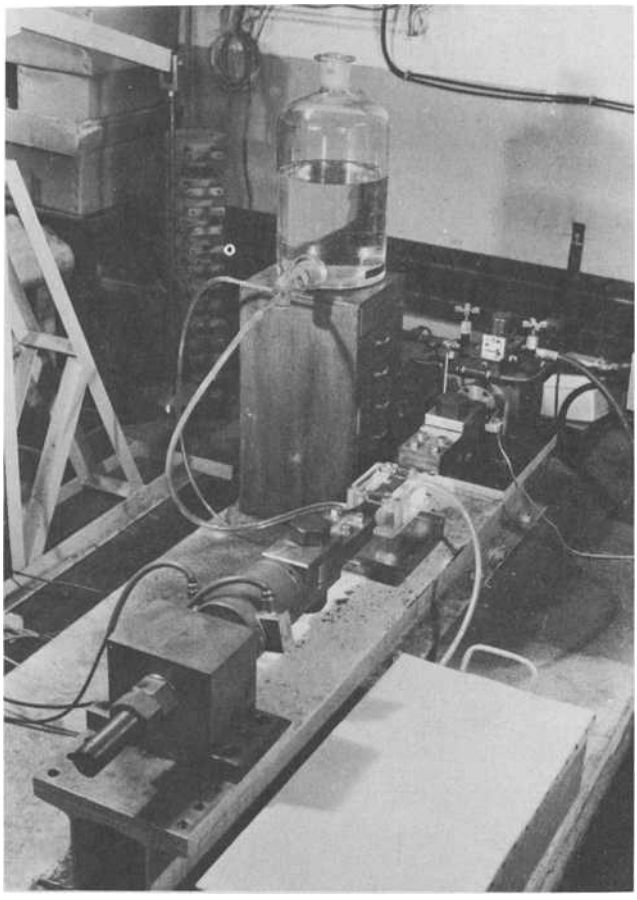

FIG. 3—*Experimental setup for the corrosion fatigue tests.*

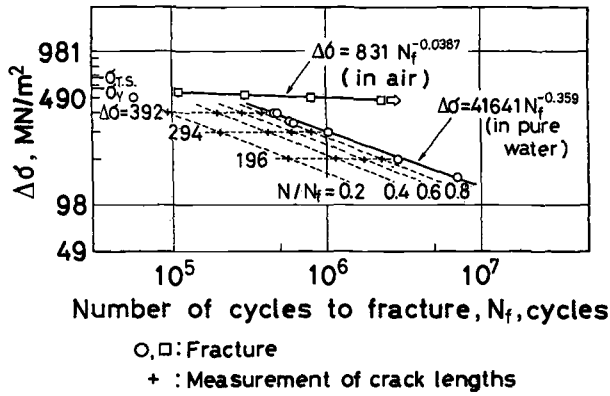

FIG. 4—S-N *curves for the fatigue of HT 60 steel in air and in pure water (10 Hz;* R = *0.04).*

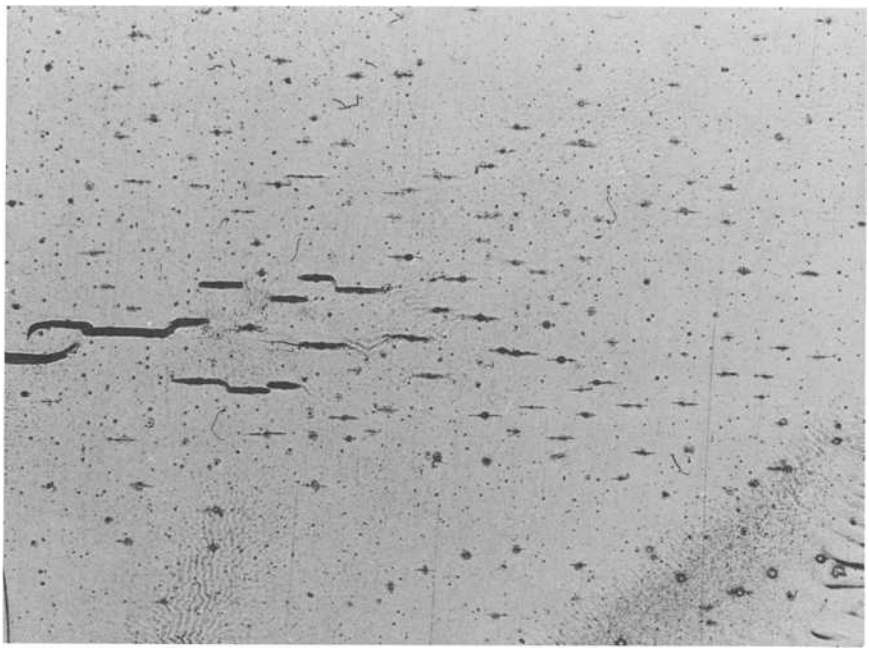

FIG. 5—*Small surface cracks randomly distributed over a specimen surface subjected to corrosion fatigue in pure water environment (taken on an acetyl cellulose thin film).*

(range) levels of $\Delta\sigma$ = 196, 294, and 392 MPa. N_f is the number of load cycles to fracture. After a corrosion fatigue experiment had been terminated at each load cycle ratio at each applied stress level, the corrosion-fatigued specimen was taken out from the fatigue machine and its surface was cleansed,

and then a moiré grid of 0.5-mm mesh was photoprinted onto the specimen surface. This moiré grid facilitated an effective determination of the locations and density of pits and cracks. The sizes of the pits and the cracks within a 10 by 10 mm square region determined by this grid were measured in the manner described subsequently. Figure 6 shows an example of a moiré grid photoprinted onto one of the corrosion-fatigued specimens.

The other procedure was used for investigating the individual growth behav-

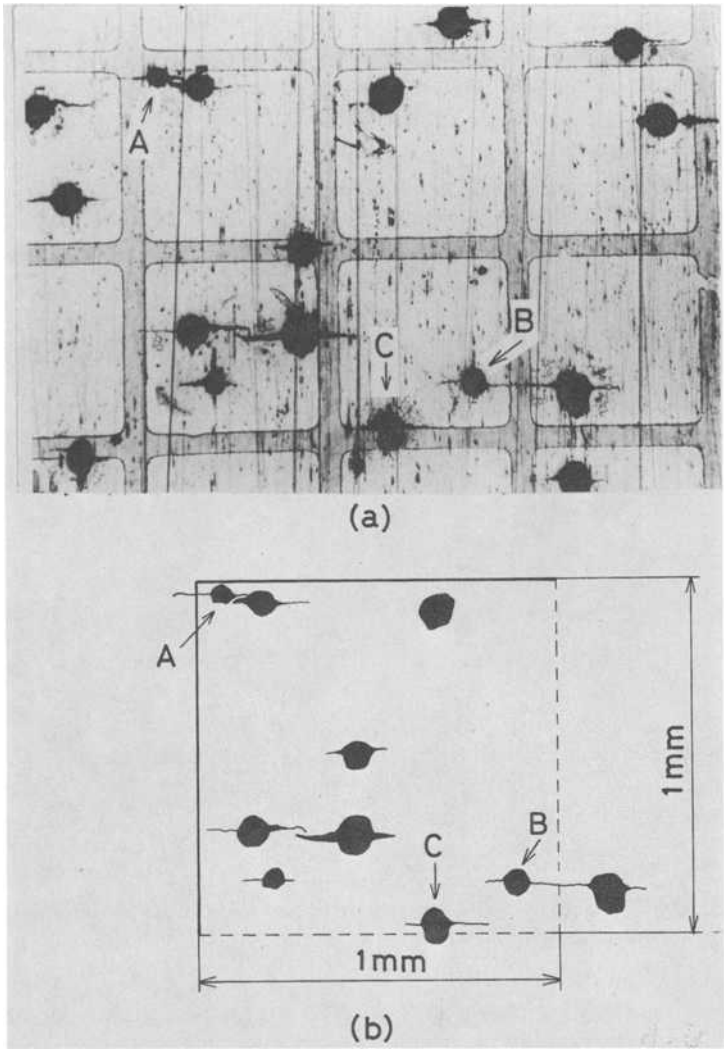

FIG. 6—*Moiré grid photoprinted onto a corrosion-fatigued specimen surface over which small surface cracks initiated from corrosion pits.*

ior of distributed small surface cracks (and their statistical distribution functions). In this procedure (right-hand side of Fig. 1*a*) surface lengths of numerous small cracks were measured by a surface replication technique throughout the corrosion fatigue process by using a single specimen for each applied stress level. The corrosion fatigue experiment of each specimen was paused at adequate load cycle intervals to take replicas of distributed small cracks until fracture occurred. The crack lengths were measured from these replicas by an off-line operation described subsequently. The growth rate of each crack along the specimen surface was determined by the seven-point incremental polynomial method from its surface length ($2a$) versus number of load cycles (N) diagram (the $2a$-N diagram) obtained by the off-line operation.

Data were taken either from corrosion-fatigued specimens directly or from surface replicas by using an x-y table attached to a metallographic microscope and a "surface flaw graphic data processing system" (an improved image-analyzing computer having a television monitor; see Fig. 7). The data taken were as follows: the coordinates of both the right and the left tip of each small crack, (x_R, y_R) and (x_L, y_L); those of each pit center (also regarded as a crack center), (x_C, y_C); both the maximum and the minimum abscissa of each pit projected onto the x-axis, (x_{max}, x_{min}); and the maximum pit depth of each pit, C. With the y-axis of the Cartesian coordinates system set parallel to the loading direction, a projected surface crack length and a projected pit diameter onto the x-axis perpendicular to the loading axis were regarded as crack length ($2a$) and pit diameter (d), respectively; that is, $2a = x_R - x_L$ and $d = x_{max} - x_{min}$. For cracks coalescing to form one large crack, each crack length and location were measured separately if they were distinguishable.

Third Step: Analysis of Data, Fatigue Damage Evaluation, and Life Prediction

This section describes the method of analysis of the data necessary for fatigue damage evaluation and residual-life prediction (or final fracture time prediction) (Fig. 1*b*). Some of the results of the analysis are also described. Although other data obtained in this study are not presented in detail here, those data produced important conclusions: (*1*) little correlation could be found between distributed small cracks and their sources (that is, corrosion pits) in terms of their sizes, and (*2*) the locations of cracks and pits were generally regarded to follow uniformly random distributions [*1*].[4]

Fatigue Damage Evaluation and Life Prediction Based on the Variation of the Statistical Distribution of Crack Surface Lengths with the Number of Load Cycles—The crack surface length ($2a$) versus cumulative relative frequency relations were plotted on normal-distribution probability papers for different load cycle ratios (N/N_f) and for different applied stress (range)

[4]The italic numbers in brackets refer to the list of references appended to this paper.

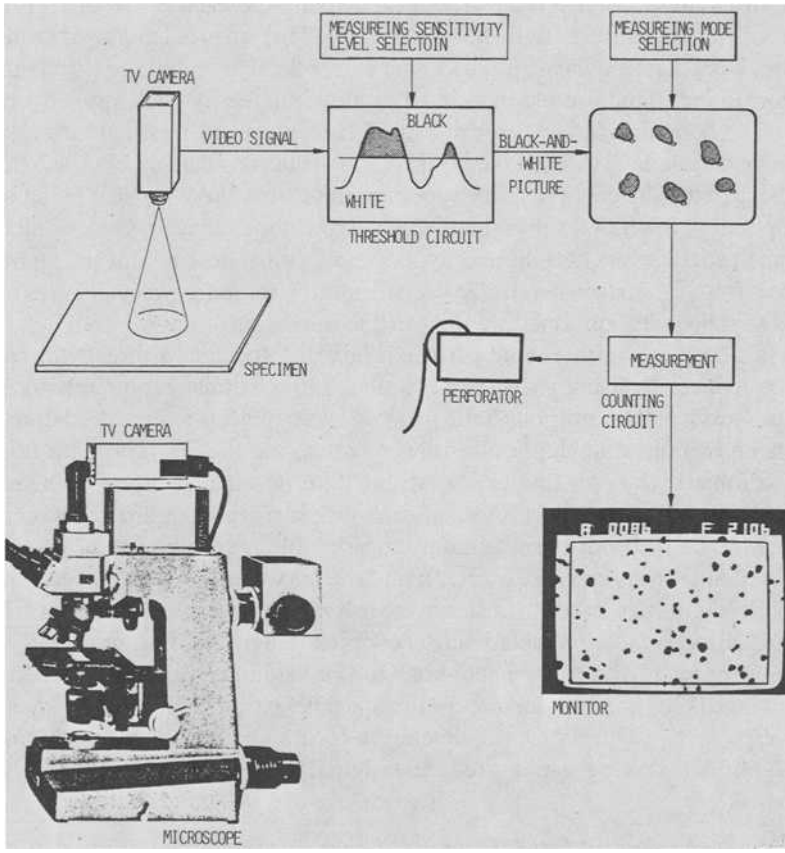

FIG. 7—*Block diagram of a "surface flaw graphic data processing system" (by courtesy of Nihon Regulator Co. Ltd.).*

levels ($\Delta\sigma$), where N and N_f are the number of load cycles and the averaged number of load cycles to fracture, respectively. The results are shown in Figs. 8*a* to 8*c*. The solid lines indicate measured cumulative normal distributions, and the dotted lines indicate cumulative truncated normal distributions.

These graphs show that crack surface lengths followed normal distributions for all the load cycle ratios and all the stress levels tested, which implies that fatigue damage evaluation and life prediction can be easily performed even with a relatively small amount of data.

The mean crack surface length ($2\bar{a}$), the standard deviation for the crack surface length distribution (s_{2a}), and the maximum crack surface length ($2a_{max}$), within an observed area of 10 by 10 mm, increased with load cycle ratio (N/N_f); all the logarithms of $2a$, s_{2a} and $2a_{max}$ increased almost linearly with N/N_f (Figs. 9 to 11). Little difference can be recognized in the relations

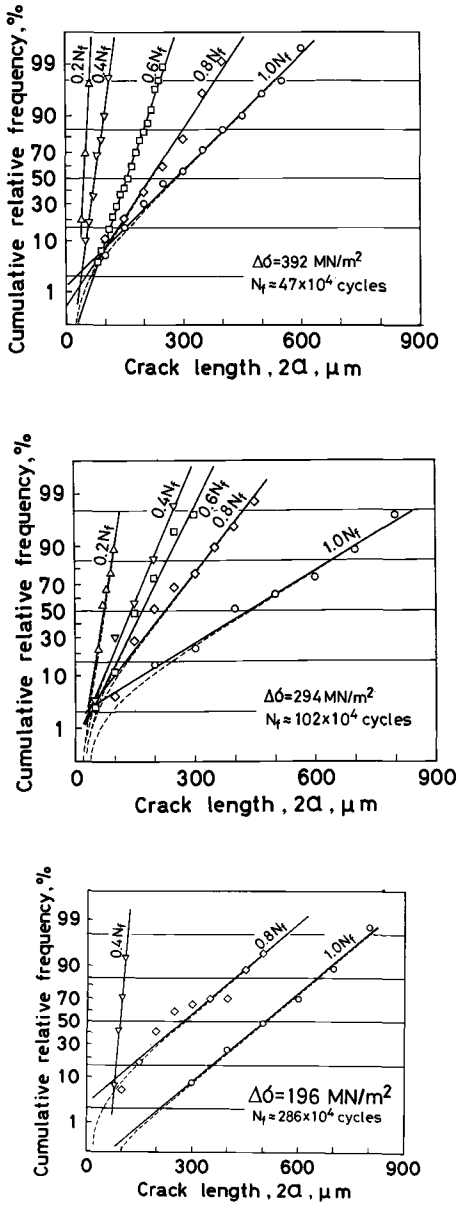

FIG. 8—*Plottings on normal probability papers, showing the variation of the surface length distribution of distributed small cracks in corrosion fatigue of HT 60 steel in pure water environment.*

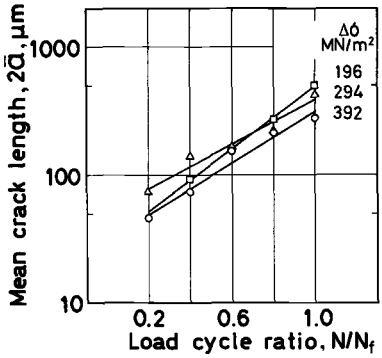

FIG. 9—*Relationship between the logarithm of the mean crack surface length and the load cycle ratio (log 2ā versus* N/N_f *relationship).*

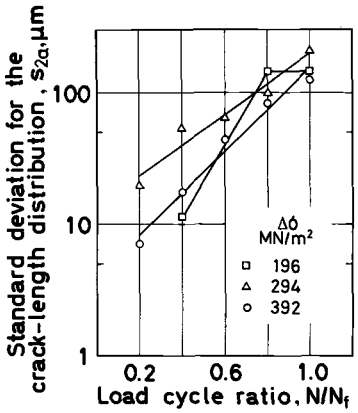

FIG. 10—*Relationship between the logarithm of the standard deviation for the crack surface length distribution and the load cycle ratio (log* s_{2a} *versus* N/N_f *relationship).*

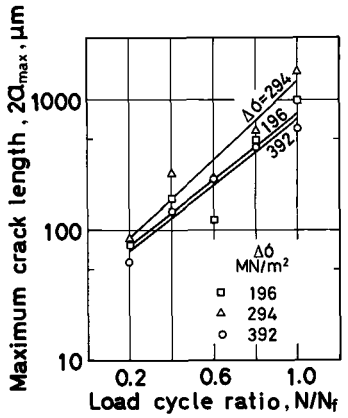

FIG. 11—*Relationship between the logarithm of the maximum crack surface length and the load cycle ratio (log* $2a_{max}$ *versus* N/N_f *relationship).*

for different stress levels ($\Delta\sigma$). These tendencies are equivalent to the case where equi-crack-length curves on a log $\Delta\sigma$ versus log N graph (that is, log $\Delta\sigma$ versus log $[N]_{2a}$ curves) are almost parallel to the S-N curve (that is, the log $\Delta\sigma$ versus log N_f curve).

Consequently, once these relations are obtained, the stage that a structure in a fatigue fracture process has reached can be estimated simply by measuring a mean or a maximum length of distributed small cracks in an observation area. If the S-N curve is known or stress analysis is made for the structure, its residual life can also be estimated. Thus the method has merit in that it does not require any laborious work to find a predominantly growing crack (the largest crack over a dangerous portion of a structure which possibly causes the fatigue fracture of the structure). This is a benefit brought about by statistical regularity which seemingly irregularly distributed cracks have. For fatigue damage evaluation and life prediction of real structures, however, further investigations need to be made (*1*) to clarify what kind of data should be prepared and the limitations of the application of the data, and (*2*) to develop an efficient measurement system.

Fatigue Damage Evaluation and Life Prediction Based on the Relation Between the Growth Rate of Each Crack and the Crack Surface Length Distribution—Figures 12 and 13 show typical examples of the growth behavior of a pioneer crack which contributed final fracture of a specimen. Except for the final stage of acceleration, the growth behavior characterizing small surface cracks can be represented by the formula

$$da/dN = C(\Delta\sigma\sqrt{\pi a})^2 \tag{1}$$

which corresponds to the power law relationship

$$da/dN = C'(\Delta K)^{m'} \tag{2}$$

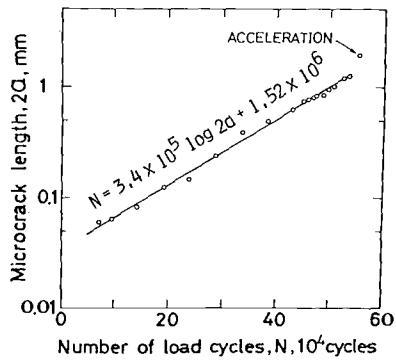

FIG. 12—*Growth characteristic of a crack causing fracture (log* 2a *versus* N *relationship).*

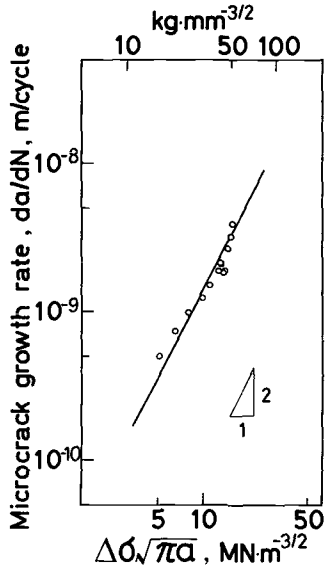

FIG. 13—*Growth characteristic of a crack causing fracture* (da/dN) *versus* $\Delta\sigma\sqrt{\pi a}$ *relationship).*

where $m' = 2$, da/dN is the growth rate of the surface length of a crack, and ΔK is the stress intensity factor range. In corrosion fatigue of the same material in the same environment, the growth behavior along a specimen surface of nonsmall surface cracks has been found to give different values of the coefficient and the exponent than Eq 1 [*2*]; that is,

$$da/dN = C''(\Delta\sigma\sqrt{\pi a})^{4.5} \tag{3}$$

A parameter $\Delta\sigma\sqrt{\pi a}$ instead of ΔK was used in this paper for a practically allowable data-processing of the growth behavior of distributed small "surface" cracks; actually, it is practically impossible to measure the variations of the shapes of all the randomly distributed small surface cracks in order to calculate the ΔK-values of the cracks. The experimental result assuring the good linear relation of the da/dN of distributed small surface cracks and the parameter $\Delta\sigma\sqrt{\pi a}$ on a logarithmic graph (Eq 1 or Fig. 13) is another reason for selecting the parameter $\Delta\sigma\sqrt{\pi a}$ to describe the growth behavior of the cracks.

Figure 14 shows a typical example of the growth behavior along a specimen surface of distributed small cracks other than "a pioneer crack" defined before in relation to Figs. 12 and 13. These cracks exhibited growth behavior similar to that of a pioneer crack (Fig. 12). Different behavior was also observed only in the final stage of the corrosion fatigue process; that is, some cracks showed hesitation caused by a negative interference with one another and some kept the linear relationship between log $2a$ and N.

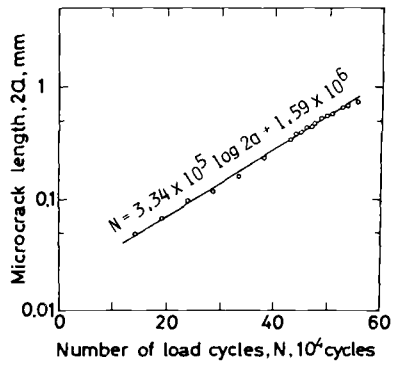

FIG. 14—*An example of the growth characteristics of distributed small surface cracks which did not cause fracture (log* 2a *versus* N *relationship).*

When surface lengths of distributed cracks follow a normal distribution $\phi_0(2a)$ with a mean, $2\bar{a} = 2\bar{a}_0$, and a standard deviation, $s_{2a} = [s_{2a}]_0$, at a given number of load cycles, N_0; that is,

$$\phi_0(2a) = \frac{1}{\sqrt{2\pi}\,[s_{2a}]_0} \exp\left\{-\frac{(2a - 2\bar{a}_0)^2}{2[s_{2a}]_0^2}\right\} \tag{4}$$

individually following Eq 1, the power relationship of crack growth rate with an exponent of two, it can be verified by using a simple transformation formula of random variables that the crack lengths follow a normal distribution $\phi(2a)$ at an arbitrary number of load cycles $N(>N_0)$ [*1*]. This result agrees well with Figs. 8*a* to 8*c*. The mean, $2\bar{a}$, and the standard deviation, s_{2a}, at $N(>N_0)$ can be obtained as

$$2\bar{a} = 2\bar{a}_0 \exp[\pi C(\Delta\sigma)^2(N - N_0)], \tag{5}$$

$$s_{2a} = [s_{2a}]_0 \exp[\pi C(\Delta\sigma)^2(N - N_0)] \tag{6}$$

In these calculations, it is assumed that there are no further crack initiations after $N = N_0$, and that crack coalescence can be neglected. Even when crack initiation after $N = N_0$ is taken into consideration, the variation of crack length distribution with the number of load cycles is not so much affected at $\Delta\sigma = 30$ and 40 MPa; this can be confirmed by experimental results and a computer analysis. On the other hand, this assumption does not hold true at $\Delta\sigma = 20$ MPa. Equations 5 and 6 agree well with the results obtained in the present corrosion fatigue experiments at higher stress levels (Figs. 9 and 10). In the present corrosion fatigue, the number of coalescing cracks remained so small until the last stage of the fatigue process that the crack coalescence was

not considered to affect crack length distribution. Fracture occurred immediately after cracks started to coalesce frequently. An example of this tendency of crack coalescence behavior is shown in Table 1 in Reference *3*. Consequently, the variation of the crack surface length distribution with the number of load cycles as shown in Figs. 8 to 10 can be calculated, when a surface length distribution with the number of load cycles as shown in Figs. 8 to 10 can be calculated, when a surface length distribution at a given number of load cycles and the crack growth rate of each crack are known. Fatigue damage evaluation and life prediction of structures can be performed based on these results. The crack surface length distribution need not be measured throughout the corrosion fatigue process.

The experimental results on the growth behavior of more than 30 distributed small cracks for each stress level tested showed that the coefficient, C, in Eqs 1, 5, and 6 can be regarded as a random variable following statistically the same normal distribution at different stress levels tested (Fig. 15). Therefore life prediction based on, say, a mean crack length requires a statistical consideration of C as well. In this study, the scattering of the C-values can be considered to involve partly those of the correction factor values of the stress intensity factor range $F(a) = \Delta K/(\Delta\sigma\sqrt{\pi a})$.

A Statistical Simulation of the Fracture Process (Due to Distributed Cracks)—A Test of the Model and Data of the Fatigue Procedure

A Monte Carlo simulation analysis of a fracture process caused by distributed small cracks has been previously proposed by one of the authors [*3*]. In that analysis, distributed small cracks continued initiating to coalesce with

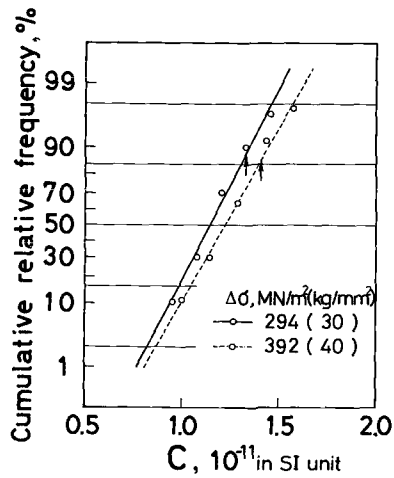

FIG. 15—*Plottings on a normal probability paper, showing the distribution of the coefficient,* C, *in the power law relationship. (The arrows in the figure indicate the values of* C *of the pioneer cracks which contributed to the final fracture.)*

one another until the final fracture was induced. On the other hand, in the present corrosion fatigue, which can be observed typically at stress levels lower than the in-air fatigue limit, a major portion of the corrosion fatigue life was occupied by successive initiations and "growth" of numerous distributed small cracks, which caused fast crack growth in the final stage of the corrosion fatigue process. More specifically, once distributed cracks coalesce with one another in a later stage of corrosion fatigue, even small cracks of less than 1 mm in surface length can produce a large crack or large cracks which grow so fast that it or they can suddenly cause final fracture.

In the present study, a new Monte Carlo simulation program has been developed on the basis of the old one [*3*]. The new simulation program can analyze fatigue fracture process of unnotched smooth materials, including the present corrosion fatigue process, in which cracks initiate randomly distributed over the material surface, grow, and coalesce. Figure 16 shows the flow chart of the program. The cracks (*1*) initiate one after another and are randomly distributed over an imaginary two-dimensional plane on a digital computer, following a given initiation behavior; (*2*) grow individually, following a growth rate law; and (*3*) coalesce to suddenly increase in length every time they satisfy a coalescence condition. Whenever the length of at least any one of such growing cracks exceeds a critical crack length $2a_c$(= 10 mm in the present analysis), fracture is judged to take place on a digital computer.

The procedures of the present Monte Carlo simulation analysis are as follows:

1. *Input Data of Crack Initiation Time (Data on a Variation of the Number of Cracks with the Number of Load Cycles)*—In the present simulation analysis, crack initiation time was determined by a variation of the number of existing cracks, n_c, with the number of load cycles, N; that is, a n_c versus N relation. This crack initiation behavior was modeled after the n_c/n_p (n_p = the number of corrosion pits) versus N/N_f relations obtained for different stress levels in the present corrosion fatigue experiments (Fig. 17). The value of n_p showed a drastic increase in a very early stage of the corrosion fatigue process, so that n_c/n_p can be considered to be replaced by n_c. In the corrosion fatigue experiments, all the cracks were observed initiating from corrosion pits; therefore n_c remained smaller than n_p; that is, $n_c/n_p < 1$ throughout the whole corrosion fatigue process. The n_c/n_p ratio increased monotonically with N, depending on the applied stress levels (Fig. 17).

2. *Input Data of Crack Surface Lengths*—Surface crack lengths were generated on a digital computer, regardless of initiation time, following the normal distribution having the mean and standard deviation which were obtained by extrapolating the $2\bar{a}$ versus N/N_f and the s_{2a} versus N/N_f straight lines (Figs. 9 and 10 respectively) to $N/N_f = 0$.

3. *Input Data of Crack Initiation Sites*—In the present corrosion fatigue experiments, crack initiation sites were statistically judged to follow the uni-

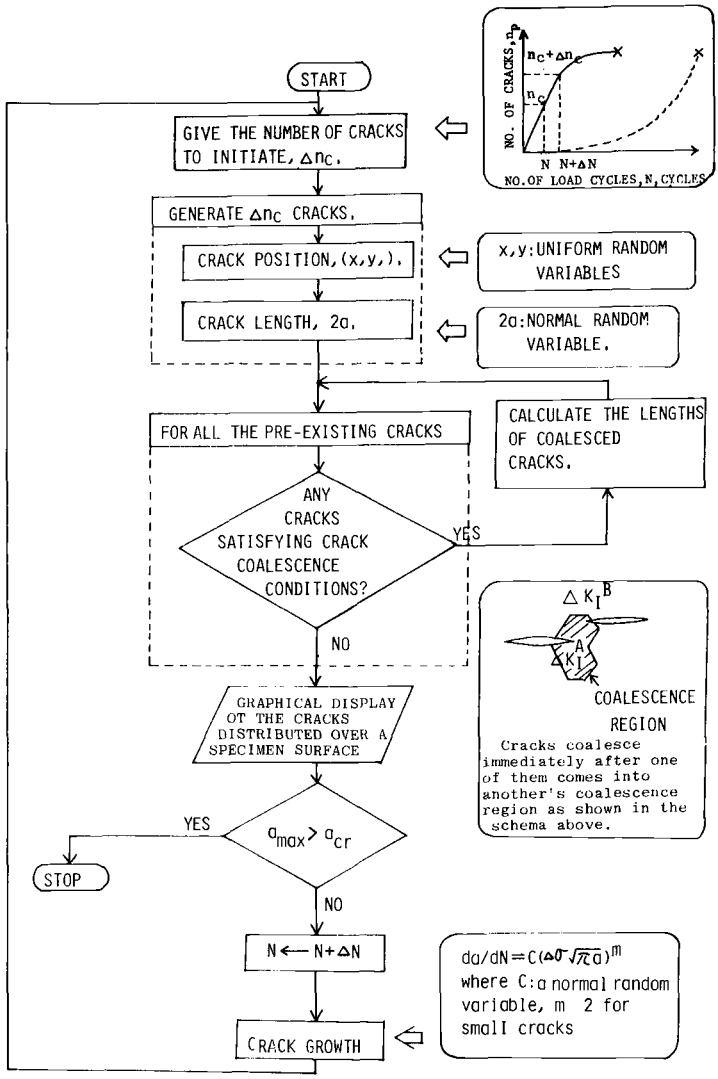

FIG. 16—*Flow chart of a Monte Carlo simulation analysis of fatigue fracture caused by the initiation, growth, and coalescence of distributed cracks.*

form random two-dimensional spatial distribution after crack initiations had sufficiently advanced; therefore, in the simulation analysis, crack coordinates (x,y) on an imaginary plane were generated by uniform random numbers on a digital computer.

4. *Crack Coalescence Criterion*—In real corrosion fatigue, as shown in Fig. 5, crack coalescence behavior seems to have such a complex nature that

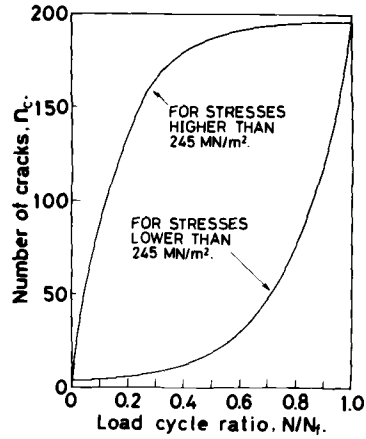

FIG. 17—*Variation of the number of distributed cracks with the load cycle ratio.*

it is hard to analyze. Therefore, in the present simulation analysis, when a Mode I stress intensity factor range, ΔK_I^A, at a tip of a crack (say, crack A) is increased by a factor of more than 1.5 due to the existence of a tip of another crack (say, crack B) in a coalescence region established at the tip of crack A, the two cracks are to coalesce immediately on a computer. The coalescence region was obtained by a calculation chiefly based on Isida's Laurent expansion method. For a detailed explanation of the calculation, see Ref [*3*].

5. *Crack Growth Rate Data*—In the present corrosion fatigue experiments, all the cracks observed, including those on the order of 60 μm in surface length, were found to show continuous growth behavior. Thus, in the present simulation analysis, all the small cracks initiated were made individually to grow on a digital computer following Eq 1, in which the coefficient, C, is a normal random variable, without imposing any threshold condition on the crack growth behavior such as the threshold intensity factor range, ΔK_{TH}. For purposes of comparison, the growth data along a specimen surface of a nonsmall surface crack which emanated from an artificial hemispherical pit-like notch of approximately 500 μm in diameter—that is, $da/dN = C''(\Delta\sigma\sqrt{\pi a})^{4.5}$—was also fed into a computer.

By using the aforementioned model and data, fatigue fracture processes, in which randomly distributed cracks are initiating, and coalescing to cause fracture, were simulated. The resultant S-N relations for the exponents in the power law relationship, $m = 2$ and 4.5, are represented by solid circular symbols (●) and by open square symbols (□) respectively in Fig. 18, with the experimental results shown by open circular symbols (○). Compared with the S-N curve obtained by the growth data of a crack emanating from an artificial pit-like notch, the S-N curve obtained by distributed small cracks data agreed sufficiently well with the corrosion fatigue test results of an un-

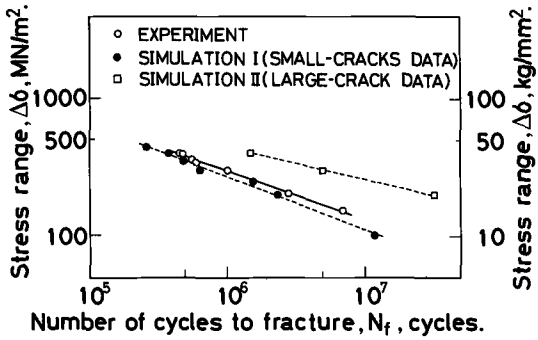

FIG. 18—*An* S-N *curve obtained by a Monte Carlo simulation analysis compared with the corresponding* S-N *curve by corrosion fatigue experiments.*

notched smooth material. Each of these *S-N* curves was no more than a single trial; nevertheless, it is quite interesting that the *S-N* curve predicted by using distributed small cracks data agreed well with the experimental results.

It is clear from these results that the statistical simulation analysis, in which the distributed small cracks data were used, provides a test of goodness of the description of the real corrosion fatigue phenomenon by the model and data used in the fatigue damage evaluation and life prediction in the section on the third step of the method.

Quantitative Measurement of Fatigue Damage by Randomly Distributed Small Cracks Data

This section proposes two methods for the damage evaluation and residual-life prediction of smooth unnotched materials subjected to fatigue. A wide and general application of the present method, however, requires basic data storage on different materials and on different environments.

Procedure 1

For a material and environment combination of interest, make laboratory experiments to record the *S-N* and crack length distribution data. The crack length distribution data should be taken for more than two stress levels from, say, a region of 10 by 10 mm on the material surface. Calculate the mean of the measured crack lengths to draw a $2\bar{a}$ versus N/N_f graph. Take crack length distribution data from a portion or portions of interest in a real structure being subjected to (corrosion) fatigue by, say, a surface replication technique; then the N/N_f ratio at the time of the data sampling can be estimated. If the $2a$ versus N/N_f graph is combined with the *S-N* curve, the residual life of the structure (that is, $N_f - N$) can be estimated.

Procedure 2

For a material and environment combination of interest, make laboratory experiments to record the *S-N* data and the growth rate data of distributed cracks (Figs. 12 to 14 or Eq 1). Take crack length distribution data, at an arbitrary time, N_0, from a portion or portions of interest in a real structure being subjected to (corrosion) fatigue. Calculate Eqs 1, 5, and 6 by using the growth rate and the crack length distribution data to predict the variation of crack length distribution with time or the number of load cycles and the $2\bar{a}$ versus $(N - N_0)$ graph. This graph provides an information on the (corrosion) fatigue initiation time. The residual life of the structure $(N_f - N_0)$ can then be estimated by a procedure such as Procedure 1.

Characteristics of the Method

The proposed method has the following characteristics:

1. In low-cycle in-air fatigue, in corrosion fatigue, or in elevated-temperature fatigue of unnotched smooth materials, cracks are found initiating even in early stages of the fatigue process; thus a major portion of the fatigue life is occupied by the initiation, growth, interference, and coalescence of the cracks [*4-7*]. The role of cracks in the mechanism of such fatigue fracture process has not yet been clarified; nevertheless, the method can be used for the quantitative evaluation of fatigue damage in unnotched smooth materials.

2. The method uses various statistical methods in the measurement of corrosion pits and distributed small cracks, fatigue damage evaluation, and residual-life prediction. For this reason, the method requires effective applications of computer techniques; for example, data-processing techniques for handling vast amounts of measured data, a two-dimensional image analysis technique, a statistical simulation analysis technique, etc.

3. The present study is a practical treatment of the most important but difficult problems in fracture mechanics that distributed small surface cracks have; that is, the surface crack problem, the multiple cracks problem, and the small crack problem. These problems are approached from the standpoint that engineering approximation is enough for practical fatigue damage evaluation, residual-life prediction, etc.

4. The method "directly" evaluates fatigue damage of materials with data on cracks, which can be considered to be observable measures of the accumulation of the fatigue damage. The accumulation of fatigue damage has been evaluated since early in the study of the fatigue of materials by measuring variations in, say, electric, magnetic, radiological, and thermodynamic properties of materials subjected to fatigue. In many cases, however, those conventional measurements seem to be "indirect" measurements of the degree of the progress of fatigue via metallurgical or crystallographical changes of the

materials. Quantitative relations must be obtained between the degree of fatigue damage and the variations in each of the aforementioned properties of materials (Fig. 19) in these cases.

Objectives of the Method and Notes on Its Applications to Other Fatigue Processes

What types of fatigue fracture processes and what portions of structures subjected to fatigue can this method be applied to?

The method can be applied to damage evaluation and life prediction of macroscopically homogeneous portions of metallic structures, even if they really are intrinsically inhomogeneous from the microscopic point of view. It does not matter whether the structures were cast or forged. The method can be applied to unnotched smooth portions of structures where neither sharp deep notches nor initial cracks exist. This method is applicable to a notch bottom and to any other surface which has enough flat area for statistical measurements or countings of distributed small cracks. The surface above, however, must be "metallurgically, mechanically and environmentally homogeneous," which means that sizes, shapes, locations, etc., of distributed small cracks should not show drastic changes within the target area to measure due to the effects of changes in material, stress, and environment. Therefore, in real complex structures having limited dangerous portions in them, the target area must be small. To structures having no predominant stress concentrations in them, on the other hand, an approach such as the statistics of extremes may be useful. Anyhow, the number of distributed small cracks should be large enough for statistical treatment.

Surfaces to measure require as large an area as usual strain gages of various sizes; that is, an area of 30 by 30 mm to 1 by 1 mm seems suitable for surfaces to measure.

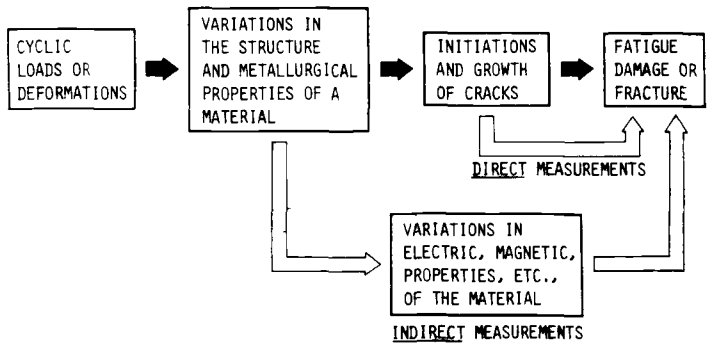

FIG. 19—*Comparison between conventional (indirect) methods and the present (direct) method for measuring fatigue damage.*

Selection of target surfaces to measure in larger structures or structural components is another problem worth examining. The target surfaces should be portions in structures where fatigue fracture is most likely to occur, and may be determined by, say, combining simulation tests, experimental as well as numerical stress analyses, experience in failures of structures, etc. If several portions in structures were estimated to have a fracture probability of the same degree, then the proposed method should be applied to all these portions.

It is clear that the method is applicable to various types of fracture processes in which multiple small cracks initiate and are randomly distributed over material surfaces, grow, and occasionally interfere and coalesce with one another suddenly to form large cracks or to start the critical fast growth. Such fracture processes can be found in (low-cycle) in-air fatigue, corrosion fatigue, (cyclic) stress corrosion cracking, elevated temperature fatigue, fretting fatigue, etc. Figure 20 shows one of the examples found in fatigue of mild steel in air. All the fracture processes cannot necessarily be classified into this category of fracture. From the authors' experience, the fracture processes mentioned previously were observed in fatigue of unnotched smooth structural steels having a tensile strength of 343 to 785 MPa in various fatigue test conditions such as axial tension, plane bending and rotary bending fatigue in air, pure and salt water, and in dilute hydrochloric acid solution environment.

The present method cannot be applied to the following cases without any modification or improvement:

1. Fatigue fracture caused by the growth of a nonsmall single crack.
2. Fatigue fracture in which the crack initiation process occupies a major portion of the whole fatigue life.
3. Fatigue fracture caused by any other reason than distributed small surface cracks' initiation, growth, and coalescence, if they are observed to occur.
4. Cases where the sampling of distributed small cracks data is impossible.

Listed below are some sample cases where modifications need to be made for practical applications of the method:

1. In in-air fatigue of unnotched smooth materials at room temperature, crack lengths generally follow asymmetric distributions such as log-normal or Weibull distributions (see, for example, Fig. 21 [*4*]), probably because distributed small cracks always need applied stress levels higher than the fatigue limit to initiate, and probably because particularly small cracks are successively initiating. When the applied stress level is reduced to be slightly higher than the fatigue limit, crack initiation times are retarded and frequent crack coalescence can hardly occur, so that the probability of fracture due to the independent growth of a small number of cracks becomes higher.

2. In cases where a peak stress, σ_{max}, exceeds the yield strength, σ_{ys}, even from a very early stage of fatigue, crack density is so high that crack coalescence can occur from a relatively early stage of fatigue. These cases can be

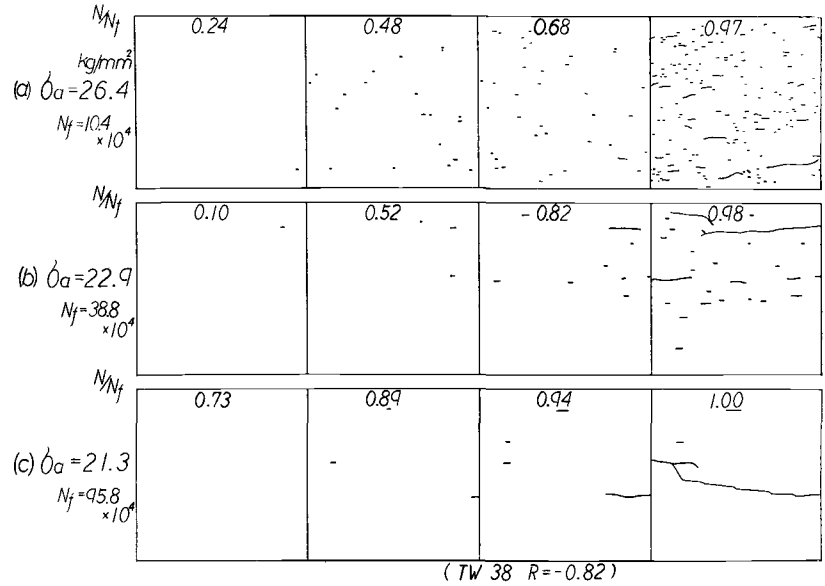

FIG. 20—*Distributed small cracks in in-air fatigue of a mild steel.*

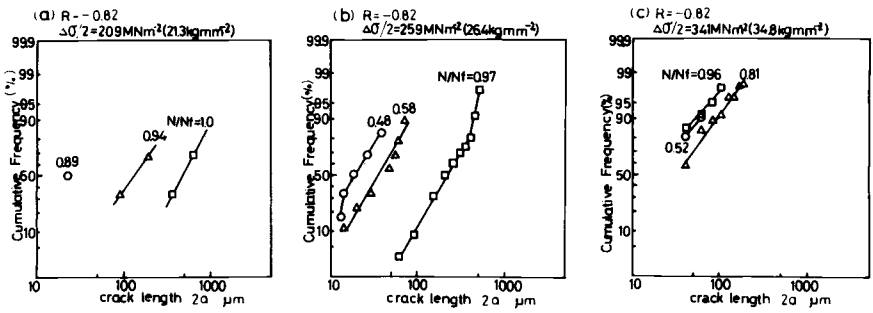

FIG. 21—*Plottings on log-normal probability papers, showing the surface length distribution of distributed small cracks in in-air fatigue of a mild steel.*

found in fatigue at higher stress ratios, in fatigue of lower strength steels, in low-cycle fatigue, etc. Such crack coalescence can not only cause final fracture, but can accelerate the growth of cracks, so that the growth behavior of those cracks are considered to be different from that shown in Figs. 13 to 15.

3. In the present corrosion fatigue, all the cracks initiated from corrosion pits; therefore crack initiation sites were relatively easy to recognize. In general, however, crack initiation sites are hard to recognize, so that suitable techniques are required for the sampling of data on distributed small cracks.

4. Growth behavior of small cracks initiating on unnotched smooth material

surfaces was found to vary with environment (Fig. 22 [*2*]); thus fatigue crack growth behavior data should be obtained for different environment-material systems.

5. Large amounts of growth rate data have been accumulated for surface cracks emanating from artificial notches. The growth rate along a material surface, da/dN, of small cracks distributed over the surface was found to be different from that of nonsmall surface cracks emanating from artificial notches, when da/dN is represented by a parameter $\Delta\sigma\sqrt{\pi a}$ (Fig. 22 [*2*]). Great care must be taken for applications of the growth behavior data of nonsmall cracks emanating from artificial notches to small distributed cracks.

Conclusion

A quantitative method for the fatigue damage evaluation and residual-life prediction of unnotched smooth metallic materials has been proposed. The

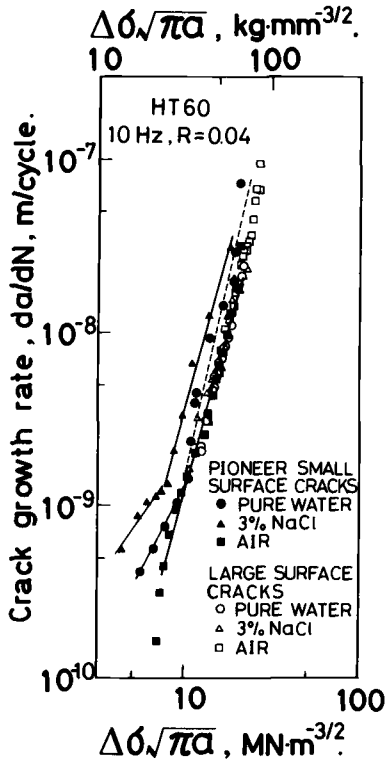

FIG. 22—*Comparison of the growth behavior of small surface cracks initiating from corrosion pits to cause fracture with that of nonsmall surface cracks initiating from artificial hemispherical notches in corrosion fatigue of HT 60 steel in various environments* (da/dN *versus* $\Delta\sigma\sqrt{\pi a}$ *relationship).*

method is based on the statistical treatments of small surface cracks which often initiate, grow, and coalesce, randomly distributed over unnotched smooth surfaces.

The methodology and the procedures of the method, composed of three steps, were described by taking an example of corrosion fatigue of a structural steel in a certain condition. The results of the application suggest the possibility that, by the present method, quantitative fatigue damage evaluation and residual-life prediction might be made for such a fatigue process as the sample corrosion fatigue.

For applications of the method to other fatigue processes than the aforementioned example, however, some modifications and improvement suitable for each case need to be made. Some of these cases were described.

It was also shown that, in this method, a Monte Carlo simulation analysis can be useful for the test of the goodness of the model and data obtained.

References

[1] Nakasone, Y., "A Statistical Investigation on Corrosion Pits and Distributed Small Cracks in Corrosion Fatigue of Smooth Unnotched Steel," Doctoral thesis, University of Tokyo, 1981 (in Japanese).

[2] Kitagawa, H., Nakasone, Y., and Shimodaira, M., to be published.

[3] Kitagawa, H., Fujita, T., and Miyazawa, K. in *Corrosion-Fatigue Technology, ASTM STP 642*, H. L. Craig, Jr., et al, Eds., American Society for Testing and Materials, 1978, pp. 98-114.

[4] Kitagawa, H., Takahashi, S., Suh, C. M., and Miyashita, S. in *Fatigue Mechanisms, ASTM STP 675*, J. T. Fong, Ed., American Society for Testing and Materials, 1979, pp. 420-449.

[5] Kitagawa, H. and Nakasone, Y. in *Proceedings*, 25th Japan Congress on Materials Research, Society for Materials Science, Japan, 1982, pp. 69-73.

[6] Kitagawa, H., Suh, C. M., Nakasone, Y., and Takahashi, S. in *Mechanics of Fatigue*, T. Mura et al, Eds., ASME, 1981, pp. 167-184.

[7] Kitagawa, H., Yuuki, R., Suh, C. M., and Mochida, I. in *Proceedings*, 1st Symposium on Fracture Mechanics, Society of Materials Science, Japan, 1981, pp. 116-120 (in Japanese).

DISCUSSION

E. E. Underwood[1] *(written discussion)*—The authors have contributed greatly to our detailed understanding of small crack behavior in fatigue. Although they have painstakingly measured the lengths of individual surface cracks and obtained distribution curves, in some cases it is possible to use the *mean* values in plotting curves. For example, their plot of $\overline{2a}$ versus N/N_f utilizes the *mean* crack length derived from their distribution curves.

[1]Chemical Engineering/Metallurgy Department, Georgia Institute of Technology, Atlanta, Ga. 30332.

The mean crack length can be obtained directly[2,3] by simple intersection counts of a test line (or parallel grid) placed randomly over the microstructure; that is,

$$L_A = \left(\frac{\pi}{2}\right) P_L \tag{7}$$

where L_A is the crack length per unit area and P_L is the number of grid intersections with the cracks per unit length of test lines. Then, a simple count of discrete cracks in a selected test area gives N_A, the ratio of number of cracks to test area. Dividing L_A by N_A gives the mean crack length $\bar{L}$ (or the authors' $\overline{2a}$). These two simple counting measurements are performed quickly and efficiently, and are free of any assumptions concerning crack size, location, or complexity.

Although this procedure applies equally to random or oriented crack traces, there are special procedures for oriented linear traces in a plane[2] that give additional information. For example, the degree of orientation is a powerful, yet simple, parameter for quantitatively expressing the fraction of a linear system that lies in a particular direction.

Perhaps in future studies some of these quantitative stereological relationships for the complete characterization of fatigued microstructures will prove useful.[4]

H. Kitagawa et al (authors' closure)—In our method the use of a mean crack length, $2\bar{a}$, is important. Fatigue damage evaluation and residual-life prediction can be made by the $2\bar{a}$ versus N/N_f relation, and, in general, a $2\bar{a}$-value can be easily calculated as the arithmetic mean of measured crack lengths.

Your quantitative stereological method for obtaining $2\bar{a}$ makes our method more efficient and practical. We consider a quick and efficient approach such as yours one of the most desirable techniques for obtaining data on cracks. Statistical methods generally require a vast amount of data; therefore a moiré grid, an x-y table, an image-analyzing computer [or a quantitative television microscope (QTM)], etc., were used by us to reduce laborious work as much as possible. If these techniques or equipment had been combined with your method, the time-consuming task of measuring locations and sizes of pits/cracks could have been greatly reduced.

In our study we were interested in not only the mean length, but also in the crack length distribution and, if any, quantitative relationship between small cracks and corrosion pits as crack initiation sites etc. Crack length distribu-

[2]Underwood, E. E., *Quantitative Stereology*, Addison-Wesley, Mass., 1970.

[3]Watanabe, H., *Journal of the Research Association of Powder Technology*, Vol. 8, No. 3, June 1971, p. 195 (in Japanese).

[4]Underwood, E. E. and Starke, E. A., Jr., in *Fatigue Mechanisms, ASTM STP 675*, American Society for Testing and Materials, 1979, pp. 633-682.

TABLE 1—*Crack length/depth distributions under various fatigue conditions.*

Material	σ_y (or $\Delta\sigma_w$), MPa[a]	Applied Stress, MPa[b]	Loading Condition	Environment	Object	Type of Distribution	Reference (Footnote number on p. 262)
Mild steel (SB-22)	279 (221)	294, 333	rotary bending 1450 rpm	air	surface length/ depth	compound Weibull	6
Mild steel (SAPH38)	265 (211)	209, 259, 341	antiplane bending 1500 rpm	air	surface length	logarithmic normal	7
Mild steel (S10C)	(181)	186 to 235 137 to 196 49 to 177	rotary bending 2220 rpm	air water 3% NaCl	surface length	Weibull	8
	(118)	127 to 177 98 to 132 69 to 118	torsion 2000 rpm	air water 3% NaCl			
Al-alloy	...	...	plane bending 3600 rpm	air 3% NaCl	surface length	compound Weibull	9
				air 3% NaCl	depth	Weibull	

Carbon steel (SS41)	175	127	plane bending 3600 rpm	3% NaCl	surface length	mixed Weibull	10
Mild steel (0.07 to 0.16C%)	227 to 233	255, 314, 333	rotary bending 3000 rpm	air	depth	compound Weibull	11
Structural steel (HT60)	559 (470)	196, 294, 392	zero-to-tension 600 cpm	water	surface length	normal	...
Stainless steel (SUS304)	328 (275)	265, 294	cantilever-type rotary bending 3600 rpm	air (electrochemical pit formation before tests)	surface length	$F(2a;N) = \int_0^a f(x;N)\,dx$ (see Footnote *c*)	12

[a] σ_y is the yield strength, $\Delta\sigma_w$ is the fatique strength in air.

[b] *Applied stress* is here defined as the applied nominal stress range, in the case of zero-to-tension cyclic loading, and otherwise the applied nominal stress amplitude.

[c] The equation is

$$f(2a;N) = \frac{g}{h}\left[\frac{N}{h} - \frac{1}{hC_1}[(2a)^{m_1} - (2a_0)^{m_1}] - \frac{k}{h}\right]^{g-1} \times \exp\left\{\left\{-\left[\frac{N}{h} - \frac{1}{hC_1}[(2a)^{m_1} - (2a_0)^{m_1}] - \frac{k}{h}\right]^{g}\right\}\right\} \left|\frac{m_1}{C_1}(2a)^{m_1-1}\right|$$

where g, h, k, and $2a_0$ are some constants; m_1, C_1 are constants related to the crack growth law; and $2a$ and N are crack length and number of load cycles respectively.

tion, for instance, may reflect the mechanism of crack formation, and may provide important information on fatigue-life prediction. Crack length/depth distribution has been found to differ in various types of fatigue experiments (Table 1).[5] Some investigators explained crack length/depth distribution from the viewpoint of fatigue mechanism; for example, the compound Weibull distribution of crack depths was regarded as resulting from the different crack growth mechanisms of Stages I and II,[6,11] and the mixed Weibull distribution was considered to be composed of the crack length distribution of coalesced cracks and of noncoalesced cracks.[10] Residual fatigue life may be predicted by using the variation of crack length distribution with the number of load cycles, as described in this paper, and the statistics of extremes can be applied to crack length distribution for predicting fatigue life distribution.[13]

W. L. Morris[14] (*written discussion*)—For aluminum alloys fatigued at high cyclic stress amplitude, it appears that crack formation within a grain enhances the probability of crack initiation in neighboring grains at the crack tip. Have you noticed such short-range correlations of crack location in your experiments?

H. Kitagawa et al (*authors' closure*)—We regard the phenomenon you pointed out as one of the most important phenomena for clarifying fatigue mechanisms.

The short-range correlations you mentioned are most likely to be found in high-cyclic-stress-range (or -amplitude) fatigue in air. Although we have made fatigue experiments of steels at high cyclic stress ranges or amplitudes

[5]Masuko, N. in *Proceedings*, 5th International Congress on Metallic Corrosion, NACE, 1972, pp. 1051-1055.

[6]Suh, C. M., "A Study on the Fracture Mechanics Analysis of Fatigue Process of Unnotched Smooth Steels," Doctoral Thesis, University of Tokyo, 1981 (in Japanese).

[7]Kitagawa, H., Takahashi, S., Suh, C. M. and Miyashita, S. in *Fatigue Mechanisms, ASTM STP 675*, American Society for Testing and Materials, 1979, pp. 420-449.

[8]Tokaji, K., Ando, Z., Sugimoto, M., and Nakano, N., *Journal of the Society of Materials Science*, Japan, Vol. 30-328, Jan. 1981, pp. 15-20 (in Japanese).

[9]Ishihara, S., Shiozawa, K., and Miyao, K., *Preprint of JSME Meeting*, Japanese Society of Materials Science, No. 780-13, Oct. 1978, pp. 13-15 (in Japanese).

[10]Ishihara, S., Shiozawa, K., and Miyao, K., "Growth and Coalescence Behavior of Multiple Surface Cracks in Plane Bending Corrosion Fatigue," Preprint of the Subcommittee for Studies of Environmental Effects on Fatigue, The Committee for Studies of Fatigue, The Society of Materials Science, Japan, 1980, pp. 1-16 (in Japanese).

[11]Sasaki, S. and Ochi, Y., *Preprint of JSME Meeting*, Japanese Society of Materials Science, No. 790-9, July 1979, pp. 13-18 (in Japanese).

[12]Tanaka, T., Sakai, T., and Okada, K., *Journal of the Society of Materials Science*, Japan, Vol. 30-332, May 1981, pp. 483-489 (in Japanese).

[13]Ishihara, S., Shiozawa, K., and Miyao, K., *Preprint of JSME Meeting*, Japanese Society of Materials Science, No. 810-11, Oct. 1981, pp. 161-163 (in Japanese).

[14]Rockwell International Science Center, Thousand Oaks, Calif. 91360.

in air, we could not make an observation on these correlations, because we have not made any surface treatment for visualizing grain boundaries.

In our corrosion fatigue experiments in the present paper, the phenomenon you pointed out was not observed, probably because (*1*) the applied cyclic stress ranges were lower than the fatigue limit in air and (*2*) all of the cracks initiated from corrosion pits. Actually, in the present experiment, numerous corrosion pits distributed over specimen surfaces played a significant role in crack initiations; that is, at applied (nominal) stress ranges of $\Delta\sigma =$ 294 and 392 MPa, the ratio of the number of distributed small cracks to that of corrosion pits from which the cracks initiated, n_c/n_p, reached higher than 60% at a load cycle ratio $N/N_f = 0.4$. For load cycle ratios higher than 0.6, the n_c/n_p ratio was converged to a value higher than 90%.[5] Corrosion pits or distributed small cracks themselves may have affected the probability of crack initiations from neighboring corrosion pits.

R. A. Smith[1]

Short Fatigue Cracks

REFERENCE: Smith, R. A., **"Short Fatigue Cracks,"** *Fatigue Mechanisms: Advances in Quantitative Measurement of Physical Damage, ASTM STP 811*, J. Lankford, D. L. Davidson, W. L. Morris, and R. P. Wei, Eds., American Society for Testing and Materials, 1983, pp. 264-279.

ABSTRACT: Short fatigue cracks are the linkage of the initiation stage to the long crack growth which can be described by linear elastic fracture mechanics. Because some cracks can initiate then cease to grow, short cracks are important in the definition of fatigue limits. This paper reviews the fatigue limits of plain and notched components and concludes that this particular short crack problem can be overcome by macroengineering parameters. So far as the growth of short cracks is concerned, their interaction with microscopic metallurgical features can be treated quantitatively only in a local sense. However, their growth in large plastic strain regions, which typically occur at a notch root, can be described by semiempirical macromechanics parameters. Finally, it is shown that in many practical circumstances the bulk of the fatigue life can be considered to be either initiation or long crack propagation, thus bypassing the short crack problem.

KEY WORDS: crack size, long crack growth, short crack growth, crack initiation, slip bands, linear elastic fracture mechanics, elastic-plastic fracture mechanics, notches, plain fatigue limits, crack growth threshold, notch plasticity, crack tip plasticity

At the time of the Comet failures in 1954, fatigue was still thought to result in a rapid crack propagation to failure. Since that time the cycle-by-cycle nature of progressive crack propagation has been recognised and, for many circumstances, correlated by the stress intensity factor range parameter ΔK. Indeed, this approach has so dominated fatigue thinking over the last decade, that it has come as a surprise to many that the early stages of the fatigue process have proved difficult to describe by linear elastic fracture mechanics (LEFM). Short cracks are said to be "anomalous" because their behaviour is not always predicted by LEFM. In a sense we are relearning the lessons of many years ago: that often the vast majority of the cycles to failure can be consumed in developing an "observable" crack. However, modern observational techniques are capable of monitoring the development of smaller and smaller

[1]Lecturer, Cambridge University Engineering Department, England.

cracks, which in turn has led to a desire to model their growth. Thus short cracks are now seen as the linkage of initiation (understood in a micromechanistic sense, but not quantified by mechanics parameters) and long crack propagation (largely understood and relatively easily quantifiable).

Short Crack Problems

It may be convenient to identify several short crack problems and discuss them separately. A suggested division is:

1. The intrusion, extrusion mechanism of initiation in a surface grain.
2. The cracks that are found to be present just below or at a stress level equal to the plain fatigue limit.
3. Nonpropagating cracks found in notched geometries.
4. For finite growth rates at higher than fatigue limit stress levels:
   (a) Slower than LEFM predictions for microcracks in plain specimens.
   (b) Faster than LEFM predictions for microcracks in plain specimens and macrocracks in notched geometries.

In this discussion growth rate is defined as rate of propagation of a crack into the load-bearing area of the structure. This follows from an engineering definition of fatigue damage as reduction of load-bearing area of the structure by crack growth. Care should be taken in interpreting other works where the development of short cracks is defined in terms of their surface length, since there may in some circumstances be a simple correlation between surface length and penetration depth.

Intrusions and Initiation

It is now accepted that the process of initiation in nominally smooth material consists of the irreversible movement of dislocations on slip planes in surface grains to form persistent slip bands. The moment at which one of the persistent slip bands becomes a single Mode II crack is a philosophical point not worth pursuing in engineering terms. Alternative mechanisms include crack nucleation at particles near an alloy surface, fracture of the particle being followed by propagation into the matrix (see, for example, Morris and James [*1*]).[2] It is clear that the slip process can only be regarded as "macro" within the grain in which it occurs, since the slip steps (typically 0.1 μm wide) are clearly of continuum scale with respect to the atomic size ($\sim$0.5 nm). Thus an application of fracture mechanics can only be local (Fig. 1), since the operative stress field, the shear on the slip plane, and the crack length, the grain diameter along the active crystallographic plane, are local to the single grain. So despite advancing knowledge of the mechanisms of initiation

[2]The italic numbers in brackets refer to the list of references appended to this paper.

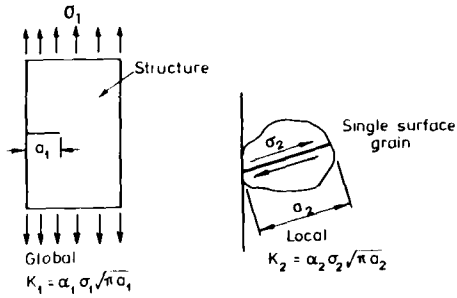

FIG. 1—*Schematic of global and local levels of application of fracture mechanics.*

in single crystals (see, for example, Mughrabi [*2*]), the way is not yet clear to applying this knowledge to a global application of fracture mechanics to a complete specimen or structure (Fig. 1), where the reference stress is the applied stress remote from the crack and the crack is a single dominant crack, of continuum size with respect to the microstructure, growing in Mode I, normal to the principal applied stress.

The engineer is therefore left with the single macroparameter, the plain fatigue limit $\Delta\sigma_0$, as a measure of the bulk stress level needed to activate the initiation process, but quantitative assessments of the number of cycles to cause crack formation are still empirical for real bulk materials.

Short Cracks at the Plain Fatigue Limit and the Relationship with the Long Crack Threshold

If a structure is known to be cracked, the combination of stress level and crack length needed for continued crack growth can be found from the long crack threshold ΔK_{TH}. This parameter is usually measured for cracks of such a length—say 15 mm—that any breakdown of continuum ideas and global fracture mechanics is inconceivable, and the threshold is found to be independent of crack length. If smaller cracks are used to define the threshold, however, the applied stress needed to cause the crack to grow increases to values greater than the plain fatigue limit (Fig. 2*a*). By definition, cracks, however small, grow when the plain fatigue limit is exceeded, so that the intersection of the plain fatigue limit and the stress component of the long crack threshold define a limiting crack size a_0 when global fracture mechanics begins to fail, a point first noted by Kitagawa [*3*]. Smith [*4*] coupled these observations with the apparent decrease in ΔK_{TH} measured for short cracks (Fig. 2*b*), while making an estimate of the shortest cracks to which LEFM can be applied by considering the minimum amount of material which might yield and limiting this to a small fraction of the crack length. The experiments of Lankford [*5*] (Fig. 3) clearly emphasize this material depen-

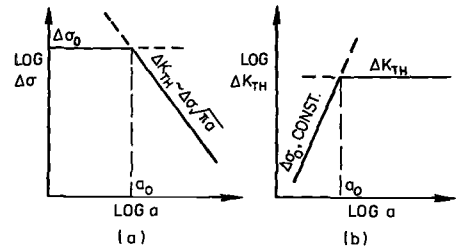

FIG. 2—*Effect of crack length on long crack threshold.*

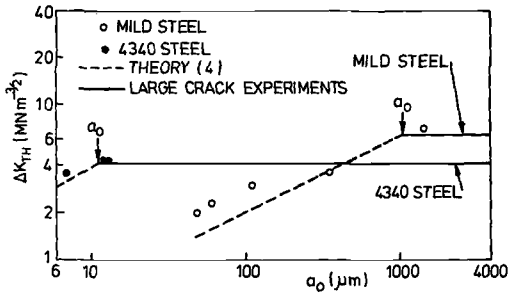

FIG. 3—*Limits of global fracture mechanics for mild steel and 4340* [5].

dence. The minimum crack size in a mild steel (1 mm) is shown to be some two orders of magnitude larger than the minimum crack size in hard 4340 steel (10 μm). Both Tanaka [*6*] and Elsender et al [*7*] have collected considerable data from the literature to substantiate this view. Tanaka [*6*] attempted to model the changeover from plain fatigue limit to long crack threshold by considering initial slip bands to be blocked at grain boundaries. The idea of the influence of grain boundaries affecting the behavior of short cracks reoccurs in several explanations of the anomalous behavior of short cracks.

In engineering terms, therefore, a global measure of the crack sizes to which LEFM can be applied is given by

$$1.12\,\Delta\sigma_0\sqrt{\pi a_0} \leq \Delta K_{TH}$$

that is,

$$a_0 \leq 0.25\left[\frac{\Delta K_{TH}}{\Delta\sigma_0}\right]^2 \tag{1}$$

and the absolute value of this critical size is extremely material dependent. We further conclude that the presence of cracks smaller than this size will not seriously decrease the plain fatigue limit. Thus harder materials are very much more sensitive to surface conditions than relatively soft mild steels. The surface condition will greatly affect the fatigue life, however, since large surface roughness may completely eliminate the cycles needed to form a crack by a slip mechanism. El Haddad et al [*8*] have associated a_0 with a measure of the reduced flow resistance of surface grains due to their lack of constraint. They also used a_0 to increase the effective lengths of short cracks to force their behaviour to conform to LEFM.

Nonpropagating Cracks and Notched Fatigue Limits

The importance of notches in real structures cannot be overemphasised. Notches are the sites where stress is locally enhanced and may be macroscopic, such as bolt holes, screw threads, welding defects, or microscopic-like scratches or metallurgical-like inclusions.

In many cases the phenomena of fatigue observed in small-scale carefully prepared laboratory specimens are modified by the notch. In particular the process of initiation may be considerably shortened. The bulk measure of the severity of a notch is the elastic stress concentration factor K_T. Since the local stress at the notch root is K_T times the nominal stress, an estimate of the stress level required to initiate a crack at a notch root $\Delta\sigma_i$ is simply $\Delta\sigma_0/K_T$ (Fig. 4). The classic early investigations of Frost [*9*], however, demonstrated that for sharp notches a higher stress level $\Delta\sigma_p$ was needed to propagate the initiated crack to failure. Further, this propagation stress level appeared to be independent of K_T but very dependent on size, being higher for physically smaller notches. Examination of unfailed specimens of notches subjected to stress levels between $\Delta\sigma_i$ and $\Delta\sigma_p$ revealed the presence of nonpropagating cracks, sometimes several millimetres in length.

This type of behaviour is impossible to explain on the basis of LEFM. Figure 5 shows that the stress intensity factor for a crack growing from a

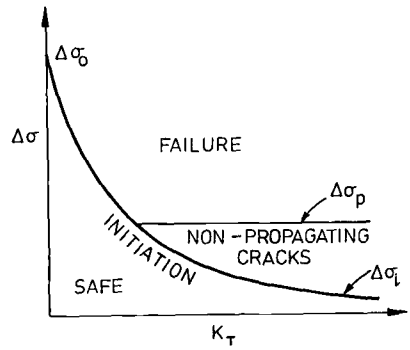

FIG. 4—*Fatigue regimes in notched components.*

notch root starts from zero and rapidly attains a value such that its actual length is enhanced by the notch depth. The important point is that the stress intensity factor increases continuously with crack length, thus providing no stopping mechanism for an initiated crack. A plasticity based argument is illustrated in Fig. 6. If the initiation stress level is to be exceeded over a finite distance ahead of the notch root, a greater than initiation stress must be applied at the surface, since the elastic stress distribution decays ahead of the notch. (This is in contrast to a plain specimen where the stress level is assumed to be uniform throughout.) This causes a zone of material, of an extent controlled by the notch geometry, to be yielded. Therefore the initiation and early growth are considered to be controlled by the notch-generated plastic strains (though these inestastic strains might occur only on a metallurgical scale in very hard materials subjected to low stresses). When the crack reaches the edge of the notch plastic zone, it must have developed enough plasticity at its own tip to carry it through the elastic stress field remote from the notch. Thus at a critical value of applied stress, the crack initiates at the notch root, grows at a decreasing rate because of the falling notch strain field and stops

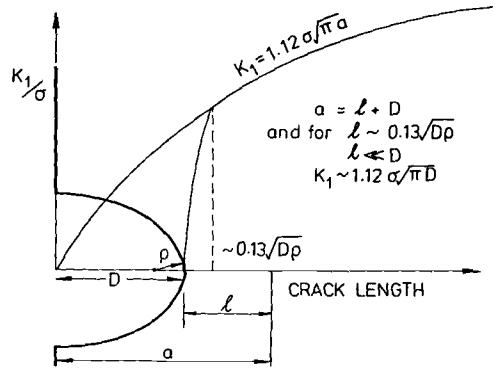

FIG. 5—*Elastic stress intensity factor for elliptical notches.*

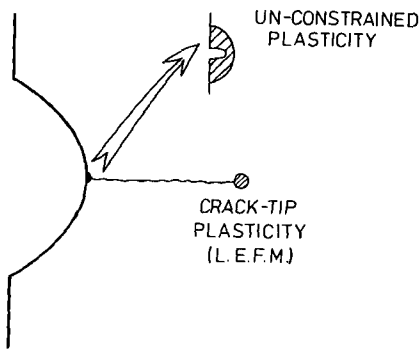

FIG. 6—*Plasticity regimes in notched components.*

at a length ℓ, corresponding to the boundary of the notch plastic zone (Fig. 7). An estimate of the stress intensity factor for such a crack is

$$\Delta K = 1.12\,\Delta\sigma\sqrt{\pi(\ell + D)} \tag{2}$$

assuming an elliptical edge notch of depth D (Fig. 5). Since $\ell \ll D$ and ΔK is insensitive to the actual value of ℓ (and hence the plastic zone size) (Fig. 5), the critical condition for continued propagation is

$$\Delta K = 1.12\,\Delta\sigma\sqrt{\pi D} \; > \Delta K_{TH} \tag{3}$$

Thus the stress level based on propagation to failure $\Delta\sigma_p$ is given by

$$\Delta\sigma_p = 0.5\,\frac{\Delta K_{TH}}{\sqrt{D}} \tag{4}$$

Typical verification of this simple equation is given on Fig. 8, in which the solid lines represent the theoretical fatigue limits calculated as above and the points are experimental values; other examples are in Smith and Miller [*10*].

It is worth noting that the traditional empirical approaches to notch fatigue, through the use of strength reduction factors, notch sensitivity factors, and size effects (see, for example, Forrest [*11*]) can all be predicted from the foregoing equation. Thus the "bulk" parameters of plain fatigue limits and long crack thresholds can be used to explain known facts of the fatigue limits of notched components.

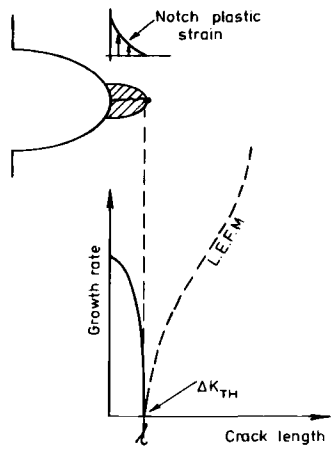

FIG. 7—*Nonpropagating crack at the edge of the notch plastic zone.*

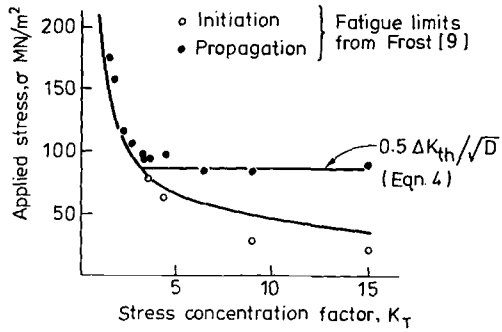

FIG. 8—*Comparison of experimental and theoretical fatigue limits* [10].

Short Cracks at Higher Than Fatigue Limit Stress Levels

Slower Than LEFM Growth Rates—Slower crack growth due to the deceleration of cracks at grain boundaries has been reported by, for example, Lankford et al [*12*] and Morris [*13*]. A comparison of the crack tip plastic zone size and the grain size appears to be important because if the plastic zone is larger than the grain size the disturbing influence of grain boundaries is lost. Some data by Lankford et al [*12*] are shown in Fig. 9. The initial high growth rate was assumed to be caused by a specimen artifact, but the lower than long crack data rates were genuine for this Ni-based superalloy with grain size on the order of 3 to 5 μm. Note that the growth rates are very low, about 5×10^{-9} m/cycle. Other causes of slower growth rate have been given by Schijve [*14*] and Truyens [*15*] and are due to irregular crack surfaces and interaction of multiple initiation sites respectively. Clearly, all these suggested mechanisms are microscopic effects operative at a length scale of about the grain size, and successful correlation by a global "macro" parameter seems to be very unlikely.

Faster Than LEFM Growth Rates—In many studies of growth rates in plain specimens initial growth rates have been reported to be high and caused by initiation of cracks at subsurface intermetallic particles (see, for example, De Lange [*16*]). Pearson [*17*] has reported data from nominally elastic microcrack growth in smooth specimens of aluminum alloys which was much faster than corresponding macrogrowth. This is assumed to be caused by the lack of constraint near the surfaces giving much enhanced crack opening. Similar behaviour of elastic cracks exploiting weak microstructural features was observed by Taylor and Knott [*18*]. Morris [*13*] concluded that crack opening (and hence growth rate) depended on the location of the crack tip relative to the grain boundaries when the crack was smaller than the grain size and, further, that the size of the plastic zone was independent of the microcrack length and of the externally applied load. Thus the continuum rates predicted by LEFM can be either faster or slower than those observed, depending on the crack tip position. Dowling [*19*] subjected smooth steel speci-

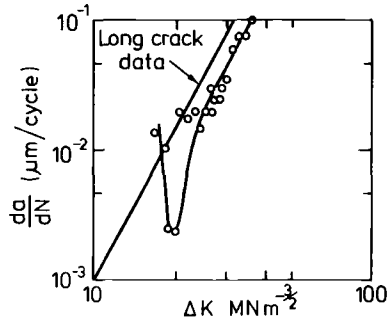

FIG. 9—*Non-LEFM behaviour of microcracks* [12].

mens to completely reversed strain cycling under elastic-plastic conditions, again achieving much enhanced growth rates; these were successfully related to LEFM data by using a ΔJ-parameter, based on J-integral concepts.

Much faster growth than LEFM rates, however, has been demonstrated for cracks growing at notches (Figs. 10 and 11) [*20,21*]. Figure 10 [*20*] shows a pronounced dip in growth rates for cracks growing away from large elliptical notches in a mild steel. The notch depth D was 16 mm and its root radius ρ was 0.3 mm, giving an elastic stress concentration $K_T = 15$. The minimum growth rates occur at considerable crack lengths ($\sim$2 to 3 mm) and relatively high growth rates in the order of 5×10^{-7} m/cycle, which contrast with microcrack data [*12*] discussed previously. Similar effects can be seen in the data from El Haddad et al [*21*], which are plotted in Fig. 11 on the conventional LEFM basis, thus somewhat masking the crack length relationship.

The arguments proposed in the section on nonpropagating cracks can be applied here when the remote applied stress has been increased so that there is an overlap between the initial decreasing notch plastic strain control and the subsequent increasing crack tip plasticity control (Fig. 12). Other slightly different arguments have been advanced. Schijve [*22*] suggests that the cause of the growth dip is increasingly effective closure of the crack during part of the loading cycle as the crack grows from the surface where the closure is small. Eventually maximum closure level is reached and the growth rate increases with length in the usual way. This argument is probably true, but like all closure explanations of growth phenomena, difficult to quantify without detailed measurements because present closure prediction models are not satisfactory. Leis and Forte [*23*] argue that the notch plastic zone is in effect a displacement control situation whose driving strength is diminished by the opening produced by the advancing crack, only to be succeeded by normal load control as the crack reaches the unyielded material away from the notch. It is, however, quite clear that the limited crack tip plasticity arguments of LEFM are violated because the crack is initially completely sur-

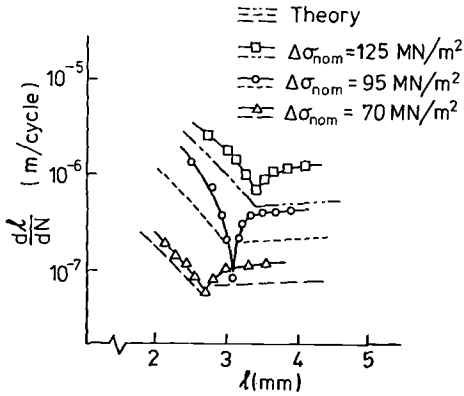

FIG. 10—*Non-LEFM behaviour of macrocracks at notches* [20].

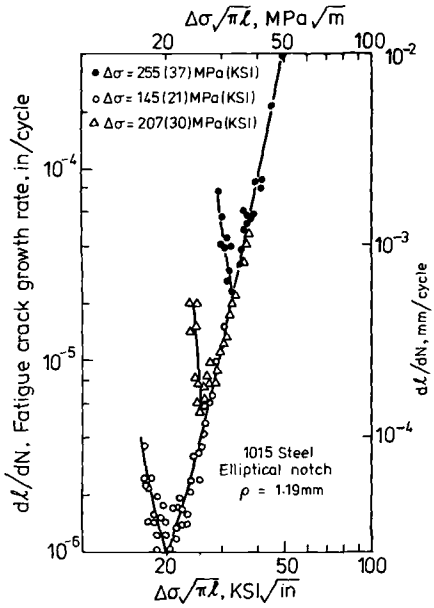

FIG. 11—*Non-LEFM behaviour of macrocracks at notches* [21].

rounded by unconstrained plasticity and the ΔK parameter is unable to correlate the experimental data.

Various other mechanics parameters have been proposed to describe crack growth in this notch plasticity region. Hammouda et al [*24*] computed plastic shear deformation at the crack tip by an elastic-plastic finite-element analysis.

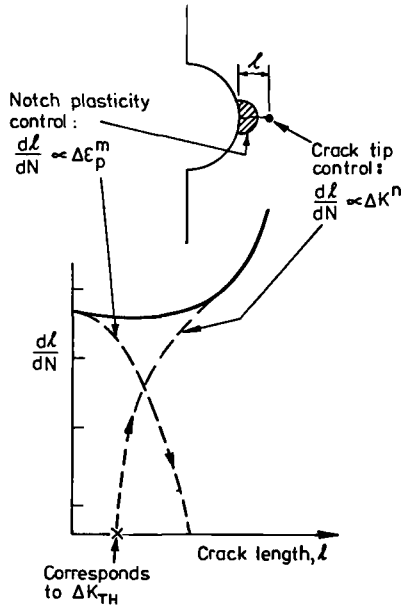

FIG. 12—*Changeover of control at notches at higher than threshold stress levels.*

El Haddad et al [*21*] used an artificially modified crack length and a cyclic *J*-integral analysis. Following a similar approach by El Haddad et al [*25*], Cameron and Smith [*20*] combined a cyclic stress-strain relationship with Neuber's rule to approximate the strain range within the yielded notch field. A strain intensity factor was then used in place of the usual stress intensity factor by replacing the nominal stress by the product of the local strain concentration factor multiplied by the nominal strain remoted from the notch. All these procedures appear to successfully reduce elastic-plastic crack propagation data to a single base. But since the data generated so far are limited, there is no reason other than computation preference for favouring one method at the expense of another—all are essentially empirical approximations.

The Relative Importance of Initiation and Short Crack Propagation in Notched Components

In order to calculate the total life of a notched component, several investigations (for example, [*26-28*]) have found it convenient to divide the total life, N_T into three parts:

1. Initiation (N_1).
2. Plastic crack growth in the notch yield zone (N_2).
3. Long LEFM growth under crack tip plasticity control (N_3).

Thus, in general, $N_T = N_1 + N_2 + N_3$. To illustrate this approach, some calculations made for elliptically notched mild steel plates [*20*] will be discussed. The notches were all 16 mm deep and had root radii of 16, 2.3, and 0.32 mm corresponding to elastic stress concentration factors of 3, 6.5, and 15 respectively. Initiation data were obtained by matching the strain range on smooth hourglass specimens to the maximum strain at the notch root, following the method described, for example, by Topper et al [*29*], and were arbitrarily defined to mean initiation plus growth to length a_0. The plastic crack growth from a length equal to a_0, defined in Eq 1 and equal to 0.2 mm in this study, was computed by the previously described strain intensity method until the crack had grown to the edge of the notch cyclically yielded zone. The subsequent elastic crack propagation calculation followed the usual Paris Law LEFM technique. The ability of Steps 2 and 3 to follow the growth rate dips is clearly shown for three stress levels in Fig. 10. In this way the fraction of total life, N/N_T, occupied by each stage, at a variety of stress levels, was found for the three notch geometries (Fig. 13 to 15).

It must be remembered that the engineering definition of "initiation"—that is, initiation and growth to 0.2 mm depth—is necessary because some experimentally determinable definition is needed for the strain-controlled experiments used to collect data. If in the future some reliable theoretical method is found to calculate initiation lives or more sensitive crack detection techniques are found they can be incorporated as Stage 1 in the above approach. Also, further caution is advised since the results depend on material, geometry, and size. For the very sharp notch, $K_T = 15$, Fig. 13, it can be seen that for all but the lowest stress levels initiation occurs at an extremely low life fraction. At very high stress levels the crack is propagating in plastically strained material because general yield is being approached, but when the notch yield zone is more contained the proportion of life spent in the notch zone decreases to about 20%. Finally, at stress levels just above the

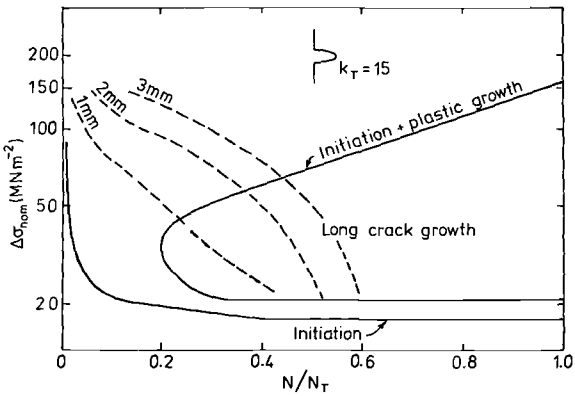

FIG. 13—*Stress versus life fractions:* $K_T = 15$.

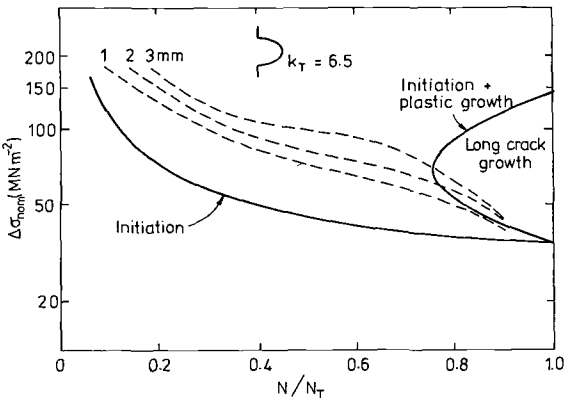

FIG. 14—*Stress versus life fractions:* $K_T = 6.5$.

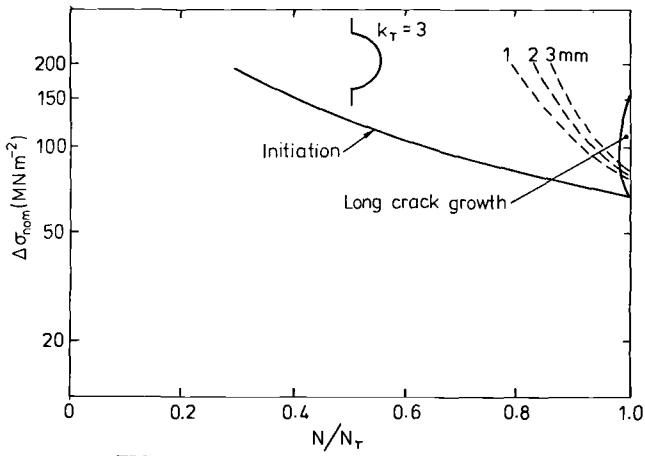

FIG. 15—*Stress versus life fractions:* $K_T = 3$.

lowest initiation level, the notch plastic zone again becomes important since the whole of the life is then consumed in the nonpropagating crack regime. Similar trends are followed by the two blunter notches, but, of course, the proportion of life spent initiating the crack becomes larger, until it consumes nearly the life at most stress levels for the $K_T = 3$ notch, and the proportions of life in the long crack growth region becomes increasingly less important, and negligible for the bluntest notch.

Superimposed on these plots are lines representing cracks of 1, 2, and 3 mm depth, representing a defect at the notch root which is typically a problem of real engineering concern. For the sharpest notch, a 1-mm defect at worst only reduces the life by about 40%, and, as might be expected, remaining life estimates could be made by LEFM calculations for a wide range of stresses. For the bluntest notch, defects of this size have an overwhelming effect on life, reducing the remaining life almost to zero.

It is clear that for certain regimes of stress and notch actuity any one of the three stages—initiation, notch plastic growth, or long crack growth—can dominate the whole of the life. This is illustrated in Fig. 16, where the region marked LEFM growth has been calculated by computing the cycles consumed by a crack growth law extending to the threshold region, and the initial crack length corresponds to ΔK_{TH}. The elastic stress intensity factors were corrected to account for the notch geometry. This produces a much larger LEFM contribution than the previous calculations which used the edge of the notch plastic zone as an initial crack length. The bounds of this region were drawn when the life estimate was in 50% error from observed experimental values (note this is a small error for a *life* estimate). The other regions were then designated by the stage which would dominate the life. At the higher stress levels and for nonpropagating cracks, growth in the notch plastic zone is important. But the short crack problem in this area can be overcome by the analytical "macro" techniques described. For blunter notches at stresses just above the initiation stress level an estimate for initiation life along is sufficient. This can be made using the strain-matching (strain/cycles to initiation) approach, again overcoming the short crack problem in a practical way. Only in the stress region just above the nonpropagating crack area is an estimate of all three stages required. Again, caution should be sounded about the generalisation of these results. They only apply (*1*) to a mild steel and (*2*) to elliptical notches. Evidence is just emerging that for equivalent stress concentration factors in welded joints, the stress gradient below the notch is much steeper, thus further reducing initiation effects and reinforcing the LEFM contributions.

The Local Nature of Some Short Crack Problems

The foregoing discussion has shown how many short crack problems can be overcome by a macroscopic approach. Because of the local nature of other short crack problem areas, however, it is worth detailing those features which make a macroscopic global approach difficult if not impossible.

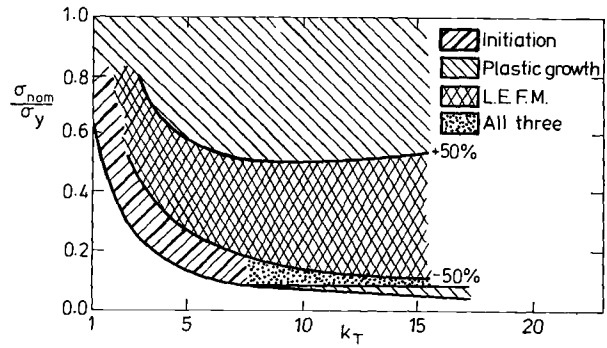

FIG. 16—*Dominant stage in life calculations.*

The statistical nature of competing multiple initiation sites is well known (see, for example, Refs *1* and *30*). This is clearly much influenced by surface condition which, in general, is much more carefully controlled in laboratory specimens than real components. The difficulties of measurement of such small cracks is complicated by the need to understand their progress into the interior as well as development along the surface. The three-dimensional nature of such situations has been receiving increasing attention recently. The volume of material sampled by small cracks (for example, measured by the crack front length/grain diameter ratio) is small. The restraint on slip on small cracks can differ from those of large cracks. Schijve [*22*] has presented an extended discussion of these features. Other reviews of the short crack problem have been published (for example, by Hudak [*31*] and Dowling [*32*]), each providing its own particular slant on the problems discussed here.

Conclusions

1. The "smallness" of a fatigue crack depends on material and stress level. No single length value can therefore be given to define this property.

2. Two main reasons can be identified as causes of the deviation of short cracks from predictions based on long crack (LEFM) behaviour. These are:

   (a). Interactions of cracks and their tip plastic zones with microstructural features of the material, such as grain boundaries or inclusions.

   (b). The situation of cracks in regions of plasticity comparable or greater than the crack length, thus violating the limited plasticity assumptions of LEFM.

3. The effects of short cracks on the fatigue limits of plain and notched components can be adequately described by a combination of the engineering macroparameters of plain fatigue limits, threshold stress intensity factors, and stress concentration factors.

4. The prediction of crack growth rates or cycles to failure is much more difficult. The "initiation" stage is at present impossible to predict using bulk engineering parameters, but empirical approaches can correlate data if similarity rules are observed. Cracks in large plastic zones can also be dealt with by empirical methods. The interaction of cracks with microstructural features is not yet sufficiently understood for a global fracture mechanics approach to be useful.

Acknowledgments

Acknowledgments are due British Gas Engineering Research Station, G.K.N. Technology Centre, and the Science and Engineering Research Council, who have partially funded this work. Dr. A. D. Cameron, now with Lloyds Register of Shipping, conducted the experiments and analysed the notched fatigue tests.

References

[1] Morris, W. L. and James, M. R., *Metallurgical Transactions*, Vol. 11A, No. 5, 1980, pp. 850-851.

[2] Mughrabi, H. et al, this publication, pp. 5-45.

[3] Kitagawa, H. and Takahashi, S. in *Proceedings*, Second International Conference on Mechanical Behavior of Materials, Boston, Mass., 1976, pp. 627-631.

[4] Smith, R. A., *International Journal of Fracture*, Vol. 13, No. 5, 1977, pp. 717-720.

[5] Lankford, J., *International Journal of Fracture*, Vol. 16, No. 1, 1980, pp. R7-9.

[6] Tanaka, K., Nakai, Y., and Yamashita, M., *International Journal of Fracture*, Vol. 17, No. 5, 1981, pp. 519-533.

[7] Elsender, A., Hopkins, P., and Batte, A. D., *Metals Technology*, Vol. 15, June 1980, pp. 256-258.

[8] El Haddad, M. H., Saith, K. N., and Topper, T. H., *Journal of Engineering Materials and Technology*, Vol. 101, No. 1, 1979, pp. 42-46.

[9] Frost, N. E., *Proceedings of the Institution of Mechanical Engineers*, Vol. 173, No. 35, 1959, pp. 811-827.

[10] Smith, R. A. and Miller, K. J., *International Journal of Mechanical Sciences*, Vol. 20. No. 4, 1978, pp. 201-206.

[11] Forrest, P. G., *Fatigue of Metals*, Pergamon Press, Oxford, 1962.

[12] Lankford, J., Cook, T. S., and Sheldon, G. P., *International Journal of Fracture*, Vol. 17, No. 2, 1981, pp. 143-155.

[13] Morris, W. L., *Metallurgical Transactions*, Vol. 11A, No. 7, 1980, pp. 1117-1123.

[14] Schijve, J., *Engineering Fracture Mechanics*, Vol. 14, No. 3, 1981, pp. 467-475.

[15] Truyens, P., "Crack Growth under Variable Loads in Ships," Doctoral thesis, University of Ghent, Belgium, 1976.

[16] De Lange, R. G., *Transactions of the Metallurgical Society*, Vol. 230, No. 4, 1964, pp. 644-648.

[17] Pearson, S., *Engineering Fracture Mechanics*, Vol. 7, No. 2, 1975, pp. 235-247.

[18] Taylor, D. and Knott, J. F., *Fatigue of Engineering Materials and Structures*, Vol. 4, No. 2, 1981, pp. 147-155.

[19] Dowling, N. E. in *Cyclic Stress-Strain and Plastic Deformation Aspects of Fatigue Crack Growth, ASTM STP 637*, American Society for Testing and Materials, 1977, pp. 97-121.

[20] Cameron, A. D., and Smith, R. A., *International Journal of Pressure Vessels and Piping*, Vol. 10, No. 2, 1982, pp. 205-217.

[21] El Haddad, M. H., Dowling, N. E., Topper, T. H., and Smith, K. N., *International Journal of Fracture*, Vol. 16, No. 1, 1980, pp. 15-30.

[22] Schijve, J., Delft University of Technology Report LR-327, The Netherlands; also in *Proceedings*, International Symposium on Fatigue Thresholds, Stockholm, EMAS, Warley, U.K., 1982.

[23] Leis, B. N. and Forte, T. P. in *Fracture Mechanics, ASTM STP 743*, American Society for Testing and Materials, 1981, pp. 100-124.

[24] Hammouda, M. M., Smith, R. A., and Miller, K. J., *Fatigue of Engineering Materials and Structures*, Vol. 2, No. 2, 1979, pp. 139-154.

[25] El Haddad, M. H., Smith, K. N., and Topper, T. H. in *Fracture Mechanics, ASTM STP 677*, American Society for Testing and Materials, 1979, pp. 274-289.

[26] Coffin, L. F. in *Proceedings*, 1971 International Conference on the Mechanical Behaviour of Materials, The Society of Materials Science, Japan, Vol. 2, 1971, pp. 516-529.

[27] Dowling, N. E., *Fatigue of Engineering Materials and Structures*, Vol. 2, No. 2, 1979, pp. 129-138.

[28] Socie, D. F., Morrow, J., and Chen, W., *Engineering Fracture Mechanics*, Vol. 11, No. 4, 1979, pp. 851-859.

[29] Topper, T. H., Wetzel, R. M., and Morrow, J. D., *Journal of Materials*, Vol. 4, No. 1, 1969, pp. 200-209.

[30] Kitagawa, H., Nakasone, Y., and Miyashita, S., this publication, pp. 233-263.

[31] Hudak, S. J., *Journal of Engineering Materials and Technology*, Vol. 103, No. 1, 1981, pp. 26-35.

[32] Dowling, N. E. in *Fracture Mechanics, ASTM STP 677*, American Society for Testing and Materials, 1979, pp. 247-273.

Fatigue Crack Growth

A. J. McEvily[1]

On the Quantitative Analysis of Fatigue Crack Propagation

REFERENCE: McEvily, A. J., **"On the Quantitative Analysis of Fatigue Crack Propagation,"** *Fatigue Mechanisms: Advances in Quantitative Measurement of Physical Damage, ASTM STP 811*, J. Lankford, D. L. Davidson, W. L. Morris, and R. P. Wei, Eds., American Society for Testing and Materials, 1983, pp. 283-312.

ABSTRACT: The literature on the subject of the mechanism of fatigue crack growth is reviewed. Historically two different mechanisms have been proposed. One is based upon the concept of damage accumulation, the other on a plastic sliding-off process at the tip of the advancing crack. The experimental evidence supports the latter mechanism as the basic process of crack growth. Damage due to static modes of separation can also be important, however, particularly in low-toughness materials. In addition, localized soft zones such as persistent slip bands can be construed as a type of damage if they form at a crack tip and facilitate crack advance.

A method for the quantitative analysis of fatigue crack growth based on a sliding-off process which is related to the crack tip opening displacement is described. The method includes consideration of R-effects, the threshold and cyclic fracture toughness. The method is potentially of use in both the elastic and plastic ranges.

KEY WORDS: fatigue, fatigue crack growth, fatigue threshold, crack-opening displacement, mean stress effects in fatigue, fatigue damage

Since the mid-1950s there has been considerable interest in the growth of fatigue cracks, an interest stimulated by the realization that fatigue crack growth can comprise a significant portion of the fatigue lifetime of a cyclically loaded structure. In addition, the treatment of this subject has been advanced by developments in the field of fracture mechanics, the introduction of servohydraulic test systems, and the availability of transmission and scanning electron microscopes for fractographic examination. A most important experimental finding stemming from early use of these two tools was the observation of Forsyth and Ryder [*1*] that a fatigue crack advances by an increment, Δa, in each cycle.[2] However, while this is still a generally accepted

[1]Professor, Department of Metallurgy, University of Connecticut, Storrs, Conn. 06268.
[2]The italic numbers in brackets refer to the list of references appended to this paper.

characteristic of the fatigue crack growth process, except at very low growth rates in the near-threshold region, there is a lack of agreement as to the mechanism involved in the growth step. As was pointed out in the 1966 ASTM Symposium on Fatigue Crack Propagation [*2*], there are two ways of viewing the cause for increment of crack growth: one is in terms of damage accumulation, the other in terms of a plastic sliding-off process at the crack tip. In the intervening years it seems surprising that the issue has not been resolved to the satisfaction of all concerned, and in fact the papers in this conference reflect the continuing diversity of views on this matter.

To illustrate the nature of these differences in terms of interpretation of results, the log of the rate of fatigue crack propagation, da/dN, for two sets of data is plotted in Fig. 1 in the manner of Paris et al [*3*]; that is, as a function of the log of the range of the stress intensity factor, ΔK. A straight line on this plot is given by the Paris equation

$$\Delta a/\Delta N = C(\Delta K)^m \tag{1}$$

In Fig. 1*a* it is seen that over a relatively narrow range of data the value of m is about 4, and this has been taken to be supportive of a damage accumulation mechanism for fatigue crack growth [*4*]. In Fig. 1*b* the slope over a region is also about 4, but this has been interpreted to indicate support for a sliding-off process of crack growth for which a slope of 2 is expected. It has been contended, however, that the added influence of static modes of separation brings about an increase in slope from 2 to 4 [*5*].

These two approaches are not the only approaches proposed for the analysis of fatigue data. For example, Fig. 2 shows a plot based upon the use of J as a correlating parameter for crack growth in both the elastic and plastic ranges [*6*], and Fig. 3 shows a master curve for crack growth in terms of ΔK_{eff}, where ΔK_{eff} is defined as $K_{\max} - K_{\text{op}}$, an approach aimed at taking into account the effect of mean stress on crack propagation through consideration of crack closure [*7*]. Both of these approaches will be considered further herein, but neither is directly concerned with the mechanism of crack growth.

This sampling indicates something of the range of views which have been developed in the quest for quantitative analyses of crack growth. To the extent that useful engineering results are potentially obtained from any of these approaches perhaps one need not be concerned about basic differences. However, it seems *a priori* that if we are to predict the effects of microstructure, environment, and variable-amplitude loading on the fatigue crack growth process, then it is still necessary to understand the basic nature of fatigue crack growth in ductile materials. In line with this objective, the aim of this paper is to review the current state of knowledge of the processes occurring at the crack tip and to identify the mechanisms involved. The reader is forewarned that this may not be an unbiased presentation because of the

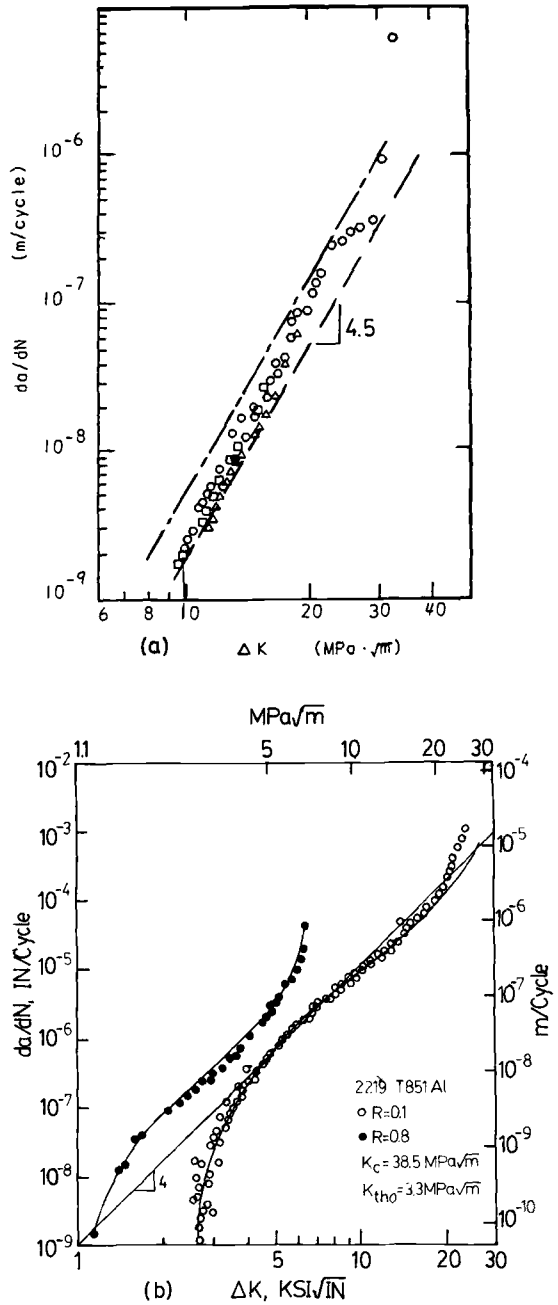

FIG. 1—*Fatigue crack growth rates versus cyclic stress intensity factor for* (a) *annealed Fe-0.64C* [4] *and* (b) *2219-T851 aluminum alloy* [88]. *Solid lines in* (b) *are based on Eq 10.*

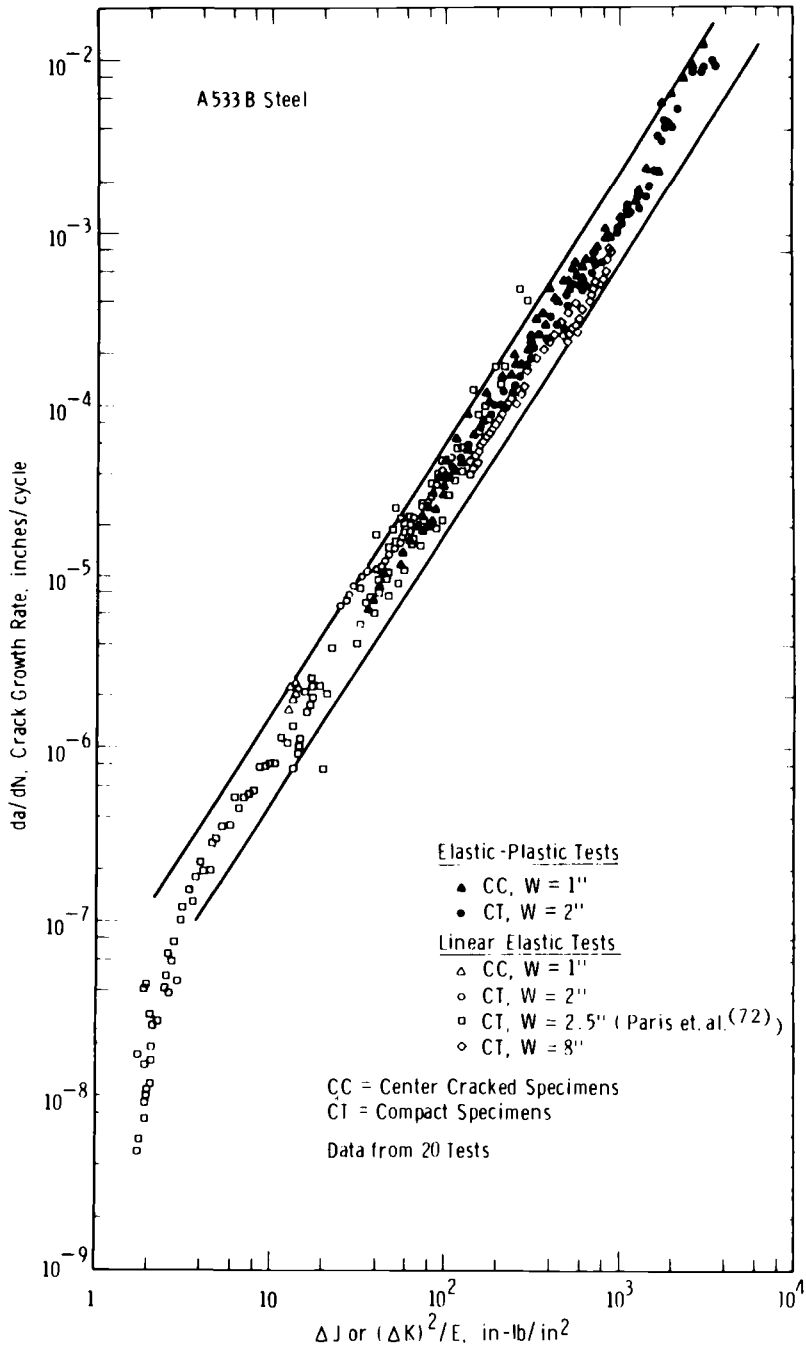

FIG. 2—*Fatigue crack growth rate versus cyclic J-range for various geometries* [6].

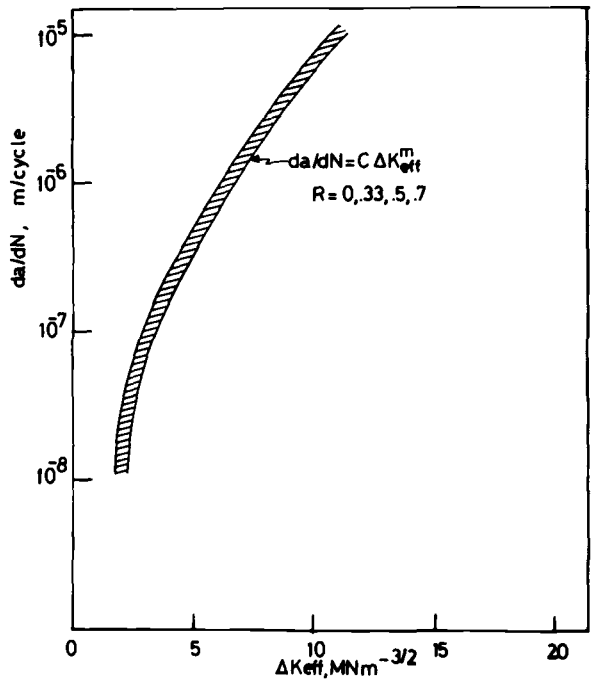

FIG. 3—*Relationship between the crack propagation rate and the effective stress intensity range for 2024-T3* [7].

author's prior involvement with the sliding-off approach. Other positions will be put forth by advocates of other approaches during this conference, and it is hoped that a clearer understanding of the true state of affairs will emerge. However, on a less sanguine but more realistic note, we may be involved in a situation wherein "old theories never die, only their proponents do".

The Fatigue Crack Tip

Shortly after Forsyth and Ryder [*1*] found that a fatigue crack advanced an increment per cycle, Laird and Smith [*8*] developed what is now referred to as the plastic blunting model of fatigue crack growth. An example of this model, which involves the opening, advance, and blunting of a crack tip in the loading portion of a cycle and the resharpening of the crack in the unloading portion of the cycle, is shown in Fig. 4 [*9*]. In this type of model crack advance cum blunting occurs continuously during the loading portion of a cycle as soon as the crack tip opening load has been exceeded. Incidentally, note that the fatigue striations in this model are formed on unloading, a process clearly seen during fatigue crack growth in polymers [*10*] where rather large deformations per cycle can be imposed. Nevertheless, there is

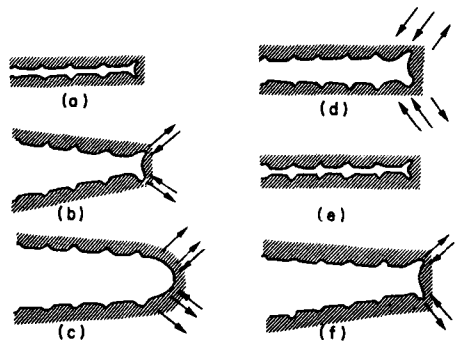

FIG. 4—*Schematic of the plastic-blunting process during a loading cycle* [9].

still controversial discussion in the literature (see, for example, Ref *11*) on this topic. It is also known that the environment, that is, ambient air versus vacuum, can influence the appearance of striations. In air they can be quite well defined, whereas in vacuum they are much less so. Lynch [*12*] has suggested that in vacuum dislocation egress at fracture surfaces during unloading will not be impeded by oxide films, so that all the fracture surface produced on loading may be deformed on unloading.

With respect to the details of plastic blunting in terms of slip processes a number of simple models have been proposed. For example, Fig. 5 shows how a crack tip might open by slip on one system and close by slip on another [*13*]. An important feature of such a model is the irreversibility of the process introduced by making use of different loading paths on the loading and unloading portions of the cycle. This type of model has been advanced by Pelloux [*14*] and by Neumann [*15*]. The work of Neumann is of particular interest in that it has involved direct observation of the slip processes occurring at crack tips during cyclic loading.

Neumann [*16*] made use of copper single crystals tested in bending or push-pull. In order to obtain a simple process of fatigue crack growth confined to a single macroscopic plane, specimens with the principal stress direction in the [100] were used. The bend specimens were notched with the base of the notch in either the [001] or [011] direction. Notched [100] crystals were also used for push-pull tests with the base of the notch in the [011]. Under these conditions, although slip occurred on {111}, the macroscopic plane of growth was the {001}. These tests demonstrated in a striking way the nature of the deformation at a crack tip during cycling; Fig. 6 provides a schematic of the deformation process during loading. Neumann summed up his observations as follows:

1. The slip near the crack tip is almost perfectly confined to two slip systems.
2. The slip traces emanate from the sides of the crack such that on each side of the crack there is mainly one slip system active.

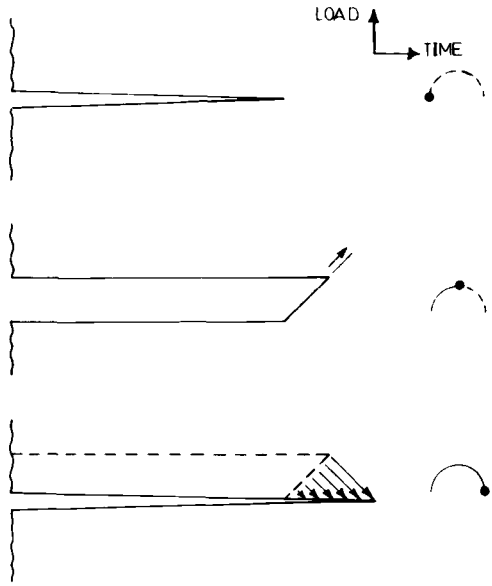

FIG. 5—*A simple sliding-off process at a crack tip* [13].

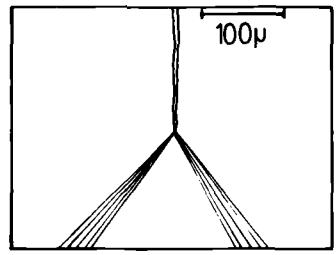

FIG. 6—*Sliding-off process of blunting a fatigue crack in a copper single crystal* [16].

3. There is an almost slip-free triangular area in front of the crack.

4. At any instant only the slip planes emanating from the crack tip are active. (The maximum distance between the active slip plane and the crack tip vertex was estimated to be less than 5000 Å.)

5. The open crack tip is a V-groove with a constant angle at the tip. The process of "blunting" the tip by plastic deformation is a widening of the "V" at constant crack tip angle. Mowbray [*17*] has pointed out that the V-tip shape will develop when the dislocations emerging from the tip can move freely away from the tip. This process is facilitated when slip lines can spread to the back surface of a tension specimen. In a bend specimen, on the other hand, the formation of a blunted tip is more likely. Similarly, at low stress

amplitudes the dislocations will be relatively close to the tip and blunting will be favored over V-tip formation.

6. The crack closes in compression by slip reversal at the current tip of the open part of the crack, leaving the angle of the tip at the open part of the crack unchanged.

After unloading a crystal from a 170-μm opening, a relatively large value, Neumann observed that the tip closed for a distance of 6 μm back from the tip. For a 40-μm opening, the tip was blunt after unloading and closure was not evident. Figure 7 shows Neumann's model of the opening and closing process. In this process of crack closure, shear strains on the order of unity are required on either side of the crack. Further, the crack advance per cycle is on the order of the crack-opening displacement. It is also interesting to note that by keeping the plastic strain amplitude constant in the push-pull tests, since all the plastic deformation occurred at the crack tip, the rate of crack advance could also be maintained constant.

In subsequent work, Neumann et al [*18*] made use of an SEM and directly observed the alternating slip process of crack growth in Fe-3Si crystals. They also noted in fatigue crack growth studies of [100] copper single crystals that Stage I growth, that is, macroscopic growth parallel to the most highly stressed slip plane, was not observed in a vacuum of 1.3 MPa (10^{-5} torr) at growth rates down to 0.1 nm/cycle, although this mode of growth was found in air at growth rates below 30 nm/cycle. This result was interpreted to indicate that the environment promoted Stage I growth in copper.

Direct evidence of rewelding of the fracture surfaces of copper crystals during tests in vacuum was also obtained in this study. This subject of rewelding of fracture surfaces has long been a matter of interest. Some time ago, evidence of reweldment under a heavy compressive loading was found in stainless steel, copper, and aluminum, but not in carbon steels. Nevertheless, the fatigue properties of all these were better in vacuum than in air. Reweldment was therefore considered to be a contributing but not controlling factor [*19*]. In a recent paper, Kikukawa et al [*20*] studied crack tip deformation pro-

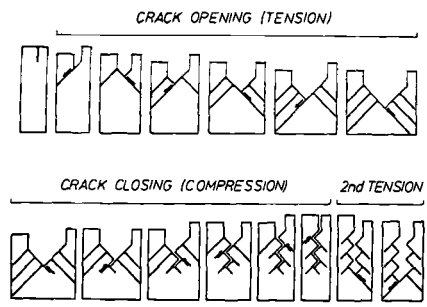

FIG. 7—*A model of the slip processes during a loading cycle* [16].

cesses in an SEM in grain-oriented silicon iron under pulsating tension test conditions ($R = 0$) at lower amplitudes than in Neumann's tests. The specimens were only one grain in thickness. They found evidence for rewelding on unloading in vacuum, although it is not clear how the distinction between crack closure, which might be greater in vacuum [*21*], and rewelding was made. Fractographic studies may be helpful in making this distinction, and recent work with a titanium alloy tested in the near-threshold region in vacuum has shown that portions of the fracture surface are not planar as in air tests, but consist of an assemblage of fine dimples, an indication that rewelding may have occurred in Stage I growth [*22*]. In general Kikukawa's results substantiated the Neumann model except that the crack tip was not a well-defined "V" as in Neumann's case, but appeared somewhat more blunt, an indication that a well defined "V" tip may be established only at high COD values. They found that the amount of crack advance per cycle, Δa, could be expressed as

$$\Delta a = (0.5 \text{ to } 0.6)\,\text{CTOD} - \Delta a_w \tag{2}$$

where Δa_w is the length of rewelding in vacuum. It is noted that a factor of 0.5 to 0.6 is consistent with a value of one half of the CTOD for the extent of crack advance [*23*].

Kikukawa et al also observed that the growth of a Stage I crack is a difficult process. They found the ratio of crack advance to crack-tip shearing displacement to be small compared with the ratio of crack propagation length to CTOD for a Stage II crack under Mode I loading. In addition, rewelding was found to occur to about the same extent in air as in vacuum in this mode. It is not apparent why, in vacuum, Stage I cracks were found to grow in Fe-3Si but not in copper. Certainly Stage I cracks grow in aluminum alloys in vacuum, a fact pointed out by Schijve [*24*] and by Pelloux [*25*], both of whom studied the Stage I growth of subsurface cracks in high-strength aluminum alloys. Wilhelm [*26*] has shown that in Al-Zn-Mg and Al-Cu alloys single-crystal Stage I growth occurs in air at room temperature but not in liquid nitrogen (77K). This finding was attributed to an absence of persistent slip bands at 77K along which Stage I cracks might propagate. In laboratory air a change in frequency from 50 to 5 Hz also impeded Stage I crack growth, a reflection of a reduced tendency for Stage I growth when corrosion processes are given time to be of influence, in seeming contradiction to Neumann's observations with copper.

In crack tip sliding-off models with all the plastic deformation occurring at the crack tip itself the rate of crack growth should be on the order of one half of CTOD. It has been recognized for some time, however, that in polycrystalline alloys tested in the LEFM range that the rate of crack growth is a much smaller fraction of CTOD. In a variety of polycrystalline alloys Robinson and Tetelman [*27*] have measured CTOD values in the range from 25 to 75 μm

and have shown that under monotonic loading of a specimen containing a fatigue crack that the CTOD closely approximates the expected value; namely

$$\text{CTOD} = \frac{K^2(1 - \nu^2)}{\sigma_y E} \tag{3}$$

We therefore have confidence in the expression for the CTOD, at least in the range measured. A lessening of the discrepancy between measured $\Delta a/\Delta N$ values and the CTOD values can be obtained by substituting the range of stress required for cyclic yielding, σ_{yc}, for σ_y, since $\sigma_{yc} = 2\sigma_y$ [*28*], but a large discrepancy still remains. This discrepancy is largest in the LEFM range and decreases at large CTOD values (Fig. 8) [*29*]. The underlying cause of this discrepancy appears to relate to the degree of strain localization at the crack tip as a function of the amplitude of the CTOD. One argument is that in the low growth rate region, that is, below 10^{-4} mm per cycle, in Fig. 8 not all the plastic deformation at a crack tip contributes to crack advance although it does contribute to the CTOD. For example, Tomkins and Biggs [*30*] and Lankford and Kusenberger [*31*] have pointed out that the lack of

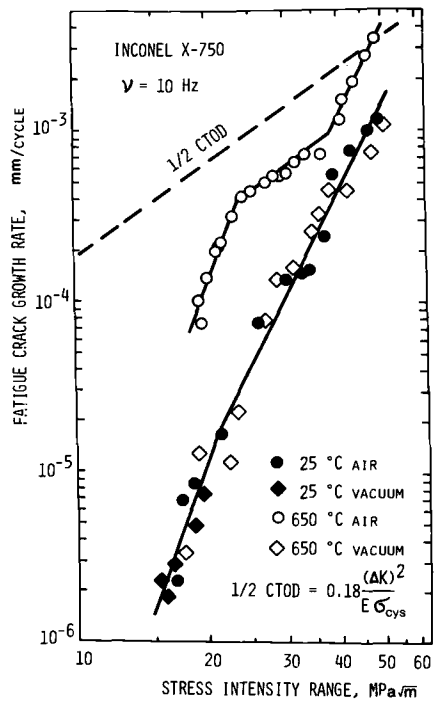

FIG. 8—*Effect of temperature test and environment on the fatigue crack growth rate of Inconel X-750 (triangular waveshape,* R = *0.05)* [29].

correlation between the CTOD and $\Delta a/\Delta N$ is probably related to the fact that crack tip flow bands are of finite width and can involve deformation in the crack flanks formed in previous cycles. Thus the amount of new crack surface formed at the edge of the flow band is in general less than the CTOD. With $\sigma\alpha\epsilon^n$, the flow band width decreases with work-hardening exponent n, and a closer correlation between CTOD and $\Delta a/\Delta N$ might therefore be expected for materials of low n in the LEFM range [*32*]. On the other hand, at high amplitudes the strain hardening which results in the lateral spread of deformation is overcome and deformation processes are relatively more concentrated at crack tip, as in the case of Neumann's large-amplitude studies of single crystals previously described [*16*].

Kuo and Liu [*33*] have developed what they refer to as the unzipping model of crack growth for the LEFM range. They maintain that their calculation includes only the crack-opening increments that contribute to crack growth and excludes the increments that only blunt the crack tip and do not cause a crack to grow (Fig. 9). They obtained the relation

$$\frac{da}{dN} = 0.02(1 - \nu^2)\frac{\Delta K^2}{E\sigma_{yc}} = 0.02\frac{\Delta J}{\sigma_{yc}} \tag{4}$$

This value for da/dN is a small fraction of the CTOD expression given in Eq 3 and is of the right order of magnitude for the LEFM range. From a quite different viewpoint, Weertman [*34*] has also developed an expression for the increment of crack growth per cycle which is a small fraction of the conventional COD. He assumed that an elastic crack tip enclave exists and that dislocations emitted from the tip result in blunting which stabilizes the crack during loading. The stress intensity for crack advance of the crack tip increases with blunting and is given as

$$K = K_{cs}\sqrt{\rho/b}$$

where K_{cs} is the critical stress intensity required the emission of dislocations from the crack tip region, ρ is the tip radius, and b is the interatomic spac-

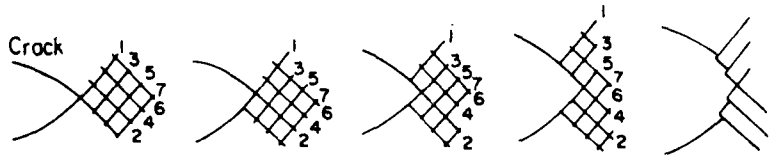

FIG. 9—*Unzipping model for crack opening and crack growth. The discrete slip bands are shown* [33].

ing. If ρ is set equal to Δa, the increment of crack advance, and with ΔK taken to be $2K$ in a push-pull test, then

$$\frac{\Delta a}{\Delta N} = \frac{b\Delta K^2}{4K_{cs}^2}$$

The value of K_{cs} is taken to be $0.8\,K_{cb}$, the critical stress intensity for brittle fracture. With $K_{cb} = (2E\gamma)^{1/2}$ and with $\gamma \simeq Eb/10$, where γ is the stress energy, then

$$\frac{\Delta a}{\Delta N} = \frac{(\Delta K)^2}{0.3E^2}$$

a value which compares favorably with the finding of Donahue et al [*35*]. However, the predicted crack tip radius appears to be much smaller than experimentally determined by Bowles [*36*].

In addition to the direct observation of slip at a crack tip, useful observations of crack tip deformation processes have also been carried out by other methods, such as the strain mapping and electron channeling techniques [*37,38*]. A number of researchers have also studied the crack tip region by transmission electron microscopy. Katagiri et al [*39*] have examined the dislocation structures in polycrystalline iron in the early stages of crack growth (up to 170 μm). Dislocation cells were observed ahead of the crack tip, with crack growth along primary slip planes and penetrating the cells, but with no difference in structure found around these cracks and away from them. In earlier work [*40*] these researchers had found that Stage I cracks grew along persistent slip bands in copper and along the primary slip plane in α-brass [*41*]. Persistent slip bands might be regarded as a form of matrix damage developed as the result of cycling prior to the appearance of a crack, since they are soft zones which facilitate dislocation motion and sliding off at the crack tip. With respect to Stage II growth the researchers concluded that the process was not substantially different from Stage I growth. Two operative slip planes were needed in each case, but more equally so for Stage II growth. Aside from the increase in dislocation density ahead of a crack tip, there remain no features evident which might be explicitly identified as fatigue damage.

The nature of the fatigue plastic zone has been investigated in a different manner by Bathias and Pelloux [*42*]. Microhardness measurements were used to determine the plane strain plastic zone sizes (the specimens were sectioned) in an annealed and in an aged maraging steel and in three different austenitic steels. Their interesting and important finding was that within the cyclic plastic zone of the fatigue crack tip the two maraging steels had cyclically softened whereas in the same region the austenitic stainless steels had cyclically hardened (Fig. 10). The importance of these observations is that it is assumed in some approaches to be discussed that cyclic hardening at a crack

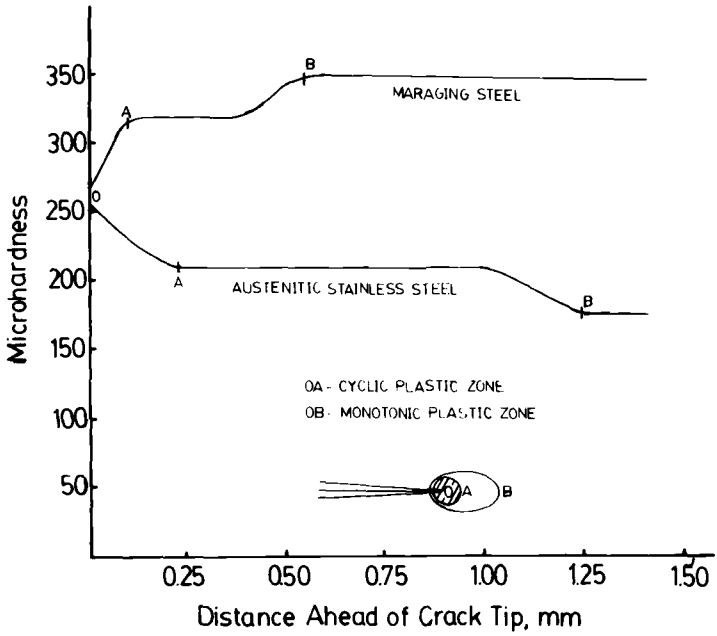

FIG. 10—*Microhardness readings ahead of fatigue cracks in* (a) *a maraging steel and* (b) *an austenitic stainless steel* [42].

tip is essential to crack propagation. Evidently this is not necessarily the case.

Models of Crack Growth

Yokobori [*43*] has prepared a recent listing of some of the models for fatigue crack growth which have been developed. A review of several of these approaches is given in this section.

An early model was proposed by Head [*44*], who assumed that the material ahead of a crack work-hardened progressively until the ductility was exhausted in an element immediately ahead of the tip and fracture ensued, a concept which in one form or another is still present. Head predicted that da/dN should be proportional to $a^{3/2}$. On the other hand, Frost and Dugdale [*45*] and later Liu [*46*] reasoned, on the basis of geometric similarity, that da/dN should be proportional to a.

Paris and Erdogan [*47*] analyzed the data for aluminum alloys and found that the rate of crack growth could be expressed as $da/dN \alpha \Delta K^4$, a finding which stimulated interest in the cause for such a relationship. At about this time, McClintock [*48*] concluded that there were two limiting kinds of mechanisms by which fatigue cracks might grow. If cracks grew as the result of damage or crack renucleation related to the area of the crack tip plastic zone

ahead of an approaching crack then a fourth-power dependency on ΔK would be expected, whereas if crack advance occurred by kinematically irreversible plastic deformation at the crack tip a second-power dependency would be expected. A fourth-power dependency was also predicted by Weertman [*49*], who made use of the Bilby-Cottrell-Swinden [*50*] model of a crack tip and a total critical displacement criterion. Weertman [*51*] has recently pointed out that an accumulated plastic work criterion is equivalent to an accumulated plastic displacement criterion and will lead to a ΔK^4 dependency. On the other hand, an accumulated plastic strain criterion for crack advance is the same as an accumulated plastic work density criterion and a ΔK^2 dependency is generally derived.

In 1959 Cottrell [*52*] pointed out that the view of ductile fracture as a process in which each element of material in front of the crack must first be worked plastically to change the stress or strain therein to meet some fracture criterion before it breaks seems wrong. In such a view, the material is supposed to have a finite capacity for plastic deformation, so that its ductility has to be "exhausted" before it can break, which suggests a critical strain as the criterion for fracture. However, as Orowan et al [*53*] have emphasized, although a bar of a ductile material may break in tension at a certain reduction in area, the same material can be plastically worked to a much greater extent without breaking if there is a compressive stress present, as in wire drawing or in the Bridgman high-pressure apparatus. Furthermore, if a tension specimen is then cut from this highly deformed and work-hardened material, it will not break until it has undergone a reduction of area almost as large as that of the unworked sample. Cottrell emphasized that the important function of plastic strain in ductile fracture is not to cause the material in front of the fracture to break, but rather to simply recede away from the fracture by plastic distortion.

Later, Garrett and Knott [*54*] attempted to resolve the matter of sliding-off versus ductility exhaustion by carrying out the following experiments. A fatigue crack propagation test was interrupted, the specimen was re-heat-treated to anneal-out fatigue damage, and the test was restarted at the same applied stress level. If the amount of crack advance per cycle depended upon a sliding-off process, the crack would be expected to grow immediately. If a damage theory held, a period of cyclic work-hardening should occur before further crack extension could occur. Figure 11 shows their results for an aluminum-copper alloy (2014) in the naturally aged and peak aged conditions. No arrest occurred following the intermediate heat treatment. In fact, the naturally aged alloy showed an initial increase in growth rate which gradually dropped off to the value established before the anneal. The large increment in initial growth for the naturally aged material was associated with a period of considerable work hardening which was absent in the peak aged condition. Garrett and Knott concluded that the fatigue growth rate is controlled by the instantaneous value of the CTOD and is not fundamentally

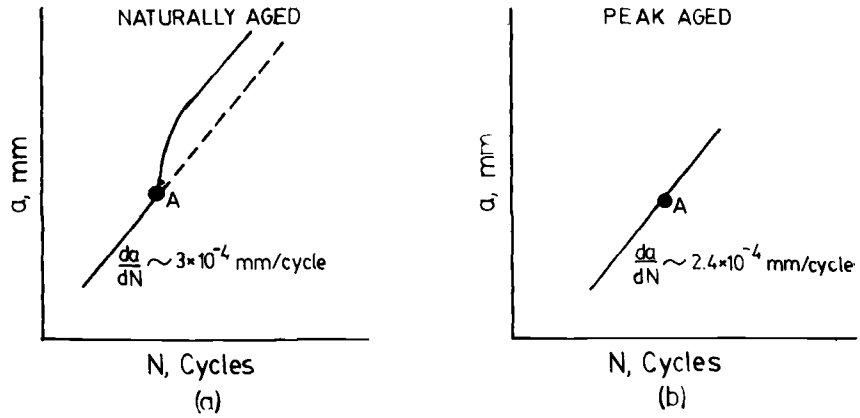

FIG. 11—*Crack growth behavior in 2014 aluminum alloy before and immediately after reheat treatment at Point A.* (a) *Naturally aged.* (b) *Peak aged. From Ref* 54.

dependent upon the build-up of a fatigue-hardened zone prior to crack advance. They did point out, however, that since work hardening controls the flow around the crack tip it has an important influence on the magnitude of the CTOD and the amount of sliding-off per cycle. Similar conclusions may also be drawn from the work of Liu and Kobayashi [*55*]. They observed that at a given reference ΔK-level in a constant-amplitude test a certain striation spacing developed. When a crack was grown at a lower ΔK-level, however, upon increasing the ΔK-level to the reference level the initial spacing of striations was greater than normally associated with the reference ΔK-level. The plastic flow process at the crack tip was evidently initially easier to operate upon increase in ΔK than subsequently when cyclic hardening at the new level had a chance to become stabilized.

A concept of "lifetime exhaustion" has also been employed, as in the work of Majumdar and Morrow [*56*], which is related to earlier work of Liu and Iino [*57*]. Figure 12 is a schematic of the strain history of a fatigue element ahead of the crack tip. An element ahead of the tip is subjected to a given magnitude of cyclic strain, and as the tip advances the strain increases and damage accumulates. In each cycle the damage accumulated is equal to $1/N_f$, the reciprocal of the number of cycles to failure at the strain range being experienced in that cycle. When $\Sigma 1/N_f = 1$ the crack tip should have arrived at the element and the failure should occur. On this basis the accumulated plastic strain model leads to the relation

$$da/dN = A(\Delta K)^2 \tag{5}$$

A major criticism of this type of model is that the $1/N_f$-values depend upon low-cycle fatigue properties of simple specimens. However, these specimens

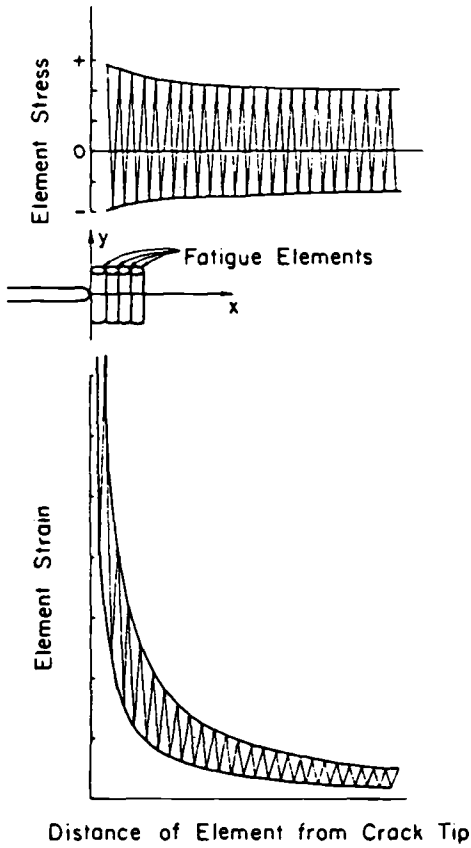

FIG. 12—*Schematic of the stress-strain history of a fatigue element ahead of the crack tip* [56].

do not fail as the result of damage accumulation. They fail because fatigue cracks are initiated early in life and grow with cycling to critical size. Weertman et al [*58*] have recently developed a new model for the process of fatigue crack growth advance for Mode II or Mode III loading. In this model dislocations are confined to two planes parallel to the plane of cracking. One of these planes is above the crack plane, the other below. During a loading portion of a cycle the dislocations moving on these planes exert a stress on the crack tip and when this stress reaches a critical value an increment of crack advance occurs. At the same time, the stress on the tip is lessened so that the crack front is stabilized against further advance. Upon reversal of the load the dislocations move in the opposite direction and are ready for participation in the next loading cycle. This model predicts a fourth-power dependency of $\Delta a/\Delta N$ on ΔK. The model as presently developed views the process

of crack advance as a brittle process, an assumption which is open to question in the case of ductile materials.

In summary, evidence has been obtained that can be interpreted to lend support to a sliding-off mechanism of crack growth. On the other hand, evidence for a fatigue-damage process that can be explicitly identified is harder to come by. The term *fatigue damage* is often used in the abstract in the sense that prior cycling causes a reduction in the residual fatigue life. It is of interest that in Frost, Marsh, and Pook's [*59*] comprehensive treatment of fatigue the term is not defined but is used in the sense indicated previously. They note that the fatigue strength of a specimen cut from the interior of the test section of a larger specimen which had failed in fatigue is not inferior to that of the virgin material. In the search for specific examples of damage one might identify the development of persistent slip bands along which Stage I cracks propagate as a form of damage in the sense that the presence of these bands facilitates the growth of cracks. However, the growth process within these bands appears to be a sliding-off process at the crack tip. In the same sense, the whole cyclic plastic zone is conditioned by prior cycling, whether it hardens or softens, to influence the sliding-off process. Further, if local cyclic softening at a crack tip were to be considered to be a form of damage since it facilitates crack growth, then what term should be applied to cyclic hardening which retards crack growth? For such cases it may be simpler to avoid the term *damage* altogether, and instead describe the specific microstructural features of import.

The term *damage* might, however, be applied to the static modes of separation, whether they be intergranular or between particles and matrix, which occur as the maximum stress intensity of a cycle, K_{max}, approaches the cyclic fracture toughness, K_{cc}. However, since these separation processes occur under the influence of the high tensile stresses and strains associated with the advancing crack tip, they are not considered to result from a cyclic process and are therefore referred to as static modes of separation. These static modes are superimposed upon the basic mechanism of crack advance. If static separation occurs ahead of the crack tip, damage exists in the form of microcracks which grow with cycling and join the main crack.

A Proposed Approach

In terms of modeling the process of crack growth, since the experimental findings lend support to a mechanism based on sliding off at the crack tip—that is, the Laird-Smith-Neumann mechanism—this feature should be incorporated in the model. On this basis one would expect to find through an assumed relationship between Δa and the CTOD that the rate of crack growth could be expressed as $da/dN \propto \Delta K^2$. In this approach, however, one must include the fact that there is a bounded region on the log $\Delta a/\Delta N$ versus log

ΔK plot within which the data must lie. The lower bound is given in ΔK_{TH} and the upper bound by the cyclic fracture toughness K_{cc}. The presence of these bounds can have an important influence on the slope of the line through the points on a log da/dN versus log ΔK plot. Donahue et al proposed that the rate of fatigue crack growth in the linear elastic range should be related to the CTOD in each cycle [*35*]. This would lead to a crack growth relation of the type

$$\frac{da}{dN} \alpha \text{CTOD} = \frac{\Delta K^2}{\sigma_y E} \tag{6}$$

The equation was modified to account for the presence of a threshold for fatigue crack growth as follows:

$$\frac{da}{dN} = A(\text{COD} - \text{COD}_{TH}) = \frac{A}{\sigma_y E}(\Delta K^2 - \Delta K_{TH}^2) \tag{7}$$

Further, upon examination of available data for inert environments it was found that the constant A could be expressed as

$$A \alpha \sigma_y / E \tag{8}$$

Since the work-hardening rate decreases with increase in yield strength, their finding was interpreted to indicate that high σ_y/E (the yield strain) ratios would lead to less lateral spread of deformation and blunting and hence more advance per cycle. This still seems to be a reasonable interpretation. Upon substitution of σ_y/E for A there results

$$\frac{da}{dN} = \frac{A'}{E^2}(\Delta K^2 - \Delta K_{TH}^2) \tag{9}$$

It is noted that Bates and Clark [*60*] observed a $(\Delta K/E)^2$ dependency away from threshold in steel, and that Frost and Dixon [*61*] and Frost and Pook [*62*] had suggested such a dependency.

A later version of Eq 9 took into account that the cyclic fracture toughness K_{cc} introduced an upper bound to the level of ΔK that can be reached. The manner of dealing with the threshold was also modified to provide a better fit to available data over a wide range. The equation became

$$\frac{da}{dN} = \frac{A'}{E^2}(\Delta K - \Delta K_{TH})^2 \left(1 + \frac{\Delta K}{K_{cc} - K_{max}}\right) \tag{10}$$

We are still learning more about the threshold level and how to deal with it in this type of equation. The threshold region is more complicated than initially

envisioned because of high closure levels and the operation of a Mode II (Stage I) crack growth process [*63*]. The initial form of the relationship, Eq 9, has the advantage that no cross-product terms are present. Further, in the initial form it has been shown that the expression is equivalent to an rms treatment of variable-amplitude loading, provided that the range of loading is not too great [*64*]. We have also used the relation

$$\Delta K_{TH} = \sqrt{\frac{1 - R}{1 + R}}\ \Delta K_{TH_0} \tag{11}$$

to relate the threshold level as a function of R to that at R equal to zero, a relation based upon CTOD equivalency [*65*]. Although Eq 11 does provide a reasonable indication of the trend of the threshold level with R, it is an oversimplification of the processes occurring at threshold since it neglects the contribution of Mode II, for example.

In the high ΔK level range the $\Delta K/(K_{cc} - K_{max})$ term of Eq 10 takes on greater significance as it accounts for the contribution of static modes to the crack growth processes. These modes are a form of damage (previously discussed) and are responsible for the increase in slope in the crack growth plot as the peak K-value, K_{max}, approaches K_{cc}. It is again noted that a form of damage capable of definition can develop if separation occurs ahead of the fatigue crack at a weak interface. In Eq 10, K_{cc} represents the fracture toughness under cyclic conditions. In the plane strain region of a crack growth test K_{cc} may be equal to K_{Ic}. However, if cyclic softening occurs, K_{cc} may be greater than K_{Ic} [*66*]. Further, as the crack progresses, if plane stress conditions develop at the tip then the value of K_{cc} should be modified accordingly. In practice we have used a single value for K_{cc} which may be treated as an adjustable parameter. The influence of mean stress on crack growth away from threshold is contained in the term $\Delta K(K_{cc} - K_{max})$ since

$$K_{max} = \frac{\Delta K}{1 - R} \tag{12}$$

In materials of high toughness mean stress effects are not pronounced; this is seen for the unembrittled steel in Fig. 13. However, in low-toughness materials where K_{max} approaches K_{cc}, the mean stress is a much more important factor (Figs. 1*b* and 13). In Fig. 13 the data and calculated curve for $R = 0.05$ for the embrittled steel lie just above the dashed band. We note also that as K_{cc} decreases the value of the Paris exponent m has been observed to increase. Ritchie and Knott [*67*] state that this is largely due to the increase in the contribution of static modes of separation with decrease in toughness. This trend of m with toughness is shown in Fig. 14. Therefore it is not surprising to find slopes of 4 for low toughness materials (as in Fig. 1*b*) even

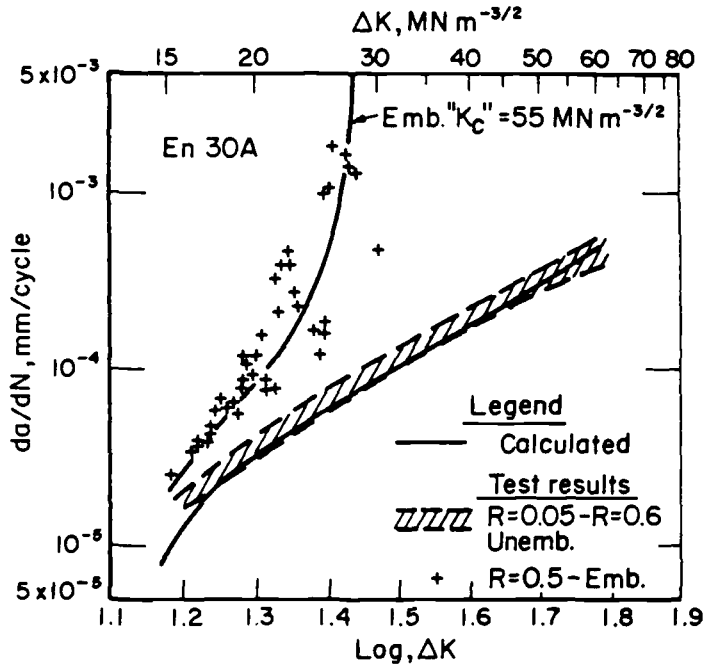

FIG. 13—*Comparison of experimental* [67] *and calculated growth rates* [5] *(Eq 10) for En 30a steel (0.35C-4.23Ni-1.43Cr-0.13Mo-0.14Si-0.44Mn.)*

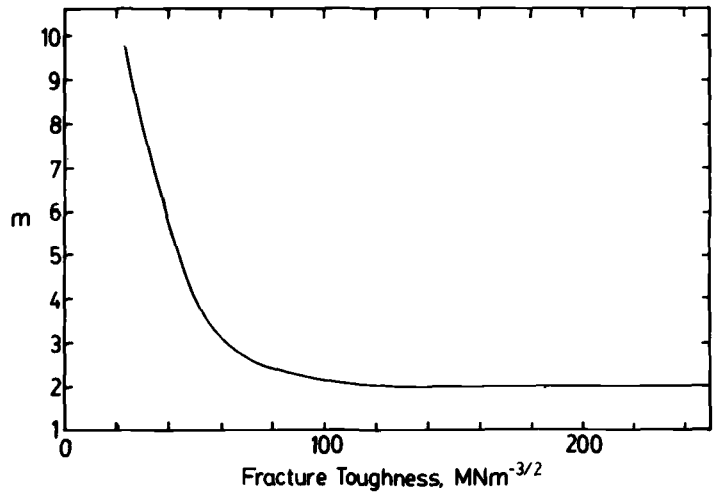

FIG. 14—*Variation of the exponent* m *of the Paris equation with static fracture toughness* K_{Ic} *for a number of medium and high strength steels* [67].

though the basic striation mode involves a slope of 2. The steepening of the curves is due to the operation of additional modes of crack advance (Fig. 15). Further, it is sometimes argued that there is a fundamental relationship between the constants c and m of the Paris equation. They can certainly be interrelated, as shown in Fig. 16, but this is an expected trend, as indicated in Fig. 15, where C is seen to be the rate of crack growth for a ΔK of unity. As m increases due to the operation of static modes C will decrease as shown. Use of the modified COD equation avoids this matter, however, since m always equals 2 and we are dealing with a three-parameter equation involving the constants A, ΔK_{TH} and K_{cc}. Work such as that of Kuo and Liu [*33*] appears useful in fixing the value of A at the appropriate level, and the work of Morris et al [*68*] and Tanaka and Taira [*69*] may be useful in determining ΔK_{TH} from a knowledge of the fatigue strength of smooth specimens.

The ΔJ-Approach

As shown in Fig. 2, the rate of fatigue crack growth can be expressed in terms of the parameter ΔJ in the elastic-plastic range or $\Delta K^2/E$ in the linear elastic range [*70, 71*]. Obviously the latter parameter is proportional to the K^2/E^2 parameter discussed previously. Where static modes of separation are not important, one might expect to find a slope of 1.0 in Fig. 2, but in fact the slope is higher, about 1.6. The reason for the higher slope is not apparent.

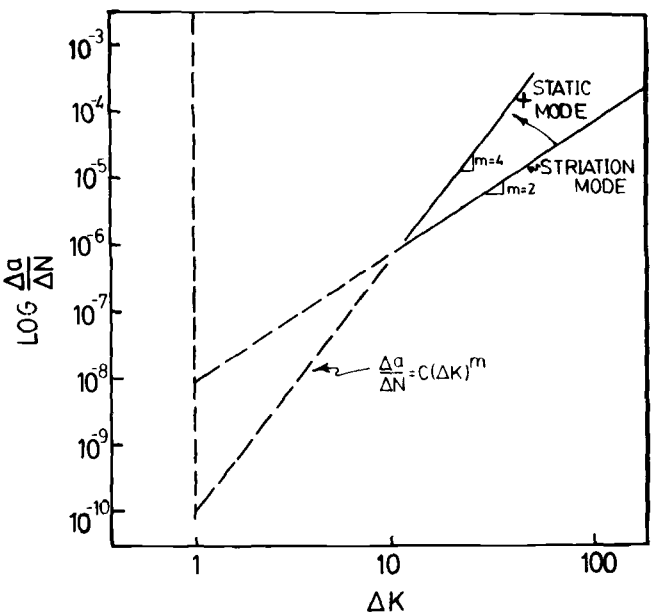

FIG. 15—*Schematic showing effect of static modes on slope* m *and* C *values.*

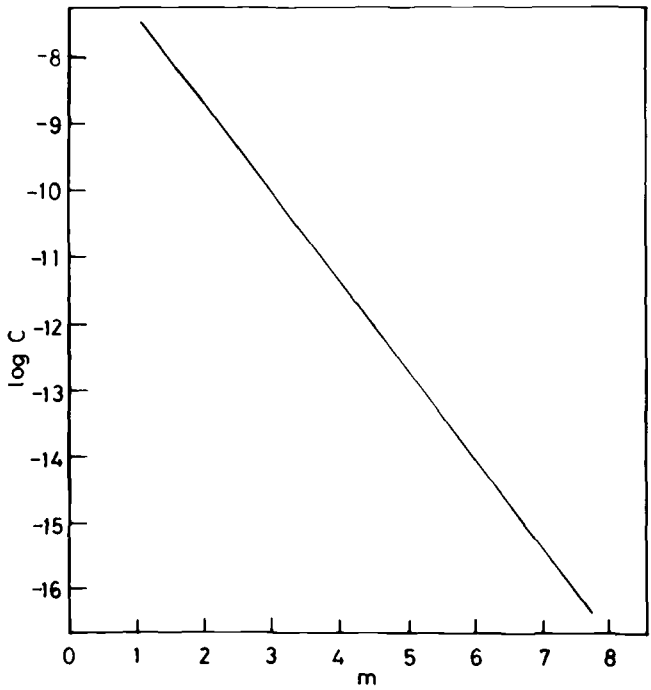

FIG. 16—*Relationship between the constants* C *and* m *of the Paris equation,* $\Delta a/\Delta N = C(\Delta K)^m$, *for a variety of steels* [67].

When extensive plastic deformation occurs, the rate of crack growth accelerates compared with linear elastic behavior [*72*], and this circumstance is nicely dealt with by means of the ΔJ-approach. It is noted that use of ΔJ is equivalent to the use of the COD concept in that for a non-work-hardening material of yield strength σ_0 the two are related by

$$\text{COD} = \frac{J}{\sigma_0} \tag{13}$$

The influence of work hardening on this relation is to reduce the level of the COD [*73, 74*]. The COD approach has been used successfully in the analysis of crack growth in steels where net section stresses approached yield and elastic-plastic conditions developed [*75*]. A main advantage of the ΔJ-approach is that values for J for different specimen configurations and strain-hardening characteristics are becoming available [*74*].

Crack Closure

As shown in Fig. 3, the concept of crack closure has been used in an attempt to rationalize fatigue crack growth behavior as a function of mean

stress [*76*] through relations of the type $\Delta K_{eff} = (0.5 + 0.4R)\Delta K$, where ΔK_{eff} is defined as $K_{max} - K_{op}$ and K_{op} is the stress intensity factor associated with opening. A number of theoretical studies have lent credence to the occurrence of closure under plane stress conditions, for example, those of Budiansky and Hutchinson [*77*] and Newman [*78*]. However, one can have doubts about the significance of closure in affecting the process of fatigue crack growth. For example, for the material of Fig. 13, though there is a strong R-effect in the low-toughness alloy, it is absent in the alloy of high toughness, a trend not anticipated in the ΔK_{eff}-approach. In the interpretation given with respect to Eq 10, however, R-effects are related to K_{cc} and the presence or absence of static modes of separation, rather than to closure. Further, studies have indicated that closure is primarily a surface layer phenomenon, as is particularly evident after an overload. If surface closure were important in affecting crack growth one might expect to find a thickness effect. However, the studies of Frost and Denton with mild steel [*79*] and those of Broek with aluminum alloys [*80*] have shown that if the crack propagates in a flat mode, there is no effect of thickness on the rate of crack growth. It also is likely that some of the data on closure effects have been obtained in the range where surface shear lips form [*76*]. In such a case, closure measured with a surface gage might be detected at a high ratio of K_{op}/K_{max} but the effective range of the cycle may not be completed at contact if the surfaces slide over each other after making contact. In fact, Hertzberg's fractograph of a slant fracture developed in fatigue (Fig. 17) [*81*] is consistent with this view. Our own work with a crack mouth gage has usually shown a fairly high ratio (>0.5) of K_{op}/K_{max} in the near-threshold region at $R = 0$, but the ratio falls off to a value on the order of 0.1 in the intermediate range of crack growth for $R = 0.05$ loading (Fig. 18), the range in which most crack growth measurements have been taken, with the closure effect decreasing with increase in R [*82*]. The high closure levels of low ΔK values are associated with a Mode II deformation process and consequent roughening of the fracture surface. More work is needed to define clearly the nature of the closure process to settle the matter, and in this regard the work of Bowles and Schijve [*83*] is of interest.

Low-Cycle Fatigue

Thus far we have discussed crack growth primarily in the LEFM range. However, since Mode I fatigue crack growth comprises a major portion of the fatigue lifetime in low cycle fatigue, we will consider analytical approaches to the determination of the low-cycle fatigue lifetime based upon crack growth.

In an initial empirical approach to the analysis fatigue crack growth in the low-cycle range [*84*], the rate of fatigue crack growth was approximated by

$$\frac{da}{dN} = (\Delta\epsilon_p)^2 a \tag{14}$$

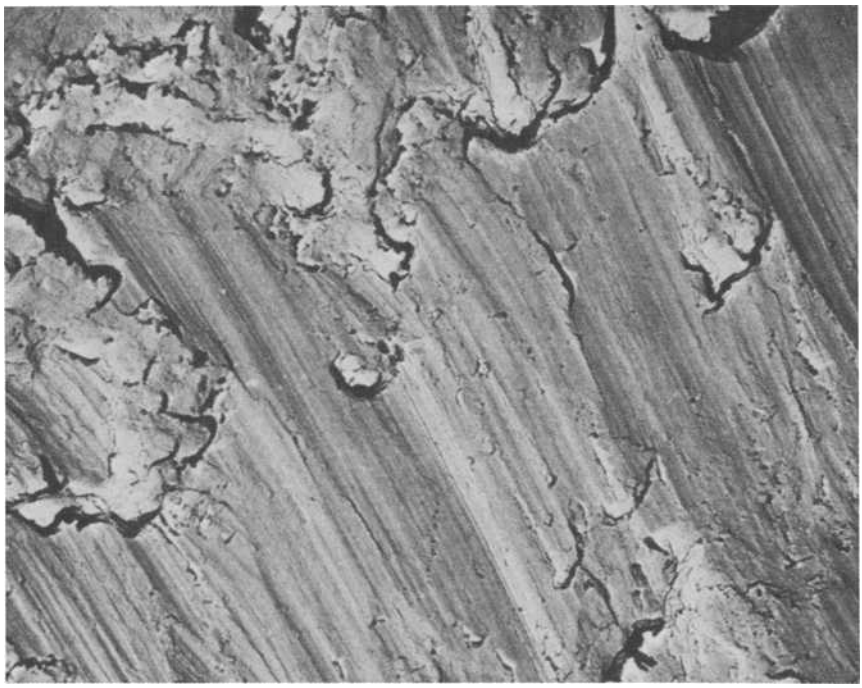

FIG. 17—*Appearance of slant fatigue fracture surface in a 2024-T3 aluminum alloy* [81].

A more considered approach to crack growth in the plastic range was developed by Tomkins [*85*], who proposed that crack advance occurred by a sliding-off process. Tomkins idealized the crack tip deformation field by two plastic hinges at ± 45 deg to the crack tip, with no deformation in the area around and within the hinges. The extent of the hinges, D, was assumed to be proportional to the Dugdale [*86*] plastic zone size for

$$D = \sqrt{2}\left(\frac{\pi^2 \sigma^2}{4T^2}\right)a \tag{15}$$

where T was taken to be the cyclic tensile strength rather than the yield strength.

With the cyclic stress and strain related by

$$\sigma = K\,\Delta\epsilon_p{}^n \tag{16}$$

the expression for D becomes

$$D = \sqrt{2}\left(\frac{\pi^2 \ell^2}{4}\,\frac{\Delta\epsilon_p{}^{2n}}{T^2}\right) \tag{17}$$

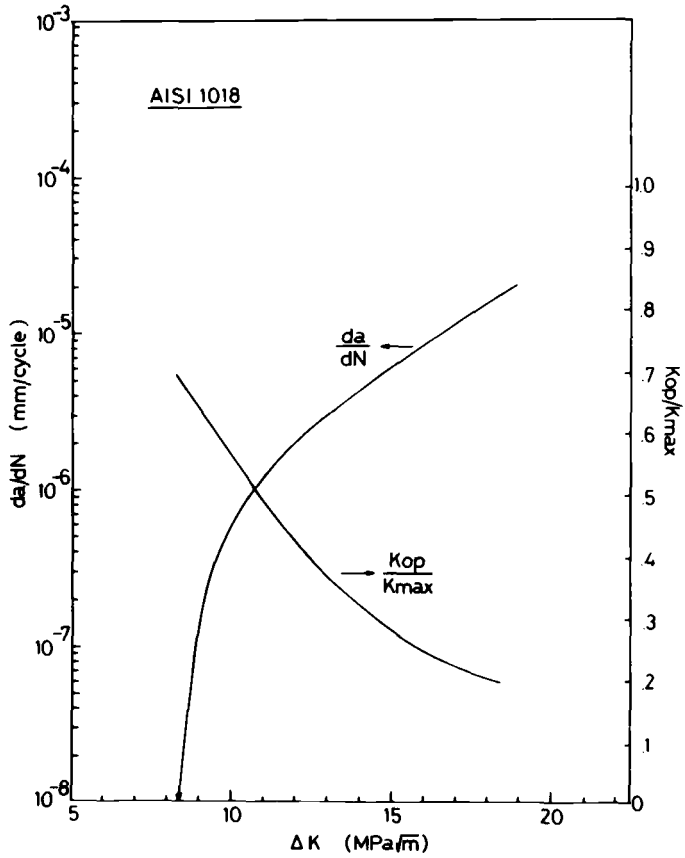

FIG. 18—*Variation of* K_{op}/K_{max} *and* da/dN *as a function of* ΔK *for AISI 1018 steel* [22].

One might expect the amount of sliding off, δ, on the plastic hinge to be proportional to the extent of the hinge; that is,

$$\delta \propto D \tag{18}$$

However, Tomkins elected to put the increment of sliding-off, $d\delta$, as

$$d\delta \simeq D d\epsilon_p \tag{19}$$

This choice allowed a simple estimate of the crack opening to be made, and this opening was related to the increment of growth per cycle. The choice does ensure that the rate of advance per cycle will be a small fraction of the plastic zone size in accord with experience. Once these assumptions are made the Tomkins expression for the rate of crack growth becomes

$$\frac{da}{dN} = \frac{\delta}{\sqrt{2}} = \frac{\pi^2}{8}\left(\frac{\Delta\sigma}{2T}\right)^2 \frac{\Delta\epsilon_p}{(2n+1)}\, a \tag{20}$$

The appeal of this approach is that it deals with a sliding-off process and incorporates the cyclic stress-strain characteristics of the material. An alternative approach which contains the same features is simply to put the rate of crack advance proportional to the CTOD [5]; that is,

$$\frac{da}{dN} = C_2 \text{CTOD} = C_2 \frac{16}{\pi} \frac{T_{1a}}{E} \ell\text{n sec} \frac{\pi}{2} \frac{\sigma}{T_1} \tag{21}$$

In the fully plastic range T_1 is taken to be the true cyclic tensile stress at necking instability given by

$$T_1 = k'(n')^{n'} \tag{22}$$

and E is taken to be the secant modulus measured from the zero stress point on the compression side of the cyclic stress-strain loop to the peak tensile stress, neglecting the elastic strain. With

$$\sigma = k'\left(\frac{\Delta\epsilon_p}{2}\right)^{n'}$$

we obtain

$$\frac{\Delta a}{\Delta N} = C_2 \text{CTOD} = C_2 \frac{16}{\pi}(n')^{n'}\left(\frac{\Delta\epsilon_p}{2}\right)^{1-n'} \times a\, \ell\text{n sec}\left[\frac{\pi}{2}\left(\frac{\Delta\epsilon_p}{2n'}\right)^{n'}\right] \tag{23}$$

Integration of this equation leads to

$$\ell\text{n}\frac{a_f}{a_i} = \frac{8}{\pi}(n')^{n'}\left(\frac{\Delta\epsilon_p}{2}\right)^{1-n'} \ell\text{n sec}\left[\frac{\pi}{2}\left(\frac{\Delta\epsilon_p}{2n'}\right)^{n'}\right] N \tag{24}$$

with the value of C_2 taken to be one half.

A comparison with Tomkins's Eq 20 can be made if we set

$$D = \frac{\pi^2}{4}\frac{\sigma^2}{T_1^2}\, a = \frac{\pi^2}{4}\frac{\left(\frac{\Delta\epsilon_p}{2}\right)^{2n'}}{n'^{2n'}}\, a \tag{25}$$

According to Eq 19 the ratio $D/(d\delta/d\epsilon_p)$ should be close to unity. For the above relation this ratio is

$$D \Big/ \frac{d\delta}{d(\Delta\epsilon_p)} = \frac{\sqrt{2}\pi}{8} \frac{1}{(1+n')} n'^{-3n'} \left(\frac{\Delta\epsilon_p}{2}\right)^{n'} \tag{26}$$

The following table lists the values of the ratio for several values of $\Delta\epsilon_p$ and typical values of n':

$\Delta\epsilon_p$	$n' = 0.1$	$n' = 0.2$
0.005	0.55	0.33
0.01	0.59	0.37
0.02	0.64	0.43

The values are fairly constant for a given value of n' and are on the order of unity, thereby lending support to Tomkins' hypothesis as evaluated by the use of the COD approach.

In making use of Eq 24 to predict the low-cycle fatigue lifetime it is necessary to integrate from an initial crack length a_i to a final crack length a_f. For a value of a_i equal to 1 μm and a value of $\Delta\epsilon_p$ of 0.01, for n' equal to 0.1 the rate of crack growth is about 2×10^{-5} mm/cycle (8×10^{-7} in./cycle). For a value of a_f equal to 5 mm the rate is higher by the ratio a_i/a_f or 5×10^3 times, so that the rate is 0.1 mm/cycle. Over this range of growth rates static modes of separation will become increasingly important. Their operation would serve to accelerate the rate of growth, decrease the fatigue lifetime, and to decrease the predicted slope on the Coffin-Manson plot. To account for static modes of separation in LCF, Eq 23 should be multiplied by a factor such as $1 + [\Delta J/(J_{cc} - J_{max})]$ by analogy with the LEFM equivalent, Eq 10. It is also noted that Kaisand and Mowbray [*87*] have developed relationships between low-cycle fatigue and fatigue crack growth rates based upon the use of the J-integral and strain energy density concepts.

Concluding Remarks

1. A review of the literature on the mechanisms of fatigue crack growth supports a mechanism of crack advance by a sliding-off process. Cyclic loading can either harden or soften the cyclic plastic zone to influence the sliding-off process, but no evidence for a specific form of cyclic damage was uncovered. Static modes of separation can accelerate the rate of crack growth, particularly as the cyclic fracture toughness is approached.

2. Since the extent of sliding-off in a cycle is related to the CTOD, an analytical approach can be developed. From the hysteresis loops for axially loaded specimens, elastic and plastic ranges can be determined and the crack growth behavior in terms of the elastic and plastic components can be expressed as

$$\frac{\Delta a}{\Delta N} = \left(\frac{\Delta a}{\Delta N}\right)_e + \left(\frac{\Delta a}{\Delta N}\right)_p$$

where

$$\left(\frac{\Delta a}{\Delta N}\right)_e = \frac{A}{E^2}(\Delta K - \Delta K_{TH})^2\left(1 + \frac{\Delta K}{K_{cc} - K_{max}}\right)$$

and

$$\left(\frac{\Delta a}{\Delta N}\right)_p = \frac{8}{\pi}(n')^{n'}\left(\frac{\Delta \epsilon_p}{2}\right)^{1-n'} \ell n \sec\left[\frac{\pi}{2}\left(\frac{\Delta \epsilon_p}{2n'}\right)^{n'}\right] f(J_{cc})$$

3. For nonuniformly loaded specimens such as the compact specimen the use of the ΔJ-approach appears to be most useful, particularly since J-determinations for a variety of standard specimen types are now available.

Acknowledgments

The constructive comments of a number of colleagues, namely Drs. S. D. Antolovich, D. L. Davidson, N. E. Dowling, K. Katagiri, J. Lankford, H. W. Liu, D. F. Mowbray, P. Neumann, B. Tomkins and J. R. Weertman, are gratefully acknowledged, as is the support provided by the Air Force Office of Scientific Research, Grant No. 81-0046.

References

[1] Forsyth, P. J. E. and Ryder, D. A., *Metallurgica*, Vol. 63, March 1961, pp. 117-124.
[2] *Fatigue Crack Propagation, ASTM STP 415*, American Society for Testing and Materials, 1967.
[3] Paris, P. C., Gomez, M. P., and Anderson, W. E., *The Trend in Engineering*, Univ. of Washington, Seattle, Vol. 13, No. 1, 1961, p. 9.
[4] Aita, C. R. and Weertman, J., *Metallurgical Transactions*, Vol. 10A, 1979. p. 535.
[5] McEvily, A. J. in *Proceedings*, Third International Conference on the Strength of Metals and Alloys, Vol. 2, Inst. of Metals, Cambridge, Eng., 1973, p. 204.
[6] Dowling, N. E. in *Cyclic Stress-Strain and Plastic Deformation Aspects of Fatigue Crack Growth, ASTM STP 637*, American Society for Testing and Materials, 1977, pp. 97-121.
[7] Elber, W. in *Damage Tolerance in Aircraft Structures, ASTM STP 486*, American Society for Testing and Materials, 1971, pp. 230-242.
[8] Laird, C. and Smith, G. C., *Philosophical Magazine*, Vol. 8, 1963, p. 1945.
[9] Laird, C. in *Fatigue Crack Propagation, ASTM STP 415*, American Society for Testing and Materials, 1967, p. 131.
[10] McEvily, A. J., Boettner, R. C., and Johnston, T. L. in *Fatigue: An Interdisciplinary Approach*, J. J. Burke and V. Weiss, Eds., Syracuse Univ. Press, Syracuse, N.Y., 1964, p. 95.
[11] Wanhill, R. J. H., *Metallurgical Transactions*, Vol. 6A, 1975, p. 1587.
[12] Lynch, S. P. in *Fatigue Mechanisms, ASTM STP 675*, American Society for Testing and Materials, 1979, pp. 174-213.
[13] McEvily, A. J. and Boettner, R. C., *Acta Metallurgica*, Vol. 11, 1963, p. 725.
[14] Pelloux, R. M. N., *Transactions of ASM*, Vol. 62, 1969, p. 281.
[15] Neumann, P., *Acta Metallurgica*, Vol. 17, 1969, p. 1219.
[16] Neumann, P., *Acta Metallurgica*, Vol. 22, 1974, p. 1155.
[17] Mowbray, D. F., private communication, 1982.
[18] Neumann, P., Verhoff, H., and Fuhlrott, H. in *Fracture 1977*, Proceedings of Fourth International Conference on Fracture, Univ. of Waterloo Press, Waterloo, Ont., Canada, Vol. 2, 1977, p. 1313.
[19] Martin, D. E., ASME Paper No. 65 — Met. 5, 1965.

[20] Kikukawa, M., Jono, M., and Adachi, M. in *Fatigue Mechanisms, ASTM STP 675*, American Society for Testing and Materials, 1979, pp. 234-253.
[21] Buck, O., Frandsen, J. D., Ho, C. L., and Marcus, H. L. in *Proceedings*, Third International Conference on the Strength of Metals and Alloys, Vol. 1, 1973, Inst. of Metals, Cambridge, Eng., p. 462.
[22] Minakawa, K. and McEvily, A. J. in *Fatigue Thresholds*, J. Bäcklund et al, Eds., Proceedings of the First International Conference on Fatigue Thresholds, EMAS Ltd., U.K., Vol. 1, 1981, p. 373.
[23] McClintock, F. A. in *Fatigue Crack Propagation, ASTM STP 415*, American Society for Testing and Materials, 1967, p. 170.
[24] Schijve, J., Report LR-240, Delft Univ. of Technology, Delft, The Netherlands, Jan. 1977.
[25] Was, G. S. and Pelloux, R. M., *Metallurgical Transactions A*, Vol. 10A, 1979, p. 656.
[26] Wilhelm, M., Nageswararao, M. and Meyer, R. in *Fatigue Mechanisms, ASTM STP 675*, American Society for Testing and Materials, 1979, pp. 214-233.
[27] Robinson, J. N. and Tetelman, A. S. in *Fracture Toughness and Slow-Stable Cracking, ASTM STP 559*, Part 1, American Society for Testing and Materials, 1974, pp. 139-158.
[28] Rice, J. R. in *Fatigue Crack Propagation, ASTM STP 415*, American Society for Testing and Materials, 1967, p. 247.
[29] Gabrielli, F. and Pelloux, R. M., *Metallurgical Transactions*, Vol. 13A, 1982, p. 1083.
[30] Tomkins, B. and Biggs, W. D., *Journal of Materials Science*, Vol. 4, 1969, p. 544.
[31] Lankford, J. and Kusenberger, F. N., *Philosophical Magazine*, Vol. 26, 1972, p. 1485.
[32] Tomkins, B., *Transactions of ASME*, Vol. 97, Series H, 1975, p. 289.
[33] Kuo, A. S. and Liu, H. W., *Scripta Metallurgica*, Vol. 10, 1976, p. 723.
[34] Weertman, J., *Three Dimensional Constitutive Relations and Ductile Fracture*, S. Nemat-Nasser, Ed., North-Holland, Leyden, The Netherlands, 1981, p. 111.
[35] Donahue, R. J., Clark, H. M., Atanmo, P., Kumble, R., and McEvily, A. J., *International Journal of Fracture Mechanics*, Vol. 8, 1972, p. 209.
[36] Bowles, C. Q., Report LR-270, Delft University of Technology, Delft, The Netherlands, May 1978.
[37] Davidson, D. L. in *Fatigue Mechanisms, ASTM STP 675*, American Society for Testing and Materials, 1979, pp. 254-275.
[38] Davidson, D. L. and Lankford, J., this publication, pp. 371-399.
[39] Katagiri, K., Awatani, J., Omura, A., Koyanagi, K., and Shiraishi, T. in *Fatigue Mechanisms, ASTM STP 675*, American Society for Testing and Materials, 1979, pp. 106-128.
[40] Katagiri, K., Omura, A., Koyangi, K., Awatani, J., Shiraishi, T. and Kaneshiro, H., *Metallurgical Transactions*, Vol. 8A, 1977, p. 1769.
[41] Katagiri, K., Omura, A., Koyanagi, K., Awatani, J., Shiraishi, T., and Kaneshiro, H. in *Fracture 1977*, Proceedings of the Fourth International Conference on Fracture, University of Waterloo Press, Waterloo, Ont., Canada, Vol. 2, 1977, p. 695.
[42] Bathias, C. and Pelloux, R. M., *Metallurgical Transactions*, Vol. 4, 1973, p. 1265.
[43] Yokobori, T. in *Fatigue Mechanisms, ASTM STP 675*, American Society for Testing and Materials, 1979, pp. 683-706.
[44] Head, A. I., *Philosophical Magazine*, Vol. 44, 1953, p. 925.
[45] Frost, N. E., and Dugdale, D. S., DSIR. MERL Rep. No. PM218, 1957.
[46] Liu, H. W., *Journal of Basic Engineering, Transactions of ASME*, Vol. 83, 1961, p. 23.
[47] Paris, P. C. and Erdogan, F., *Transactions of ASME, Series D*, Vol. 85, 1963, p. 528.
[48] McClintock, F. A. in *Fracture of Solids*, D. C. Drucker and J. J. Gilman, Eds., Interscience Publishers, New York, 1963, p. 65.
[49] Weertman, J. in *Proceedings*, First International Conference on Fracture, Sendai, Japan, Vol. 1, 1965, p. 153.
[50] Bilby, B. A., Cottrell, A. H., and Swinden, K. H., *Proceedings of the Royal Society*, Vol. 272A, 1963, p. 304.
[51] Weertman, J. in *Fatigue and Microstructure*, ASM, Metals Park, Ohio, 1979, p. 279.
[52] Cottrell, A. H. in *Fracture*, B. L. Averbach, D. K. Felbeck, G. T. Hahn, and D. A. Thomas, Eds., Wiley, New York, 1959, p. 20.
[53] Orowan, E., Nye, J. F., and Cairns, W. J., *Strength and Testing of Materials*, Part I, H.M. Stationery Office, London, 1952, p. 127
[54] Garrett, G. G. and Knott, L. F., *Metallurgical Transactions*, Vol. 7a, 1976, p. 884.
[55] Liu, H. W. and Kobayashi, H., *Scripta Metallurgica*, Vol. 14, 1980, p. 525.

[56] Majumdar, S. and Morrow, J. in *Fracture Toughness and Slow-Stable Cracking, ASTM STP 559*, American Society for Testing and Materials, 1974, pp. 159–182.
[57] Liu, H. W. and Iino, N. in *Proceedings*, Second International Conference on Fracture, Chapman and Hall, London, 1969, p. 812.
[58] Weertman, J., Lin, I.-H., and Thomson, R., to be published in *Acta Metallurgica*.
[59] Frost, N. E., Marsh, K. J., and Pook, L. P., *Metal Fatigue*, Clarendon Press, Oxford, 1974.
[60] Bates, R. C. and Clark, W. G., *Transactions of ASM*, Vol. 62, 1969, p. 380.
[61] Frost, N. E. and Dixon, J. R., *International Journal of Fracture Mechanics*, Vol. 3, 1967, p. 301.
[62] Pook, L. P. and Frost, N. E., *International Journal of Fracture*, Vol. 9, 1973, p. 53.
[63] Minakawa, K. and McEvily, A. J., *Scripta Metallurgica*, Vol. 15, 1981, p. 633.
[64] McEvily, A. J. in *Mechanical Failure: Definition of the Problem*, NBS Special Publication 425, Washington, D.C., 1976, p. 13.
[65] McEvily, A. J. and Groeger, J. in *Fracture 1977*, Proceedings of the Fourth International Conference on Fracture, Waterloo, Ont., Canada, Vol. 2, 1977, p. 1293.
[66] Roman, I., Ono, K., and Tetelman, A. S., *Engineering Fracture Mechanics*, Vol. 14, 1981, p. 155.
[67] Ritchie, R. O. and Knott, J. F., *Acta Metallurgica*, Vol. 21, 1973, p. 639.
[68] Morris, W. L., James, M. R., and Buck, O., *Engineering Fracture Mechanics*, to be published.
[69] Taira, S., Tanaka, K., and Hoshina, M. in *Fatigue Mechanisms, ASTM STP 675*, American Society for Testing and Materials, 1979, pp. 135–173.
[70] Dowling, N. E. and Begley, J. A. in *Mechanics of Crack Growth, ASTM STP 590*, American Society for Testing and Materials, 1976, pp. 82–103.
[71] Mowbray, D. F. in *Cracks and Fracture, ASTM STP 601*, American Society for Testing and Materials, 1976, pp. 33–46.
[72] Paris, P. C., Bucci, R. J., Wessel, E. T., Clark, W. G., and Mager, T. R. in *Stress Analysis and Growth of Cracks, ASTM STP 513*, American Society for Testing and Materials, 1972, pp. 141–176.
[73] Rice, J. R. in *Fracture*, H. Liebowitz, Ed., Vol. 2, Academic Press, New York, 1968, p. 191.
[74] Shih, C. F., Andrews, W. R., de Lorenzi, H. G., German, M. D., Van Stone, R. H., and Mowbray, D. F., "Methodology for Plastic Fracture," EPRI Report NP-1735, March 1981.
[75] McEvily, A. J., Beukelmann, D., and Tanaka, K. in *Strength and Structure of Solid Materials*, H. Miyamoto et al, Eds., 1976, Noordhof, The Netherlands, p. 265.
[76] Elber, W., *Engineering Fracture Mechanics*, Vol. 2, 1970, p. 37.
[77] Budiansky, B. and Hutchinson, J. W., *Transactions of ASME, Series A*, Vol. 45, 1978, p. 267.
[78] Newman, J. C., Jr., in *Mechanics of Crack Growth, ASTM STP 590*, American Society for Testing and Materials, 1976, pp. 281–301.
[79] Frost, N. E. and Denton, K., *Journal of Mechanical Engineering Science*, Vol. 3, 1961, p. 295.
[80] Broek, D., *Elementary Engineering Fracture Mechanics*, Noordhof, The Netherlands, 1974, p. 238.
[81] Hertzberg, R. W., in *Fatigue Crack Propagation, ASTM STP 415*, American Society for Testing and Materials, 1967, p. 205.
[82] Minakawa, K. and McEvily, A. J. in *Strength of Metals and Alloys*, Proceedings of the Sixth International Conference on the Strength of Metals and Alloys, Pergamon Press, Elmsford, N.Y., Vol. 2, 1982, p. 845.
[83] Bowles, C. Q. and Schijve, J., this publication, pp. 400–426.
[84] Boettner, R., Laird, C., and McEvily, A. J., *Transactions of AIME*, Vol. 233, 1965, p. 379.
[85] Tomkins, B., *Philosophical Magazine*, Vol. 18, 1968, p. 1041.
[86] Dugdale, D. S., *Journal of the Mechanics and Physics of Solids*, Vol. 8, 1960, p. 100.
[87] Kaisand, L. R. and Mowbray, O. F., *Journal of Testing and Evaluation*, Vol. 7, 1979, p. 270.
[88] Creager, M. and Sommer, A. W., Technical Report AFML-TR-77-193, Nov. 1977.

J.-P. Baïlon[1] *and Stephen D. Antolovich*[2]

Effect of Microstructure on Fatigue Crack Propagation: A Review of Existing Models and Suggestions for Further Research

REFERENCE: Baïlon, J.-P. and Antolovich, S. D., **"Effect of Microstructure on Fatigue Crack Propagation: A Review of Existing Models and Suggestions for Further Research,"** *Fatigue Mechanisms: Advances in Quantitative Measurement of Physical Damage, ASTM STP 811*, J. Lankford, D. L. Davidson, W. L. Morris, and R. P. Wei, Eds., American Society for Testing and Materials, 1983, pp. 313-349.

ABSTRACT: Systematic improvements in the fatigue crack propagation (FCP) properties of metal alloys through combinations of heat treatment, processing, and composition control depend on identifying the basic processes and parameters that are involved. Towards that end, numerous models have been developed. These models generally fall into three classes: (*1*) macroscopic, in which bulk properties are used to fit a modified Paris equation; (*2*) microscopic, in which dislocation deformation processes are incorporated into a criterion for crack advance; and (*3*) low-cycle fatigue (LCF) based, in which crack propagation is assumed to result from failure of a microscopic LCF ligament defining a process zone directly ahead of the propagating crack. This paper reviews the basic assumptions underlying these models. Their implications are discussed and compared with experimental data, both numerical and microstructural. Various experimental procedures are reviewed and some suggestions are made for research that could be used to verify the validity of these models.

KEY WORDS: fatigue crack propagation, low-cycle fatigue, fatigue models, microstructure, fatigue damage dislocations, nickel-base superalloys, copper alloys, aluminum alloys, steels

Nomenclature

E Young's modulus
G Shear modulus

[1]Department of Metallurgical Engineering, Ecole Polytechnique, Montreal, Quebec, Canada.
[2]Director and Professor of Metallurgy, Fracture and Fatigue Research Laboratory, Georgia Institute of Technology, Atlanta, Ga. 30332.

σ_{ys} Yield strength
σ_{yc} Cyclic yield strength
σ_u Ultimate tensile strength
ϵ_f True fracture strain
$\epsilon_{f'}$ Fatigue ductility
n Strain-hardening exponent
n' Cyclic strain-hardening exponent
K_{IC} Plane strain fracture toughness
G_{IC} Plane strain crack extension force
ΔK $K_{max} - K_{min}$ in a fatigue cycle
ΔK_{th} Threshold stress intensity
R Load ratio (minimum load/maximum load)
a Crack length
K_c Plane stress fracture toughness
R_p^f Reversed plastic zone size
N_i, N_f Cycles to initiation, cycles to failure
$\Delta\epsilon_p$ Plastic strain range
ρ Crack tip radius of curvature

In most structures, especially large structures involving fabrication processes such as welding and riveting, cracks or crack-like defects are likely to be present. In one study 700 cracks were found in the skin of the underside of an aircraft wing [*1*].[3] Modern design practice is to consider the rate at which these flaws grow to some specified failure condition in order to determine the cyclic life, and in recent years considerable effort has been expended to develop experimental and analytical methodologies to reach this goal. A prime impetus for this approach has been the U.S. Air Force, and numerous Air Force reports are available on this subject. The engineering aspects of the problem such as nondestructive inspection (NDI), finite element stress analyses, and stress intensity parameter solutions have been advanced to the point where the concept of "retirement for cause" has become an attainable goal [*2*]. The basic idea of the concept is that critical components, such as disks in jet engines, will be removed from service only when the damage state as exemplified by crack size becomes critical.

From the preceding comments it is obvious that improved fatigue crack propagation (FCP) resistance is desirable since in many applications the life is FCP limited. While the *engineering* aspects of the problem appear to be reasonably well under control, the same cannot be said about the current level of understanding of the basic processes that cause a crack to propagate in fatigue. Yet a fundamental understanding of these processes must be developed if improvements in FCP behavior are to be put on a rational basis and not merely result from empirical approaches. The most fundamental ap-

[3]The italic numbers in brackets refer to the list of references appended to this paper.

proach to improving FCP behavior in alloys is to develop models in which the microstructural parameters that control fatigue are identified. These models, if in agreement with experimental results, can then be used as a guide in developing fatigue-resistant alloy systems.

In this paper we will review various models that have been proposed and which are representative of a general philosophy or approach. We will then compare these models with available experimental data and identify what further information is necessary to either substantiate or refute these models.

Description of FCP Models

A model for FCP should ideally take into account the influence of all the parameters that affect the propagation of a fatigue crack in a given material under given conditions. Unfortunately, such a comprehensive model has not yet been developed, primarily because of the large number of parameters involved. These parameters may be divided into two classes: the first includes "intrinsic" parameters which characterize the material itself (E, G, σ_{ys}, σ_{yc}, σ_u, ϵ_f, ϵ_f', n, n', K_{IC}, ΔK_{th}, ...), the second being the "extrinsic" parameters such as temperature, frequency, environment, specimen geometry, K_{max}, K_{min}, ΔK, R-ratio, overload ratio, etc. Careful and systematic experimental studies of the dependence of FCP on these numerous parameters requires a great effort, the success of which in developing an ideal model is absolutely without guarantee. Scientists and engineers must critically design and carry out some specific experiments and then compare the experimental data with the models. The models may vary from purely empirical to very fundamental. In this paper we have arbitrarily decided to divide the large spectrum of models into three parts: (*1*) phenomenological models, developed essentially on an empirical basis, of which crack tip opening displacement (CTOD) models are representative; (*2*) dislocation-based models, which give a specific process for crack advance in term of a micromechanism; and (*3*) models based on the micro low-cycle fatigue (LCF) process, which try to correlate FCP to LCF.

Each class will be briefly presented using typical examples, and the most salient characteristics of the class will be pointed out. It is not our intent to present an exhaustive compilation of all the models, since in the interest of clarity and brevity we have attempted to simplify the original analyses and have deliberately omitted numerous related models which differ only slightly. Recent proceedings of seminars or conferences devoted to this subject are available and the reader is invited to refer to them (for example, Refs *3* to *5*).

Phenomenological Models

Looking back on the historical development of FCP models, one may easily discern two distinctive periods, the B.P. and A.P. eras (before and after Paris), the watershed between them being 1963.

Before this date, FCP was generally treated in terms of extrinsic parameters such as crack length (a), applied stress (σ), mean stress (σ_m), and R-ratio. An example of such models is that proposed by Schijve [*6*]:

$$da/dN = C\sigma^m a^p \tag{1}$$

where C, m, and p are experimental constants.

Other authors have attempted to incorporate the influence of some intrinsic parameters in their equations, as done by Weertmen [*7*]:

$$da/dN = \frac{C\sigma^2 a}{E\,G_{Ic}\,\sigma_u{}^2} \tag{2}$$

or by McEvily and Johnston [*8*]:

$$da/dN = \left\{\sigma\sqrt{a}\Big/\left[\left(\frac{\sigma_{ys} + \sigma_u}{2}\right)\epsilon_u\,\sigma_u{}^2 E\right]^{1/4}\right\}^m \tag{3}$$

In 1963, Paris and Erdogan [*9*] applied the recently developed concepts of linear elastic fracture mechanics (LEFM) to FCP and suggested that the experimental data fit the empirical equation

$$da/dN = C\Delta K^m \tag{4}$$

where C and m are constants, and ΔK is the stress intensity parameter range.

Since this date, the development and refinement of LEFM concepts [*10*] as well as the accumulation of numerous experimental data have encouraged many investigators to propose modified forms of Eq 4. It was soon recognized that Eq 4 is only valid in a limited range of ΔK-values, bounded at high ΔK by K_{max_c}, the critical value of specimen toughness, and at low ΔK by ΔK_{th}, the threshold stress intensity factor below which a long fatigue crack appears not to propagate. K_{max_c} and ΔK_{th} are therefore the asymptotic limits of Eq 4.

Many further attempts were made in order to take into account the influence of extrinsic and intrinsic parameters (such as R-ratio, E, σ_{ys}, σ_{yc}, etc.) on da/dN.

To illustrate this point, Masounave et al in 1978 [*11*] have compiled over 40 modified versions of Eq 4. Among them are the following examples:

Forman's equation [*12*]:

$$da/dN = \frac{C\Delta K^m}{(1 - R)K_c - \Delta K} \tag{5}$$

The agreement between this equation and experimental data appears to be fair, especially for aluminum alloys.

Nicholson's equation [*13*]:

$$da/dN = A\frac{(\Delta K - \Delta K_{th})^m}{(K_c - K_{max})} \tag{6}$$

Frost/Dixon equation [*14*]:

$$da/dN = \frac{C}{\sigma_{ys}E}[\Delta K - \Delta K_{th}]^2\left[1 + \frac{\Delta K}{K_{Ic} - K_{max}}\right] \tag{7}$$

Mention should also be made of empirical models [*15,16*] proposed to take into account the phenomenon of crack closure as revealed by Elber's work [*17*].

Dislocation-Based Models

Weertman's Model—Among the different models proposed by Weertman [*18*], the one which gives rise to an accumulated plastic work criterion will be briefly presented.

The basic assumption is that a fatigue crack will grow an incremental length δa if a critical value D_c of the accumulated displacement is reached. D_c is given by the equation

$$D_c = \sum_n |D_n| \tag{8}$$

where D_n is the displacement increment that occurs across the crack plane at a fixed point in a stationary coordinate system during the n^{th} cycle.

Weertman assumes that the dependence of plastic displacement on the distance from the crack tip is approximately given by a linear relationship

$$D(x) = (2K^2/\pi\sigma_{ys}{}^2G)\,[1 - (\pi\sigma_{ys}{}^2x/K^2)] \tag{9}$$

where

$D(x)$ = plastic displacement at a point located at a distance x in front of the crack tip on the crack plane,
σ_{ys} = monotonic yield stress,
G = shear modulus, and
K = stress intensity factor.

Equation 2 is in fact an approximation derived from the BSC-Dugdale model of the plastic zone. Since the BSC-Dugdale model for the plastic zone is based on the continuous dislocation formalism (not crystal dislocation theory), Weertman's model can thus be classified as a dislocation-based model for fatigue crack growth.

If Eq 9 is substituted into Eq 8 with the assumption that $\delta a \ll R_0$ (R_0 is the plastic zone size) so that the summation in Eq 1 can be replaced with an integration, the following equation is obtained for push-pull loading ($R = -1$):

$$D_c = \left(\frac{2K^2/\pi\sigma_{ys}G}{\delta a/2}\right)[2x_0 - (\pi s_{ys}^2/K^2)\,x_0R_0] \tag{10}$$

Since the center of the plastic zone is located at $x = x_0 = R_0/2 = \frac{1}{2}(\pi K^2/8\sigma_{ys}^2)$ for the BSC-Dugdale model and for a crack in a perfectly plastic solid, Eq 10 can thus be rewritten as

$$da/dN = \Delta K^4/8\pi^2 G\sigma_{ys}^3 D_c \tag{11}$$

which is valid even if the loading is not push-pull.

In the case where the material is not perfectly plastic and is characterized by a strain-hardening exponent $n \neq 0$, the center of the plastic zone is given by

$$x_0 = R_0(1 - n)/2(1 + n) \tag{12}$$

and the crack growth rate is then given by

$$da/dN = \Delta K^4(1 - n)/8(1 + n)\pi^2 G\sigma_{ys}^3 D_c \tag{13}$$

Equations 11 and 13 indicate that an accumulated displacement criterion leads to a 4th-power Paris equation. Such a criterion is in fact equivalent to an accumulated plastic work criterion, since the plastic work U done per unit distance of crack advance is equal to $D_c\sigma_{ys}$. Hence Eqs 11 and 13 take the simplified form

$$da/dN = A\Delta K^4/G\sigma_{ys}^2 U \tag{14}$$

where A is a constant which depends on the strain-hardening behavior of material.

Fine and co-workers [*19-21*] have attempted to measure directly the energy term U, employing very small strain-gages glued in front of the crack tip or very near the crack path. For several materials (aluminum alloys, steels, and Ni-7Al), the experimental values of A are in the range of 1.6 to 6.3×10^{-3}, which is two to ten times lower than the predicted theoretical value ($\frac{1}{8}\pi^2$ for $n = 0$).

Yokobori's Model—The approach employed by Yokobori for the development of a dislocation-based model of fatigue crack growth is essentially summarized in Ref *22*. This analysis is based on a treatment of the instability of

dislocation emission from the crack tip and on dislocation group dynamics, taking into account the macro fracture mechanics concept.

As a first step, Yokobori and co-workers consider the balance of three forces (applied shear stress, image force, and ledge force) acting on a dislocation segment lying near the crack tip on a glide plane under Mode I. They conclude that spontaneous generation of dislocations will occur for very small values of K_I ($K_I > 1.07$ MPa $\sqrt{m}$ for iron and $K_I > 0.26$ MPa $\sqrt{m}$ for aluminum).

Furthermore, the authors show that the emission of dislocation loops will be spontaneous (that is, no activation energy). Thus it is concluded that, both in body-centered-cubic (BCC) and face-centered-cubic (FCC) metals, dislocation emission is spontaneous during the tensile cycle for the case of a crack under alternating stress, and fatigue blunting will occur under Mode I opening.

With the assumption that the FCP rate is equal to half of the crack-opening displacement (COD), which is equal to $2nb$ where b is the Burgers vector and n is the number of dislocations emitted from the crack tip, the FCP rate is given by

$$da/dN = nb \tag{15}$$

The number n of emitted dislocations is calculated according to dislocation group dynamics and is equal to

$$n = \gamma(p)\left(\frac{4fb}{v_0}\right)^{-(p+1/p+2)}\left(\frac{\tau_0^*}{G}\right)^{-(p(p+1)/p+2)}\left(\frac{\tau_a}{G}\right)^{(p+1)^2/p+2} \tag{16}$$

for large values of n, where

f = loading frequency,
τ_a = applied shear stress,
G = shear modulus,
p = the exponent on the stress in the equation for dislocation velocity,
v = $v_0\,(\tau_a/\tau_0^*)^p$ in which $v_0 = 1$ cm/s and
τ_0^* = the stress required to give $v = 1$ cm/s for the dislocation, and
$\gamma(p)$ = dimensionless parameter depending on p.

Assuming that the applied stress near the crack tip is averaged over some distance s and the applied shear stress $\tau_a = \Delta K_I/\sqrt{s}$, then combining Eqs 15 and 16 gives

$$da/dN = b\gamma(p)\left(\frac{4fb}{v_0}\right)^{-(p+1/p+2)}\left(\frac{\tau_0^*}{G}\right)^{-(p(p+1)/p+2)}\left(\frac{\Delta K_I}{G\sqrt{s}}\right)^{(p+1)^2/p+2} \tag{17}$$

Equation 17 is only valid for a perfectly plastic material. For strain-hardening materials the applied stress τ_a in Eq 16 is replaced by

$$\sigma = f(n')\sigma_{cy}\left(\frac{\Delta K}{\sigma_{cy}\sqrt{s}}\right)^{2n'/1+n'} \tag{18}$$

where

σ_{cy} = initial cyclic yield stress,
n' = cyclic strain-hardening exponent, and
$f(n')$ = some function of n'.

Thus the FCPR becomes

$$da/dN \propto \left(\frac{\Delta K}{\sigma_{cy}\sqrt{s}}\right)^{2n'(p+1)^2/(1+n')(p+2)} \tag{19}$$

Yokobori has also extended the theory to the case in which the COD has some finite value at the instant of tensile stroke. The following equation is obtained:

$$da/dN \propto \left(\frac{\Delta K}{\sigma_{cy}\sqrt{s}}\right)^{2n'(p+1)^2/(1+n')(p+2)+1/1+n'} \tag{20}$$

From Eqs 19 and 20, it can be concluded that m, the exponent of Paris's equation, should depend on fundamental deformation behavior as characterized by the strain rate exponent p and the strain-hardening behavior of material. For $p = 4$ to 10 and $n' = 0.08$ to 0.3, calculated values of m are in the range of 0.6 to 5.

Gerberich and Moody [*23*] found fair agreement between calculated and experimental values of m for pure iron and some iron alloys tested at room and low temperatures.

Models Based on a Micro Crack Tip LCF Process

General Comments—One point of view that has been proposed is that FCP is caused by damage accumulation in small elements ahead of the main crack that are subjected to reversed yielding. The crack then advances by some distance when sufficient damage has been accumulated, the distance generally being termed the "process zone" in which the micro LCF process is presumed to operate. The notion appears to have been put forth by McClintock [*24*] without any interpretation as to the significance of the process zone. Other investigators have made modifications of this basic idea and in particular have tried to attach microstructural significance to the process zone concept [*25-28*]. In the following section examples of LCF-based FCP

models are reviewed. In later sections of the paper their implications are pointed out and they are compared with available experimental data. Finally, their strengths and weaknesses are discussed and further experimental approaches are suggested.

Specific Models

Antolovich/Saxena/Chanani—Following some earlier work by McClintock [*24*], in this model [*25*] the LCF process is assumed to occur in some region "ℓ" ahead of the main crack and the crack advances "ℓ" units in ΔN cycles, where ΔN represents the number of cycles to crack initiation[4] at an average plastic strain range $\Delta\epsilon_p$ in the process zone. The plastic strain is related to the stress intensity parameter using the Mode I analogy of the Hull-McClintock Mode III solution for plastic strain as a function of plastic zone size and distance. This is essentially a modification of an earlier model put forth by two of the authors [*26*] in which some of the restrictions in the Coffin-Manson equation, process zone shape and crack tip singularly are removed. For a given plastic strain range (zero-tension-zero) the "life" of the element is calculated from the Coffin-Manson equation

$$(\Delta N_i)^\beta \Delta\epsilon_p = C_0 \epsilon_f' \tag{21}$$

where

ΔN_i = cycles to initiate crack in process zone,
$\Delta\epsilon_p$ = plastic strain range,
ϵ_f' = fatigue ductility, and
C_0 = constant.

Going through the indicated operations, the following equation results:[5]

$$\frac{da}{dN} = \frac{C}{(\sigma_{yc}' \epsilon_f' E)^{1/\beta}} \cdot \frac{1}{\ell^{1/\beta - 1}} \cdot \Delta K^{2/\beta} \tag{22}$$

[4]In the initial paper it was suggested that ΔN was associated with the number of cycles to failure in a macroscopic LCF test. This is not consistent and the model is modified in this paper in this respect.

[5]In the original model a crack sharpness parameter S was included to accommodate reversed plastic zone sizes R_p^f that did not follow

$$R_p^f = A\left(\frac{\Delta K}{\sigma_{ys'}}\right)^2$$

This term should be small and is not generally available in any event. For purposes of this paper it is assumed to be zero.

where

σ'_{yc} = cyclic yield,
E = Young's modulus,
C = constant,

and all other parameters are as previously defined.

Lanteigne and Baïlon—Lanteigne and Baïlon [27] have developed a model whose primary objective is to take into account the existence of the threshold stress intensity factor ΔK_{th} for FCP.

The basic assumptions of this model are as follows:

1. The crack tip is assumed to be a semicircular notch with a finite radius ρ.
2. Incremental crack growth occurs within a distance $\simeq 4\rho$ from the crack tip. This value is deduced from LEFM analysis, which indicates that the triaxiality factor reaches its maximum value at this distance.
3. The dependence of the strain gradient amplitude on ΔK ahead of the crack tip is then calculated.
4. The rate of FCP is given by

$$da/dN = 4\rho/N_f \tag{23}$$

where N_f is the number of cycles required to produce incremental crack growth along the distance 4ρ for a plastic strain range $\Delta\epsilon_p$ at the crack tip. N_f is given by the Manson-Coffin relation[6]

$$\Delta\epsilon_p \cdot N_f^{\beta} = \frac{\epsilon_f'}{2} \tag{24}$$

5. The existence of ΔK_{th} is taken into account by assuming that N_f is sufficiently high for da/dN to be less than 10^{-8} to 10^{-7} mm/cycle. In other words, there exists a critical value $\Delta\epsilon_0$ of the strain amplitude at the crack tip which does not contribute to damage responsible for crack growth.

According to this model, the FCPR is given by

$$da/dN = \frac{4}{\rho^{1/\beta-1}} \left[\frac{0.2(1-\nu^2)(\Delta K^2 - \Delta K_{th}^2)}{\pi\sqrt{3}\, CE\sigma_{ys}\epsilon_f'} \right]^{1/\beta} \tag{25}$$

where ν is Poisson's coefficient and C is the triaxiality factor. From this model, a theoretical value of ΔK_{th} (in SI units) can be deduced and is given by

$$\Delta K_{th} \simeq 12.4\sqrt{\rho\sigma_{ys}E\Delta\epsilon_0} \tag{26}$$

if $\nu = 0.3$ and $C \simeq 2.7$.

[6]As previously discussed, cycles to initiation can be used instead of cycles to failure.

As pointed out by the authors [*27*], in its present form the model is only valid for a stress ratio $R = 0$. Secondly, the model was developed assuming a perfectly elastic-plastic material and no consideration is given to real materials which have a cyclic strain hardening exponent $n' \neq 0$. Thirdly, this model is only valid for values of FCPR less than a critical value for which $N_f = 1$ or ¼ in Eq 24. Below this critical value, fatigue crack growth requires damage accumulation governed by the Coffin-Manson relation, whereas, above this critical value, the fatigue crack can grow each cycle by an incremental value which may be deduced from the crack tip opening displacement. In other words, if one fatigue striation *could* be formed during one fatigue cycle (continuum regime), it is not always true that one cycle leads to the formation of one striation, particularly at low ΔK levels (noncontinuum regime), which is the case treated by Lanteigne and Baïlon and indeed by any of the LCF-based damage accumulation models.

In a recent study Heikkenen et al [*29*] have introduced the threshold effect into the Chakrabortty model. This was done by modifying the Coffin-Manson equation to take into account what effectively is an endurance limit. This endurance limit is identified with the plastic strain range at which persistent slip bands begin to form and can be obtained experimentally from the cyclic stress-strain curve as the start of Stage II deformation. Using these ideas, and correcting for crack closure, a value of 2.0 MPa$\sqrt{\text{m}}$ is obtained for an underaged Al-6Zn-2Mg-0.1Zr alloy tested in laboratory air. This compares favorably to the closure-corrected experimental value of 2.9 MPa$\sqrt{\text{m}}$.

Analysis and Critique of Models

Phenomenological Models

It must be stressed that the Paris equation (Eq 4) was proposed on a purely empirical basis. Therefore the primary use of this equation and of its derived versions is to provide a data correlation scheme and a means to conveniently represent FCP data for engineering calculations. The values of the parameters C and m are experimentally determined, and predictions cannot be made if the mechanical properties of material are changed or the extrinsic parameters (R, temperature, frequency) vary. These equations should be viewed as simply proposing a *form* for the FCP curves and not as prediction tools. In as much as the intrinsic parameters that they do identify are monotonic tensile and fracture properties they implicitly assume that FCP behavior is controlled by these processes. As we have seen, it is not clear that this is the case. With these restrictions, such equations can be useful to the design engineer for the computation of structural resistance to fatigue crack propagation. They do not, however, provide guidance to the materials engineer for the development of alloy compositions and thermomechanical treatments which would enhance FCP resistance.

Finally, the strongest criticism which can be addressed to any phenomenological model comes from a dimensional analysis of Eq 4 or of its derived versions. As readily seen, the dimension of C in Eq 4 must depend on the value of the exponent m. If, in the absence of any theoretical model, FCPR values should depend on the stress intensity factor, such a dependence must at least agree with the empirical equation

$$da/dN = V_0 \left(\frac{\Delta K}{\Delta K_0} \right)^m \tag{27}$$

where V_0 is the value of the FCP rate corresponding to ΔK_0.

Empirical relationships with the form of Eq 27 have already been proposed by Yokobori et al [*30*] and Baus et al [*31*]. As shown later, this empirical relationship between the C and m parameters of Paris's equation for a given material is in fact experimentally verified for several materials and can therefore be considered to be a valuable criterion to qualify the dimensional soundness of any empirical or theoretical FCP equation.

Dislocation-Based Models

Credit should be given to the authors who have proposed dislocation-based models for their attempt to address the problem along guidelines which are physically sound and based on fundamental mechanisms. In these approaches, however, the crack advance mechanism is highly idealized and the assumptions (necessary to obtain solutions) are often over simplified, if not too simplistic. For example, Weertman's model [*18*] requires the shape of the plastic zone to be perfectly circular, with its size R_0 being equal to $K^2/\pi\ \sigma_{ys}^2$ (perfectly plastic) or to $\pi\ K^2/8\sigma_{ys}^2$ (BSC-Dugdale Model). It should be noted that these equations imply that plane stress conditions prevail, whereas most FCP test results are obtained for plane strain. Furthermore, the displacement D at a given point located at a distance x in front of the crack tip is assumed to depend linearly on x. As recognized by Weertman himself, such assumptions have to be made, since "a completely developed analytical solution of the stress-strain field for a monotonically growing crack or the growing fatigue crack in an elastic-plastic solid has not yet been developed." What then results is a mixed micro/macro model with a somewhat artificial linking between them. Furthermore, Weertman's theory and indeed any theory based on crack blunting and COD approach generally leads to a fixed value of the exponent m in the Paris equation, a conclusion which is clearly in conflict with the experimental values of m varying generally in the range of 2 to 6 depending on material and testing conditions.

Theoretical models based on crystal dislocation theory, such as that proposed by Yokobori et al [*22*], appear too simplistic, inasmuch as the emission of dislocations from the crack tip is assumed to occur during tensile loading

with no provision for reversed straining occurring during the compressive stroke. These models ignore in fact the existence of the reversed (or cyclic) plastic zone ahead of the crack tip and do not take into account the to-and-fro motion of dislocations which occurs during fatigue cycling with the resulting formation of sub cells or persistent slip bands in the reversed plastic zone.

The models have the advantage, however, of predicting a theoretical value of exponent m which will change from one material to another, depending on the basic properties of dislocation motion in material.

Equation 27 implies that both C and m in the Paris equation must be related in the following way:

$$C = V_0/\Delta K_0{}^m \tag{28}$$

Rearranging the relation gives

$$m = a \ln C + b \tag{29}$$

with

$$a = 1/\ln \Delta K_0$$

and

$$b = \ln V_0/\ln \Delta K_0$$

The fact that experimental data gathered for several materials agrees well with Eq 29 (see, for example, Refs *32* to *35*) indicates that this must be considered when comparing a theoretical model to experimental data.

Application of this dimensional analysis to Eq 17 leads to

$$m = \alpha(p + 1) \tag{30}$$

and

$$C = b\,\gamma(p)\left(\frac{4fb}{v_0}\right)^{-\alpha}\left(\frac{\tau_0{}^*}{G}\right)^{-\alpha p}\left(\frac{1}{G\sqrt{s}}\right)^{\alpha(p+1)} \tag{31}$$

with

$$\alpha = (p + 1)/(p + 2)$$

The theoretical values of C and m deduced from Eqs 30 and 31 are indeed mutually dependent and agree with Eq 29 for which the theoretical values of a and b are

$$a = -1/\ln(G\sqrt{s}) \tag{32}$$

and

$$b = \frac{\ln\left[b\gamma(p)(4fb/v_0)^{-\alpha}(\tau_0^*/G)^{-\alpha p}\right]}{\ln(G\sqrt{s})} \tag{33}$$

Finally, Eq 28 implies that "$\ln(da/dN)$ versus $\ln(\Delta K)$" curves have a pivot point at $da/dN = V_0$ and $\Delta K = \Delta K_0$ where all curves intersect each other. The existence of this pivot point has already been proposed by some authors [*30,32,36-38*] and appears to be well supported experimentally. Since Eq 18 for strain-hardening materials predicts the existence of this pivot point located at $\Delta K_0 = \sigma_{yc}\sqrt{s}$, it is worth calculating the value of the "appropriate length s" (which can be considered as the size of a process zone ahead the crack tip) by using the experimental values of ΔK_0 and σ_{yc}, as shown in Table 1. In this table, the abscissa ΔK_0 of the pivot point has been deduced from an extensive compilation of experimental data for several materials [*39*] and the values of σ_{yc} are either those given in the literature [*37,40*] or realistically estimated. In Table 1, the value R_p of the monotonic plastic zone size as given by $R_p = (1/3\pi)\,(K_{max}/\sigma_{ys})^2$ is also calculated with $\Delta K_0 = K_{max}$ $(R = 0)$, and σ_{ys} is given in the literature or assumed to be equal to σ_{yc}. The ratio s/R_p is approximately equal to $10(3\pi$ if $\sigma_{ys} = \sigma_{yc})$, and one can therefore conclude that the magnitude of the "appropriate length" proposed by Yokobori [*22,32*] is physically unrealistic since it is ten times larger than the monotonic plastic zone size and in some cases approaches 0.3 m.

Apparently, the "appropriate length" has no physical meaning and cannot be considered as the dimension of a process zone in which rupture of the material occurs during FCP.

TABLE 1—*Comparison between the monotonic plastic zone size and the "appropriate length s" proposed by Yokobori et al* [22].

Material	ΔK_0, MPa$\sqrt{m}$	σ_{cy}, MPa	s, mm	R_p, mm
Aluminum alloy	22.32	200	12.5	1.32
		500	2.0	0.21
90-10 brass	32.36	50[a]	418	44.4
		100[a]	108	11.1
70-30 brass	19.78	240[b]	6.8	0.21
		450[b]	1.9	0.21
Stainless steels	54.08	250[b]	46.8	4.96
		600[b]	8.1	0.86
Structural and alloy steels	22.98	200	13.2	1.4
		1000	0.53	0.056

[a] Reference *39* for 90-10 α-brass (0 and 25% cold worked).

[b] Reference *36* for 70-30 α-brass (0 and 82% cold worked) and 305 stainless steel (0 and 50% cold worked).

LCF-Based FCP Models

Implications—In these models the Paris exponent m in the midlife da/dN versus ΔK regime is related to the Coffin-Manson exponent through the equation

$$m = 2/\beta \tag{34}$$

Thus one check of their validity is to use Eq 34 for various alloy systems. This is done for a number of alloy systems in Fig. 1. It can be seen that to a reasonably good approximation Eq 34 is obeyed, especially when it is realized that much of the data used to make these comparisons was generated in different laboratories.

A further implication is that for a given class of materials there should be a relationship between the Paris equation exponent and constant. We have seen previously that such a relationship is required on purely dimensional

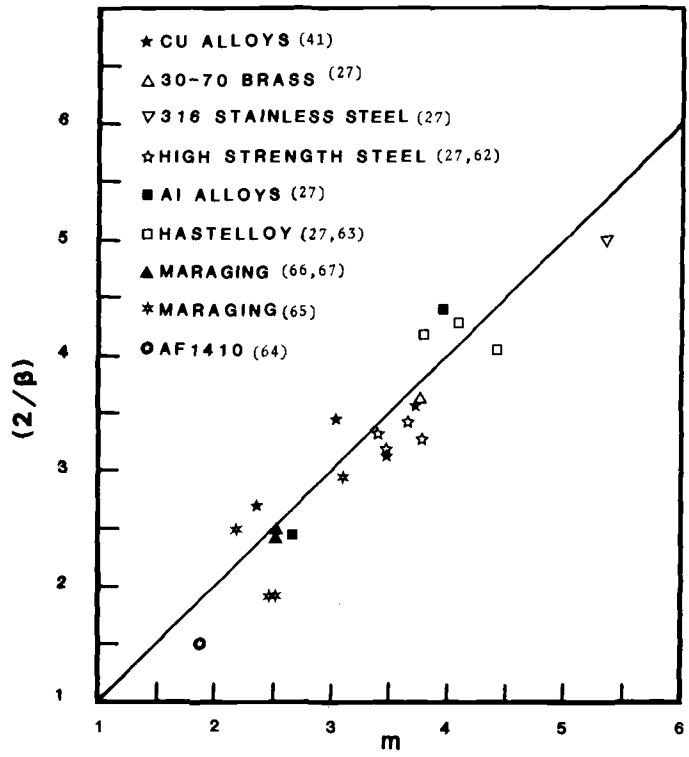

FIG. 1—*Predicted* $(2/\beta)$ *versus observed* (m) *Paris equation exponent.* β *is the Coffin-Manson exponent.*

grounds and was predicted by Yokobori's model. Using as an example the model developed by Antolovich et al [25] in its original form, the following equation results:

$$m = a \ln R - b \tag{35}$$

where

$$a = 2/\ln \left\{ \frac{c}{\sigma_{yc} \epsilon_f E \ell} \right\}$$

and

$$b = a \ln (4\ell)$$

For a given class of materials, a and b should be virtually constant. Experimental results for Waspaloy of various heat treatments are shown in Fig. 2 and it can be seen that the form of Eq 35 is followed.

A further implication of such models is that large process zone sizes should be associated with improved fatigue properties. The idea that has been advanced for this behavior is that the larger the process zone, the smaller the average strain and the greater the number of cycles for a crack to advance one process zone size [28]. The increased crack advance length is more than offset by the *greatly* increased number of cycles for a smaller plastic strain. It should be noted that this idea is really inherent in the basic assumptions on

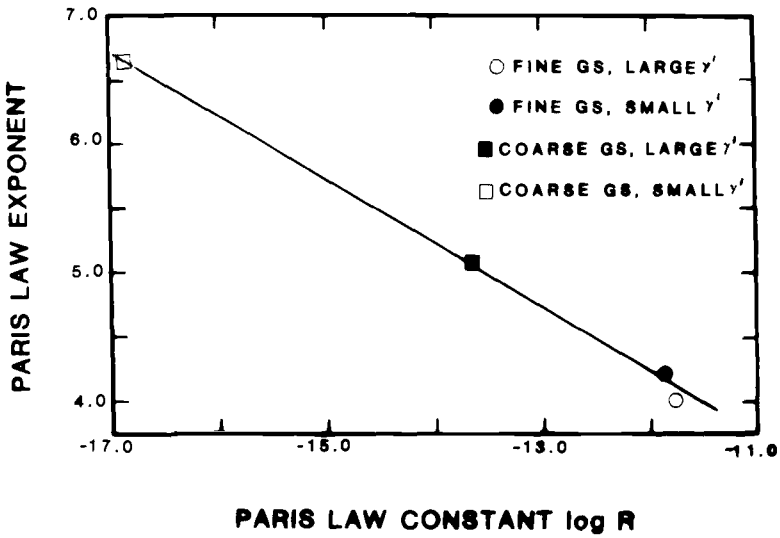

FIG. 2—*Relationship between Paris equation constant* (R) *and exponent* (m) *for Waspaloy having different heat-treatments* [46].

which all these models are based. In some cases a high degree of slip reversibility is associated with a large process zone and this may be a further contributing factor to larger FCP lives being associated with large process zones. In an investigation of the microstructural implications of the model [*41*], the effect of lowering the stacking fault energy (SFE) was studied for solid solution copper-aluminum alloys. It was found that the lower the SFE, the larger the process zone and the lower the FCP rate. The results for the process zone are shown in Table 2 and the FCP results are shown in Fig. 3. In this study the notion of slip reversability was discussed and related to the average plastic strain range. For lower strain ranges the dislocation debris tended to be contained in well-defined slip planes and dislocation/dislocation interactions were minimized. The basic idea was that if cross-slip does not occur the to-and-fro motion of dislocations would be less impeded and the fatigue resistance should be higher. For the lower SFE alloys, the process zone was approximately equal to the grain size. Typical transmission electron micrographs of the low SFE material are shown in Fig. 4. For the higher SFE alloys (lower aluminum), deformation resulted in the formation of well-defined cells, and the process zone was approximately equal to the cell size. In this case the FCP rate was higher as shown in Fig. 3. The deformation substructure Cu-2.2Al is shown in Fig. 5. It is interesting to note that there may be no *a priori* process zone as implied by one author [*28*]. Instead, in some cases there is an interaction between the imposed strain range and deformation mode that results in the development of a process zone *as the fatigue process occurs*.

Another reason that has been advanced for improved FCP behavior with increasing slip planarity has been that the crack, in following crystallographic planes, deviates from a plane normal to the stress axis and the stress intensity drops off significantly. While this is true for *macroscopic* cracks [*42*] the effect is much less pronounced for small deviating segments at the tip of a macroscopically normal crack. In the latter case, the stress intensity depends on both the deviation angle as well as the ratio of the length of the deviating segment to the overall crack length [*43*]. Typically, for a 45-deg deviation the deviating segment must be 10 to 20% of the total crack for significant reductions in K to occur. It thus appears that this effect is

TABLE 2—*Process zone size for copper-aluminum alloys* [41].

Alloy Composition, wt. %	Calculated Process Zone Size, μm	Measured Cell Size or Grain Size, μm
Cu	1.32	0.7 to 1.1
Cu-2.2Al	1.31	0.7 to 0.8
Cu-4.2Al	1.51	...
Cu-6.3Al	190	32

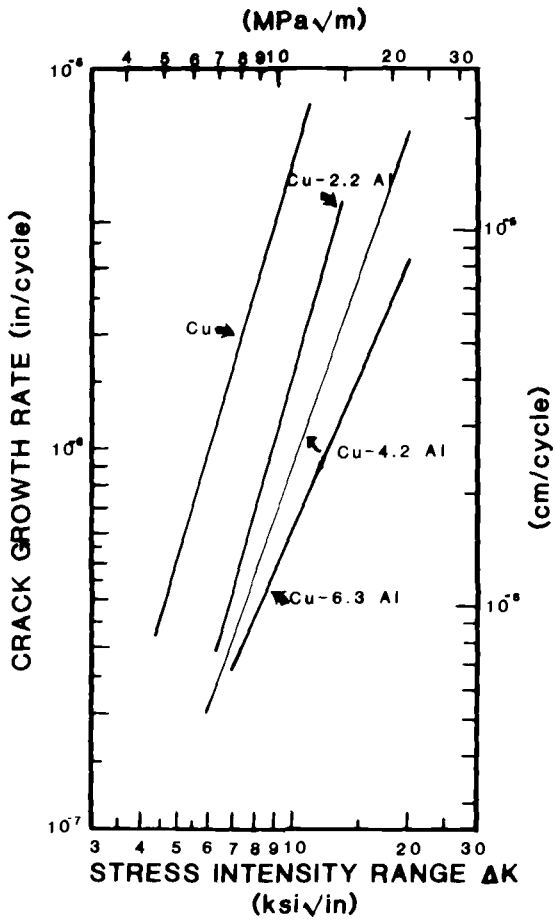

FIG. 3—*Comparison of FCP behavior of various copper-aluminum alloys* [41].

relatively small on the microstructural scale. In addition, when the crack tip deviates, there is a net increase in the total crack path and even though the intrinsic crack growth rate is unaltered, the *effective* rate is reduced. This effect seems to be realized to a significant degree in some titanium alloys [*44*] and has also been suggested for In 718 [*45*].

Some recent experiments were carried out using Waspaloy, a nickel-base superalloy, to study the effects of slip mode on FCP behavior [*46*]. Two grain sizes (ASTM #3 and ASTM #9) were chosen and, for each grain size, the γ' precipitate size was either 1000 or 100 Å. The basic idea was to have virtually equivalent strengths but different slip modes for each grain size. For small γ', deformation will occur by shearing, whereas for larger γ', deformation will have a more significant degree of looping. Thus the slip will be either in-

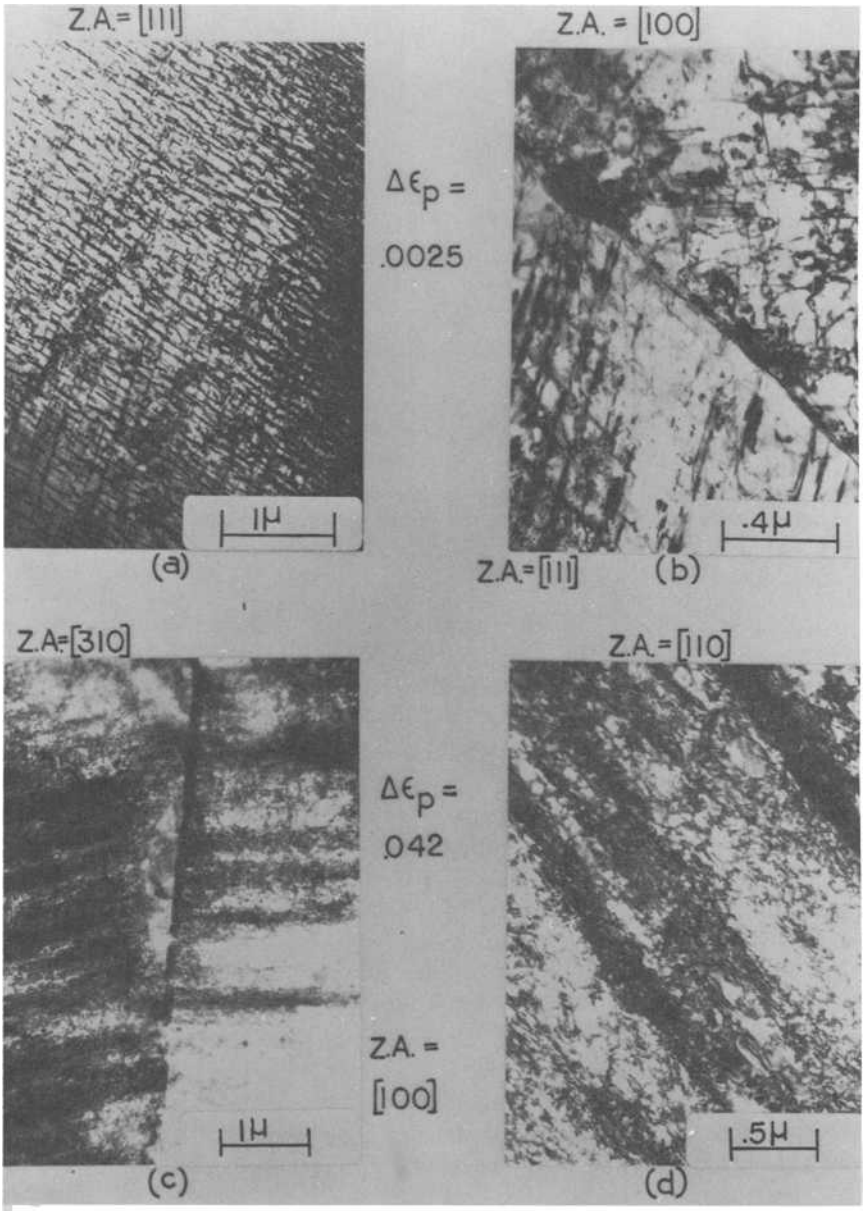

FIG. 4—*Transmission electron micrographs showing deformation substructures for Cu-6.3Al. The plastic strain level is indicated by* $\Delta\epsilon_p$ *and the diffracting conditions are given by the zone axis (ZA)* [41].

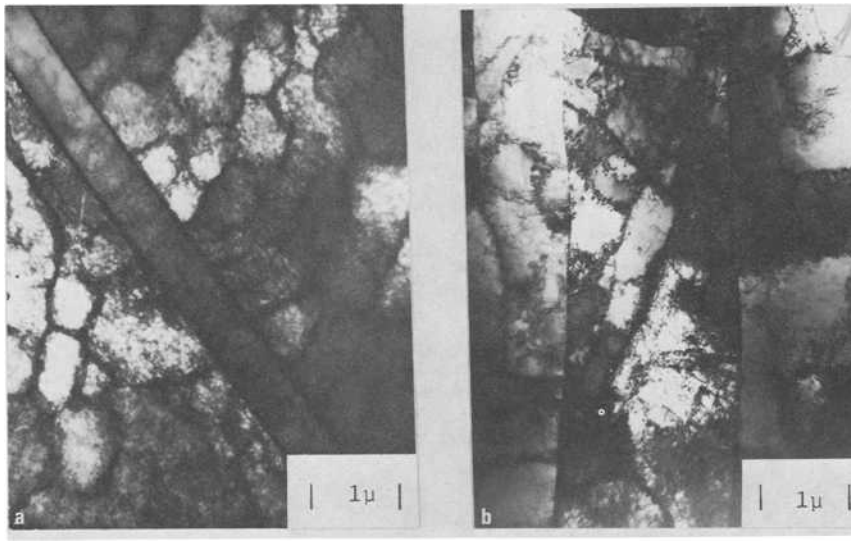

FIG. 5—*Transmission electron micrographs showing LCF substructure* (a) *and FCP substructure* (b) *of a Cu-2.3Al alloy. In* (a) *the plastic strain range was 0.003; in* (b) *the stress intensity parameter was 21 MPa$\sqrt{m}$.*

homogeneous (small γ') or homogeneous (large γ'). By increasing the grain size the inhomogeneity of deformation can be accentuated. The results of the constant-amplitude fatigue tests are shown in Fig. 6. For the coarsest grains, the FCP rates are lowest for the fine precipitates in which deformation takes place by precipitate shearing. Well-defined shear bands are seen in the transmission electron micrographs of Figs. 7*a* and 7*b* for the fine γ', and in Figs. 8*a* and 8*b* looping of the coarse γ' precipitates can be seen. Figures 9*a* to 9*d* show the surface topography, and for the fine and coarse γ' again significant differences can be seen at the same stress intensity level. In this case the lower FCP rate is probably due to increased slip reversibility and an increased crack path, with reductions in stress intensity parameter being relatively minor. Other investigators have also observed improved FCP properties with more planar slip [*47,48*] and these findings merit close scrutiny by the research community.

Critique of LCF-Based FCP Models—In the preceding section we have seen that, at least for some systems, there is a reasonable correlation between FCP performance and the appropriate LCF parameters. It is important to note that this does not imply a one-to-one correspondence between LCF and FCP behavior.

This approach is intermediate in its degree of fundamentalism between the more macroscopic models and the dislocation-based models. As such it is really a phenomenological rather than a mechanistic representation. How-

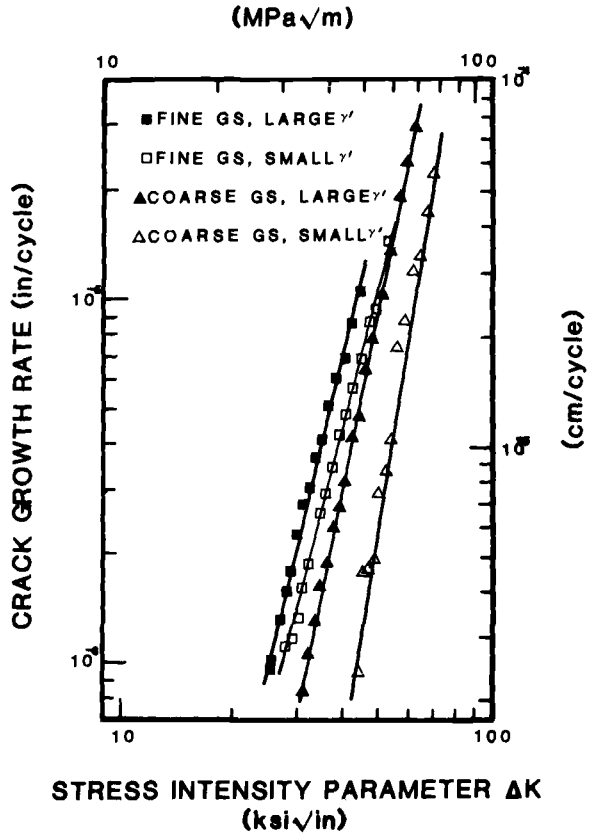

FIG. 6—*FCP behavior of Waspaloy heat-treated to produce different deformation modes* [46].

ever, mechanisms can be inferred from the damage processes associated with LCF and to this extent guidance in materials development is provided.

The question is sometimes raised as to why the same fatigue damage process observed in a uniaxial LCF test should also be the limiting factor ahead of a propagating fatigue crack, where there is a high degree of triaxiality and a large plastic constraint factor. It is the authors' opinion that the adequacy of the correlation depends very much on factors such as temperature, stacking fault energy, strain rate, and purity (to name only a few). For example, consider a single phase alloy of low stacking fault energy tested at low temperature. Here damage would be associated with dislocation debris and should be the same in FCP as in LCF at the same equivalent plastic strain. Next consider a system of high stacking fault energy tested at high temperature and low strain rates where creep and grain boundary sliding are important. In this case the hydrostatic stress component is important and there

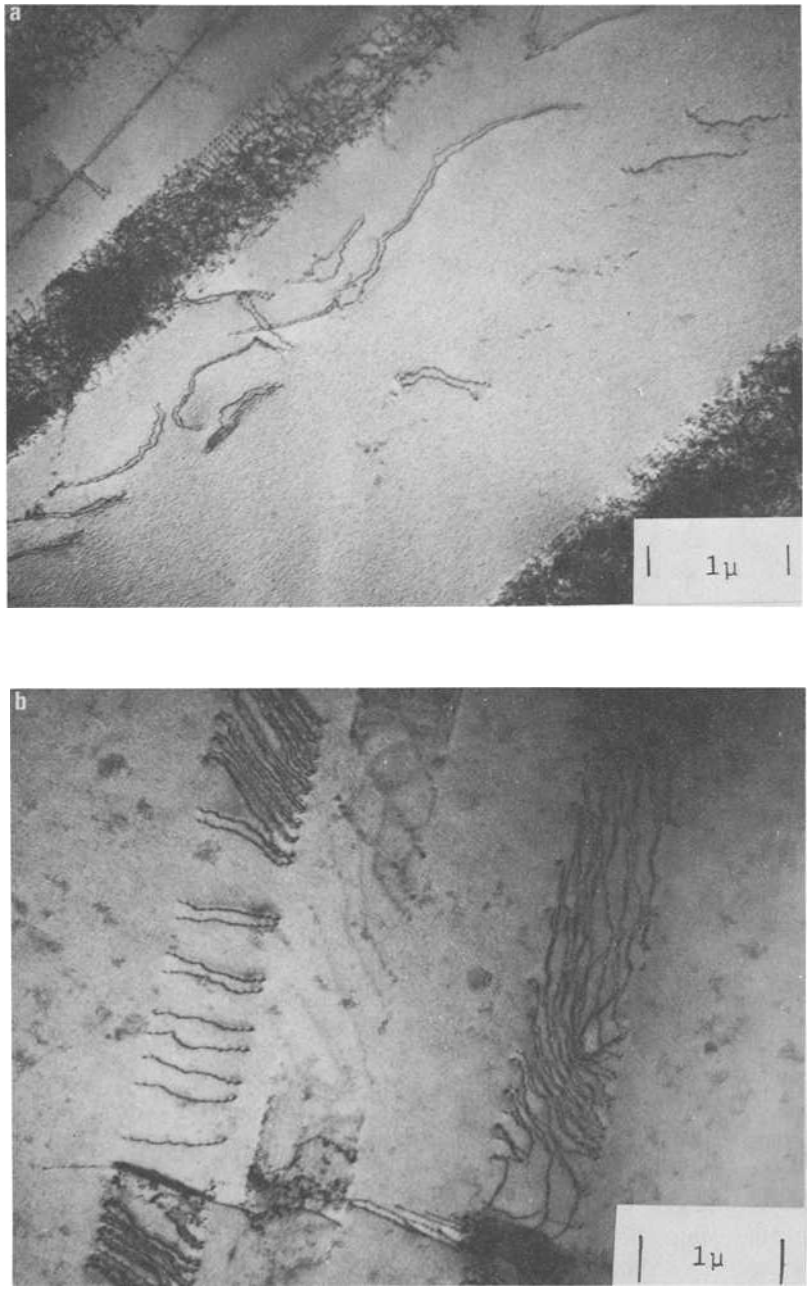

FIG. 7—*Transmission electron micrographs showing LCF substructure* (a) *and FCP substructure* (b) *for Waspaloy having large grains (ASTM #3) and fine* γ' *precipitates (~100 Å). In* (a) *the plastic strain range was 0.3%; in* (b) *the stress intensity parameter was 79 MPa*$\sqrt{m}$. *The paired dislocations are indicative of precipitate shearing. In* (a) *the diffraction vector was* [*200*] *while in* (b) *it was* [*111*] [51].

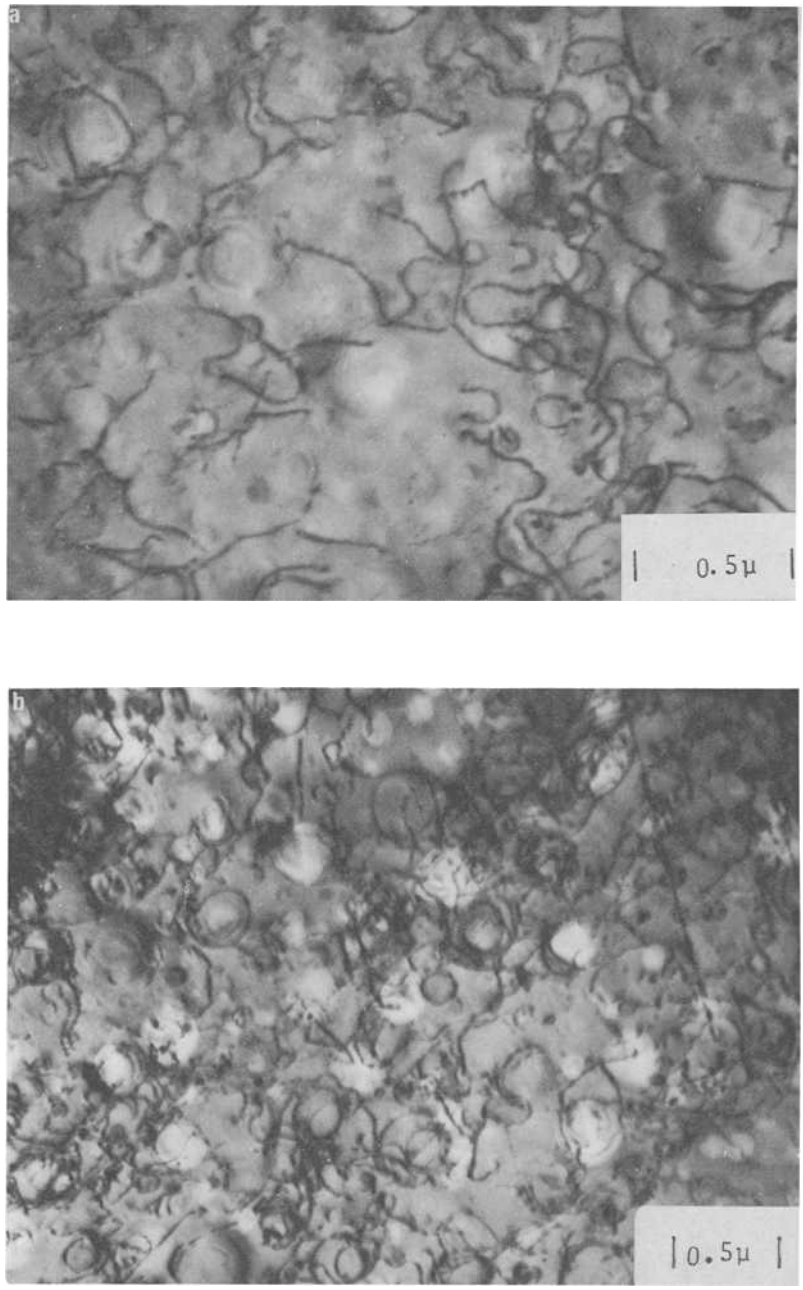

FIG. 8—*Transmission electron micrographs showing LCF substructures* (a) *and FCP substructure* (b) *for Waspaloy having fine grains (ASTM #9) and large* γ' *precipitates (~1000 Å). In* (a) *the plastic strain range was 0.072%; in* (b) *the stress intensity parameter was 50 MPa*$\sqrt{m}$*. In both cases looping was the predominant deformation mode. In both* (a) *and* (b) *the diffraction vector was* [*111*] [51].

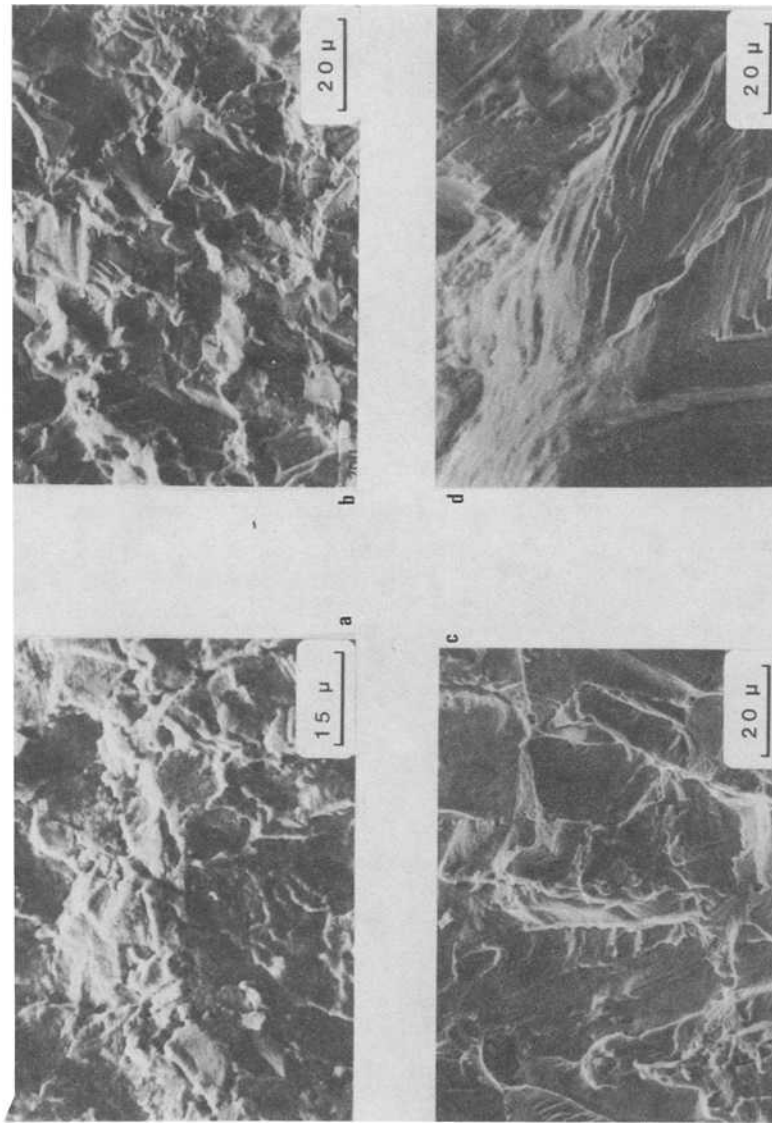

FIG. 9—*Scanning electron micrographs of the fracture surfaces of Waspaloy specimens. FCP data are shown in Fig. 6. In all cases the stress intensity parameter was 46 MPa√m. The microstructures associated with the fractographs are* (a) *fine grain (ASTM #9), large γ′ (~1000 Å);* (b) *fine grain (ASTM #9), small γ′ (~100 Å);* (c) *coarse grain (ASTM #3), large γ′ (~1000 Å); and* (d) *coarse grain (ASTM #3), fine γ′ (~100 Å).*

could be significant differences in the damage process (or the rate of damage accumulation) that occurs in LCF and FCP.

It should be recognized that these models are limited to the regime in which crack growth is discontinuous and not controlled by COD processes in which there is apparently a close correlation between the cyclic growth rate and the striation spacing. Furthermore, the Coffin-Manson equations that are used should be for initiation, not failure, since failure of a macroscopic LCF specimen integrates a considerable amount of crack propagation. While this fact does not appear to have been taken into account by the authors of the models discussed in this paper, it does not represent a major limitation to the underlying basis of these models.

The next stage in the development of these models would be to express the Coffin-Manson parameters in terms of microstructural features related to the damage process. In doing this, a greater degree of fundamentalism would be achieved and there would tend to be a convergence of the dislocation and LCF-based models.

Direct Experimental Verification of Models

Necessary Information

One of the major problems to be dealt with relates to actually identifying "damage" ahead of a propagating crack. To do this, structural changes have to be correlated to crack advance. Presumably such changes are related to plastic strain levels ahead of propagating cracks, and it is thus important to determine the plastic strain distribution. Such information is clearly necessary if the LCF/FCP models are to be verified. Another important parameter, presumably related to the deformation behavior, is crack closure. Crack closure effects must be incorporated into models where appropriate and this effect must be studied. Another useful approach, especially for verification of the LCF/FCP models, would be to have a consistent set of both LCF and FCP experiments in which the same alloy heats, test machines, etc., were employed. In the following section some experimental techniques emphasizing the microscopy approach are briefly discussed and some experimental results are cited.

Experimental Approaches

Optical Microscopy—This tool, although not glamorous, can yield very significant results and be of real value in the evaluation of fatigue behavior. For example, in a study of overload fatigue behavior [*49*] in aluminum alloys, intermetallic cracking as a result of the overloads was identified by this technique. In this case, cracking of the intermetallics relaxed the stresses around the main crack front, and the improved FCP performance for spec-

trum loads that were dominated by a tensile portion could be understood. In some cases plastic strain induces phase changes and these changes can be used to outline plastic zones. An example is shown in Fig. 10 for IN 718 in which γ'' (a bct phase) is converted to δ which is orthorhombic [*50*].

Sometimes it is possible to gain some insight into the plastic strain levels around a fatigue crack by optical microscopy methods even when there is no strain-induced phase change. In Fig. 11, optical micrographs illustrate the effect of plastic strain on slip band density in Waspaloy that has been heat-treated to deform by planar glide and tested in LCF [*51*]. The quantitative relationship between slip band spacing (density) and plastic strain range is shown in Fig. 12. Each point represents anywhere from 43 to 383 measurements, and the graph may be considered accurate to a high degree of confidence. As partial confirmation of the trend, data from another recent study are included [*52*]. If an FCP specimen is now examined, the slip band spacing can be related to the "calibration" curve shown in Fig. 12. Scanning electron micrographs of the region around a crack tip are shown in Fig. 13, and quantitative results are shown in Fig. 14 where a curve based on Rice's equation is included for comparative purposes. The data in Fig. 14 clearly show that the strain decreases with increasing distance from the fracture surface. However, the strain appears to vary from grain to grain, and a more complete statistical characterization is required to increase the degree of confidence. It is noteworthy, however, that the maximum strain was about 4%, with an average over the plastic zone (which was measured to be 84 μm and calculated using Ref *41* to be 105 μm) of 0.42%. This low average strain range is consistent with the excellent FCP properties observed for this alloy.

Use of such techniques is obviously limited to materials in which there is some special or easily identifiable feature associated with the deformation process.

Scanning Electron Microscopy (SEM)—Direct observation of deformation mechanisms occurring at or near the crack tip can be carried out by SEM techniques. Subgrains which are found in the highly strained regions around the crack tip can be detected in SEM using back-scattered electrons. Use of electron channeling and pseudo-Kikuchi lines allow evaluation of the amount of strain. Crack closure phenomenon can also be observed and eventually quantified. Finally, quantitative stereography coupled with SEM observations of displacements near the crack tip lead to the calculation of five of the nine components of the strain tensor. All these applications of SEM to the study of mechanisms occurring at the crack tip have been extensively developed by Davidson and Lankford and a detailed review of that work is given in their article in this volume.

It should however be pointed out that experimental data obtained by SEM techniques are restricted to plane stress conditions, since only the specimen surface can be observed and space limitations in SEM working chambers generally require thin specimens to be observed.

FIG. 10—*Optical micrograph showing plastic zone in In 718 as delineated by δ-phase* [50].

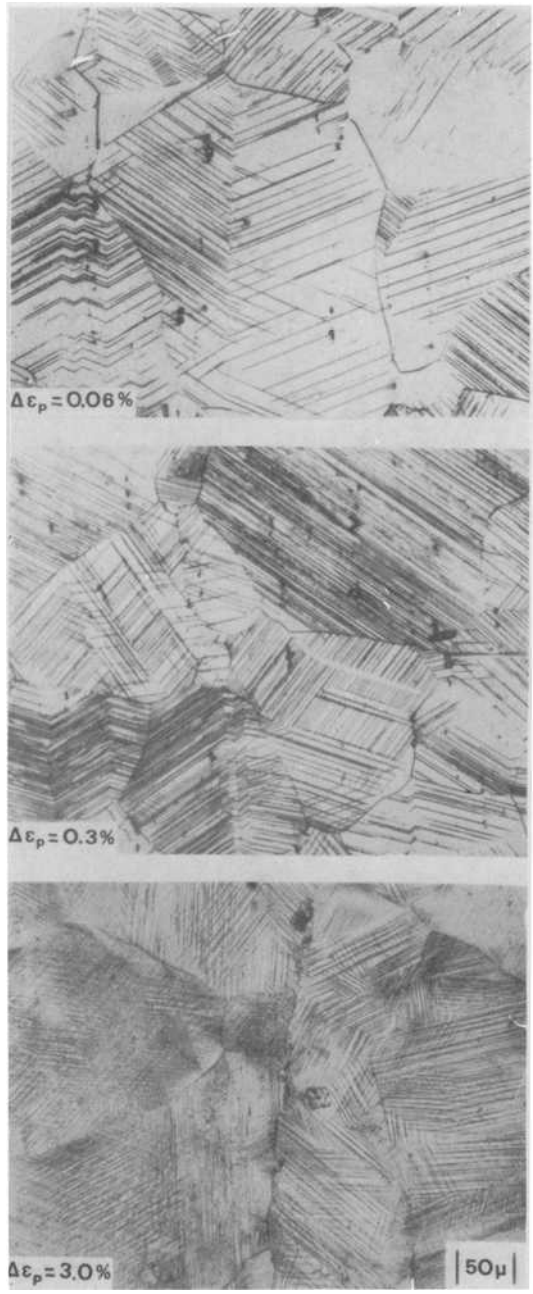

FIG. 11—*Slip band spacing for large-grain (ASTM #3), fine* γ' *(~100 Å) Waspaloy. The plastic strain range is indicated on each micrograph* [51].

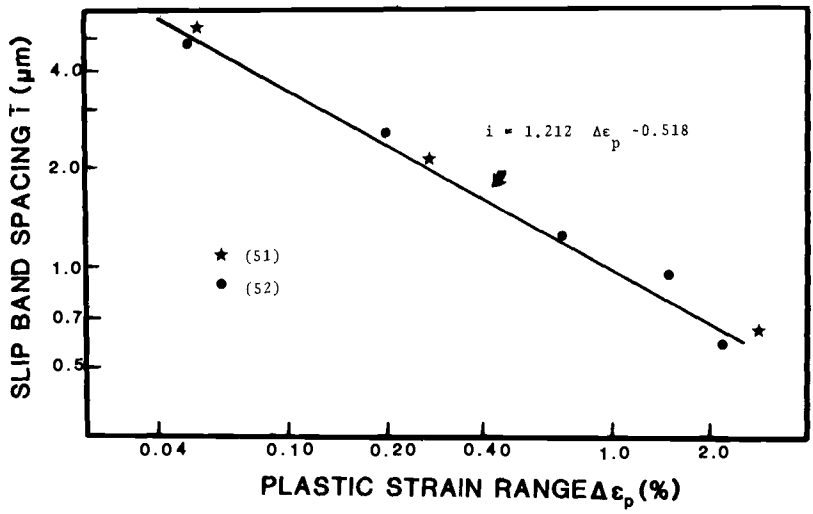

FIG. 12—*Relationship between slip band spacing and plastic strain range for Waspaloy.*

Microhardness—The extent of plastic deformation at the tip of fatigue cracks may be evaluated by measuring the microhardness ahead of the crack tip perpendicular to the crack plane. This technique was extensively employed by Bathias and Pelloux [*53*] and further developed by several investigators, most recently in France [*54*]. A calibration curve of microhardness versus cyclic plastic strain has to be established by measuring the microhardness of LCF specimens tested under controlled conditions. In this respect, the technique is similar to the measurement of plastic strain by metallography, as discussed previously.

Results obtained by this technique indicate that the level of cyclic plastic strain very near the crack tip remains low ($\Delta\epsilon_p \simeq 4$ to 10%) and are in good agreement with experimental data obtained by other methods such as quantitative metallography [*50,55-57*] or holography and Moiré fringes [*58,59*]. Microhardness was used to study the Waspaloy described previously, and the results were in reasonable agreement with the metallographic study as far as plastic zone size was concerned. The microhardness approach was less sensitive in terms of the plastic strain distribution than was the measurement of slipband density.

The microhardness technique is not limited to plane stress conditions, since carefully polished sections can be made at various depths through the thickness of the specimens, in which plane strain conditions prevail. One limitation of this technique comes from the finite size of microhardness indentations, which may be in the range of 1 to 5 μm even with very small loads (1 or 2 g). Furthermore, for low strain hardening, small hardness errors

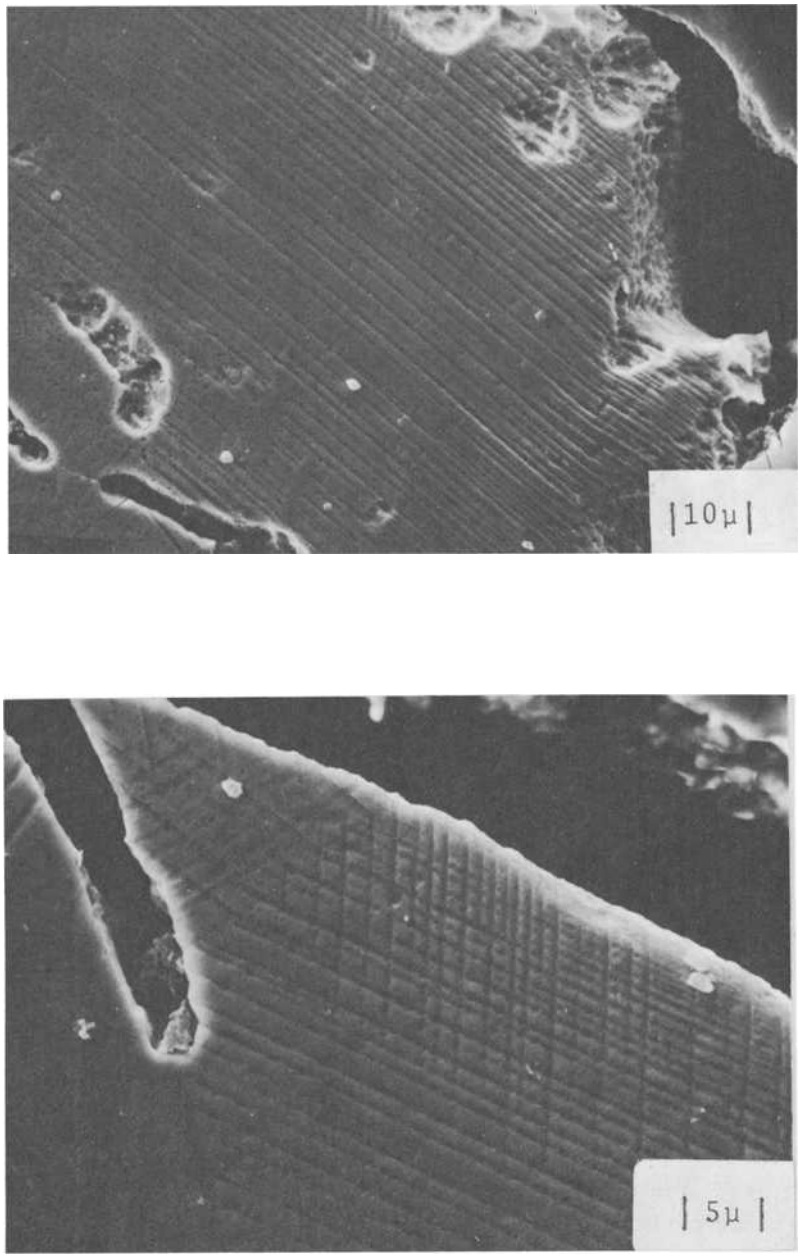

FIG. 13—*Scanning electron micrographs showing the variation in slip band spacing around the fatigue surface of a Waspaloy specimen. The grain size was ASTM #3 and the precipitate size was ~100 Å* [51].

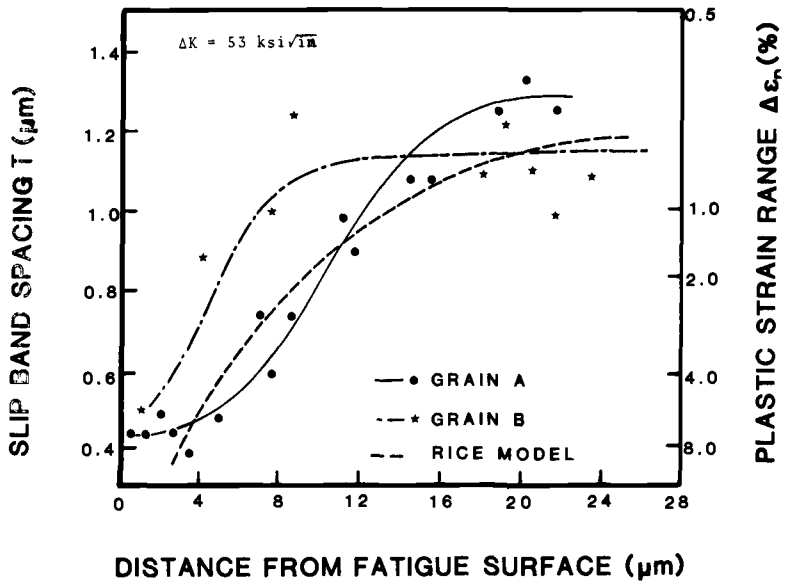

FIG. 14—*Slip band spacing as a function of distance from the fatigue surface for the specimen shown in Fig. 13. The corresponding plastic strain is also given and was derived from Fig. 12* [51].

will lead to large uncertainties in strain. Of course, it is difficult to investigate the "process zone" where fatigue cracking is assumed to occur according to several theoretical models, since the size of this process zone is generally very small (on the order of microns). Some limitations are also encountered at low ΔK levels, for which the size of the plastic zone may be very small, particularly in high-strength materials. Finally, at low ΔK levels in coarse-grained materials, anisotropy effects may lead to large scatter of experimental data.

Transmission Electron Microscopy (TEM)—For dislocation-based models as well as LCF-based models electron microscopy experiments provide much useful information. In the first case detailed processes can be observed, while in the latter comparisons between the deformation debris associated with LCF and FCP can be made to see if similar processes are operating. To the extent that similar processes are observed, one can have a degree of confidence that the basic assumptions inherent in the LCF-based models are really correct. The fatigue plastic zones are generally very small, so that obtaining foils within the fatigue plastic zone is usually difficult experimentally. However, some success has been achieved along these lines (see, for example, Refs *41,51,60,* and *61*), and typical micrographs showing crack tip deformation debris have already been shown in Figs. 5, 7, and 8. These micrographs show that, at least in a qualitative sense, the deformation debris in LCF and FCP are equivalent.

The cell structure for copper fatigued by LCF and FCP is shown in Fig. 15, and again the type of deformation process in both LCF and FCP is similar. The information contained in the micrographs is essentially qualitative; it would be useful to develop techniques in which foils could be obtained from very precise locations ahead of fatigue cracks in order to make quantitative evaluations of the fatigue "damage" (for example, cell size, subgrain misorientation, dislocation density, etc.).

Concluding Remarks

The real usefulness of theoretical model development is not so much to provide a predictive tool for FCP properties (obviously FCP curves can always be measured much more accurately than they can be predicted), but to assess the relative importance of various intrinsic and extrinsic parameters which can then be used to develop superior heat treatments and alloy compositions. At present, there is a multitude of models having various levels of refinement. Provided that the critical damage process for crack advance assumed (either implicitly or explicitly) for these models is followed, then they are likely to be in agreement with experiment. The weakness of these fundamental models is that they are not based on observed damage processes. It must be recognized that these processes are likely to be different for different materials and that a single FCP model is probably not a realistic expectation. Materials should be grouped into classes for which crack tip damage mechanisms have been identified by experiment to be similar.

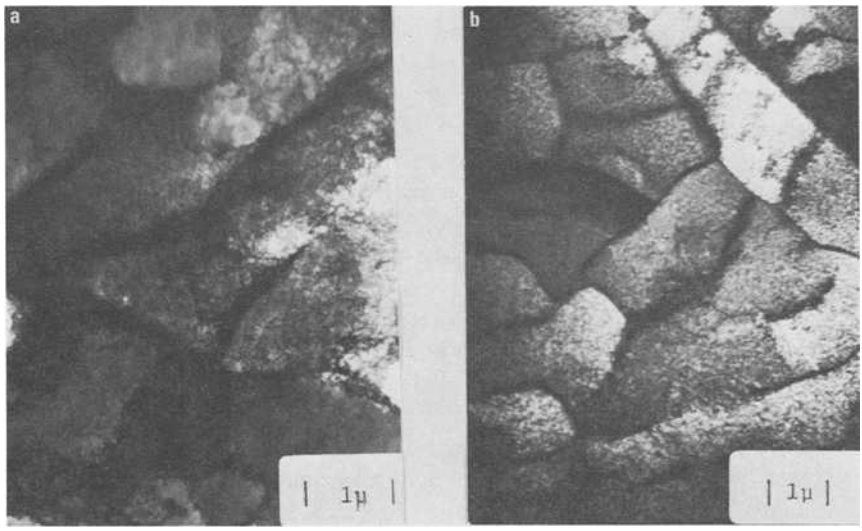

FIG. 15—*Comparison of cell structures in copper deformed by* (a) *LCF* ($\Delta\epsilon_p = 0.002$) *and by* (b) *FCP* ($\Delta K = 11$ *MPa* $\sqrt{m}$). *In both cases the deformation substructure was similar* [41].

A precise knowledge of the stress and strain gradients ahead the crack tip as well as microfracture mechanisms occurring in the process zone are clearly necessary for a better understanding of the fatigue cracking phenomenon. It is our view that most emphasis must be placed on the experimental approach. Data may come from different experimental techniques which have to be applied or adapted to this specific problem. Optical microscopy (interferometry or Moiré fringes), quantitative metallography (strain etching, recrystallization, phase changes, twinning, etc.), quantitative SEM observations, microhardness techniques, dislocation density measurements from quantitative TEM, microfocus X-Ray diffraction, and acoustic emission are among the most promising experimental techniques and are discussed by various contributors to this conference. While each of these techniques has some limitations and drawbacks, the combination of them should be very fruitful for a better modeling of the FCP process based on a deeper understanding of the mechanisms occurring at a fatigue crack tip. This applies both to Stage II crack growth (as empirically described by the Paris equation) and to low crack growth rates (threshold region).

References

[1] Cooper, T. D. and Kelto, C. A., "Fatigue in Machines and Structure-Aircraft," *Fatigue and Microstructure*, ASM, Metals Park, Ohio, 1979, pp. 29-56.

[2] Hill, R. J., Reimann, W. H., and Ospey, J. S., "A Retirement-for-Cause Study of an Engine Turbine D1512," AFWAL-TR-81-2094, Air Force Wright Aeronautical Laboratories, 1981.

[3] *Fatigue Mechanisms, ASTM STP 675*, J. T. Fong, Ed., American Society for Testing and Materials, 1979.

[4] *Fatigue and Microstructure*, ASM Publication, Metals Park, Ohio, 1979.

[5] *La Fatigue Des Matériaux et Des Structures*, C. Bathias and J. -P. Baïlon, Eds., Maloine S. A., Paris, 1980.

[6] Schijve, J., NLR Report MP 195, 1960.

[7] Weertman, J. in *Proceedings*, First International Conference on Fracture, Japanese Society of Strength and Fracture of Materials, Sendai (Japan), 1965, p. 153.

[8] McEvily, A. J. and Johnston, T. L. in *Proceedings*, First International Conference on Fracture, Japanese Society of Strength and Fracture of Materials, Sendai (Japan), 1965, p. 515.

[9] Paris, P. and Erdogan, F., *Journal of Basic Engineering, Transactions of ASME, Series D*, 1963, Vol. 85, pp. 528-539.

[10] Rice, J. R. in *Fatigue Crack Propagation, ASTM STP 415*, American Society for Testing and Materials, 1967, p. 247.

[11] J. Masounave, J. -P. Baïlon and J. I. Dickson, Chap. 6 in "*La Fatigue Des Matériaux et Des Structures*", C. Bathias and J. -P. Baïlon, Eds., Maloine S. A., Paris, 1980.

[12] Forman, A. G., *Journal of Basic Engineering*, Vol. 89, 1967, pp. 459-469.

[13] Nicholson, C. E. in *Proceedings*, Conference of Mechanics and Mechanisms of Crack Growth, Churchill College, Cambridge, England, April 1973.

[14] Frost, N. E. and Dixon, J. R., *International Journal of Fracture*, Vol. 9, 1967, pp. 301-316.

[15] Fitzgerald, J. M., *Journal of Testing and Evaluation*, Vol. 5, 1977, pp. 343-353.

[16] Sullivan, A. M. and Crooker, T. W., *Transactions of ASME*, Vol. 98, 1976, pp. 179-184.

[17] Elber, W. in *Damage Tolerance in Aircraft Structures, ASTM STP 486*, American Society for Testing and Materials, 1971, pp. 230-242.

[18] Weertman, J., "Fatigue Crack Propagation Theories," in *Fatigue and Microstructure*, ASM, Metals Park, Ohio, 1979, pp. 279-306.

[19] Ikeda, S., Izumi, Y., and Fine, M. E., *Engineering Fracture Mechanics*, Vol. 9, 1977, pp. 123-136.
[20] Liaw, P. K., and Fine, M. E., *Metallurgical Transactions*, Vol. 12A, 1981, pp. 1927-1937.
[21] Fine, M. E. and Izumi, Y. in 4th International Conference on the Strength of Metals and Alloys, Vol. 2, Laboratoire de Physique du Solide, Nancy, France, 1976, p. 468.
[22] Yokobori, T., Konosu, S., and Yokoburi, A. T. Jr., in *Fracture 1977*, ICF4, D. R. M. Taplin, Ed., Waterloo, Canada, Vol. 1, 1977, pp. 665-681.
[23] Gerberich, W. W. and Moody, N. R. in *Fatigue Mechanisms, ASTM STP 675*, J. T. Fong, Ed., American Society for Testing and Materials, 1979, pp. 293-334.
[24] McClintock, F. A., *Fracture of Solids*, Wiley, New York, pp. 65-102.
[25] Antolovich, S. D., Saxena, A., and Chanani, G. R., *Engineering Fracture Mechanics*, Vol. 7, 1975, pp. 649-652.
[26] Chanani, G. R., Antolovich, S. D., and Gerberich, W. W., *Metallurgical Transactions*, Vol. 3, 1972, pp. 2661-2672.
[27] Lanteigne, J. and Baïlon, J. -P., *Metallurgical Transactions*, Vol. 12A, 1981, pp. 459-466.
[28] Chakrabortty, S. B., *Fatigue of Engineering Materials and Structures*, Vol. 2, 1979, pp. 331-344.
[29] Heikkenen, H. C., Starke, E. A., Jr., and Chakrabortty, S. B., *Scripta Metallurgica*, Vol. 16, 1982, pp. 571-574.
[30] Yokobori, T., Kawada, I., and Hata, T., *Reports of the Research Institute of Strength and Fracture of Materials*, Tohoku University, Japan, Vol. 11, 1973, pp. 35-64.
[31] Baus, A., Charbonnier, J. C., Lieurade, M. R., Marandet, B., Roesch, L., and Sanz, G., *Revue de Métallurgie*, Vol. 92, 1975, pp. 891-935.
[32] Yokobori, T. in *Fatigue Mechanisms, ASTM STP 675*, J. T. Fong, Ed., American Society for Testing and Materials, 1979, pp. 683-701.
[33] Niccolls, E. M., *Scripta Metallurgica*, Vol. 10, 1976, p. 295.
[34] Baïlon, J. -P., Masounave, J., and Bathias, C., *Scripta Metallurgica*, Vol. 11, 1977, p. 1101.
[35] Tanaka, K., Masuda, C., and Nishijima, S., *Scripta Metallurgica*, Vol. 15, 1981, pp. 259-264.
[36] Aubert, M., Laniesse, J., and Pigoury, M., "Propriétés en fatigue des tôles selon le travers court," Soudage et Techniques Connexes, Vol. 33, 1979, pp. 285-295.
[37] Hickerson, J. P. and Hertzberg, R. W., *Metallurgical Transactions*, Vol. 3, 1972, pp. 179-189.
[38] Tanaka, K. and Matsuoka, S., *International Journal of Fracture*, Vol. 13, 1977, p. 563.
[39] Baïlon, J. -P., Masounave, J., and Bathias, C., to be published.
[40] Ishii, H. and Yukaua, K., *Metallurgical Transactions*, Vol. 10A, 1979, pp. 1881-1887.
[41] Saxena, A. and Antolovich, S. D., *Metallurgical Transactions*, Vol. 6A, 1975, pp. 1809-1828.
[42] Paris, P. C. and Sih, G. C., in *Fracture Toughness Testing and Its Applications, ASTM STP 381*, American Society for Testing and Materials, in 1965, pp. 30-83.
[43] Kitagawa, H., Yuuki, R., and Ohara, T., *Engineering Fracture Mechanics*, Vol. 7, 1977, pp. 515-529.
[44] Eylon, D., Hall, J. A., Pierce, C. M., and Ruckle, L., *Metallurgical Transactions*, Vol. 7A, 1976, pp. 1817-1826.
[45] Clavel, M. C., Levaillant, C., and Pineau, A. in *Creep-Fatigue Environment Interactions*, R. M. Pelloux and N. S. Stoloff, Eds., Metals Society, AIME, Warrendale, Pa., 1980, pp. 24-45.
[46] B. Lawless, "Correlation Between Cyclic Load Response and Fatigue Crack Propagation in the Ni-Base Superalloy Waspaloy", Ms. thesis, University of Cincinnati, Ohio, Aug. 1980.
[47] Merrick, H. F. and Floreen, S., *Metallurgical Transactions*, Vol. 9A, 1978, pp. 231-233.
[48] Mills, W. J. and James, L. A., ASME Publication 7-WA/PUP-3, 1979.
[49] Sanders, T. H., Sawtell, R. R., Staley, J. T., Bucci, R. J., and Thakker, A. B., "The Effect of Microstructure on Fatigue Crack Growth of 7XXX Aluminum Alloys under Constant Amplitude and Spectrum Loading," NADC Contract N00019-76-6-0482, 1978.
[50] Clavel, M., Fournier, D., and Pineau, A., *Metallurgical Transactions*, Vol. 6A, 1975, pp. 2305-2307.
[51] Diederich, D., "A Study of Fatigue Plastic Zones in Waspaloy," Senior thesis, University of Cincinnati, Ohio, June 1981.

[52] Clavel, M., "Fatigue Plastique et Fissuration de Deux Alliages Base Nickel Durcis par des Précipités Cohérents Étude Comparative des Mécanismes," Ph.D. thesis, École des Mines de Paris, 1980.
[53] Bathias, C. and Pelloux, R. M. N., *Metallurgical Transactions*, Vol. 4, 1973, pp. 1265-1273.
[54] Fatigue Committee, Task Group 3, Société Française de Métallurgie, DGRST Report 78-7-2435, 1980 (Délégation générale à la recherche scientifique et technique).
[55] Hahn, G. T., Hoagland, R. G., and Rosenfield, A. R., *Metallurgical Transactions*, Vol. 3, 1972, pp. 1189-1202.
[56] Hornbogen, E., Minuth, E., and Stanzl, S. T., *Materials Science Engineering*, Vol. 43, 1980, pp. 145-150.
[57] Chalant, G. and Remy, L., *Materials Science Engineering*, Vol. 50, 1981, pp. 253-261.
[58] Ohta, A., Kosuge, M., and Sasaki, E., *International Fracture*, Vol. 13, 1977, pp. 289-300.
[59] Liu, H. W. and Kuo, A. S. in *Proceedings*, Conference on Fracture Mechanics and Technology, G. S. Sih and C. L. Chow, Eds., Hong Kong, 1977, pp. 893-906.
[60] Kitagiri, K., Omura, A., Koyanagi, K., Awatani, J., Shiraishi, T., and Kaneshiro, H., *Metallurgical Transactions*, Vol. 8A, 1977, pp. 1769-1773.
[61] Purcell, A. H. and Weertman, J., *Metallurgical Transactions*, Vol. 4, 1973, pp. 349-353.
[62] Brinkman, C. R. et al, "Application of Hastelloy-X in Gas Cooled Reactors," ORNL-TM 5405, Oak Ridge National Laboratory, Tenn., Oct. 1976.
[63] Jablonsky, D. A., "Fatigue Evaluation of Hastelloy X at Elevated Temperature in Air, Vacuum and Oxygen Environment," Ph.D. thesis, Massachusetts Institute of Technology, Cambridge, Mass., Feb. 1978.
[64] Antolovich, S. D., "Fatigue Crack Propagation and Corrosion Fatigue of AF-1410 Steel," AFML-TR-79-4209, Air Force Materials Laboratory, 1979.
[65] Aizaz, A., "A Study of Low Cycle Fatigue, Fatigue Crack Propagation and Microstructure in High Purity and Commercial 300 Grade Maraging Steel," Ms. thesis, University of Cincinnati, Ohio, June 1978.
[66] Antolovich, S. D., Saxena, A., and Chanani, G. R., *Metallurgical Transactions*, Vol. 5, 1974, pp. 623-632.
[67] Van Swam, W. F., Pelloux, R. M., and Grant, N. J., *Metallurgical Transactions*, Vol. 6A, 1975, pp. 45-54.

DISCUSSION

A. J. McEvily[1] (*written discussion*)—In your comparison of the crack growth resistance of copper and its alloys, I wonder if LEFM is an appropriate basis. In particular, a ΔJ-approach might be more suited to the case of copper if plastic zone sizes are large.

Also, we know that near the threshold, closure is important, and at high ΔK's, the fracture toughness is sensitive to microstructure. Some of the shift in the position of curves might be associated with the positions of the extremes of the curves. Therefore I think we should attempt to develop a comprehensive treatment of the entire curve rather than just a portion thereof.

[1]Professor, Department of Metallurgy, University of Connecticut, Storrs, Conn. 06268.

J. P. Baïlon and S. D. Antolovich (authors' closure)—All tests were carried out so that plane strain conditions prevailed. For example, samples 23 mm thick were used for testing below about 10 MPa$\sqrt{m}$. For higher stress intensities, the specimen thickness was increased to 57 mm. From this point of view LEFM seems an appropriate basis of representation. With respect to using ΔJ, there appears to be some as yet unanswered difficulties with this concept and, in any event, its use usually affects only the high ΔK regime.

The points about closure near the threshold and fracture toughness in the higher ΔK regime are important. The closure effect, if any, is expected to be of more importance for the pure copper than for the alloys. If a ΔK_{eff} representation were used, the copper would exhibit an even more rapid crack growth rate than the alloys near threshold. Similarly, at high ΔK the crack growth of the copper would be slowed down more than the alloys because of a toughness effect. Thus the differences that were observed in FCP rates would be expected to be *even greater* if these effects were taken into account, and we can be quite sure that the differences in FCP behavior relate to differences in microstructure and slip mode.

We would, of course, agree that a comprehensive treatment of the whole FCP curve is desirable, but especially so for the low-to-mid ΔK regime where most of the life is spent. This, as is pointed out in the paper, is being done for the LCF-based models by introducing threshold and closure effects.

J. T. Fong[2] *(written discussion)*—You disagree with Professor McEvily on the significance of microstructural changes ahead of the crack tip in defining fatigue damage. Please amplify your position, and comment on the possibility of quantifying the complex state of the damage microstructure.

J. P. Baïlon and S. D. Antolovich (authors' closure)—We disagree with Professor McEvily primarily with respect to the sliding off models he has presented. These models attempt to explain fatigue crack propagation behavior in terms of monotonic tensile and fracture properties. Thus they do not appear to account for the fact that repeated loadings induce a different dislocation substructure and, inferentially, different deformation modes and mechanisms of damage accumulation. They further seem to require cycle-by-cycle crack extension. However, as we have seen in the film presented by Dr. Davidson, in many instances the crack does not move on each cycle. This observation is more consistent with a damage accumulation mechanism than with a sliding off process.

As to the possibility of making quantitative advances in understanding the complex damage state ahead of propagating cracks, we are guardedly optimistic. The modern tools at our disposal for making such advances have been

[2]National Bureau of Standards, Washington, D.C. 20234.

discussed extensively at this conference and we are sure that many new applications will be forthcoming.

Another factor that must be considered are the systems that are being used to study fatigue damage. As we have seen in this conference, not only is *quantification* of fatigue damage an elusive goal, but *defining* damage is open to considerable speculation. In our opinion we would make much more progress if microstructurally simple systems, in which important parameters could be varied systematically, were more extensively used. We would then begin to more fully understand the importance of slip mode, precipitate coherency, and crystal structure (to name only a few) as they affect fatigue damage. The problem with complex systems, as implied by some of Professor McEvily's comments, is that numerous mechanisms may operate, making it difficult to make a correct assessment of any one. Along these lines, it is important for the funding agencies to provide the support for the *fundamental* studies that will give us the information necessary to economically produce more fatigue-resistant materials.

A. K. Chakrabarti[3] (*written discussion*)—The damage in front of a fatigue crack should be a maximum near the crack tip, and would decrease with distance away from the crack tip. Did you observe this to be the case in the nickel-base superalloy?

J. P. Baïlon and S. D. Antolovich (author's closure)—If it is assumed that damage is related to the density of deformation debris, then Fig. 14 shows that the slip band density increases for Waspaloy as the crack surface is approached.

[3]Materials Research and Engineering, Detroit Diesel Allison, Division of General Motors Corporation, Indianapolis, Ind. 46206.

Morris E. Fine[1] *and David L. Davidson*[2]

Quantitative Measurement of Energy Associated with a Moving Fatigue Crack

REFERENCE: Fine, M. E. and Davidson, D. L., **"Quantitative Measurement of Energy Associated with a Moving Fatigue Crack,"** *Fatigue Mechanisms: Advances in Quantitative Measurement of Physical Damage, ASTM STP 811*, J. Lankford, D. L. Davidson, W. L. Morris, and R. P. Wei, Eds., American Society for Testing and Materials, 1983, pp. 350-370.

ABSTRACT: Energy must be supplied to accomplish the processes which occur in the plastic zone ahead of the crack during fatigue crack extension. This energy has been measured (*1*) by using foil strain gages (Ikeda, Izumi, and Fine), (*2*) from electron-channeling patterns (Davidson and Lankford), (*3*) by stereoimaging (Davidson and Lankford), and (*4*) from calorimetric measurement of the heat generated during crack propagation (Gross and Weertman). The experimental results to date are presented and discussed. Both the hysteretic and permanent plastic work have been measured by strain gages. The permanent plastic work and the stored energy from cyclic plastic work are negligible. The work done numerically equals the heat evolved. The crack propagation rate data fit an equation $dC/dN = A\Delta K^4/\mu\sigma_y' U$, where A is a universal constant, μ is the shear modulus, σ_y' is the cyclic yield stress, and U is the energy per unit area of fatigue crack. The latter is a function of ΔK except when the exponent in the Paris equation is 4.

KEY WORDS: fatigue crack propagation, energy, hysteretic plastic work, heat evolved

The purpose of this paper is to examine the fatigue crack growth rate from a thermodynamics viewpoint. The crack growth is discussed from an energetics viewpoint based on an energy balance between mechanical energy input and heat energy dissipated. The energy balance is justified through irreversible thermodynamics. The stored energy is shown to be small. The methods which have been used to determine the hysteretic work done in the crack growth and the heat dissipated will be reviewed. This term has been correlated with crack

[1]W. P. Murphy Professor of Materials Science and Engineering, Department of Materials Science and Engineering and Materials Research Center, Northwestern University, Evanston, Ill. 60201.

[2]Staff Scientist, Southwest Research Institute, San Antonio, Tex. 78284.

growth in both theoretical and experimental treatments, and that relation will be examined from the viewpoint of its use, both as a tool in determining the effects of variables on crack growth and as an assist to the design of materials for better resistance to fatigue crack growth.

Basic Energetics of Crack Growth as Derived from Thermodynamics

From the second law of thermodynamics, the extension of a fatigue crack during a cycle of constant stress amplitude loading (δD) requires that

$$\delta G \leqq 0 \tag{1}$$

where G is the Gibbs free energy. The equality holds for reversible crack growth, but since crack growth is spontaneous and irreversible δG must be less than zero or the crack will not grow.

If the system does not deviate much from equilibrium during each loading cycle, that is, the crack growth rate is slow, then irreversible thermodynamics is applicable and following Prigogine [*1*] the system tends to approach equilibrium at a rate which minimizes the entropy production rate.[3] By de Donder's theorem [*2*]

$$\left(\frac{dS}{dt}\right)_{ir} = -\frac{1}{T}\left(\frac{dG}{dt}\right)_{ir} \tag{2}$$

and at constant T, the rate of crack propagation is expected to occur by that process which minimizes the reduction in Gibbs free energy per cycle and δG is expected to be small. In condensed systems δG is approximately equal to δF, the change in Helmholtz free energy per cycle. Then

$$\delta F = \delta E - T\delta S \cong 0 \tag{3}$$

where δE is the change in internal energy. With δS being small, $\delta F \cong \delta E$ and the First Law of thermodynamics leads to the conclusion that the work done per cycle on the sample DW equals the heat dissipated per cycle DQ; that is,

$$\delta E = DW - DQ \cong 0 \tag{4}$$

Derivation of Fatigue Crack Propagation Rate Equation from Energy Balance

A number of investigators [*3-7*] have derived a rate equation for fatigue crack propagation based on an energy balance. The reader is referred to the

[3]The italic numbers in brackets refer to the list of references appended to this paper.

references for detailed derivations. The following qualitative derivation will suffice for conceptual purposes. The basis for the energy balance, of course, is that δE is negligibly small and $DW = DQ$ during each cycle. This has been experimentally proved by the stored-energy measurements (see the next section).

U is defined as the energy required to make a unit area of fatigue crack by propagation of an already existing crack. The energy required to produce a unit area of fatigue crack by propagation of an already existing crack may also be thought of as twice an effective surface energy Γ (two surfaces are created); that is, $U = 2\Gamma$. As subsequently discussed, U is almost completely hysteretic in nature, in line with δE being negligibly small, and either goes to heat the specimen or is converted to heat lost to the surroundings. Thus for a specimen of unit thickness $DQ = U\delta C$. From Eq 4 the work done on a specimen of unit thickness $DW = U\delta C$. The quantity DW has been computed at several levels of approximation by using the Dugdale model [*5*], assuming Rice's elastoplastic analytical result for Mode III two-dimensional cracks [*6*], and from the continuous dislocation theory [*7*].

For present purposes an even simpler approximation will be made; DW is equated to the maximum stored elastic energy at K_{max}. The maximum value of stress in the plastic zone is σ_u, the ultimate tensile strength; σ_y, a "yield" stress, may be regarded as the average stress value giving an average value of shear strain σ_y/μ where μ is the shear modulus. The plastic zone radius at maximum stress intensity K_{max} is proportional to $(K_{max}/\sigma_y)^2$. Then the maximum stored energy is proportional to $K_{max}^4/\mu\sigma_y^2$. When K_{min} is small $\Delta K \cong K_{max}$ and

$$\delta C = \frac{dC}{dN} = A\frac{\Delta K^4}{\mu\sigma_y^2 U} \tag{5}$$

where A is a dimensionless constant. All the references cited give Eq (5) as the result when K_{min} is small. In addition, other theoretical treatments [*8–12*] based on other criteria besides on energy balance similarly predict an equation of the form of Eq 5.

Recognizing that δA must be less than zero for crack growth, Izumi et al [*6*] introduced a proportionality factor in the energy balance (Eq 4), which equals one for reversible crack growth and less than one for irreversible crack growth. Measurement of DQ and DW gives by difference the deviation from reversibility. This difference is essentially the stored internal energy per cycle (δE), which is small.

Equations of the form of Eq 5 have been criticized because exponents on ΔK of other than 4 are frequently observed when fitting experimental results for dC/dN to the Paris relation $dC/dN = M(\Delta K)^m$. Such deviations can be accommodated by allowing U to be a function of ΔK. If the processes by which the crack extends change with ΔK, then certainly U will be a function of ΔK.

Taking U to be a function of ΔK and allowing m in the Paris equation to vary leads to

$$\frac{dC}{dN} = \frac{A}{\mu\sigma^2} \frac{(\Delta K)^4}{B(\Delta K)^n} = M\Delta K^m \tag{6}$$

where $m = 4 - n$. If n is zero, that is, U is constant with respect to ΔK, m becomes 4.

Weertman [*12,13*] has derived a general equation for fatigue propagation based on an elastic crack-tip enclave model. For propagation by a cleavage mode the fatigue crack is assumed to propagate when the true stress intensity K_t in a very small elastic region assumed to be at the tip of the crack (which is surrounded by a plastic region) equals the critical stress intensity factor K_{cb} for a perfectly brittle solid. For propagation by shear sliding, K_{cs} replaces K_{cb}. Both cases give propagation equations in which the Paris exponent is variable. If K_{max} is large compared with K_{cs} or K_{cb} then m in Eq 6 is 2. If K_{max} is not large compared with K_{cs} or K_{cb} then larger values of m are predicted. Weertman [*13*] suggested that the cleavage mode is favored as K_{max} is increased because of work hardening in the plastic zone.

Procedures for measuring DW [*14-19*] and DQ [*20*] have recently been developed. The present paper reviews the methods, results, and their application to computing U for testing Eq 5.

Energy Stored During Cyclic Deformation

As is well known, during monotonic plastic deformation the stored energy or increase of internal energy is generally only a few percent of the energy expended. Clarebrough et al observed that much less energy is generally stored by long-lived fatigue specimens than by specimens failed monotonically [*21,22*]. The stored energy of 99.6% nickel fatigued to failure in 10^6 cycles was only 0.05 cal/g, which is small compared with the estimated total hysteresis energy dissipated, 2400 cal/g [*23*]. Thus the stored energy was only 0.002% of the dissipated energy.

Halford [*24*] made an extensive study of the stored energy from cyclic deformation on OFHC copper tubes deformed in torsion. Stored energy was determined during half cycles by measuring the temperature rise. Net changes in the level of stored energy were determined after a selected number of cycles in a differential annealing microcalorimeter. During each completely reversed cycle, a storage-release-storage-release sequence was observed. In annealed OFHC copper the storage portion exceeded the release so that a net amount of energy was stored per cycle. The reverse was true for cold-worked OFHC copper. With repeated deformation of annealed OFHC copper the rate of energy storage decreased with the number of cycles and approached zero early in the fatigue life. With increase in plastic strain amplitude the initial rate of increase and stable value of stored energy increased, but stabilization was reached in fewer cycles and the stored energy-total work done ratio decreased. For exam-

ple, the stable value of stored energy at a strain amplitude of 0.006 was approximately 0.75 cal/g, with saturation being reached prior to 10^3 cycles.

During fatigue crack propagation, a given element of material in the crack path will experience ever-increasing strain amplitude as the crack approaches. When it finally fails, the stored energy in the element is only a tiny fraction of the total work done. Integration over all the elements in the plastic zone yields a similar conclusion for the energy stored in the plastic zone and δE (per cycle) in Eq 4 must be very small compared with DW or DQ. As will be discussed subsequently in this paper, this has been verified further by direct measurement [*15,18,19*].

Measurement of Energy Required to Produce a Unit Area of Fatigue Crack by Propagation (U)

Since $DW \cong DQ$, the energy required to make a unit area of fatigue crack by propagation may be measured from the mechanical response of the specimen or by calorimetry. Several such methods have been devised and these will now be described.

Strain-Gage Method

Ikeda et al [*14*] devised a method for measuring DW by strategically cementing tiny foil strain gages (200 × 210 μm in size) ahead of a fatigue crack and determining the nominal stress versus local strain curves as the crack approaches under constant ΔK loading. Thus the specimen's mechanical response to the work done on it is measured and the net work, obtained by integrating over a full cycle, is numerically equal to DW which in turn equals δCU assuming the specimen is of unit thickness. Since the integration is over a full cycle, U represents plastic work; the elastic work is eliminated by the integration.

Figure 1 shows some typical results. X is defined as the distance from the center of the gage to the crack tip along the crack plane, and Y is defined as the distance from the center of the gage to the crack plane. Nominal stress-local strain curves of decreasing X for two different Y-values are shown. While the initial curves, A and G, do not close, the subsequent curves do close to a first approximation forming loops. The curves have been arbitrarily shifted to the right on the strain axis for clarity. When the gages are far from the crack tip, the loop width is too small to be shown on the scale of the curves (B and H). Curves D and I show slight hysteresis and this increases with decrease of X, as shown by Loops E, F, and J. When the crack enters the gage, it is broken. The crack bypasses the gage when Y is large, and Loop K results.

For determination of U, local stress is needed rather than nominal stress. Local stress was determined from the stress-strain hysteresis loops for unnotched specimens by using strain amplitudes determined with foil strain gages.

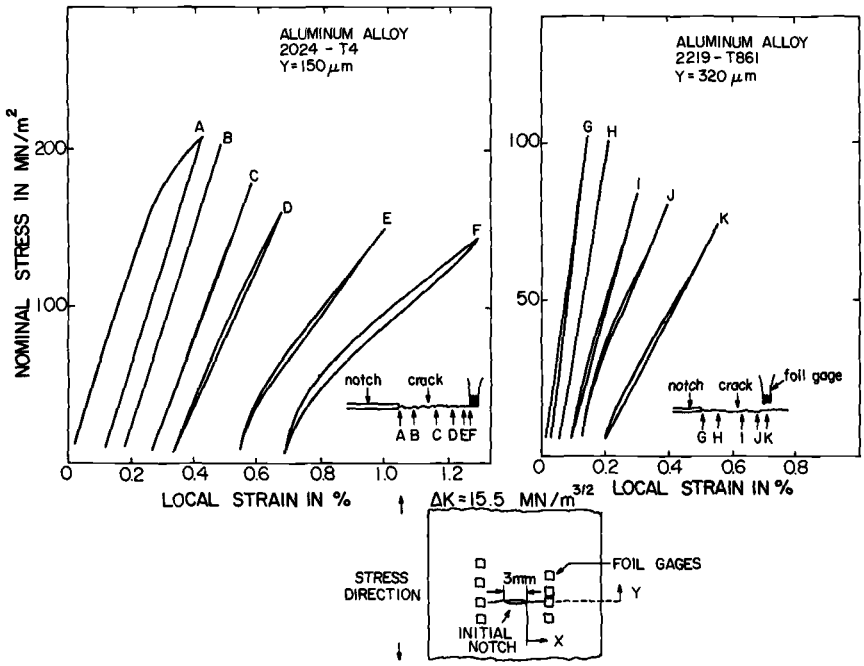

FIG. 1—*Typical nominal stress-local strain curves versus distances from crack tip determined by using 200 μm foil strain gages. The distances A-F and G-K are approximately 2 mm. Center notch is 3 mm long and 0.2 mm wide. R was 0.05. Specimens were 3 mm thick. From Izumi and Fine* [15].

The plastic work U is made up of two parts: hysteretic (U^h) and permanent (U^p). The latter was measured in several alloys and found to be much less than 1% of U. The values of U^p which have been determined [*15,18,19*] will be discussed later in light of Eq 4, but U^p was thus a negligible part of U.

From the local stress versus local strain hysteresis loops, (U_{XY}), the local plastic work per unit area of crack advance for the coordinates in the plastic zone X and Y was determined:

$$U_{XY} = \frac{\int_{\epsilon_1}^{\epsilon_2} \sigma_u d\epsilon - \int_{\epsilon_1}^{\epsilon_2} \sigma_\ell d\epsilon}{\delta C} \tag{7}$$

where σ_u and σ_ℓ refer to local stresses in the upper and lower curves of the hysteresis loop. Since the experiment is done at constant ΔK, according to linear elastic fracture mechanics a plastic zone of constant size and shape advances with the crack. A contour map of U_{XY} in the plastic zone may thus be drawn; that shown in Fig. 2 is for HY 80 and HY 130 pressure vessel steels [25]. The

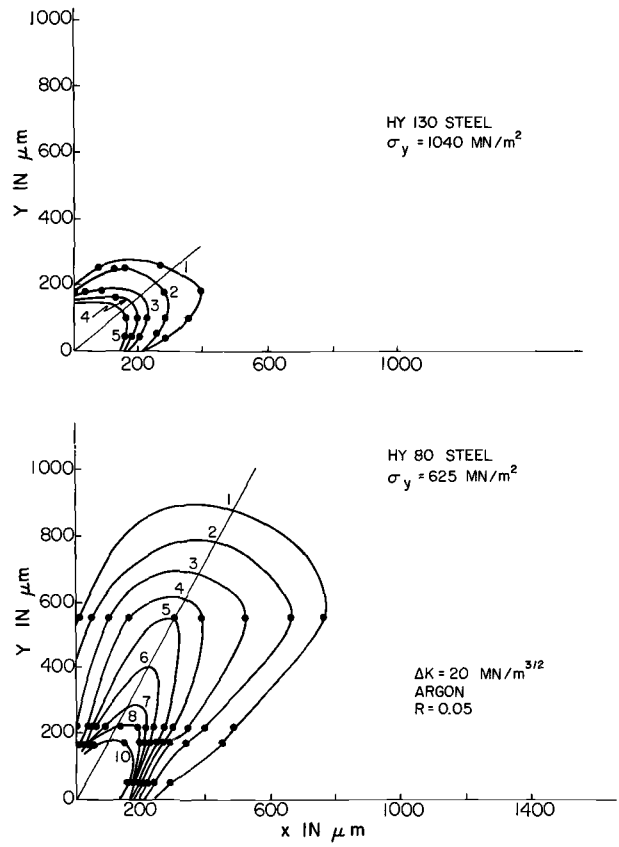

FIG. 2—*Contour maps of plastic zones at* ΔK *of 20 MN/m$^{3/2}$ in pressure vessel steels HY 80 (0.16 C-3 Ni-1.5 Cr-0.4 Mo, tempered 1 h at 700°C) and HY 130 (0.10 C-3 Ni-0.5 Cr-0.45 Mo-0.10 V, tempered 1 h at 600°C). Specimens were 3.5 mm thick. The contour lines are lines of equal local plastic work* (U_{XY}) *in units of 10^{11} J/m^4 as indicated by the numbers. From Kwun and Fine* [25].

plastic zones are butterfly-wing shaped, since the maximum shear stress is 45 deg from the loading direction and the crack plane. As expected, the plastic zone size increases with decrease in yield stress.

The plastic work per unit area of fatigue crack propagation was obtained by integrating over the plastic zone:

$$U = \int\int U_{XY}\, dX dY \tag{8}$$

Because the foil gage fails when the crack enters it, U_{XY} closer than 100 μm to the crack tip cannot be measured directly and was determined by an extrapolation method [*15, 18*]. U_{XY} for a constant small Y was extrapolated to small

X on a log-log scale. Following Rice's [8] solution for a Mode III crack (the present case is of course Mode I) the contour lines were assumed to be circles touching the crack tip and symmetrical to it. Using this method of extrapolation, U is finite because X approaches zero faster than U_{XY} approaches infinity. For convenience U was divided into two parts, U_c and U_f, where U_c, determined by extrapolation, is for the region of the plastic zone less than 100 μm from the crack tip, and U_f, determined by measurement, is the remainder. U_c was in the range of 5 to 40% of U.

To determine the effect of specimen thickness on U, the fatigue crack propagation rates of 3 and 6 mm thick specimens of 2219 aluminum alloy were compared for both the T861 and overaged heat treated condition. In the ΔK range of 7 to 20 MN/m$^{3/2}$, the dC/dN curves were essentially identical for both thicknesses. Additionally, a 1-mm-thick specimen was investigated. While dC/dN's at 7 and 8 MN/m$^{3/2}$ were the same as for the thicker specimens, the rate was much slower at 20 MN/m$^{3/2}$. It was thus concluded that U is independent of specimen thickness as long as ΔK is not too high or the specimen too thin. The measurements of U by using strain gages are summarized in Table 1.

Electron-Channeling Methods

The phenomena of electron channeling may be used in two ways to determine the plastic work dissipated by fatigue crack growth.

Channeling-Contrast Micrographs—Some materials form subcells within the plastic zone of the fatigue crack. The size distribution of subcells caused by crack growth can be measured nondestructively and easily from micrographs made in the scanning electron microscope. Contrast is developed because of the change in back-scattered electron yield from the differences in orientation of the subcells. Once detected and recorded, subcell sizes may be used together with information derived from bulk specimens to determine the work dissipated in fatigue crack growth. From bulk specimens, stress range and plastic work per cycle (hysteresis loop area) have been correlated with the size of the subcells formed by the repeated loading. These measurements are combined with the subgrain size distribution measured around the fatigue crack tip to compute the work dissipation term [16]. Some results are given in Table 2.

The work dissipated during fatigue crack growth has been measured for low-carbon steel by using subgrain size information determined from channeling contrast; the effects of both ΔK and environment have been studied [26]. At $\Delta K = 8$ MN/m$^{3/2}$ this method was compared with the strain gage method. The latter method actually measures the work outside a region roughly comparable to one half the strain gage size, with information nearer to the crack being obtained by extrapolation, as explained in the previous section; conversely, the region of subcell formation for this crack growth condition is approximately within 100 μm of the crack tip. Values of plastic work within 100 μm of the crack tip as determined by both techniques were found to be approx-

TABLE 1—*Compilation of results on plastic work of fatigue crack propagation and testing of Eq 5.*

Alloy	ΔK, $MN/m^{3/2}$	$dC/dN\|_{\Delta K}$, 10^{-8} m/cycle	U, 10^5 J/m^2	Method[a]	Ref.	m[b]	σ_y',[c] MN/m^2	A[d]
0.05C steel, annealed	8.0	15	53	2	17	4.6	170	4.3×10^{-3}
HY80 steel	20	3.5	7.7	1	23	3.4	520	3.6
HY130 steel	20	5.0	2.2	1	23	3.6	870	4.0
Nb-HSLA steel								
Hot-rolled	12.4	0.8	12	1	13	...	340	3.5
Hot-rolled	15.5	1.7	8	1	13	3.5	340	2.1
Hot-rolled	19.5	3.7	12	1	13	...	340	2.7
400°C temper	20	0.6	30	1	28	3.9	600	3.2
550°C temper	20	1.5	7.6	1	28	4.1	690	2.6
4140-650°C temper	20	4.9	3.6	3	18	2.7	540	2.5
	40	32	11.4	3	18	...	540	3.2
99.99$^+$ Al, cold-rolled	2.5	16	18	1	27	4.0	42	3.3
1100 Al, annealed	2.8	29	12	1	27	4.2	49	3.5
2219 Al-T861	7.8	1.5	2.4	1	14	4.0	370	3.5
	15.5	25	1.6	1	14	...	370	2.5
2219 Al, overaged	9.3	6.8	2.1	1	14	4.0	260	3.4
	15.5	32	1.4	1	14	...	260	1.4
2024 Al-T4	7.8	1.6	2.6	1	14	3.0	390	4.4
	15.5	14	3.2	1	14	...	390	3.1
Al-6.3Cu-T4	10.8	2.0	6.1	1	14	4.0	230	1.2
	12.4	4.7	5.8	1	14	...	230	1.6
7050 Al-T6	12.4	30	0.5	1	13	3.5	410	2.8
7050 Al-T76	15.5	30	0.6	1	13	4.0	510	2.3
X7091	10	0.16	0.17	1	12	2.3	550	2.2
	17	0.56	0.43	1	12	...	550	2.3

[a]Method for measuring U: 1—strain gage; 2—electron-channeling contrast plus strain gage; 3—heat evolved.
[b]$dC/dN = M(\Delta K)^m$ where m is the Paris exponent.
[c]0.2% offset cyclic yield stress.
[d]$dC/dN = A(\Delta K)^4/\mu\sigma_y'^2\, U$; mean value $A = [2.9 \pm 0.8\ (\text{S.D.})] \times 10^{-3}$.

TABLE 2—*Results of measurement of* U *by electron-channeling patterns and by stereoimaging.*

Alloy	ΔK, $MN/m^{3/2}$	U, 10^5 J/m^2	Method[a]	Ref.	Atmosphere
0.05 C,					
Steel-annealed	8	18	4	27	dry N_2
Steel-annealed	12	10	4	27	dry N_2
Steel-annealed	8	1.5	4	27	wet air
Steel-annealed	12	5.6	4	27	wet air
7075-T6	9.3	0.042	5	28[b]	water vapor
6061-T6	10.5	0.026	5	28[b]	water vapor
2024-T4	11	0.059	5	28[b]	water vapor
7075-T6	6	9.4	6	unpublished	vacuum
7075-T6	8	2.3	6	unpublished	vacuum
7075-T6	10	2.1	6	unpublished	vacuum

[a]Method for measuring U: 4—channeling contrast micrographs (cell size); 5—selected area electron-channeling pattern; 6—stereoimaging.
[b]Recomputed from data given in Ref *28*.

imately the same [*18*], with the strain gage technique determining additional work dissipation out to a distance as far as about 1500 μm at an angle of 50 deg to the crack plane [*18*]. Only a limited number of materials form subcells around fatigue cracks; thus the foregoing technique has limited application. But it has been used to advantage in verifying one of the assumptions of computing work dissipation by the strain gage technique and in the study of environmentally assisted fatigue crack growth (see subsection on Effects of Environment in section on Compilation of Measured Data for U).

Selected Area Electron-Channeling Patterns—For those materials which do not form subgrains, it is often possible to obtain strains within the plastic zone of a fatigue crack indirectly from changes in selected area electron-channeling patterns (SACP). These channeling pattern changes are due to the presence of dislocations within the plastic zone, but it is difficult to measure dislocation density directly by SACP. Rather, SACP changes have been correlated to plastic strains in a tensile calibration specimen of the same material [*27*]. The resulting plastic zone size and strain distribution information may then be related to the work associated with the residual deformation or stored energy (U^p) in growing the fatigue crack by use of the stress-strain curve [*28*]. The resulting computed values of plastic work are presented in Table 2 and are seen to be quite small in keeping with the factor U^p being small.

Stereoimaging Method

The stereoimaging method is a high spacial resolution method for measuring displacements caused by loading a crack [*29*]. From these measured displacements, three elements of the symmetric strain range tensor can be deter-

mined for many locations near the crack tip [*30*]. This information may be combined with data relating plastic strain range to work dissipation per cycle, as determined from bulk specimens, to calculate the work dissipated in one loading cycle or in growing the crack a unit distance. The method for computing U from information derived by stereoimaging is presented by Davidson and Lankford.[4] Values derived by this method for 7075-T6 for fatigue cracks grown in vacuum are shown in Table 2, and are seen to be of comparable magnitude to those measured by the strain gage technique.

Calorimetric Measurement of DQ

Recently Gross and Weertman [*20*] developed a calorimetric technique for measuring DQ whereby the heat generated each cycle is determined by measuring the temperature gradient away from the crack plane in an insulated sample whose ends are maintained at a constant temperature. The temperature gradient was measured with thermistors cemented to the sample with thermally conducting paste. They were located far enough away from the crack so that the heat flow was unidirectional. In practice the specimen was stress cycled until a constant temperature gradient was reached, then the cycling was ceased and the decay of the temperature gradient was measured. The heat evolved per cycle

$$DQ = -\frac{k}{N\Delta X}\int_0^{\infty} \Delta T(t)dt \tag{9}$$

where k is the thermal conductivity, t is time, N is the number of cycles, ΔX is the distance between thermistors, and ΔT is the temperature difference between thermistors. Equation 9 assumes ΔX is small enough so that dT/dX at $\Delta X/2$ equals $\Delta T/\Delta X$ to a good approximation.

Gross and Weertman implicitly assumed that δE (Eq 4) is negligible and equated U to $DQ/\delta C$. For 4140 steel tempered at 650°C at ΔK of 20 MN/m$^{3/2}$ they obtained U of 4×10^5 J/m^2 (Table 1). As will be discussed subsequently, this is in the range of values determined previously for some other steels by using the strain-gage technique.

Comparison of Hysteretic and Permanent Contributions to U

The energy required to form a unit area of fatigue crack by propagation (U) was divided into two parts: hysteretic (U^h) and permanent (U^p). During fatigue crack propagation U^h is converted to heat and raises the specimen temperature or is dissipated to the surroundings; U^p is stored as an increase in in-

[4]This publication, pp. 371-399.

ternal energy. Thus measurement of U^p and its magnitude compared with U^h is a test of Eq 4.

By using strain gages, U^p as well as U^h may be measured [*15,18,19*]. Measurements of U^p were made by Izumi and Fine [*15*] on binary Al-6.3Cu aged at room temperature. This alloy was selected because the permanent plastic strain is larger than in the other alloys studied by them. These were commercial precipitation-hardened aluminum alloys. The procedure used was very similar to that employed for U^h in that the local permanent plastic work density (U_{xy}^p) around the crack tip was integrated to give U^p. As for U^h, an extrapolation was used to determine the contribution close to the crack tip. At ΔK of 12.4 MN/m$^{3/2}$, U^p was found to be 2×10^3 J/m^2 compared with 6×10^5 J/m^2 for U^h. Thus U^p is 300 times smaller than U^h.

Liaw et al [*18*] used a similar procedure to determine U^p in low-carbon steel. It was found to be 3×10^2 J/m^2 compared with 5×10^6 J/m^2 for U^h, or a factor 1700 times smaller. Liaw and Fine [*19*] also compared U^p and U^h in cold-rolled 99.99$^+$ aluminum and annealed 1100 aluminum with similar results. U^p is negligibly small for determining the fatigue crack propagation rate. Equation 4 is a very good approximation. Further confirmation comes from the electron-channeling pattern measurements in Table 2.

Compilation of Measured Data for U

In this section the values of U determined by the various methods described are tabulated and compared.

Effects of Stress Intensity Variation

While DW or DQ per cycle is expected to increase with ΔK since the fracture area per cycle increases with ΔK, normalizing them by dividing by the fracture area per cycle might be expected to result in a parameter independent of ΔK. As already discussed, this is not the case; U in general is a function of ΔK (following Eq 6) unless the exponent of the Paris equation is 4. Although a Paris exponent of 4 is very often observed, other values such as near 2 or 3 are also frequently observed.

Recently Kwun and Fine [*31*] observed that in overaged rapidly solidified powder metallurgy aluminum alloy X7091 for ΔK of 7 to 20 MN/m$^{3/2}$ the Paris exponent was 2.3 (Fig. 3). By using the strain-gage technique, U was measured at ΔK of 10 and 17 MN/m$^{3/2}$. The values were 1.7×10^4 and 4.3×10^4 J/m^2, respectively. From Eq 6, $U = B(\Delta K)^n$, which predicts that

$$\frac{U_{17}}{U_{10}} = \left(\frac{17}{10}\right)^{1.7} = 2.5$$

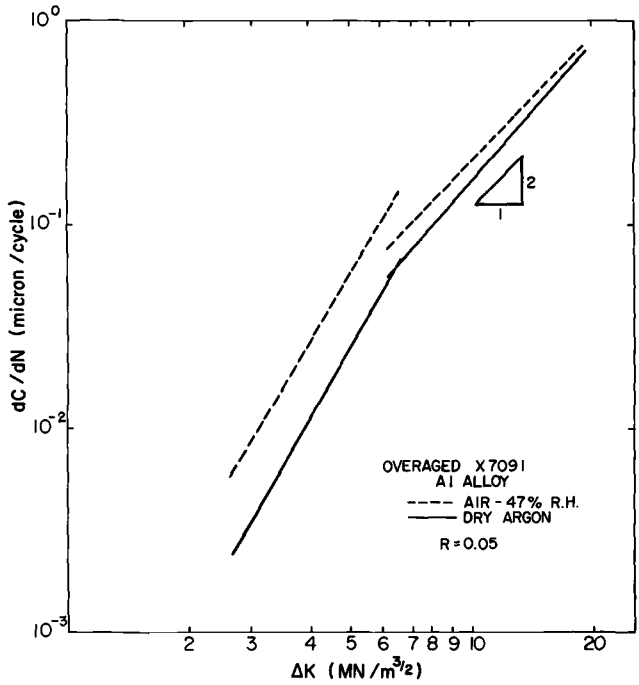

FIG. 3—*Fatigue crack propagation rate versus* ΔK *in X7091 aluminum alloy (overaged) in air (47% relative humidity) and in dry argon. From Kwun and Fine* [25].

The actual ratio of U_{17}/U_{10} is 2.3, which is in remarkably good agreement with the predicted ratio.

Gross and Weertman [*20*] obtained the empirical equation $dC/dN = 1.61 \times 10^{-11}\ \Delta K^{2.7}$ (in units of m/cycle) for 4140 steel quenched and tempered at 650°C tested in air. They also measured U versus ΔK using the DQ method. The results are shown in Fig. 4. The predicted ratio is

$$\frac{U_{40}}{U_{20}} = \left(\frac{40}{20}\right)^{1.3} = 2.5$$

A ΔK of 40 was selected for the upper limit of the comparison because at high ΔK static fracture modes become important. The actual ratio of U_{40}/U_{20} is approximately 3, which is in reasonably good agreement. Both experiments support Eq 6.

Effects of Alloying and Heat Treatment and Testing of Eq 5

A compilation of results on measurements of U by using strain gages and by the heat evolved are given in Table 1. The strain-gage measurements were

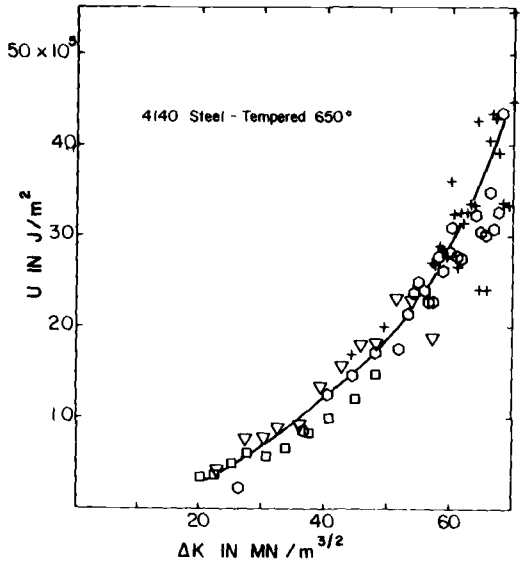

FIG. 4—*Plot of* U *as a function of* ΔK *in 4140 steel quenched and tempered 1 h at 650°C. Measurements were made by the calorimetric method of Gross and Weertman* [20]. *The symbols represent different tests.*

done in an argon environment; the heat-evolved measurements were done in air. The reproducibility and accuracy of the measurement of U need to be discussed. Considering aluminum alloy 2219 with T861 and overaged heat treatments where m was 4, the U-values at two different ΔK's for each differed by 40%. Systematic errors in the strain-gage measurement of U were analyzed by Izumi and Fine [*15*] who concluded they were no more than 20%. As discussed later, at low ΔK the crack may have a Stage I character which contributes to U.

According to Eq 5, A is a universal constant with no adjustable parameters. All quantities except A may be measured. Thus Eq 5 may be tested for a set of metals and alloys if σ_y', μ, and $dC/dN|_{\Delta K}$ have been measured for all of them with ΔK being the controlled variable. Since, in general, U is a function of ΔK, pairs of U and ΔK values need to be inserted into Eq 5. The data set presented in Table 1 gives a remarkably good confirmation of Eq 5. Data from two very different methods of measurement of U are included. Further, $dC/dN|_{\Delta K}$ varies from 0.16 to 32 $\times$ 10^{-8} m/cycle, σ_y' from 42 to 690 MN/m^2, and U from 0.17 to 53 $\times$ 10^5 J/m^2. The alloy set includes iron and aluminum base alloys; the shear modulus for the latter is smaller by a factor of 3. Yet for the 12 alloys, some with several treatments and several different ΔK values, $A = (2.9 \pm 0.8) \times 10^{-3}$ with 2.9 being the mean value and 0.8 the standard deviation. We consider Eq 5 to be very well substantiated. Also, measurements of U by using strain gages and from the heat evolved are in very good agreement.

Recently Mura and Vilmann [7] simulated plastic flow ahead of a crack tip by using a two-dimensional distribution of dislocations. They were able to calculate G for the cracked system. Assuming $\Delta G = 0$ as the condition for crack propagation, A was predicted to be in the range 1.7×10^{-3} to 2.2×10^{-3}, which is very close to the experimental results.

As already mentioned, the U-values determined from selected area electron-channeling patterns, given in Table 2, are quite small compared with those given in Table 1. While the effect of the water-vapor environment is partially responsible for the low U-values, the major reason is that the SACP changes are related to strain, as previously explained, by comparison to similar changes in a tensile calibration specimen [27]; thus only the residual deformation is measured and not the total energy dissipation related to arriving at that final state.

The stereoimaging results, for tests done in vacuum (Table 2) are approximately the same as values measured by the strain-gage technique for the 2XXX aluminum alloys. The decrease in U which occurs with increasing ΔK for 7075-T6 is attributed to the fact that in the range of measurements $6 < \Delta K < 10$ MN/m$^{3/2}$ there is a large Mode II component, which gives the crack a large Stage I characteristic. The transition to Stage II crack growth has not yet occurred. Davidson [32] has previously explained this behavior in terms of change in crack growth mode and its effect on energy dissipation. Similar decreases in U with increasing ΔK may be found in Table 1 for 2219 and Al-6.3Cu aluminum alloys; this behavior may also possibly be attributed to similar changes in crack growth mode.

Effects of Environment

The work dissipated in growing a fatigue crack in low-carbon steel (0.5 C) in a very dry nitrogen environment (<5 ppm water vapor) and a humid air (50 to 100% relative humidity) environment was measured by using the electron-channeling contrast technique [26]. This information, together with other observations on crack growth, was interpreted in terms of Eq 5 [32]. For the humid environment, U increased with increasing ΔK up to $\Delta K \cong 14$ MN/m$^{3/2}$, where it approximately equaled U-values measured in the dry environment; at higher ΔK, indications were that U for both environments became independent of ΔK. Values at ΔK of 8 and 12 MN/m$^{3/2}$ are shown in Table 2. This information coincided with crack-tip strain measurements which indicated that water vapor lowered the strain at the crack tip and resulted in a smaller plastic zone size [26]. Another finding which correlates with the foregoing information is that the crack grows much straighter in the humid environment than in the dry environment. Concomitantly, the crack growth rate is faster in humid air than in the dry nitrogen, and the slope of the dC/dN versus ΔK curve is lower in the former than in the latter.

The changes in crack-tip plasticity caused by humid air have been ration-

alized through the use of Eq 5, since no other basis could be found which incorporated all the findings into a description of crack growth.

Discussion

The advantages of using Eq 5 to describe fatigue crack growth are several. The equation relates the crack-forcing function (ΔK) to the material response (U) and two macroscopic materials characterization parameters (σ_y' and μ). Thus the equation is able to relate macroscopic and microscopic parameters, which is essential to a description of fatigue crack growth in terms of metallurgical structures and in terms of the way in which damage accumulates. It is not specific to any mechanism or model.

If U in Eq 5 is to be considered as a fundamental materials characterization parameter, it is expected to depend on changes in metallurgical structure due to such factors as alloying, deformation mechanisms, and heat treatments. Therefore the concept embodied in U is of value to the materials scientist trying to develop new materials, probably more so than to persons trying to predict structural lifetimes.

To obtain lower crack growth rates, Eq 5 states that U and σ_y' must be increased. Thus an alloy designer must learn how to increase both σ_y' and U. To a first approximation σ_y' and U are inversely related because as σ_y' increases the plastic zone size for a given ΔK decreases. Recall that the local plastic work is integrated over the plastic zone to obtain U. Liaw et al [*33*] examined the relation between σ_y' and U for data determined with strain gages as shown in Figs. 5 and 6 for steels and aluminum alloys. While a general hyperbolic decrease of U with increase of σ_y' is observed, there are some interesting exceptions; for instance, the U-values for the steel tempered at 400°C, 2024-T4 aluminum, and Al-6.3 Cu-T4 lie above the curves. The latter two materials contain dispersed phases which homogenize the plastic deformation so that it is not so highly localized in the plastic zone. The origin of the effect for the 400°C tempered Nb-HSLA (high-strength, low-alloy) steel is not known. These concepts need to be further explored to see if such indications can lead to design of better alloys.

The local plastic work density for the coordinates X and Y in the plastic zone (U_{XY}) is approximately

$$U_{XY} = \frac{|\sigma^\ell \epsilon^\ell|_{XY}}{|dC/dN|} \tag{10}$$

where σ^ℓ is the maximum local stress and ϵ^ℓ is the local plastic strain range. Even though $\sigma_{XY}{}^\ell$ increases with σ_y' because the plastic zone can sustain higher stresses, U_{XY} for constant value of X and Y is usually smaller for higher strength alloys. This is because $\epsilon_{XY}{}^\ell$ is smaller [*33*]. Liaw et al [*33*] have given the following example. A comparison of HY 130 and hot-rolled Nb-HSLA steel

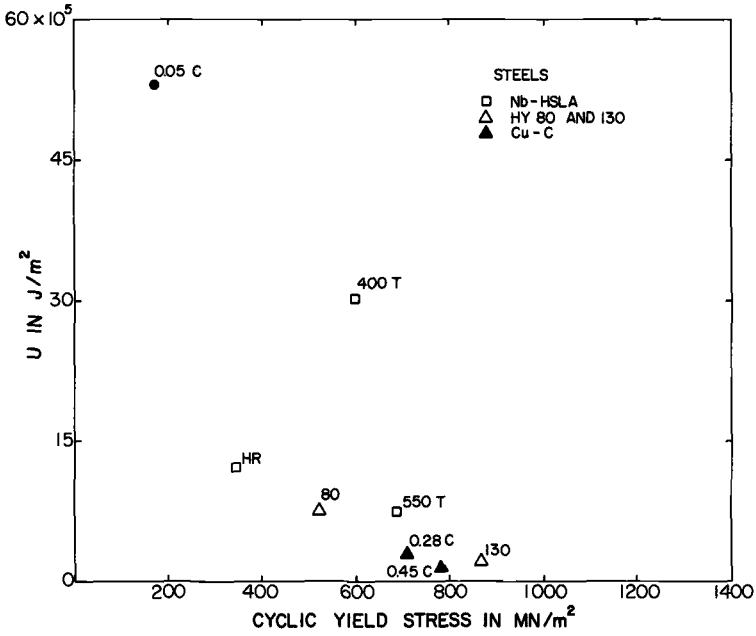

FIG. 5—*Examination of* U *as a function of 0.2% offset cyclic yield stress* (σ_y') *in steels. Average values of* U *are plotted where there are measurements for more than one* ΔK. *From Liaw et al* [33].

(Table 1) shows that the former has higher strength and lower U. The values of dC/dN at ΔK of 20 MN/m$^{3/2}$ are comparable. For $X = 100$ μm and $Y = 30$ μm, $\sigma_{XY}{}^{\ell}$ for HY 130 is 540 MN/m^2 and $\epsilon_{XY}{}^{\ell}$ is 0.012. On the other hand, for the hot-rolled Nb-HSLA steel, at the same X and Y, $\sigma_{XY}{}^{\ell}$ is 270 MN/m^2 and $\epsilon_{XY}{}^{\ell}$ is 0.094. We need to have a better understanding of the factors which determine $\epsilon_{XY}{}^{\ell}$. The hysteresis loop width versus stress range $\Delta\sigma$ in uncracked-unnotched specimens, a much easier set of measurements to obtain than those to determine U, should quantitatively indicate how $\sigma_{XY}{}^{\ell}$ and $\epsilon_{XY}{}^{\ell}$ vary in the plastic zone ahead of a fatigue crack. Such a study versus microstructure would appear to be very helpful towards developing alloys which have low fatigue crack propagation rates.

Thus Eq 5 points the alloy designer towards the development of increasing hysteresis loop area, as measured on smooth specimens, while not allowing much change in σ_y'. Likewise, an increase in modulus, for example, through fiber reinforcement, should also decrease crack growth rates, if all other factors are kept equal.

Since measurement of U takes considerable time, it is desirable to compute it from other measurements. This may possibly be done from hysteresis loop areas versus $\Delta\sigma$ determined on a smooth specimen, provided the distribution of $\Delta\sigma$ versus X and Y ahead of a Mode I fatigue crack can be calculated includ-

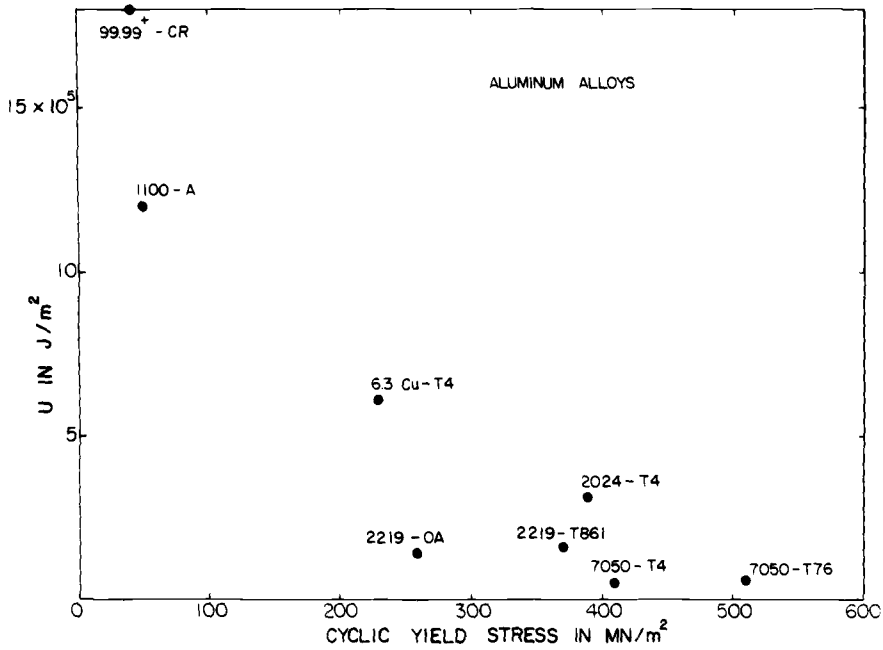

FIG. 6—*Examination of* U *as a function of 0.2% offset cyclic yield stress* (σ_y') *in aluminum alloys. Average values of* U *are plotted where there are measurements for more than one* ΔK. *From Liaw et al* [33].

ing plasticity. As a crude first approximation, following the strain exhaustion treatments of fatigue crack propagation by Majumdar and Morrow [*34*] and Chakrabortty [*35*], the stress distribution solution of Rice for a stationary Mode III crack may be assumed.

It should be emphasized that since U^p was found to be much smaller than U^h, the accumulation of damage as measured by increase in internal energy (E) in the plastic enclave at the crack tip does not control the crack propagation rate. Most of the work done in crack propagation goes to back and forth motion of the dislocations involved in the extension process. In severely cold-worked metals the stored energy in the plastic enclave around the crack tip may actually be reduced by the stress-strain cycling. Cherepanov and Halmanov [*11*] pointed out that there are two contributions to U, one from the processes which occur near the crack tip and the other from advancing the plastic zone.

If U is a material characteristic, then variations of Eq 5 can be used to predict crack growth. An example where this may be useful is in the analysis of the effect of microstructure in growth retardation after an overload. Assuming that an effective ΔK in the overload plastic zone could be computed, then, knowing U, subsequent crack growth through this overload region could be

predicted. It has not been experimentally determined, though, how U is affected by R-ratio, spectrum loading, and overloads. It is not clear at this time how Eq 5 is to be modified to take these into consideration.

Energy considerations should also control the near-threshold region of fatigue crack propagation, and evidence is presented to show that U does increase considerably as ΔK is decreased in the low ΔK region. However, it is not clear how to modify Eq 5 to satisfactorily apply to the near-threshold region. Firstly, the crack propagation is not continuous and it is not possible to ascribe a δC to each cycle. Also, the crack closure stress becomes large as the threshold is approached so that closure effects must be included.

Thus the concepts embodied in Eq 5 have both advantages and limitations. The purpose of this paper has been to develop the concepts and indicate how U may be determined. The use of U to designers is still being explored and examined, and it may be some time until it is clear as to the long-term value of these concepts to the prevention of fatigue failures other than for design of better alloys.

Acknowledgments

The preparation of this paper was supported in part (MEF's contribution) by the Northwestern University Materials Research Center under NSF-MRL Grant DMR79-23573 and in part (DLD's contribution) by the Office of Naval Research.

References

[1] Prigogine, I., *Thermodynamics of Irreversible Processes*, Wiley-Interscience, New York, 1955.
[2] de Donder, T., *L'Affinite*, Gautier-Villars, Paris, 1936.
[3] Cherepanov, G. P., *International Journal of Solid Structures*, Vol. 4, 1968, p. 811.
[4] Raju, K. N., *International Journal of Fracture*, Vol. 8, 1972, p. 1.
[5] Irving, P. E. and McCartney, L. N., *Metal Science*, Vol. 11, 1977, p. 351.
[6] Izumi, Y., Fine, M. E., and Mura, T., *International Journal of Fracture*, Vol. 17, 1981, p. 15.
[7] Mura, T. and Vilmann, C., "Fatigue Crack Propagation Related to a Dislocation Distribution," in Proceedings of Symposium on *Defects and Fracture*, G. C. Sih, Ed., Noordhoff, Leyden, The Netherlands, 1981; Vilmann, C., Ph.D. thesis, "A Dislocation Density Approach to Fracture and Fatigue," Northwestern University, Evanston, Ill., 1979.
[8] Rice, J. R. in *Fatigue Crack Propagation, ASTM STP 415*, American Society for Testing and Materials, 1967, p. 247.
[9] Weertman, J., *International Journal of Fracture*, Vol. 9, 1973, p. 125.
[10] Mura, T. and Lin, C. T., *International Journal of Fracture*, Vol. 10, 1974, p. 284.
[11] Cherepanov, G. P. and Halmanov, H., *Engineering Fracture Mechanics*, Vol. 4, 1972, p. 219.
[12] Weertman, J. in *Fracture Mechanics*, N. Perrone, H. Liebowitz, D. Mulville and W. Pilkey, Eds., University Press of Virginia, Charlotteville, 1978, p. 193; *Fatigue and Microstructure*, ASM Materials Science Seminar volume, American Society of Metals, Metals Park, Ohio, 1979, p. 279.
[13] Weertman, J. in *Three Dimensional Constitutive Relations and Ductile Fracture*, S. Nemat-Nasser, Ed., North-Holland, Amsterdam, The Netherlands, 1981, pp. 111-122.

[14] Ikeda, S., Izumi, Y., and Fine, M. E., *Engineering Fracture Mechanics*, Vol. 9, 1977, p. 123.
[15] Izumi, Y. and Fine, M. E., *Engineering Fracture Mechanics*, Vol. 11, 1979, p. 791.
[16] Davidson, D. L. and Lankford, Jr., J., "Determination of the Energy of Fatigue Crack Propagation and its Alteration by Wet Air," in *Proceedings*, Symposium on Environment Sensitive Fracture of Engineering Materials, 1977, TMS-AIME (in press).
[17] Davidson, D. L. and Lankford, Jr., J., "Crack Tip Plasticity Associated with Corrosion Assisted Fatigue," Interim Report of 31 May 1978, Contract N00014-75C-1038, Southwest Research Institute, San Antonio, Texas, and unpublished data.
[18] Liaw, P. K., Fine, M. E., and Davidson, D. L., *Fatigue of Engineering Materials and Structures*, Vol. 3, 1980, p. 59.
[19] Liaw, P. K. and Fine, M. E., *Metallurgical Transactions*, Vol. 12A, 1981, p. 1927.
[20] Gross, T. and Weertman, J. (to be published); T. Gross, Ph.D. thesis, "Calorimetric Measurement of the Plastic Work of Fatigue Crack Propagation in Quenched and Tempered 4140 Steel," Northwestern University, Evanston, Ill., Aug. 1981.
[21] Clarebrough, L. M., Hargreaves, M. E., Head, A. K., and West, G. W., *Transactions of the Metallurgical Society of AIME*, Vol. 203, 1955, p. 99.
[22] Clarebrough, L. M., Hargreaves, M. E., West, G. W., and Head, A. K., *Proceedings of the Royal Society (London)*, Vol. A242, 1957, p. 160.
[23] Halford, G. R., *Journal of Materials*, Vol. 1, 1966.
[24] Halford, G. R., Ph.D. thesis, "Stored Energy of Cold Work Changes Induced by Cyclic Deformation," University of Illinois, Urbana, Ill., 1966.
[25] Kwun, S. I. and Fine, M. E., *Fatigue of Engineering Materials and Structures*, Vol. 3, 1980, p. 367.
[26] Davidson, D. L. and Lankford, Jr., J., *International Journal of Fracture*, Vol. 17, 1981, pp. 257-275.
[27] Davidson, D. L., *Scanning Electron Microscopy 1974*, IITRI, Chicago, Ill., 1974, pp. 927-934.
[28] Davidson, D. L. and Lankford, Jr., J., *Fatigue of Engineering Materials and Structures*, Vol. 3, 1980, pp. 289-303.
[29] Davidson, D. L., *Scanning Electron Microscopy 1979*, Vol. II, SEM Inc., AMF O'Hare, Ill., 1979, pp. 79-86.
[30] Williams, D. R., Davidson, D. L., and Lankford, Jr., J., *Experimental Mechanics*, Vol. 20, 1980, pp. 134-139.
[31] Kwun, S. I. and Fine, M. E., *Scripta Metallurgica*, Vol. 14, 1980, pp. 155-158.
[32] Davidson, D. L., *Fatigue of Engineering Materials and Structures*, Vol. 3, 1981, pp. 229-236.
[33] Liaw, P. K., Kwun, S. I., and Fine, M. E., *Metallurgical Transactions*, Vol. 12A, 1981, pp. 49-55.
[34] Majumdar, S. and Morrow, J. in *Fracture Toughness and Slow-Stable Cracking, ASTM STP 559*, American Society for Testing and Materials, 1974, p. 159.
[35] Chakrabortty, S. B., *Fatigue of Engineering Materials and Structures*, Vol. 2, 1979, pp. 331-344.

DISCUSSION

H. Mughrabi[1] *(written discussion)*—You mentioned that A should be a universal constant. In your experiments you determined $A = 2.9 \times 10^{-3}$ with a mean standard deviation of $\pm 0.8 \times 10^{-3}$. What were the largest and smallest values of A?

[1]Max-Planck-Institut für Metallforschung, Institut für Physik, Stuttgart, Federal Republic of Germany.

M. E. Fine and D. L. Davidson (authors' closure)—Time did not allow us to present this detail orally. Table 1 indicates that, for this data set, A varies from 1.2 to 4.3 $\times 10^{-3}$.

S. D. Antolovich[2] *(written discussion)*—In your equation for FCP you have indicated that U is a function of ΔK. In order to show a threshold, U must increase very rapidly in some low ΔK range yet, if I correctly recall your data, you show a tendency for U to *increase* with increasing ΔK. Can you explain this apparent contradiction?

M. E. Fine and D. L. Davidson (authors' closure)—As shown in Table 2, in fact, U does increase on lowering ΔK in the low ΔK region, provided the measurements are made in an inert environment; however, we do not know how to modify the theory to include the threshold region, because of large crack closure effects and because crack propagation is not continuous.

J. T. Fong[3] *(written discussion)*—In your thermodynamic formulation, it was assumed $\delta E \approx 0$. For what materials, and at what temperatures, were experiments done to justify this assumption? How small was the δE measured? Is it 1% or 5%?

M. E. Fine and D. L. Davidson (authors' closure)—As stated in the text but not given orally, in Al-6.3Cu aged at room temperature, U^h/U^p, measured by strain gages, is 300 for $\Delta K = 12.4$ MN/m$^{3/2}$. This factor is 1700 in annealed low-carbon steel at ΔK of 8 MN/m$^{3/2}$. Similar results were obtained for cold-rolled 99.99$^+$ aluminum and annealed 1100 aluminum alloys where the ratios measured were 2×10^4 at ΔK of 2.5 MN/m$^{3/2}$ and 1×10^3 at ΔK of 2.8 MN/m$^{3/2}$, respectively. Further, U^p measured by selected area electron-channeling patterns is quite small in several aluminum alloys (Table 2). All these measurements were made at room temperature.

[2]University of Cincinnati, Cincinnati, Ohio.
[3]National Bureau of Standards, Washington, D.C. 20234.

David L. Davidson[1] *and James Lankford*[1]

Fatigue Crack Tip Strains in 7075-T6 Aluminum Alloy by Stereoimaging and Their Use in Crack Growth Models

REFERENCE: Davidson, D. L. and Lankford, J., **"Fatigue Crack Tip Strains in 7075-T6 Aluminum Alloy by Stereoimaging and Their Use in Crack Growth Models,"** *Fatigue Mechanisms: Advances in Quantitative Measurement of Physical Damage, ASTM STP 811*, J. Lankford, D. L. Davidson, W. L. Morris, and R. P. Wei, Eds., American Society for Testing and Materials, 1983, pp. 371-399.

ABSTRACT: Detailed quantitative measurements of crack tip strains have been made for near-threshold fatigue cracks in 7075-T6 aluminum specimens grown in a vacuum environment. In addition, crack tip opening displacements and crack growth rates have been measured. These data are used in three related models which examine cumulative and critical strain and critical energy dissipation as criteria for crack advance. These models are then examined in light of observed crack growth patterns.

KEY WORDS: fatigue crack growth, strain, aluminum alloy, modeling, crack tip plasticity, crack tip opening displacement

The development of a quantitative model that will predict the rate of growth of a fatigue crack can be divided into two subtasks. The first is to establish a quantitative criterion (failure condition) according to which the crack extends; the second is to quantify the extent of incremental crack advance (the distance over which the failure condition has been exceeded).

Most efforts to model fatigue crack growth have invoked the concept of the material ahead of the crack being "damaged," which is considered to manifest itself microstructurally (as dislocations, subcells, slip bands, voids, or microcracks). It has proven difficult to incorporate these microstructural details into tractable predictive models. In the case of aluminum alloys at low homologous temperatures, voids and microcracks appear to be irrelevant to

[1]Staff Scientist, Southwest Research Institute, San Antonio, Tex. 78284.

crack advancement, but within the crack tip plastic zone, the dislocation density does gradually increase as the crack tip is approached, and the dislocation arrangements may be altered as well.

Rather than use this knowledge of dislocation microstructure directly, it may be possible to treat crack growth in an equally valid way by considering the local mechanical factors (stress, strain, energy density) represented by the presence of the dislocations. This approach has in fact been the basis for many models, but most such efforts have greatly suffered from a lack of knowledge regarding the near-crack-tip mechanical parameters. It has been assumed in many models [*1–3*] that low-cycle fatigue measurements made on bulk specimens, which provide information such as Coffin-Manson exponents and strain-hardening coefficients, are likewise relevant in the local vicinity of a crack tip.[2] Alternatively, far field measurements or estimates [*4–7*] of crack tip strains or stress have been extrapolated to the near-crack-tip region; this kind of extrapolation is extremely questionable, since the state of stress and scale of yielding differ greatly for the two regimes.

The present paper reports the results of an effort to bypass the intrinsic difficulties in describing crack tip "damage" in a microstructural sense. Instead, the very local crack tip deformation field is quantified, and is itself considered to be the "damage" caused by the cyclic loading. These crack tip strains are, of course, due to the generation and motion of dislocations, but by describing "damage" as strain instead of in terms related to the description of dislocations, a macroscopic parameter results, even though the measurement of this parameter is on a very localized basis (micrometres). This information has been incorporated into quantitative models for crack growth. In addition, information derived from direct, dynamic observation of fatigue crack growth at high resolution within the scanning electron microscope (SEM) have been incorporated in the model formulations.

Determination of Strains

Single-edge notch specimens were fabricated from a commercially obtained, 6.25-mm-thick plate of 7075-T6 aluminum alloy. The specimens, 54 mm in length by 20 mm wide by 3 mm thick, were pinhole-loaded at frequencies of 0.3 or 5 Hz, and at a stress ratio of 0.15 to 0.2, in either of two equivalent inert environments: dry N_2,[3] and a vacuum of $\sim 1 \times 10^{-6}$ torr. No differences in crack growth behavior were detected between the two frequencies or environments. All cracks were oriented perpendicularly to the rolling direction; after initiating and growing each crack under the desired conditions within an environmental cell housed in a laboratory test machine, specimens were transferred to a special loading stage for observation within

[2]The italic numbers in brackets refer to the list of references appended to this paper.

[3]Dry means less than 10 ppmv of water vapor in nitrogen gas, as measured by a dew-point indicator located within 2 cm of the crack tip.

the scanning electron microscope [*8*]. Using this stage, cyclic deformation and extension of the crack tip may be observed and recorded. Still photographs were made at maximum, minimum, and intermediate loads, and videotapes were made of some of the cracks, so that cyclic crack growth could be observed dynamically. Specimens which had been cracked in the laboratory machine were either immediately placed in the SEM and observed, or, if the rest time between cycling in the laboratory and transferal to the SEM had been more than 2 h, the crack was cycled an additional 100 cycles within the SEM prior to observation. This precaution was taken because of crack tip relaxation effects which we have observed for this material, and which would have affected the observations and measurements.

The stereoimaging technique [*9,10*] was used to observe and measure the crack tip displacements which occurred upon changing the applied load. This technique utilizes the capabilities of the eye-brain system to visualize in-plane displacements in the eye axis as displacements out of the plane of the photographs. Consequently, the techniques and equipment used in making relief maps from aerial photographs may be used to quantify the displacements caused by loading the crack. Displacements of points on the specimen surface near the crack tip were determined at regular intervals in the x and y directions, thereby allowing strains to be determined both in line with the loading axis (x), and normal to it (y), which was approximately in the direction of crack growth. With this technique, it is not necessary to impose a grid network on the specimen (the measurements do not require it); thus, spatial resolution is not limited by the ability to attach a very fine grid.

Strain is computed from the measured displacement distribution by differentiating the displacement functions in mutually perpendicular directions, thereby allowing determination of both the normal strains ϵ_{xx} and ϵ_{yy}, and the shear strain γ_{xy}. These are the total in-plane strains, elastic plus plastic, and constitute essentially everything which may be experimentally determined regarding the crack tip deformation field without recourse to assumptions. z-axis displacements could also be measured by conventional stereophotography, but gradients of these displacements cannot be computed; therefore z-axis strains cannot be obtained. Computational techniques for the separation of the total strain into elastic and plastic components exist, as do techniques for the calculation of stresses from the measured strains [*11*], but these will not be used in this paper.

From the computed normal strains, a Mohr's circle construction may be used to compute the magnitude and direction of the maximum (ϵ_{11}) and minimum (ϵ_{22}) principal strains, and the maximum shear strain (γ_{max}).

Experimental Results

The stereoimaging technique produces extensive data for each crack tip. However, since the normal strain ranges $\Delta\epsilon_{xx}$, $\Delta\epsilon_{yy}$, and $\Delta\gamma_{xy}$ frequently

were observed to show little systematic dependence upon x and y, much of the analytical effort has been based instead on the maximum shear strain range $\Delta\gamma_{max}$, and the principal strain ranges $\Delta\epsilon_{11}$ and $\Delta\epsilon_{22}$. Results have been presented through the use of displacement diagrams and Mohr's circles of strain [*10*]. Displacement diagrams, in particular, demonstrate a dramatic and general observation: cracks open in such a way as to give rise to mixed mode (I and II) deformation. Figure 1 represents a typical displacement field, showing that displacements occur both parallel and perpendicular to the loading axis, even though the loading is nominally pure Mode I. Why the deformation field is asymmetric with respect to the plane of the crack is not known, but possible reasons will be discussed later. Also, no method has yet been devised to separate the displacements observed into those associated with pure Mode I and those due to pure Mode II; thus, the observed mixed mode deformation must remain qualitative at this time.

Strains derived from such displacement diagrams are presented here as spatial distributions of $\Delta\gamma_{max}$. Figures 2 to 6 are for the stress intensity factor range $6 \leq \Delta K \leq 10$ MN m$^{-3/2}$. Two strain distributions are shown at $\Delta K =$ 10 MN m$^{-3/2}$ in order to indicate the variability in magnitude, but qualitative similarity, of the observations. (Note changes in the vertical scales in the different figures.) These figures show a strain concentration at the crack tip, with the strain decreasing with distance from the crack tip. In general, the strain intensity peaks forward of the crack, approximately along the y-axis, although there may be a tendency to form a bimodal distribution along x some distance ahead of the crack tip. Cross sections through Figs. 2 to 6 are shown in Figs. 7 to 11; these confirm the general pattern of deformation described previously. These data will be used later in the models developed.

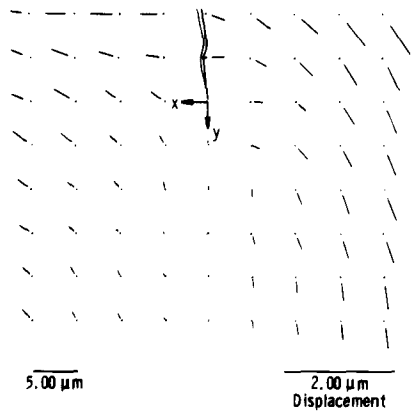

FIG. 1—*Displacements due to the loading portion of the cycle near a fatigue crack grown in 7075-T6 in vacuum at* $\Delta K = 6.2$ *MN/m*$^{3/2}$. *Note the asymmetry of material motion about the crack plane, resulting in considerable shear, even though the loading was Mode I along the x-axis. Displacement magnitude is enhanced relative to the spacing of the measurements.*

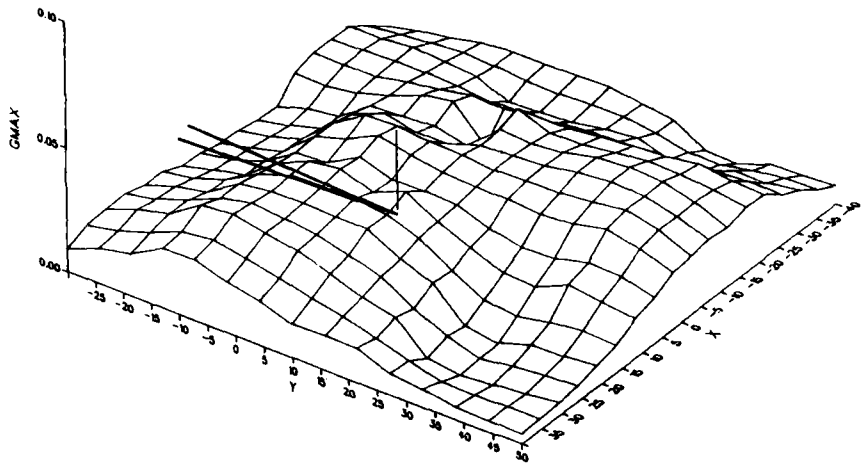

FIG. 2—*Distribution of maximum shear strain at* $\Delta K = 6\ MN/m^{3/2}$. *Location of the crack is on the* x-y *plane. View is 35 deg around from the* y-*axis and 30 deg in elevation;* x *and* y *are in micrometres.*

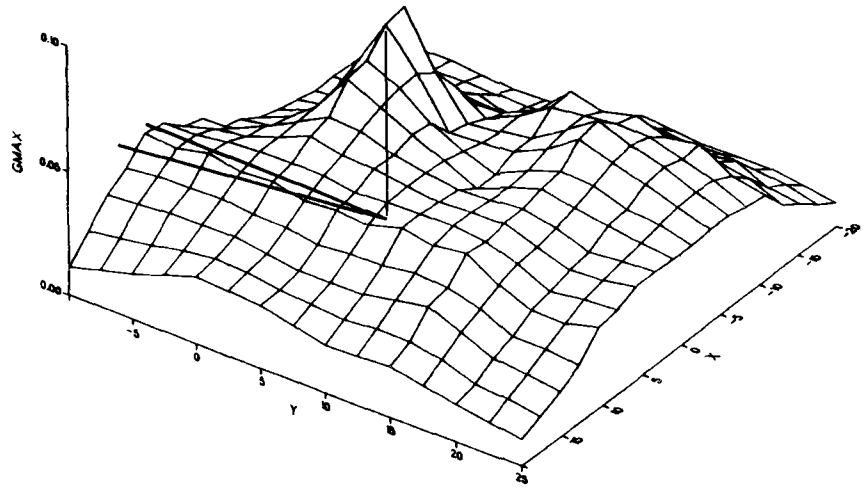

FIG. 3—*Distribution of maximum shear strain at* $\Delta K = 6.2\ MN/m^{3/2}$.

It should be noted that very narrow lines of intense slip, or slip lines, have not been observed; rather, strain is distributed around the crack tip in a broad region, homogeneous on a scale of 0.5 to 1 μm. It should be emphasized that narrow slip bands can exist, and have been seen in other materials using stereoimaging; they have not been observed during the course of the present study.

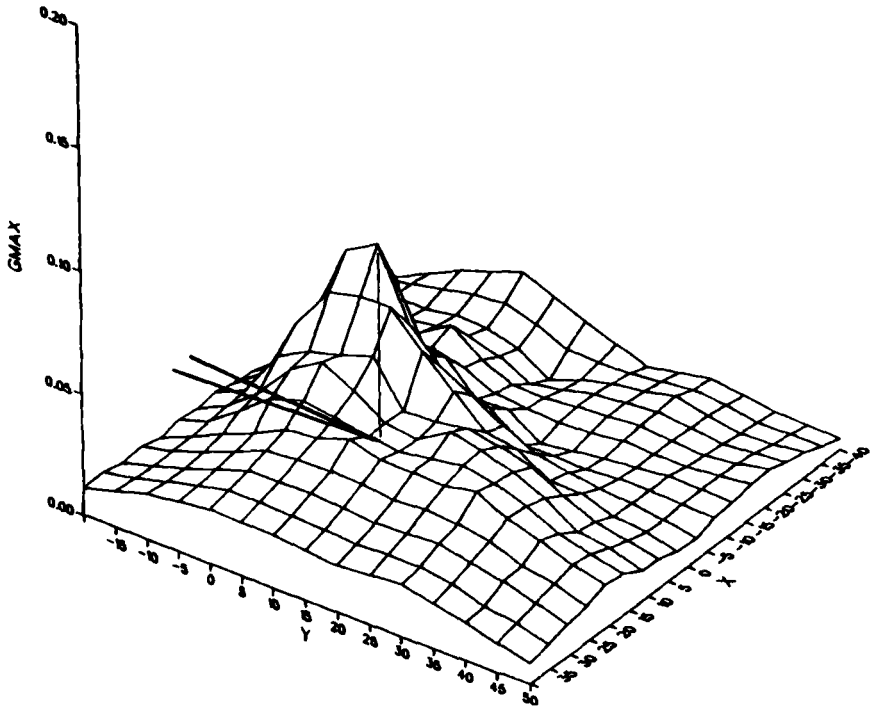

FIG. 4—*Distribution of maximum shear strain at* $\Delta K = 8\ MN/m^{3/2}$.

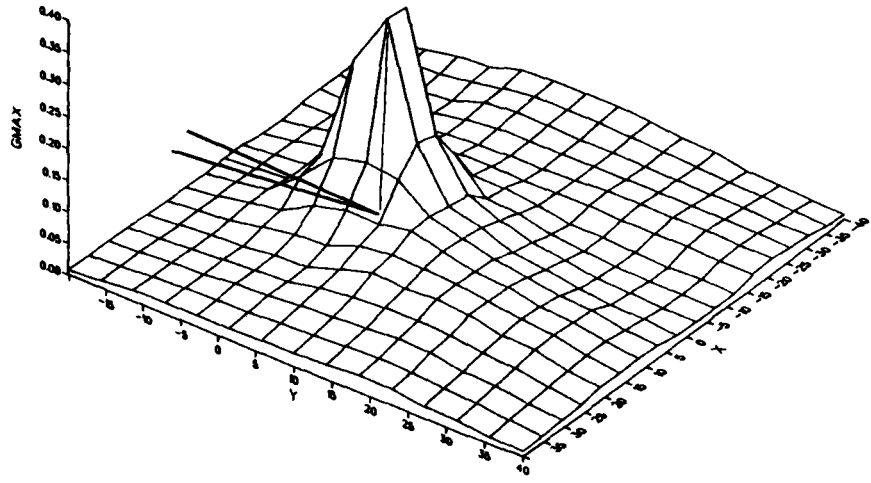

FIG. 5—*Distribution of maximum shear strain at* $\Delta K = 10\ MN/m^{3/2}$.

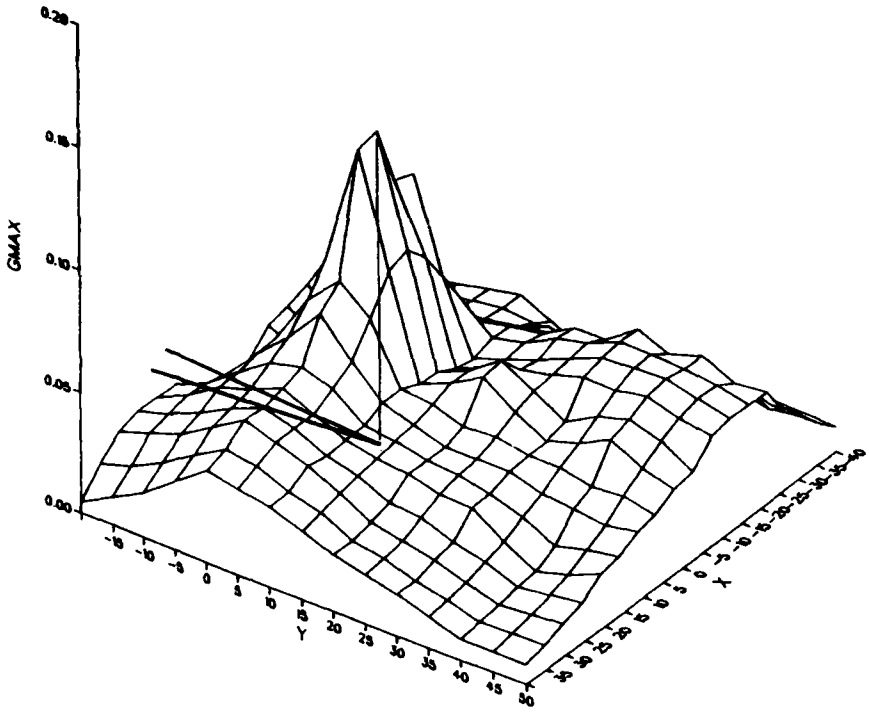

FIG. 6—*Distribution of maximum shear strain at* $\Delta K = 10\ MN/m^{3/2}$.

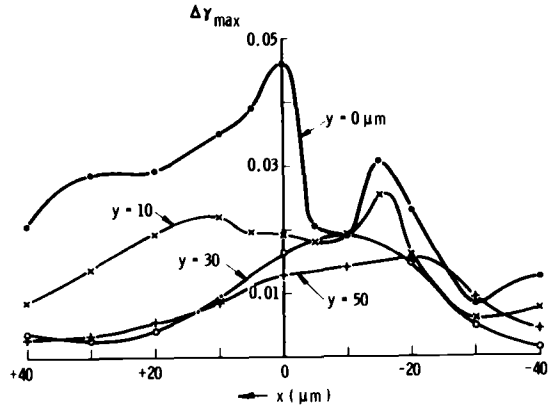

FIG. 7—*Maximum shear strain distributions along x for several y;* $\Delta K = 6\ MN/m^{3/2}$.

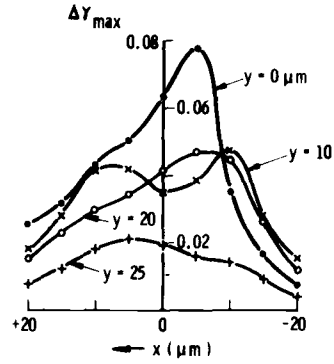

FIG. 8—*Maximum shear strain distribution along* x *for several* y; $\Delta K = 6.2\ MN/m^{3/2}$.

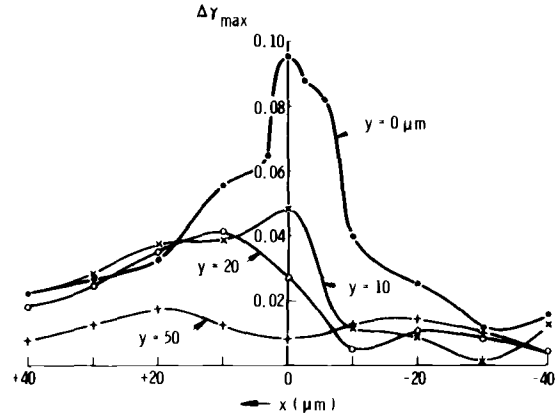

FIG. 9—*Maximum shear strain distribution along* x *for several* y; $\Delta K = 8\ MN/m^{3/2}$.

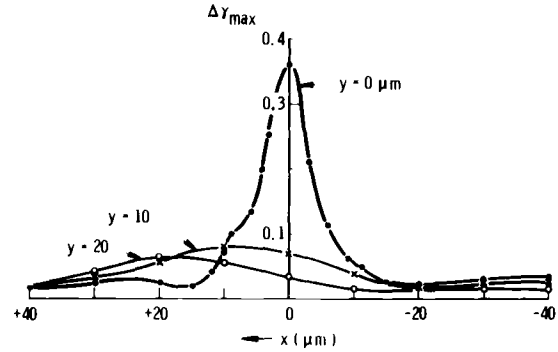

FIG. 10—*Maximum shear strain distribution along* x *for several* y; $\Delta K = 10\ MN/m^{3/2}$.

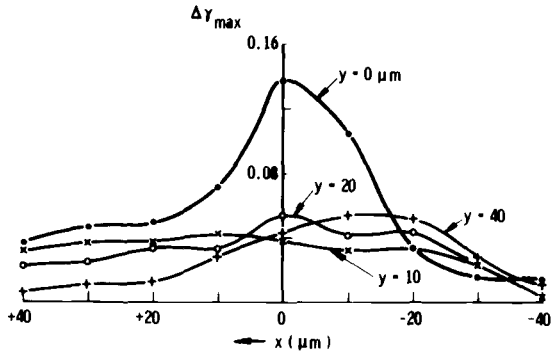

FIG. 11—*Maximum shear strain distribution along* x *for several* y; $\Delta K = 10\ MN/m^{3/2}$.

Another strain parameter which has been found useful in characterizing the strain range distribution is the effective total strain range, defined here as

$$\Delta\epsilon_t^{\text{eff}} = \frac{2}{\sqrt{3}}(\Delta\epsilon_1^2 + \Delta\epsilon_1\Delta\epsilon_2 + \Delta\epsilon_2^2)^{1/2} \tag{1}$$

The advantage of this relation is that it combines the principal strain ranges into one term. (Numerically, $\Delta\epsilon_t^{\text{eff}}$ is nearly equal to $\Delta\gamma_{\max}$ in many instances, although some exceptions have been noted.) The distribution of $\Delta\epsilon_t^{\text{eff}}$ ahead of the crack along the maximum strain region has been examined in considerable detail. The data can be fit into two equations:

$$\Delta\epsilon_t^{\text{eff}} = \Delta\epsilon_0 - m\ln(r + A) \tag{2}$$

where $\Delta\epsilon_0$, m, and A are fitting constants, and

$$\Delta\epsilon_t^{\text{eff}} = \frac{E}{(A + r)^{\ell}} \tag{3}$$

where E, A, and ℓ are fitting constants. Equation 2 generally fits the data much better than does Eq 3, a result in agreement with previous data derived by analysis of selected area electron channeling patterns [*12*]. Equation 2 has the general form derived by Rice [*13*] for a moving crack, while Eq 3 has the general form of that derived by Hutchinson [*14*] and Rice and Rosengren [*15*] for a unidirectionally loaded crack in a work-hardening material. Both equations have been modified, in order to provide finite strain values at $r = 0$, by inclusion of the parameter A. However, since the experimental data fit Eq 2 better than Eq 3, and since the cracks in question are indeed moving (albeit rather slowly), results are subsequently analyzed by Eq 2.

Values of the parameters characterizing the measured crack tip strain range distributions are listed in Table 1. All the data obtained have been included, although some of it is not considered "typical." The data thought to be "best" are labeled by an asterisk; the rationale behind this decision will be discussed later. Trends in all the factors appear to correlate with changes in ΔK, with the exception of A, for which no trend is discernible. The computed plastic zone size, r_p, is the value of r derived by setting $\Delta\epsilon_t^{\text{eff}} = 0.0065$ in Eq 2, where 0.0065 is approximately twice the shear strain at yield in a tension specimen. Thus r_p really should be considered to be an estimate of the cyclic plastic zone size ahead of the crack tip. Data in the table indicate that r_p decreases with increasing ΔK, which is thought to occur because of the changing stress stage as ΔK increases.

The correlation between crack tip plastic strain range $\Delta\epsilon_p$ and ΔK is shown in Fig. 12. Although considerable scatter exists in the data, the "best" data fit along a line having a slope of 2.5 to 3.5. Part of the reason for this scatter may be understood by considering the crack tip opening displacements corresponding to the measured crack tip strains.

Several measurements of crack-opening magnitude at various distances behind the crack tip are shown in Fig. 13. These data, in agreement with similar information for 304SS [*16*] obtained within 1 μm of the crack tip, indicate that the crack-opening displacement (COD) is a power function of the distance behind the crack tip, $-y$, so that

$$\text{COD} = C_0|-y|^p \tag{4}$$

Values of C_0 and p are listed in Table 1. From the data available, no correlation exists between p and ΔK; the mean value and standard deviation is $p = 0.6 \pm 0.16$. However, correlation of C_0 with ΔK gives

$$C_0 = C\,\Delta K^q \tag{5}$$

where $C = 8 \times 10^{-11}$ m and $q = 4.0$. This is a very useful and interesting result, since C_0 basically represents the crack tip opening displacement (at $y = 1$ μm behind the tip).

By comparing C_0 and the crack tip plastic strain range $\Delta\epsilon_p = \Delta\epsilon_t^{\text{eff}} - 0.0065$, it is clear that the two are correlated, as shown in Fig. 14. All the data reported in Table 1 are shown in the figure, as well as an additional point obtained from strain measurements after an overload to $K_{\max} = 24$ MN/m$^{3/2}$, demonstrating that the range of the correlation extends beyond the data of Table 1. The line shown in the figure has been statistically fit to the data with a correlation coefficient of 0.97. The equation is

$$\Delta\epsilon_p = 2.8 \times 10^3\, C_0^{0.69} \tag{6}$$

TABLE 1—*Crack-opening, crack tip strain, and strain distribution parameters.*

	$\text{COD} = C_0\lvert -y\rvert^p$			$\Delta\epsilon_t^{\text{eff}} = \Delta\epsilon_0 - m\ln(y + A)$ ahead of crack				
		Crack Tip			Strain Distribution			
Data Set	ΔK, MN/m$^{3/2}$	C_0, μm	p	$\Delta\epsilon_t(0)$	m	$\Delta\epsilon_0$	A, μm	r_p,[a] μm
34	6[b]	0.15	0.67	0.040	0.0068	0.0416	1.26	175
35	6	0.18	0.64	0.054	0.0113	0.0606	1.8	119
36	6.2[b]	0.11	0.60	0.048	0.0075	0.0463	0.76	200
39	8	0.097	0.72	0.040	0.0052	0.0306	0.15	100
40	8	0.07	0.77	0.049	0.0082	0.0446	0.59	104
41	8[b]	0.25	0.81	0.094	0.0310	0.1372	4.0	64
43	10[b]	1.59	0.34	0.295	0.0738	0.2802	0.81	40
44	10	0.52	0.60	0.163	0.0342	0.1444	0.58	56

[a] r_p = value of r when $\Delta\epsilon_t^{\text{eff}} = 0.0065$.
[b] "Best" data.

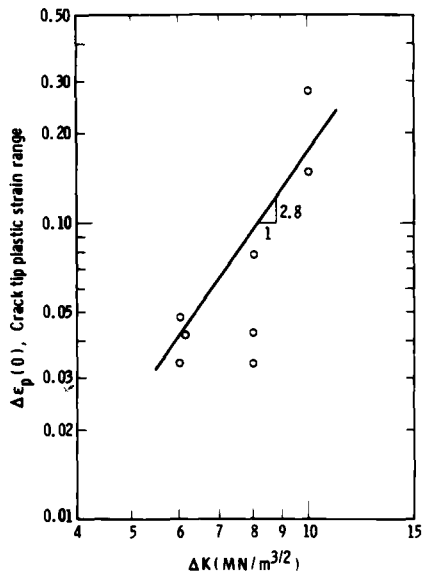

FIG. 12—*Crack tip plastic strain range versus* ΔK. *The line shown is consistent with the critical strain model.*

The correlation between crack tip opening displacement (CTOD) and crack tip strain (Fig. 14) is considered to be very good, and it certainly is reasonable that these two factors should be closely related. In fact, a simple model based solely on the measured crack tip opening [*17*] leads to an accu-

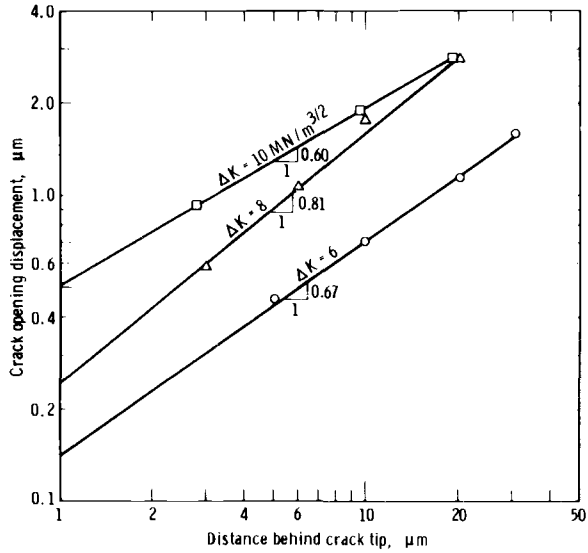

FIG. 13—*Crack-opening displacement as a function of distance behind crack tip.*

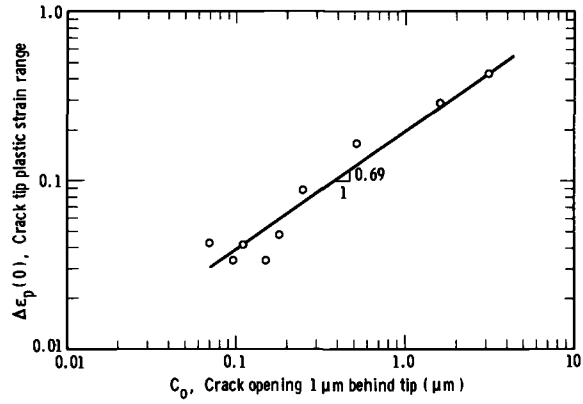

FIG. 14—*Crack tip plastic strain range versus crack tip opening displacement.*

rate estimate of crack tip shear strain. The correlation also indicates that the scatter shown in Fig. 12 between ΔK and crack tip strain is a consequence of the actual fatigue process, and not an artifact of strain measurement by the stereoimaging technique. Reasons for a variable CTOD and crack tip strain at a constant ΔK are becoming clearer, as will be discussed later.

The equations developed to this point relate crack tip opening, crack tip strain, and ΔK (Eqs 5 and 6). The relationship with the highest correlation

coefficient is Eq 6; therefore, numerical values of the coefficient and exponent in Eq 6 will be considered to be fixed in relating all three factors. Substituting amongst the equations gives

$$\Delta\epsilon_p = 2.8 \times 10^3 [C(\Delta K)^q]^{0.69} \tag{7}$$

and

$$\Delta\epsilon_p = K_0(\Delta K)^r \tag{8}$$

For the equations to be self-consistent, it is necessary that

$$K_0 = 2.8 \times 10^3 C^{0.69} \tag{9}$$

and

$$r = 0.69q \tag{10}$$

The values chosen for K_0, C, r, and q will be those which are most consistent with these relations and the data presented in the foregoing figures and tables.

To put the CTOD and da/dN measurements in perspective, it is interesting to note the results of fractographic analysis of failed specimens. Although the specimens were fatigued in vacuum, some striations were observed. This is not as surprising as it might seem, since Kirby and Beevers [*18*] have shown clearly that in 7075-T6, striations are formed in the near-threshold region (other work [*19*] suggests that in this alloy striations may not be formed in vacuum at higher ΔK-values). Kirby and Beevers reported striation spacings on the order of 1 μm for the crack growth rate of 4×10^{-11} m/cycle; our tests gave striation spacings of 0.5 to 2 μm for slightly higher crack growth rates. These spacings are 2 to 5 times the corresponding measured maximum crack tip opening displacements (C_0 in Table 1), and are several orders of magnitude in excess of the observed crack growth rates.

Models for Crack Growth

Cyclic deformation of the material through which a crack is advanced causes microstructural damage to that material. Within the spatial resolution level relevant to the present strain determinations (nominally 3 to 5 μm), strain accumulation is the measure of this microstructural damage. Strain accumulation occurs within a given volume element of the material as a consequence of the increasing incremental plastic strain which occurs on each cycle as the crack approaches the element. How this process of incremental strain accumulation actually causes material failure and the ultimate formation of two new surfaces (crack extension) is not well understood.

The concept of a criterion for failure of an element at the crack tip has been postulated since the earliest studies of crack growth. Such failure cri-

teria, for example, have considered incremental crack growth to occur upon the attainment of either a critical strain, a critical stress, or a critical energy, within a small region of material at the crack tip. The data presented in the figures and tables of this paper can be used to assess the relevance of these possible failure criteria.

From Table 1 and Figures 2 to 6 and 12, it is clear that the strain range at the crack tip is strongly dependent upon the stress intensity factor, and, therefore, with crack growth rate. Moreover, as might be expected, the computed stress range increases with the measured crack-tip strain range [*11*]. Therefore, neither of these incremental (per cycle) factors can be considered as a failure criterion, since neither is independent of loading conditions or the rate of crack growth. Rather more likely are those failure criteria dependent upon an accumulation (to the point of "exhaustion" or "criticality") of strain or plastic work.

Consequently, the models developed here will examine the attainment of a critical cumulative plastic strain at the crack tip as a criterion for crack advance, and also the concept of the necessity of expending a critical, cumulative amount of plastic work in order to extend the crack. A natural by-product of these calculations will be the predicted amount of incremental crack extension (directly related to crack growth da/dN) which occurs when the crack tip failure criteria are exceeded. Strain and energy accumulation models are, of course, variants of the same basic idea of combining strain range and number of cycles into a factor which can serve as a criterion for crack growth, but there are differences in the approaches, and these will be discussed after the model development.

Critical-Strain-to-Fracture Model

Average crack growth per cycle da/dN (the usual macroscopically measurable parameter) is assumed to correspond to crack extension by an amount Δa after a critical number of cycles ΔN_c, so that

$$\frac{da}{dN} = \frac{\Delta a}{\Delta N_c} \tag{11}$$

It should be noted that $\Delta a/\Delta N_c$ is the true, physical representation of crack extension, while da/dN describes the average amount by which the crack would grow if it did so on every cycle.

The critical strain for fracture ϵ_c is reached when

$$\Delta N_c \Delta \epsilon_p = \epsilon_c \tag{12}$$

where $\Delta \epsilon_p$ is the plastic strain range experienced by the element Δa. Substituting gives

$$\frac{da}{dN} = \frac{\Delta a \Delta \epsilon_p}{\epsilon_c} \tag{13}$$

If this relationship is valid, da/dN should vary with Δa and $\Delta \epsilon_p$, and these, like da/dN, must depend upon ΔK. In addition, the correlating term in the relationship, ϵ_c, must be independent of ΔK (constant). This requirement can be verified by solving Eq 13 for ϵ_c, substituting the appropriate ΔK-dependent relationships for Δa and $\Delta \epsilon_p$, and inserting for da/dN an empirical relationship in ΔK based on experiment.

From Fig. 12,

$$\Delta \epsilon_p = K_0(\Delta K)^r \tag{14}$$

where $K_0 \simeq 2.8 \times 10^{-4}$ and $r \simeq 2.7$. Determination of Δa requires the additional assumption that the incremental crack extension is proportional to the crack tip opening; that is,

$$\Delta a = \alpha C_0 \tag{15}$$

Combining this with Eq 5 yields

$$\Delta a = \alpha C(\Delta K)^q \tag{15a}$$

where $C = 7 \times 10^{-11}$ m and $q \simeq 4.0$ (consistent with Eqs 9 and 10 in relating K_0 to C and r to q).

Because of the wide variability in fatigue crack growth rates reported for 7075-T6, and the paucity of data representative of truly inert environmental conditions, crack growth rates were measured for the particular specimen design, material microstructure, load conditions, and environment corresponding to the crack tip deformation measurements. These results are shown in Fig. 15, which by a linear regression fit to the data yields

$$da/dN = B(\Delta K)^s \tag{16}$$

where $B = 1.3 \times 10^{-14}$ m/cycle and $s = 6.7 \pm 0.1$ with a correlation coefficient of 0.9 for $6 < \Delta K < 10$ MN/m$^{3/2}$.

Combining Eqs 11 to 16 and solving for ϵ_c gives

$$\epsilon_c = \frac{\alpha C K_0}{B} \Delta K^{q+r-s} \tag{17}$$

Substituting the appropriate values for q, r, and s, we obtain

$$\epsilon_c \simeq \frac{\alpha C K_0}{B} \tag{18}$$

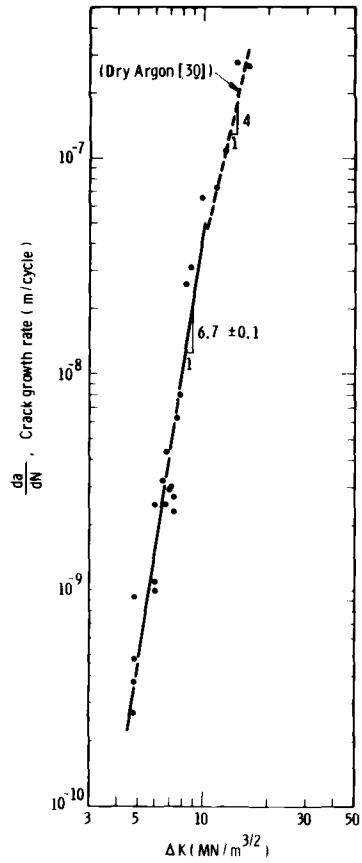

FIG. 15—*Crack growth rate versus* ΔK, *7075-T6, no environment effect.*

which is a constant, independent of ΔK. This result is encouraging evidence of the possible validity of critical cumulative strain as a criterion for crack growth. Substituting the aforementioned values of C, K_0 and B into Eq 18, and assuming $\alpha = 0.5$,[4] gives $\epsilon_c \cong 0.75$. This value is reasonable when we consider the uncertainty in values of the constants.

This model may be compared with the well-known Coffin-Manson description of cumulative strain, in which cycles to failure ΔN_f, for a specimen loaded through the plastic strain range $\Delta\epsilon_p$, is given by the relation [*20*]

$$\Delta\epsilon_p \Delta N_f^{\beta} = \epsilon_c$$

[4]Numerous models relating crack growth rate to CTOD make this assumption, and it appears valid at a higher growth rate; thus it is assumed here to be consistent with those results.

where for 7075-T6, $\beta \cong 0.5$. (This relation is similar to Eq 12 if β is set equal to 1.) When $\beta \simeq 0.5$, Eq 13 becomes

$$\frac{da}{dN} = \Delta a \left(\frac{\Delta \epsilon_p}{\epsilon_c} \right)^2$$

Solving for ϵ_c and combining with Eqs 14 to 16 gives

$$\epsilon_c{}^2 = \frac{\alpha C K_0{}^2}{B} \Delta K^{q+2r-s}$$

which is the equivalent of Eq 17. For ϵ_c to be independent of ΔK, based on known values of q and s, r must be 1.4, which is much lower than measured (Fig. 12), and ϵ_c must equal 0.02, which is also unrealistically low. Thus it is concluded that $\beta = 1$ is much more realistic than the value derived from the Coffin-Manson relationship.

Cumulative Damage Model

This model, essentially that of Jablonski and Pelloux [*20*], presumes that a small element of material well ahead of the crack tip begins to accumulate damage as soon as plastic flow begins. Damage accumulates increasingly with each cycle as the element moves through the plastic zone toward the crack tip until sufficient damage occurs and the element fails at a critical damage strain ϵ_{cd}. The per-cycle strain range distribution ahead of the crack tip is $\Delta\epsilon(r)$; thus the cumulative damage is represented by

$$\epsilon_{cd} = \frac{1}{da/dN} \int_0^{r_p} \Delta\epsilon(r) dr \tag{19}$$

where $dr/(da/dN)$ is the number of cycles experienced at the strain range during the period it is in the increment dr, and r_p is the plastic zone dimension. Substituting Eq 2 into Eq 19 gives

$$\epsilon_{cd} = \frac{1}{da/dN} \int_0^{r_p} [\Delta\epsilon_0 - m \ln (r + A)] dr \tag{20}$$

$$\epsilon_{cd}(da/dN) = [\Delta\epsilon_0 r_p - m(r_p + A)\ln(r_p + A) + m r_p + mA \ln A] \tag{21}$$

For the ΔK-range being modeled, $r_p \gg A$, which allows Eq 21 to be simplified to

$$\epsilon_{cd}(da/dN) \cong r_p[\Delta\epsilon_0 + m(1 - \ln r_p)] \tag{22}$$

The data of Table 1 may be used to evaluate Eq 21 or 22; results are shown in Table 2. It is apparent from Column 6 of the table that the right-hand side of Eq 21 is nearly constant, and that $\epsilon_{cd} \propto dN/da$ rather than being a constant. Also, $\epsilon_{cd}(da/dN)$ is a very large value (average = 212%), which does not seem realistic. One is led to conclude from the numerical evaluation of this model that it does not yield reasonable results, a point to be further expanded in the Discussion section of this paper.

Critical-Work-to-Failure Model

This model provides a method for computing the work expended in growing the crack an incremental distance Δa, whereby the cracked area increases an amount Δa per unit depth into the material. Figure 16*a* shows the plastic zone ahead of the fatigue crack, together with the idealized strain distribution within the zone. The plastic zone is divided into strips of width d_i, in which the maximum incremental strain range is $\Delta\epsilon_{p_i}$. The energy dissipated in crack growth Δa is illustrated in Fig. 16*b*. Two vertical axes are shown; on the left is $\Delta\epsilon_{p_i}$, and on the right is W_c, the work per cycle dissipated within the hysteresis loop at a given spatial location. By measuring, through stereoimaging, the cyclic strain at a point ahead of the crack tip, the corresponding W_c can be calculated, based on push-pull tests of uncracked specimens cycled to saturation stress under strain-controlled conditions. Correlation of strain and work within the hysteresis loop for the smooth specimens gives

$$W_c = W_0(\Delta\epsilon_p)^n \tag{23}$$

For 7075-T6, $W_0 = 1.346 \times 10^3$ J/m^3 and $n = 1.0615$.

TABLE 2—*Evaluation of cumulative damage integral.*

Data Set	ΔK, MN/m$^{3/2}$	$\Delta\epsilon_0 r_p$, μm	$m(r_p + A)\ln(r_p + A)$, μm	mr_p, μm	$\int\Delta\epsilon(r)dr$	da/dN, $10^{-2}\mu$m/cycle
34	6	7.28	6.20	1.20	2.27	0.15
35	6	7.21	6.54	1.34	2.02	0.15
36	6.2	9.26	7.95	1.50	2.78	0.2
39	8	3.06	2.40	0.52	1.18	1
40	8	4.64	3.96	0.85	1.50	1
41	8	8.78	8.89	1.96	2.05	1
43	10	11.2	11.1	2.96	2.97	5
44	10	8.10	7.80	1.90	2.20	5
				Average=	2.12	

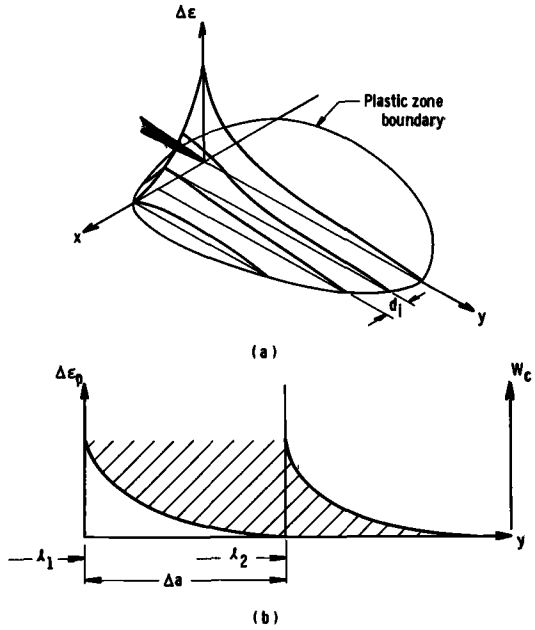

FIG. 16—*Schematic showing how work was computed.* (a) *Division of the plastic zone into strips.* (b) *Changes of cyclic plastic strain range and work dissipated with crack length. Hatched area is representative of the total work dissipated in a strip* d_i *in growing the crack an increment* Δa.

The hatched area in Fig. 16*b* represents the total work expended in growing the crack, because Δa is proportional to the number of cycles

$$\Delta N = \Delta a/(da/dN) \tag{24}$$

required to cause a crack extension of Δa. Thus the area of the hatched region is $\Delta N W_c$ within the strip d_i:

$$W_i = W_0(\Delta\epsilon_p{}^m)^n \, \Delta N \, d_i \tag{25}$$

where $\Delta\epsilon_p{}^m$ is the maximum value of $\Delta\epsilon_p$ within d_i. The total work expended is

$$W = \sum_i W_i = W_0 \frac{\Delta a}{(da/dN)} \sum_i (\Delta\epsilon_{p_i})^n \, d_i \tag{26}$$

where W is the work expended in growing the crack a distance Δa. The specific work, U, is the work expended per unit area of new crack, and is given by

$$U = \frac{W}{\Delta a} = \frac{W_0}{(da/dN)} \sum_i (\Delta \epsilon_{p_i})^n d_i \tag{27}$$

Computational results for U are given in Table 3, which uses the cyclic strain data already presented.

Weertman [*21*] has shown theoretically that the relationship between crack growth rate, driving force (ΔK), material parameters, and U is

$$da/dN = A \frac{\Delta K^4}{\sigma_y^2 \mu U} \tag{28}$$

where μ is the shear modulus, σ_y is the cyclic yield stress, and A is a constant. In this equation, it is assumed that U is a constant, and that da/dN is related to ΔK by a fourth-power exponent; that is, the crack is growing in the Paris regime. The data in Table 3, however, show that in the present instance U is not independent of ΔK, suggesting that if an equation like Eq 28 is to be used, a more general form should be employed:

$$da/dN = A \frac{\Delta K^4}{\sigma_y^2 \mu U_0 (\Delta K)^m} = \frac{A(\Delta K)^{4-m}}{\sigma_y^2 \mu U_0} \tag{29}$$

where U_0 is an empirically determined constant.

Note that in this equation the assumption is made that the exponent on the driving force is equal to 4. Since da/dN is proportional to $(\Delta K)^{6.7}$ (Fig. 15), it is clear that $4 - m = 6.8$, or $m = -2.8$. This means that

$$U = U_0 (\Delta K)^{-2.8} \tag{30}$$

Thus the work expended per unit area of crack advance decreases with increasing ΔK, a result to be discussed later.

TABLE 3—*Computation of total work expended per unit crack growth.*

Data Set	ΔK, MN/m$^{3/2}$	da/dN, 10^{-8}m/cycle	$\Sigma(\Delta\epsilon_{p_i}{}^m)d_i$, ($10^{-6}$m)	W, 10^{-3}J/m	U, 10^5J/m^2
34	6	0.15	1.19	1.6	10.6
35	6	0.15	0.71	0.95	6.4
36	6.2	0.2	1.3	1.75	8.7
39	8	1	0.87	1.2	1.2
40	8	1	2.2	2.9	2.9
41	8	1	2.31	3.1	3.1
43	10	5	4.44	6	1.2
44	10	5	3.73	5	1.0

Another equally valid way to consider this situation is to permit a variable driving-force exponent. In this case, an even more general form of Eq 29 results:

$$da/dN = A \frac{\Delta K^n}{\sigma_y^2 \mu U_0 (\Delta K)^m} = A \frac{\Delta K^{n-m}}{\sigma_y^2 \mu U_0} \tag{31}$$

As noted before da/dN is proportional to $\Delta K^{6.8}$. However, if the ΔK dependence of U is analyzed (Table 3), it is found that a better representation than Eq 30 is

$$U = U_0(\Delta K)^{-4.1}$$

Again, m is negative, but now the driving-force exponent is only 2.7. The significance of these various possibilities will be discussed later.

Discussion

The discussion is divided into two sections, one examining the experimental results themselves, and the other exploring the consequences of the models presented.

Experimental Results

Based on the cyclic stress intensity exponent of 6.7 which correlates the experimental crack growth rates, it is apparent that the ΔK-range studied (6 to 10 MN $m^{3/2}$) corresponds to the near-threshold, or transition, crack growth regime. This is below the so-called Paris regime, characterized by a ΔK-exponent of 4. Some of the crack tip phenomena observed in this study can be explained by considering the factors thought to control crack growth in this region. Crack tip opening displacement (CTOD) as characterized by C_o, was found to be proportional to approximately $(\Delta K)^3$, while some crack growth models assume a relationship of the form CTOD$\alpha(\Delta K)^2$. However, these models generally assume operation within the Paris regime, in which the crack opens predominantly in Mode I. For the present experiments, that region is for $\Delta K > 10$ MN/$m^{3/2}$.

The crack growth rate in the near-threshold region is less than would be implied by extrapolation of the Paris region, just as the CTOD is lower. This is a consequence of the changing mode of deformation from predominantly Mode I in the Paris region to an increasingly Mode II-dominated mix as ΔK is decreased toward threshold. This tendency suggests that much of the crack-driving force is dissipated in shear strain, rather than in tensile (Mode I) opening of the crack; the amount of Mode I opening generally governs the amount of actual crack extension.

Observed crack tip strain fields (Figs. 2 to 6) support this view. In particular, it is evident that the strain field peaks ahead of the crack tip, rather than within two shear bands at ~45 deg to the crack plane. The location of the peak, and the orientation of the principal strains, strongly support the concept of in-plane (Mode II) sliding, as suggested previously. This strain field would tend to minimize crack opening normal to the fracture plane.

Some of the data presented in Table I are considered to be "best" for the purpose of characterizing crack tip during crack extension. This judgement was based on the following reasoning. During the past four years, we have observed, at high resolution in the SEM, cracks growing in various aluminum alloys at relatively low stress intensities. It has become increasingly apparent that crack extension does not occur on every cycle [*22*]. Instead, as cycling progresses, the tip generally blunts to an ever increasing extent (but does not grow), while the crack tip opening likewise increases, until the crack extends upon reaching some critical state which our data suggest corresponds to a critical cumulative strain. This sharp-blunt sequence is then repeated. With this observation in mind, it is our opinion that the "best" strain and CTOD data are those which are the larger of the measured values for a given ΔK, since these values usually will be most characteristic of the critical condition just prior to crack extension.

The crack-opening relationship which describes the present results has been shown (Eq 4) to be

$$C = C_0|-y|^p$$

where $p = 0.6 \pm 0.16$. Finite-element analysis of monotonic crack tip opening in power-law hardening materials has been carried out by Dean and Hutchinson [*23*]; when strain-hardening values characteristic of aluminum alloys are used, their analysis predicts $p = 0.75$. This is well within the uncertainty band of the present experimental data. An important point to consider, however, is that during fatigue, C is not a constant on each load cycle at a given value of ΔK, and although Eq 4 with $p \simeq 0.7$ does describe the shape of the crack profile, the CTOD amplitude has a range of possible values, depending upon the immediate history of the crack tip in the sharp-blunt sequence.

Crack Growth Models

The critical-strain-to-fracture model and the cumulative damage model are very similar in concept and will be compared first. The cumulative damage model considers an element of material ahead of the crack tip to accumulate damage on each cycle as the crack tip moves toward the element. Conversely, the critical-strain-to-failure model considers an element of material immediately ahead of the crack tip which is accumulating strain at approxi-

mately the cyclic strain range at the crack tip through sufficient cycles that the sum reaches a critical value, and the element breaks. Numerical evaluation of these two failure criteria indicates that the critical strain model, which gives a failure strain of about 75%, is more reasonable than the cumulative damage model, which yields a cumulative strain >230%. The reason for this may be that the cumulative damage model assumes damage to occur equally at both low and high strains (when the product of strain range and number of cycles remains constant); evidently, this is a poor assumption. Examination of the strain distribution indicates that the strain is relatively low within the plastic zone, peaking strongly at the crack tip (Figs. 3 to 6). This trend increases at higher ΔK. Thus damage to the material is apparently likewise distributed. The size of the critical element in which strain is accumulating is given by Eq 15 as approximately half the crack tip opening displacement. This small element of material has been referred to as the "process zone" in other theoretical models.

The concept of a critical strain to fracture, supported by the present results, is certainly not new; it has been used as a failure criterion in a number of theoretical treatments of fracture, including Weertman's adaptation of the Bilby-Cottrell-Swinden dislocation theory of fatigue crack growth [*24*]. In the case of the BCS theory and adaptations of it, the failure criterion is actually a critical displacement, but this could be thought of as a critical strain. Other theoretical models use critical strain, either directly or indirectly. For example, the model of Lanteigne and Baïlon [*25*] obtains the critical number of cycles and strain for crack advance from low-cycle fatigue data.

Critical strain as a failure criterion has been used extensively in the modeling of high-temperature crack growth, where the damage mechanism is mainly creep cavitation. Recent examples of this are the models of Cocks and Ashby [*26,27*]. Thus, an advantage of describing fatigue crack growth through a critical strain model is the common link it provides with another physical damage mechanism.

An alternative way of utilizing strains at the crack tip is through the expression derived by Weertman [*21*] (Eq 28), where stress and strain are combined into an energy term U. The seemingly curious observation that U decreases with increasing ΔK (Table 3) has also been shown by Fine [*28*] for several aluminum alloys and by Davidson [*29*] for low-carbon steel. The latter observation was explained in terms of the effects of crack-opening mode on the mechanisms of energy dissipation, and the same general observations appear relevant to the aluminum alloys. The concepts are schematically shown in Fig. 17. The range of the present measurements are in the near-threshold region *A-B*. The ΔK_{TH} is defined as the loading condition when U becomes extremely large, and, through Eq 28, da/dN becomes very small. The line *ABC* represents the decrease in U which would occur if the fatigue crack continued to keep the same mix of Mode I and Mode II as ΔK increased. But at some point, *B*, the mode mix begins to change, with Mode I becoming much more

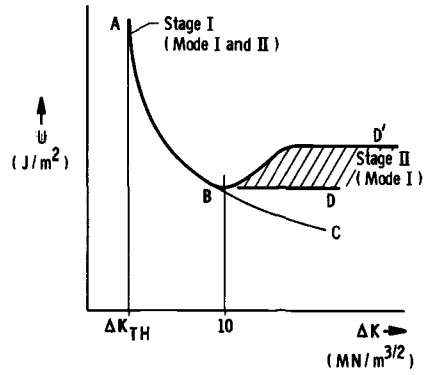

FIG. 17—*Schematic of the energy change with* ΔK, *showing the effect of change in crack tip deformation mode.*

dominant. At higher ΔK, the value of U may continue constant, as along line BD, or rise, as along line BD'. The latter change was observed in low-carbon steel; exactly what occurs for the aluminum alloys is not clear, but Fine's data [*28*] indicate some increase (as along BD') may also occur. The point of transition, B, is thought to be determined by the slip characteristics of the material, perhaps the stress state, and such metallurgical factors as grain size, shape, and texture. For 7075-T6 in the present study, $\Delta K = 10$ MN/m$^{3/2}$ appears to be the beginning of the transition region, because the crack tip strain distribution is starting to change; compare Figs. 5 and 6 to Figs. 2 and 3. The detailed analysis of Koss and Chan [*30*] provides a model by which some aspects of the crack tip mechanics may be related to metallurgical characteristics as the transition between Stages I and II occurs.

Final Remarks

Fatigue damage may be described by the actual microstructural changes (increase in dislocation density, formation of cell walls, etc.) which occur near the crack tip, or by the mechanics of crack tip yielding caused by loading the crack. The macroscopic loading parameters control, to some degree, the crack tip stresses and strains, but they are also influenced by slip characteristics and other metallurgical characteristics such as grain size and texture. This paper has concentrated on the description of fatigue damage in terms of crack tip mechanics, and has shown, through the models presented, that this description has merit, even though neither the underlying characteristics of the microstructure nor the damage caused by cyclic deformation is described. The next task will be to connect a description of microstructure (slip characteristic, texture, etc.) with the mechanics description of damage, so that the design of materials resistant to fatigue crack growth may be advanced.

Summary and Conclusions

Measurements of crack tip opening displacements and strains have been made for fatigue cracks in 7075-T6 grown in the absence of environment mental influence in the near-threshold region. The following conclusions have been drawn:

1. Crack opening is mixed Mode I and Mode II.
2. Crack tip strain range is proportional to crack tip opening displacement.
3. The distribution of crack tip strain range within the plastic zone peaks at, and ahead of, the crack tip.
4. Crack tip strain range and crack tip opening are power functions of cyclic stress intensity factor (ΔK).
5. The experimental findings indicate that the fatigue crack is growing with a strong Stage I crack growth component in the near-threshold region.
6. A model is presented which assumes a critical strain must be reached before crack growth can occur. The experimental data support this model and indicate that the critical strain is independent of ΔK. Another model, assuming cumulative cyclic damage, is shown to provide an inadequate failure criterion.
7. The critical strain crack growth model also requires a critical number of cycles prior to crack advance. Experimental observations of intermittent crack growth support this concept.
8. The energy dissipated in growing the crack a unit area, U, is computed, and found to be inversely related to ΔK. A rationale for this result, based on the observed mode of crack growth, is offered.

Acknowledgments

Support for this work by the Air Force Office of Scientific Research (Dr. Alan H. Rosenstein, Technical Monitor) is gratefully acknowledged. Prof. Rishi Raj suggested the form of the critical strain model in discussions while visiting the Southwest Research Institute, and we are pleased to acknowledge his contribution.

References

[1] Chakrabortty, S. B., *Fatigue of Engineering Materials and Structures*, Vol. 2, 1979, pp. 331-344.
[2] Antolovich, S. D., Saxena, A., and Chanani, G. R., *Engineering Fracture Mechanics*, Vol. 7, 1975, pp. 649-652.
[3] Chanani, G. R., Antolovich, S. D., and Gerberich, W. W., *Metallurgical Transactions*, Vol. 3, 1972, pp. 2661-2672.
[4] Liu, H. W. and Iino, N., *Fracture 1969*, Chapman and Hall, New York, 1969, pp. 812-823.
[5] Ohta, A., Kosuge, M., and Sasaki, E., *International Journal of Fracture*, Vol. 13, 1977, pp. 289-300.
[6] Shimada, H. and Furuya, Y., *Experimental Mechanics*, Vol. 21, 1981, pp. 423-428.
[7] Kang, T. S. and Liu, H. W., *International Journal of Fracture*, Vol. 10, 1974, pp. 201-222.

[8] Davidson, D. L. and Nagy, A., *Journal of Physics E*, Vol. 11, 1978, pp. 207-210.
[9] Davidson, D. L., *Scanning Electron Microscopy/1979/II*, Scanning Electron Microscopy Inc., AMF O'Hare, Ill., pp. 79-86.
[10] Williams, D. R., Davidson, D. L., and Lankford, J., *Experimental Mechanics*, Vol. 20, 1980, pp. 134-139.
[11] Davidson, D. L., Williams, D. R., and Buckingham, J., *Experimental Mechanics* (in press).
[12] Davidson, D. L. and Lankford, J., *Fatigue of Engineering Materials and Structures*, Vol. 3, No. 4, 1980, pp. 289-303.
[13] Rice, J. R. in *Fracture V*, Vol. II, H. Liebowitz, Ed., Academic Press, New York, 1968; see Equation 289, p. 287.
[14] Hutchinson, J. W., *Journal of the Mechanics and Physics of Solids*, Vol. 16, 1968, pp. 13-31.
[15] Rice, J. W. and Rosengren, G. F., *Journal of the Mechanics and Physics of Solids*, Vol. 16, 1968, pp. 1-12.
[16] Davidson, D. L., *Micro- and Macro-Mechanics of Crack Growth*, AIME, Warrenville, Pa., 1982, pp. 161-176.
[17] Davidson, D. L., *Scripta Metallurgica*, Vol. 16, No. 3, 1982, pp. 281-283.
[18] Kirby, B. R. and Beevers, C. J., *Fatigue of Engineering Materials and Structures*, Vol. 1, 1979, pp. 203-215.
[19] Pelloux, R. M. N., *Fracture 1969*, Chapman and Hall, London, 1969, pp. 731-744.
[20] Jablonski, D. A. and Pelloux, R. M., *Metallurgical Transactions A*, Vol. 10A, 1979, pp. 63-70.
[21] Weertman, J., *International Journal of Fracture*, Vol. 9, 1973, pp. 125-131.
[22] Davidson, D. L. and Lankford, J. in *Fatigue Mechanisms, ASTM STP 675*, American Society for Testing and Materials, 1979, pp. 277-284.
[23] Dean, R. H. and Hutchinson, J. W. in *Fracture Mechanics: Twelfth Conference, ASTM STP 700*, American Society for Testing and Materials, 1980, pp. 383-405.
[24] Bilby, B. A., Cottrell, A. H., and Swinden, K. H., *Proceedings of the Royal Society*, Vol. A272, 1963, pp. 304-314.
[25] Lanteigne, J. and Baïlon, J.-P., *Metallurgical Transactions A*, Vol. 12A, 1981, pp. 459-466.
[26] Cocks, A. C. F. and Ashby, M. F., *Metal Science*, Vol. 14, 1980, p. 395.
[27] Cocks, A. C. F. and Ashby, M. F., *Scripta Metallurgica*, Vol. 16, 1982, pp. 109-114.
[28] Liaw, P. K., Kwan, S. I., and Fine, M. E., *Metallurgical Transactions A*, Vol. 12A, 1981, pp. 49-55.
[29] Davidson, D. L., *Fatigue of Engineering Materials and Structures*, Vol. 3, 1981, pp. 229-236.
[30] Koss, D. A. and Chan, K. S., *Acta Metallurgica*, Vol. 28, 1980, pp. 1253-1263.

DISCUSSION

R. W. Hertzberg[1] *(written discussion)*—The authors have commented on the fact that fatigue crack growth is discontinuous in the low FCP regime. This should come as no surprise when one compares the macroscopic growth rates in the threshold regime with the Burgers vector for a dislocation. We find that $(da/dN)_{macro}$ is less than $\bar{b}$ so that growth must be discontinuous. Furthermore, there is direct proof that discontinuous crack extension occurs in numerous polymeric solids. In these materials a plastic zone, described by the Dugdale model, is found to grow continuously but then break down sud-

[1]Department of Metallurgy and Materials Engineering, Lehigh University, Bethlehem, Pa. 18015.

denly during one loading cycle. The resulting fracture band is equal in length to the size of the plastic zone.[2]

D. W. Cameron[3] (*written discussion*)—I agree with the intermittent nature of crack propagation based on similar studies in aluminum alloys, as well as Mode I-Mode II mixing during the process. We apparently have similar experimental problems with specimen movement in the SEM field and focussing.

What was the grain size of the material examined? In observing the intermittent nature of propagation, was there evidence of microstructural interference (grain boundary constituent particles) in these effects? With the magnification levels associated with the observations, do the continuum parameters (strain, stress, stress intensity) provide reasonable quantifiable descriptions of the process?

D. L. Davidson and J. Lankford (*authors' closure*)—Thank you for making your observation of intermittent crack growth known to us. It helps to reinforce the validity of the concept that crack growth is not occurring on each cycle. The aluminum alloys reported on here had a pancake grain structure with the large dimension of the pancake being 200 μm on average, and the short dimension averaging 22 μm. The line of the crack front was oriented in the short direction of the grain. Occasionally, crack growth behavior near a grain boundary is observed to be altered, but no grain boundary constituent particles seem to be related to this. We believe this alteration in crack growth behavior near grain boundaries is due to the degree of misorientation between adjacent grains. This would cause a difference in compliance between the two grains, and a difference in the slip systems relative to the crack front which are active in the two grains. We are still investigating the effects of grain boundaries on crack growth behavior.

The continuum parameters stress and strain do appear to provide quantifiable descriptions of the fatigue crack growth process, in our opinion, if (*1*) measured on the appropriate scale, and (*2*) combined properly with descriptions of material behavior and driving force (stress intensity). This belief should not be interpreted as proof that the description, or model, which we have offered in this paper is a perfect description of the events accompanying fatigue crack growth, even though it does appear that we may be on the correct track.

A. K. Chakrabarti[4] (*written discussion*)—The intermittent nature of crack growth indicates a critical damage accumulation at the crack tip prior to a

[2]Hertzberg, R. W., Skibo, M. D., and Manson, J. A. in *Fatigue Mechanisms, ASTM STP 675*, J. T. Fong, Ed., American Society for Testing and Materials, 1979, pp. 471-500.

[3]Structural Integrity Laboratories, University of Toronto, Ontario, Canada.

[4]Materials Research and Engineering, Detroit Diesel Allison, Division of General Motors Corporation, Indianapolis, Ind. 46224.

stepwise extension of the crack. This also shows that continuous growth in every cycle is not needed, as has been suggested in various models and observations. Were any microscopic observations made to determine the nature of the damage? If so, what was the nature of the damage? Does the extent of damage reach a critical value prior to the stepwise extension of the crack?

D. L. Davidson and J. Lankford (authors closure)—The microscopic measurements we made were of strain (considering strain measured with a gage length of 5 μm to be microscopic). Strain derived over such small distances reflects the movement of dislocations on a relatively local basis; thus one would expect dislocation density in the vicinity of a crack tip to reflect the intermittent nature of the crack advance. Although we have not made such measurements, C. Q. Bowles and D. Broek observed the dislocation structure just beneath and parallel to the fatigue fracture surface in 7075-T6 aluminum by transmission electron microscopy and found a periodic variation in dislocation density which approximately equals the striation spacing.[5] In our opinion, each of these dense tangles probably represents a location where strain at the crack tip was building up during the blunting portion of the cycle. Thus "damage" in this situation could be defined as an increase in dislocation density, or an increase in strain, and our interpretation of this information would be that a critical value of one of these parameters is required before crack growth can occur.

R. A. Bayles[6] *(written discussion)*—Are you sure that the whole crack front (through the thickness of the specimen) moves intermittently, and that you are not seeing the crack pinned, and then released, at the surface?

D. L. Davidson and J. Lankford (authors' closure)—Yes, that is, we are as sure as we can be from the evidence at hand. Let us restate the evidence which leads us to believe crack growth in the near-threshold region is not continuous throughout the specimen thickness:

1. We directly observe it to be intermittent on the surface.
2. Striation spacing on the fracture surface is much larger than the growth rate per cycle.
3. Dislocation density, as measured near the fracture surface by C. Q. Bowles and D. Broek,[5] is periodic, which indicates that a nonuniform buildup of strain accompanies crack growth.
4. For the loading conditions we are using—that is, low ΔK, which produces a small plastic zone size-to-specimen thickness ratio—, the constraint is such that the fracture surface does not have a shear lip and exhibits the same

[5]*International Journal of Fracture*, Vol. 8, 1972, p. 75.
[6]Naval Research Laboratory, Washington, D.C. 20375.

features near the surface as in the interior. From this we conclude that the surface is behaving much the same way as the interior.

5. Striations on the fracture surface indicate somewhat different directions and spacings on different grains, and steps between adjacent grains are not uncommon. These observations have been made in numerous fractographic examinations by many investigators. They indicate that a unified crack front advancing the same on each cycle is unlikely.

In summary, we can think of no reason why, in fact, what is being observed on the surface should be any different from what is occurring in the interior, not forgetting that a free-surface, plane-stress condition exists at the plane of observation.

C. Q. Bowles[1] *and J. Schijve*[2]

Crack Tip Geometry for Fatigue Cracks Grown in Air and Vacuum

REFERENCE: Bowles, C. Q. and Schijve, J., **"Crack Tip Geometry for Fatigue Cracks Grown in Air and Vacuum,"** *Fatigue Mechanisms: Advances in Quantitative Measurement of Physical Damage, ASTM STP 811*, J. Lankford, D. L. Davidson, W. L. Morris, and R. P. Wei, Eds., American Society for Testing and Materials, 1983, pp. 400-426.

ABSTRACT: Plastic castings of fatigue cracks were produced by a process of vacuum infiltration and subsequently examined in a scanning electron microscope. Study of the castings revealed that the crack tip geometry in the 2024-T3 and 7075-T6 alloys was essentially the same. Crack advance in air is initially "brittle" in both alloys, with the crack tip subsequently blunting to an elliptical geometry at maximum load. Brittle crack extension presumably results from tensile rupture due to the presence of water vapor. At minimum load the crack tip has been resharpened but remains generally elliptical and singly notched.

In contrast, crack advance in vacuum appears to result solely from slip activity in the absence of any active species to promote failure by tensile rupture. Crack branching is believed to be a significant means of accommodating plastic flow near the maximum of the load cycle. The crack front itself appears to be highly disorganized due to crack propagation at different levels and on different slip systems in adjacent grains of the polycrystalline materials.

Castings of air fatigued specimens also shed some new light on plasticity just behind the crack tip and on contact between the two fracture surfaces during crack closure at a larger distance behind the crack tip.

KEY WORDS: aluminum alloys, striation formation, fatigue crack growth, environment influence, crack tip geometry

There are perhaps two distinct approaches to the study of the mechanisms of fracture. One involves the study of bulk material ahead of and in the vicinity of the crack tip, while a second approach is oriented toward examination of fracture surfaces.

[1]Associate Professor of Mechanical Engineering, University of Missouri, Independence, Mo. 64050.

[2]Professor, Aeronautical Engineering Department, Delft University of Technology, Delft, The Netherlands.

One easily recognizes that a complete understanding of the fatigue mechanism will require a correlation of observations from both approaches. Indeed, many experimental programs will combine elements of the two approaches in their execution. In this paper fractographic observations are presented which were obtained from plastic castings produced by vacuum infiltration of fatigue cracks grown in air and vacuum. The infiltration technique [*1*] gives replicas with very high resolution which are studied in a scanning electron microscope.[3]

Technical Background

In 1960 Forsyth and Ryder [*2*] published results demonstrating that striations represented the propagation distance of a fatigue crack during each stress cycle. Further analysis of their observations led Forsyth and Ryder [*3*] to conclude that each striation profile most probably resulted from a brittle-fracture/ductile-fracture sequence. Examination of both laboratory and service failures showed that the ratio of ductile to brittle fracture in an individual striation depended on the ductility of the specimen.

Stubbington [*4*] studied both air and corrosion fatigue fracture surfaces of an aluminum alloy and identified two types of striations, Types A and B. Type A striations were more prevalant on fatigue fractures produced in air and were considered brittle. The striation profiles were thought to result from an initial quasi-brittle to brittle fracture during the tensile half of the load cycle which was then arrested by plastic deformation. The striations themselves were found to occur on individual fracture facets which were in turn assumed to represent the path of the fracture plane through individual polycrystalline grains. Etch pit studies and Laue photographs showed the preferred fracture plane was on or near the (100) cube plane.

Laird and Smith [*5*] published results showing crack tip profiles obtained by metallographic sectioning and optical microscopy; these were subsequently extended by Laird [*6*] to include the characterization of several types of striations. Laird postulated a "plastic blunting model" to describe crack tip geometry associated with various stages of loading.

As tensile loading is begun (Figs. 1*a* and *b*) slip is concentrated at the double notches located at ± 45 deg to the crack plane. This slip concentration is assumed to help maintain a more or less square geometry (Fig. 1*b*). According to Laird and Smith the stress concentration of the crack tip at maximum load is lessened, leading to a broadening of the slip zones and crack tip blunting (Fig. 1*c*). On unloading, slip in the zones is reversed, the crack faces are brought together, and the new crack surface just created is folded by buckling at the crack tip, producing the two ears which result in the doubly notched condition. An alternative representation given by Schijve [*7*] (Figs.

[3]The italic numbers in brackets refer to the list of references appended to this paper.

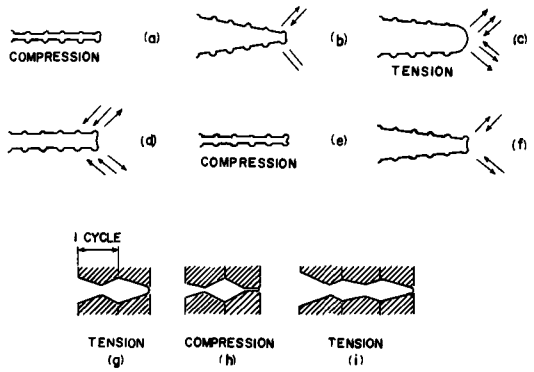

FIG. 1—(a-f) *Crack tip geometry as visualized by Laird and Smith* [5] *from optical photographs of fatigue crack cross sections.* (g-i) *Alternative crack tip geometry suggested by Schijve* [7].

1*g*, *h*, and *i*) requires that, after unloading, the crack tip be singly notched and fully sharp; the sawtooth profile shown schematically is supported by the requlary repeating character of striations.

Pelloux [*8,9*] suggests a crack tip profile similar to that of Schijve and has formulated a model of crack extension by alternating shear in which a small region at the crack tip deforms plastically while the remainder of the sample behaves elastically. In theory plastic deformation should be reversible. However, there are several reasons why cyclic slip can be only partly reversible during unloading. Pelloux proposes that the newly formed oxide layer can provide the necessary obstacle; the resulting crack growth schematic is shown in Figs. 2*a-j*.

Meyn [*10*] first observed that striations were not formed on the fracture surfaces of aluminum alloy specimens fatigued in vacuum. Meyn and others have also observed that the crack growth rate in vacuum is much less than in air at comparable cyclic stress intensities. Pelloux has suggested that the alternate shear model can explain these results, since in the absence of an oxide layer one would expect partly reversed slip (Figs. 2*f-j*).

Tomkins [*11*] and Tomkins and Biggs [*12*] set forth a different picture of the shear flow process (Figs. 3*a-g*). Tensile loading initiates plastic flow in two narrow shear bands at 45 deg to the crack tip. Continued loading to the tensile strain limit produces a new crack surface which is formed by shear decohesion along the inner edges of the flow bands where the shear gradient is the largest (Fig. 3*b*).

If strain hardening occurs in the flow bands before the strain limit is reached, then rupture can be expected at the tip of the blunt crack (Fig. 3*c*). Rupture at the crack tip will expose new flow bands, allowing the process to repeat. Unloading procedures reversed shear flow and the crack closes but without any significant recohesion.

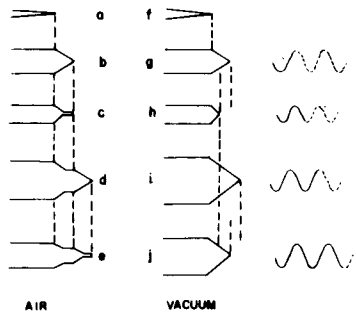

FIG. 2—*Alternate shear mechanisms of crack tip advance for air and vacuum proposed by Pelloux* [8,9].

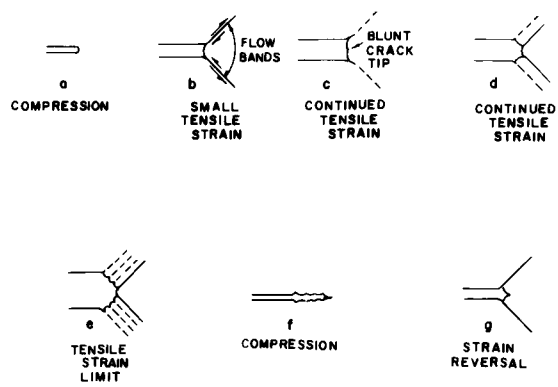

FIG. 3—*Fatigue crack tip advance by plastic flow proposed by Tomkins and Biggs* [11,12].

According to Tomkins and Biggs, at low crack tip strains all the deformation at the crack tip may be accommodated by an initial flow-off producing a single ripple which is a deep valley (Fig. 3*b*). As the strain increases each ripple is succeeded by finer "striations," which are shallower valleys formed by intermediate flow-off (Fig. 3*e*). In their test, ripples varied from 1 to 300 μm wide. One can only assume that ripples described by Tomkins and Biggs represent the usual striations observed by other workers. The markings they term striations are presumably the rumpled side of the striation described by McMillan and Pelloux [*13*].

Replicas for electron microscopy are shadowed in the direction of crack propagation, resulting in contrast on the trailing side of the striation, or in the direction opposite crack propagation, resulting in enhancement on the leading side of the striation. McMillan and Pelloux reported results of shadowing in both directions and observed that the leading edge of striations

are heavily rumpled and deformed, whereas the trailing edges are much more smooth and featureless, having only occasional wavy slip lines. They have explained these observations by suggesting that the leading edge of the striation, which is nearest the crack tip, is heavily deformed as a result of plasticity during unloading; this is in contrast to the mechanism of formation suggested by Tomkins and Briggs.

The Tomkins and Biggs proposal for crack growth differs on one major point from the other models of Laird and Smith and Pelloux. All agree that striations have a general sawtooth shape consisting of hills and valleys. For the Tomkins and Biggs case, however, valleys result from flow-off during the initial part of tensile load, whereas the other cases require the valley to be formed during unloading.

The present authors have attempted to resolve differences between the current models for crack tip advance by using a technique of *in situ* vacuum infiltration with plastic to produce a casting of the crack. Although a new specimen must be used for each infiltration, plastic castings provide a means of studying fracture events occurring at the crack tip at any point on the load cycle curve. The infiltration technique has also been used for *in situ* infiltration of fatigue cracks grown in vacuum.

Experimental Procedures

Infiltration Technique

Experimental details of the infiltration technique have been previously reported [*1*]. Therefore the following paragraphs provide only a summary of the procedures. Figure 4 is a diagram of the main components. Silicone rubber cups (A) cover the crack and are held in place by heavy rubber bands. Glass stopcocks (B,C) lead to a mechanical vacuum pump and to a funnel which holds plastic to be infiltrated. Tubing is used for connecting lines, and hose clamps are used to ensure a good vacuum seal.

The fatigue crack is grown to desired length and the infiltration apparatus is positioned while the specimen is still under load. After approximately 5 min of evacuation with the mechanical pump, plastic is mixed and introduced into the funnel. The plastic is allowed to flow into the system and to harden for approximately 16 h while the load on the specimen is maintained.

After the plastic has hardened, part of the sample consisting of the crack, the plastic casting, and approximately 1 cm of material surrounding the crack is cut from the bulk specimen. The whole is now cured for an additional 3 h at 60°C to improve temperature stability in the scanning electron microscope. The remaining metal surrounding the casting is removed in a solution of 50% HCl, 50% H_2O, and a few drops of H_2O_2. Finally, the castings are coated with gold for scanning electron microscopy.

To facilitate *in situ* infiltration of fatigue cracks in vacuum, a Perspex win-

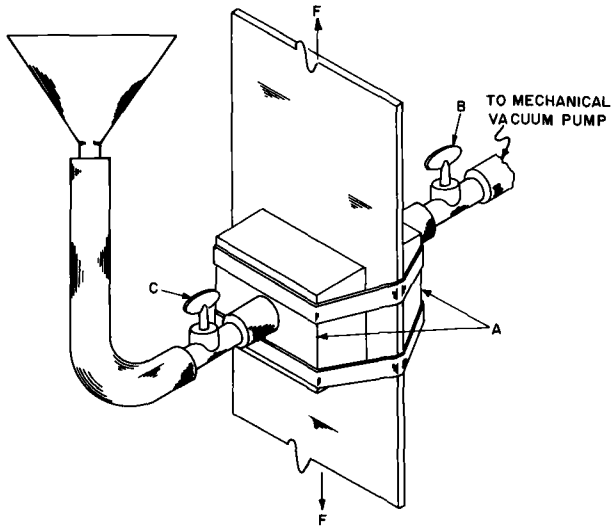

FIG. 4—*Schematic of infiltration technique.*

dow was provided in one of the cups to allow visual observation of crack growth and the second was given a 35-mm round outlet to aid vacuum pumping. The sample and rubber cups were then connected through a glass valve and 30-cm flexible tube to an oil diffusion pump. Pressure at the end of the flexible tubing was always 1.1×10^{-3} Pa (8×10^{-6} torr) before testing was begun, and corrections for conductance of the flexible tube [*16*] gave an estimated pressure of 9.3×10^{-3} Pa (7×10^{-5} torr) at the sample.

The pressures obtained were not comparable with vacuum tests of other workers. However, crack growth rates of vacuum tests were 0.06 to 0.08 μm/cycle, and crack growth rates in air at comparable stress intensities were 0.3 to 0.5 μm/cycle.

We also note that mass spectrometry [*14,15*] tests have shown the major gas species in a normal diffusion pumped vacuum system to be residual water vapor. Thus if we assume that all the residual gas at the sample is water vapor we are led to a conservative estimate of less than 1 ppm H_2O.

Materials and Tests

The alloys studied were 2024-T3 and 7075-T6 in the clad condition. Specimen size was 200 mm long, 100 mm wide, and 4 mm thick with a center crack starter of $2a = 6$ mm consisting of 3 mm hole and 1½ mm jewelers saw cuts.

Tests were stopped while the crack was still in the tensile mode but with some development of shear lips and usually corresponded to a crack length of

approximately $2a$ of 16 mm. Vacuum tests were also stopped at a $2a$ of approximately 16 mm, giving the same nominal K-value as obtained for air tests.

Three basic load programs were used to characterize the crack tip profile (Fig. 5). The load level was chosen as 78.4 ± 39.2 MPa, which gave a stress ratio of $R = 1/3$. Sine wave loading was employed at a frequency of 20 Hz for all tests by a closed-loop hydraulic fatigue machine. When a test was stopped the sine wave being executed was completed, always ending at mean load, as shown by the heavy arrows in Fig. 5. Any one of the points chosen for infiltration (also shown in Fig. 5) was then reached by executing the additional sine waves. A total of 48 specimens were infiltrated and examined in the scanning electron microscope.

Experimental Results

Fatigue of 2024-T3 in Laboratory Air

Optical photographs of plastic castings produced at maximum load (Point 3, Fig. 5*a*) are shown in Figs. 6*a* and *b*. Curvature of the crack front is apparent, and the beginning development of shear lips appears to be slanted and does not carry over the curvature of the tensile portion of the crack front. Castings produced at minimum load (Fig. 6*c*) again show the general crack front curvature, whereas the shear lips are again straight with no apparent change in the angle of slant.

The Fig. 6*c* photograph was taken with lighting from below to accent holes in the castings. These holes were never observed in castings produced by in-

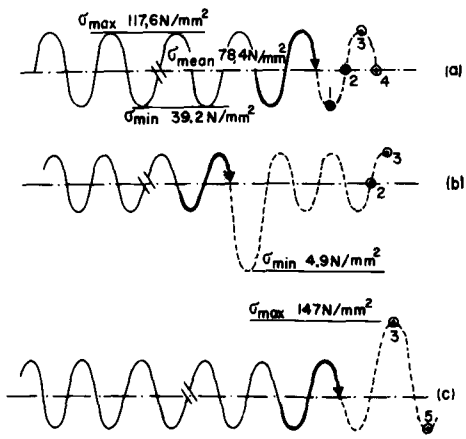

FIG. 5—*Load programs with points of plastic infiltration indicated by number.*

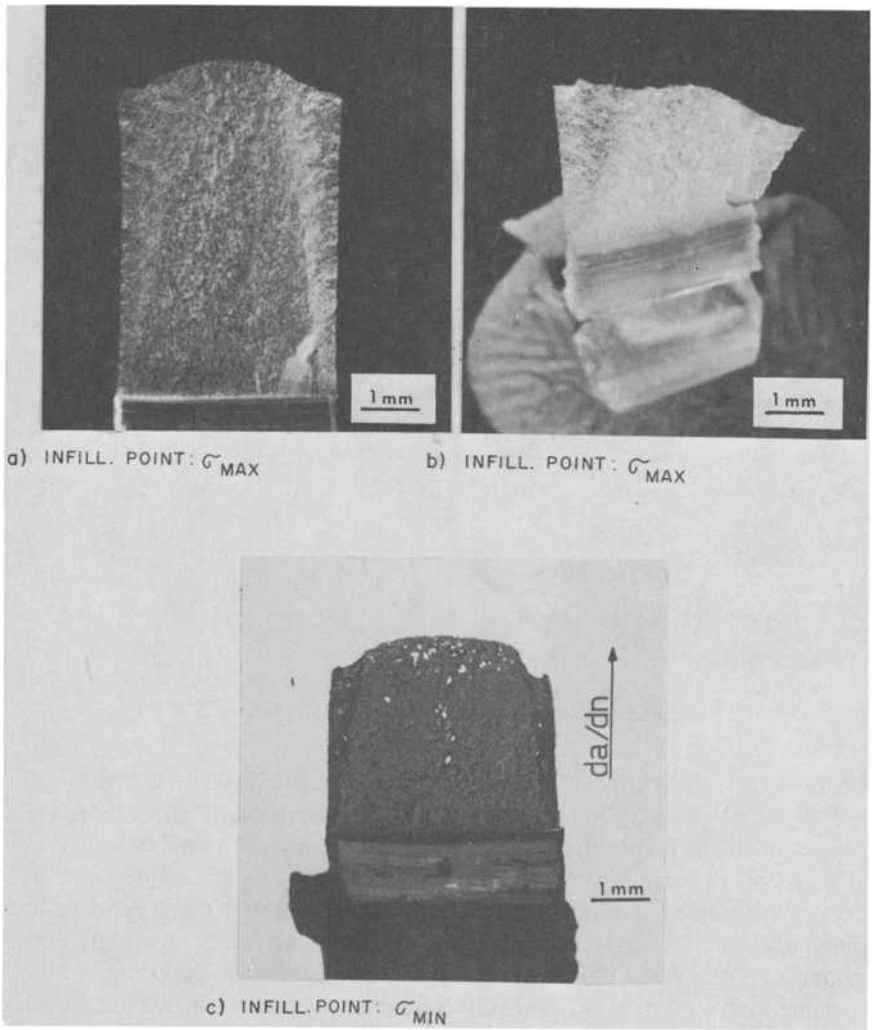

FIG. 6—*Optical photographs of castings produced at maximum and minimum loads in 2024-T3.*

filtration at σ_{mean} or σ_{max} and it is assumed they represent points of crack closure; this will be discussed later.

The fairly regular appearance of the crack front seen at the optical level begins to disappear at higher magnifications, as shown by the SEM micrograph of Fig. 7. Differences in elevation of the crack propagation path are clearly evident.

Figure 8*a* shows the crack tip at maximum load. The tip is generally blunt, but appears to be more elliptical rather than circular in shape. At minimum

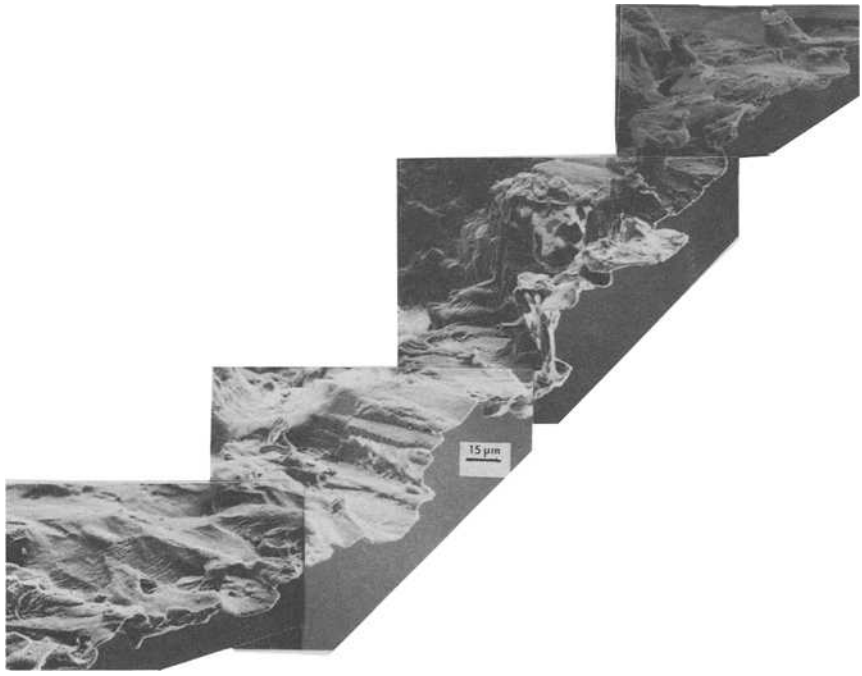

FIG. 7—*Montage of crack tip infiltrated at maximum load in 2024-T3.*

load the crack tip is much sharper; however, Fig. 8*b* shows that it remains generally elliptical and the last striation is distinctly visible. Figures 8*c* and *d* again show the striking difference between maximum and minimum load.

Results of a program with one negative peak load (Fig. 5*b*) are shown in Fig. 9*a* (infiltration at mean load). The wide striation (A) corresponding to uploading from 4.9 to 117.6 MPa and one additional striation at (B) corresponding to the last full load cycle are clearly visible. A second sample with the same load program but with infiltration at σ_{max} again shows the broad striation as well as the striation resulting from the next load cycle (Fig. 9*b*). However, now the last striation is not so sharply defined due to the rounded crack tip accompanying crack extension on uploading from Point 2 to 3 (Fig. 5*b*).

Measurements of the crack tip opening displacement (CTOD) at maximum load from photographs similar to Fig. 8*c* give an average value of 1.0 μm. One is cautioned, however, that the last striation formed at minimum load is carried upward by both sides of the crack face, thus adding to the apparent CTOD measurement. It is suggested that the value of CTOD at minimum load (0.2 μm), which represents the thickness of both halves of the striation, must be subtracted from the actual CTOD measurement at maxi-

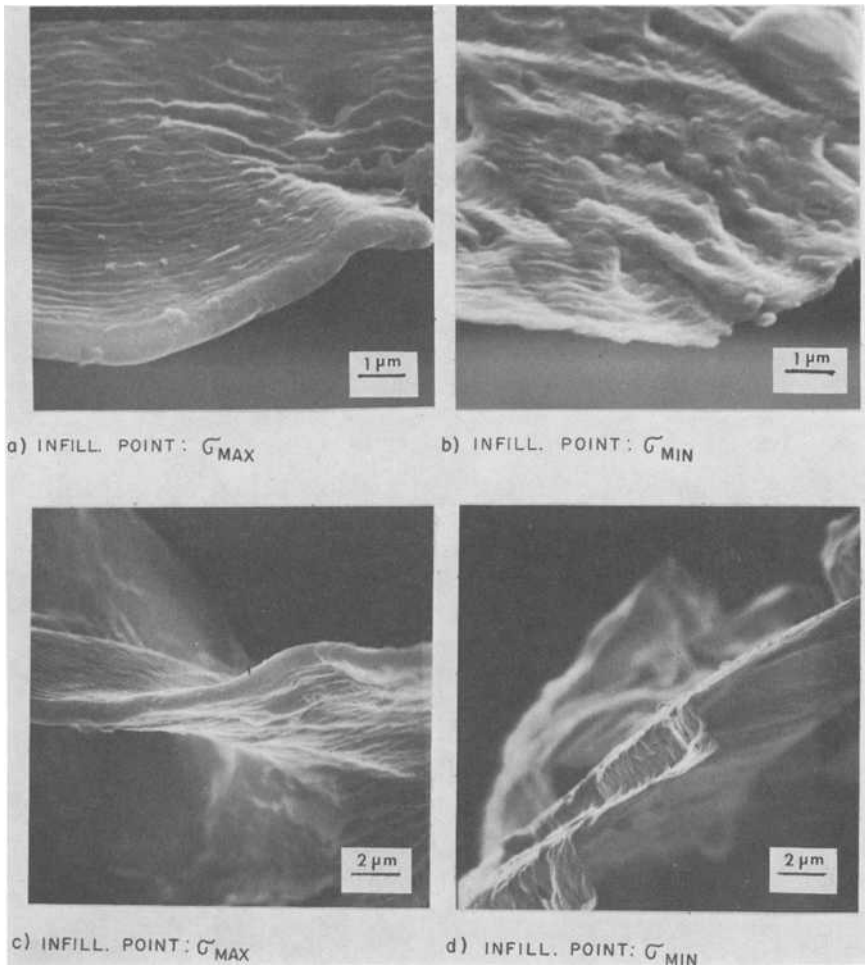

FIG. 8—(a,b,c,d) *SEM micrographs of fatigue crack tip in 2024-T3.* (c,d) *Viewed perpendicular to the crack front.*

mum load, giving an actual CTOD at maximum load of approximately 0.8 μm.

The evidence so far presented does not allow us to choose between the various models of crack propagation which were discussed. To do so, one must locate with some certainty the point at which cracking begins and how it proceeds.

A program similar to Fig. 5*b* but consisting of a negative peak load followed by ten load cycles, and then an overload of 25% was used to further check the behavior of the last striation formed. The result is shown in Figs.

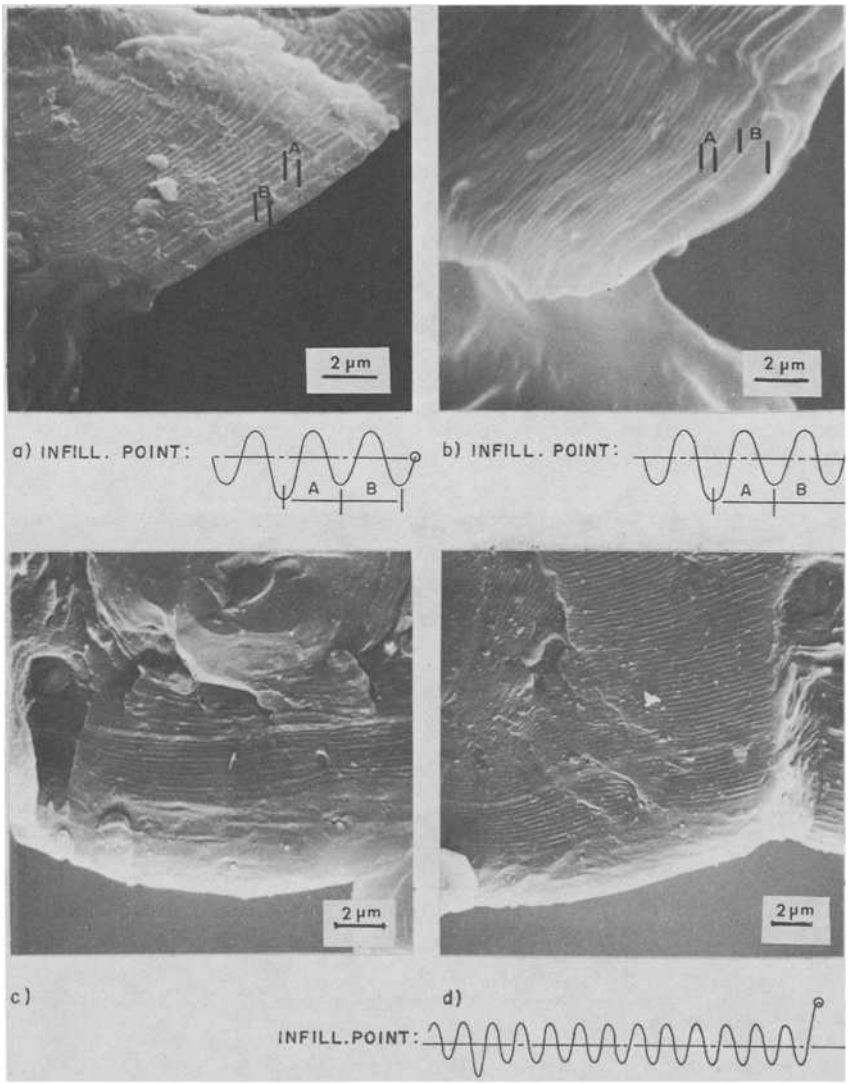

FIG. 9—(a,b) *Crack tip in 2024-T3 at mean and maximum load after indicated load sequence.* (c,d) *Crack tip in 2024-T3 resulting from load sequence shown with infiltration at 25% overload.*

9*c* and *d*, where ten striations are seen following the large striation produced by the negative peak load. Even though considerable crack extension has occurred from the overload the last striation appears to be fully undisturbed. One can only conclude that during a rising load, cracking begins precisely at the very apex of the crack tip, with very little initial plastic flow at the tip. Thus the last striation formed is left completely undisturbed.

The manner in which initial crack propagation occurs was investigated further by infiltrating a sample at a point just above the mean load when coming from minimum load. Figures 10*a* and *b* show what appear to be initial stages of "brittle" crack extension at Points C. One further notes that this initial stage of fracture appears to be not yet fully continuous along the crack front. Numerous other examples were found where the initial crack extension had not occurred along the entire crack front. Since in most cases the crack tip was observed to be fully rounded at mean load, we must assume that crack extension apparently does not begin in a fully synchronized manner along the crack front.

An explanation is best obtained by considering crack closure, first reported by Elber [*16,17*]. The relative displacement of the crack faces is recorded as a function of applied stress on an X-Y plot. The curve which is obtained, in general, has two straight portions corresponding to a fully closed crack and to a fully opened crack. The transition region between the two straight portions is due to a gradual loss of contact between the crack faces during the load rise. The completion of the transition marks the point where the crack faces are assumed to be fully opened, and the corresponding stress level is called the opening stress or σ_{op}. The actual difficulties in measuring crack closure and in data analysis are certainly real but not relevant to this work.

The crack closure model generally assumes that the crack faces mate evenly over the entire fracture surface. Optical photographs of castings produced at minimum load, however, indicate that crack closure is a result of individual

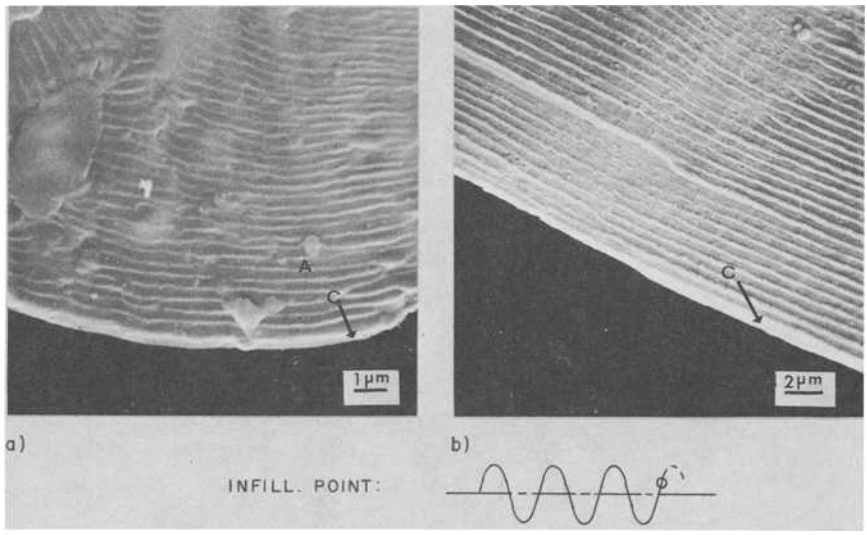

FIG. 10—(a,b) *Evidence of brittle crack extension in 2024-T3 shown by infiltration at a point just above mean load.*

contact points caused by a mismatch of the fracture surfaces (Fig. 6*c*). Many additional points of contact between the fracture surfaces become visible when the casting are viewed in the SEM. Figure 11*a* represents such an area in the fracture region near the center of the plate, and Fig. 11*b* is a similar region in the shear lip (points of contact are indicated at (x)).

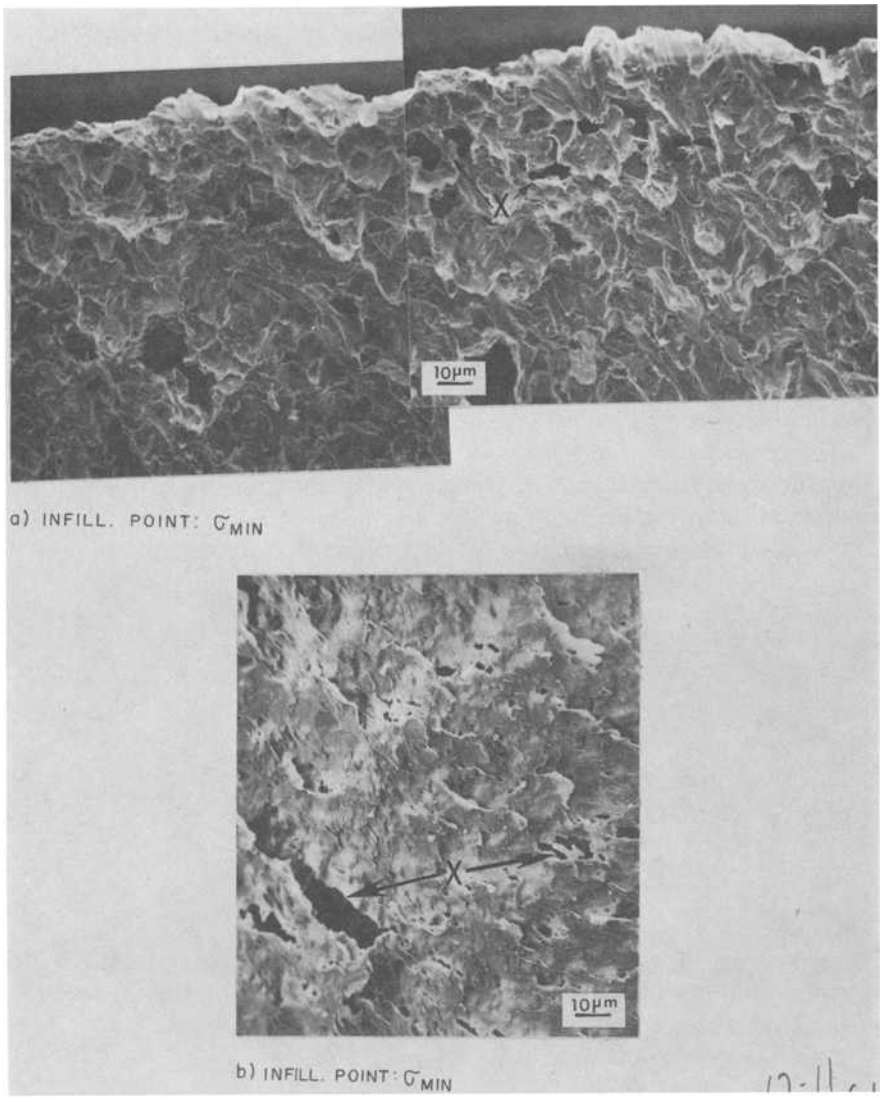

FIG. 11—*Crack closure occurring near the crack tip in 2024-T3.* (a) *Plane strain region near center of plate.* (b) *Plane stress region in the shear lip.*

A qualitative evaluation of a number of photographs indicates the relative amount of surface contact in the shear lips is about the same as that in the interior of the specimen. One must point out, however, that the relative amounts of fracture surface contact give no indication of the amount of load being transferred.

For very thin sheets crack closure may occur through the entire thickness, whereas for thick sheets crack closure may be predominately a surface effect. However, the significant point borne out by the present experiments is that closure is not an event which occurs uniformly over the entire surface. Instead, it occurs only locally, which on a microscopic level explains why initial crack extension does not start simultaneously at all points along the entire crack front.

Thus during load rise we expect that crack growth will occur first at those places on the crack tip where the opening stress has been reached and will proceed somewhat discontinuously until the crack is fully open. The time span of these events will be nearly instantaneous and will only be observed when an experimental technique such as plastic infiltration is used.

At the beginning it was noted that at the optical level the tensile portion of the crack front was curved while the shear lips appeared slanted and did not carry over the crack front curvature. One might suspect that a distinctly different mode of cracking was operating, and this fact is generally supported by the micrographs of Fig. 12.

In every case we observed a shear mode of failure and at no time did we observe characteristic fatigue striations. Figures 12*a* and *b* taken from a sample infiltration at σ_{max} indicate that the crack tip in the shear lip is much sharper than in the plate interior (compare with Figs. 8*a* and *b*). Although no explanation is available for the observed increase in sharpness of the crack tip, we expect it is associated with the fact that the plate interior is undergoing primarily Mode I opening while the shear lips are undergoing a mixed Mode I and III opening. Figure 12*c* was taken just behind the crack tip and very small secondary cracks are indicated at (E). Figure 12*c* can be compared with Fig. 11*b* which is from a sample infiltrated at minimum load. Numerous secondary shear cracks are still present in Fig. 11*b*, however, indicating again that crack closure is macroscopically not complete.

Fatigue of 7075-T6 in Laboratory Air

Fatigue crack tips found in the 7075 alloy have basically the same geometry as found in the 2024 alloy. Consequently micrographs verifying all points discussed in the preceding paragraphs have been omitted; however, several photographs demonstrating the equivalence mentioned are presented.

Figure 13*a* is an optical photograph of a casting produced at maximum load. Some crack tip curvature is evident, but it is not as pronounced as that in 2024. Furthermore, although the crack length is the same as that in 2024,

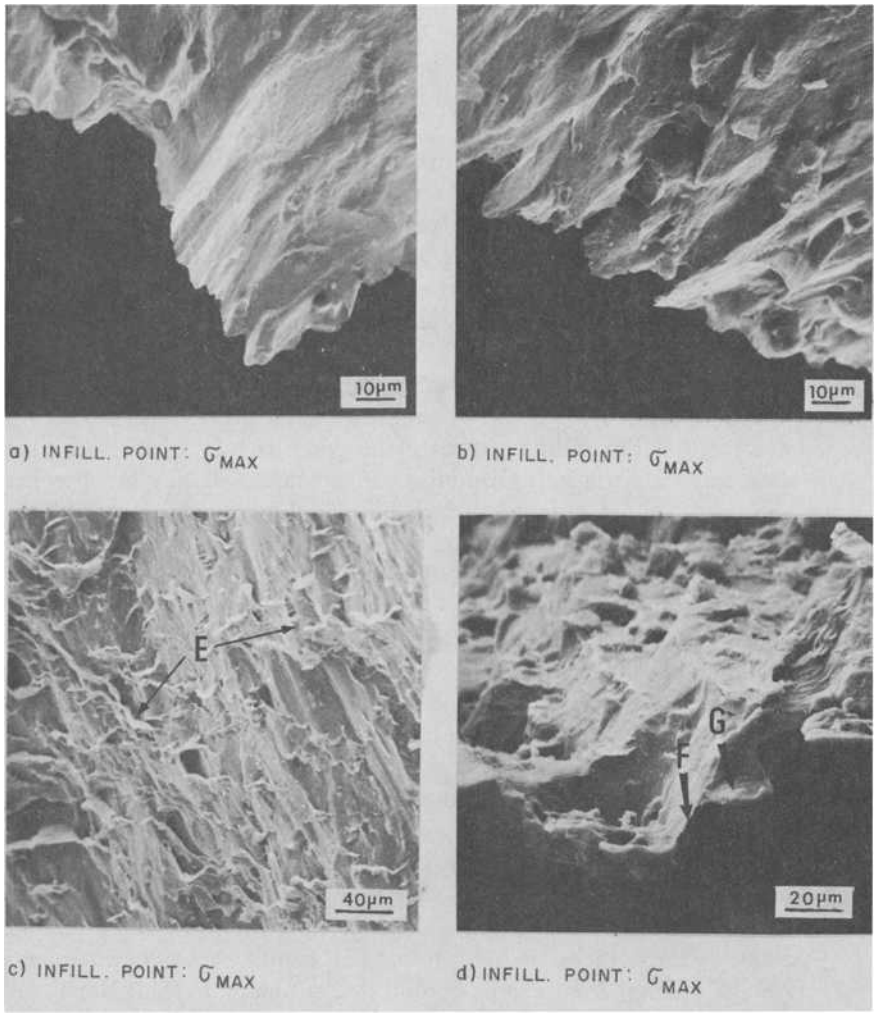

FIG. 12—(a,b,c,d) *SEM micrographs of shear lip fracture in 2024-T3.*

the shear lips have not reached the same stage of development. Both differences may be associated with lower ductility of the 7075 alloy, which further implies that the plastic zones are smaller. As a consequence, a state of plane strain will apply over a larger part of the thickness and crack closure will occur to a lesser extent at the surface. The casting produced at minimum load showed the same characteristic holes corresponding to crack closure in both the shear lips and the plate interior. Figures 13*b* and *c* show the crack tip at maximum load and demonstrate there is very little to choose between the crack tips of 2024 and 7075.

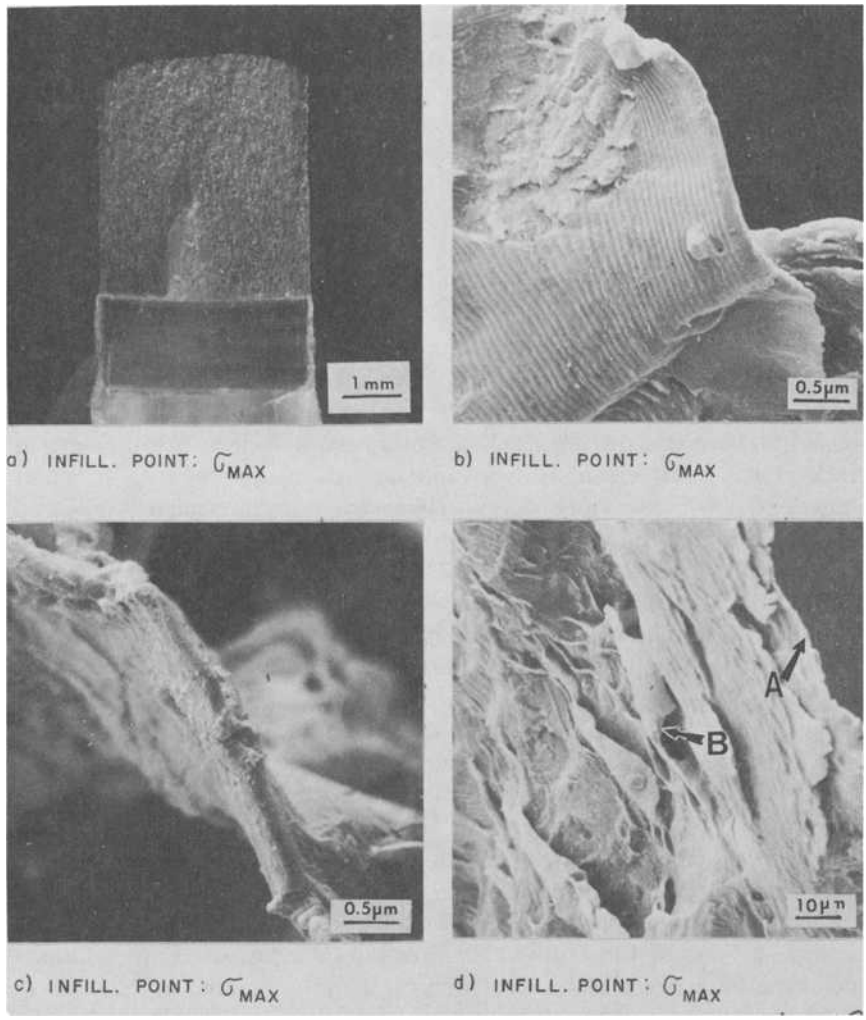

FIG. 13—(a,b,c,d) *Representative photographs of crack tip geometry found in 7075-T6.*

Figure 13*d* is an area of the shear lip from the 7075 sample infiltrated at maximum load; a portion of the crack tip is indicated at (A). The completely different mode of failure is evident from the presence of secondary shear cracks indicated at (B), which is again similar to the differences observed for the 2024 alloy.

Crack tip opening displacement measurements in 7075 were approximately 1.4 μm at maximum load and 0.4 μm at minimum load; surprisingly, these are larger than the values found for 2024. A comparison of the values of

ΔCTOD in air with the average crack growth rates in the two alloys (Table 1) indicates that da/dn is approximately 0.5 ΔCTOD for 2024 and 0.7 ΔCTOD for 7075. Although it should be pointed out that sufficient data are not available for an accurate quantitative comparison, it appears that in air the ratio $\alpha = da/dn/\Delta\text{CTOD}$ is larger for the 7075 alloy. In other words, there is more crack extension in this alloy for the same amount of incremental crack tip opening.

Fatigue of 2024-T3 and 7075-T6 in Vacuum

Whereas fatigue fractures produced in laboratory air are always characterized by distinctive striation patterns, fracture surfaces produced in vacuum are invariably void of striations or are at best marked by what are termed ill-defined slip patterns. It has also been known for some time that crack growth rates in an inert environment are much less than in air at equivalent ΔK-levels. Thus Meyn's [*10*] results were immediately criticized based on the fact that his observations may not have been at high enough crack rates for striations to be visible in vacuum. This criticism has since been rejected by various workers such as Pelloux [*8*], Broek et al [*18*], and Wanhill [*19*], who have conducted investigations where the crack growth rate was high enough to produce visible striations.

Results of the present investigation confirm the much lower crack rate in vacuum (Table 1) and also indicate that the difference in appearance of fracture surfaces formed in the two environments is caused by a fundamental difference in the deformation at the crack lip in vacuum. This difference is shown in Fig. 14, which is taken from a sample infiltrated at maximum load. The branched crack tip shown is not an isolated occurrence; rather, it is easily observed at many locations along the crack front. Furthermore crack branching was systematically reproducible in several samples tested in vacuum. It is natural to assume that once the branched crack tip is formed one of the branches will quickly dominate, leaving the other in the wake of the crack. An example of this behavior is shown in Fig. 15*a*. As soon as the dominating branch has propagated a short distance, however, it may again

TABLE 1—*Crack growth rates and ΔCTOD values found for 2024 and 7075 at* $\Delta K = 13.3\ MN/m^{3/2}$.

	2024-T3	7075-T6
Macroscopic crack growth rates		
Air	0.43 μm/cycle	0.73 μm/cycle
Vacuum	0.07 μm/cycle	0.10 μm/cycle
ΔCTOD (in air)	0.08 μm	1.0 μm
$da/dn = \alpha\Delta\text{CTOD}$ (in air)	$\alpha = 0.54$	$\alpha = 0.73$

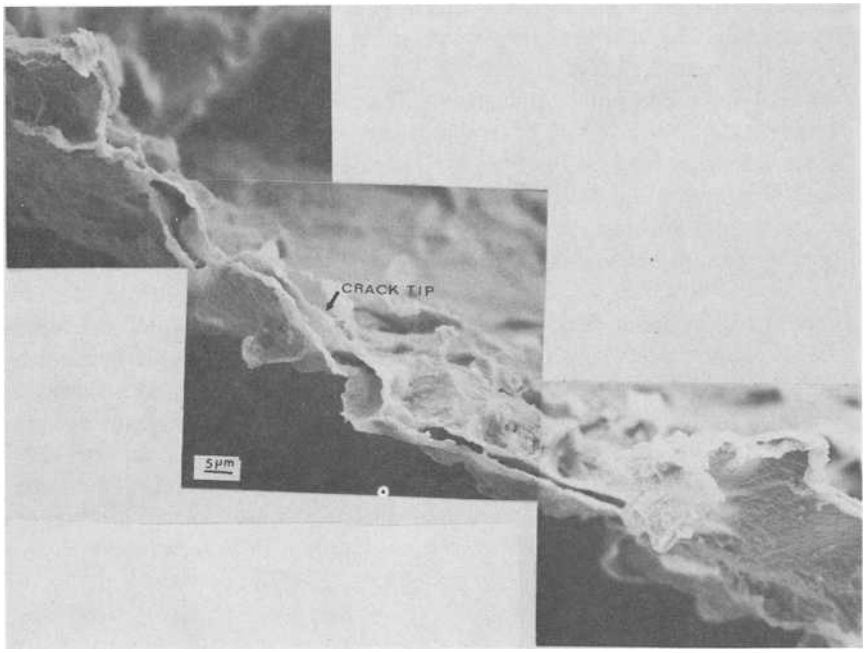

FIG. 14—*Montage of crack tip branching occurring at maximum load and resulting from crack growth in vacuum. Material: 2024-T3.*

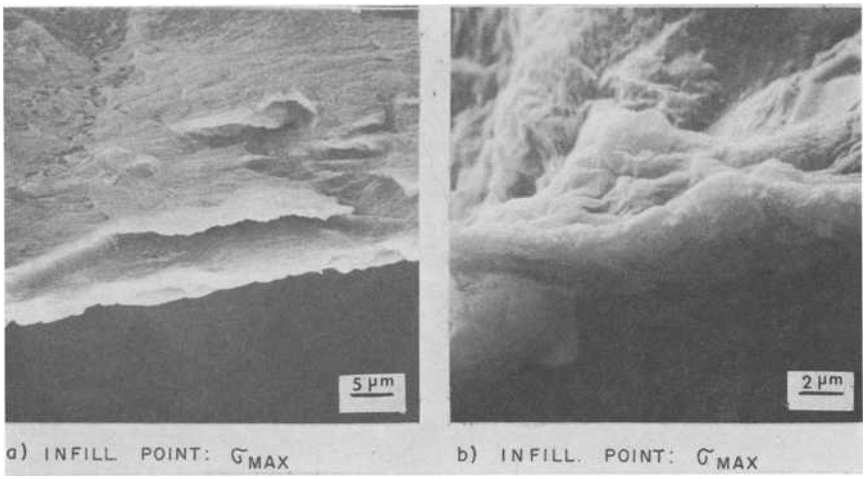

FIG. 15—*Fatigue crack growth in 2024-T3 in vacuum.* (a) *Crack branches left in the wake of the propagating crack tip.* (b) *Unbranched crack resulting presumably from alternate shear.*

begin to branch. The simple unbranched crack tip was also observed and is shown in Fig. 15*b*. Perhaps the most significant observation was that there was no apparent preferential mode of failure. Crack closure is again identified at well-defined points of surface contact.

The crack tip found in 7075 samples fatigued in vacuum was again much the same as the crack tip of 2024. There were areas of branching bordered by areas of both alternate shear and mixed Modes I and III shear failure, and, as before, there appeared to be no preferential mode of failure. An apparent alternate or single shear mode is shown in Fig. 16.

From a macroscopic standpoint the fracture surface produced in vacuum is much more irregular than fracture in air. The fact that any one of several modes of failure are operating simultaneously along the crack front is undoubtedly a contributing factor. However, as long as only shear failure operates, a path will be chosen for crack advance which most easily accommodates slip, thus resulting in wide variations from grain to grain in elevation of the crack front. Subsequent linking of these differences in elevation result in a crack front which is highly irregular and unorganized.

Discussion of Results

An unexpected observation in the present experimental program was the occurrence of an initially quasi-brittle crack extension during the rising part of the load cycle for both alloys tested.

The cause of initial brittleness observed is presumed to be water vapor; this

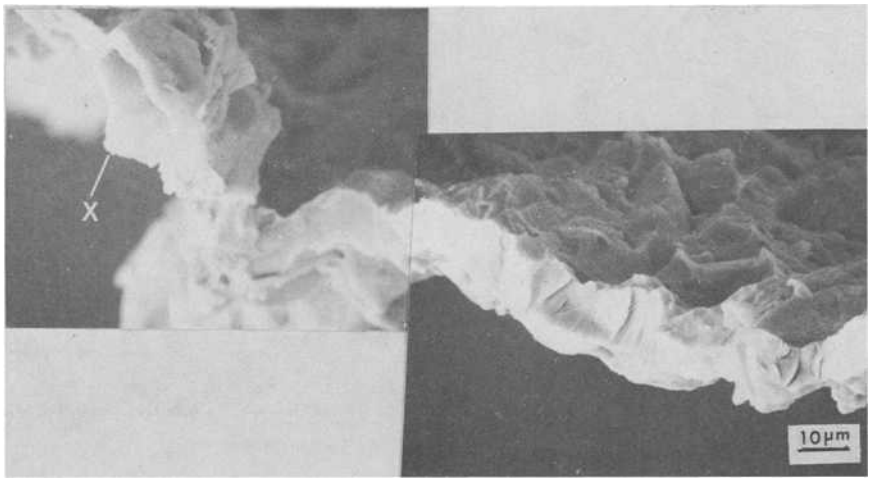

FIG. 16—*Region of alternate shear with adjacent region of branching in 7075-T6 in vacuum.*

has been amply demonstrated by Broom and Nicholson [*20*], Hartman and Jacobs [*21*], Bradshaw and Wheeler [*22*], and many others. Vogelesang [*23*] has suggested that in corrosion fatigue a crack will propagate by cleavage or shear, depending on whether the tensile fracture stress σ_{cr} or the shear stress τ_{cr} is reached first. The tendency for cleavage will increase if the value of the ratio σ_{cr}/τ_{cr} is lowered.

In normal air fatigue tests there are two ways of lowering the value of the ratio σ_{cr}/τ_{cr}. First by increasing τ_{cr} by work hardening; however, it is difficult to predict whether cyclic slip in the reversed plastic zone will result in cyclic work hardening or softening. The second method of lowering σ_{cr}/τ_{cr} is by reducing the stress required to break atomic bonds, σ_{cr}. Tyson and Alfred [*24*] have shown that theoretically σ_{cr} is on the order of ten times greater than τ_{cr}, which has been known for some time to be the cause of the bulk plastic behavior of metals. However, the discontinuity of a free surface lowers τ_{cr} for atoms at the surface, and the presence of a corrosive environment at the surface lowers σ_{cr} even further. The precise manner in which water vapor reduces σ_{cr} is not known, but the most widely accepted explanation is that water vapor reacting with freshly exposed metal at the crack tip releases hydrogen which in turn is responsible for reducing bond strength.

One should not expect that σ_{cr} and τ_{cr} represent two competing processes in which one mode of fracture is fully excluded in favor of the other. We must expect that crack extension from bond rupture during the initial load rise is also accompanied by some plastic deformation. As discussed by Vogelesang and Schijve [*25*], environmentally assisted tensile decohesion at the crack tip will initiate some shear decohesion as well. However, the tensile decohesion is the controlling factor. During further increase of the crack tip stress intensity more plastic deformation will occur, which is the beginning of the blunting process. The effectiveness of a mildly corrosive environment in promoting tensile rupture will then be reduced and plastic flow will ultimately dominate, leading to the crack tip geometry found at maximum load (Fig. 8*a*).

Bowles and Broek [*26*] studied the dislocation structures associated with fatigue by removing disks from the fracture surface which was then carefully protected with a resistant paint and electropolished from one side only. Thin foils produced in this manner showed a distinctly periodic array of light and dark bands, with a spacing corresponding to striation spacing as determined from replicas. Simple tilting experiments showed that the dark bands corresponded to dense unresolvable dislocation tangles which at times formed into subgrains. In contrast, the light areas showed very little dislocation structure regardless of the tilt angle employed. An example of the structure observed by Bowles and Broek is shown in Fig. 17 for 7075-T6.

Wanhill [*19*] confirmed the observations of Bowles and Broek for 7075-T6 and extended the technique to include fractures in 2024 as well as fractures of both alloys in vacuum. An unexpected observation was that seldom did

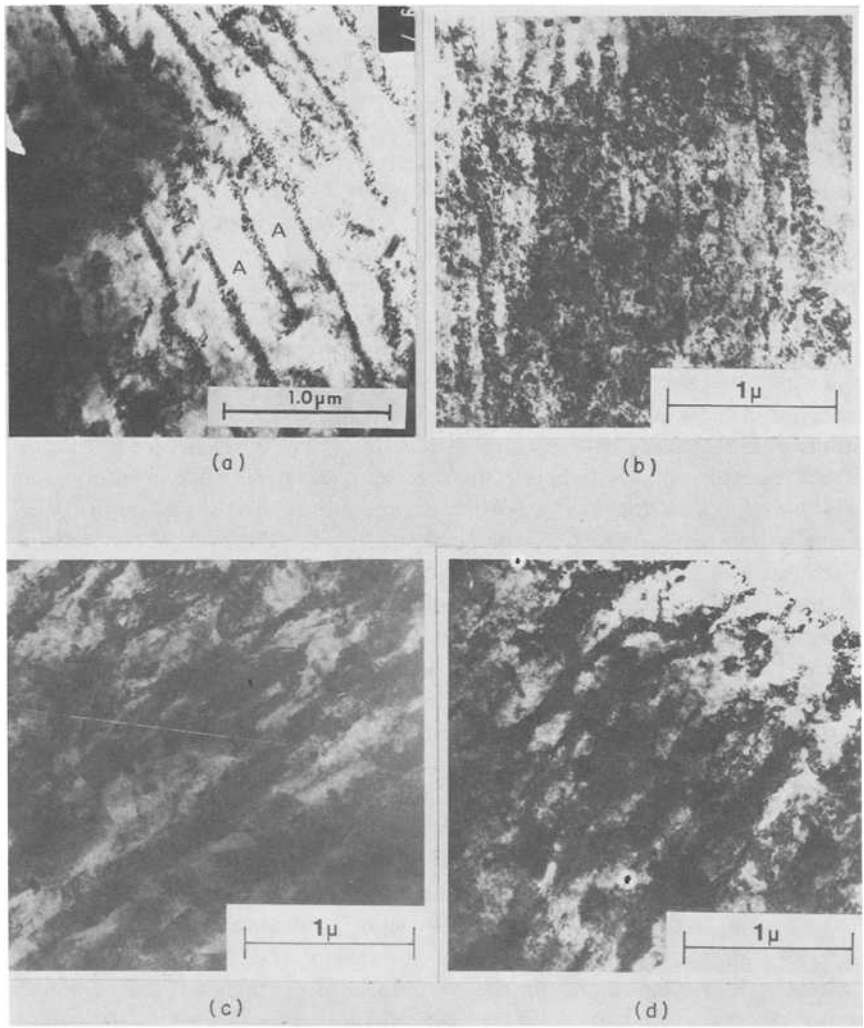

FIG. 17—*Transmission electron micrographs of fatigue fracture in air indicating characteristic light areas and dark bands of dislocation tangles and subgrains.* (a) *7075-T6.* (b) *2024-T3.* (b,c) *Transmission electron micrographs of fatigue fracture in vacuum showing only dark, ill-defined bands of dislocations.* (c) *7075-T6.* (d) *2024-T3.* (a) *Bowles and Broek* [26]. (b,c,d) *Wanhill* [19].

any periodic array of dislocations appear in vacuum. On the occasions that a periodic structure was found it was very ill defined and had no correlation with crack growth rates.

At the time of their observations Bowles and Broek suggested the dark bands of dislocations were produced by some type of spontaneous dislocation rearrangement into a cell structure as a result of the high stress intensity at

the crack tip at maximum load. However, no satisfactory explanation could be given for the presence of light areas which were relatively free from dislocations. In contrast, Wanhill suggested that the absence of any periodic structure in vacuum was the result of excessive crack tip blunting because of ease of slip activity.

A more plausible explanation of the preceding results is now possible based on the present study. To begin with we believe that the rather puzzling light areas (indicated at Points A in Fig. 17*a*) which are relatively void of dislocation structure are simply a result of the initially brittle crack extension shown at Points C in Figs. 10*a* and 10*b*. In contrast, the dense bands of dislocations result as plastic deformation dominates near the maximum of the load cycle. Because no component of brittle fracture occurs in vacuum and crack extension results from one of several different modes of alternate shear, it is natural to expect that the dislocation structure would be more or less uniform over the entire fracture surface.

Striation spacings on fracture surfaces produced in air are expected to correlate with the dislocation band structure of Fig. 17. At the same time the continuous plastic deformation producing crack extension in vacuum can be expected to give a more or less even dislocation structure, with no correlation with crack growth rates.

Geometry of Fatigue Crack Advance in Laboratory Air

In the discussion which follows we have combined observations from 2024 and 7075 to give a general picture of the geometry of fatigue crack advance.

Scanning electron micrographs taken at minimum load show that the fatigue crack tip is singly notched and, although resharpening occurs, the profile remains elliptical, a result of well-behaved reversed plasticity (Fig. 8). During the rising portion of the load cycle, initial crack extension appears to be quasi-brittle in nature. The initial extension is not fully synchronized along the crack front (Figs. 10*a* and *b*) and appears to result from a nonuniform release of contact between points on the fracture surfaces near the tip which are presumed to be locations where crack closure occurs. As the closure stress is exceeded and the crack faces are opened, crack extension ultimately becomes synchronized along the crack front.

At maximum load the fatigue crack is generally blunt and smooth, with a profile which is still more elliptical than circular (Fig. 8*a*). The crack tip geometry just described is shown in Fig. 18, where each of the sequences are only schematic representations resulting from a large number of observations.

A plastic flow or alternate shear model of crack advance should result in the crack tip geometry suggested by Pelloux. At no time did we observe this geometry in constant-amplitude tests; however, the geometry was observed in several samples which were given an overload. Figures 19*a* and *b* were taken from castings produced at a maximum overload of 25% (Fig. 5c) and in-

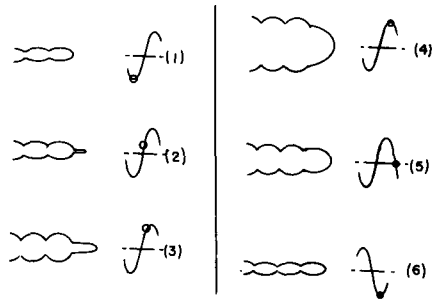

FIG. 18—*Representation of fatigue crack advance mechanism and associated crack tip geometry derived from plastic castings of specimens fatigued in air.*

dicate a CTOD of approximately 7 μm with a geometry strikingly similar to that suggested by Pelloux. As soon as a very small overload was applied the crack tip tended to conform to the alternate shear geometry, as shown in Figs. 9*c* and *d*, which represent a 25% overload.

The geometry of the crack tip at minimum load after an overload is shown in Figs. 19*c* and *d*, where the crack tip is seen to be blunt and heavily deformed with a CTOD of 4 μm. Furthermore, the ratio of $(CTOD)_{max}/(CTOD)_{min}$ for the peak overload and subsequent minimum load in 2024 is 7/4 or 1.75. In contrast, the ratio of $(CTOD)_{max}/(CTOD)_{min}$ for constant-amplitude tests in the same materials is 1.0/0.2 or 5.0. In other words, the resharpening mechanism after the overload cycle was much less effective, thus leaving the crack tip open to a considerable extent.

The preceding observations on crack tip geometry also appear to be in agreement with some recent results of Schijve and Arkema [*27*]. In a series of constant-amplitude tests with a single peak load, the crack closure stress was measured before and immediately after the peak load. It was systematically found that the peak load decreased the closure stress, although it significantly increased after further crack growth. At the same time, crack growth retardation was generally observed (reviewed in Ref *27*), but the initial drop of the closure stress caused a delay of the retardation. It was suggested that peak loads will open the crack and thus reduce the closure stress. The present results confirm the larger opening of the crack tip after application of an overload, and the crack tip geometry at minimum load just after overload indicates that considerable additional negative stress is required to resharpen the crack. The magnitude of the negative stress required is not known, although it should be related to the size of the plastic zone produced by the overload at the tip of the crack.

Fatigue Crack Advance in Vacuum

The inability to account for environmental effects is a fundamental weakness of all crack growth models invoking slip or τ_{cr} as a mechanism for crack

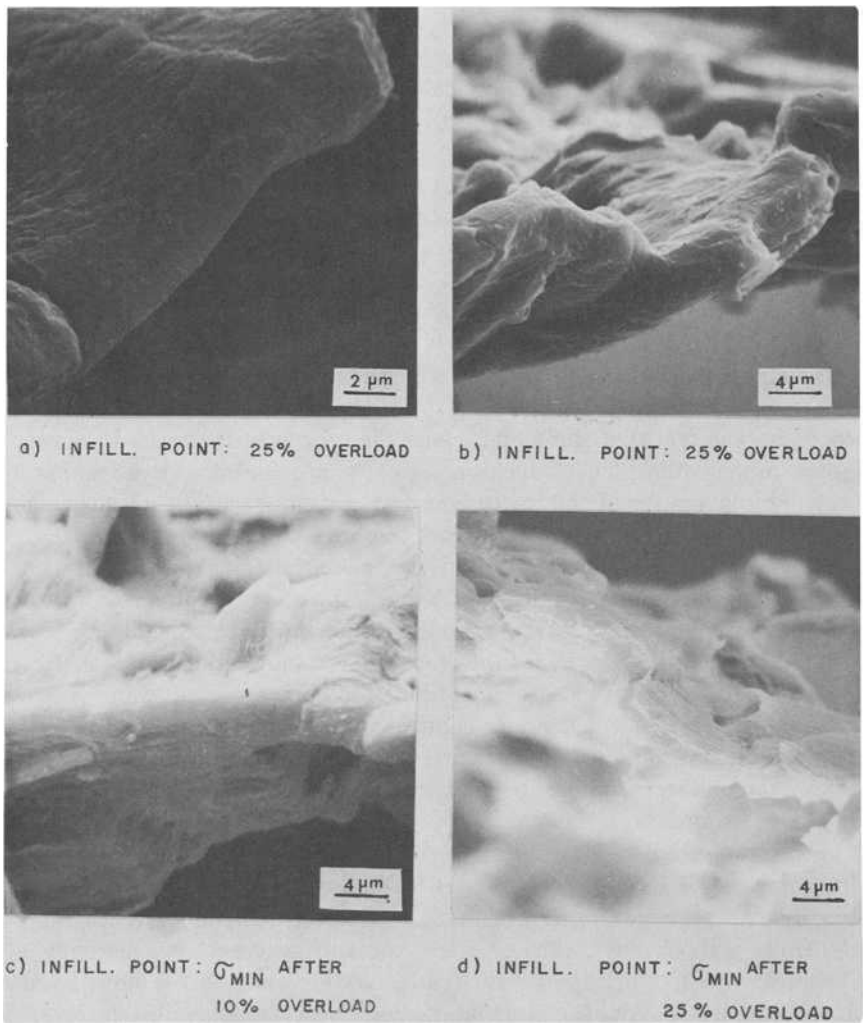

FIG. 19—(a,b) *Crack tips in 2024-T3 after indicated overloads.* (c,d) *Crack tips in 2024-T3 at minimum load after indicated overloads. All samples tested in air.*

advance. Pelloux and others have attempted to overcome this difficulty by suggesting that the crack extension during load rise may be the same for both air and vacuum. Because of the absence of an oxide layer in vacuum, however, reversed slip during unloading may in essence allow the crack tip to "back up", giving a resultant crack advance which is less in vacuum than air (Figs. 2*i* and *j*). Nevertheless, slip activity cannot account for the increasing crack growth rates accompanying increased activity of the environment. Moreover, the low crack rates in very dry oxygen, comparable to those in vacuum [*21,22*], are also hard to reconcile with any rebonding concept.

In the opinion of the present authors the slower crack growth rates in vacuum result from a competitive interaction of the crack modes which were observed. The variety of cracking modes occurs because in the absence of any environmental influence the ratio of σ_{cr}/τ_{cr} is sufficiently large that only slip modes of crack advance operate.

The mode of cracking observed most often was crack tip branching, which occurred over large portions of the crack front. It would be difficult to describe the mechanism for branching at the level of the crack tip geometry. However, it may well be possible that excessive slip activity in two different directions could initiate branching in a way somewhat similar to the model of Tomkins.

Branching alone could account for a slower crack rate because the energy associated with crack advance is essentially divided between the two branches. The fact that slip modes cause the growth of the crack, however, implies propagation planes which vary greatly in angle and elevation. As a result the topography of the fracture surface is much coarser than for crack growth in humid air. The much rougher fracture surface involves a relatively poorly organized crack front, and in fact a longer crack front. The two-dimensional stress intensity concept should therefore be affected by this three-dimensional behavior and, although no solutions are available for such a three-dimensional character of the crack, it seems logical that a lower stress intensity will be the result. In conclusion, the lower crack rate in vacuum stems from several supplementary contributions: (*1*) the absence of the environmental contribution, (*2*) crack branching, and (*3*) a longer and poorly organized crack front, where the latter two contributions cooperate in lowering the stress intensity.

In the literature it has been suggested that fatigue crack growth in an inert environment (for example, vacuum) should serve as a reference for crack growth in an aggressive environment. It now seems that the reference is not an unequivocal reference, because apart from differences in the environmental contribution to crack growth there are also differences in the stress intensity associated with changed cracking modes.

Conclusions

An infiltration technique has revealed essentially new information about cyclic crack extension in aluminum alloys, indicating that previous crack growth models were rather speculative. In air crack growth in each cycle starts with a quasi-brittle extension followed by crack tip blunting. This is an environmentally controlled process, especially for the quasi-brittle contribution. During unloading crack tip sharpening does occur, but the tip remains in a flat semielliptical shape.

In vacuum the mechanism is completely different. Crack growth occurs due to slip induced shear decohesion. Crack branching was systematically

found. In addition, the topography of the fracture surface was much more irregular than for fatigue in air. Both factors cooperate in reducing the crack tip stress intensity. Crack growth in vacuum is much slower, partly because of the absence of environmentally assisted tensile decohesion. However, the lower stress intensity is also a significant contribution.

References

[1] Bowles, C. Q., Report LR-249, Delft University of Technology, Delft, The Netherlands, 1977.

[2] Forsyth, P. J. E. and Ryder, D. A., *Aircraft Engineering*, Vol. 32, 1960, pp. 96-99.

[3] Forsyth, P. J. E. and Ryder, D. A., *Metallurgia*, Vol. 63, 1961, pp. 117-124.

[4] Stubbington, C. A., Report CPM-4, Royal Aircraft Establishment, Farnborough, England, 1963.

[5] Laird, C. and Smith, G. C., *Philosophical Magazine*, Vol. 7, 1962, pp. 847-857.

[6] Laird, C. in *Fatigue Crack Propagation, ASTM STP 415*, American Society for Testing and Materials, 1967, pp. 131-168.

[7] Schijve, J., Discussion to the paper of J. C. McMillian and R. M. N. Pelloux, in *Fatigue Crack Propagation, ASTM STP 415*, American Society for Testing and Materials, 1967, p. 533.

[8] Pelloux, R. M. N., *Transactions of ASM*, Vol. 62, 1969, pp. 281-285.

[9] Pelloux, R. M. N., *Engineering Fracture Mechanics*, Vol. 1, 1970, pp. 697-704.

[10] Meyn, D. A., *Transactions of ASM*, Vol. 61, 1968, pp. 52-61.

[11] Tomkins, B., *Philosophical Magazine*, Vol. 18, 1968, pp. 1041-1066.

[12] Tomkins, B. and Biggs, W. D., *Journal of Materials Science*, Vol. 4, 1969, pp. 544-553.

[13] McMillan, J. C. and Pelloux, R. M. N. in *Fatigue Crack Propagation, ASTM STP 415*, American Society for Testing and Materials, 1967, pp. 505-532.

[14] Dushman, S., *Scientific Foundations of Vacuum Techniques*, 2nd ed., Wiley, New York, 1962.

[15] Gutshall, P. G. and Bowles, C. Q., Final Technical Report of NASA Contract NASA-CR-114719, 1974.

[16] Elber, W., *Engineering Fracture Mechanics*, Vol. 2, 1970, p. 37.

[17] Elber, W. in *Damage Tolerance in Aircraft Structures, ASTM STP 486*, American Society for Testing and Materials, 1971, p. 230.

[18] Broek, D., Hartman, A., and Nederveen, A., Report NLR-TR-71032-U, National Aerospace Laboratory, Amsterdam, The Netherlands, 197i.

[19] Wanhill, E. J., Report NLR-TR-74094-C, National Aerospace Laboratory, Amsterdam, The Netherlands, 1974.

[20] Broom, T. and Nicholson, A., *Journal of the Institute of Metals*, Feb. 1961, pp. 183-190.

[21] Hartman, A. and Jacobs, F. A., Report NLR-TN-M 2123, National Aerospace Laboratory, Amsterdam, The Netherlands, 1964.

[22] Bradshaw, F. J. and Wheeler, C., *Applied Materials Research*, April 1966, p. 112.

[23] Vogelesang, L. B., Report LR-222, Department of Aerospace Engineering, Delft University of Technology, Delft, The Netherlands, 1976.

[24] Tyson, W. R. and Alfred, L. C. R. in *Corrosion Fatigue: Chemistry, Mechanics and Microstructures*, NACE-2, 1971, pp. 281-288.

[25] Vogelesang, L. B. and Schijve, J., *Fatigue of Engineering Materials and Structures*, Vol. 3, 1980, pp. 85-98.

[26] Bowles, C. Q. and Broek, D., *International Journal of Fracture Mechanics*, Vol. 8, No. 1, 1972, pp. 75-85.

[27] Schijve, J. and Arkema, W. J., Report VTH-217, Department of Aerospace Engineering, Delft University of Technology, Delft, The Netherlands.

DISCUSSION

H. Mughrabi[1] *(written discussion)*—You have made the most interesting observation that, in aluminum alloys, the fatigue crack advances during every cycle in air first by a quasi-brittle and subsequently by a ductile mode. Could this imply that the crack advance in air per cycle is roughly the sum of a quasi-brittle increment and a plastic increment, and that the difference between fatigue lifetimes in air and in vacuum can be understood by saying that in vacuum it is only the plastic increment which plays a role? If so, it would be most interesting to know whether you believe that this behavior is general to a wider class of materials or just peculiar to the alloys you have studied.

C. Q. Bowles and J. Schijve (authors' closure)—Professor Mughrabi poses an interesting possibility. The experimental results certainly imply that some type of partitioning of crack growth between the two observed modes could be used. However, we feel that the transition from a quasi-brittle to ductile mode is not marked by a sharp dividing line. Thus we see no way to quantify the two portions.

In the main body of the paper we point out that the quasi-brittle increment of crack growth is totally absent in vacuum. Thus one can say that its absence is responsible for the increased lifetime of specimens fatigued in vacuums. In somewhat more detail we have suggested that the increased fatigue lifetime is owing to three things: (*1*) the ductile increment leads to rapid crack tip blunting; (*2*) crack branching leads to a reduction of the crack tip stress intensity factor; and (*3*) the multitude of crack front geometries resulting from the ductile mode produces an extremely irregular crack front.

The authors indeed believe that the observed behavior is general to a wider class of materials. We have no evidence to that effect, however, and are planning some experiments on ferrous materials.

[1]Max-Planck-Institut für Metallforschung, Institut für Physik, Stuttgart, Federal Republic of Germany.

C. Loye,[1] *C. Bathias,*[1] *D. Retali,*[2] *and J. C. Devaux*[2]

The Plastic Zone Ahead of a Fatigue Crack in 316 Stainless Steel

REFERENCE: Loye, C., Bathias, C., Retali, D., and Devaux, J. C., **"The Plastic Zone Ahead of a Fatigue Crack in 316 Stainless Steel,"** *Fatigue Mechanisms: Advances in Quantitative Measurement of Physical Damage, ASTM STP 811*, J. Lankford, D. L. Davidson, W. L. Morris, and R. P. Wei, Eds., American Society for Testing and Materials, 1983, pp. 427-444.

ABSTRACT: After a short review of different experimental methods used for studying the plastic zone ahead of a crack tip, the capabilities of the microhardness method are analyzed in detail. A finite-element calculation, which takes the cyclic hardening of 316 stainless steel into account, permits a thorough study of plastic deformation at the crack tip. The microhardness technique is a good method of studying the shape of the plastic zone and the deformation around the tip of the crack.

KEY WORDS: fatigue, plastic zone, stresses, strains, experimental techniques, plastic analysis

The plastic zone at the tip of a fatigue crack is difficult to observe because of its small size (usually less than 1 mm). Observations are also complicated by the shape of the crack tip. Techniques presently being used are performed after fatigue testing and usually in a destructive manner. The development of the plastic zone inside a material cannot be observed concurrently with crack propagation. Observations are performed for a particular crack length either by stereographic or interferomic methods on the surface, or on a cross section by metallographic methods.

The nature of surface plastic zones formed ahead of cracks has been well established by the work of Davidson and Lankford [*1-3*].[3] They studied plastic zones in Fe-3Si steel, 304 stainless steel, and in aluminum alloy 6061 T6 by an electron-channeling method. They found the maximum dimension of the surface plastic zone to be equal to $\alpha(K/\sigma_y)^2$, where the coefficient α is 0.09 for Fe-3Si steel and 0.14 for the other two alloys.

[1]Université de Technologie de Compiègne, Compiegne, France.
[2]Framatome, Chalon, France.
[3]The italic numbers in brackets refer to the list of references appended to this paper.

Davidson and Lankford also used a sophisticated stereographic technique to study plastic strain at the fatigue crack tip. They found that the maximum nominal strain in the loading direction was about 12% in vacuum and about 6% in humid air. The strain in the region of the crack tip was found to be described by the function

$$\Delta\epsilon_p = E/(A + Br)^m$$

where A is the dislocation cell size, B is the slope of $A = f(r)$, r is the distance from the crack tip, $m = 0.74$ for low-carbon steel, and E is related to the maximum shear strain experienced by the material at the crack tip.

Greater difficulty is met in determining the nature of the plastic zone inside a material, particularly in the case of the plane strain condition. Generally, metallographic etching, X-ray diffraction, and other methods are not of sufficient precision. The microhardness technique, however, provides interesting results for all materials which cyclicly harden or soften.

The results presented in this paper are those of a Working Group of the French Metallurgical Society.

Quantitative Comparison of Experimental Techniques

Microhardness Technique

Cyclic loading of the plastic zone ahead of a fatigue crack leads to either hardening or softening of the metal. Microhardness, which depends on the density and arrangement of dislocations and consequently on the strain history, can be used to reveal the size and shape of the plastic zone. Hardness is generally measured in the 0, 45, and 90 deg directions with respect to the crack propagation direction. Following the Rice model [*4*] it is possible to distinguish between the monotonic and cyclic plastic zones as shown in Figs. 1 to 3.

The monotonic zone is characterized by a nearly constant microhardness while it increases parabolically in the cyclic zone. Consequently, the cyclic plastic zone is defined to be the distance between the crack tip and the first change of slope (r_c^y). The monotonic plastic-zone radius corresponds to the transition between the plateau and the basic material hardness value (r_m^y). Figure 1 also shows the scatter in results obtained by several laboratories[4] using a Reichert or Leitz microscope with a 25-g load.

[4]Centre d'Etudes du Bâtiment et des Travaux Publics, Commissariat à l'Energie Atomique, Creusot Loire, Ecole Nationale Supérieure des Mines de Paris, Ecole Nationale Supérieure de Mécanique et d'Aérotechnique, Institut de Recherches de la Sidérurgie Française, Société Nationale Industrielle Aerospatiale, Service Technique des Constructions et Armes Navales, and Université de Technologie de Compiégne.

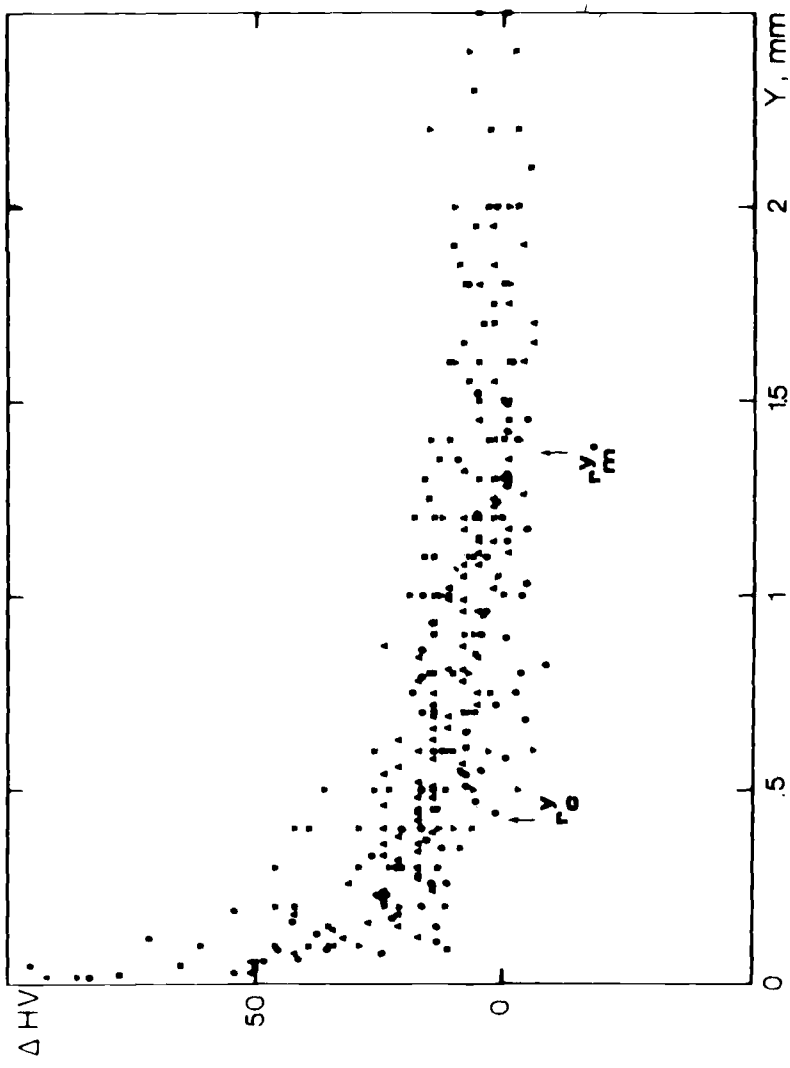

FIG. 1—*Summary of microhardness values* (ΔHv) *versus distance* (Y) *to the crack tip for 316 stainless steel; results from six laboratories;* $\Delta K = 40\ MPa\sqrt{m}$; $R = 0.1$.

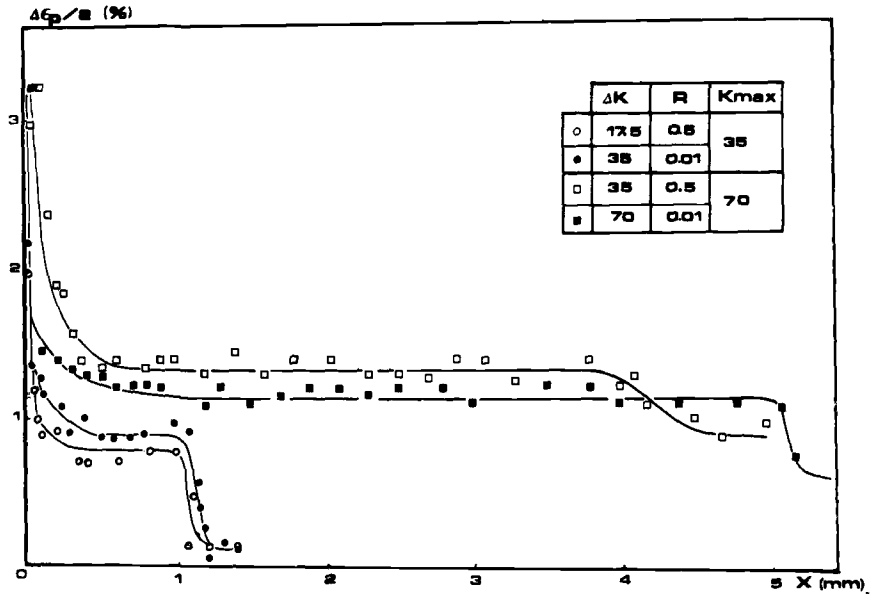

FIG. 2—*Plastic strain as a function of distance from crack tip in 316 stainless steel.*

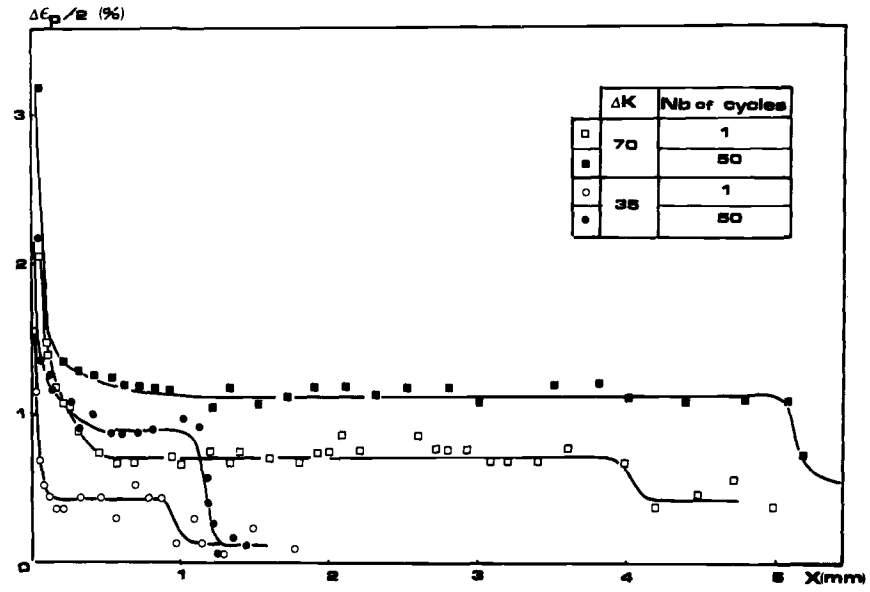

FIG. 3—*Strain gradient in the crack propagation direction. Influence of cycle number on the plastic zone formation in 316 stainless steel.*

Etching Techniques

Many etching procedures have been used for revealing the plastic zone. Etching techniques generally serve as a means to study the cyclic plastic zone. One notable work is that of Hahn et al on a Fe-3Si steel [5]. By etching, they determined not only the shape and dimensions of the plastic zone which enclosed the fatigue crack, but also an estimate of the plastic strain therein. The measured dimensions of the plastic zone are approximately the same as those calculated by Rice [4]. The principal disadvantage of this method is that it is not suitable for other alloys.

A general method that can be used for many alloys (iron and steels, stainless steels [6], copper and superalloys [7]) employs polishing and electrolytic etching. By measuring the dislocation cell size or the distance between twins, it is possible to determine the magnitude of strains by comparison with materials from low-cycle fatigue specimens. Hahn et al [5] found an equivalent plastic strain between 1 and 6% in silicon steels. Clavel et al [7] corroborated these values with measurements of mechanical twin densities in INCO 718. Metallographic etching techniques are useful for studying the cyclic plastic zone; however, they are incapable of revealing the monotonic zone in which the dislocation and defect densities are lower than in the cyclic zone.

Other Experimental Techniques

Among other experimental techniques that have been used to reveal the plastic zone in 316 stainless steel, channeling contrast in scanning electron microscopy seems to be an interesting prospect for the future. After careful electrolytic polishing, channeling contrast is influenced by the matrix disorientations. In material taken from low-cycle fatigue specimens of 316 stainless steel, only one glide system was revealed for $\Delta\epsilon_p = 0.3\%$, two systems for $\Delta\epsilon_p = 0.5\%$, and three systems for $\Delta\epsilon_p = 2.5\%$ [8]. The channeling-contrast method is not better than etching techniques for a morphological study of the plastic zone, but it gives an accurate determination of plastic strains in the cyclic plastic zone.

Japanese authors have used X-ray diffraction with a 200-μm-diameter monochromatic beam to measure strains in the plastic zone [9]. This method is less accurate than microhardness and has not been successful in measuring cyclic plastic strains less than 0.8% in 316 stainless steel.

To be complete it is necessary to mention that other techniques used to study the surface plastic zone include holography, moiré, and stereography (notably the work of Davidson [10]).

Determination of the Plastic Zone by the Microhardness Technique

After comparing many experimental techniques, it was concluded that microhardness is the most effective method of studying the plastic zone in aus-

tenitic stainless steels. The chemical composition and mechanical properties of the 316 stainless steel studied in this investigation are given in Tables 1 and 2 respectively. Compact tension specimens ($W = 75$ mm, $H/W = 0.6$, and $10 < B < 20$ mm) were subjected to fatigue loading. From microhardness measurements the radius r_c and r_m of the cyclic and monotonic plastic zones were determined in three directions (0, 45, and 90 deg) in the specimen midplane. This information was used to deduce the approximate shape of the plastic zones. The monotonic plastic zones were found to be approximately circular. Their shape evolves with cyclic loading and is dependent on K_{max}. For low values of K_{max} two wings were observed which merged into one circular zone for high values of K_{max}. These observations were made for ΔK between 17 and 70 MPa$\sqrt{m}$. The cyclic plastic zone was observed to assume the shape of two wings for all values of ΔK (Fig. 4).

The values of the cyclic and monotonic plastic zone radii along the x and y axes are reported in Table 3 and compared with values calculated according to the formula of Irwin [*11*]:

$$r = \frac{1}{6\pi}\left(\frac{K}{\sigma_y}\right)^2$$

Experimental results show that the monotonic zone radius is a function of K_{max} (Fig. 5) for an R-ratio between 0 and 0.5:

$$r_m^y = 0.052\left(\frac{K_{max}}{\sigma_y}\right)^2$$

$$r_m^x = 0.072\left(\frac{K_{max}}{\sigma_y}\right)^2$$

TABLE 1—*Chemical composition of 316 stainless steel by weight percent.*

C	Cr	Ni	Mo	Mn	Si	S	P	N
0.029	17.54	12.60	2.38	1.80	0.50	0.012	0.032	0.077

TABLE 2—*Mechanical characteristics of 316 stainless steel after quenching from 1070°C.*[a]

σ_y	UTS	A	Z	K_{cu}
280 MPa	590 MPa	52%	80%	250 J/cm^2

[a] A = elongation; Z = necking coefficient; and K_{cu} = impact energy.

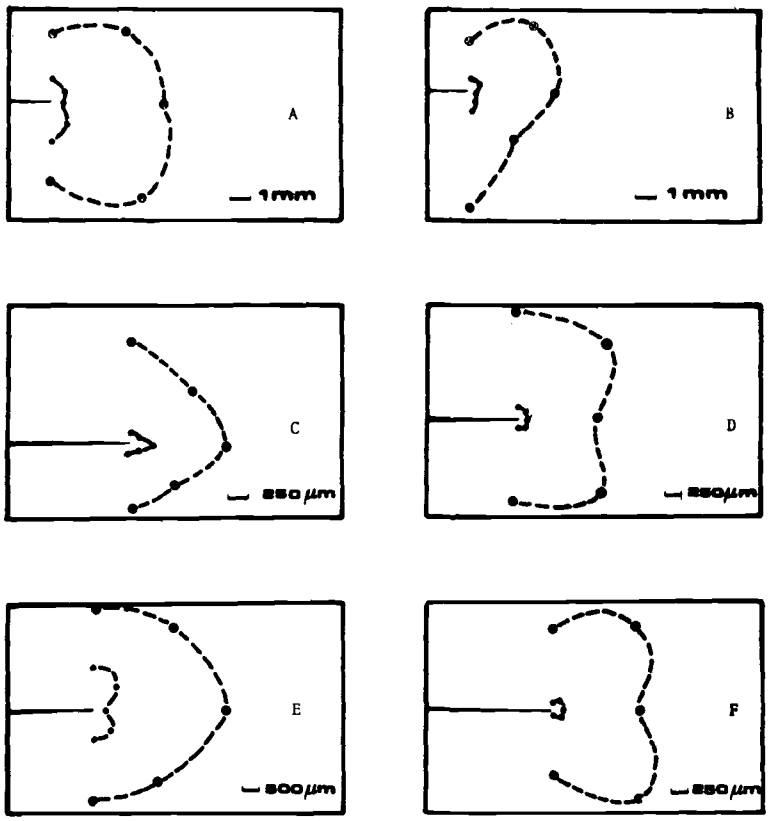

A : ΔK = 70 MPa$\sqrt{m}$, R = 0.01, N = 50 cycles
B : ΔK = 70 MPa$\sqrt{m}$, R = 0.01, N = 1 cycle
C : ΔK = 35 MPa$\sqrt{m}$, R = 0.01, N = 50 cycles
D : ΔK = 35 MPa$\sqrt{m}$, R = 0.01, N = 1 cycle
E : ΔK = 35 MPa$\sqrt{m}$, R = 0.5 , N = 50 cycles
F : ΔK = 17,5 MPa$\sqrt{m}$, R = 0.5, N = 50 cycles

FIG. 4—*Plastic-zone shapes, in 316 stainless steel, obtained by microhardness.*

The R-ratio has no significant influence on the cyclic zone radius. For 316 stainless steel it was found that

$$r_c^y = 0.104 \left(\frac{\Delta K}{2\sigma_y} \right)^2$$

$$r_c^x = 0.043 \left(\frac{\Delta K}{2\sigma_y} \right)^2$$

TABLE 3—*Comparison of experimentally determined plastic zone size data to Irwin relation.*[a]

ΔK, MPa$\sqrt{m}$	R	N, cycles	Cyclic Zone, μm			Monotonic Zone, μm		
			r_c^y	r_c^x	r_{calc}	r_m^y	r_m^x	r_{calc}
70	0.01	1	800	400	829	3850	4000	3380
		50	1400	800	829	3350	5150	3380
35	0.01	1	125	100	207	1100	950	850
		50	125	275	207	975	1120	850
35	0.5	50	1000	350	207	3130	4400	3310
17.5	0.5	50	75	100	50	870	1025	829

[a]The equations are

$$r_c = \frac{1}{6\pi}\left(\frac{\Delta K}{2\sigma_y}\right)^2$$

and

$$r_m = \frac{1}{6\pi}\left(\frac{K_{max}}{\sigma_y}\right)^2$$

Note that the coefficient in this experimentally determined relationship for r_c^y is greater than that of the Irwin relationship for plane strain (0.053) and less than that of the Rice relationship [*4*] (0.15).

These experimental results show that the ratio between the radii of the monotonic and cyclic zones is nearer 3 than the value of 4 obtained theoretically by Rice by neglecting the effect of cyclic hardening [*4*].

Estimation of Deformation Inside the Plastic Zone

Microhardness is a successful method for evaluating strain hardening or softening in metals. In order to quantitatively evaluate the magnitude of plastic deformation inside the plastic zone, microhardness was correlated with equivalent plastic deformation in low-cycle fatigue specimens.

Specimens of 316 stainless steel were cycled until stabilization of hysteresis loops for values of equivalent longitudinal plastic deformation ($\Delta\epsilon_p/2$) between 0.4 and 1.8%. After stabilization, each specimen was dismounted, sectioned longitudinally, then mechanically and electrolytically polished. Microhardness measurements were performed at the minimum specimen cross section. Thus, for each specimen, the value of Vickers microhardness (Hv), was associated with a corresponding equivalent plastic deformation ($\Delta\epsilon_p/2$) (Fig. 6).

By using this technique, the equivalent plastic strain in the monotonic zone was determined to be about 1% in copper, brass, and ferritic and austenitic steels. In the cyclic plastic zone it is a maximum of 10% near the crack tip. These results corroborate those of Clavel et al [*7*] and Lankford et al [*3*].

It is appropriate to investigate the precision of the microhardness tech-

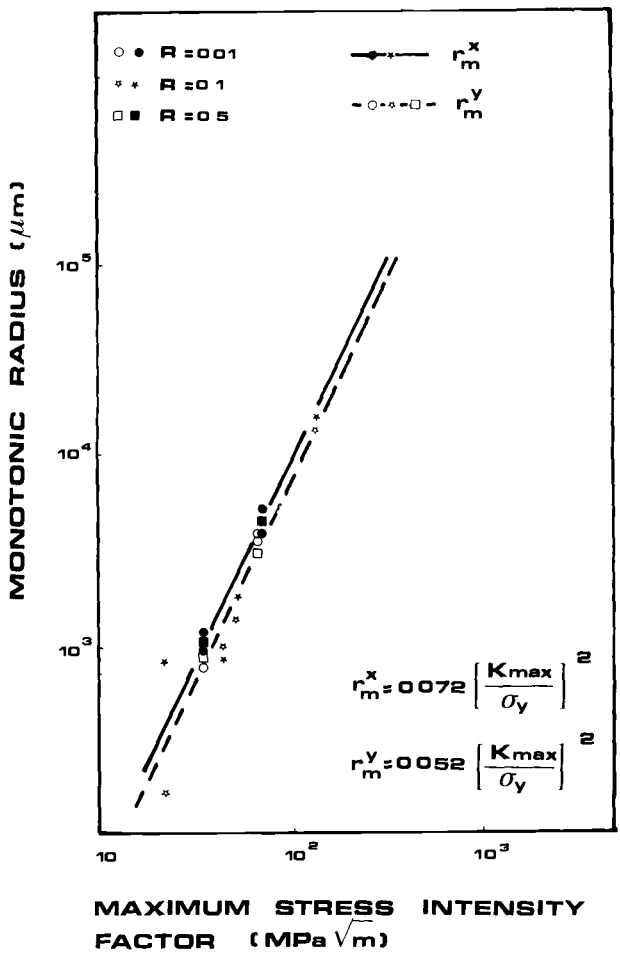

FIG. 5—*Monotonic plastic-zone dimensions measured by microhardness versus* K_{max} *in 316 stainless steel.*

nique. In the case of 316 stainless steel, microhardness is a sensitive method for measuring equivalent plastic strain. After stabilization of mechanical hysteresis loops, an imposed cyclic plastic strain of 1.8% resulted in a microhardness increase of 50%, and the minimally detectable cyclic plastic strain resulted in an increase of 0.1 to 0.2%. Even considering the experimental uncertainties, there exists a linear relationship between Vickers microhardness and imposed strain on low-cycle fatigue specimens. Comparing the results obtained in different laboratories of our Working Group, we found that a simple vertical shifting of the origin brings all the data into coincidence. This means that dispersion between laboratories is essentially due to calibration of

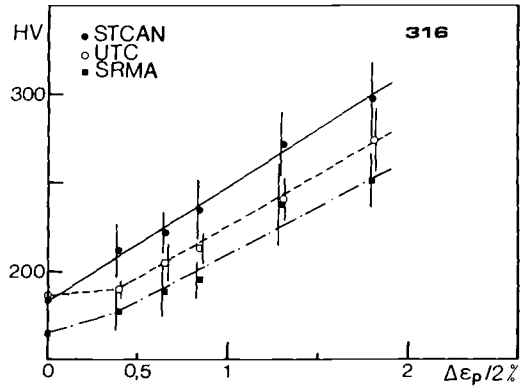

FIG. 6—*Microhardness* (Hv) *versus imposed plastic strain* ($\Delta\epsilon_p/2$). *Scatter in results obtained by three laboratories.*

microhardness (Fig. 6). Considering that Hv_0 depends on the laboratory, we obtain

$$Hv - Hv_0 = f\left(\frac{\Delta\epsilon_p}{2}\right)$$

Consequently, results from different laboratories can be easily compared.

Calculation of Deformation Inside the Plastic Zone

After correlating microhardness values with equivalent plastic strain, isostrain contours can be plotted around the crack tip. Figure 7 shows the strain profile inside the plastic zone for $K_{max} = 70$ MPa$\sqrt{m}$ and $R = 0.01$. The presence of a plateau is evident where the strain decreases slowly in the monotonic zone. The corresponding equivalent plastic strain is about 1%. This value depends on the value of K_{max} and is nearly independent of ΔK between 17 and 70 MPa$\sqrt{m}$ for 316 stainless steel (Fig. 2). This observation confirms that the cyclic hardening of the monotonic zone is weakly cyclic and is due principally to the opening of the crack; hence it is a function of K_{max}.

Accommodation of the elastic singularity near the crack tip is manifested by an increase in the basic material hardness value from 162 to 170. The strain gradient decreases sharply in the vicinity of the crack tip. Comparing microhardness values measured at a distance of 10 and 100 μm from the crack tip, which corresponds to the grain diameter, we observed that the strain decreased from 3.58 to 1.76% for $\Delta K = 70$ MPa$\sqrt{m}$ and from 2.14 to 1.18% for $\Delta K = 35$ MPa$\sqrt{m}$. Consequently, the strain gradient inside the grain containing the crack is extremely high.

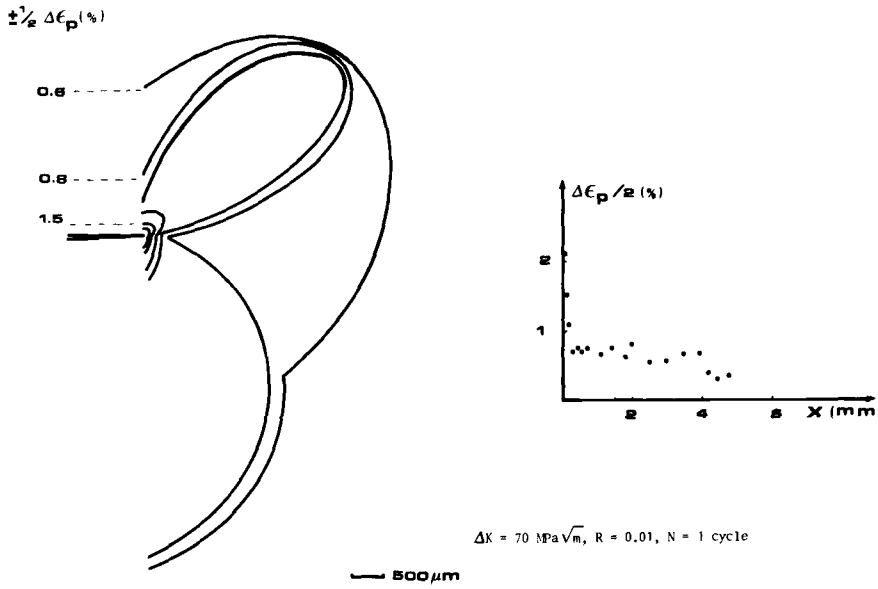

FIG. 7—*Strain profile at the crack tip after one loading cycle in 316 stainless steel;* $\Delta K = 70$ *MPa*$\sqrt{m}$*;* $R = 0.01$.

To better understand the relationship between strain accumulation at the crack tip and cycle number, plastic zones were studied after 1 loading cycle and after 50 cycles with the same loading. In both cases, the imposed cyclic loading amplitude was reduced until the crack reached the fatigue threshold. Experimental results showed that the first cycle likely is more damaging than the following cycles (Fig. 3 and Table 3). For example, for $\Delta K = 70$ MPa$\sqrt{m}$ the maximum strain detected at the crack tip was 2% after 1 cycle and 3% after 50 cycles. Correspondingly, the strain plateau of the monotonic zone was observed to increase from 0.8 to 1.2%. Such studies of strain accumulation at the crack tip improve the possibility of using a Coffin-Manson-type damage law [*12,13*] to express crack growth rate.

Consider a linear cumulation:

$$D = \sum_i \frac{n_i}{N_i}$$

$$n_i = \frac{\Delta x}{da/dN}$$

and

$$A(N_i)^\beta = \frac{\Delta \epsilon_p}{2}$$

where

N_i = cycles to initiation in low-cycle fatigue,
$\Delta\epsilon_p$ = plastic strain range, and
β, A = constants.

By using the Coffin relationship, the damage D experienced by the plastic zone can be expressed in terms of plastic strain range as

$$D = A^{1/\beta} \int_0^{r_c} \frac{(1/2\,\Delta\epsilon_p)^{-1/\beta}}{da/dN}\, dx$$

When $D = 1$, the crack growth rate becomes

$$da/dN = A^{1/\beta} \int_0^{r_c} (\Delta\epsilon_p/2)^{-1/\beta}\, dx$$

With experimental measurements of the plastic zone size and the equivalent plastic strains therein, the crack growth rate can be determined with good accuracy (Table 4).

These results confirm the previously proposed models [*14,15*], which provide the validity of expressing the crack growth rate as a function of a localized low-cycle fatigue. On the other hand, our studies permit us to furnish a significant interpretation to the equivalent strain determined by the measurement of microhardness. This equivalent plastic strain is to be compared with that defined by the Manson-Coffin relation.

Comparison Between Experimental Results and Calculation

Different numerical simulations of a Mode I CT75 specimen have been performed in plane strain with the TITUS finite-element computer code of Framatome. By simulation, the specimens were loaded to a maximum value and then unloaded to zero load. The cyclic and monotonic stress-strain curves

TABLE 4—*Example of damage cumulation.*

ΔK, MPa$\sqrt{m}$	R	da/dN(Microscopic), mm/c[a]	da/dN (Macroscopic, mm/c	da/dN (Calculated), mm/c
70	0.01	1.88×10^{-3}	5.4×10^{-3}	1.76×10^{-3}
35		...	1.95×10^{-4}	3.5×10^{-4}
40	0.1	2.2×10^{-4}	3.7×10^{-4}	1.76×10^{-4}
20		...	1.35×10^{-4}	2.9×10^{-5}
35	0.5	8×10^{-4}	...	2×10^{-3}
17.5		...	...	1.8×10^{-4}

[a]Striation spacing.

are shown in Fig. 8 with the kinematic model. The yield stress (σ_y) is 270 MPa for the two hardening curves. Even for $K = 70$ MPa$\sqrt{m}$, the plastic zone remains confined and the loading curve is almost linear; therefore the linear stress intensity factor (K_I) can be used to define the load level. Figure 9 is a plot of the plastic-zone size for the two different stress strain curves as a function of $(\Delta K/\sigma_y)^2$ during loading. The monotonic plastic zone size developed during loading up to 70 MPa$\sqrt{m}$ was found to be proportional to $(K/\sigma_y)^2$ and independent of a detailed description of the hardening curve. The reverse plastic zone created during unloading (cyclic zone) was found to be well correlated with $(\Delta K/\sigma_y)^2$ and roughly independent of the maximum value of K. The reverse plastic zone is also independent of a detailed description of the hardening curve. The size of the cyclic plastic zone was calculated to be 0.3 times the size of the monotonic plastic zone and not 0.25 as generally reported. The results are plotted in Fig. 9.

Monotonic zone:

$$R_m{}^i = \alpha_m{}^i \left(\frac{K}{\sigma_y}\right)^2$$

where

$$\alpha_m{}^x = 0.025$$

$$\alpha_m{}^y = 0.119$$

$$\alpha_m\,(\max) = 0.127$$

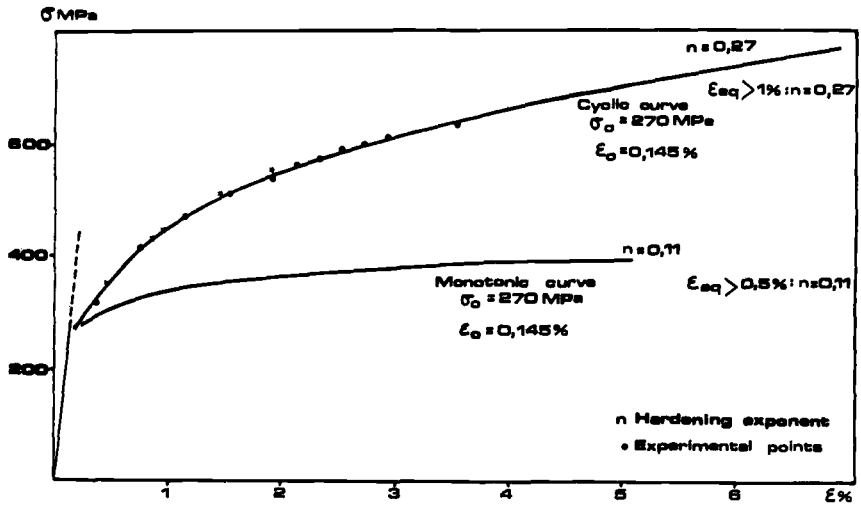

FIG. 8—*Monotonic and cyclic stress-strain curves of 316 stainless steel.*

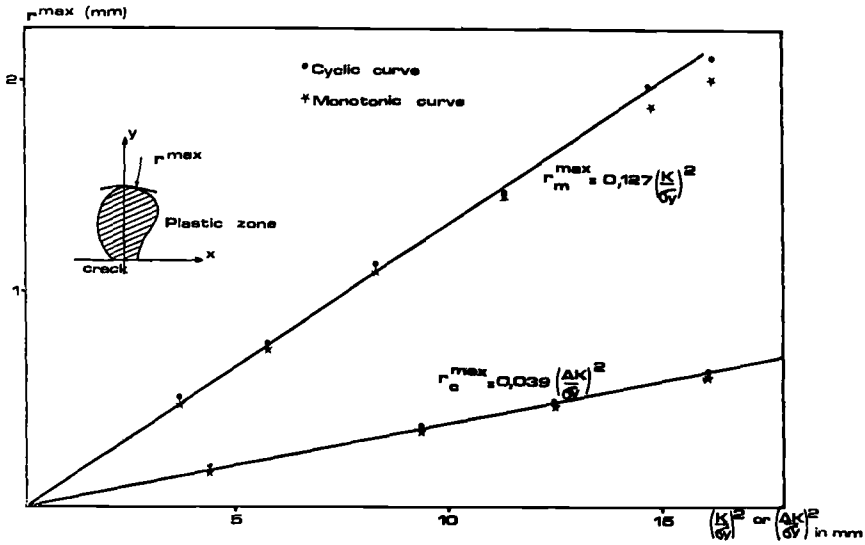

FIG. 9—*Finite-element calculation of maximum plastic-zone sizes for two hardening curves in 316 stainless steel.*

Cyclic zone:

$$R_c^i = \alpha_c^i \left(\frac{\Delta K}{\sigma_y} \right)^2$$

where

$$\alpha_c^x = 0.007$$

$$\alpha_c^y = 0.036$$

$$\alpha_c \text{ (max)} = 0.039$$

The results obtained for the monotonic zone are consistent with the results of Rice and co-workers [*16*]. They considered a circular mesh with a crack. The crack was loaded with the elastic asymptotic solution. In our calculation, we have considered the whole specimen and taken into account the far field. On the macroscopic level, the difference between the two hardening curves (monotonic and cyclic) is almost negligible up to 35 MPa$\sqrt{\text{m}}$. The loading curves differ by less than 0.5%. The far fields are alike. The plastic zones are equivalent. The J-integrals differ by less than 0.7%. The J-integral was calculated for different contours around the crack tip. Except for the first contour, 1 mm from the crack tip, the J-integral was found to be independent of the dif-

ferent contours. All of these calculations are governed by σ_y, the yield stress for small scale yielding up to 35 MPa$\sqrt{m}$. However, the stress and strain evolutions inside the plastic zone, very near the crack tip, are different. The angular distribution of the calculated equivalent plastic strain at the crack tip is presented with polar coordinates in Fig. 10. The equivalent strain is a maximum at $\theta = 110$ deg. This observation is well known. The true strain at the crack tip will probably be an average value of equivalent strains [*17*].

For the monotonic plastic zone size (r_m^y) the coefficient in the y-direction was found to be 0.119 by finite-element calculation, 0.150 by Rice, and 0.052 experimentally. The discrepancies between calculated and experimental values cannot be attributed to error or imprecision, but may be related to two complications. Firstly, calculations were performed considering a purely plane strain condition, whereas in reality a plane stress factor exists. Secondly, there exists a closure effect at the crack tip which appears to reduce the effective stress intensity factor range and consequently the size of the plastic zone in the y-axis direction. This closure effect has not been considered in calculations. Assuming that the effective stress intensity factor range is 60% of its nominal value, the coefficient α_m^y determined experimentally becomes 0.12%, the calculated numerical value. Thus, it is clear that one cannot compare calculations with experimental results without considering the effective stress intensity factor and closure effect which reduce the singularity.

The finite-element calculations for the 316 stainless steel showed that in

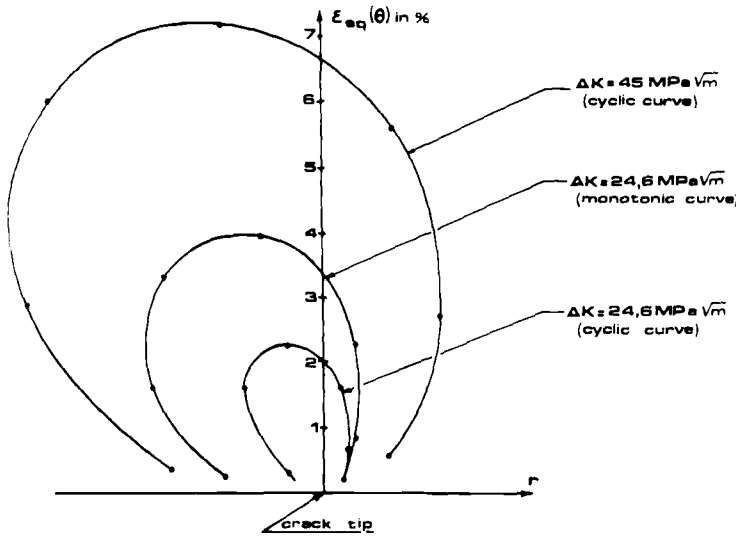

FIG. 10—*Polar distribution of the equivalent strain calculated by the finite-element method.*

plane stress, the plastic-zone size in the x-direction is much more greater than in plane strain:

$$\alpha_m{}^x = 0.224$$

$$\alpha_m{}^y = 0.120$$

Thus it seems that there exists an effect of plane stress even in the through thickness of a 20-mm-thick specimen. This may explain the noncoincedancy between measured and calculated dimensions of the plastic zone in the x-direction.

Conclusions

Comparing the results obtained by finite-element calculations and those by different experimental methods, we can notice that the microhardness technique offers a particular interesting method of studying the plastic zone at the tip of a fatigue crack in 316 stainless steel. The microhardness technique is of very good help in studying the plastic zone in plane strain states. It allows us to measure the plastic-zone dimensions, its form and contour, and the distribution of plastic strain within it.

Acknowledgments

We thank Glenn Romanoski (University of Cincinnati) and Luc Remy (Ecoles des Mines de Paris) for their helpful discussions.

References

[1] Davidson, D. L. and Lankford, J., *Journal of Engineering Materials and Technology, Transactions of ASME*, Jan. 1976, pp. 24-29.

[2] Davidson, D. L. and Lankford, J., "Crack Tip Plasticity Associated with Corrosion-Assisted Fatigue," SWR Report 14-75-C-1038, Southwest Research Institute, San Antonio, Tex., 31 May 1979.

[3] Lankford, J., Davidson, D. L., and Cook, T. S., in *Cyclic Stress-Strain and Plastic Deformation Aspects of Fatigue Crack Growth, ASTM STP 637*, American Society for Testing and Materials, 1977, pp. 36-55.

[4] Rice, J. R. in *Fatigue Crack Propagation, ASTM STP 415*, American Society for Testing and Materials, 1967, pp. 247-311.

[5] Hahn, G. T., Hoagland, R. G., and Rosenfield, A. R., *Metallurgical Transactions*, Vol. 3, No. 5, May 1972, pp. 1189-1202.

[6] Bathias, C. and Pelloux, R. M., *Metallurgical Transactions*, Vol. 4, No. 5, May 1973, pp. 1265-1274.

[7] Clavel, M., Fournier, D., and Pineau, A., *Metallurgical Transactions*, Vol. 6A, Dec. 1975, pp. 2305-2307.

[8] Benoit, D., Meny, L., and Reponty, M., "The Study of Deformation Mechanisms in an Austenitic Stainless Steel with Crystalline Contrast: Preliminary Results," presented at 16th Annual Conference of the Microbeam Analysis Society of America, Vail, Colo., 13-17 July 1981.

[9] Taira, S. and Honda, K., *Transactions of the Japan Society of Mechanical Engineers*, Vol. 4, No. 14, 1961, pp. 230-237.
[10] Davidson, D. L., "The Observation and Measurement of Displacements and Strain by Stereoimaging, "*Scanning Electron Microscopy*, Vol. 2, 1979, pp. 79-86.
[11] Irwin, G. R., "Plastic Zone Near a Crack and Fracture Toughness," in *Proceedings of the Sagamore Conference*, 1960, pp. 10-63.
[12] Coffin, L. F., *Transactions of ASME*, Vol. 76, 1954, pp. 931-950.
[13] Manson, S. S., NASA Report TN 2933, 1953.
[14] Chakrabortty, S. B., *Fatigue of Engineering Materials and Structures*, Vol. 2, 1979, p. 331.
[15] Majumdar, S. and Morrow, J. in *Fracture Toughness and Slow-Stable Cracking, ASTM STP 559*, American Society for Testing and Materials, 1974, pp. 159-182.
[16] Levy, N., Margal, P. V., Ostergree, W. J., and Rice, J. R., *International Journal of Fracture Mechanics*, Vol. 7, 1971, p. 143.
[17] McClintock, F. A., "On the Plasticity of the Growth of Fatigue Cracks," *Fracture of Solids*, Wiley, New York, 1963.

DISCUSSION

L. F. Coffin[1] (*written discussion*)—How is the microhardness technique used to determine the *active* plastic zone in relation to the prior hardness history?

C. Loye et al (*authors' closure*)—To reduce the effect of prior hardness history on the plastic zone at the fatigue crack tip, tests were started by advancing the crack near the threshold stress intensity factor range. Under these preliminary conditions the crack rate was about 10^{-7} mm/cycle and the plastic-zone radius was less than 0.1 mm. Subsequently, one or several fatigue cycles were applied with a stress intensity factor between 17 and 70 MPa$\sqrt{\text{m}}$.

The precracking was obtained under the following conditions: initiation = 13 MPa$\sqrt{\text{m}}$; arrest of the crack = 8 MPa$\sqrt{\text{m}}$; R-ratio = 0.01; a/W = 0.55; and frequency = 50 Hz.

W. J. Baxter[2] (*written discussion*)—The active rate-controlling plastic zone at the tip of a fatigue crack can be imaged by exoelectron emission. The emission caused by all prior deformation can be suppressed by permitting reoxidation of the microcracks in the oxide film. Then, upon resumption of fatigue cycling, new microcracks are created in the oxide, and the associated exoelectron emission images only the active region of plasticity at the crack tip.[3] For large plastic zones ($\sim$5 mm), such as described by Schuster and Alstetter,[4] it would be straightforward to make quantitative measurements of the distribution of

[1]General Electric Company, Schenectady, N.Y. 12301.
[2]General Motors Research Laboratories, Warren, Mich. 48090.
[3]*Metallurgical Transactions*, 1976.
[4]This publication, pp. 445-463.

damage within the zone by scanning the surface with a focused laser beam and increasing the exoelectron current.[5]

E. E. Underwood[6] *(written discussion)*—Microhardness measurements are of considerable value in defining the conditions ahead of a crack. When crack propagation is studied at elevated temperatures, however, the results may differ considerably from those obtained at room temperature. In one study,[7] a microhardness survey was conducted around a high-temperature crack both laterally and ahead of the crack tip. A gradient in the microhardness readings was obtained, with hardness decreasing from the unaltered matrix surrounding the crack at a distance, to low values as the crack surface was approached. This softening was attributed to an increase in the vacancy concentration in the vicinity of the crack. Thus it is important when studying crack propagation to define the conditions under which the crack is propagating.

[5]*Journal of Testing and Evaluation*, 1975.
[6]Georgia Institute of Technology, Chemical Engineering/Metallurgy, Atlanta, Ga. 30332.
[7]Mirkin, I. L. and Trunin, I. I., *Metallovedenie i Obrabotka Metallov*, Vol. 6, 1957, pp. 2-7.

Gary Schuster[1] *and Carl Altstetter*[2]

Comparison of Fatigue Damage in Stable and Unstable Stainless Steels

REFERENCE: Schuster, G. and Altstetter, C., **"Comparison of Fatigue Damage in Stable and Unstable Stainless Steels,"** *Fatigue Mechanisms: Advances in Quantitative Measurement of Physical Damage, ASTM STP 811*, J. Lankford, D. L. Davidson, W. L. Morris, and R. P. Wei, Eds., American Society for Testing and Materials, 1983, pp. 445-463.

ABSTRACT: As a result of the stress-induced martensitic transformation of certain austenitic stainless steels their fatigue behavior is modified. A number of experimental techniques have been applied in order to understand why this occurs. The methods used include metallography of various types, electron diffraction, magnetic permeability, and local mechanical property determination. The advantages and disadvantages of the various techniques are discussed, and by a combination of techniques various hypotheses to explain the fatigue phenomena are examined and reinforced or rejected. It is concluded that the volume expansion resulting from the phase transformation causes a favorable residual stress state at the crack tip.

KEY WORDS: stainless steel, fatigue crack propagation, residual stress, fatigue life, fractography, metallography, martensitic transformation

In the course of a continuing study of fatigue behavior and environmentally induced cracking of austenitic stainless steels [*1-7*] a number of techniques have been employed in an effort to assemble comprehensive knowledge of the changes which took place in the material as a result of cyclic or static loading.[3] Some of the less highly alloyed of the stainless steels undergo stress-induced phase transformation of the face-centered-cubic (FCC) austenite to body-centered-cubic (BCC) α'-martensite or hexagonal-close-packed (HCP) ϵ-martensite or both. It is well established that these stainless steels can have a very high work-hardening rate which makes them

[1]Owens Corning Fiberglas Technical Center, Granville, Ohio 43023; formerly at Department of Metallurgy, University of Illinois at Urbana-Champaign, Ill. 61801.

[2]Professor of Physical Metallurgy, Department of Metallurgy, University of Illinois at Urbana-Champaign, Ill. 61801.

[3]The italic numbers in brackets refer to the list of references appended to this paper.

highly formable and capable of large increases in yield strength through cold working. One of the objects of the program was to determine whether this transformability of the austenite would also provide improved fatigue behavior in either the annealed or the cold-worked starting condition. If such benefits could be demonstrated, then austenite stability could be used as a design parameter for proper choice of a steel for a given application. Thus the first step was to explore the phenomenology of cyclically loaded stable and unstable alloys; that is, to determine the degrees of instability which could lead to improved fatigue behavior under various conditions of cyclic load or strain amplitude. In order to develop the concept of utilization of austenite instability as a beneficial factor in fatigue design, however, it was necessary to complement the phenomenological studies with mechanistic studies. These were directed to answering the question "Why are unstable austenites better or worse than stable austenites?"

The experimental techniques used in this program were chosen to measure property and phase changes in the vicinity of a propagating crack, without any attempt to define the conditions leading to the initiation of cracking. In addition to the more macroscopic quantities of load and crack length or strain amplitude and life, which were used to establish the phenomenological da/dN versus ΔK or strain versus life curves, the following techniques were employed:

1. Optical metallography.
2. Interferometry.
3. Transmission electron metallography.
4. Glancing incidence electron diffraction.
5. Scanning electron fractography.
6. Selected-area electron channeling.
7. Magnetic phase analysis.
8. Microhardness profiling.
9. Crack tip extensometry.
10. Residual stress analysis.

As will be seen, some of these techniques give essentially the same information as others, some give unique information, and some are just not worth the trouble. It is the intention of this paper to outline the utility of the techniques and to demonstrate how they can be used to interpret mechanical test results in mechanistic terms. A description of the techniques and comments on their general usefulness will follow the order given above.

Experimental Materials

Several different types of austenitic stainless steel have been used throughout this study and in some cases there was more than one composition within a single alloy designation. Among AISI alloys used are 201, 202,

301, 302, 304, 310, and 316, as well as the proprietary alloy, Nitronic 40. Alloy composition change is a basic way to change austenite stability, but it is not the only way. Others are test temperature, precipitation heat treatment to change local chemistry (sensitization), state of stress (for example, hydrostatic compression inhibits the $\gamma \rightarrow \alpha'$ transformation), and prior cold work. It is unfortunate that from the viewpoint of austenite stability the AISI composition ranges are so broad that the alloy designations only roughly indicate austenite stability. For example, Fig. 1 shows the ranges of chromium and nickel equivalent encompassed by AISI specifications for 301, 302, and 304 stainless steels superimposed on a Schaeffler diagram, which is a type of room-temperature section through a multicomponent phase diagram for weld metal [*8*]. Clearly, AISI 302 austenites considerably overlap 301 and 304, and some 301 alloys would be more stable than 304 austenites. M_S and M_D temperatures are also possible ways to indicate austenite stability,[4] but they are laborious to determine, somewhat uncertain to calculate from chemical analysis, and are of unproven validity for gaging mechanical behavior effects. A technique which has been found useful for purposes of

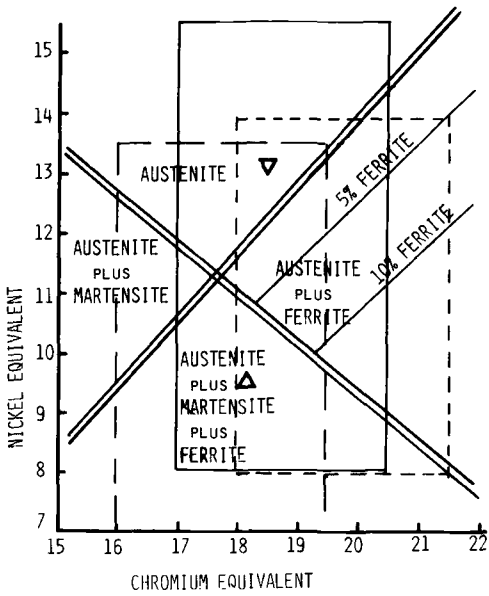

FIG. 1—*Schaeffler diagram with AISI composition limits of 301, 302, and 304 austenitic stainless steels.* ——— ——— *301,* ——— *302,* — — — — *304. Nickel equivalent = Ni + 30C + 0.5Mn. Chromium equivalent = Cr + Mo + 1.5Si + 0.5Nb (element symbols are concentrations in weight percent.)* Δ *= 301 alloy and* ∇ *= 302 alloy used for Figs. 2, 3, and 5 to 11.*

[4]The M_S temperature is the temperature at which martensite begins to form on cooling. The M_D temperature is the highest temperature at which martensite forms during plastic deformation.

characterizing austenite stability is the measurement of α' phase content simultaneously with stress-strain response in a tension test. The amount of α' is measured magnetically by placing on the tension specimen a probe sensitive to magnetic permeability changes. Typical results are shown in Fig. 2 for AISI 301 and 302 alloys. The triangle points in Fig. 1 represent these two alloys. A single number summarizing the transformability would be the % α' at fracture. Unfortunately, this does not say anything about the $\gamma \rightarrow \epsilon$ transformation. Diffraction techniques and Mossbauer spectroscopy are the best ways to detect the ϵ-phase, but it is difficult to get quantitative, bulk analyses by these methods.

Metallographic Techniques

For studies of changes attending the initiation and propagation of fatigue cracks optical metallography is probably the most powerful and easily used technique. The scale on which changes occur during fatigue is ideally matched to the technique. Of course, there are limitations to surface observations on flat surfaces and resolutions of a few tenths of a micrometre. Yet the alternative of transmission electron microscopy (TEM), though extremely useful for examining the details, is laborious and incapable of revealing

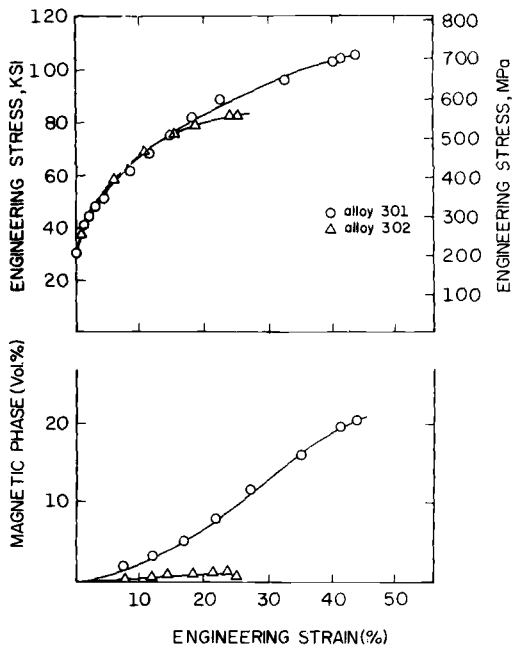

FIG. 2—*Engineering stress versus strain and percent magnetic phase versus strain for tension test of 1.5-mm-thick steel strips of AISI 301 and 302* [6].

general behavior. Scanning electron microscopy (SEM) has contrast problems on relatively smooth surfaces, but is superb and ideally suited for fractography. Furthermore, by use of more refined SEM techniques, described later, other kinds of information about fatigue processes can be collected.

For the particular problem at hand—detection of phase transformation in stainless steels—preparation of surfaces for optical microscopy is critical, because unstable austenite can be easily transformed by grinding and mechanical polishing [*1*]. For preparation of fatigue specimen surfaces we have used grinding through 600 grit SiC papers, followed by electropolishing for 5 min at 23 V in a chilled solution of 4:1 glacial acetic acid : perchloric acid. This was routinely followed by baking at 200°C for 30 min. For the most critical application, the recording of electron channeling patterns, the specimens were rough ground, then vacuum annealed at 1050°C and water quenched. The surface was then very lightly ground with 600 grit SiC to remove the oxide and then electropolished for 75 min [*5*]. For interferometry extreme flatness was necessary, requiring mechanical polishing down to 0.03-μm Al_2O_3 slurry. Fringe patterns at up to $\times 100$ were observable by viewing the specimen through a half-silvered cover glass in sodium vapor light. Magnifications up to $\times 450$ were made with a two-beam interference microscope and thallium vapor light. Interferometry, though having the potential for quantitative strain measurement normal to the surfaces, is not recommended for crack propagation studies, because there is too much deformation and the surface distortions are not sharp enough. Equivalent results at low magnifications could be obtained by oblique illumination and slight over focusing. The Nomarski contrast technique suffered from some of the same problems as the other interference techniques. An etchant of 10-mL nitric acid (HNO_3): 10-mL glacial acetic acid (HAc): 15-mL hydrochloric acid (HCl) plus a drop of glycerine was used for determining grain structures. The α'-martensite could be easily discerned by stain-etching for 1 to 3 h in a boiling solution of 36-g chromium trioxide (CrO_3) and 160-g sodium hydroxide (NaOH) in 175 mL of distilled water. A number of experiments were performed using a colloidal suspension of magnetite in water (Ferrofluid AO1) [*7,9*]. In this method the polished specimen was placed in a solenoid after spreading a thin layer of suspension under a cover glass. The α' could be clearly seen due to the collection of dark magnetite particles, even when the solenoid was not used. The resolution was not as good as with the stain-etching method, but it was used to check the reliability of staining. Quantitative phase analysis was done by placing a grid over projected images or photomicrographs and counting the number of grid intersections falling in each phase. This technique was difficult to carry out on α'/ϵ phase mixtures because of the difficulty of distinguishing the ϵ-phase from the α'-phase (see below).

The use of transmission electron microscopy was very straightforward and, in conjunction with diffraction and dark field imaging, was found to be in-

valuable for observing the morphology and formation sequence of the α' and ϵ phases. As concluded from both TEM and optical microscopy, the ϵ formed as thin, parallel-sided platelets on $\{111\}_\gamma$, frequently extending across grains [*1*]. From these platelets the α' spread into both the ϵ and parent γ phases. Thus the α' tended to be distributed as clusters of laths in parallel, linear arrays across the grains. Another, more massive or blocky form of α' occurred in certain grains, apparently depending on the relation of the grain orientation to the stress axis [*1*]. The α' was initially distributed quite heterogeneously, but with increasing degrees of deformation became more homogeneous, finally replacing both γ and ϵ phases in the more unstable alloys. Glancing incidence electron diffraction was performed on fracture surfaces using an SEM instrument [*3–5*]. In this application the specimen surface is nearly parallel to the electron beam and diffraction occurs from thin edges or protrusions from the fracture surface. Generally, spotty ring patterns were obtained due to the extreme amounts of local deformation. By moving the beam from point to point (beam size < 1 μm) the phase fractions were determined as the fraction of points having a given type of diffraction pattern. Oxide patterns and mixed patterns were occasionally seen, but were not counted in the determination of phase fractions. Obviously this technique is biased in favor of the protrusions versus the flat facets, but it gives unique information for a less than 1-μm-thick volume at the fracture surface. Thus, in effect, the phase associated with crack propagation can be determined. Caution must be used in this interpretation, because it is not always certain whether the α'-phase, for example, is the cause or the effect of a sharp crack. An entire specimen surface can be easily surveyed by this technique.

There is no need to elaborate on the use and the usefulness of SEM for fractography. It has allowed a quantum jump in our understanding of fracture processes, particularly on the more ductile rupture surfaces, which are impossible to see with light microscopy and for which replica TEM is often inadequate and at times even misleading. The use of stereo pairs is encouraged, and photogrammetric procedures to determine fracture facet crystallography have been described in hydrogen embrittlement and stress corrosion cracking studies [*4,10*]. In the present research program extensive use has been made of selected-area electron channeling patterns to survey the deformation in the vicinity of a propagating fatigue crack [*5*]. The channeling pattern consists of pairs of parallel dark and light lines [*11*], similar to a Kikuchi pattern in TEM. At low index crystallographic directions many pairs intersect at angles which can be indexed to determine the indices of the direction. The sharpness of the lines is determined by the perfection of the crystal within the micron or less depth by 12-μm-diameter volume on which the electron beam impinges. In order to make semiquantitative measurements of strain, patterns recorded at various points around a fatigue crack are compared with patterns taken on a calibration specimen of the same material strained by a known amount [*12*]. Figure 3 shows such patterns

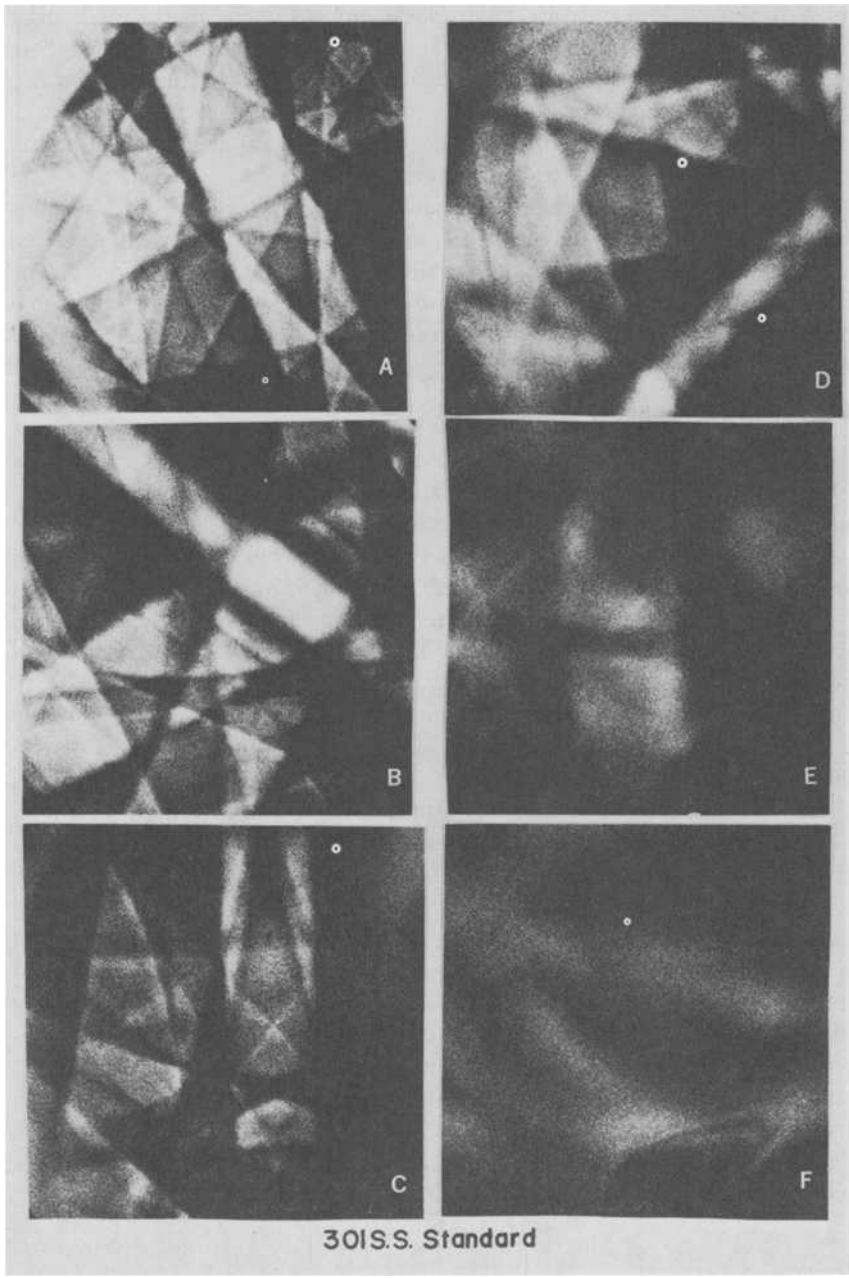

FIG. 3—*Selected area channeling patterns from various points on an AISI 301 tapered specimen tested in air. Plastic strains were* (a) *0%*, (b) *1%*, (c) *1¾%*, (d) *3¼%*, (e) *6½%, and* (f) *8½%* [5].

from a tapered tension specimen. Each pattern was taken from a region whose strain was known from the displacement of fiducial marks made prior to the plastic deformation [5]. As the amount of plastic strain increases there is a gradual deterioration in the sharpness of the pattern until, at about 8% strain, only indistinct streaks can be seen (Fig. 3*f*). The technique has the advantage of a spatial resolution smaller than the usual austenite grain size, but the inhomogeneity of strain from grain to grain makes it difficult to get representative values of strain. The method is somewhat subjective in interpretation and is also limited to initially annealed material, carefully prepared surfaces, small strains, and, in the present research, the austenite phase. The chief advantages of the technique are that in a small, precisely located volume it is semiquantitative, nondestructive, and sensitive to small strains.

Magnetic Measurements

Based on the fact that the α'-phase is ferromagnetic whereas γ and ϵ are paramagnetic, relatively simple, nondestructive, and *in situ* magnetic permeability or magnetic saturation measurements can be calibrated for phase analysis. An instrument (Model E-2 Ferritemeter, Twin City Testing Co., N. Tonawanda, N.Y.) sensitive to permeability changes was used in this work. It was calibrated by quantitative metallography and magnetic saturation measurements for α'-contents up to 100%, with an indication sensitivity of ± 0.1 volume percent at low α'-contents [2]. A probe consisting of two hemispherical contact points spaced 5.2 mm apart sampled a volume estimated to be 2×10 by 1 mm deep. A 1-μm-thick layer of iron on copper was detectable [3]. Although sensitive and easy to use, this instrument had to be used with caution on fatigue cracked specimens due to the extreme localization and inhomogeneity of the α'-phase. Another problem stems from its sensitivity to specimen configuration, edge effects, and "lift-off" effects in which rough surfaces or poor surface contact gave erratic readings. A standardized test procedure for partially cracked specimens was to position the probe with each hemispherical tip straddling the crack and then, maintaining this orientation, to move the probe various distances from the crack. In this way only crude averages are obtained from cracked specimens, but for the applications involving tension testing or for crack initiation studies the magnetic method is quite sensitive. As an aside, it might be pointed out that this is a very sensitive and practical method for the detection of the onset of fatigue damage in slightly unstable austenitic alloys. It should be developed into a quantitative NDE technique for unstable austenites.

Mechanical Tests

Microhardness measurements were made on a number of fatigue-cracked specimens using a 136-deg diamond indenter and a 50-g load [5,6]. Before

making measurements the specimens were mounted in bakelite to provide solid support, because this was found to decrease the scatter in the measurements. In making hardness profiles normal to the crack some scatter was inevitable due to the inhomogeneity of slip and transformation and due to grain boundary influences. The selected load was a compromise between spatial resolution (better at low loads) and scatter (smaller at large loads). Microhardness is an extremely useful technique capable of spatial resolutions of 100 μm or so, sufficient to define plastic zone sizes. By making profiles at various points along a fatigue crack, zone size versus ΔK may also be estimated. To a large extent, microhardness, for large strains, and channel pattern analysis, for small strains, are complementary techniques.

In a number of tests the crack-opening displacement (COD) was measured as a function of stress intensity during a loading cycle. In the manner of Elber [*13*] an effective stress intensity was defined as that which was in excess of the stress intensity at which the crack opens. This point is determined by noting a compliance change during the loading or unloading cycle. The COD was measured by bonding a resistance strain gage directly over the tip of the crack in a notched strip specimen. Prior to attachment a 3.2-mm (0.125-in.) strip of tape was used to cover the crack so that the gage was not bonded in the region of the crack and acted as an extensometer for that region. The output of the strain gage was plotted against the applied load on either an X-Y recorder (at 0.03 Hz) or on an oscilloscope (at 3 Hz), both of which gave essentially the same results. In addition to the strain gage a clip-on extensometer was attached to the notch at the edge of the specimen.

An indication of the residual axial stress at the tip of the crack was obtained from a foil strain gage bonded to the face of a strip specimen at the tip of the crack. The active area of the gage was 0.5 by 0.6 mm (0.02 by 0.025 in.). Strain readings were taken before and after the specimen was sliced axially at a distance of 2.54 mm (0.1 in.) in front of the crack tip using a slow-speed diamond saw. The resistance change readings were converted to stress by assuming that only longitudinal stress relaxation occurred. Although such measurements gave approximate stress values over a relatively large volume, they were quite useful in corraborating our conclusions based on other measurement techniques.

Interpretation of Fatigue Results

This section describes some examples of the application of the previously discussed techniques. Firstly the phenomena must be presented. Figure 4 shows strain-life relationships determined for several stainless steel compositions in constant total strain amplitude tension-compression tests on smooth, round specimens in air. The AISI 304 alloy had the least stable and the 21-6-9 alloy the most stable austenite of the group. In this type of test, austenite instability is definitely detrimental at high strain amplitudes, but at

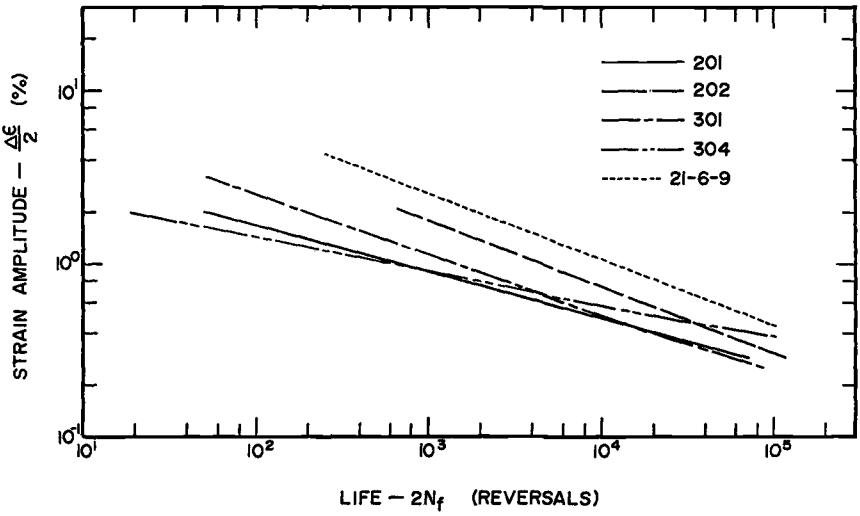

FIG. 4—*Total strain amplitude versus fatigue life relations for several austenitic stainless steel alloys* [2].

low strain amplitudes there is a tendency for the curves to cross over; that is, a longer fatigue life might be the result of austenite instability at small strain amplitudes. Figure 5 compares the fatigue crack growth rate versus stress intensity relations for two alloys of different austenite stabilities. The data are for controlled-load amplitude tests at $R = 0.05$ on single V-notched strip specimens tested in air. The more unstable alloy, AISI 301, is clearly superior to the more stable alloy, AISI 302. The two alloys behave the same, however, when tested at a higher mean stress (Fig. 6); that is, in Fig. 6 a given value of stress intensity is obtained with a high peak load and a short crack versus a low peak load and long crack for Fig. 5. Finally, in Fig. 7 the behavior of these two alloys is compared for tests in hydrogen gas at 1 atm.

There are several reasons why austenite instability might be responsible for this behavior:

1. Transformation-induced crack tip plasticity (TRIP).
2. Enhanced work-hardening rate.
3. More stable work-hardened state, that is, less tendency for plastic instability.
4. Lower fatigue crack growth in martensite or in a two or three phase mixture.
5. Residual compressive stress at the crack tip due to the volume increase when γ transforms to α.
6. Hydrogen could influence any of these factors and, in addition, could lead to a hydrogen-induced change in crack advance mechanism.

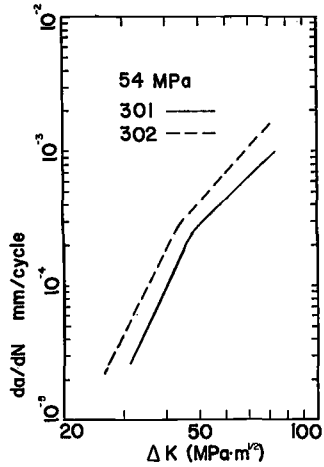

FIG. 5—*Fatigue crack growth rate versus stress intensity amplitude for AISI 301 and 302 strips tested in air. Mean stress = 54 MPa.*

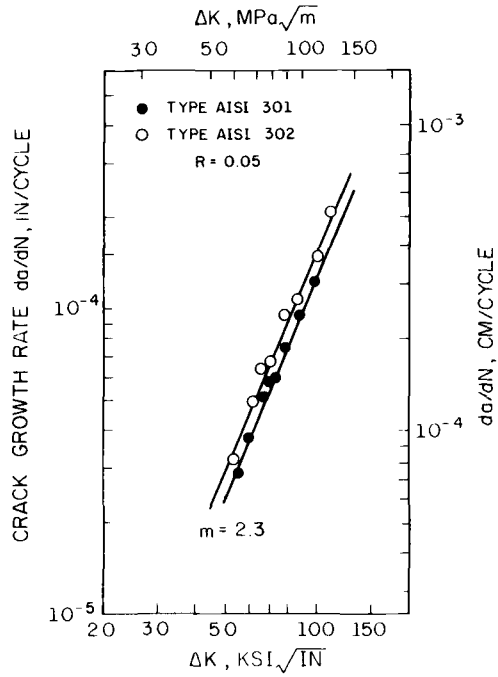

FIG. 6—*Fatigue crack growth rate versus stress intensity amplitude for AISI 301 and 302 strips tested in air. Mean stress = 90 MPa* [6].

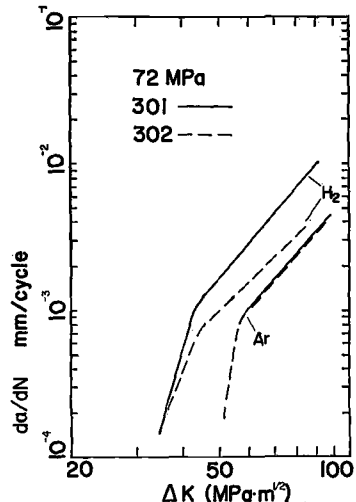

FIG. 7—*Fatigue crack growth rate versus stress intensity amplitude for AISI 301 and 302 strips tested in H_2 or argon at 1 atm pressure. Mean stress = 72 MPa.*

These points will be referred to by number in the discussion which follows.

It is the goal of this research to try to distinguish between these various possibilities and select the reason or reasons why transformation might lead to inferior fatigue behavior as well as to improved behavior. Ultimately, austenite instability might be used as a basis for selection of a given alloy for a given fatigue application. At the outset it is desirable to characterize the degree of austenite instability. Figure 2 shows the tensile results for the two alloys represented in Figs. 5 to 7. The γ-ϵ transformation is difficult to characterize, as discussed before, but could well be an important factor. Figure 2 clearly shows that the high rate of work hardening is due to phase transformation in these alloys. Figure 8 shows that phase transformation is localized at the fatigue crack tip, and Fig. 9 indicates that hardness differences can be considerable. They are correlated with the crack tip phase transformation, just as in a monotonic tension test. Magnetic permeability phase content data are in agreement with those obtained by optical metallography. Channeling pattern studies are illustrated in Fig. 10. The plastic zone sizes can be estimated from all of these techniques, and they are tabulated in Table 1. It must be noted that each technique assesses slightly different characteristics at different sensitivities, with different criteria for defining the zone size. In fact, it is clear from these observations that the plastic zone is not sharply defined, as it usually is when making elastic/plastic calculations.

All of these observations demonstrate that Points 1 and 2, above, are valid, in themselves, but one must question whether they can explain the fatigue behavior. Indeed, single-phase austenite alloys are quite plastic regardless of

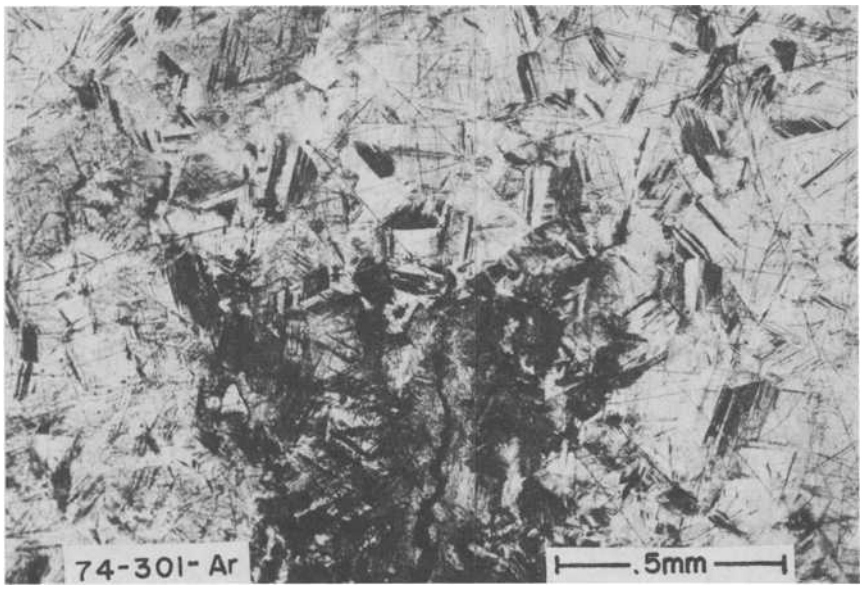

FIG. 8—*Optical micrograph of a fatigue crack in a strip of AISI 301 tested in argon at a mean stress of 54 MPa. Blackened regions are α'-martensite stain-etched in boiling sodium chromate.*

whether they transform or not. Thus the TRIP effect (Point 1) is probably of minor importance in these alloys. The enhancement of work-hardening rate (Point 2) is considerable, as Fig. 9 shows, but this effect is observed both at high and at low mean stresses. Thus neither of these reasons explains the enhancement or degradation of fatigue life at small and large strain amplitudes respectively (Fig. 4) nor the effect of mean stress (Figs. 5 and 6). The stability of the work-hardened state (Point 3) can be compared for AISI 301 and 302 in Fig. 11 for specimens cold-rolled by 26% and then fatigued at constant-load amplitude. The cyclic softening adjacent to the fatigue crack in the relatively stable 302 alloy is a manifestation of plastic instability. Corroborating evidence is found in the marked stress amplitude decrease in a constant strain amplitude fatigue test of cold-worked stable austenite [7]. Transformation of austenite tends to continue throughout the fatigue life of unstable austenite alloys. Thus martensite transformation leads to stable cyclic hardening just as it leads to stable work hardening in a monotonic test or forming operation. This has been observed to be a less important factor at high strain amplitudes than at low amplitudes [7]. Fatigue crack growth rate measurements on stable and unstable steels cold-rolled up to 40% reduction in thickness indicate that the crack propagation rate can be halved by cold work, but both steels have very nearly the same crack growth characteristics in the cold-worked state [5]. Thus we are forced to conclude that although

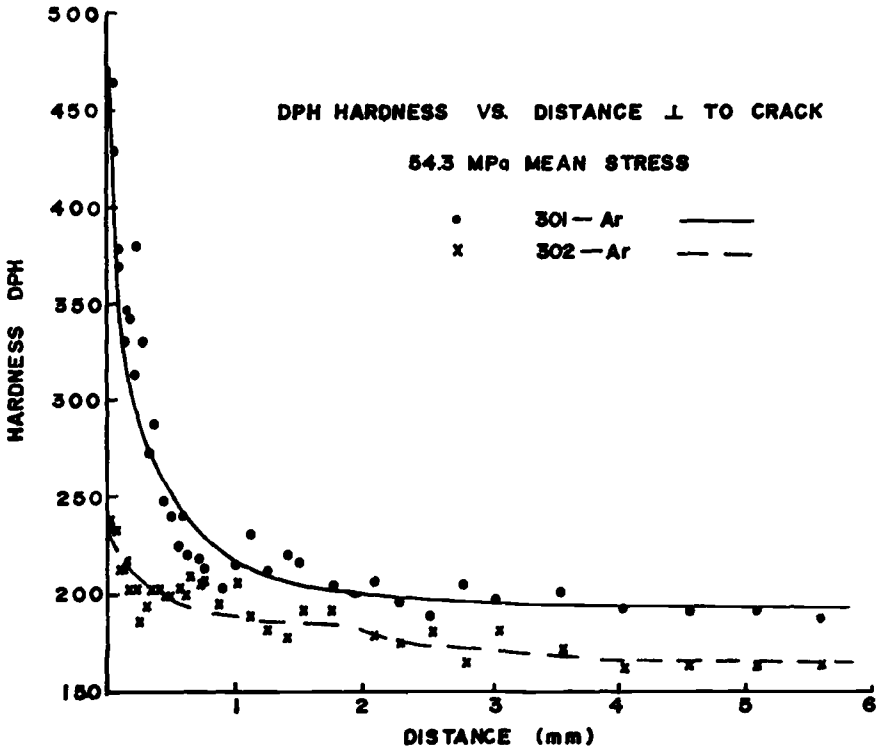

FIG. 9—*Microhardness versus distance normal to fatigue cracks in AISI 301 and 302 tested in argon at a mean stress of 54 MPa.*

the unstable alloy has a more stable work hardened state than does the stable alloy (Point 3), this does not lead to a lower fatigue crack growth rate. A similar argument discounts Point 4, which concerns crack growth rate in the multiphase cold-worked unstable austenites.

Two types of measurement, COD and residual stress, were made to examine Point 5, the residual stress explanation for the differences in fatigue behavior. For the constant-load amplitude tests we employed in this program there was no observed difference in the COD of stable and unstable alloys for either large or small mean stresses. This is partly due to the insensitivity of the COD test, where it is required that deviations from linear unloading behavior must be identified. This is difficult to do precisely. The direct measurement of residual stress did show marked differences in the residual compressive stress at the crack tip for the 301 and 302 alloys at low mean stress (186 versus 52 MPa), but no difference at high mean stress (38 versus 38 MPa). As Hornbogen has shown, in order for the volume increase due to the $\gamma \rightarrow \alpha$ transformation to effectively alter the crack tip stress state and

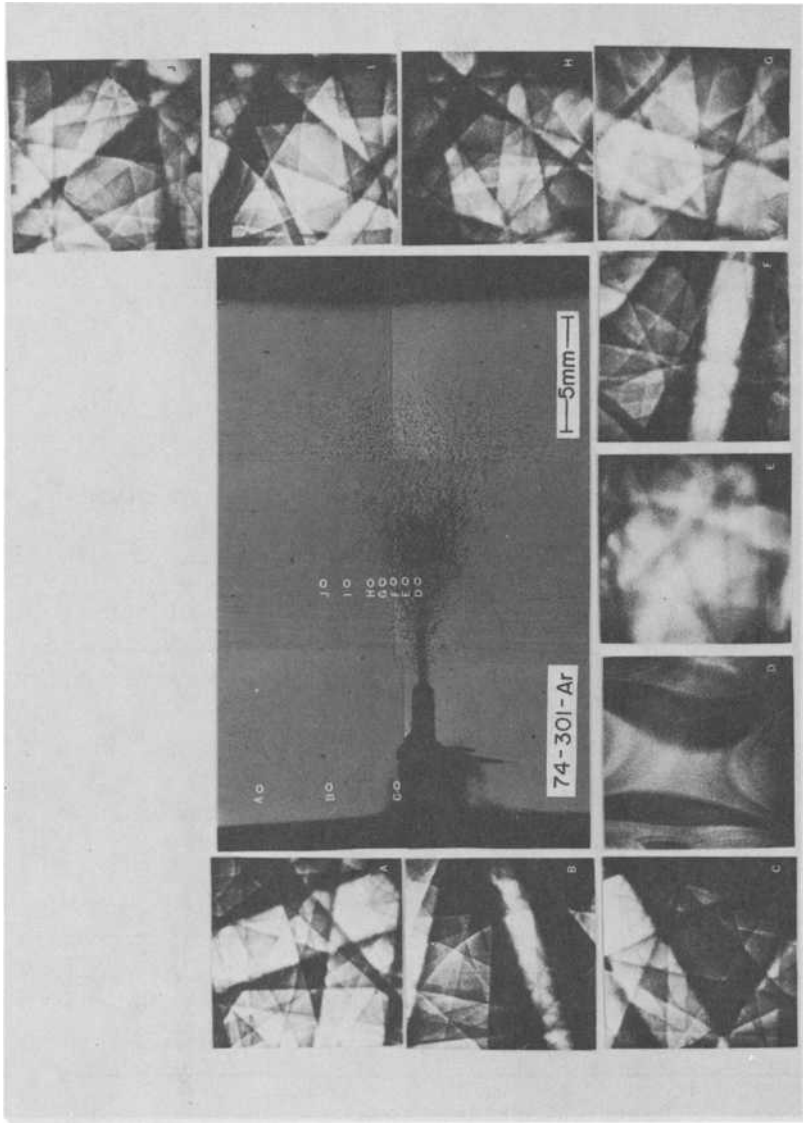

FIG. 10—*Selected area channeling pattern changes in the vicinity of a fatigue crack in AISI 301 steel tested in argon at a mean stress of 54 MPa. Estimated amounts of deformation are as follows:* (a,b,c) *0.* (d) *8%.* (e) *4%.* (f) *½%.* (g) *1%.* (h) *½%.* (i,j) *0%. Same specimens as Fig. 8.*

TABLE 1—*Plastic zone size measurements by using different techniques.*[a]

Steel	Atmosphere	Plastic Zone Size (R_p), mm		
		Microhardness	Electron Channeling	Photomacrograph
301	Ar	3.6	3.1	3.1
	H_2	1.7	1.1	2.1
302	Ar	3.8	>4.1	3.6
	H_2	2.8	1.8	2.6
301, 26% CW[b]	Ar	3.0	...	...
301, 40% CW	Ar	3.0	...	...
302, 26% CW	Ar	3.0	...	...
302, 40% CW	Ar	3.0	...	...

[a]Mean stress = 54 MPa; ΔK = 38 MPa $\sqrt{m}$.
[b]CW = cold-worked.

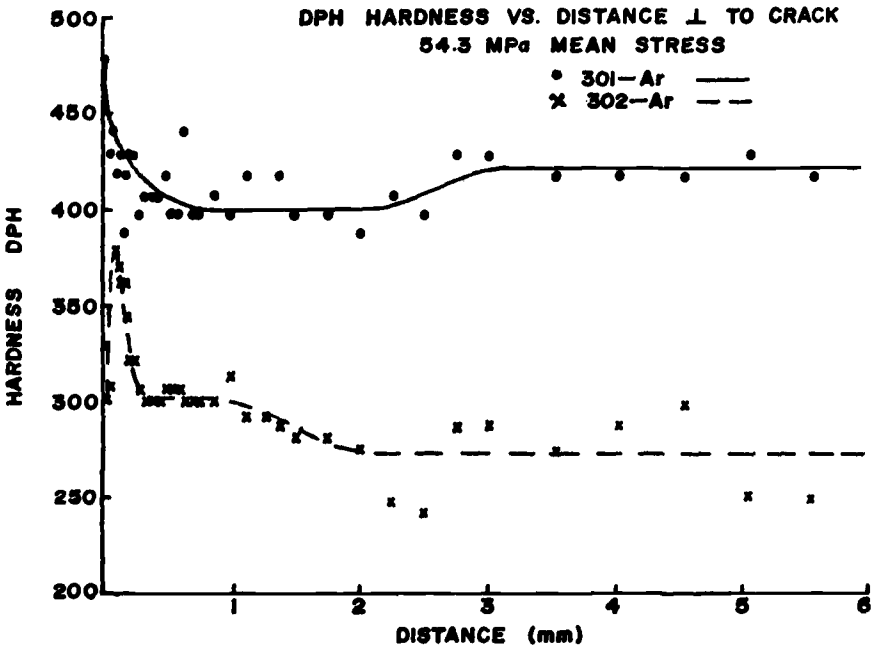

FIG. 11—*Microhardness versus distance normal to fatigue cracks in AISI 301 and 302 cold-rolled by 26% before testing in argon at a mean stress of 54 MPa.*

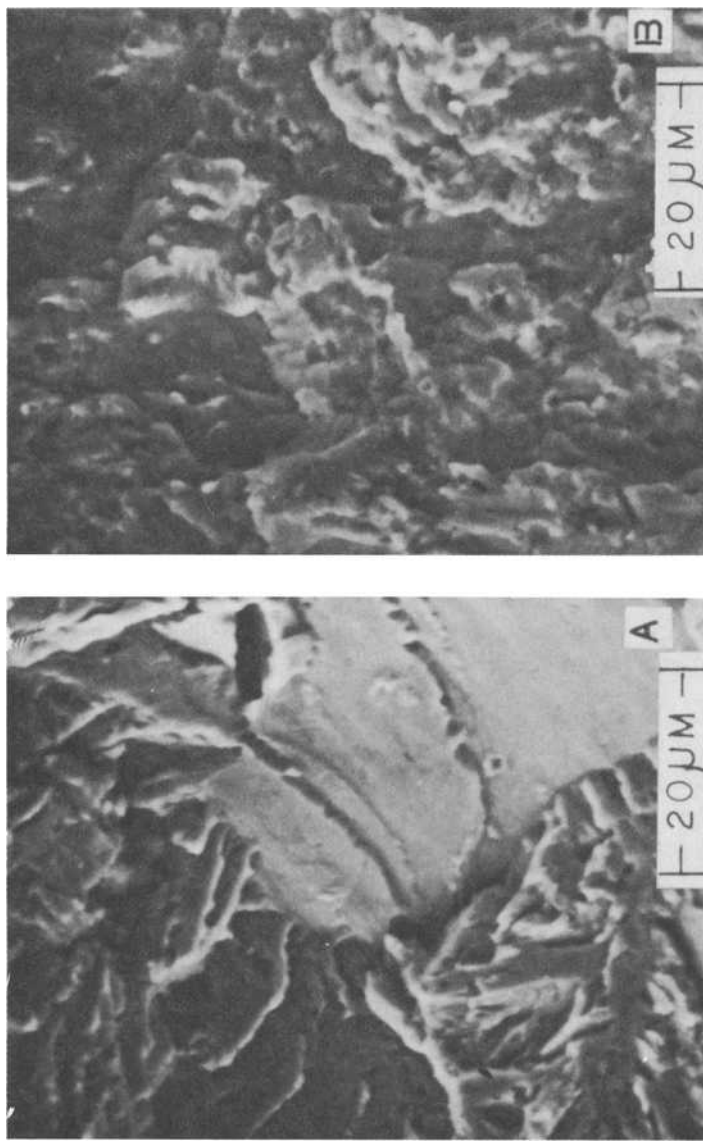

FIG. 12—*SEM fractographs of* (a) *AISI 301 and* (b) *AISI 302 fatigue-tested in H_2 gas at 1 atm pressure. Mean stress = 54 MPa.*

thereby decrease the crack growth rate, the transformed zone must be confined by the surrounding material [*14*]. At low mean stresses this is the case, whereas at high mean stresses net section yielding is possible, and large, favorable compressive stresses at the crack tip do not occur.

A final mechanistic question to be answered is the marked effect of a hydrogen gas atmosphere on the fatigue behavior of stable and unstable austenitic alloys, shown in Fig. 7 for AISI 301 and 302. Effects of hydrogen testing can be seen with many of the experimental techniques described previously; the details are reported elsewhere [*15,16*]. The most telling differences are in the fractographic features of the two alloys (Fig. 12). Large, flat facets can be seen in the hydrogen-tested AISI 301, while the fatigue crack growth rate is observed to increase markedly over the argon-tested specimens. This is not true for AISI 302. Thus it seems clear that hydrogen effects a change in the basic crack advance mechanism (Point 7).

Summary

We have tried to demonstrate the benefits of making careful observations and measurements of various types in order to interpret fatigue behavior. In the particular problem of understanding fatigue of unstable austenitic stainless steels, the residual stress measurements were invaluable. For the effects of hydrogen, fractography provided key clues to the interpretation. In other instances, other techniques may have been required. It is not always possible to predict which technique is going to be the best, and only after several are used does it become apparent.

Acknowledgments

This work was supported by U.S. Army Research Office (Durham) Grant DAAG29 76G 0278. Use of unpublished results from the M.S. theses of R. Bianchetta and Z. Khan is appreciated. William Powers assisted in making some of the measurements, and the advice of Darrel Socie, Peggy Mochel, and John Woodhouse in some of the experimental details was helpful. The facilities of the Materials Research Laboratory (supported by Department of Energy Contract DOE-EY-C-OZ-1198) and the Materials Engineering Research Laboratory were invaluable in the conduct of this research.

References

[*1*] Hennessy, D., Steckel, G., and Altstetter, C., *Metallurgical Transactions A*, Vol. 7A, 1976, p. 415.

[*2*] Franke, G. and Altstetter, C., *Metallurgical Transactions A*, Vol. 7A, 1976, p. 1719.

[*3*] Eliezer, D., Chakrapani, D., Altstetter, C., and Pugh, E. N., *Metallurgical Transactions A*, Vol. 11A, 1980, p. 1563.

[4] Liu, R., Narita, N., Altstetter, C., Birnbaum, H., and Pugh, E. N., *Metallurgical Transactions A*, Vol. 11A, 1980, p. 1563.
[5] Schuster, G., "The Effects of Phase Transformation on the Fatigue Crack Growth Rate of Austenitic Stainless Steels Tested in Argon and Hydrogen Atmospheres," Ph.D. dissertation, University of Illinois at Urbana-Champaign, 1980.
[6] Zhan, Z., "A Study of Fatigue Crack Growth Rate in Metastable Stainless Steels," M.S. thesis, University of Illinois at Urbana-Champaign, 1977.
[7] Bianchetta, R., "The Effect of Prestrain on Low Cycle Fatigue of Unstable Austenitic Stainless Steel," M.S. thesis, University of Illinois at Urbana-Champaign, 1977.
[8] Schaeffler, A. L., *Metal Progress*, June 1973, p. 207.
[9] Gray, R., Sikka, V., and King, R., *Journal of Metals*, Nov. 1978, p. 18.
[10] Nelson, J. L. and Beavers, J., *Metallurgical Transactions A*, Vol. 10A, 1979, p. 658.
[11] VanEssen, C., Schulson, E., and Donaghay, R., *Journal of Materials Science*, Vol. 6, 1971, p. 213.
[12] Davidson, D. in *Fatigue Mechanisms, ASTM STP 675*, American Society for Testing and Materials, 1979, pp. 254-275.
[13] Elber, W. in *Damage Tolerance in Aircraft Structures, ASTM STP 486*, American Society for Testing and Materials, 1971, pp. 230-242.
[14] Hornbogen, E., *Acta Metallurgica*, Vol. 26, 1978, p. 147.
[15] Schuster, G. and Altstetter, C., "Hydrogen-Enhanced Fatigue Crack Growth in Unstable and Stable Stainless Steels," presented at Third International Conference on Effect of Hydrogen on Behavior of Metals, Jackson Hole, Wyo., Aug. 1980.
[16] Schuster, G. and Altstetter, C., submitted to *Metallurgical Transactions A*.

DISCUSSION

R. W. Hertzberg[1] *(written discussion)*—I would like to call your attention to a parallel study involving fatigue crack propagation (FCP) in MP35N, another unstable alloy.[2] This material undergoes an FCC to HCP transformation when stressed. The FCP response was found to depend on the cyclically stabilized properties of the material in the plastic zone and on the timing of the strain-induced phase transformation. Specifically, the slope of the da/dN-ΔK plot varied with the log of the pre-exponential constant, and the slope decreased with increasing cyclic yield strength and cyclic strain-hardening exponent.

[1]Department of Metallurgy and Materials Engineering, Lehigh University, Bethlehem, Pa. 18015.
[2]Hickerson, J. and Hertzberg, R. W., *Metallurgical Transactions*, Vol. 3, 1972, p. 179.

N. Ranganathan[1] *and J. Petit*[1]

Quantitative Measurements in the Plastic Zone Caused by a Single Overload in Air and Vacuum

REFERENCE: Ranganathan, N. and Petit, J., **"Quantitative Measurements in the Plastic Zone Caused by a Single Overload in Air and Vacuum,"** *Fatigue Mechanisms: Advances in Quantitative Measurement of Physical Damage, ASTM STP 811*, J. Lankford, D. L. Davidson, W. L. Morris, and R. P. Wei, Eds., American Society for Testing and Materials, 1983, pp. 464-484.

ABSTRACT: Plastic deformations near the crack tip following overload tests in air and vacuum on 2024-T351 aluminum alloy were measured by interferential-contrast, interferometry, and microhardness methods. The evolution of the plastic zone sizes in the overload-affected zone is described. Quantitative analysis of the results obtained show that plastic zone sizes are higher in vacuum and the distribution of plastic strains are different than in air. Differences in plastic zones between plane stress and plane strain conditions are also shown. These results, complemented with macrofractographic and microfractographic measurements and the calculation of the *J*-integrals, suggest an explanation for the differences in material behavior in air and vacuum.

KEY WORDS: fatigue delay, environmental effect, plastic zones, plastic strain distribution

The effect of a single spike overload on constant-amplitude fatigue crack growth has been described in several studies [*1-3*] which have led to different models being proposed [*4-6*].[2] In previous work [*7*] conducted on a high-strength aluminum alloy, it was shown that the application of an overload in air and vacuum caused a similar delayed crack growth retardation in both environments. The study, however, brought out important quantitative differences due to the environment, characterized in vacuum by stronger delaying effects. To gain new insight into the influence of environment on this phenomenon, a study of the quantitative evolution of fatigue damage was undertaken. This paper presents and discusses measurements of crack-tip plasticity parameters by three different techniques.

[1]Laboratoire de Mécanique et de Physique des Matériaux, ENSMA, Poitiers, France.
[2]The italic numbers in brackets refer to the list of references appended to this paper.

Experimental Procedure

The overload tests were conducted on 10- and 4-mm-thick compact tension specimens of 2024-T351 aluminum alloy in air and in vacuum by using an environmental chamber [*7-8*]. The specimen surface was polished up to 1 μm before the test to facilitate crack length measurement by a traveling microscope ($\times$25). During all overload tests the evolution of crack mouth opening displacement with respect to the load was recorded. Table 1 recapitulates the test conditions.

Plastic strain fields near the crack tip were measured by three techniques: inferential contrast, interferometry, and microhardness.

Nomarski Interferential Contrast

The specimen surface after the fatigue test is examined under polarized light through an interferential contrast indicator. Changes in flatness give rise

TABLE 1—*Test conditions.*[a]

Test	Thickness, mm	$R = P_{min}/P_{max}$	Environment	ΔK_i, MPa$\sqrt{m}$
A_{11}	10	0.01	air	13.10
A_{12}	10	0.01	air	14.90
A_{13}	10	0.01	air	18.00
A_{21}	10	0.1	air	12.70
A_{22}	10	0.1	air	13.50
A_{23}	10	0.1	air	15.70
A_{24}	10	0.1	air	20.20
A_{31}	10	0.1	air	15.70
A_{32}	10	0.1	air	20.20
A_{41}	4	0.1	air	18.89
V_{11}	10	0.01	vacuum	15.70
V_{12}	10	0.01	vacuum	18.38
V_{21}	10	0.1	vacuum	12.70
V_{22}	10	0.1	vacuum	13.50
V_{23}	10	0.1	vacuum	15.70
V_{24}	10	0.1	vacuum	20.98
V_{31}	10	0.1	vacuum	16.00
V_{41}	10	0.1	vacuum	13.45
V_{42}	10	0.1	vacuum	18.53
V_{51}	4	0.1	vacuum	15.67
V_{52}	4	0.1	vacuum	20.60
V_{61}	4	0.1	vacuum	18.89

[a]The overload ratio was

$$\tau = 2\left(= \frac{\Delta K_{peak}}{\Delta K_i}\right)$$

where ΔK_{peak} is stress intensity factor range due to the overload, and ΔK_i is initial stress intensity factor range. The frequency was 20 Hz, or 35 Hz (vacuum), and 0.2 Hz (overloading cycle). The signal was sinusoidal, the vacuum was 5.10^{-3} Pa, and the relative humidity was about 50% in air.

to either Newton's interference patterns under polychromatic light or to zones of different light intensity under monochromatic light.

Nomarski Interferometry

In this case, the deformed surfaces are observed under monochromatic light ($\lambda = 546$ nm) by using an interferometer. Interferences are produced by comparing an area of the object with a slightly displaced image of the same area. An undeformed, optically flat zone thus gives parallel and equi-spaced fringes. Changes in flatness in the plastic zone lead to differences in fringe spacing.

Theoretically, the minimum detectable limit is on the order of $\lambda/2$ (that is, 273 nm), but the practical scatter is higher due to polishing and is on the order of 1 μm.

Microhardness

After overload tests, the specimen surfaces were repolished up to 1 μm (the surface removed was on the order of 15 μm), and microhardness measurements were carried out on the specimen surface at different distances from the overload application point under 25 or 50 g load.

Hardness tests were conducted on Specimen V_{42} at 2 and 5 mm from the crack surface after cutting across the specimen thickness.

To correlate the hardness values to equivalent strain levels two series of tests were conducted:

1. Small specimens were tested in tension to different monotonic plastic strain levels (ϵ_M), and hardness measurements were carried out on each of them. For each strain level at least 30 measurements were made in order to obtain the mean and standard deviation values of hardness.
2. Low-cycle fatigue specimens were tested at different total strain levels ($\Delta\epsilon_t$). After stabilization of the hysteresis loops corresponding to a plastic strain half range $\Delta\epsilon_p/2$, hardness values were measured at the center of the specimen at about midthickness.

The calibration curves thus obtained (Fig. 1) compare equivalent hardness values in monotonic tension ϵ_M and imposed total strain half range $\Delta\epsilon_t/2$. Figure 2 correlates hardness values to plastic strain half range $\Delta\epsilon_p/2$. Considering the scatter, we find that minimum equivalent strain levels detectable are 0.7% for ϵ_M and 0.2% for $\Delta\epsilon_p/2$.

After these measurements had been completed, the fracture surfaces were examined in an optical microscope and in a scanning electron microscope (SEM) to measure macroscopic tear sizes and microscopic stretch zone widths.

Experimental Results and Analysis

Typical evolutions of the crack growth rates with respect to the crack length for two tests conducted at the same conditions in air and in vacuum are shown

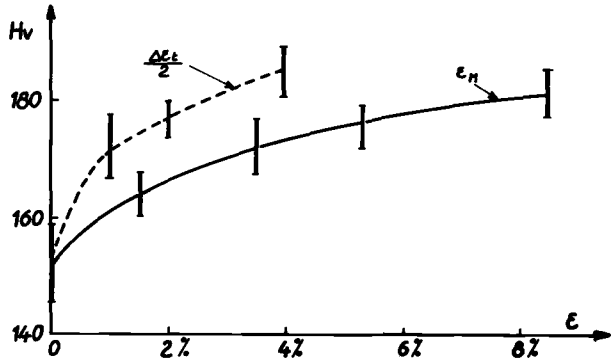

FIG. 1—*Relationship between microhardness and monotonic strain and imposed total strain half range.*

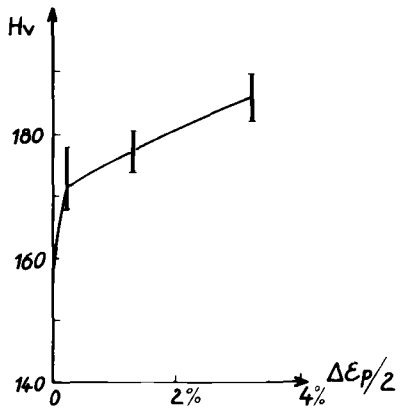

FIG. 2—*Relationship between microhardness and plastic strain half range.*

in Fig. 3 and the major parameters are defined in Fig. 4. The environmental effect is essentially characterized by stronger delay effects and by a lower minimum growth rate at the end of the deceleration period in vacuum. The crack length over which the retardation is observed (a_d) also is longer in vacuum (see also Ref 7).

Nomarski Contrast and Interferometry

Fig. 5 gives a typical result obtained by optical contrast on a 10-mm-thick specimen tested in vacuum (No. V_{42}) and shows the characteristic points (S, A, M, and F) in the delay periods (also see Fig. 4). The observed plastic zone consists of two wings on either side of the crack. The maximum size ($2r_y$) of this zone is also indicated. When the crack is in the deceleration phase (that is, be-

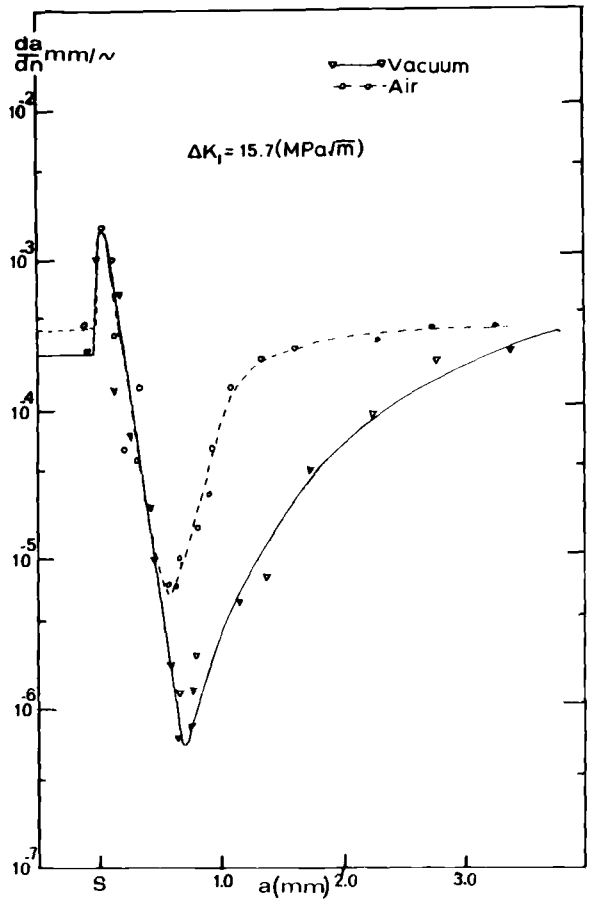

FIG. 3—*Comparison between the evolution of the crack growth rate* (da/dN) *with respect to the crack length for Tests* A_{23} *and* V_{23} *at the same* ΔK_i.

tween Points A and M), plastic deformation is not detectable near the crack plane. At a well-defined distance from S, a new plastic zone reappears on the surface, the size of which increases as the crack advances in the acceleration phase, between Points M and F.

Figure 6 illustrates a typical example of the development of interference fringe patterns in the overload plastic zone (Test A_{41}). Again the reference points S, A, M, and F are indicated. At a first approximation the limit of the plastic zone is defined where fringe spacings start changing drastically.

A comparison of these two optical methods shows that the plastic zones determined by interferometry are slightly higher, which indicates that the interferometric method has a better resolution. Particularly, in the deceleration

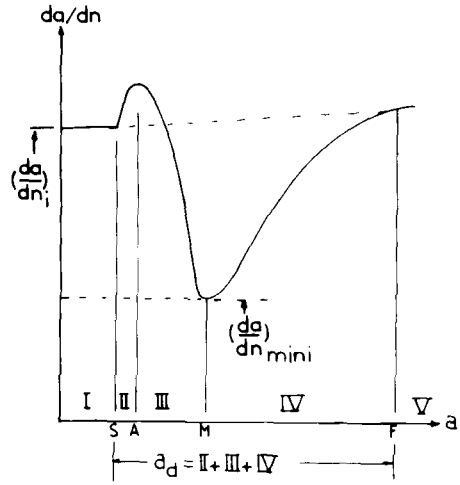

S = Point of overload application
A = Point of maximum acceleration
M = Point of minimum growth rate
F = End of delay period
$(da/dN)_i$ = Initial crack growth rate
$(da/dN)_{mini}$ = Crack growth rate at M
a_d = Affected crack length

FIG. 4—*Definition of major parameters during an overload test.*

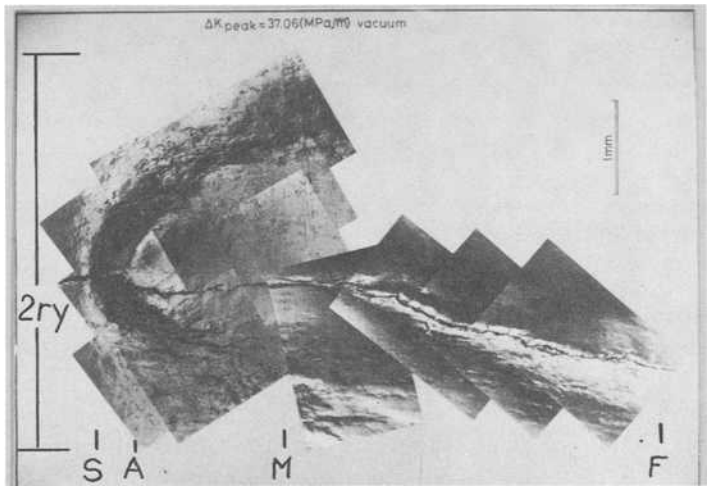

FIG. 5—*Typical result obtained by interferential contrast, showing the development of the plastic zone (Test V_{42}).*

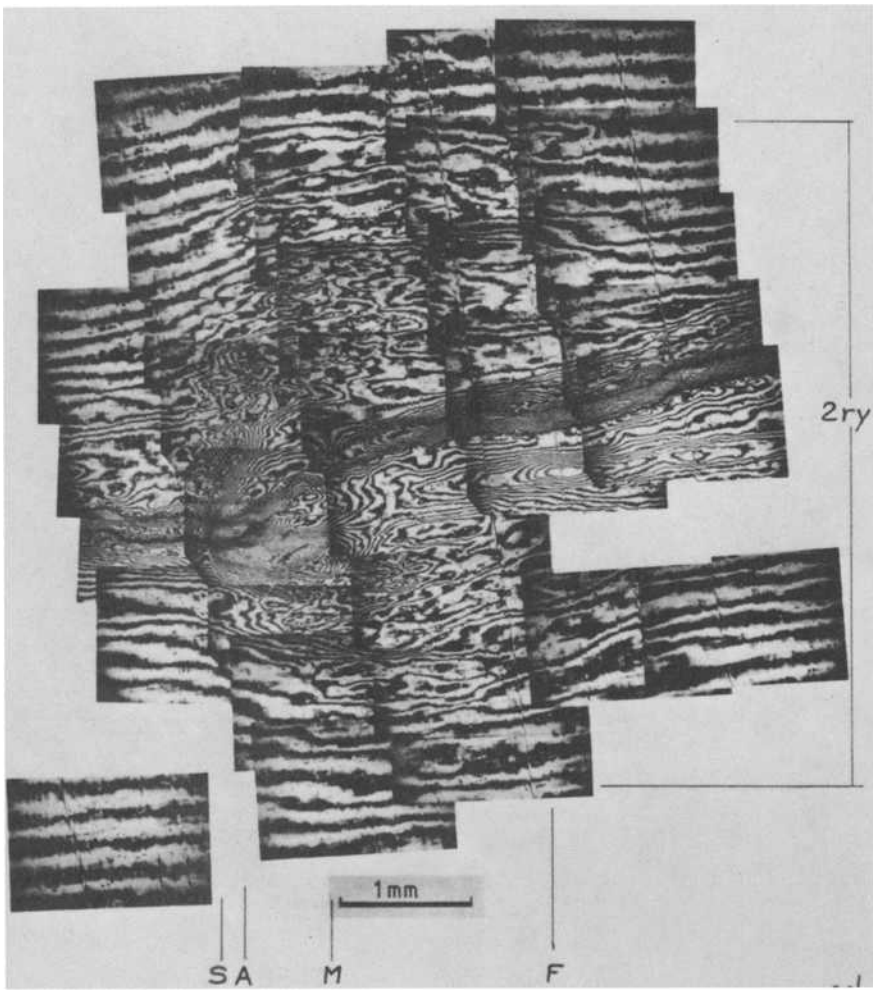

FIG. 6—*Interferences fringes in the overload plastic zone for Test* A_{4l}. *The small rectangle on the left indicates fringes in an optically flat zone.*

phase (that is, between Points A and M) it is possible to detect the presence of plastic deformation close to the crack. The development of the plastic zone detected by interferometry after Point M, however, is comparable with that obtained by optical contrast.

Figures 7*a* and 7*b* compare plastic zone sizes measured by interferential contrast at different values of K_{max} for constant ΔP tests and overload tests, in vacuum and air. For overload tests the K_{max} value corresponds to the peak load P_{peak}.

The measured values in the two environments are consistent with the esti-

mations according to the models of Rice [*9*] or Irwin [*10*] only in the low-value range of K_{max} corresponding to constant ΔP tests. For higher values of K_{max} (that is, just after the overload), the plastic zone sizes in vacuum are generally greater than those in air, reaching a factor of about 1.5; the comparison with the aforementioned models gives an acceptable correlation only for the tests in vacuum.

Quantitative evaluation of the interference fringe spacing changes in the overload-affected region is difficult due to the complexity of the fringes topography. In the zone at constant ΔP and for a ΔK of 18.8 MPa$\sqrt{m}$, the changes in fringe spacings are analyzed in terms of w-displacements (in the thickness direction), and are plotted with respect to y (distance perpendicular to the crack plane) in Fig. 8 in both air and vacuum. Point L marked on these curves is defined later.

Microhardness

Figures 9*a* to 9*d* show the typical evolution of microhardness perpendicular to the crack plane on the surface of specimens A_{41} and V_{61}. The asymmetry of

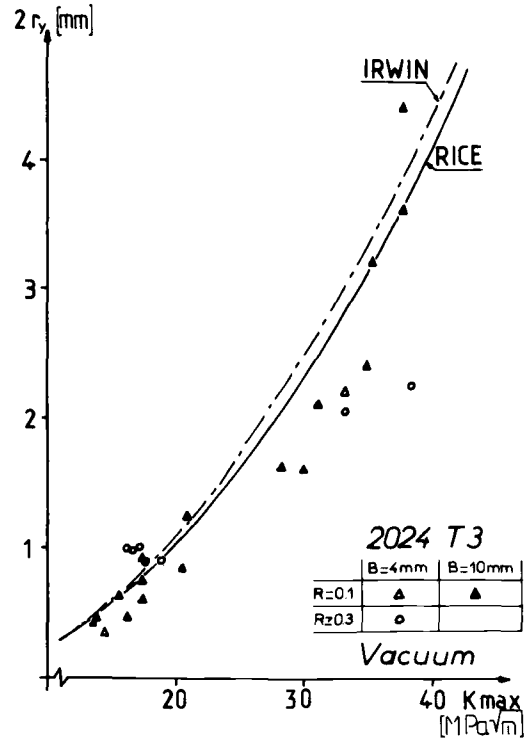

FIG. 7*a*—*Comparison between measured plastic zone sizes and those calculated by models of Rice and Irwin (in vacuum).*

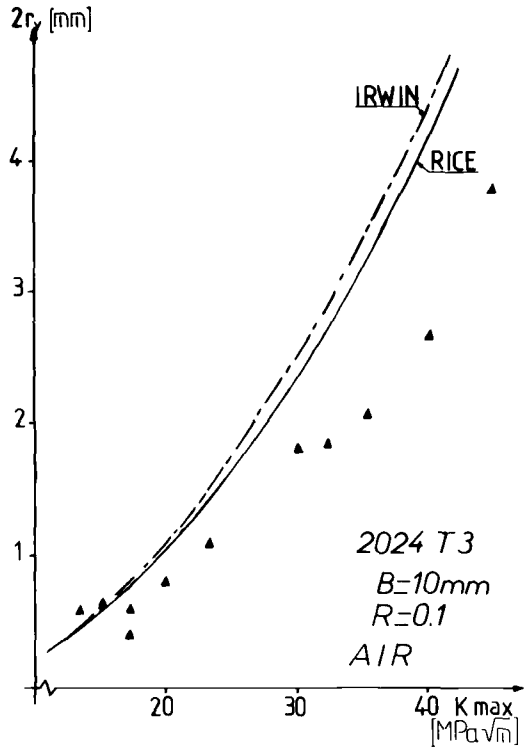

FIG. 7*b*—*Comparison between measured plastic zone sizes and those calculated by models of Rice and Irwin (in air).*

the plastic deformation on either side of the crack is evident especially in vacuum.

The results reveal the following points: (*1*) the maximum of ΔH_v near the crack is on the order of 25 in both the environments, and (*2*) the deformation profiles in the affected zones in vacuum are significantly different from those in air.

Measurements made in the plastic zone associated with the crack before the point of overload give detectable deformations only in vacuum (Fig. 10).

A comparison of microhardness measurements with those made by interferometry (Fig. 8) leads us to observe that the plastic zone size detected by microhardness (that is, 0.6 mm) corresponds to Point L on the (W-Y) curve. Thus Point L appears to be boundary between elastic and plastic regions. Applying the same concept in the case of the (W-Y) profile in air, we see that this elastic-plastic limit is situated at 0.12 mm from the crack. This explains why any change in microhardness values cannot be detected in air.

Figures 11*a* to 11*c* present the microhardness measurements made on Speci-

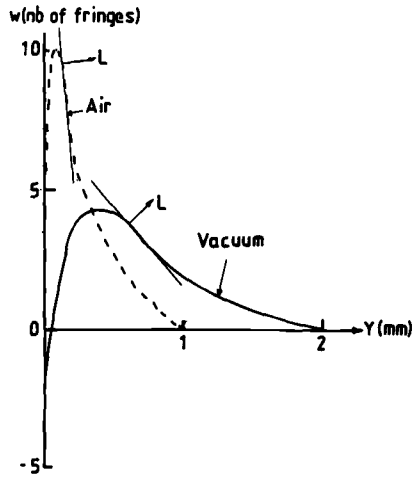

FIG. 8—*Evaluation of displacements in the thickness direction in the plastic zone, obtained by interferometry.*

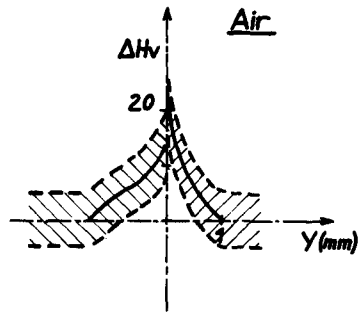

FIG. 9*a*—*Microhardness perpendicular to the crack plane at Point S (Test* A_{41}*).*

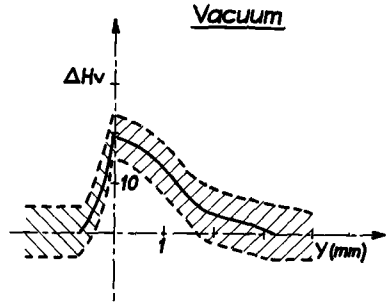

FIG. 9*b*—*Microhardness perpendicular to the crack plane at Point S (Test* V_{61}*).*

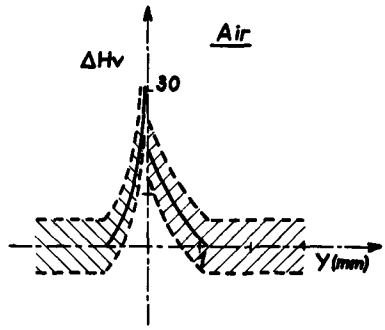

FIG. 9c—*Microhardness perpendicular to the crack plane at Point S + 0.30 (Test A_{41}).*

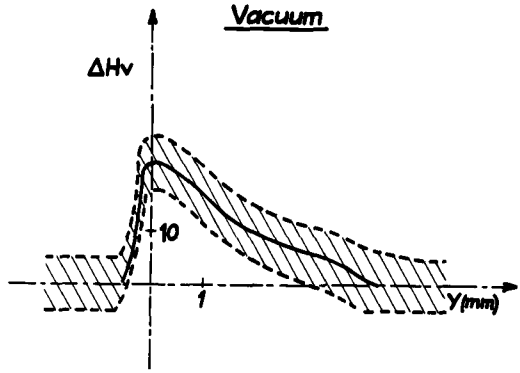

FIG. 9d—*Microhardness perpendicular to the crack plane at Point S + 0.37 (Test V_{61}).*

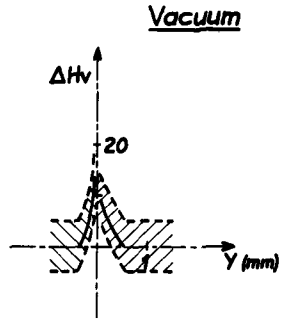

FIG. 10—*Hardness variation near the crack in vacuum before the overload application point (Test V_{61}).*

men V_{41} on the surface and in cross sections at 2 and 5 mm from this surface. Figure 11*a* compares the evolution of microhardness with the boundary of the plastic zone obtained by optical contrast (in broken lines); a good correlation is indicated. The decrease of the plastic zone when approaching the plane strain region is seen in Fig. 11*b*. The intensity of deformation is three times lower at the specimen center and the plastic zone is about four times smaller (Fig. 11*c*).

Tear and Stretch Zone

Figure 12 compares the evolution of macroscopic tear sizes in air and vacuum for Tests A_{21} to A_{24} and Tests V_{21} to V_{24} conducted at comparable values of ΔK_i. The tear size is systematically larger in vacuum than in air [*7*]. Since the tear can be related to the state of triaxiality at the crack tip [*11*] it can be surmised that strain distributions at the crack tip are not the same in air and vacuum. Such a result has also been reported by Davidson [*12*], where the strain ϵ_{yy} perpendicular to the crack plane measured on the specimen surface by stereo-imaging techniques was shown to be an order of magnitude higher in vacuum than in air at 100% relative humidity.

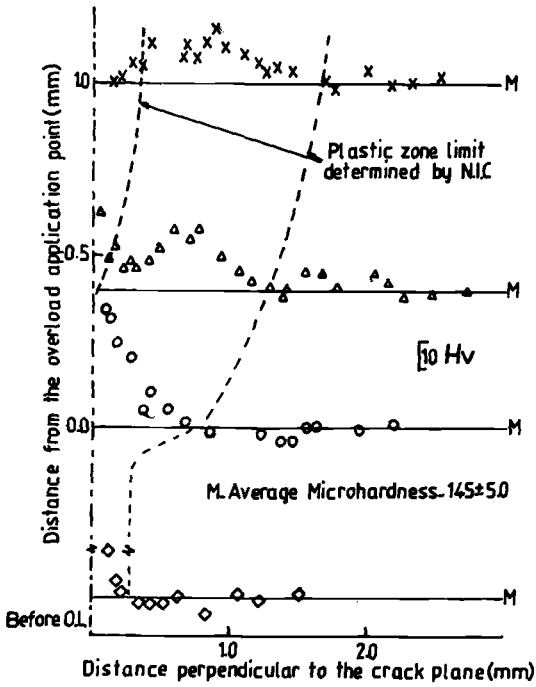

FIG. 11*a*—*Evolution of microhardness in the plastic zone on the surface (Test V_{41}).*

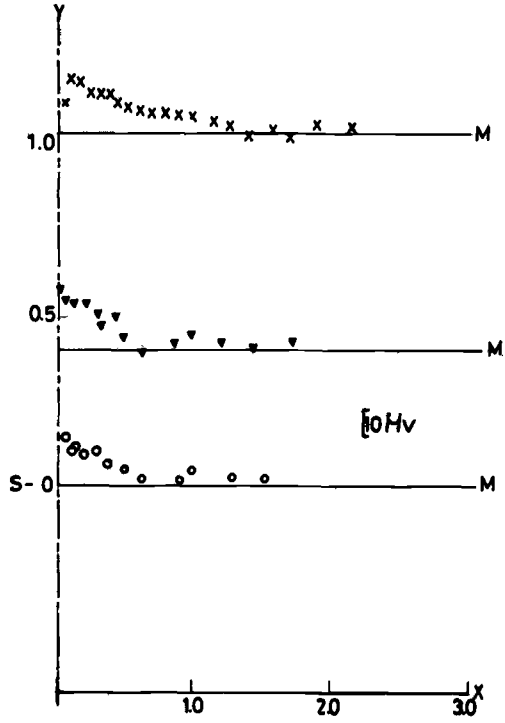

FIG. 11*b*—*Evolution of microhardness in the plastic zone at 2 mm from the surface (Test* V_{41}*).*

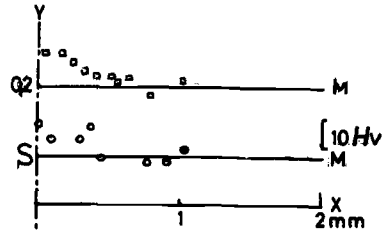

FIG. 11*c*—*Evolution of microhardness in the plastic zone at the center of the specimen (Test* V_{41}*).*

Figure 13 shows examples of microphotographs of the stretch zones observed at the overload application point S in air and in vacuum at the same K_{peak} value, where K_{peak} is the stress intensity factor at the peak load. Stereographic measurements indicate that the stretch zone size is smaller in vacuum than in air.

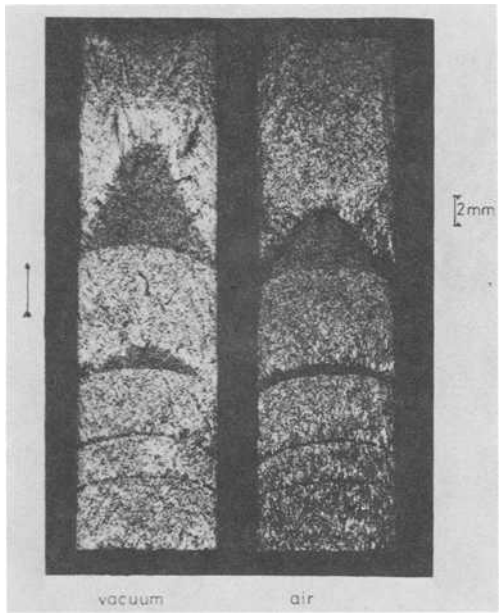

FIG. 12—*Comparison of macroscopic tear sizes in vacuum (left) and air (right) for Tests* V_{21} *to* V_{24} *and Tests* A_{21} *to* A_{24} *respectively, looking from bottom to top.*

This stretch zone size being related to crack-tip opening displacements [*13*], it can be supposed that the crack tip opens to a smaller extent in vacuum than in air. Such a result has also been obtained by Bowles [*14*] by an infiltration technique.

The test conditions in this study do not correspond to usual J_{IC} test procedure, especially with respect to conditions of precracking [*15*]. Nevertheless, an approximate J_{IC} value is estimated by the following method:

1. The crack-mouth opening values are converted to load-line opening values V_{LL} according to the correction proposed by Landes [*16*].
2. J-values are calculated from the area under the load V_{LL} diagram [*17*].
3. The so-obtained J-values are plotted as a function of the maximum crack advance Δa measured at midthickness for each overload.

The critical crack extension Δa_c, and hence J_{IC}, is deduced using the criterion proposed by Paris [*18*]:

$$\Delta a_c = 0.025 \frac{K_{IC}}{\sigma_{YS}^2 (1 - \nu^2)}$$

where σ_{YS} is the yield strength and ν is Poisson's ratio.

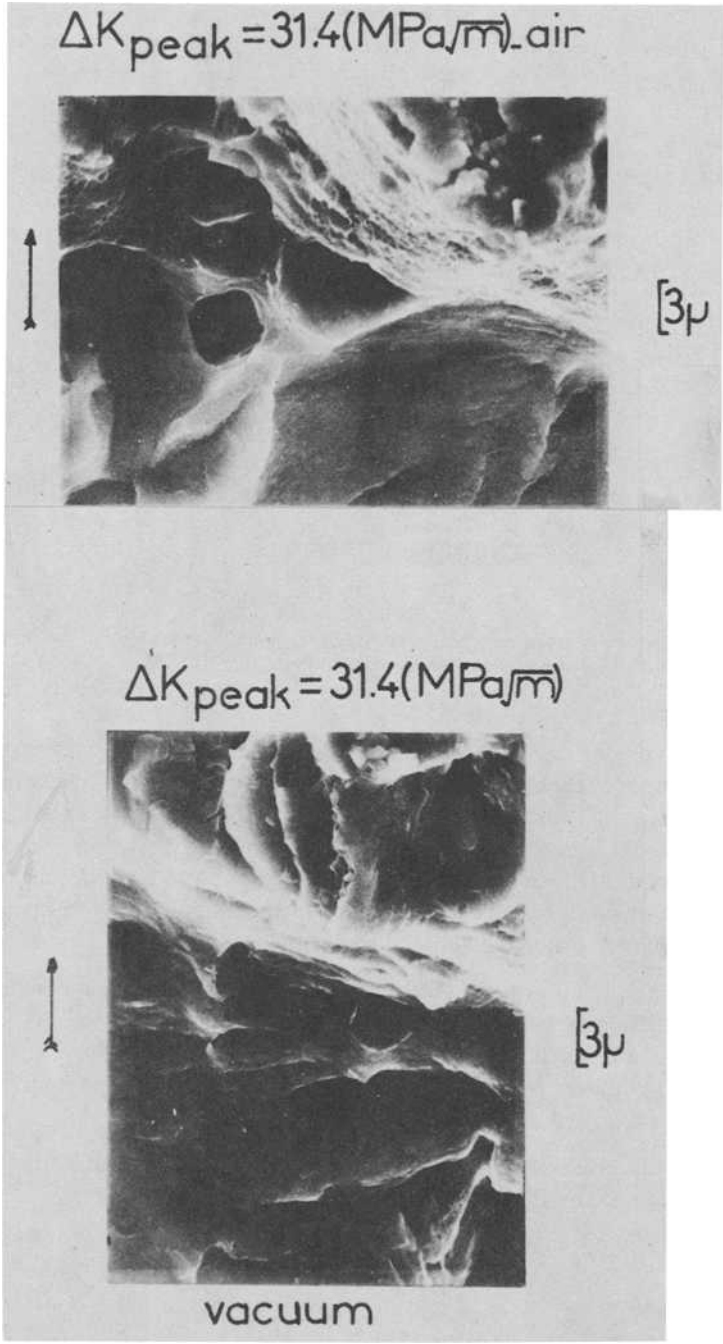

FIG. 13—*Microscopic stretch zones at the overload application point in the two environments.*

Substituting the K_{IC} value for the considered alloy [*19*]—that is, $K_{IC} = 36$ MPa$\sqrt{m}$ and $\sigma_{ys} = 320$ MPa in the foregoing equation—, we obtain a value for Δa_c of 0.32 mm.

The J-Δa curve thus obtained (Fig. 14) shows that the data points in air and in vacuum fall in the same scatter band. The J_{IC} value determined by the aforementioned procedure is 11 000/m^2; this corresponds to an equivalent K_{IC} of 31 MPa$\sqrt{m}$ independent of the environment, which is consistent with the value of K_{IC} given earlier. An identical value in air and in vacuum of K_{IC} has been previously reported for another aluminum alloy [*20*].

Discussion

Table 2 compares plastic zone sizes defined by the three techniques used for Tests A_{41} and V_{61}. The information obtained by the three methods, though complementary in nature, are different in the following respects:

1. The optical contrast method provides essentially qualitative information on the intensity of deformation and gives an overall picture of the deformed zone.

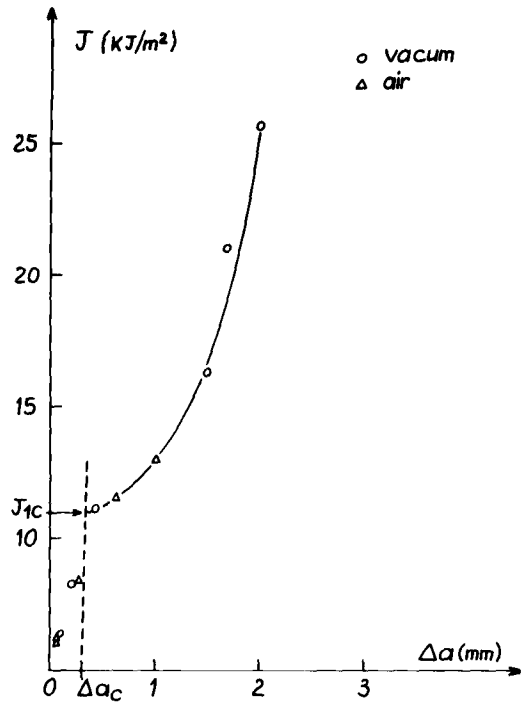

FIG. 14—*J-integral versus cracked ligament size in air and vacuum.*

TABLE 2—*Comparison between plastic zone sizes determined by the three methods.*

Test	Distance with Respect to Point S, mm	Plastic Zone Size (mm) Perpendicular to the Crack Plane		
		Optical Contrast	Interferometry	Microhardness
V_{61}	S − 0.53	1.67	1.62	1.10
V_{61}	S	1.74	2.53	3.3
V_{61}	S + 0.2	3.53	4.43	...
V_{61}	S + 0.37	2.63	2.92	3.50
V_{61}	S + 0.58	3.23	4.02	3.6
A_{41}	S − 0.5	0.41	1.13	...
A_{41}	S	1.28	2.85	1.72
A_{41}	S + 0.15	2.33	2.93	2.75
A_{41}	S + 0.5	2.58	2.93	1.10

2. Changes in the interference fringe spacing relate to displacements in the thickness direction and hold only an indirect relation to in-plane deformations. In highly deformed zones these changes are extremely complex and difficult to analyze. Thus a correlation between these interferometric measurements and microhardness has been proposed only in the case of monotonic loading before the overload. This optical technique is convenient for studying small plastic zones.

3. Quantitative evaluation by microhardness evaluation of plastic strain levels appears to be possible on the surface as well as at different distances from it inside the specimen, even though the low variations of microhardness with respect to plastic consolidation in the case of the studied alloy tend to limit the possibilities of this technique.

The measurements made in the plastic zone corresponding to the monotonic loading before the overload show that significant results are obtained only in vacuum.

The plastic zone associated with the overload corresponds essentially to monotonic deformation. An analysis of the microhardness results from the calibration curve presented in Fig. 1 has provided a deformation map for Specimens A_{41} (Fig. 15) and V_{61} (Fig. 16). In both environments, maximum ϵ_M appears to be about 5%. In the vicinity of the crack there exists a cyclic plastic zone, and the observed peak values of microhardness can be associated with cyclic deformation. From the calibration presented in Fig. 2, $\Delta\epsilon_p/2$ appears to be on the order of 0.5%. But it is not possible from the measurements made on this alloy to determine the boundary between cyclic and monotonic zones.

An examination of the results obtained by the three techniques as a whole shows that the deformation profiles and the plastic zones are not the same at a given value of K in air and in vacuum. On the other hand, the J-integral analysis indicates that there is no appreciable difference in the fracture toughness due to the environment. Consequently, the observed differences in material behavior should be examined from another angle.

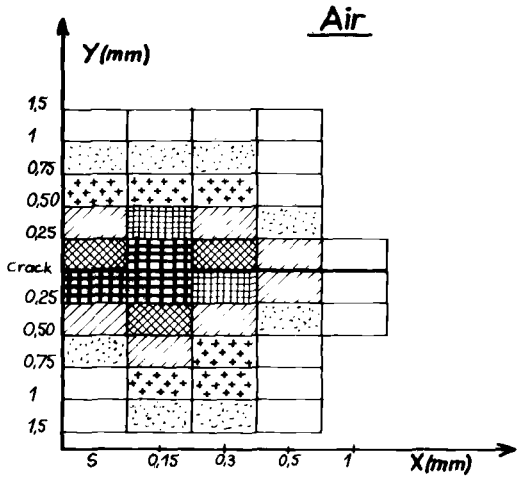

FIG. 15—*Strain distribution in the plastic zone (Test A_{41}).*

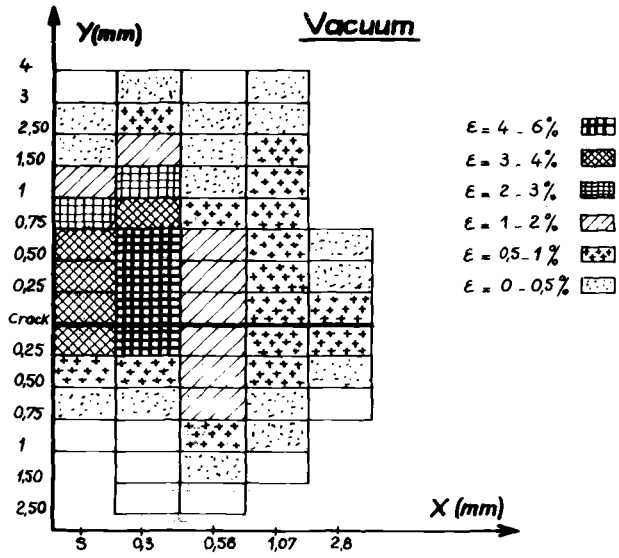

FIG. 16—*Strain distribution in the plastic zone (Test V_{61}).*

The fracture during the overload takes place in mixed plane stress and plane strain modes in the specimen thickness range studied. Just before the application of the overload where crack growth rates are almost equivalent, the accumulated plastic strain is higher in vacuum, especially on the surface [*21*]. Consequently, under the same peak load, the crack advance is lower in the plane

stress region near the surface, and conversely the crack tunneling at the specimen center is more pronounced in the specimen tested in vacuum; this can be seen for Tests A_{23} and V_{23} in Fig. 12 (third overloads from the bottom).

It has also been observed that the stretch zone width (SZW) is smaller in vacuum. This zone represents a transition between the fatigue precrack and the overload fracture regions, and is formed by alternating shear along slip bands originating from the crack tip [*22*].

Although attempts to correlate SZW with fracture toughness parameters have not yet produced a completely unified approach, it has been proposed that SZW reaches a critical value before fracture (SZW_C) and that this value is proportional to the factor (K_{IC}/σ_{yS}) where K_{IC} is the plane strain fracture toughness and σ_{yS} is the yield strength [*22,23*].

Comparing the crack-tip conditions in air and vacuum, we find that the cyclic consolidation is higher in vacuum, which leads to a higher yield strength. Since the K_{IC} value is not affected by the environment, the factor K_{IC}/σ_{yS} is smaller in vacuum, resulting in a smaller stretch zone.

Conclusions

1. The crack-tip plasticity induced by a single spike overload depends upon environmental conditions.
2. The monotonic deformation levels extend over larger distances in vacuum than in air, while the maximum values near the crack tip are on the same order.
3. The static J_{IC} value is the same in air and vacuum.
4. The obtained results and their analysis show that the three-dimensional strain distributions are different in the studied environments.
5. An explanation of the differences in environmentally induced material behavior is offered based on the obtained results.

Acknowledgments

The authors wish to thank Professor J. de Fouquet, Director, Ecole Nationale Supérieure de Mécanique et d'Aérotechnique, who by his critical appreciation helped us to revise this paper.

References

[*1*] Schijve, J., Broek, D., and de Rijk, P., "Fatigue Crack Propagation under Variable Amplitude Loading," Report NLR MP 2094, Delft University of Technology, Delft, The Netherlands, 1961.
[*2*] Corbly, D. M. and Packman, P. F., *Engineering Fracture Mechanics*, Vol. 5, 1973, p. 473.
[*3*] Probst, E. P. and Hillberry, B. M., *AIAA Journal*, Vol. 73, 1973, p. 325.
[*4*] Wheeler, O. E., *Journal of Basic Engineering, Transactions of ASME*, March 1972, pp. 181-186.

[5] Matsuoka, S., Tanaka, K., and Kawahara, M., *Engineering Fracture Mechanics*, Vol. 8, 1976, p. 507.
[6] McCartney, L. N., *International Journal of Fracture*, Vol. 14, No. 2, 1978, p. 213.
[7] Ranganathan, N., Petit, J., and Bouchet, B., *Engineering Fracture Mechanics*, Vol. 11, 1979, p. 775.
[8] Petit, J., Nadeau, A., Lafarie, M. C., and Ranganathan, N., *Revue de Physique Appliquee*, Vol. 15, 1980, p. 919.
[9] Rice, J. R. in *Fatigue Crack Propagation, ASTM STP 415*, American Society for Testing and Materials, 1967, p. 267.
[10] McClintock, F. A. and Irwin G. R. in *Fracture Toughness Testing and Its Applications, ASTM STP 381*, American Society for Testing and Materials, 1965, pp. 84–113.
[11] Knott, J. F., *Fundamentals of Fracture Mechanics*, Butterworth, London, 1973, p. 243.
[12] Davidson, D. L. and Lankford, J., "Crack Tip Plasticity Associated with Corrosion-Assisted Fatigue," Interim Report O2-4268, Southwest Research Institute, San Antonio, Tex., 1979.
[13] Liu, H. W. and Kobayashi, H., *Scripta Metallurgica*, Vol. 14, 1980, p. 525.
[14] Bowles, C. Q., "The Role of Environment Frequency and Wave Shape During Fatigue Crack Growth in Aluminum Alloys," Report LR-270, Delft University of Technology, Delft, The Netherlands, 1978.
[15] "The Determination of J_{IC}, a Measure of Fracture Toughness," working document of ASTM Subcommittee E24.08 on Elastic-Plastic and Fully Plastic Fracture Mechanics Terminology, American Society for Testing and Materials, 1980.
[16] Landes, J. D., *International Journal of Fracture*, Vol. 16, 1980, p. R183.
[17] Landes, J. D. and Begley, J. A. in *Fracture Analysis, ASTM STP 560*, American Society for Testing and Materials, 1974, pp. 170–186.
[18] Paris, P. C., discussion presented at meeting of *J*-Integral Task Group, American Society for Testing and Materials, 10 Oct. 1973, Carnegie-Mellon University, Pittsburgh, Pa.
[19] Bucci, R. J., *Engineering Fracture Mechanics*, Vol. 12, 1979, p. 407.
[20] Hudson, C. M. and Seward, S. K., *Engineering Fracture Mechanics*, Vol. 8, 1976, p. 315.
[21] Verkin, B. I. and Grinberg, N. M., *Material Sciences Engineering*, Vol. 41, 1979, p. 149.
[22] Hopkins, P. and Jolley, G., *Fracture 1977*, Vol. 3, 1977, p. 329.
[23] Kobayaski, H., Nakamura, H., and Nakazawa, H., *Recent Research in Mechanical Behavior of Solids*, University of Tokyo Press, Tokyo, 1979, p. 341.

DISCUSSION

A. J. McEvily[1] *(written discussion)*—What is the reason for the larger amount of crack advance in vacuum as compared to air for the last of the series of overloads applied?

N. Ranganathan and J. Petit (authors' closure)—For the last overload in the two specimens the K_{peak} values are not the same. The value in vacuum is 44.3 MPa$\sqrt{m}$ and in air is 42.6 MPa$\sqrt{m}$. This factor enhances any differences in the tear size and shape due to environment.

Considering the third overloads in the two specimens which were conducted at the same K_{peak} of 33.08 MPa$\sqrt{m}$, one notices the tear in vacuum extends over a larger distance and the shape of this zone is different from that in air.

The fracture in these specimens takes place in mixed plane strain and plane

[1]Professor, Department of Metallurgy, University of Connecticut, Storrs, Conn. 06268.

stress modes. To the authors' knowledge no rigorous treatment exists in the literature regarding this type of fracture.

As has been previously reported [*12,21*], the accumulated plastic strain is higher in vacuum than in air, especially on the specimen surface. This means that the pinching effect is greater in vacuum near the surface, thus inhibiting crack advance in the plane stress region during the overload; conversely, the crack tunneling at the center is higher.

Summary

Summary

A period was set aside at the end of the conference for open discussion. The discussions centered around the question "What is fatigue damage?" Written contributions provided by some of the authors and other participants, both during the conference and after further reflection, are excerpted here. These contributions reflect, more or less, the spirit and essence of these discussions. In light of these discussions, a few closing comments are offered by the editors with respect to the conference and to the future direction of fatigue research.

To place the discussions in perspective, one might first respond to the question "Why should one be concerned with the understanding of mechanisms for fatigue and, more specifically, with the definition of fatigue damage?" A response might be gleaned from the following rhetorical question: How else can one provide assurance or reliable estimates of *long* fatigue lives on the basis of *short-term* data? This assurance can be derived only through a suitable blending of testing with mechanistic understanding and modeling of the processes of fatigue damage accumulation. Another response may be found in the closing remarks by J. C. Grosskreutz for a session on Direct Observations from Slipbands to Nucleation of Microcracks at the 1978 ASTM Symposium on Fatigue Mechanisms:

> The reasons why we do this work to understand the mechanisms of fatigue are so that we can do a better job of predicting fatigue life, of finding ways of nondestructive testing for fatigue damage, and of developing new materials which will be fatigue resistant. In the final analysis, that is why we do the work; or why you do the work now.[1]

One cannot begin to understand the mechanisms of fatigue without knowing what is fatigue damage. One certainly cannot make *quantitative* measurements unless fatigue damage is first *quantitatively* defined. Hence the central question of the discussion: "What is fatigue damage?"

Contributions During Conference

W. J. Baxter (author), General Motors Research Laboratories, Warren, Michigan: [I would define] fatigue damage [as] localized irreversible slip

[1] *Fatigue Mechanisms, ASTM STP 675*, J. T. Fong, Ed., American Society for Testing and Materials, 1979, p. 276.

which nucleates a crack. Quantitative measurement [of this damage can be made by measuring the] associated rupture of a thin surface oxide film [using a] gel electrode or exoelectrons.

R. N. Pangborn (author), Penn State University, University Park, Pennsylvania: [I would define] fatigue damage [as] reduction in life (fraction of life expended). The parameters [that can be] used to monitor (not measure) fatigue damage (prior to crack initiation) [include] change in surface and subsurface microplasticity, residual stress, and dislocation density. These parameters can be measured quantitatively, but since they are material and stress dependent, the relative changes during fatiguing must be evaluated.

We cannot directly measure damage defined in this manner. We can only monitor microstructural changes that contribute collectively to the accumulation of damage.

Julia R. Weertman (author), Northwestern University, Evanston, Illinois: The most significant damage produced in many metals and alloys fatigued at elevated temperatures occurs in the form of grain boundary cavities, whose nucleation, growth, and coalescense can lead to intergranular failure. Small-angle neutron scattering (SANS) measurements of single-phase materials fatigued at elevated temperature produce values for void volume fraction, number, density, and size distribution of voids. From this information can be calculated void nucleation rates and individual void growth rates as functions of loading parameters (T, $\Delta\sigma$ or $\Delta\epsilon$, ν, R, etc.).

H. Mughrabi (author), Max-Planck-Institut für Metallforschung, Institut für Physik, 7000 Stuttgart 80, Federal Republic of Germany: The wide span of topics considered at this conference can be taken as an indication that it may not be wise to attempt a general definition of fatigue damage. Hence I find myself less ambitious than most of the earlier speakers and plead that, in any particular instance, it is essential to assess whether, and what type of, fatigue damage prevails. That done, one has to go into the details of that particular fatigue damage, as exemplified in some of the earlier presentations. I find a clarification of such details more rewarding than a search for a general but almost necessarily unspecific definition of a complex phenomenon.

My co-authors and I wished to consider the following types of fatigue damage: (1) *persistent slip bands* (PSBs) characterized by extrusion shape and height; roughness profile of extrusion; and microcracks formed (*a*) at the interfaces between PSB and matrix, and (*b*) in valleys of surface roughness of PSB-surface profile (2) *Surface roughness* originating from (random) irreversible slip within PSBs and in planar slip materials without PSBs. For lack of more pertinent, less easily accessible parameters, we characterized the surface roughness by the mean width $\bar{w}$ of the surface profile, referred to as a certain thickness h of the slip region considered. A more desirable

parameter would be the probability of finding a notch of a certain depth and sharpness. (3) Fatigue damage at grain boundaries (GBs) due to impinging PSBs in the form of (*a*) slip step formation at GBs, and (*b*) PSB-GB cracks. In a related sense, I would like to mention the sharp slip offsets in planar slip precipitation-hardened alloys.

S. D. Antolovich (author), University of Cincinnati, Cincinnati, Ohio: If we have difficulty defining damage in a quantitative sense (and that is certainly clear from the various presentations), it seems equally clear that some qualitative distinctions can be made. I suggest the following qualitative distinctions: (1) Persistent slip bands in materials such as copper (high stacking fault energy solid solutions). (2) Shearing of precipitates in nickel-base alloys. (Here the amount of reversibility is certainly a consideration.) (3) Generation of irreversible dislocation debris in fcc metals of low stacking fault energy. By this, I mean Cottrell-Lomer locks and their associated tetrahedral defects. (4) In alloys that deform by planar glide (either low stacking fault energy solid-solution alloys or [alloys that contain] coherent ordered precipitates) but contain embrittling agents on the boundaries (that is, carbides, dissolved oxygen, etc.), damage results from a pile-up of dislocations at the boundary and occurs as an intergranular crack; this is a static mode. (5) Another static mode is cracking of brittle particles in the plastic zone at high ΔK as a result of critical strain criterion. (6) In bcc metals at low temperatures, it would seem (speculation) that damage would be an accumulation of $a[100]$ dislocations which coalesce into a microcrack. Their formation is driven by plastic deformation according to the reaction

$$\underset{\text{glide}}{\frac{a}{2}[11\bar{1}]} + \underset{\text{glide}}{\frac{a}{2}[\bar{1}\bar{1}\bar{1}]} \rightarrow \underset{\text{sessile}}{a[001]}$$

P. Abelkis (discusser), Douglas Aircraft Company, Long Beach, California: From a practical point of view, as we design structures to carry loads, the stage of damage at which the structure is unable to carry the design static load may be considered to be one important aspect of damage. The other is the life remaining to reach that stage. Damage [may be considered as] anything that leads to crack formation and propagation and reduction of static strength. Let us identify these items and define their importance quantitatively and qualitatively to the fatigue failure process. Some of these items will only be important for estimating life, others for predicting residual strength. [I would like to ask the following] questions: (1) Is intermittent crack growth referring basically to near-threshold growth under constant-amplitude loading? (2) Where is all this basic research in materials fatigue failure processes (damage measurements) leading to? (*a*) Improved fatigue materials? and (*b*) Improved life prediction? Where are we at this stage with respect to these questions?

A. K. Chakralearti (discusser), Detroit Diesel Allison (GMC), Indianapolis, Indiana: Damage is defined as the process by which ductility exhaustion takes place ahead of the crack tip on a microlevel so that the crack can propagate or grow intermittently. Moreover, discussors feel that a critical damage [state] is required at the growing crack tip after every stepwise growth at the end of which the crack can progress by another step again. Mechanistic studies and definition of damage process may help in understanding the role of fundamental material parameters related to crack growth processes, and this in turn will help develop better material.

C. E. Jaske (discusser), Battelle Columbus Laboratories, Columbus, Ohio: Fatigue damage is a physical change in a material resulting from cyclic loading that reduces the ability of the material to perform its intended function. We need damage studies at the long lives and low growth rates most relevant to many engineering applications. Too many studies are at short times for the convenience of investigation in the laboratory.

Post-Conference Contributions

P. E. Bretz (discusser), Aluminum Company of America, Alcoa Technical Center, Pennsylvania: [The situation, I believe, indicates] that the problem of fatigue damage needs to be brought into perspective a little better than we were able to do in the heat of discussion. In my mind, the relevant question is "Why do we need to measure fatigue damage?" One reason is certainly to predict remaining lives in structures. The other is to understand damage from a microstructural point of view, so that the metallurgist may build into new alloys those features which inhibit fatigue damage. We must ask ourselves whether our definitions and measurements of fatigue damage will help either the design engineer or the metallurgist do his job. Probably no single definition or measurement will fulfill both requirements, but certainly we ought to keep at least one of these two goals in mind at all times. It would be interesting to hear each of the conference authors relate his work to one of these goals.

E. E. Underwood (discusser), Georgia Institute of Technology, Atlanta, Georgia: It is apparent that this audience represents many diverse views on the definition of damage, as reflected in the philosophy, background, or practical requirements of each participant. Out of the gamut of definitions offered, however, it appears that two broad categories are possible: one based on mechanical properties and another based on microstructural deterioration.

I would like to offer a list of microstructural damage events that could collectively define damage: (1) *The Fatigue Crack*. This includes the main crack, branches, segments, and their planarity, jaggedness, preferred path,

degree of orientation, etc. (2) *Cavitation*. At grain boundaries: ahead of the crack tip, dimples, linking, finger growth. At particles: where particle fractures, disbonding, and shearing precede cavity formation. (3) *Microstructural Changes*. Matrix changes, including dislocation density and configurations, grain shape changes, multiple slip bands, grain boundary thickening, ledge formation, and PFZ/s. In the vicinity of the crack tip: particle damage, dimples, microcracks, particle disbonding, etc. (4) *Changes at the Specimen Surface*. Persistent slip bands, extrusions, intrusions, grain upheavals, grain boundary thickenings, etc.

These damage events can all be quantified in the sense that their size, extent, distribution, spacings, orientations, etc., can be described quantitatively,[2,3] based on quantitative stereological measurements on the plane of polish. A more difficult task is the quantification of features in the nonplanar fracture plane. A concerted effort is underway in this more difficult area, and new results are already becoming available.[3,4]

Final Remarks

What is the current state of affairs? What are the directions for fatigue research in the future? In his concluding remarks given to the 1978 ASTM symposium referred to previously, JoDean Morrow made the following statement, perhaps in frustration but which nevertheless must be taken seriously:

> Finally, I am somewhat disappointed that I don't have any better idea of what fatigue damage is than I did at the beginning of this symposium. It hasn't been defined.[5]

Similar sentiments were expressed by some at this conference as well.

More realistically and optimistically, this conference has served to open yet another dialogue between researchers in fatigue and between the scientific and engineering communities, whereby the issues of what is fatigue damage and why its quantitative understanding is important are addressed. An effort was made to directly confront the question "What is fatigue damage?" Two definitions were developed:

- Fatigue [damage] is a chemical-physical process whereby *irreversible degradation of a specific property* results from the application of cyclic stress and strain.

[2]Underwood, E. E. and Starke, E. A., Jr., in *Fatigue Mechanisms, ASTM STP 675*, J. T. Fong, Ed., American Society for Testing and Materials, 1979, p. 633-682.

[3]Underwood, E. E. and Chakrabortty, S. B. in *Fractography and Materials Science, ASTM STP 733*, L. N. Gillbertson and R. D. Zipp, Eds., American Society for Testing and Materials, 1981, pp. 337-354.

[4]Underwood, E. E. and Underwood, E. S., "Quantitative Fractography by Computer Simulation," in *Proceedings*, Third European Symposium for Stereology, M. Kališnik, Ed., Ljubljana, Yugoslavia, 1982.

[5]*Fatigue Mechanisms, ASTM STP 675*, J. T. Fong, Ed., American Society for Testing and Materials, 1979, p. 891.

- Fatigue damage is physical separation of the material (cracks, cavitation, etc.)

These definitions, along with the foregoing responses, suggest progress but, more importantly, point out the need for a continuing dialogue between researchers and engineers.

To make meaningful progress, we must make a clearer distinction between:

- *Physical* damage (cavities, microcracks, etc.).
- *Process* of damage (cyclic slip etc.)
- *Manifestation* of damage (X-ray line broadening, cyclic stress-train response, etc.)

We need to recognize the stoichastic nature of fatigue, and need more quantitative measurements that are repeatable and representative. Whatever parameter we choose to represent fatigue damage must be consistent with the desired end use; that is, for life prediction, material improvement, etc. We must also narrow the dichotomy between continuum mechanics concepts and microstructural realities, between the state variables and metallurgical approaches.

In viewing the conference in retrospect, we believe that progress *has* been made since 1978—not as much as some of us would like to see or expect, perhaps, but nonetheless noticeable and meaningful progress. With the development of more advanced instrumentation, we can look forward to more significant advances in understanding. It is clear that our efforts can be made more effective by more sharply focused questions and more critical and unequivocal experimentation.

On behalf of the sponsoring ASTM committees, we express our sincere appreciation to the authors and discussers for their contributions and for being very frank and open in sharing their views. We acknowledge the support of the Office of Naval Research and the assistance of the ASTM staff in this endeavor.

J. Lankford

Southwest Research Institute, San Antonio, Texas; symposium co-chairman and editor

W. L. Morris

Rockwell International, Thousand Oaks, California; symposium co-chairman and editor

D. L. Davidson

Southwest Research Institute, San Antonio, Texas; symposium co-chairman and editor

R. P. Wei

Lehigh University, Bethlehem, Pennsylvania; symposium co-chairman and editor

Index

E

F

V